

ANCHORAGE OF HEADED REINFORCING BARS IN CONCRETE

By

Krishna P. Ghimire, David Darwin, Matthew O'Reilly

A Report on Research Sponsored by

Electric Power Research Institute
Concrete Reinforcing Steel Institute Education and Research
Foundation

BarSplice Products, Incorporated
Headed Reinforcement Corporation
LENTON[®] products from Pentair[®]

Structural Engineering and Engineering Materials
SM Report No. 127
January 2018

THE UNIVERSITY OF KANSAS CENTER FOR RESEARCH, INC.
2385 Irving Hill Road, Lawrence, Kansas 66045-7563



ANCHORAGE OF HEADED REINFORCING BARS IN CONCRETE

By

Krishna P. Ghimire

David Darwin

Matt O'Reilly

A Report on Research Sponsored by

Electric Power Research Institute

Concrete Reinforcing Steel Institute Education and Research Foundation

BarSplice Products, Incorporated

Headed Reinforcement Corporation

LENTON[®] products from Pentair[®]

Structural Engineering and Engineering Materials

SM Report No. 127

THE UNIVERSITY OF KANSAS CENTER FOR RESEARCH, INC.

LAWRENCE, KANSAS

January 2018

ABSTRACT

Headed reinforcing bars serve as a viable alternative to hooked bars for anchorage in concrete because they provide a more efficient anchorage mechanism and limit congestion of the reinforcement. This study is part of a comprehensive study of the anchorage behavior of the headed bars. The work described in this report includes tests of 32 No. 8 headed bars anchored in simulated column-foundation joints represented by bars anchored in slabs, all but two with reinforcement in the plane of the slab, and six lapped-splice specimens without confining reinforcement containing No. 6 headed bars and an analysis of these tests along with test results from 23 studies by other researchers of 84 exterior, seven roof-level interior, and seven knee beam-column joints subjected to reversed cyclic loading. The headed bars in the column-foundation joint specimens had net bearing areas ranging from 4 to 15 times the area of the bar A_b ; some of the headed bars contained large obstructions adjacent to the bearing face of the head that exceeded the dimensional limits for HA heads in ASTM A970-16; embedment lengths ranged from 6 to 8.5 in.; reinforcement in a plane perpendicular to the headed bars included combinations of bars placed symmetrically about the headed bar, parallel and close to the long edges of the specimen, bars placed symmetrically about and close to the headed bar in the short direction of the specimen, and bars oriented in both the long and short directions of the specimen; concrete compressive strengths ranged from 4,200 to 8,620 psi; and stresses in the bars at failure ranged from 49,500 to 117,000 psi. The No. 6 headed bars had a net bearing area of $4A_b$ and a lap length of 12 in. The center-to-center spacing between the spliced bars was 1.67, 2.33, or 3.53 bar diameters d_b ; clear concrete cover to the bars was 2 in.; concrete compressive strengths averaged 6,360 and 10,950 psi; and stresses in the bars at failure ranged from 75,010 to 83,560 psi. For the beam-column joints subjected to reversed cyclic loading, headed bar sizes ranged between D12 (No. 4) and D36 (No. 11), net bearing areas ranged from 1.7 to $11.4A_b$, and embedment lengths ranged from 8 to $22.6d_b$; concrete compressive strengths ranged from 3,480 to 21,520 psi and steel yield strengths ranged from 53,650 to 149,930 psi; all but four specimens contained hoops, spaced at 2.2 to $6.8d_b$ (1.8 to 5.9 in.), as confining reinforcement parallel to the headed bar within the joint region; clear cover and minimum center-to-center spacing between the bars ranged from 1.4 to $9.9d_b$ and from 2 to $11.2d_b$, respectively.

Experimental anchorage strengths are compared with values based on descriptive equations for anchorage strength and design provisions for development length of headed bars for members with concrete compressive strengths up to 16,000 psi and steel yield strengths up to 120,000 psi that recognize the contribution of confining reinforcement without specifying minimum limits on bar spacing or clear cover. The descriptive equations and design provisions were developed based on tests of simulated beam-column joints under monotonic loading as part of the comprehensive study. The comparisons are used to expand the applicability of the descriptive equations to members subjected to reversed cyclic loading and develop simplified design guidelines allowing for the use of headed reinforcing bars in wide range of reinforced concrete members. Changes in the provisions of ACI 318-14 for the development length of headed bars and in ASTM A970 for head dimension requirements are also proposed.

The results of this study show that reinforcement perpendicular to headed bars in column-foundation joints does not improve the anchorage strength. Headed bars with obstructions exceeding the dimensional limits for HA heads in ASTM A970-16 provide adequate anchorage strength. Headed bars did not provide sufficient anchorage in knee beam-column joints subjected to reversed cyclic loading. The descriptive equations and proposed design provisions developed based headed bars in beam-column joint specimens tested under monotonic loading, in which the anchorage strength of the headed bar is a function of embedment length, concrete compressive strength, bar spacing, bar diameter, and confining reinforcement within the joint region, are applicable to a wide range of reinforced concrete members, including beam-column joints subjected reversed cyclic loading, lap splices, and column-foundation joints, and allow the minimum clear spacing of $3d_b$ between headed bars permitted in joints in special moment frames in accordance with Section 18.8.5.2 of ACI 318-14 to be reduced to $1d_b$, allowing for the use of more closely spaced headed bars. The anchorage strength of the headed bars calculated using anchorage provisions of Chapter 17 of ACI 318-14 with a strength reduction factor of 1.0 provides a very conservative and highly variable estimate of anchorage strength for headed bars compared to the proposed design provisions.

Keywords: anchorage, beam-column joint, bond and development, column-foundation joint, headed bar, high-strength concrete, high-strength steel, splice, reversed cyclic loading

ACKNOWLEDGEMENTS

This report is based on a thesis presented by Krishna P. Ghimire in partial fulfillment of the requirements for the Ph.D. degree from the University of Kansas. Support for the study was provided by the Electric Power Research Institute, Concrete Reinforcing Steel Institute Education and Research Foundation, BarSplice Products, Inc., Headed Reinforcement Corp., and LENTON[®] products from Pentair[®]. Additional materials were supplied by Commercial Metals Company, Gerdau Corporation, Nucor Corporation, MMFX Technologies Corporation, Dayton Superior, Midwest Concrete Materials, and Grace Construction Products. Thanks are due to Ken Barry, Mark Ruis, and David Scott who provided project oversight for the Advanced Nuclear Technology Program of the Electric Power Research Institute, and to Neal Anderson, Cary Kopczynski, Mike Mota, Javeed Munshi, and Conrad Paulson who served as industry advisors.

TABLE OF CONTENTS

ABSTRACT	i
ACKNOWLEDGEMENTS	iii
LIST OF FIGURES	ix
LIST OF TABLES	xviii
CHAPTER 1: INTRODUCTION	1
1.1 GENERAL	1
1.2 PREVIOUS STUDIES	2
1.2.1 Early headed stud and headed bar studies	2
1.2.2 Tests on slab and column-like specimens	3
1.2.3 Tests on headed bar splices	7
1.2.4 Tests on compression-compression-tension (CCT) nodes	12
1.2.5 Tests on beam-column joints under monotonic loading	16
1.2.6 Tests on beam-column joints subjected to reversed cyclic loading	21
1.3 CURRENT CODE PROVISIONS AND DESIGN RECOMMENDATIONS	22
1.4 NEWLY PROPOSED DESCRIPTIVE EQUATIONS AND DESIGN PROVISIONS	26
1.4.1 Descriptive Equations	26
1.4.2 Design Provisions	28
1.5 OBJECTIVE AND SCOPE	30
CHAPTER 2: EXPERIMENTAL WORK	33
2.1 MATERIAL PROPERTIES	33
2.1.1 Concrete Properties	33
2.1.2 Steel Properties	34
2.2 SLAB SPECIMENS	38
2.2.1 Specimen Design	38
2.2.2 Test Parameters	41
2.2.3 Specimen Designation	41

2.2.4 Specimen Fabrication.....	42
2.2.5 Test Procedure	43
2.3 SPLICE SPECIMENS	44
2.3.1 Specimen Design	44
2.3.2 Test Parameters.....	45
2.3.3 Specimen Designation	45
2.3.4 Specimen Fabrication.....	46
2.3.5 Test Procedure	46
2.3.6 Specimen Instrumentation	49
CHAPTER 3: TEST RESULTS	50
3.1 TESTS ON HEADED BARS ANCHORED IN SLAB SPECIMENS WITH SHALLOW EMBEDMENT	50
3.1.1 Failure Modes	52
3.1.2 Effect of Strut Angle.....	54
3.1.3 Effect of Reinforcement in a Plane Perpendicular to Headed Bar.....	56
3.1.4 Effect of Net Bearing Area of Head	60
3.1.5 Effect of Concrete Compressive Strength.....	61
3.2 HEADED BAR SPLICE TESTS.....	63
3.2.1 Failure Modes	64
3.2.2 Effects of Lapped Bar Spacing and Concrete Compressive Strength.....	65
3.2.3 Load-Deflection and Strain in Lapped Bars	68
3.3 ANALYSIS OF TEST RESULTS FROM OTHER STUDIES AND COMPARISONS WITH THE CURRENT STUDY	70
3.3.1 Headed Bars Tested in Slab and Column-like Specimens.....	73
3.3.1.1 Analysis Based on Descriptive Equations and Anchorage Provisions of ACI 318-14	75
3.3.1.2 Effect of Reinforcement in a Plane Perpendicular to the Headed Bar.....	89
3.3.2 Headed Bar Splice Specimens	91

3.3.2.1 Analysis Based on Descriptive Equations	92
3.3.2.2 Effect of Lapped Bar Spacing on Splice Strength	96
CHAPTER 4: ANALYSIS OF BEAM-COLUMN JOINT SPECIMENS SUBJECTED TO REVERSED CYCLIC LOADING	99
4.1 INTRODUCTION	99
4.2 ANALYSIS BASED ON NEWLY PROPOSED DESCRIPTIVE AND DESIGN EQUATIONS	100
4.2.1 Descriptive Equations and Design Provisions Proposed by Shao et al. (2016).....	100
4.2.2 Exterior and Roof-level Interior Beam-Column Joints.....	103
4.2.2.1 Specimens with $d/\ell_{eh} \leq 1.5$ and $\ell_{eh}/\ell_{ehy} < 1.0$	114
4.2.2.2 Specimens with $d/\ell_{eh} \leq 1.5$ and $\ell_{eh}/\ell_{ehy} \geq 1.0$	115
4.2.2.3 Specimens with $d/\ell_{eh} > 1.5$	119
4.2.2.4 Headed bar spacing.....	126
4.2.2.5 Summary	131
4.2.3 Knee Beam-Column Joints	132
4.3 EFFECT OF HEAD SIZE	140
4.3.1 Specimens with bearing area $A_{brg} \geq 3.7A_b$	142
4.3.2 Specimens with bearing area $A_{brg} < 3.7A_b$	145
4.4 ANALYSIS OF HEADED BARS IN BEAM-COLUMN JOINTS USING ANCHORAGE PROVISIONS IN ACI BUILDING CODE.....	148
CHAPTER 5: DESIGN PROVISIONS	155
5.1 DESIGN EQUATION	155
5.1.1 Confinement and spacing factor, ψ_{cs}	156
5.1.2 Bar location factor, ψ_o	158
5.1.3 Comparisons of test results	158
5.1.4 Range of specified yield strength.....	165
5.1.5 Stress multiplier	165
5.1.6 Further simplification of design equation	166

5.1.7 Head size	166
5.2 PROPOSED CODE PROVISIONS.....	172
5.2.1 Proposed Changes in ACI 318.....	172
5.2.2 Proposed Changes in ASTM A970.....	183
5.3 EXAMPLE DESIGN PROBLEMS.....	187
CHAPTER 6: SUMMARY AND CONCLUSIONS	189
6.1 SUMMARY.....	189
6.2 CONCLUSIONS.....	190
6.3 FUTURE WORK.....	191
REFERENCE	193
APPENDIX A: NOTATION.....	199
APPENDIX B: DETAILS OF SLAB AND SPLICE SPECIMENS TESTED IN THE CURRENT STUDY	205
B.1 STRESS-STRAIN CURVES FOR HEADED BARS	205
B.2 SCHEMATICS OF SLAB SPECIMENS.....	206
B.3 CROSS-SECTIONS OF HEADED SPLICE SPECIMENS.....	213
B.4 STRAIN IN LAPPED BARS IN HEADED SPLICE SPECIMENS	215
APPENDIX C: TEST RESULTS AND SPECIMENS FROM OTHER STUDIES INCLUDED IN THE CURRENT STUDY.....	218
C.1 SLAB AND COLUMN-LIKE SPECIMENS.....	218
C.2 EXTERIOR AND ROOF-LEVEL INTERIOR BEAM-COLUMN JOINT SPECIMENS....	223
C.3 KNEE BEAM-COLUMN JOINT SPECIMENS.....	247
APPENDIX D: SUMMARY OF STUDIES ON BEAM-COLUMN JOINTS TESTED UNDER REVERSED CYCLIC LOADING.....	250

LIST OF FIGURES

Figure 1.1 Types of beam-column joints studied in the current study.....	2
Figure 1.2 (a) Unbonded and (b) bonded lengths of the headed bar tested by DeVries et al. (1999).....	4
Figure 1.3 Slab specimens tested by Choi et al. (2002).....	6
Figure 1.4 Column-like specimens tested by Choi et al. (2002) and Choi (2006).....	6
Figure 1.5 Reinforcement detail of splice specimens (a) top view and (b) side view (Thompson et al. 2002)	8
Figure 1.6 Detail of headed splice confinement using hairpin and hoop tie-downs, after Thompson et al. (2002).....	8
Figure 1.7 Force transfer mechanism in lapped bars (struts in the picture are marked for this report), Thompson et al. (2002)	9
Figure 1.8 CCT node specimens (a) without and (b) with confining reinforcement, after Thompson (2002).....	14
Figure 1.9 CCT node specimens tested by Shao et al. (2016)	16
Figure 1.10 Crack pattern of a specimen at failure (headed bar and cracks in the picture are highlighted for this report), Bashandy (1996).....	18
Figure 1.11 Critical section for headed bar in Type 1 and Type 2 joints.....	24
Figure 1.12 Effective confining reinforcement within the joint region of beam-column joints suggested by Shao et al. (2016)	30
Figure 2.1 (a) Left to right: cold-swaged threaded coupling sleeve, friction-forged, taper-threaded, and cold-swaged No. 8 headed bars (figure from Shao et al. 2016); (b) and (c) obstruction adjacent to the bearing face of the friction-forged heads; and (d) gap in the obstruction adjacent to the bearing face of the cold-swaged threaded coupling sleeve heads (taper-threaded and cold-swaged heads had no obstructions)	35
Figure 2.2 Friction-forged obstruction adjacent to the bearing face of F4.1 and F9.1 headed bars (also see Figures 2.1b and c).....	36
Figure 2.3 Schematic view of slab specimens in Series 1 to 5 (a) front view, (b) side view	39
Figure 2.4 Schematic view of slab specimens in Series 6 (a) front view, (b) side view.....	40

Figure 2.5 Slab specimen designation.....	42
Figure 2.6 Slab specimen formwork	43
Figure 2.7 Splice test specimen detail and test configuration.....	44
Figure 2.8 Lap configuration of headed splice specimens.....	45
Figure 2.9 Splice specimen designation.....	46
Figure 2.10 Schematic view of splice test (a) front view and (b) side view	48
Figure 2.11 Location of infrared markers marked by circles.....	49
Figure 3.1a Breakout failure of slab specimen 8-5-S14.9-6#5-6 from test Series 5 with one of the supports within the failure region	52
Figure 3.1b Breakout failure of slab specimen 8-5-F4.1-6#5-6 from test Series 5 with both supports outside the failure region (specimen contained a single bar anchored at the middle of the slab)	53
Figure 3.1c Breakout failure of slab specimen 8-5-F4.1-0-6 from test Series 6 with both supports outside the failure region (location of the headed bar is shown)	53
Figure 3.2 Compression region between anchored headed bar and nearest support	54
Figure 3.3 Bar force at failure normalized with respect to a concrete compressive strength of 5,000 psi and an embedment length of 6 in. T_N versus the ratio h_{cl}/ℓ_{eh} [T_N is calculated using Eq. (3.1), only specimens with A_{brg} ranging from 4 to $9.5A_b$ are included].....	55
Figure 3.4 Dowel action of reinforcement perpendicular to the headed bar.....	56
Figure 3.5 Location of headed bars and reinforcement in a plane perpendicular to the headed bar: (a) front and (b) side views of specimens in the first five series, (c) front and (d) side views of specimens in Series 6 (details of reinforcement configuration for all specimens are provided in Section B.2 of Appendix B).....	57
Figure 3.6 Slab specimens in Series 1 and 2 that contained No. 4 and No. 5 bars perpendicular to the headed bar distributed evenly along the long and short direction of the specimen	58
Figure 3.7 Bar force at failure normalized with respect to a concrete compressive strength of 5,000 psi and an embedment length of 6-in. T_N versus area of reinforcement A_{st} , within a $1.5\ell_{eh}$ radial distance from the center of and in a plane perpendicular to the headed bar, normalized with respect to the area of the headed bar A_b [T_N is calculated using Eq. (3.1); specimens with A_{brg} ranging from 4 to $9.5A_b$ and h_{cl}/ℓ_{eh} ranging from 1.24 to 2.79 are included]	59

Figure 3.8 Bar force at failure normalized with respect to a concrete compressive strength of 5,000 psi and an embedment length of 6 in. T_N versus the net bearing area of the head A_{brg} [T_N is calculated using Eq. (3.1); only specimens with h_{cl}/ℓ_{eh} ranging from 1.24 to 2.79 are included]	61
Figure 3.9 Bar force at failure normalized with respect to an embedment length of 6 in. T_N versus concrete compressive strength f_{cm} [T_N is calculated using Eq. (3.2), only specimens with h_{cl}/ℓ_{eh} ranging from 1.24 to 2.79 and A_{brg} ranging from 4 to $9.5A_b$ are included]	62
Figure 3.10 Bar force at failure normalized with respect to an embedment length of 6 in. T_N versus concrete compressive strength f_{cm} [T_N is calculated using Eq. (3.3), only specimens with h_{cl}/ℓ_{eh} ranging from 1.24 to 2.79 and A_{brg} ranging from 4 to $9.5A_b$ are included]	63
Figure 3.11 (a) Cracking pattern and failure mode of headed splice specimens (top view) (b) cracking patterns and failure mode of Specimen (3) 6-12-S4.0-12-0.5	65
Figure 3.12 Stress-strain behavior for headed bars used in splice specimens	66
Figure 3.13 Average maximum force T in spliced headed bars versus the center-to-center spacing and concrete compressive strength	67
Figure 3.14 Average maximum stress f_{su} in spliced headed bars versus the center-to-center spacing and concrete compressive strength	68
Figure 3.15 Load-deflection diagram for Specimen (3) 6-12-S4.0-12-0.5	69
Figure 3.16 Strain in lapped bars in specimen (3) 6-12-S4.0-12-0.5 as a function of total applied load P	70
Figure 3.17 (a) Unbonded and (b) bonded lengths of the headed bar tested by DeVries et al. (1999)	74
Figure 3.18 Slab specimens tested by Choi et al. (2002)	75
Figure 3.19 Column-like specimens tested by Choi et al. (2002) and Choi (2006)	75
Figure 3.20 Bar force at failure T versus anchorage strength T_h calculated using Eq. (3.4) for slab specimens tested by DeVries et al. (1999) and Choi et al. (2002), and in the current study; a modification factor of 0.8 for headed bars with concrete cover less than $8d_b$ is applied to T_h as appropriate (for specimens tested in the current study, only those with A_{brg} ranging from 4 to $9.5A_b$ are included)	79
Figure 3.21 Bar force at failure T versus the anchorage strength T_h calculated using Eq. (3.4) and (3.5) for column-like specimens tested by Choi et al. (2002) and Choi (2006); a modification factor of 0.8 for headed bars with concrete cover less than 2.5 in. is applied to T_h	82

Figure 3.22 Column ties as anchor reinforcement and column longitudinal bars as reinforcement in a plane perpendicular to the headed bars in column-like specimens tested by Choi et al. (2002) and Choi (2006)	83
Figure 3.23 Bar force at failure T versus the anchorage strength T_{anc} calculated using Eq. (3.9) for slab specimens tested by DeVries et al. (1999), Choi et al. (2002), Choi (2006), and in the current study.....	84
Figure 3.24 Bar force at failure T versus the anchorage strength T_{anc} calculated using Eq. (3.9) for column-like specimens tested by Choi et al. (2002) and Choi (2006)	85
Figure 3.25 Distribution of ratios T/T_h and T/T_{anc} for headed bars in slab specimens tested by DeVries et al. (1999).....	87
Figure 3.26 Distribution of ratios T/T_h and T/T_{anc} for headed bars in slab specimens tested by Choi et al. (2002)	87
Figure 3.27 Distribution of ratios T/T_h and T/T_{anc} for headed bars in column-like specimens tested by Choi et al. (2002) and Choi (2006).....	88
Figure 3.28 Distribution of ratios T/T_h and T/T_{anc} for headed bars in slab specimens tested in the current study.....	88
Figure 3.29 Ratio of bar force at failure T to the force calculated using Eq. (3.4) and (3.5) T_h versus reinforcement in a plane perpendicular to the headed bar A_{st} normalized to the total area of the headed bars sharing that reinforcement nA_b for column-like specimens tested by Choi et al. (2002) and Choi (2006) and slab specimens tested in the current study [for specimens tested in the current study, only those with h_{cl}/ℓ_{eh} ranging from 1.24 to 2.79 and A_{brg} ranging from 4 to $9.5A_b$ are included].....	90
Figure 3.30 Bar force normalized to 5,000 psi concrete compressive strength and 12 in. lap length T_N versus lapped bar spacing for specimens tested by Thompson et al. (2002) and Chun (2015) containing no confining reinforcement and all specimens tested in the current study	97
Figure 4.1 Types of beam-column joints studied in the current study.....	99
Figure 4.2 Effective confining reinforcement within the joint region of beam-column joints suggested by Shao et al. (2016)	102
Figure 4.3 M_{peak}/M_n versus ℓ_{eh}/ℓ_{ehy} for specimens with $d/\ell_{eh} \leq 1.5$ and $V_p/V_n < 1.0$. M_{peak}/M_n is the ratio of peak moment to nominal flexural strength, and ℓ_{eh}/ℓ_{ehy} is the ratio of embedment length to the embedment length required to yield the headed bar calculated using the descriptive equations, Eq. (4.1) and (4.2).....	112

Figure 4.4 M_{peak}/M_n versus ℓ_{eh}/ℓ_{ehy} for specimens with $d/\ell_{eh} \leq 1.5$ and $V_p/V_n \geq 1.0$. M_{peak}/M_n is the ratio of peak moment to nominal flexural strength, and ℓ_{eh}/ℓ_{ehy} is the ratio of embedment length to the embedment length required to yield the headed bar calculated using the descriptive equations, Eq. (4.1) and (4.2).....	113
Figure 4.5 V_p/V_n versus ℓ_{eh}/ℓ_{ehy} for specimens with $d/\ell_{eh} \leq 1.5$. V_p/V_n is the ratio of peak joint shear to nominal joint shear strength, and ℓ_{eh}/ℓ_{ehy} is the ratio of embedment length to the embedment length required to yield the headed bar calculated using the descriptive equations, Eq. (4.1) and (4.2).....	118
Figure 4.6 M_{peak}/M_n versus V_p/V_n for specimens with $d/\ell_{eh} \leq 1.5$ and $\ell_{eh}/\ell_{ehy} \geq 1.0$. M_{peak}/M_n is the ratio of peak moment to nominal flexural strength, and V_p/V_n is the ratio of peak joint shear to nominal joint shear strength.....	119
Figure 4.7 Ratio of test-to-calculated failure load T/T_h versus ratio of effective beam depth to embedment length d/ℓ_{eh} for specimens without confining reinforcement [T_h is calculated using Eq. (4.1)] (Shao et al. 2016).....	120
Figure 4.8 Ratio of test-to-calculated failure load T/T_h versus ratio of effective beam depth to embedment length d/ℓ_{eh} for specimens with confining reinforcement [T_h is calculated using Eq. (4.2)] (Shao et al. 2016).....	121
Figure 4.9 Ratio of test-to-calculated failure load T/T_h versus normalized confining reinforcement A_{tt}/A_{hs} for specimens with $d/\ell_{eh} \geq 1.5$ [T_h is calculated from Eq. (4.2)] (Shao et al. 2016).....	121
Figure 4.10 Load transfer within the beam-column joint based on strut-and-tie mechanism (column longitudinal reinforcement and beam compression reinforcement are not shown for clarity).....	124
Figure 4.11 M_{peak}/M_n versus ℓ_{eh}/ℓ_{ehy} for specimens with $d/\ell_{eh} > 1.5$. M_{peak}/M_n is the ratio of peak moment to nominal flexural strength, and ℓ_{eh}/ℓ_{ehy} is the ratio of embedment length to the embedment length required to yield the headed bar calculated from Eq. (4.1) or (4.2).	126
Figure 4.12 M_{peak}/M_n versus ℓ_{eh}/ℓ_{ehy} for exterior and roof-level interior beam-column joint specimens with $\ell_{eh}/\ell_{ehy} \geq 1.0$. M_{peak}/M_n is the ratio of peak moment to nominal flexural strength, and ℓ_{eh}/ℓ_{ehy} is the ratio of embedment length to the embedment length required to yield the headed bar calculated using the descriptive equations, Eq. (4.1) and (4.2).....	130
Figure 4.13 Reinforcement detail of knee beam-column joints with joint efficiency (a) 68%, and (b) 115% tested by Nilsson and Losberg (1976)	134
Figure 4.14 Reinforcement details for KJ16 knee beam-column joint specimens (McConnell and Wallace 1995).....	136

Figure 4.15 Reinforcement details for KJ17 knee beam-column joint specimens (McConnell and Wallace 1995).....	136
Figure 4.16 Reinforcement details for KJ18 knee beam-column joint specimens (McConnell and Wallace 1995).....	137
Figure 4.17 Reinforcement detail of knee beam-column joint specimens (a) JMT-No. 11-1a and JMT-No. 11-1b, and (b) JMT-No. 11-2a and JMT-No. 11-2b (Chun et al. 2007).....	137
Figure 4.18 Ratio of peak moment to nominal flexural strength M_{peak}/M_n versus ratio ℓ_{eh}/ℓ_{ehy} for knee beam-column joint specimens [ℓ_{ehy} is calculated using Eq. (4.2)]	139
Figure 4.19 Splitting failure plane and column longitudinal reinforcement as confining reinforcement for headed bars anchored in the column treated as straight bars by ignoring the head.....	142
Figure 4.20 M_{peak}/M_n versus ℓ_{eh}/ℓ_{ehy} for exterior and roof-level interior beam-column joint specimens with $A_{brg} \geq 3.7A_b$. M_{peak}/M_n is the ratio of peak moment to nominal flexural strength, and ℓ_{eh}/ℓ_{ehy} is the ratio of embedment length to the embedment length required to yield the headed bar calculated using the descriptive equations, Eq. (4.1) and (4.2).....	144
Figure 4.21 M_{peak}/M_n versus ℓ_{eh}/ℓ_{ehy} for exterior and roof-level interior beam-column joint specimens with $A_{brg} < 3.7A_b$. M_{peak}/M_n is the ratio of peak moment to nominal flexural strength, and ℓ_{eh}/ℓ_{ehy} is the ratio of embedment length to the embedment length required to yield the headed bar calculated using the descriptive equations, Eq. (4.1) and (4.2).....	146
Figure 4.22 M_{peak}/M_n versus ℓ_{eh}/ℓ_{dy} for exterior and roof-level interior beam-column joint specimens with $A_{brg} < 3.7A_b$. M_{peak}/M_n is the ratio of peak moment to nominal flexural strength, and ℓ_{eh}/ℓ_{dy} is the ratio of embedment length to the development length of straight bar (headed bars treated as straight bars by ignoring the head) calculated using Eq. (4.6) in accordance with Section 4.3 of ACI 408R-03.	147
Figure 4.23 Geometric parameters used in the anchorage analysis of beam-column joint specimens (a) front view (b) side view (column longitudinal reinforcement and beam compression reinforcement are not shown for clarity).....	150
Figure 4.24 Distribution of ratios T/T_h and T/T_{anc} for headed bars with $\ell_{eh}/\ell_{ehy} < 1.0$ in beam-column joint specimens tested under reversed cyclic loading	154
Figure 5.1 Effective confining reinforcement within the joint region of beam-column joints..	157
Figure 5.2 Effective confining reinforcement for members other than beam-column joints	157

Figure 5.3 Ratio of test-to-calculated stress $f_{su}/f_{s,calc}$ versus concrete compressive strength f_{cm} for beam-column joint specimens with widely-spaced and closely-spaced headed bars without confining reinforcement tested by Shao et al. (2016).....	159
Figure 5.4 Ratio of test-to-calculated stress $f_{su}/f_{s,calc}$ versus concrete compressive strength f_{cm} for beam-column joint specimens with widely-spaced and closely-spaced headed bars enclosed by No. 3 ties spaced at $3d_b$ in the joint region tested by Shao et al. (2016).....	160
Figure 5.5 M_{peak}/M_n versus ℓ_{eh}/ℓ_{dt} for beam-column joint specimens tested under reversed cyclic loading. M_{peak}/M_n is the ratio of peak moment to nominal flexural strength, and ℓ_{eh}/ℓ_{dt} is the ratio of embedment length to the development length calculated using Eq. (5.2).....	163
Figure 5.6 (a) Maximum dimensions and non-planner features of the obstruction (b) detail of gap in obstruction adjacent to the bearing face of the head (after Shao et al. 2016)	168
Figure 5.7 Headed bar with an obstruction not considered to detract from the net bearing area of the head.....	168
Figure 5.8 Dimensions of heads used in beam-column joint specimens tested by Chun et al. (2009) and headed splice specimens tested by Chun (2015) [figure after Hong et al. (2007)] ..	169
Figure 5.9 Beam-column joint for Example 1. (a) Plan view; (b) Section a-a (For column bars, only corner bars are shown).....	187
Figure 5.10 Beam-column joint for Example 2. (a) Plan view; (b) Section a-a (For column bars, only corner bars are shown).....	188
Figure B.1 Stress-strain curve for No. 6 headed bar	205
Figure B.2 Stress-strain curve for No. 8 headed bar	205
Figure B.3 Cross-section view of slab specimen 8-5-F4.1-0-6 with no reinforcement perpendicular to the headed bar	206
Figure B.4 Cross-section view of slab specimen 8-5-F4.1-2#5-6 with 2 No. 5 bars as reinforcement perpendicular to the headed bar.....	206
Figure B.5 Cross-section view of slab specimen 8-5-F4.1-4#5-6 with 4 No. 5 bars as reinforcement perpendicular to the headed bar.....	207
Figure B.6 End view of slab specimens 8-5-F4.1-2#8-6, 8-5-F9.1-2#8-6, 8-5-T4.0-2#8-6, and 8-5-T9.5-2#8-6 with 2 No. 8 bars as reinforcement perpendicular to the headed bar	207
Figure B.7 End view of slab specimens 8-8-O12.9-6#5-6, 8-8-O9.1-6#5-6, 8-8-S6.5-6#5-6, 8-8-O4.5-6#5-6, 8-5-S14.9-6#5-6, 8-5-S6.5-6#5-6, 8-5-O12.9-6#5-6, 8-5-O4.5-6#5-6, 8-5-S9.5-6#5-	

6, 8-5-S9.5-6#5-6, and 8-5-F4.1-6#5-6 with 6 No. 5 bars as reinforcement perpendicular to the headed bar	208
Figure B.8 Cross-section view of slab specimen 8-5-F4.1-6#5-6 with 6 No. 5 bars as reinforcement perpendicular to the headed bar.....	208
Figure B.9 End view of slab specimen 8-5-T4.0-8#5-6 with 8 No. 5 bars as reinforcement perpendicular to the headed bar	209
Figure B.10 End view of slab specimens 8-5-T9.5-8#5-6, 8-5-F4.1-8#5-6, and 8-5-F9.1-8#5-6 with 8 No. 5 bars and No. 4 bars spaced at 12 in. as reinforcement perpendicular to the headed bar	209
Figure B.11 Lapped bars with clear spacing of 0.5 in.	213
Figure B.12 Lapped bars with clear spacing of 1 in.	213
Figure B.13 Lapped bars with clear spacing of 1.9 in.	213
Figure B.14 Strain in lapped bars in specimen (3) 6-5-S4.0-12-0.5 as a function of applied load	215
Figure B.15 Strain in lapped bars in specimen (3) 6-5-S4.0-12-1.0 as a function of applied load	215
Figure B.16 Strain in lapped bars in specimen (3) 6-5-S4.0-12-1.9 as a function of applied load	216
Figure B.17 Strain in lapped bars in specimen (3) 6-12-S4.0-12-0.5 as a function of applied load	216
Figure B.18 Strain in lapped bars in specimen (3) 6-12-S4.0-12-1.0 as a function of applied load	217
Figure B.19 Strain in lapped bars in specimen (3) 6-12-S4.0-12-1.9 as a function of applied load (strains were measured when the specimen was reloaded after loading to 65 kips).....	217
Figure D.1 Reinforcement details for exterior beam-column joint specimens (Wallace et al. 1998).....	253
Figure D.2 Reinforcement details for knee beam-column joint specimens (Wallace et al. 1998)	254
Figure D.3 Side view showing configuration of beam bars in exterior beam-column joint (a) 90° standard hooks, (b) headed bars, and (c) 90° standard hooks anchored in wall (Chun et al. 2007)	266

Figure D.4 Configuration of hooked and headed bars in beam-column joints (a) standard 90° hooked bars (b) single-headed bars, and (c) double-headed bars (Lee and Yu 2009)..... 271

Figure D.5 Detail of exterior beam-column joint specimens containing hooked bars and headed bars (Kang et al. 2010)..... 273

Figure D.6 Reinforcement detail for exterior beam-column joint specimens (Kang et al. 2012) 275

LIST OF TABLES

Table 1.1 Modification factor ψ_{cs} for confining reinforcement and spacing	29
Table 2.1 Concrete mixture proportions	33
Table 2.2 Headed bar physical properties	34
Table 2.3a Details of friction-forged No. 8 headed bars (Figures are from Shao et al. 2016).....	36
Table 2.3b Details of taper-threaded and cold-swaged No. 6 and No. 8 headed bars (Figures are from Shao et al. 2016)	37
Table 2.3c Details of cold-swaged threaded coupling sleeve No. 8 headed bars (Figures are from Shao et al. 2016)	37
Table 3.1 Detail of slab specimens	51
Table 3.2 Detail of headed bar splice specimens	64
Table 3.3 Test results for headed bars in slab and column-like specimens tested by DeVries et al. (1999), Choi et al. (2002), and Choi (2006) and comparisons with descriptive equations [Eq. (3.4) and (3.5)] and anchorage provisions of ACI 318-14 (a modification factor of 0.8 is applied to T_h as appropriate)	77
Table 3.4 Statistical parameters of T/T_h values for slab and column-like specimens tested by DeVries et al. (1999), Choi et al. (2002), Choi (2006), and in the current study	80
Table 3.5 Statistical parameters of T/T_{anc} values for slab and column-like specimens tested by DeVries et al. (1999), Choi et al. (2002), Choi (2006), and in the current study	86
Table 3.6 Test results for lap splice specimens containing No. 8 headed bars tested by Thompson et al. (2002) and comparisons with descriptive equation [Eq. (3.4)] with 0.8 modification factor applied	93
Table 3.7 Test results for lap splice specimens tested by Chun (2015) and comparisons with descriptive equation [Eq. (3.4)] with 0.8 modification factor applied	95
Table 4.1 Modification factor ψ_{cs} for confining reinforcement and spacing	102
Table 4.2 Detail of exterior and roof-level interior beam-column joint specimens tested under reversed cyclic loading	104
Table 4.3 Statistical parameters for test-to-calculated ratio in beam-column joint specimens with $\ell_{eh}/\ell_{ehy} < 1.0$ tested under reversed cyclic loading and in beam-column joint specimens containing confining reinforcement tested under monotonic loading by Shao et al. (2016).....	129

Table 4.4 Statistical parameters for T'_{mod}/T_h in beam-column joint specimens with $\ell_{eh}/\ell_{ehy} \geq 1.0$ tested under reversed cyclic loading	131
Table 4.5 Detail of knee beam-column joint specimens	132
Table 4.6 Statistical parameters from the comparison of anchorage strengths of headed bars..	153
Table 5.1 Modification factor ψ_{cs} for confining reinforcement and bar spacing	156
Table 5.2 Statistical parameters of $f_{sul}/f_{s,calc}$ for headed-bar beam-column joint specimens without confining reinforcement tested by Shao et al. (2016), with $f_{s,calc}$ based on Eq. (5.2)	160
Table 5.3 Statistical parameters of $f_{sul}/f_{s,calc}$ for headed-bar beam-column joint specimens with confining reinforcement tested by Shao et al. (2016), with $f_{s,calc}$ based on Eq. (5.2)	161
Table 5.4 Statistical parameters of $f_{sul}/f_{s,calc}$ for headed-bar CCT node, splice, and shallow embedment specimens, with $f_{s,calc}$ based on Eq. (5.2)	164
Table 5.5 Coefficient k_t for headed deformed bars in tension.....	166
Table B.1 Detail of slab specimens tested in the current study	210
Table B.2 Detail of headed splice specimens tested in the current study	214
Table C.1 Data for specimens tested by Devries et al. (1999), Choi et al. (2002), and Choi (2006)	218
Table C.2 Data for beam-column joint specimens (exterior and roof-level interior joints) tested under reversed cyclic loading	223
Table C.3 Data for knee beam-column joint specimens tested by Wallace et al. (1998) and Chun et al. (2007) under reversed cyclic loading	247

CHAPTER 1: INTRODUCTION

1.1 GENERAL

Mechanical anchorage of a reinforcing bar is required when the bar cannot fully develop its yield strength with a straight length of embedment. This occurs, for example, at exterior beam-column joints where space constraints do not allow the bar to be embedded to the length required. In this case, hooked or headed bars can be used to provide anchorage.

In general, mechanical anchorage of a reinforcing bar is achieved through bearing on the concrete from a hook or head in addition to the bond along the straight portion of the bar. The use of conventional hooked bars for anchorage in heavily reinforced members often causes congestion due to the extra length needed after the bent portion of the bar (tail of the hook). Such congestion creates difficulty in fabrication, construction, and concrete placement, which may, in turn, compromise the anchorage strength. Headed bars serve as a viable alternative to hooked bars and can also eliminate problems due to congestion. Section 25.4.4 of ACI 318-14 Building Code Requirements for Structural Concrete has provisions for the development of headed deformed bars in tension. The Code, however, limits the value of concrete compressive strength to 6,000 psi and steel yield strength to 60,000 psi due to a lack of information on how headed bars perform when used with higher-strength materials. ACI 318-14 also puts limits on the clear spacing between the headed bars ($\geq 4d_b$), clear concrete cover ($\geq 2d_b$), and net bearing area of the head ($\geq 4A_b$), where d_b and A_b are the diameter and area of the bar, respectively.

The research reported here is part of a larger study that was conducted to investigate the anchorage strength of headed bars in tension for high-strength materials (up to Grade 120 steel and 16,000 psi concrete compressive strength) in exterior beam-column joints. From these tests, characteristic and design equations were developed to represent anchorage strength (Shao et al. 2016). All of the tests involved monotonic loading of specimens. The experimental work in this study specifically addresses the performance of headed bars in splice and shallow embedment tests. The current study also includes an analysis of exterior, roof-level interior, and knee beam-column joints (Figure 1.1) subjected to reversed cyclic loading. In exterior joint specimens, the beam reinforcement was anchored in the column using headed bars; in roof-level interior joint

specimens, the column reinforcement was anchored in the beam using headed bars; and in knee joint specimens, both column and beam reinforcement was anchored at the joint using headed bars.

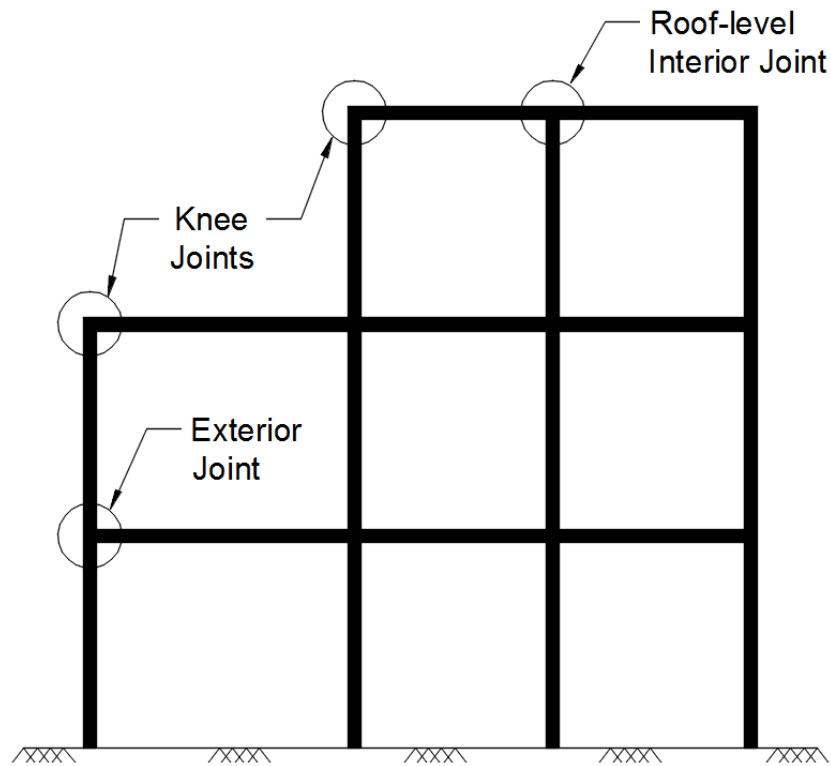


Figure 1.1 Types of beam-column joints studied in the current study

This chapter includes a detailed discussion of the state-of-the-art, relevant research work, and code provisions for headed bars, followed by the objective and scope of the current study.

1.2 PREVIOUS STUDIES

1.2.1 Early headed stud and headed bar studies

Studies of headed anchorage started as early as in 1956 when Viest (1956) tested 12 specimens in which concrete slabs were connected to wide-flange steel beams using headed steel studs with smooth shank investigate the shear transfer mechanism between the beam and slab. The test parameter was the ratio of effective depth-to-stud diameter, where the effective depth of the stud was the height measured from the base to the underside of the head. Viest (1956) proposed one of the first expressions to describe the shear strength of headed studs. McMackin et al. (1973) tested 32 concrete block specimens containing headed anchor studs loaded in direct tension or a combination of shear and tension. The headed studs had net bearing areas equal to $1.5A_b$ or $1.8A_b$, where the net bearing area of a head is the gross area of the head minus the nominal area of the bar

Ab. The study contributed to further development of design criteria for anchorage using headed steel studs. A study by Stoker et al. (1974) involved 19 shallow and deep embedment tests in concrete blocks using Grade 60 No. 11, No. 14, and No. 18 headed deformed bars with square steel plates attached to their ends with net bearing areas up to 15 times the cross-sectional area of the bar. Embedment lengths ranged from 7.8 to $33.6d_b$. The thickness of the plates was 1 in. Concrete compressive strengths ranged from 3,550 to 5,400 psi. Stoker et al. (1974) found that the embedment length required to develop a headed bar was 62% of that required for a straight bar. Dilger and Ghali (1981) studied the use of headed studs as shear reinforcement in slabs in an effort to overcome difficulties in concrete placement due to closely spaced stirrups. The test results from 40 full-scale slab-column joint specimens showed that headed studs not only facilitated easier reinforcement fabrication but also made it possible to transfer high shear stresses. Based on their study, Dilger and Ghali (1981) proposed rules for the placement and spacing of headed studs for shear. These rules have been modified over the years, codified in the present form in Section 22.6 of ACI 318-14, and are no longer in use in their original form.

1.2.2 Tests on slab and column-like specimens

DeVries et al. (1999) tested three slab specimens containing three to 11 deformed headed bars (for a total of 18 tests) embedded in concrete slabs to study the effects of embedment length, edge distance, bar diameter, head area, and aspect ratio (ratio of larger to smaller dimension of the head), confining reinforcement, concrete compressive strength, and bonded length (length over which the deformed bar is in contact with concrete) on anchorage strength. The tests included specimens containing headed bars with embedment lengths ℓ_{eh} measured from the bearing face of the head to the loaded surface of the slab that were less than five times the clear side cover to the bar. DeVries et al. (1999) tested No. 6 and No. 11 headed bars with embedment lengths ranging from $1\frac{3}{8}$ to 9 in. Fourteen of the headed bars were unbonded along the total embedment length ℓ_{eh} using a PVC pipe as a bond breaker, as shown in Figure 1.2a. Four specimens with ℓ_{eh} equal to 9-in. were bonded, as shown in Figure 1.2b. The yield strength of the headed bars was 72,000 psi. Concrete compressive strengths ranged from 3,920 to 12,040 psi. Each specimen contained three to 11 bars, four placed with clear cover of 1.6 in. from one side face and 17.6 in. from the adjacent orthogonal side face of the slab, four bars placed at the corner of the slab with 1.6 in. concrete

clear cover in two directions, and three bars placed with clear cover of 17.3 or 17.6 in. in two directions. Four headed bars contained two No. 3 bars (perpendicular to the headed bar) distributed evenly along embedment length as confining reinforcement. These headed bars were tested one at a time to investigate the effect of concrete side cover on the anchorage strength. The net bearing areas of the heads ranged from 4.7 to $7.4A_b$, while the aspect ratios ranged from 1 to 2. The thicknesses of the heads ranged from 0.5 to 1.0 in. The headed bars had no obstructions adjacent to the head. The confining reinforcement consisted of two No. 3 bars perpendicular to the headed bar distributed evenly along the embedment length. During the test, supports were placed at least 2 times the embedment length away (outside of the anticipated failure region) from the headed bars to prevent the support from affecting anchorage strength.

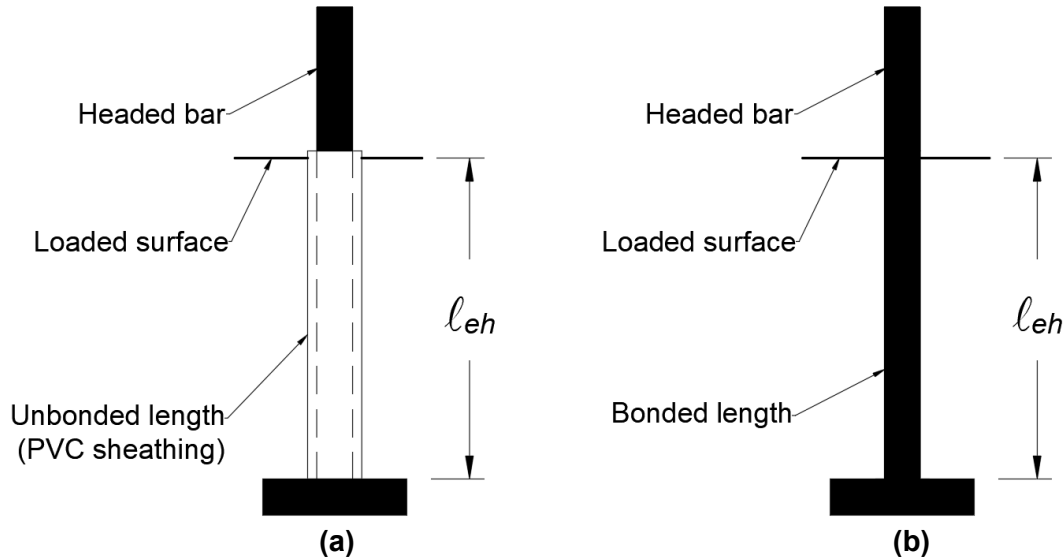


Figure 1.2 (a) Unbonded and (b) bonded lengths of the headed bar tested by DeVries et al. (1999)

DeVries et al. (1999) investigated the anchorage and displacement behavior of headed bars under direct tension. Displacement was nearly linear with the applied load at lower loads, but increased significantly close to failure. The major failure mode, concrete breakout, was sudden in nature; no cracking was observed before failure. The headed bars lost strength immediately after failure. The size of the conical region of the concrete pulled along with the headed bar (failure cone) increased with increase in the embedment length, edge distance, or head size. The presence of transverse reinforcement did not affect the anchorage strength or deflection of the headed bars, while bond along the bar in contact with concrete increased the anchorage strength and decreased

the head slip measured at the back of the head using a dial gauge. The anchorage strength was also improved by increasing the embedment length and edge distance. The aspect ratio of the head did not affect anchorage strength. DeVries et al. (1999) concluded that headed reinforcement can provide anchorage to develop the tensile strength on the bar.

Choi et al. (2002) and Choi (2006) conducted 76 tests on headed bars anchored in slab (Figure 1.3) and column-like (Figure 1.4) specimens with embedment lengths ranging from 6 to $15d_b$ to investigate the anchorage behavior of headed bars. Choi et al. (2002) tested 16 slab and 28 column-like specimens, and Choi (2006) tested 32 column-like specimens. The major test parameters included embedment length, bar size, spacing between bars, column ties parallel to the headed bar as confining reinforcement, and column longitudinal reinforcement as reinforcement perpendicular to the headed bars. Slab specimens contained headed bars anchored at the middle and close to the edge of the concrete slab, as shown in Figure 1.3. In the slab specimens, headed bars were anchored at the middle of the slab to evaluate cases where the slab boundaries would not limit the concrete breakout failure region and anchored close to the edge of the slab with cover to the bar ranging from 40 to 124 mm (1.6 to 4.9 in.) to investigate the role of edge effects on the anchorage strength. The headed bars were tested one at a time. The column-like specimens contained two to four headed bars in a layer anchored in the column, as shown in Figure 1.4. These specimens were tested to investigate the effects of spacing between the headed bars, confining reinforcement (column ties), and reinforcement perpendicular to the headed bar (column longitudinal bars) on the anchorage strength. The center-to-center spacing between the bars ranged from 3 to $15d_b$. D16 (No. 5), D19 (No. 6), D22 (No. 7), D25 (No. 8), and D29 (No. 9) headed bars with yield strengths of 360 or 420 MPa (52,200 or 60,900 psi) were tested. The net bearing area of heads A_{brg} ranged from 2.6 to $3.2A_b$ and the heads had no obstructions. D16 (No. 5), D19 (No. 6), D22 (No. 7), or D25 (No. 8) bars were used as column longitudinal reinforcement. Concrete compressive strengths ranged from 27.1 to 39.1 MPa (3,930 to 5,670 psi). In the column-like specimens, D10 (No. 3) or D13 (No. 4) ties spaced at 2.7 to $14.5d_b$ (3 to 9.1 in.) on both sides of the headed bars (Figure 1.4) were used as confining reinforcement parallel to the headed bars. Ten column-like specimens tested by Choi (2006) and all 16 slab specimens tested by Choi et al. (2002) did not contain such confining reinforcement. All specimens were cast and tested in the horizontal

position. During the test, supports were placed at least 1.5 times the embedment length away (outside of the anticipated failure region) from the headed bars to prevent the support from affecting anchorage strength.

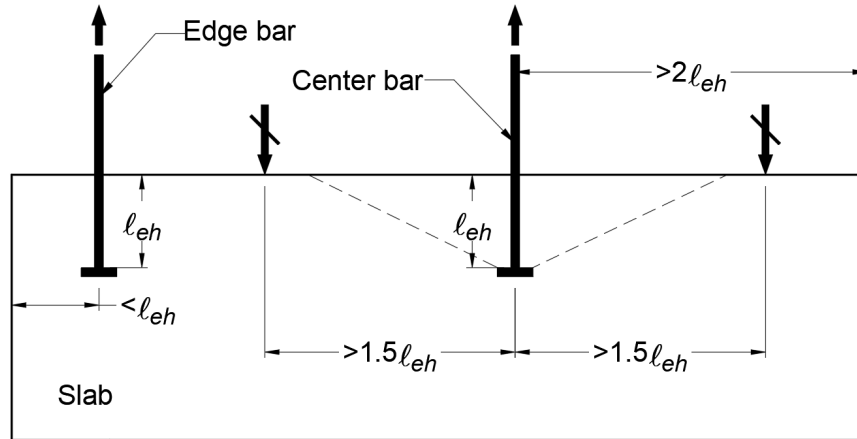


Figure 1.3 Slab specimens tested by Choi et al. (2002)

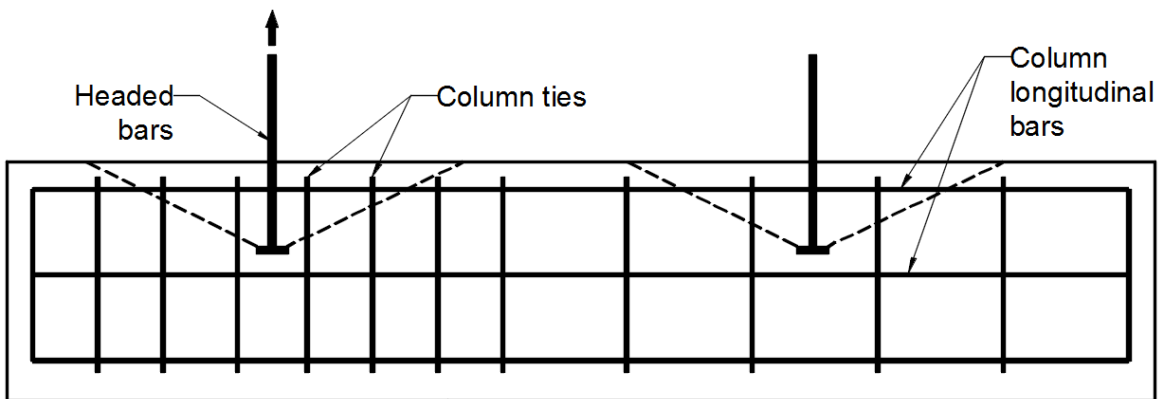


Figure 1.4 Column-like specimens tested by Choi et al. (2002) and Choi (2006)

The test results showed that the anchorage strength of the headed bars with confining reinforcement (column ties) parallel to the bars was 18 to 32% higher than the strength of the headed bars without such confining reinforcement. The confining reinforcement within 0.45 times the embedment length from the headed bar was effective in increasing the anchorage strength. Choi et al. (2002) found that reinforcement perpendicular to the headed bars (column longitudinal reinforcement) did not affect anchorage strength. Choi (2006), however, reported a 16% average increase in anchorage strength when doubling the amount of reinforcement perpendicular to the bar. Choi (2006) also observed a lower anchorage strength of headed bars with center-to-center spacing less than $8d_b$ compared to that of headed bars with the spacing greater than or equal to $8d_b$.

1.2.3 Tests on headed bar splices

Thompson et al. (2002) tested 27 beam specimens containing No. 5 or No. 8 spliced headed bars. The test parameters included lap configuration (contact and non-contact), lap length, bar spacing, head bearing area, head geometry, confining reinforcement, and concrete compressive strength. The splices were categorized as contact or non-contact depending on whether the head of a bar was in contact with the adjacent lapping bar. The center-to-center spacing between the bars being spliced was 1.24 or $2.1d_b$ for contact splices and was 3 or $5d_b$ for non-contact splices. Lap lengths ranged from 3 to $14d_b$. The headed bars contained rectangular, square, and circular heads with no obstruction adjacent to the head. The net head bearing areas ranged from 1.2 to $4.7A_b$. Four specimens contained non-headed (straight) lapped bars. To prevent shear failure, stirrups were provided away from the splice region, as shown in Figure 1.5. Specimens had widths of 25 in. for center-to center spacings of 1.24 and $3d_b$ and 36 in. for center-to center spacings of 2.1 and $5d_b$. A depth of 10.5 in. was used for all specimens. Concrete compressive strengths ranged from $3,200$ to $5,700$ psi. To study the effect of confinement on the performance of spliced headed bars, hairpin and hoop tie-downs consisting of Grade 60 No. 2, No. 3, or No. 4 bars were used in the splice region, as shown in Figure 1.6. Hairpin tie-downs consisted of two hairpin ties anchored in the slab to horizontal bars located under the splice region on each lapped bar; one located 1 in. away from the bearing face of the head and the other at the end of the spliced region. Hoop tie-downs consisted of light-gauge hoops anchored to two transverse bars placed over and two transverse bars placed under the lapped bars in the middle of the splice region. These transverse bars were anchored in the specimen using hoops.

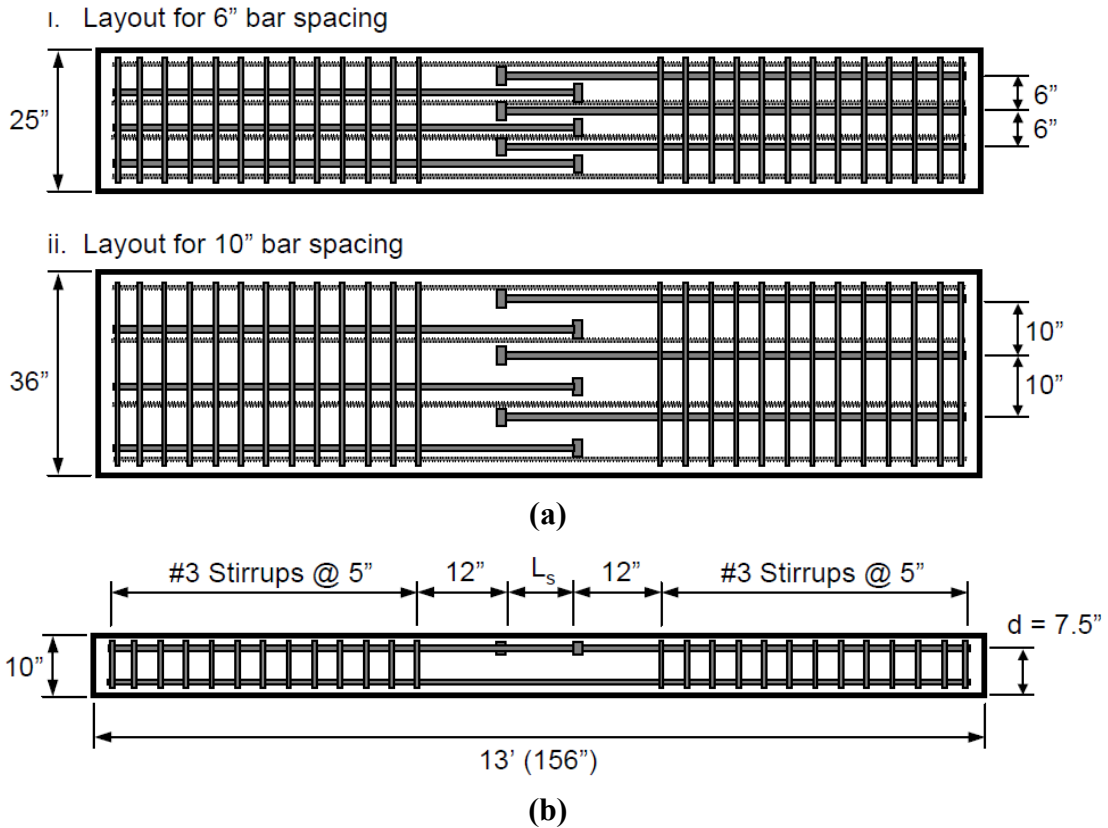


Figure 1.5 Reinforcement detail of splice specimens (a) top view and (b) side view (Thompson et al. 2002)

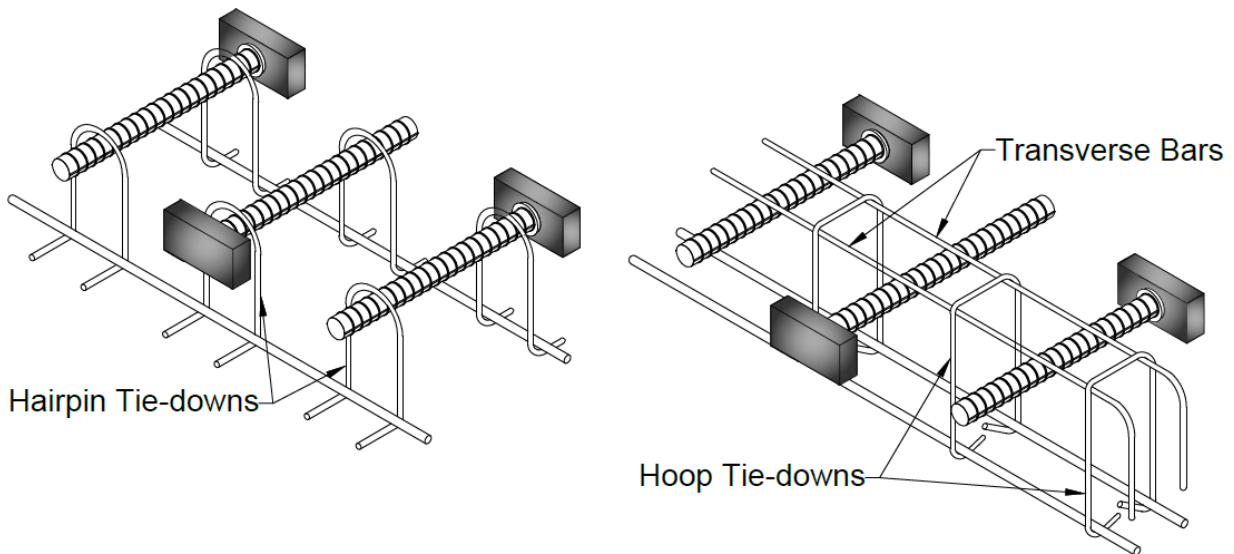


Figure 1.6 Detail of headed splice confinement using hairpin and hoop tie-downs, after Thompson et al. (2002)

As the load increased in the splice tests, cracks started in the vicinity of the head perpendicular to the lapped bars and spread within the splice region, while outside the splice region, cracks initiated at the location of the first stirrups (12 in. away from the end of splice region,

Figure 1.5). Struts were formed between the head and adjacent bars being spliced at an angle of about 55° to the bars, as shown in Figure 1.7, except in specimens with a 3 or $5d_b$ lap length where the struts were formed between the heads of adjacent lapping bars. Cracks appeared along and parallel to these struts. Specimens failed when these diagonal cracks extended the full length of the lap zone. The headed bar splice specimens exhibited diagonal cracks, while the non-headed bar splice specimens exhibited splitting cracks oriented along the lapped bars. Contact splices exhibited fewer cracks than non-contact splices. Internal cracking patterns, observed during the autopsy of the specimens, were formed along the struts. More cracks were observed, however, on the surface of the specimens with a $14d_b$ lap length than on the surface of specimens with shorter lap lengths. Cracks in the specimens containing hairpin tie-downs resembled those in specimens with no confinement. These specimens exhibited minimal increase in splice strength (5%) compared to the specimens with no confinement. In specimens containing hoop tie-downs, cracks formed along the transverse bars and compression strut between adjacent lapping bars. These specimens exhibited a more gradual failure than specimens with no confinement.

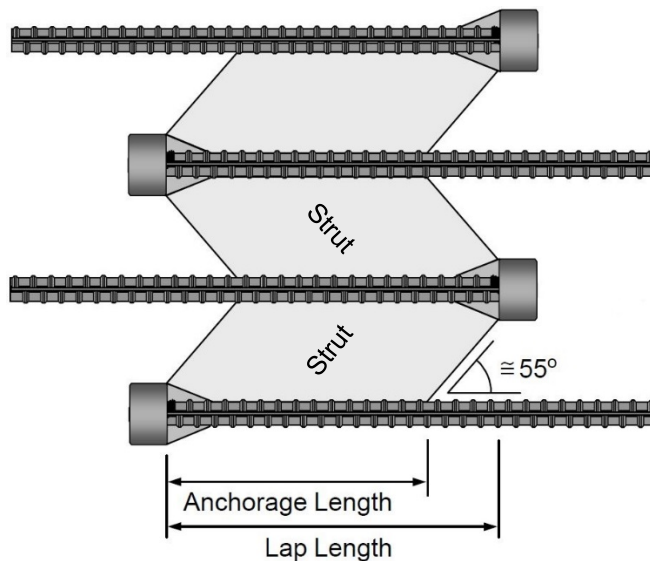


Figure 1.7 Force transfer mechanism in lapped bars (struts in the picture are marked for this report), Thompson et al. (2002)

The test results from the study also showed that increasing the net bearing area of the heads from 1.2 to $4.7A_b$ doubled the splice strength, indicating that the larger heads contributed more to splice strength than the smaller heads for a given lap length. Bond along the bar was expressed as a difference in stresses calculated from strains measured using two or three strain gauges at 1.5 to

$4d_b$ from the bearing face of the head. Thompson et al. (2002) observed a sharp decline in bond within $2d_b$ of the bearing face of the head, caused by the formation of a wedge of concrete in front of the head. In specimens containing hairpin tie-downs, concrete wedges with length up to $2d_b$ were formed because the hairpin close to the head helped to form longer wedges. Shorter wedges were formed in specimens without hairpin confinement. Based on this observation, Thompson et al. (2002) suggested excluding the part of the bar within $2d_b$ of the bearing face of the head when calculating the anchorage length (Figure 1.7) available for bond. Hoop tie-downs were more effective than hairpin tie-downs at improving splice strength. In specimens with a $12d_b$ lap length, hairpin tie-downs and hoop tie-downs increased splice strength by 5 and 11%, respectively, compared to companion specimens containing no confining reinforcement. For specimens with an $8d_b$ lap length, hairpin tie-downs increased splice strength by 22 to 43% compared to companion specimens containing no confining reinforcement. Thompson et al. (2002) suggested that this larger increase in anchorage strength in the specimens with the $8d_b$ lap length occurred because the hairpin tie-downs placed 1 in. away from the head enhanced bearing on the head. This effect, however, was not mentioned by Thompson et al. (2006b) when discussing the effects of confinement on lapped strength. In specimens with lap lengths of $5d_b$ or less, anchorage was primarily achieved through bearing on the head, with very little contribution from bond along the bar. Bearing on the head was determined based on the stress in the bar calculated from the strain measured using a strain gauge 1.5 to $2d_b$ from the bearing face of the head. Thompson et al. (2002) also found that splice strength increased with an increase in lap length due to increased bond along the bar and contribution of head bearing to splice strength.

Chun and Lee (2013) also studied headed bar splices, emphasizing the effects of confining reinforcement, lap length, bar spacing, concrete cover, bar diameter, and concrete compressive strength. Twelve beam specimens containing splices of Grade 80 No. 8 or No. 9 headed reinforcing bars were tested. The headed bars conformed to ASTM A970 and had circular heads with a gross bearing area of $5A_b$. Obstructions on the heads with a diameter d_{obs} and a length t_{obs} equal to 1.5 and $0.75d_b$, respectively, however, reduced the net bearing area adjacent to the obstruction (gross head area minus the obstruction area) to 2.7 and $2.8A_b$. Splice lengths ranged from 16 to $25d_b$, while the clear spacing between the headed bars was 2 or $4d_b$. The depth of the specimens was

13³/₄ or 17³/₄ in., depending on the maximum anticipated load to prevent a compression failure in flexure. Specimen widths ranged from 8⁷/₈ to 16 in. as a function of bar spacing. Clear concrete cover to the outside bars and heads were 1 or $2d_b$ and 0.38 or $1.38d_b$, respectively. In three specimens, the splices were confined using stirrups placed either along the entire splice region or only at the ends of the splice region; confining reinforcement was not used in the other nine specimens. Concrete compressive strengths were 3,050 and 6,090 psi.

Chun and Lee (2013) studied cracking behavior and measured the strain distribution in the lapped headed bars using strain gauges. All specimens exhibited brittle failure with a sudden loss of strength. In specimens without confining reinforcement, failure occurred due to prying action of the concrete within the splice region. An increase in the lap length from 15 to $25d_b$ increased the splice strength by 40% and an increase in concrete cover from 1 to $2d_b$ increased the splice strength by about 8%. Chun and Lee concluded that the increase in strength for splices without confining reinforcement was provided primarily by bond along the bars rather than due to any change in bearing on the heads because the stress in the bar, calculated from the strain measured using a strain gauge located $1d_b$ from the bearing face of the head, did not change as the lap length increased. Based on the observations by Thompson et al. (2002), however, it is likely that the wedge of concrete that forms adjacent to the heads shielded the strain gauge, limiting its usefulness in determining force transfer near the head. Confining reinforcement provided by two stirrups at the ends of the splice and stirrups throughout the splice limited the prying effect within the splice region and increased the splice strength compared to specimens without confining reinforcement by 33% and 59%, respectively.

Chun (2015) studied the anchorage behavior of headed splices in tests of 24 beam specimens containing splices of Grade 80 No. 8 or No. 9 headed bars, including the results from the 12 splice specimens tested by Chun and Lee (2013). The headed bars complied with ASTM A970 and had circular heads with a gross area of $5A_b$, which were similar to those used by Chun and Lee (2013). Obstructions on the heads with a diameter d_{obs} and a length t_{obs} equal to 1.5 and $0.75d_b$, respectively, reduced the net head bearing area adjacent to the obstruction (gross head area minus obstruction area) to 2.7 and $2.8A_b$. Test parameters included splice length, clear spacing between the lapped bars, concrete side cover, confining reinforcement, bar diameter, and concrete

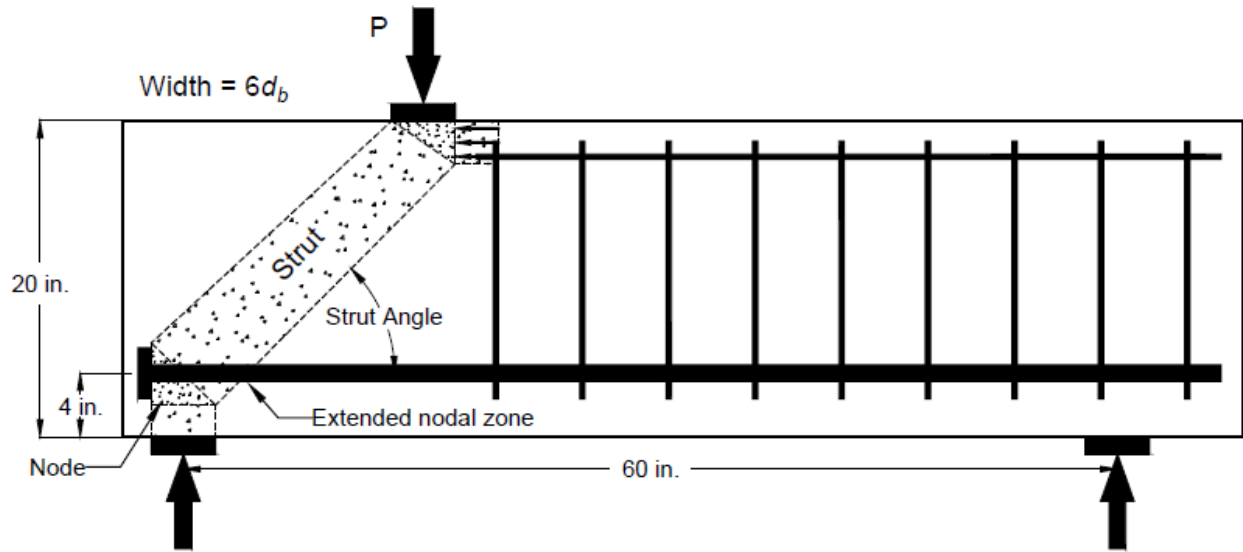
compressive strength. Splice lengths ranged from 15 to $30d_b$, the center-to-center spacing between the lapped bars was 3 or $5d_b$, where the latter complied with spacing requirements for headed anchorage in Section 12.6 of ACI 318-11. The side cover to the lapped bars was equal to half the clear spacing between the bars, except for three specimens that had a side cover of $3.5d_b$. Cover to the head ranged from 0.38 to $2.88d_b$. In six specimens, the splice region was fully confined using No. 3 stirrups placed along the entire splice region, while in two specimens, confinement was provided using No. 3 stirrups only at the ends of the splice region (described as partially confined). In other 16 specimens, no confinement was provided within the splice region. Concrete compressive strengths ranged from 2,940 to 9,120 psi.

Chun (2015) made similar observations on the cracking patterns to those by Chun and Lee (2013); flexural cracking started within the constant moment region and cracks at the end of splice were dominant. All specimens exhibited brittle failure with sudden loss of strength. At the onset of failure, longitudinal cracks formed within the splice region parallel to the lapped bars and the cover concrete was vertically separated from the beam as a result of prying action exposing the bars immediately after the failure. The specimens in which the splices were fully confined along the length exhibited more flexural and longitudinal cracking than the unconfined specimens, while the partially confined specimens fell in between. Chun (2015) observed that increasing the level of confinement increased splice strength. Additional specimens tested by Chun (2015) that contained stirrups showed that preventing the prying action increased the anchorage strength by up to 67% compared to the companion specimens containing no confinement. Chun (2015) proposed a descriptive equation for predicting the splice strength of headed bars as a function of confining reinforcement, side cover, bar spacing, lap length, bar diameter, and concrete compressive strength.

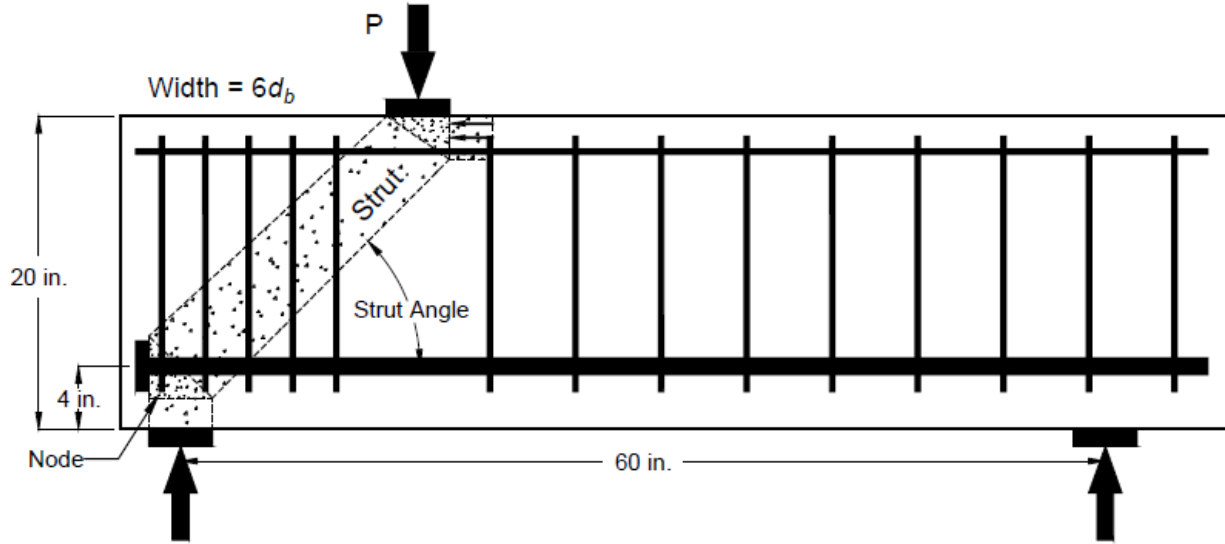
1.2.4 Tests on compression-compression-tension (CCT) nodes

Thompson et al. (2005, 2006a) studied the anchorage behavior of headed bars at compression-compression-tension (CCT) nodes in deep-beams. CCT nodes are described in Section R23.2 of ACI 318-14 as regions in a strut-and-tie model where two compressive forces and one tensile force act in equilibrium. The study involved 64 beam specimens containing a single bar anchored at a CCT node; 51 specimens contained a headed bar, 10 specimens contained a

straight bar, and three specimens contained a bar anchored with a standard 180° hook. The beams had a height of 20 in. and a width of $6d_b$. The headed bars had circular, square, or rectangular heads with no obstructions. The test parameters included bar size (No. 8 or No. 11), strut angle (30°, 45°, and 55°), head size (net bearing area ranging from 1.2 to $10.4A_b$), and head orientation (horizontal or vertical orientation of longer sides of rectangular heads). Confining reinforcement was provided within the nodal zone (Figure 1.8a) in six specimens, with No. 3 stirrups spaced at 3 or 6 in. (Figure 1.8b) in five specimens and a spiral consisting of $3/16$ in. diameter plain wire with a 1 in. pitch and 3 in. diameter along the bar within the nodal zone in one. Concrete compressive strengths ranged between 3,050 and 5,660 psi.



(a)



(b)

Figure 1.8 CCT node specimens (a) without and (b) with confining reinforcement, after Thompson (2002)

Thompson et al. (2005, 2006a) observed that the specimens containing a hooked bar and most of the specimens containing a headed bar exhibited splitting or crushing of concrete at the node. Splitting failure, characterized by cracks on a plane perpendicular to the side face of the beam along the diagonal compression strut, was generally dominant in specimens containing smaller heads ($\leq 2.9A_b$) and rectangular heads with the longer side oriented vertically. Crushing of concrete occurred near the bottom of the strut and was more dominant for larger heads ($> 2.9A_b$) and for rectangular heads with the longer side oriented horizontally. Specimens containing straight

bars experienced pullout failure characterized by extensive slip of the anchored bar relative to the surrounding concrete without significant splitting or crushing of concrete at the node. Strain gauges spaced at $2d_b$ between 1 and $20d_b$ from the bearing face of the head were used to examine the stress profile along the bar. The bond along the bar was expressed as a difference in stresses in the bar calculated from strains measured using strain gauges at 1 and $20d_b$ from the bearing face of the head. The stress along the bar at different load levels showed that bond along the bar carried most of the anchorage force at initial loads. The bond force decreased as the bar began to slip and a greater portion of the bar force was provided by bearing on the head. The maximum bar stress occurred at the intersection of the bar and the end of the extended nodal zone (right side of zone at intersection of extended nodal zone and the headed bar in Figures 1.8a and b). The extended nodal zone is defined in Section R23.2.6 of ACI 318-14 as a region bounded by the intersection of widths of the compressive strut and tie. The stirrups provided within the nodal zone (Figure 1.8b) did not increase the anchorage strength of the headed bar, but improved ductility (expressed as a ratio of displacement at loading point at peak load to the displacement at yield) compared to that of companion specimens without confining reinforcement. An increase in the contribution of bond of about 46% to anchorage strength was observed in specimens containing confining reinforcement, while the contribution from bearing on the head decreased by about 21%. Thompson et al. (2005, 2006a) suggested that this increase was because the stirrups restrained splitting of concrete, which prevented a decrease in bond along the bar, and also that the stirrups provided alternate paths for carrying the load through multiple compression struts, resulting in increased anchorage length.

Shao et al. (2016) evaluated test results of 10 CCT node specimens to investigate the anchorage behavior of headed bars at a compression-compression-tension node. Specimens were 18×20 in. beams containing two or three ASTM A1035 Grade 120 No. 8 bars, anchored by heads at one end and straight reinforcement at the other. Anchorage at both ends was tested in separate tests. The headed ends of the bars had a net bearing area of $4.1A_b$ and contained no obstructions adjacent to the head. No confining reinforcement was provided within the anchorage region (Figure 1.9). No. 4 stirrups spaced at 3.5 in. were provided outside the anchorage region to prevent shear failure. In Figure 1.9, loading point and support locations are denoted by solid arrows for

tests of headed end and dotted arrows for tests of non-headed end. Both ends of the beams were tested one at a time. Embedment length (equal for headed and non-headed ends) was measured from the extended nodal zone (Section R23.2.6 of ACI 318-14) and ranged from 9 to $14d_b$. The center-to-center spacing between headed bars was 6 or $12d_b$. The concrete compressive strengths ranged from 4,490 to 5,800 psi.

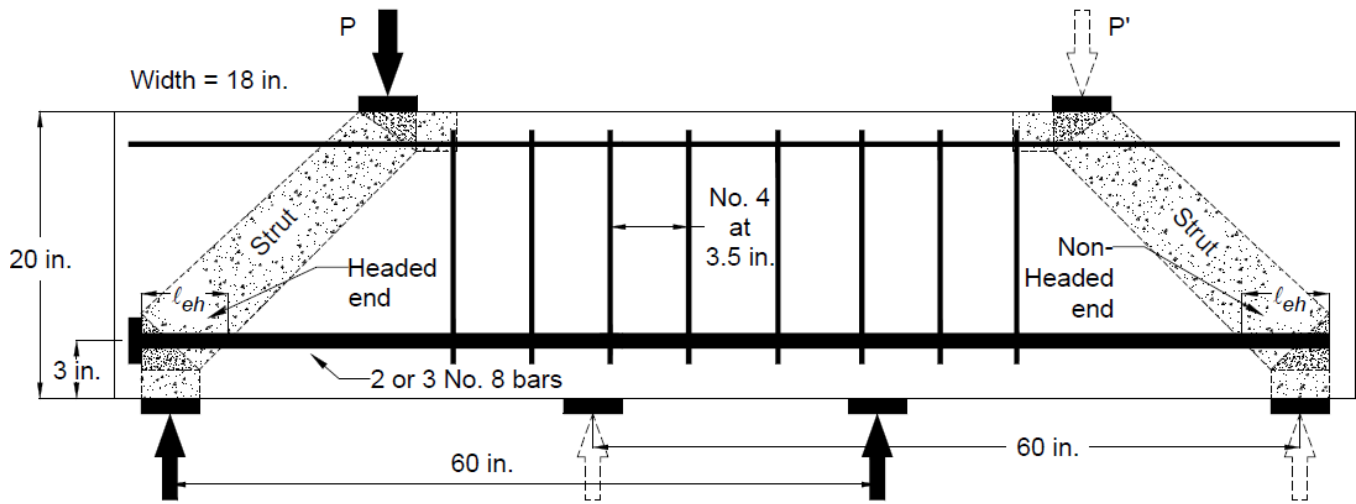


Figure 1.9 CCT node specimens tested by Shao et al. (2016)

The specimens exhibited side blowout failure mode at the headed end, characterized by a sudden separation of the side concrete cover at the anchorage region, except in one case where the concrete crushed in front of the head along the compressive strut. Non-headed end of specimens exhibited pullout in which the straight bar had significant slip relative to the surrounding concrete. The headed end had about 40% greater anchorage strength on average than that of non-headed end. Specimens generally exhibited increased anchorage strength at both headed and non-headed ends by a factor of about 2 on average with an increase in embedment length from 9 to $14d_b$.

1.2.5 Tests on beam-column joints under monotonic loading

Bashandy (1996) tested 32 simulated exterior beam-column joints to investigate the effects of embedment length, confining reinforcement, concrete cover to the bar, bar diameter, and head size on anchorage strength of headed bar. Embedment lengths ranged from 8.5 to 17 in. Six specimens with confining reinforcement within the joint region contained No. 3 ties with spacing ranging from 2 to 4 in. The balance of the specimens did not have confining reinforcement. No. 8 and No. 11 headed bars with head sizes ranging from 2 to $7.1A_b$ were tested. The heads were attached to the bar by friction welding and did not have obstructions. The width of the column was

12 in. and the depth varied depending on the embedment length. Concrete compressive strengths ranged from 3,200 to 5,800 psi. Each specimen contained two headed bars. Three specimens had headed bars placed outside the column core (a region of the column cross-section located inside the column longitudinal reinforcement) with 1.5 in. side concrete cover (1.1 in. cover to the head). The other specimens contained headed bars placed inside the column core with 3 in. side concrete cover (2.6 in. cover to the head).

Eighteen specimens failed by side blowout, which was characterized by spalling of the concrete side cover. In the other fourteen specimens, failure occurred along diagonal cracks formed in the joint region as shown in Figure 1.10. The diagonal cracks formed along the strut between the head and the top face of a bearing plate simulating the compressive zone of the beam. The test results showed that the anchorage strength of the headed bars increased with an increase in embedment length, confining reinforcement, head size, and concrete cover. Bashandy (1996) compared the anchorage strength of headed bars placed outside the column core with that of headed bars placed inside the column core. The comparison showed that the anchorage strength of the headed bars placed outside the column core was 18 to 26% lower than that of headed bars placed inside the column core. To determine the effect of bar size on anchorage strength, six No. 8 and No. 11 headed bar specimens were compared. Gross head areas of No. 8 and No. 11 bars were 4.96 and 4.84 in.², respectively. Bashandy (1996) assumed that the effect of this small difference in *gross* head area (less than 5%) would be negligible. A comparison showed that one specimen containing No. 11 headed bars had 5% greater anchorage strength (force in the bar at failure) than the companion specimen containing No. 8 headed bars, while two specimens containing No. 8 bars had about 4% greater anchorage strength than the companion specimens containing No. 11 bars. Bashandy (1996) concluded that the bar size did not have significant effect on the anchorage strength. The No. 8 and No. 11 headed bars included in this comparison, however, had net bearing areas of $5.3A_b$ (4.19 in.²) and $2.1A_b$ (3.28 in.²), respectively, suggesting that the larger bar size may have compensated for the smaller bearing area of the head.

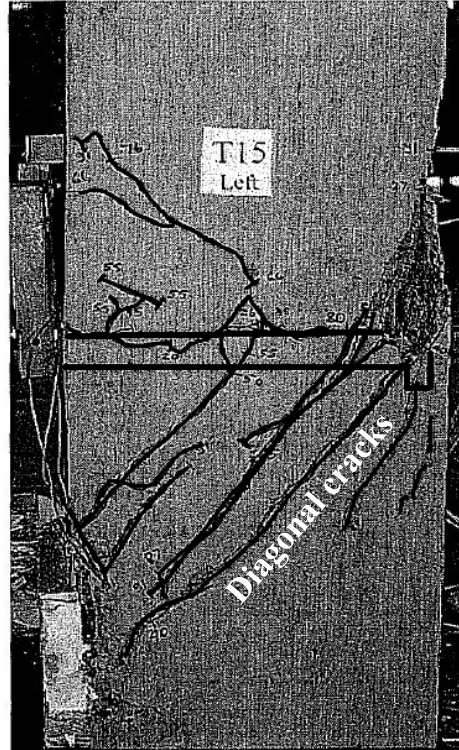


Figure 1.10 Crack pattern of a specimen at failure (headed bar and cracks in the picture are highlighted for this report), Bashandy (1996)

Hong et al. (2007) studied the stress transfer mechanism of headed bars in an exterior beam column joint using a strut-and-tie model. The model included a strut formed between the head and the compressive zone of the beam. The model considered concrete compressive strength, yield strength of the headed bar, head size, and joint dimensions as primary variables. The model also considered a fan-shaped compression field in the strut, in which the strut expands laterally towards the headed bar representing bond along the interface of the concrete and the bar. The model was validated by comparing with test results from 24 exterior beam-column joints tested by Chun et al. (2009). Although Chun et al. (2009) was published in a later date, the test results were available for comparison in Hong et al. (2007). The comparison showed that the ratio of predicted-to-test values ranged from 0.87 to 1.24 with a mean and coefficient of variation of 1.00 and 10.6%, respectively.

Chun et al. (2009) tested 30 full-scale simulated exterior beam-column joint specimens. Twenty four contained headed bars and six contained 90° hooked bars. ASTM A615 Grade 60 No. 8, No. 11, and No. 18 bars were used. Each specimen contained a single hooked or headed bar, and no confining reinforcement was provided within the joint region. Concrete compressive

strengths ranged from 3,510 to 3,640 psi. No axial load was applied on the column during the test. Embedment lengths ranged from 6.3 to $10.4d_b$ (50 to 86% of the column depth) for No. 8 and No. 11 headed bars and from 8.4 to $15.5d_b$ (50 to 93% of the column depth) for No. 18 headed bars. The headed bars contained circular heads with gross area of $5A_b$ attached to the bar using a parallel-threaded connection. These heads had obstructions with a diameter d_{obs} and a length t_{obs} equal to 1.5 and $0.75d_b$, respectively, which reduced the bearing area of the head adjacent to the obstruction to values between 2.7 and $2.8A_b$. The width of the column and side concrete cover to the headed bars were $6d_b$ and $2.5d_b$, respectively.

The specimens exhibited cracks starting at the face of the column and propagated towards the head or hook along the bar. As the cracks reached the head (or bent portion of the hooked bar), specimens containing bars with a deeper embedment length (70 to 90% of the depth of the column) exhibited diagonal cracks propagating below the anchored bar toward the bearing plate on the column face where compressive force, simulating the compressive force in the beam, was applied. Chun et al. (2009) observed that in specimens with shallow embedment (50% of the column depth), diagonal cracks extended above and below the anchored bar and failed due to concrete breakout similar to that observed in an anchorage failure. Chun et al. (2009) observed an increase in anchorage strength with increase in embedment length. Chun et al. (2009) found that the models for the anchorage strength of headed bars proposed by Thompson et al. (2006), Bashandy (1996), and DeVries (1996) based on failure modes such as side face blowout, concrete breakout, splitting, joint shear do not accurately predict the concrete contribution to anchorage strength. Chun et al. (2009), therefore, proposed a model for the anchorage strength of headed bars based on bearing on the head and bond along the bar. The contributions of head bearing and bond to the anchorage strength were determined from the measured strain distribution along the bar. Strains were measured using strain gauges spaced at $3d_b$ along the embedment length with the first gauge at $1d_b$ from the bearing face and the last gauge at the critical section (face of the column). Chun et al. (2009) expressed the anchorage strength as a sum of contributions from head bearing and bond along the bar. The bearing on the head was a function of concrete compressive strength, net bearing area of the head, and embedment length to column depth ratio, while the bond along the bar was a function of concrete compressive strength, embedment length, and bar diameter.

Shao et al. (2016) tested 202 simulated exterior beam-column joint specimens to investigate the anchorage behavior of headed bars under monotonic loading. The major test parameters were bar diameter, embedment length, concrete compressive strength, bar spacing, and confinement in the joint region. The specimens contained ASTM A1035 Grade 120 No. 5, No. 8, or No. 11 headed bars with net bearing area of heads ranging from 3.8 to $14.9A_b$. Some headed bars had obstructions adjacent to the head that were larger than those permitted by ASTM A970 and ACI 318. In these cases, the bearing area adjacent to the obstruction (gross area of the head minus the area of the obstruction) ranged from 4.5 to $12.9A_b$. Embedment lengths ranged from 6 to $14.5d_b$ (4 to 6 in. for No. 5 bars, 6 to 14.5 in. for No. 8 bars, and 12 to 19.25 in. for No. 11 bars). Concrete compressive strengths ranged from $3,960$ to $16,030$ psi. Most of the specimens had 2.5 in. side concrete cover to the headed bar; some specimens had side cover ranging from 3 in. to 4 in. The center-to-center spacing between headed bars ranged from 2.9 to $11.8d_b$ (with two to four headed bars in a specimen). Specimens contained no confining reinforcement, two No. 3 hoops, or No. 3 hoops spaced at $3d_b$ within the joint region. The confining reinforcement was parallel to the headed bars. Bars stresses at anchorage failure ranged from $26,370$ to $158,170$ psi.

The study showed that the contribution of concrete to anchorage strength could be represented more accurately by the concrete compressive strength raised to the 0.25 power than by the square root of the compressive strength, the value used currently in ACI 318. The test results showed that the headed bars containing large obstructions ($2d_b$ in diameter and $5.25d_b$ in length) with bearing areas adjacent to the obstructions of at least $4.5A_b$ performed satisfactorily. Shao et al. (2016) also developed descriptive equations and design provisions (presented in detail in Section 1.4) that safely allow the use of headed reinforcing bars with yield strengths up to $120,000$ psi and concrete compressive strengths up to $16,000$ psi. The descriptive equations and design provisions developed by Shao et al. (2016) are used in the current study to reanalyze the results of beam-column joint specimens subjected to reversed cyclic loading.

Shao et al. (2016) also analyzed the test results on headed bars in exterior beam-column joints by Chun et al. (2009) and lap splices by Chun (2015). As described in Sections 1.2.3 and 1.2.5, these tests involved headed bars with a gross area of $5A_b$ providing net bearing area of $4A_b$ in accordance with ASTM A970, but with an obstruction with a diameter d_{obs} of $1.5d_b$ (the upper

limit on diameter of obstruction permitted in ASTM A970) and a length t_{obs} of $0.75d_b$, resulting in a bearing area adjacent to the obstruction of only 2.7 and $2.8A_b$. Shao et al. (2016) did not consider Chun's lap splice specimens with confining reinforcement as being applicable for design because (1) the confining reinforcement was perpendicular to the headed bars, (2) confining reinforcement perpendicular to headed bars was shown to be ineffective in confining the bars based on findings from headed bar splice tests by Thompson et al. (2002) and CCT node tests by Thompson et al. (2005, 2006a), and (3) although the confining reinforcement was effective in Chun's tests, it is highly unlikely that spliced headed bars, as used by Chun, would be used in practice. Analysis of results from Chun et al. (2009) and Chun (2015) showed low anchorage strengths for the headed bars. Shao et al. (2016) suggested that the net bearing area of a head with an obstruction be defined as the gross area of head minus the area of the obstruction adjacent to the head and be at least $4A_b$.

1.2.6 Tests on beam-column joints subjected to reversed cyclic loading

The current study includes an analysis of the results of 84 exterior, seven roof-level interior, and seven knee beam-column joints (Figure 1.1) subjected to reversed cyclic loading by Bashandy (1996), Murakami et al. (1998), Wallace et al. (1998), Matsushima et al. (2000), Nakazawa et al. (2000), Tasai et al. (2000), Yoshida et al. (2000), Takeuchi et al. (2001), Ishibashi et al. (2003), Ishibashi and Inokuchi (2004), Kiyohara et al. (2004), Kiyohara et al. (2005), Kato (2005), Masuo et al. (2006a, 2006b), Adachi and Masuo (2007), Chun et al. (2007), Ishida et al. (2007), Tazaki et al. (2007), Lee and Yu (2009), Kang et al. (2010), Kang et al. (2012), Chun and Shin (2014), and Dhake et al. (2015). In the exterior joint specimens, the beam reinforcement was anchored in the column using headed bars; in roof-level interior joint specimens, the column reinforcement was anchored in the beam using headed bars; and in knee joint specimens, both column and beam reinforcement was anchored at the joint using headed bars. A summary of these studies is presented in this section with details of all 23 studies presented in Appendix D.

The major test parameters in these studies included embedment length, concrete compressive strength, bearing area of the head, bar spacing, bar size, and joint shear. In addition, Adachi and Masuo (2007) and Ishida et al. (2007) studied the effect of transverse beams (beams perpendicular to the test beam at the joint) and beams wider than columns, respectively, on joint performance. Seven exterior beam-column joint specimens contained transverse beams

perpendicular to the test beam at the joint. Concrete compressive strengths and steel yield strengths ranged from 24 to 148.4 MPa (3,480 to 21,520 psi) and from 370 to 1034 MPa (53,650 to 149,930 psi), respectively. Headed bar size ranged between D12 and D36. Test beams contained two to nine headed bars with net bearing area of the heads ranging from 1.7 to $11.4A_b$ in one or two layers as top and bottom beam reinforcement. Embedment lengths of the headed bars ranged from 8 to $22.6d_b$. Clear cover and minimum center-to-center spacing between the bars (minimum of vertical and horizontal center-to-center spacing) ranged from 1.6 to $9.9d_b$ (1.1 to 8.7 in.) and from 2 to $11.2d_b$ (1.6 to 12.4 in.), respectively. Hoops of D6 bars (Japanese bar with area of a single leg equal to 0.044 in.^2) to D16 (No. 5) bars spaced at 2.2 to $6.8d_b$ (1.8 to 5.9 in.) were used as confining reinforcement parallel to the headed bars within the joint region. Four out of the 98 specimens analyzed did not contain confining reinforcement parallel to the headed bars. Column axial load applied during the test ranged from none to $0.20A_g f'_c$, where A_g is gross-sectional area of the column and f'_c is concrete compressive strength (a complete description of all notation is provided in Appendix A).

Sixty out of 84 exterior joints and all seven roof-level interior joints performed satisfactorily under reversed cyclic loading. These specimens reached peak moment 1 to 41% greater than the nominal flexural strength of the member anchored at the joint using headed bars with not more than 20% reduction in peak load at 3.5% drift, indicating an acceptable level of performance. The remaining 24 (of the 84) exterior joints did not reach the nominal flexural strength of the anchored member and exhibited significant joint deterioration. All seven knee beam-column joints exhibited similar behavior under reversed cyclic loading in which the specimens reached 1.0 to 1.26 times the nominal flexural strength of the members framing into the joint at peak closing moment (top bars in tension) but reached only 0.74 to 0.86 times the nominal flexural strength of the framing members at peak opening moment (top bars in compression). A detailed analysis of the performance of these exterior, roof-level interior, and knee beam-column joints is presented in Chapter 4.

1.3 CURRENT CODE PROVISIONS AND DESIGN RECOMMENDATIONS

Design provisions for headed bars are included in ACI 318-14. Design recommendations are provided in ACI 352R-02. The development length of a headed bar is measured from the

bearing face of the head to the critical section. In accordance with Section 25.4.4 of ACI 318-14, the development length of a headed bar in tension ℓ_{dt} is given by

$$\ell_{dt} = \left(\frac{0.016 f_y \Psi_e}{\sqrt{f'_c}} \right) d_b \quad (1.1)$$

where f_y (psi) is the specified yield strength of the bar, Ψ_e is a modification factor equal to 1.2 for epoxy-coated reinforcement and 1.0 otherwise, and f'_c (psi) is the compressive strength of concrete. Yield strength f_y is limited to a maximum of 60,000 psi, and the concrete must be normalweight with compressive strength f'_c used in Eq. (1.1) limited to 6,000 psi. The development length cannot be less than the maximum of $8d_b$ and 6 in., where d_b is the diameter of the bar. The bar size for headed reinforcement may not exceed No. 11, and the clear concrete cover to the bar and clear spacing between the bars must be at least $2d_b$ and $4d_b$, respectively, except for beam-column joints designed in accordance with Section 18.8.5.2 of ACI 318-14, which allows the minimum clear spacing between the bars to be $3d_b$ for seismic designs. Unlike hooked bars, confining reinforcement is not considered in determining the development length of headed bars based on observations by Thompson et al. (2005) that confining reinforcement (in this case perpendicular to the bar) did not improve the anchorage strength of headed bars.

The design recommendations in ACI 352R-02 for beam-column connections in cast-in-place concrete frames are less stringent than those in ACI 318-14. Beam-column joints in ACI 352R-02 are classified as Type 1 and Type 2 based on the loading conditions and anticipated deformations of members connected to the joint under lateral load. Type 1 joints are detailed for non-seismic loading that is not expected to result in significant inelastic deformation, while Type 2 joints are detailed to meet the requirements for seismic loading, considering the deformation into the inelastic range that occurs under load reversals. The critical section for the transfer of member forces to the connection is taken at the joint-member interface and is defined differently for Type 1 and Type 2 joints. As shown in Figure 1.11, the critical section for hooked or headed bars is taken at the face of the column for Type 1 joints and at the outside edge of the column core (outer edge of hoops) for Type 2 joints.

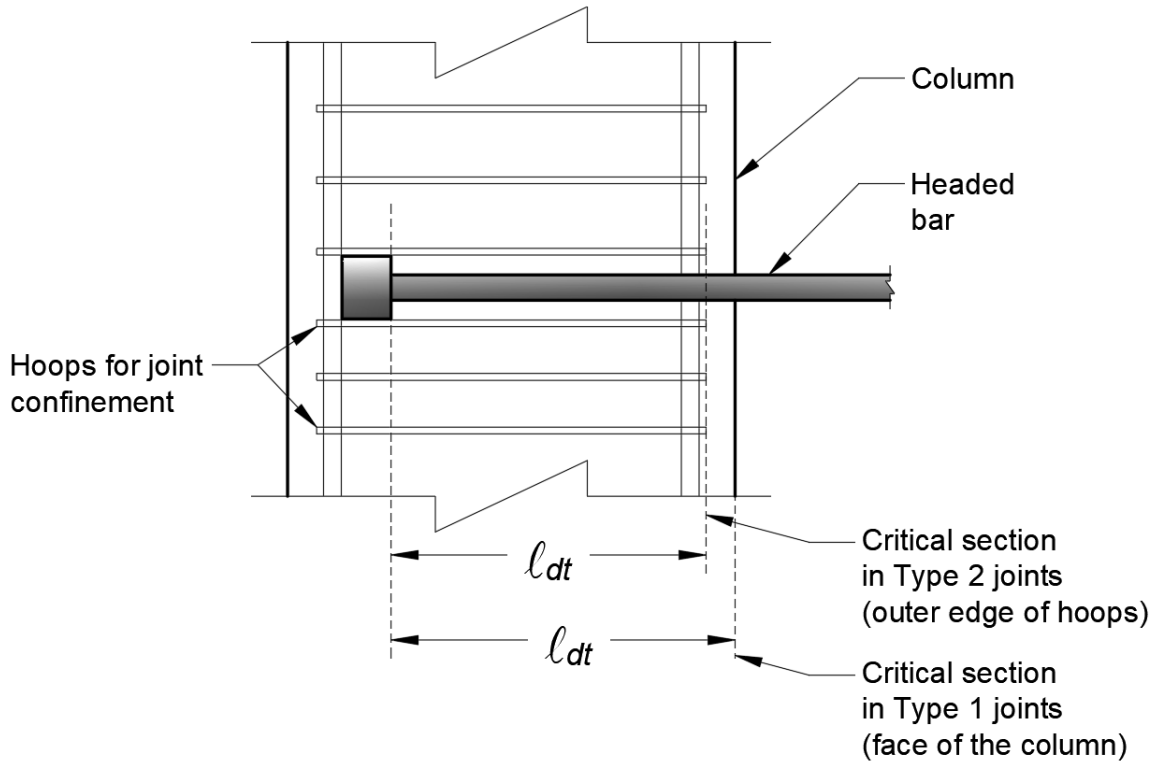


Figure 1.11 Critical section for headed bar in Type 1 and Type 2 joints

The recommendations in ACI 352R-02 for the development length ℓ_{dt} of headed bars are based on those for hooked bars. According to ACI 352R-02, the development length of a 90° standard hooked bar (standard hooks are defined in Section 25.3.1 of ACI 318-14) in tension ℓ_{dh} enclosed within the confined core of a Type 2 connection is given by

$$\ell_{dh} = \frac{\alpha f_y}{75\sqrt{f'_c}} d_b \quad (1.2)$$

where α is a stress multiplier to increase the stress under large deformation for the anchored bar at critical section. For Type 2 connections with ASTM A706 or equivalent reinforcement, α is taken as 1.25, while for other reinforcement, a value of α greater than 1.25 is recommended. The development length ℓ_{dh} should not be less than the maximum of $8d_b$ and 6 in. In accordance with Section 25.4.3.2 of ACI 318-14, a modification factor of 0.7 may be applied to the development length of standard hooked bars if No. 11 or smaller hooks have side cover not less than 2.5 in. and cover to the extension beyond the hook not less than 2 in. Since a Type 2 connection requires the hooked bar to be enclosed within the confined core with side clear cover normal to the plane of the hook not less than 2.5 in. and clear cover on the bar extension beyond the hook not less than 2

in. a modification factor to the development length of the hooked bar of 0.7 is already included in Eq. (1.2). A modification factor of 0.8 may be applied to the development length calculated using Eq. (1.2) if confining reinforcement in the joint region is provided at a spacing not greater than $3d_b$.

The development length of a headed bar in tension for both Type 1 and Type 2 joints is $3/4$ of the development length of a hooked bar in a Type 2 joint calculated using Eq. (1.2), which equals

$$\ell_{dt} = \frac{3}{4} \left(\frac{\alpha f_y}{75 \sqrt{f'_c}} \right) d_b \quad (1.3)$$

where α is the stress multiplier: for Type 1 connections, $\alpha = 1.0$, and for Type 2 connections, $\alpha = 1.25$. In ACI 352R-02, the maximum concrete compressive strength f'_c (psi) permitted for calculating development length is 15,000 psi, much higher than the upper limit of 6,000 psi in ACI 318-14 and, at the time of the development of the recommendations in ACI 352-02, not supported by experimental results. The development length should not be less than the larger of $8d_b$ and 6 in. Confining reinforcement within the joint region should be provided in accordance with the joint confinement requirements of Section 4.2 of ACI 352R-02. ACI 352R-02 further recommends that in corner beam-column joints where both beam and column terminate at the joint, headed bars adjacent to the free face of the joint with side clear cover less than $3d_b$ be confined by stirrups perpendicular to the longitudinal axis of the headed bars being developed. If the headed bars are expected to undergo significant inelastic deformations, the strength of the stirrup legs in a Type 2 corner joint should be one-half the force required to yield the headed bars adjacent to the free face of the joint. The strength of the stirrup legs in other cases should be one-quarter of the force required to yield the headed bars adjacent to the free face of the joint. If the side cover is greater than $3d_b$, minimum confining reinforcement in accordance with Section 4.2 of ACI 352R-02 should be provided.

The approaches adopted in ACI 318-14 and ACI 352R to calculate the development length of headed bars can be compared using a Type 1 joint ($\alpha = 1.0$). In this case, the respective development lengths of a headed bar without an epoxy coating ($\psi_e = 1.0$) are given by Eq. (1.4) and (1.5).

$$\ell_{dt} = \left(\frac{0.016f_y}{\sqrt{f'_c}} \right) d_b \quad (\text{ACI 318-14}) \quad (1.4)$$

$$\ell_{dt} = \left(\frac{0.01f_y}{\sqrt{f'_c}} \right) d_b \quad (\text{ACI 352R-02}) \quad (1.5)$$

The development lengths for headed bars calculated using Eq. (1.4) and (1.5) are functions of $f_y d_b / \sqrt{f'_c}$. The development length based on ACI 353-02 using Eq. (1.5), however, is 37.5% less than that required by ACI 318-14 using Eq. (1.4). The key reason is that, unlike ACI 352R-02, which incorporates the modification factors for hooked bars based on side concrete cover (0.7) and confining reinforcement (0.8), ACI 318-14 does not consider these factors when calculating the development length of headed bars. In addition, ACI 318-14 is more restrictive in the use of high-strength concrete (6,000 psi in ACI 318-14 versus 15,000 psi in ACI 352R-02).

1.4 NEWLY PROPOSED DESCRIPTIVE EQUATIONS AND DESIGN PROVISIONS

1.4.1 Descriptive Equations

Shao et al. (2016) developed descriptive equations to characterize the anchorage strength of headed bars without and with confining reinforcement in simulated beam-column joints based on tests described in Section 1.2.5 in which the bar stresses ranged from 26,370 to 158,170 psi and concrete compressive strengths ranged from 3,960 to 16,030 psi. The equations incorporate the effects of embedment length, concrete compressive strength, bar diameter, bar spacing, and confining reinforcement. Specimens included in the development of descriptive equations contained ASTM A1035 Grade 120 No. 5, No. 8, or No. 11 headed bars with net bearing areas ranging from 3.8 to $9.5A_b$ and side cover to the bar ranging from 2.5 to 4 in. The descriptive equation for the anchorage strength of headed bars without confining reinforcement in the joint region [Eq. (1.6)] was based on 30 beam-column joint specimens containing headed bars with a center-to-center spacing greater than or equal to $8d_b$ (described as widely-spaced).

$$T_c = 781 f_{cm}^{0.24} \ell_{eh}^{1.03} d_b^{0.35} \quad (1.6)$$

where T_c = anchorage strength of headed bars without confining reinforcement (lb); f_{cm} = measured concrete compressive strength (psi); ℓ_{eh} = embedment length (in.); and d_b = diameter of headed bar (in.). A complete description of all notation is presented in Appendix A.

Headed bars with a center-to-center spacing less than $8d_b$ (closely-spaced) were generally weaker than the widely-spaced headed bars. To account for the effect of bar spacing on anchorage strength, Shao et al. (2016) modified the descriptive equation to Eq. (1.7) based on the analysis of 34 beam-column joint specimens without confining reinforcement containing headed bars spaced center-to-center less than $8d_b$.

$$T_c = \left(781 f_{cm}^{0.24} \ell_{eh}^{1.03} d_b^{0.35} \right) \left(0.0836 \frac{c_{ch}}{d_b} + 0.3444 \right) \quad (1.7)$$

where $0.0836 \frac{c_{ch}}{d_b} + 0.3444 \leq 1.0$ and c_{ch} = center-to-center spacing between the bars (in.).

The descriptive equation for the anchorage strength of widely-spaced headed bars with confining reinforcement within the joint region [Eq. (1.8)] was based on 43 beam-column joint specimens containing headed bars with a center-to-center spacing greater than or equal to $8d_b$. The equation was derived assuming that the anchorage strength T_h is the sum of the contributions from the concrete T_c and the confining reinforcement within the joint region. The contribution from confining reinforcement in the joint region was found to be related to the area of confining reinforcement A_{tr} within $7.5d_b$ for No. 3 through No. 8 bars and $9.5d_b$ for No. 9 through No. 11 bars of the centerline of the headed bars in direction of the interior of the joint.

$$T_h = 781 f_{cm}^{0.24} \ell_{eh}^{1.03} d_b^{0.35} + 48,800 \frac{A_{tr}}{n} d_b^{0.88} \quad (1.8)$$

where T_h = anchorage strength of headed bars with confining reinforcement (lb); A_{tr} = total cross-sectional area of effective confining reinforcement ($NA_{tr,l}$) parallel to the headed bars being developed (in.²); N = total number of legs of effective confining reinforcement parallel to the headed bars being developed; $A_{tr,l}$ = area of a single leg; and n = number of headed bars. The first term in Eq. (1.8) is the contribution of the concrete T_c , shown in Eq. (1.6), and second term is the contribution of the confining reinforcement.

Similar to the closely-spaced headed bars without confining reinforcement, closely-spaced headed bars with confining reinforcement generally exhibited lower anchorage strength than the widely-spaced headed bars with confining reinforcement. To account for the lower anchorage strength of these closely-spaced headed bars, Shao et al. (2016) modified the Eq. (1.8) to obtain

Eq. (1.9) for headed bars with a center-to-center spacing less than $8d_b$ using the test results for 31 specimens.

$$T_h = \left(781 f_{cm}^{0.24} \ell_{eh}^{1.03} d_b^{0.35} + 48,800 \frac{A_{tt}}{n} d_b^{0.88} \right) \left(0.0622 \frac{c_{ch}}{d_b} + 0.5428 \right) \quad (1.9)$$

where $0.0622 \frac{c_{ch}}{d_b} + 0.5428 \leq 1.0$ and $\frac{A_{tt}}{n} \leq 0.3 A_b$

Shao et al. (2016) simplified these descriptive equations by adjusting the powers of the variables. The adjustments were guided by the development of a similar expression for hooked bars by Sperry et al. (2015a, 2015b). The power of f_{cm} was increased from 0.24 to 0.25 and that of ℓ_{eh} was decreased from 1.03 to 1.0. The power of d_b in the first term of Eq. (1.8) was increased from 0.35 to 0.5 and that in the second term of the same equation was decreased from 0.88 to 0.75. The coefficients were adjusted so as to obtain average values of the ratios T/T_c or T/T_h equal to 1.0, where T is the measured test failure load on the headed bar. Eq. (1.10) and (1.11) are the simplified descriptive equations.

$$T_c = \left(768 f_{cm}^{0.25} \ell_{eh} d_b^{0.5} \right) \left(0.0826 \frac{c_{ch}}{d_b} + 0.347 \right) \quad (1.10)$$

where $\left(0.0826 \frac{c_{ch}}{d_b} + 0.347 \right) \leq 1.0$

$$T_h = \left(768 f_{cm}^{0.25} \ell_{eh} d_b^{0.5} + 48,000 \frac{A_{tt}}{n} d_b^{0.75} \right) \left(0.0616 \frac{c_{ch}}{d_b} + 0.5598 \right) \quad (1.11)$$

where $\left(0.0616 \frac{c_{ch}}{d_b} + 0.5598 \right) \leq 1.0$ and $\frac{A_{tt}}{n} \leq 0.3 A_b$

A modification factor of 0.8 is applied to T_c or T_h for headed bars terminating inside a column core (a region of the column cross-section located inside the column longitudinal reinforcement) with clear side cover to the bar is less than 2.5 in., or terminating in a supporting member other than beam-column joints with side cover to the bar is less than $8d_b$.

1.4.2 Design Provisions

Shao et al. (2016) developed an equation [Eq.(1.12)] and proposed design provisions for the development length of headed bars based on the descriptive equations discussed in Section 1.4.1. The equation includes strength reduction factor to ensure that no more than 5% of the

specimens used to develop the equation have the ratio of test-to-calculated failure load less than 1.0.

$$\ell_{dt} = \left(0.0024 \frac{f_y \Psi_e \Psi_{cs} \Psi_o}{f_c'^{0.25}} \right) d_b^{1.5} \quad (1.12)$$

where ℓ_{dt} = development length of a headed bar in tension (in.) not less than the greater of $8d_b$ and 6 in.; f_y = specified yield strength of the headed bar (psi); Ψ_e = modification factor for epoxy-coated or zinc and epoxy dual-coated bars; Ψ_{cs} = modification factor for confining reinforcement and bar spacing; Ψ_o = modification factor for bar location; f_c' = concrete compressive strength (psi); and d_b = diameter of the headed bar (in.). A complete description of all notation is presented in Appendix A.

The proposed provisions apply to headed bars with yield strengths up to 120,000 psi and concrete compressive strengths up to 16,000 psi. The modification factor Ψ_e for the reinforcement coating condition is equal to 1.2 for epoxy-coated or zinc and epoxy dual-coated bars for all other conditions, and 1.0 for uncoated or zinc-coated (galvanized) bars and is retained from ACI 318-14. Values for the modification factor for confining reinforcement and bar spacing Ψ_{cs} , given in Table 1.1, are permitted to be interpolated for intermediate values of f_y , c_{ch} , and A_{tt}/A_{hs} .

Table 1.1 Modification factor Ψ_{cs} for confining reinforcement and spacing

Confinement level	f_y	c_{ch}	
		$2d_b$	$\geq 8d_b$
$\frac{A_{tt}}{A_{hs}} \geq 0.3$	$\leq 60,000$	0.6	0.4
	120,000	0.7	0.45
No confining reinforcement	all	1.0	0.5

where c_{ch} is center-to-center spacing between adjacent headed bars, A_{hs} is the total cross-sectional area of headed bars being developed, and A_{tt} is the total cross-sectional area of all confining reinforcement parallel to ℓ_{dt} for headed bars being developed in beam-column joints (Figure 1.12) and located $8d_b$ of the top (bottom) of the headed bars in direction of the interior of the joint for No. 3 through No. 8 headed bars or within $10d_b$ of the top (bottom) of the bar in direction of the interior of the joint for No. 9 through No. 11; or minimum total cross-sectional area of all confining

reinforcement parallel to headed bars being developed in members other than beam-column joints within $7\frac{1}{2}d_b$ on one side of the bar centerline for No. 3 through No. 8 headed bars or within $9\frac{1}{2}d_b$ on one side of the bar centerline for No. 9 through No. 11 headed bars. These design provisions are updated and simplified in the current study, which are presented in detail in Chapter 5.

The value for ψ_o is equal to 1.0 for headed bars terminating inside a column core (a region of the column cross-section located inside the column longitudinal reinforcement) with clear side cover to the bar ≥ 2.5 in., or terminating in a supporting member other than beam-column joints with side cover to the bar $\geq 8d_b$; in other cases, the value of ψ_o is equal to 1.25.

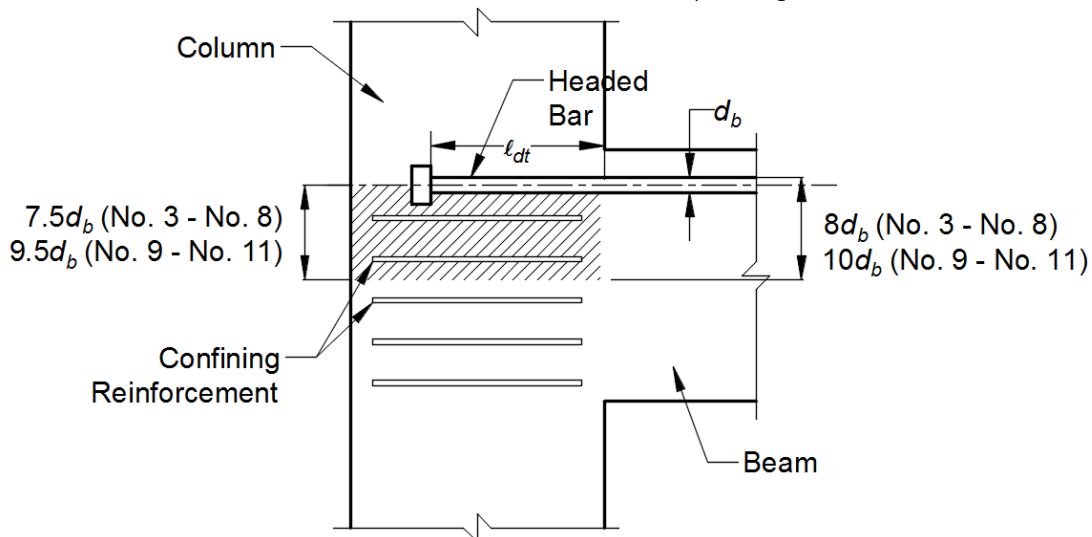


Figure 1.12 Effective confining reinforcement within the joint region of beam-column joints suggested by Shao et al. (2016)

1.5 OBJECTIVE AND SCOPE

Shao et al. (2016) developed descriptive equations and design provisions (presented in Section 1.4) that safely allow the use of headed reinforcing bars with yield strengths up to 120,000 psi and concrete compressive strengths up to 16,000 psi. The descriptive equations and design provisions were developed based on test results of 202 exterior beam-column joint specimens subjected to monotonic loading. The objective of the current study is to further improve the level of understanding of the behavior of headed bars, evaluate the applicability of the design provisions proposed by Shao et al. (2016) to a broader range of reinforced concrete members including headed bars used in splices, shallow embedment, and members subjected to reversed cyclic loading, and develop appropriate modifications to the proposed design provisions. The current study includes tests of headed splice and slab specimens subjected to monotonic loading, and an analysis of test

results of exterior, roof-level interior, and knee beam-column joint specimens subjected to reversed cyclic loading. Results from these tests are compared with the descriptive equations for anchorage strength and the proposed design provisions for the development length of headed bars. Based on these analysis, modifications to the proposed Code provisions for headed bars in members subjected to monotonic as well as cyclic loading are developed.

Specimens tested in this study include six headed bar splice specimens and 15 slab specimens (each containing one to three headed bars for a total of 32 tests). The main variables in the headed bar splice tests were spacing between bars and concrete compressive strength. Splice specimens contained ASTM A1035 Grade 120 No. 6 headed bars with net bearing area of $4A_b$ and the heads had no obstructions. The center-to-center spacing between bars ranged from $1.67d_b$ to $3.53d_b$ with side and top clear cover of 2 in. The average concrete compressive strengths were 6,360 and 10,950 psi. The tests on slab specimens were conducted to investigate the effects of concrete compressive strength, net bearing area of the head, and reinforcement in a plane oriented perpendicular to the headed bar with shallow embedment. The embedment lengths of the headed bars ranged for 6 to $8.5d_b$. Concrete compressive strengths in the slab specimens ranged from 4,200 to 8,620 psi and stress in the bar at failure ranged from 49,500 to 117,000 psi. Two to eight No. 5 or two No. 8 bars were provided as reinforcement in a plane oriented perpendicular to the headed bar placed symmetrically on both sides of the bar. Two specimens contained no such reinforcement. Each specimen contained one to three ASTM A1035 Grade 120 No. 8 headed bars with net bearing areas ranging from 4 to $15A_b$. Some headed bars had an obstruction adjacent to the head that reduced the bearing area adjacent to the obstruction to $4.5A_b$. The current study also includes an evaluation of tests on headed bar splice specimens by Thompson et al. (2002) and Chun (2015), slab specimens by DeVries et al. (1999) and Choi et al. (2002), and column-like specimens tested by Choi et al. (2002) and Choi (2006).

The analysis of beam-column joints includes 84 exterior, seven roof-level interior, and seven knee beam-column joint specimens subjected to reversed cyclic loading with considerable inelastic lateral displacement reversals. The tests include those by Bashandy (1996), Murakami et al. (1998), Wallace et al. (1998), Matsushima et al. (2000), Nakazawa et al. (2000), Tasai et al. (2000), Yoshida et al. (2000), Takeuchi et al. (2001), Ishibashi et al. (2003), Ishibashi and Inokuchi

(2004), Kiyohara et al. (2004), Kiyohara et al. (2005), Kato (2005), Masuo et al. (2006a, 2006b), Adachi and Masuo (2007), Chun et al. (2007), Ishida et al. (2007), Tazaki et al. (2007), Lee and Yu (2009), Kang et al. (2010), Kang et al. (2012), Chun and Shin (2014), and Dhake et al. (2015). Details of these studies are presented in Appendix D. The major test parameters in these studies included embedment length, concrete compressive strength, bearing area of headed bars, bar spacing, bar size, and joint shear. Bar sizes ranged from No. 4 through No. 11 with net bearing area of heads ranging from 1.7 to $11.4A_b$. Some headed bars with gross area of the head ranging from 3.9 to $9A_b$ had obstructions that reduced the bearing area adjacent to the head to values between 1.7 and $5.4A_b$. Embedment lengths ranged from 8 to $22.6d_b$. Concrete compressive strengths and steel yield strengths ranged from 3,480 to 21,520 psi and from 53,650 to 149,930 psi, respectively. The center-to-center spacing between the bars ranged from 2 to $8.8d_b$, while clear cover to the headed bars within the joint region ranged from 1.4 to $9.9d_b$. All but four specimens contained hoops, spaced at 2.2 to $6.8d_b$ (1.8 to 5.9 in.), as confining reinforcement parallel to the headed bar within the joint region. Seven exterior beam-column joint specimens contained transverse beams perpendicular to the test beam at the joint.

CHAPTER 2: EXPERIMENTAL WORK

In this Chapter, the test program and details of the specimens tested in the current study, including material properties (concrete and reinforcing steel), and the test procedures are presented. The experimental study included tests of 32 headed bars in slab specimen with shallow embedment and six tests of headed lap splices.

2.1 MATERIAL PROPERTIES

2.1.1 Concrete Properties

Non-air entrained ready-mix concrete with nominal compressive strengths of 5,000, 8,000, and 12,000 psi were used in slab and lap splice specimens. Mixture proportions of the concrete on saturated surface dry (SSD) based are presented in Table 2.1. Type I/II portland cement, crushed limestone with a maximum aggregate size of $\frac{3}{4}$ in., and Kansas River sand were used for the mixtures. In the 5,000 and 8,000 psi concrete mixtures, a mid-to-high range polycarboxylate-based water reducer was used as a water reducing agent, while in the 12,000 psi concrete mixture, a high-range polycarboxylate-based water reducer was used. The 12,000 psi concrete mixtures also contained pea-gravel to improve gradation and workability. Table 2.1 also includes the specific gravity (SG) of the portland cement and the bulk saturated surface dry specific gravity BSG (SSD) of the aggregates.

Table 2.1 Concrete mixture proportions

Material	Quantity (SSD)			SG or BSD (SSD) ^[2]
	5,000 psi w/c ^[1] = 0.44	8,000 psi w/c ^[1] = 0.32	12,000 psi w/c ^[1] = 0.29	
Type I/II Cement, lb/yd ³	600	700	750	3.2
Water, lb/yd ³	263	225	217	1.0
Kansas River Sand, lb/yd ³	1396	1375	1050	2.63
Pea Gravel, lb/yd ³	-	-	316	2.60
Crushed Limestone, lb/yd ³	1735	1683	1796	2.59
Water Reducer, oz (US)	30 ^[3]	171 ^[3]	104 ^[4]	-

^[1] w/c = Water to cement ratio

^[2] SG = specific gravity; BSD (SSD) = bulk saturated surface dry specific gravity

^[3] Mid-to-high range polycarboxylate-based water reducer

^[4] High-range polycarboxylate-based water reducer

2.1.2 Steel Properties

To ensure the anchorage failure governed by the surrounding concrete rather than tensile strength of the headed bars, ASTM A1035 Grade 120 No. 6 and No. 8 headed bars were used in headed splice and slab specimens. Stress-strain curves for the headed bars is provided in Section B.1 of Appendix B. Reinforcement in a plane perpendicular to the headed bar in slab specimens, and shear and ancillary reinforcement in lap splice specimens consisted of No. 4, No. 5, or No. 8 ASTM A615 Grade 60 bars. Physical properties of the headed bars are shown in Table 2.2. Head types used in the 32 shallow embedment tests and six splice tests are shown in Figure 2.1 and details of the heads are presented in Table 2.3. Details of these heads, including others not used in the current study, are also presented by Shao et al. (2016). A re-measurement of heads F4.1, F9.1, S4.0, S6.5, S14.9, O4.5, O9.1, and O12.9 resulted in slightly different head dimensions in Table 2.3 than reported by Shao et al. (2016).

Table 2.2 Headed bar physical properties

Bar Size	Heads	Yield Strength f_y (ksi)	Nominal Diameter d_b (in.)	Average Rib Spacing (in.)	Average Rib Height		Average Gap Width (in.)	Relative Rib Area ^[2]
					A ^[1] (in.)	B ^[2] (in.)		
No. 6	S4.0	119.8	0.75	0.475	0.053	0.052	0.293	0.096
No. 8	F4.1, F9.1	129.0	1	0.633	0.065	0.060	0.347	0.084
No. 8	T4.0, T9.5	120.0	1	0.590	0.067	0.062	0.287	0.095
No. 8	S6.5, S9.5, S14.9, O4.5, O9.1, O12.9	115.9	1	0.580	0.069	0.063	0.280	0.099

^[1] Per ASTM A615, A706; ^[2] Per ACI 408R-3

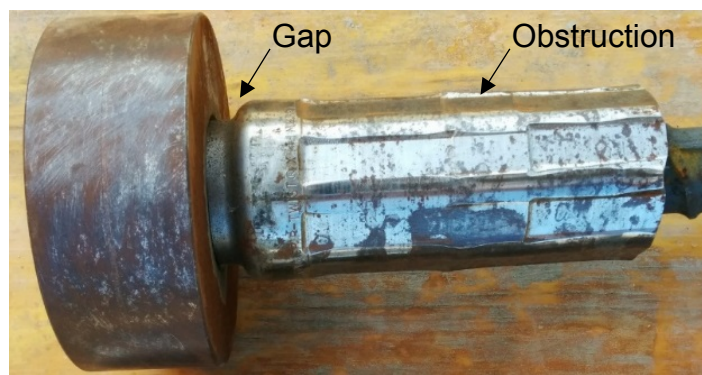
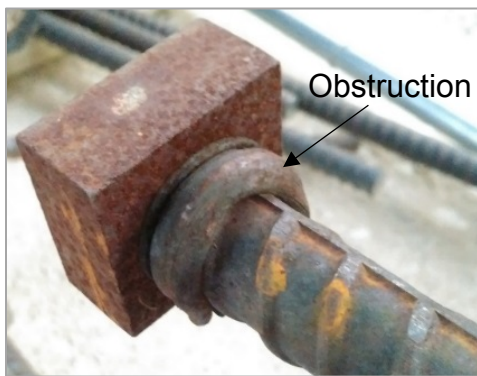
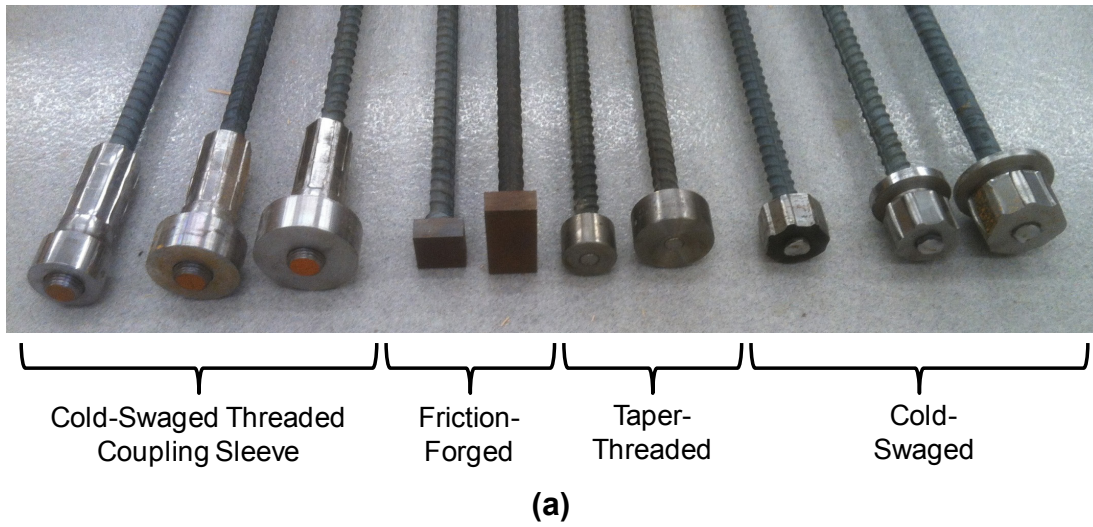
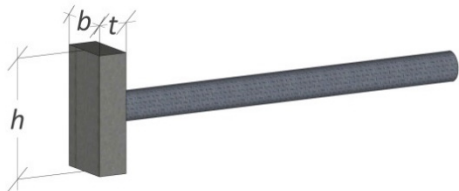


Figure 2.1 (a) Left to right: cold-swaged threaded coupling sleeve, friction-forged, taper-threaded, and cold-swaged No. 8 headed bars (figure from Shao et al. 2016); (b) and (c) obstruction adjacent to the bearing face of the friction-forged heads; and (d) gap in the obstruction adjacent to the bearing face of the cold-swaged threaded coupling sleeve heads (taper-threaded and cold-swaged heads had no obstructions)

Table 2.3a Details of friction-forged No. 8 headed bars (Figures are from Shao et al. 2016)

	Dimension Notation	Designation	b (in.)	h (in.)	t (in.)	d_{obs} (in.) ^[1]	t_{obs} (in.) ^[1]	Net Bearing Area (A_{brg}) ^[2]
Friction-Forged Headed Bars		F4.1 ^[3]	2.02	2	1	1.54	0.60	$4.1A_b$
		F9.1 ^[3]	2.03	3.98	1.02	1.58	0.62	$9.2A_b$

^[1] See Figure 2.2

^[2] Net bearing area calculated as gross head area minus bar area. These heads contained obstructions adjacent to the bearing face of the head, as shown in Figures 2.1b, 2.1c, and 2.2. These obstructions, however, did not have any detrimental effects on the anchorage strength of the headed bars and, therefore, are not considered to detract from the net bearing area of the head.

^[3] Head dimensions updated from those given by Shao et al. (2016)

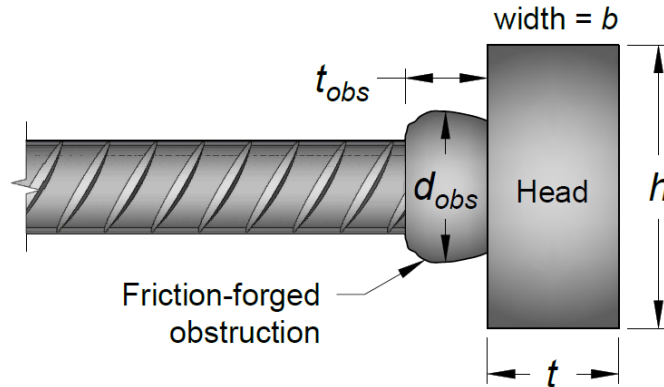
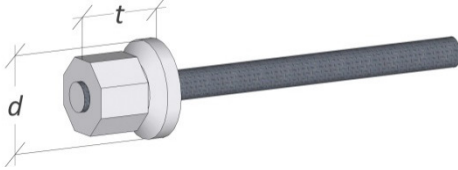


Figure 2.2 Friction-forged obstruction adjacent to the bearing face of F4.1 and F9.1 headed bars (also see Figures 2.1b and c)

Table 2.3b Details of taper-threaded and cold-swaged No. 6 and No. 8 headed bars
(Figures are from Shao et al. 2016)

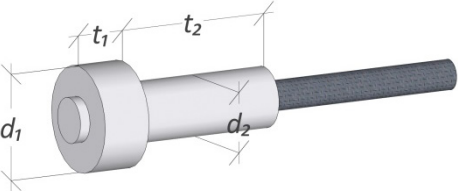
	Dimension Notation	Designation	Bar Size	d (in.)	t (in.)	Net Bearing Area (A_{brg}) ^[1]
Taper-Threaded		T4.0	No. 8	2.25	1.5	$4.0A_b$
		T9.5	No. 8	3.25	1.5	$9.5A_b$
Cold-Swaged Headed Bars		S4.0 ^{[2][3]}	No. 6	1.63	1.52	$4.1A_b$
		S6.5 ^{[2][3]}	No. 8	2.4	1.78	$5.0A_b$
		S9.5	No. 8	3.25	2.75	$9.5A_b$
		S14.9 ^[2]	No. 8	4	2.66	$15A_b$

^[1] Net bearing area calculated as gross head area minus bar area

^[2] Head dimensions updated from those given by Shao et al. (2016)

^[3] Octagonal-shape head

Table 2.3c Details of cold-swaged threaded coupling sleeve No. 8 headed bars
(Figures are from Shao et al. 2016)

	Dimension Notation	Designation	d_1 (in.)	t_1 (in.)	d_2 (in.)	t_2 (in.)	Net Bearing Area (A_{brg})
Cold-Swaged Threaded Coupling Sleeve		O4.5 ^[1]	2.76	1.625	1.72 ^[2]	5.19	$4.6A_b$ ^[2]
					2.2 ^[3]		$2.8A_b$ ^[3]
		O9.1 ^[1]	3.5	1.625	1.72 ^[2]	5.19	$9.2A_b$ ^[2]
					2.2 ^[3]		$7.4A_b$ ^[3]
		O12.9 ^[1]	4	1.625	1.72 ^[2]	5.19	$13.0A_b$ ^[2]
					2.2 ^[3]		$11.2A_b$ ^[3]

^[1] Head dimensions updated from those given by Shao et al. (2016). These heads contained obstructions with a gap (width not less than $\frac{3}{8}$ in.) adjacent to the bearing face of the head, as shown in Figure 2.1d.

^[2] Net bearing area calculated as gross head area minus area of the obstruction adjacent to the bearing face of the head

^[3] Net bearing area calculated as gross head area minus the maximum area of the obstruction

2.2 SLAB SPECIMENS

2.2.1 Specimen Design

Slab specimens were designed to investigate the anchorage behavior of headed bars in a simulated column-foundation joint. A total of 32 headed bars with shallow embedment lengths, ranging between 6 and 8.5 in., were tested to study the effects of support location (distance between the headed bar and compression reaction), head type and bearing area, and reinforcement oriented perpendicular to the headed bar.

Headed bars simulating column longitudinal reinforcement were embedded in a concrete slab, as shown in Figures 2.3 and 2.4. The slabs were designed as simply-supported beams (neglecting self-weight) to resist bending and shear at the maximum anticipated load on the anchored bar. The specimens contained two or three headed bars, which were loaded one at a time and embedded sufficiently far apart so that an anchorage failure of one bar did not interfere with the anchorage capacity of the others. The width of the specimen was chosen so that it was greater than the diameter of the anticipated concrete breakout failure surface. The depth of the specimens was sufficient to provide flexural and shear strength; only the minimum required flexural reinforcement was provided. In the first five test series, the clear distance between the nearest support and the headed bar was 10 in., while the clear distance between the farthest support and the headed bar was 44.3 in., as shown in Figure 2.3. This configuration was intended to simulate a column anchored in the foundation and subjected to bending, with the reaction support nearest to the anchored headed bar representing the compression zone of the column and the headed bar representing anchored tension reinforcement. The other reaction support was placed sufficiently far away from the anchored bar to avoid interference with the concrete breakout failure surface. In the final test series, both supports were outside the anticipated failure region. The clear distance between the supports and the headed bar in the final test series ranged from 14.5 to 16.5 in. (Figure 2.4), which is greater than the radius of the anticipated failure surface, which, using the provisions for anchors in Section 17.4.2.1 of ACI 318-14, would be located $1.5\ell_{eh}$ from the center of the headed bar.

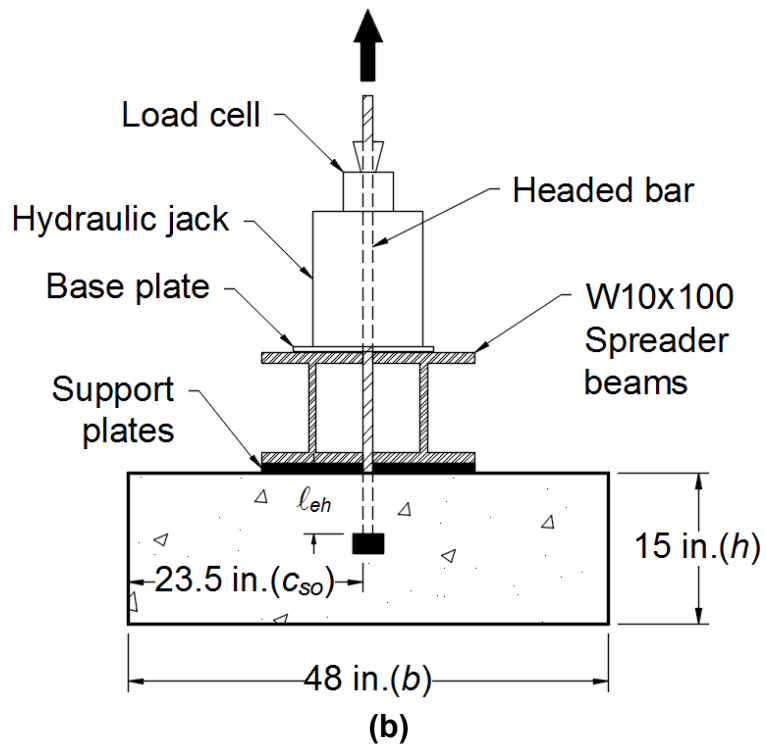
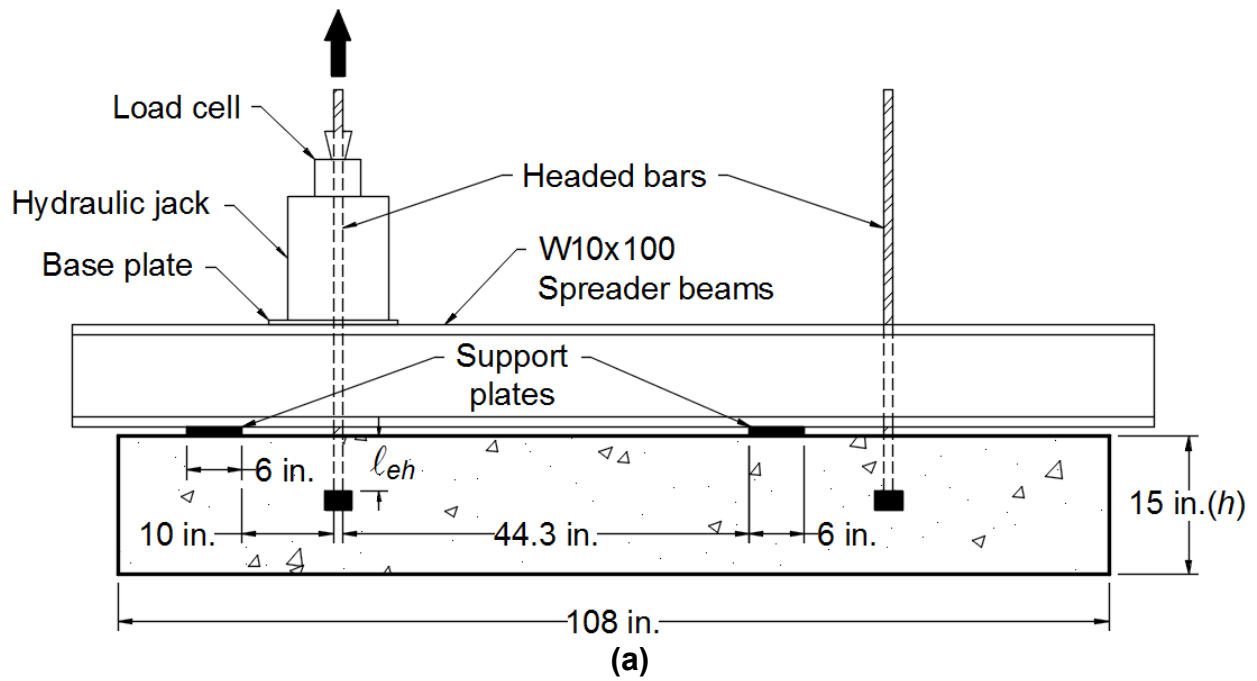


Figure 2.3 Schematic view of slab specimens in Series 1 to 5 (a) front view, (b) side view

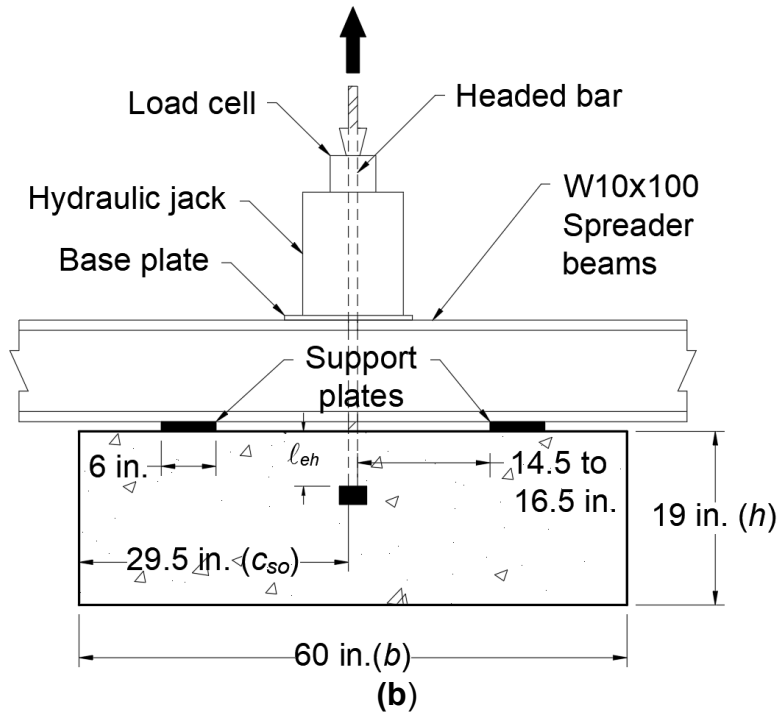
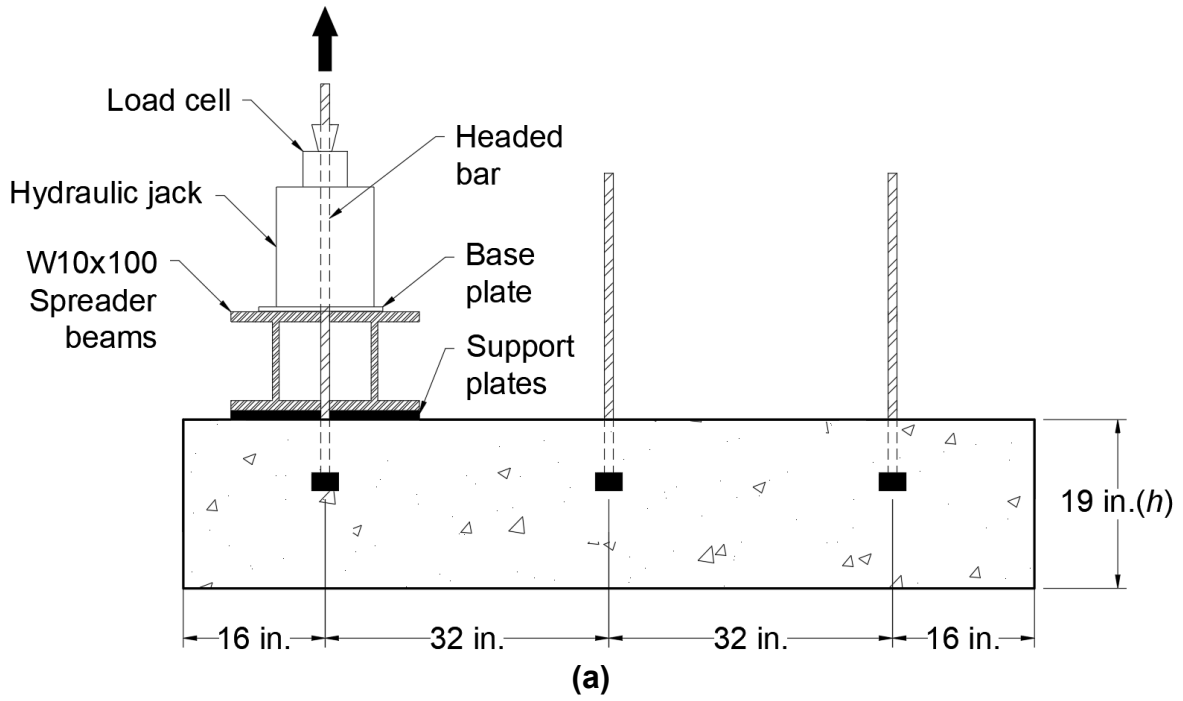


Figure 2.4 Schematic view of slab specimens in Series 6 (a) front view, (b) side view

2.2.2 Test Parameters

Headed bars: The specimens contained Grade 120 ASTM A1035 No. 8 headed bars.

Concrete compressive strength: The target concrete compressive strengths were 5,000 and 8,000 psi. Measured compressive strengths ranged from 4,200 to 8,620 psi. Concrete mixture proportions are given in Section 2.1.1.

Embedment length: Embedment lengths ranged from 6 to 8.5 in.

Reaction force placement: The distance from the center of the headed bar to the center of the closest reaction plate ranged from 12.8 to 47.3 in.

Amount of reinforcement in a plane perpendicular to the headed bar: Reinforcement in a plane perpendicular to the headed bars ranged from none to quantities including two No. 8 or six or eight No. 5 bars placed symmetrically about the headed bar, parallel and close to the long edges of the specimen; two to six No. 5 bars placed symmetrically about and close to the headed bar in the short direction of the specimen; and nine No. 4 and eight No. 5 bars distributed evenly and oriented in, respectively, the long and short directions of the specimen. All reinforcement perpendicular to the headed bars were Grade 60. Details of the reinforcement configuration are provided in Section B.2 of Appendix B.

Type of headed bar: Head types F4.1, F9.1, O4.5, O9.5, O12.9, S6.5, S9.5, S14.9, T4.0, and T9.5, presented in Table 2.3, were used in slab specimens.

2.2.3 Specimen Designation

The slab specimen designations followed the convention shown in Figure 2.5. The first and second terms indicate the bar size and the nominal concrete compressive strength, respectively. The third term represents the head type (Table 2.3). The fourth and final terms represent the amount of reinforcement in a plane perpendicular to the headed bar and embedment length in in., respectively. For example, 8-5-F4.1-2#8-6, indicates that the specimen contained a No. 8 headed bar cast in concrete with a nominal compressive strength of 5 ksi, the head was a F4.1 (friction-forged with a net bearing area of 4.1 times the area of the embedded bar), the reinforcement in a plane perpendicular to the headed bar consisted of two No. 8 bars, and headed bar had a nominal embedment length of 6 in.

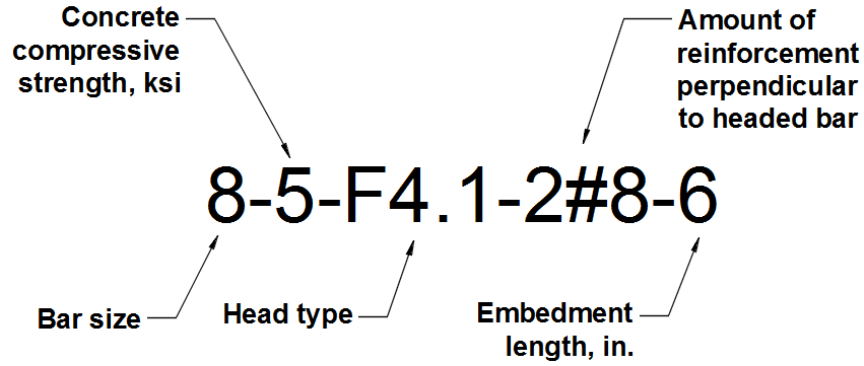


Figure 2.5 Slab specimen designation

2.2.4 Specimen Fabrication

Formwork for the slab specimens was constructed of $\frac{3}{4}$ -in. plywood and timber with nominal dimensions of 2×4 in., as shown in Figure 2.6. The headed bars were supported from below by a $1\frac{7}{8}$ -in. diameter PVC pipe; a wooden truss above the form held the bar upright until the concrete had set. Concrete was placed in two layers; each layer was consolidated with a spud vibrator. Specimens were wet-cured with burlap and plastic covering on the top surface until the compressive strength of the concrete reached 3,000 psi. The forms were then removed and the specimens were allowed to dry until they reached the target strength before testing. For high-strength concrete (nominal strengths of 12,000 psi), specimens were wet-cured immediately after demolding to allow concrete to continue to gain strength. Concrete cylinders of 4×8 in. and 6×12 in. were made and stored close to the specimens. The cylinders were cured in a similar fashion as the specimens were cured. These cylinders were used to keep track of concrete compressive strength of specimens. Steel molds were used for the 6×12 in. concrete cylinders that were tested on the same day as the embedment tests were performed. Plastic molds were used for the other cylinders.



Figure 2.6 Slab specimen formwork

2.2.5 Test Procedure

The slab specimens were tested using the self-reacting frame shown in Figures 2.3 and 2.4, which consisted of two steel spreader beams placed along the longest dimension of the specimen in Series 1 to 5 and along the shortest dimension of the specimen in Series 6 on either side of the anchored headed bar. An upward force was applied on the anchored bar using a hydraulic jack placed on top of the spreader beams. The spreader beams were selected based on the moment and shear strength demands at the maximum anticipated load applied to the specimens, so that the maximum deflection of the spreader beams was less than the thickness of the plates that served as support plates ($1 \times 6 \times 12$ in.) to prevent the beam from touching the slab. A load cell was mounted on top of the jack to measure the tensile force applied on the bar. Load was applied monotonically, pausing at regular intervals (at every 10-kip increment in load) for marking cracks. Cracks were marked until the load reached about 70% of the expected failure load, and then the specimen was loaded until failure, after which cracks were marked and photographs were taken. The tensile load applied to the headed bar was recorded during the test using a load cell placed between the

hydraulic jack and the bar grips. Specimens reached the failure load at about 15 min. once the load was started applying.

2.3 SPLICE SPECIMENS

2.3.1 Specimen Design

The splice specimens were beams tested using four-point loading to evaluate the splice strength of headed bars. The specimens were designed to ensure a failure of the splice. The test parameters included in this study were the spacing between the lapped bars and the compressive strength of the concrete. Six specimens containing No. 6 headed bars (Figure 2.7) were used to investigate lap splice performance. The 18×20 in. beams contained three bottom cast lapped bars at mid-span with a lap length l_{st} of $16d_b$ (12 in.). The tension splice length (equal to the distance between the bearing faces of adjacent headed bars) was chosen based on the results of headed bar anchorage tests in beam-column joints (Shao et al. 2016) so that the anticipated failure stress on the bar was above 60 ksi but below the strength of the bar. None of the specimens had confining reinforcement within the splice region.

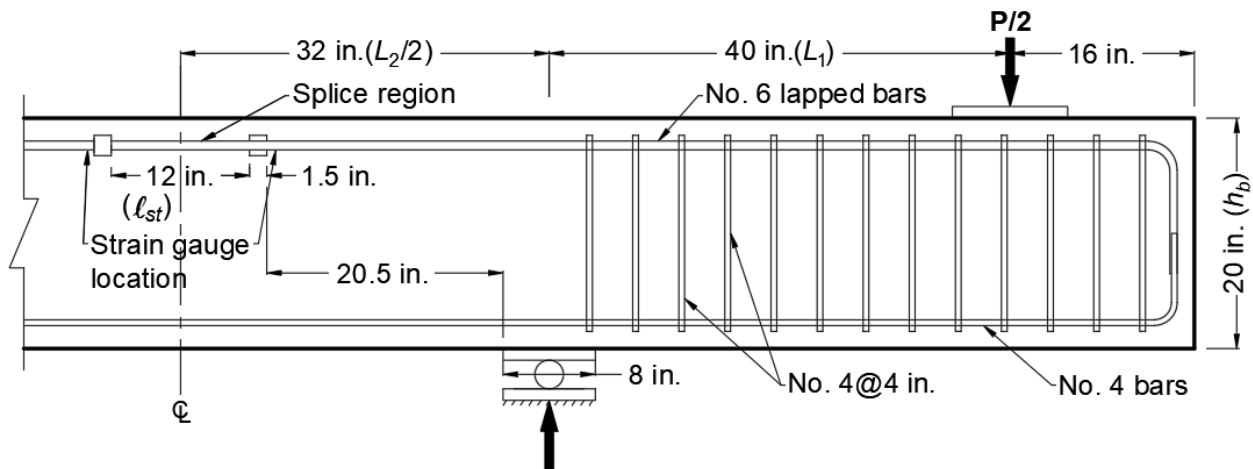


Figure 2.7 Splice test specimen detail and test configuration

Figure 2.7 shows a side view of the specimen and the test configuration. A four-point loading configuration was used to provide a uniform moment and zero shear within the splice region. Sufficient shear reinforcement was provided outside the constant moment region to prevent shear failure. The specimens were inverted (with the splice on top) and loaded symmetrically during the test.

2.3.2 Test Parameters

Bar size: The splice specimens contained Grade 120 ASTM A1035 No. 6 headed bars.

Concrete compressive strength: The target concrete compressive strengths were 5,000 and 12,000 psi, while the measured compressive strengths averaged 6,360 and 10,950 psi. Concrete mixture proportions are given in Section 2.1.1.

Lap length: The nominal embedment length was 12 in. for all specimens.

Type of headed bar: All specimens had No. 6 S4.0 heads (See Table 2.3).

Splice spacing: Three configurations of lapped bar spacings were used, as shown in Figure 2.8: (a) lapped bars placed with the heads in contact with the adjacent bar, giving a clear spacing of $1/2$ in. ($0.67d_b$) and a center-to-center spacing of $1 1/4$ in. between the lapped bars; (b) lapped bars with a clear spacing of 1 in. ($1.33d_b$) (center-to-center spacing of $1 3/4$ in.), the minimum clear distance between the parallel bars in a layer required by ACI 318 for the $3/4$ -in. maximum size aggregate used in the concrete; and (c) lapped bars spaced equally along the width of the beam giving a clear spacing of $1 7/8$ in. ($2.53d_b$) and a center-to-center spacing of $2 5/8$ in.

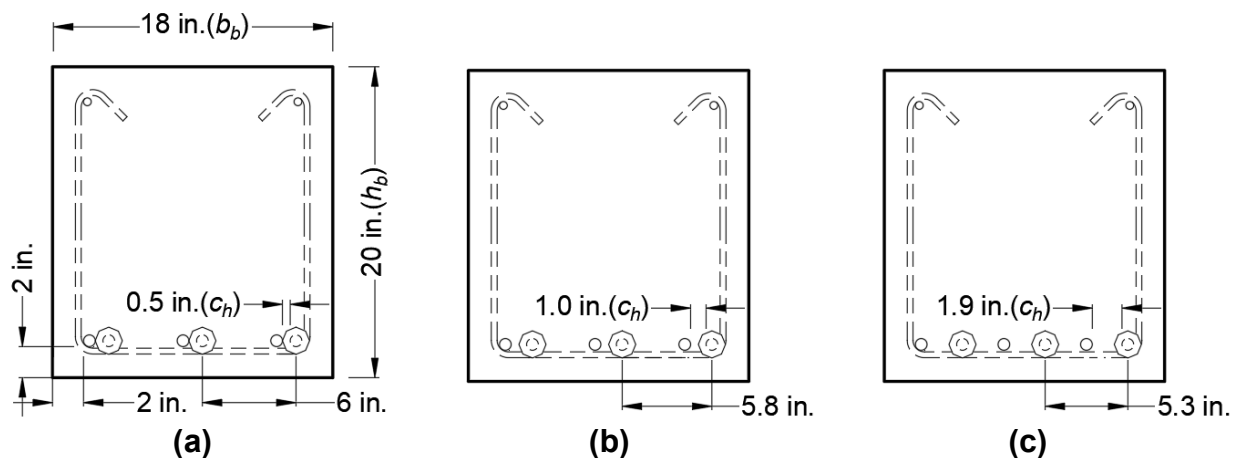


Figure 2.8 Lap configuration of headed splice specimens

2.3.3 Specimen Designation

The designations for the splice specimens were chosen so as to describe the key test parameters (Figure 2.9), as follows. The first number (in parenthesis) represents the number of lapped bars. The second and third numbers indicate the ASTM size designation for the bars and nominal concrete compressive strength in ksi, respectively. The fourth and fifth terms show the head type (Table 2.3) and the nominal lap length, in in., respectively. The last term indicates the

clear spacing between the bars in inches. For instance, specimen (3)-6-5-S4.0-12-0.5 contained three No. 6 headed lapped bars in 5 ksi nominal compressive strength concrete. The headed bars had cold-swaged heads with a net bearing area equal to four times the bar area, a lap length of 12 in., and a clear spacing between the lapped bars of 0.5 in.

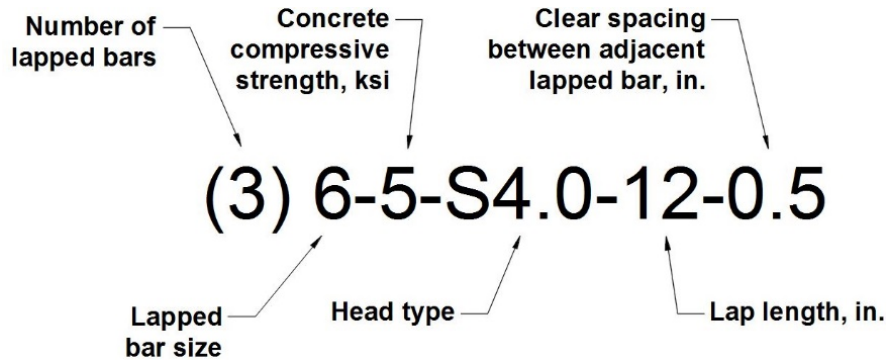


Figure 2.9 Splice specimen designation

2.3.4 Specimen Fabrication

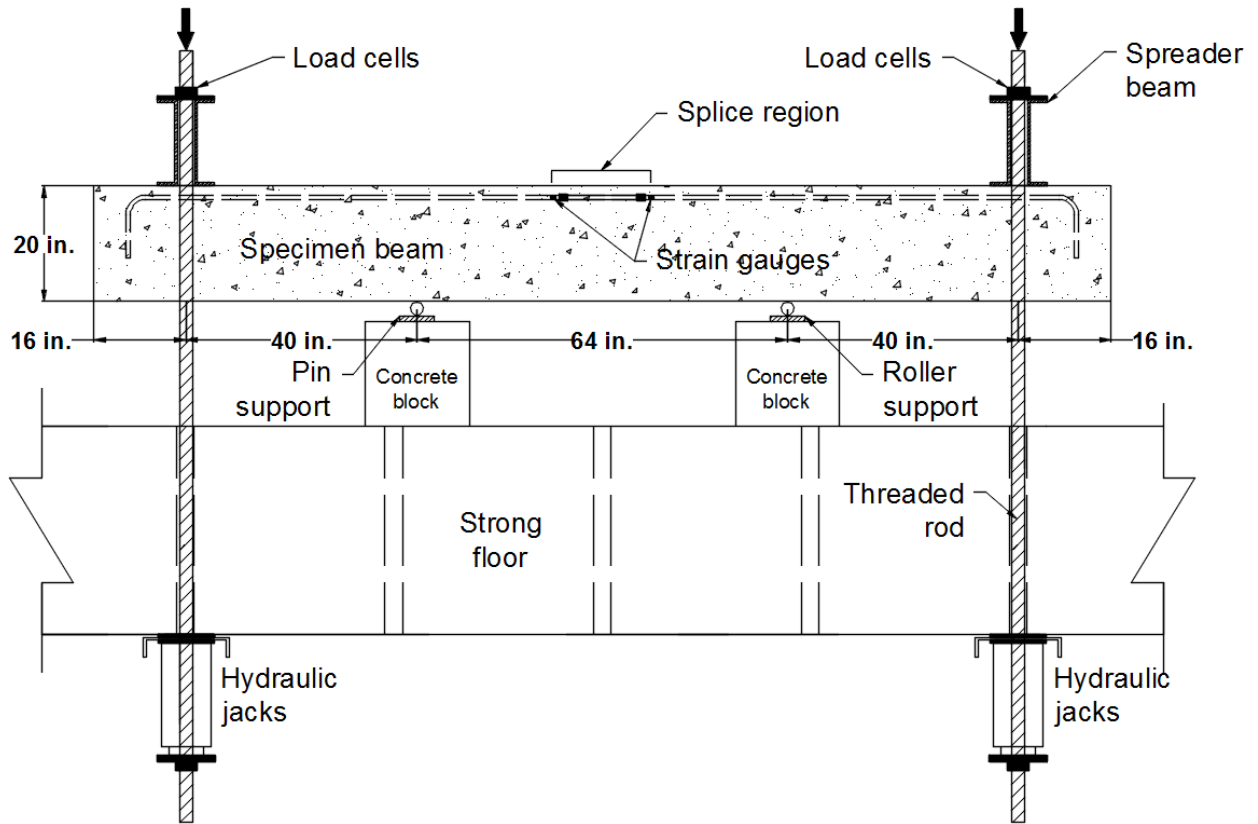
The specimens were cast in wooden forms. The bottom-cast headed-bar splices were placed symmetrically at the midspan of the beam. The concrete was placed in two lifts, with internal vibration after each lift. After finishing, the specimens were covered with wet burlap and plastic to cure. Forms were removed once the concrete compressive strength reached 3,000 psi. Specimens with a target concrete compressive strength of 5,000 psi were allowed to air dry; specimens with a target compressive strength of 12,000 psi were wrapped in wet burlap and wet-cured for approximately one month before drying and testing. As for the shallow embedment tests, cylinders were cast to keep track of the gain in concrete strength. Steel molds were used for the 6×12 in. concrete cylinders that were tested on the same day as the embedment tests were performed, and plastic molds were used for the other cylinders.

2.3.5 Test Procedure

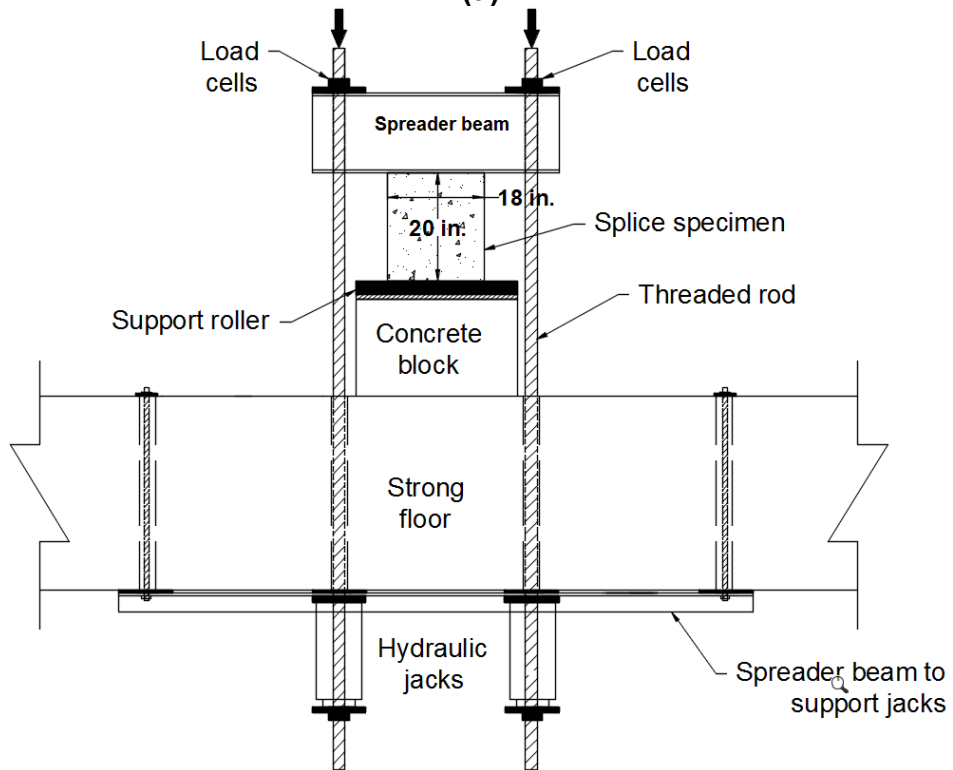
Splice specimens were inverted and placed on supports prior to testing (pin and roller supports spaced at 64 in.). Placing the splices on top facilitated inspection and marking of cracks in the splice region during tests. The specimens were then leveled, and the location of the loading points from the supports and the span length were measured. Loads were applied symmetrically at the ends of the specimen using spreader beams, each connected by two threaded rods to dual-

acting center-hole hydraulic jacks mounted under the strong floor in the laboratory, as shown in Figure 2.10. The hydraulic jacks were mounted directly to the strong floor and were not supported by the spreader beams. The spreader beams and threaded rods were designed to transfer the maximum anticipated load to the specimen without undergoing significant deflection during the test. Two concrete blocks were placed symmetrically in between the load points to serve as the middle supports (Figure 2.10a). High-strength gypsum cement paste was used to level the blocks and prevent sliding during the test. A 2.5-in. diameter steel roller was placed on a 1×10×24 in. steel base plate (also leveled using the gypsum cement) and mounted on each block. The roller on one of the concrete blocks was fixed against motion, simulating a pinned support. The roller on the other concrete block was free to roll, simulating a roller support. The supports were placed at least the depth of the beam away from the splice region. Specimens were placed symmetrically on the supports; the nominal distance between the loading point and nearest support was 40 in., and the nominal length of the central span was 64 in. The actual span measurements were recorded before each test; in all cases, actual measurements were within 0.5 in. of the nominal measurements.

Prior to testing, a small load was initially applied to the beam to ensure free motion of all portions of the test apparatus. During testing, load was applied monotonically with periodic pauses (at every 10-kip increment in load) for marking cracks. Cracks were marked until the load reached about 70% of the expected failure load, and then the specimen was loaded until failure, after which cracks were marked and photographs were taken.



(a)



(b)

Figure 2.10 Schematic view of splice test (a) front view and (b) side view

2.3.6 Specimen Instrumentation

Specimens were instrumented to measure the load and displacement, as well as the strain on the spliced bars. The loads applied through the hydraulic jacks were measured using center-hole load cells installed above the spreader beams on each threaded rod. An infrared tracking system was used to measure the displacement, rotation, and crack width during testing. Infrared markers (as shown in Figure 2.11) were installed along one of the vertical faces of the specimen so that the displacement and rotation at the loaded ends and midspan could be measured. In the first series of splice test specimens, strains in the lapped bars were measured using strain gauges mounted 1 in. outside the splice region (one on an edge bar and another on the middle bar). In the second series, a strain gauge was mounted 1 in. outside the splice region on each of the lapped bars. Load and strain measurements were recorded using a single data acquisition system. Displacements and rotations were recorded using the separate optical tracking system. An effort was made to start both systems simultaneously to avoid mismatch of load/strain and corresponding displacement data from the tests. The data were synchronized by aligning the load and displacement values at failure (the sudden drop in load after the specimen fails also causes an abrupt change in deflection). The data sampling rate for both systems was 2 Hz. Prior to testing, the beam was centered on the loading system and all measurement systems connected. To avoid interference with the displacement readings, infrared markers were installed on the vertical face of the specimen opposite to the face where cracks were marked.



Figure 2.11 Location of infrared markers marked by circles

CHAPTER 3: TEST RESULTS

In this chapter, test results from the headed bar slab and splice specimens are presented. Failure modes, effects of test parameters on the anchorage strength of headed bars, and an analysis of test results from other studies are presented.

3.1 TESTS ON HEADED BARS ANCHORED IN SLAB SPECIMENS WITH SHALLOW EMBEDMENT

Headed bars anchored in slab specimens were tested to investigate the anchorage behavior of the headed bars in a simulated column-foundation joint with the column subjected to bending. Six series of slab specimens, discussed in detail in Section 2.2, were tested to investigate the effects of support location, bearing area of the head, reinforcement in a plane perpendicular to the headed bar, and concrete compressive strength on the anchorage strength. The slab specimens contained two or three headed bars simulating column longitudinal reinforcement anchored in a foundation, except for one specimen that had a single bar anchored in the center of the slab. Only one headed bar was loaded at a time; the spacing between the bars was chosen to ensure that the failure of one headed bar would not interfere with the anchorage strength of adjacent bars. Thirty-two headed bars with shallow embedment lengths, ranging between 6 and 8.5 in., were tested. The net bearing areas of the heads A_{brg} ranged from 4 to $15A_b$. Concrete compressive strengths ranged from 4,200 to 8,620 psi and stresses in the bars at anchorage failure ranged from 49,500 to 117,000 psi. A summary of specimens is provided in Table 3.1 with complete details provided in Table B.1 of Appendix B.

Table 3.1 Detail of slab specimens ^[1]

Specimens ^[2]				ℓ_{eh}	f_{cm}	h_{cl}	$\frac{h_{cl}}{\ell_{eh}}$	$\frac{A_{brg}}{A_b}$	$\frac{A_{st}}{A_b}$	T	T_{anc}	T_h	$\frac{T}{T_{anc}}$	$\frac{T}{T_h}$
SN	Description	Head	(in.)											
Series 1	1	8-5-T9.5-8#5-6 ^[3]	A	8.00	7040	10.5	1.31	9.5	1.29	65.6	57.0	55.8	1.15	1.18
		8-5-T9.5-8#5-6 ^[3]	B	8.25	7040	10.5	1.27	9.5	1.29	67.8	60.2	57.5	1.13	1.18
	2	8-5-T4.0-8#5-6	A	8.50	7040	10.5	1.24	4.0	0	61.8	62.4	59.3	0.99	1.04
		8-5-T4.0-8#5-6	B	7.50	7040	10.5	1.40	4.0	0	56.3	51.7	52.2	1.09	1.08
Series 2	3	8-5-F4.1-8#5-6 ^[3]	A	7.44	5220	10.5	1.41	4.1	1.29	68.9	43.6	48.1	1.58	1.43
		8-5-F4.1-8#5-6 ^[3]	B	7.38	5220	10.5	1.42	4.1	1.29	64.4	43.6	47.7	1.48	1.35
	4	8-5-F9.1-8#5-6 ^[3]	A	7.13	5220	10.5	1.47	9.2	1.29	69.9	41.0	46.1	1.70	1.52
		8-5-F9.1-8#5-6 ^[3]	B	7.00	5220	10.5	1.50	9.2	1.29	54.9	40.1	45.2	1.37	1.21
Series 3	5	8-5-F4.1-2#8-6	A	6.00	7390	10.5	1.75	4.1	0	64.4	37.9	41.9	1.70	1.54
		8-5-F9.1-2#8-6	B	6.00	7390	10.5	1.75	9.2	0	65.0	37.9	41.9	1.71	1.55
	6	8-5-T4.0-2#8-6	A	6.06	7390	10.5	1.73	4.0	0	60.5	38.9	42.4	1.56	1.43
		8-5-T9.5-2#8-6	B	6.13	7390	10.5	1.71	9.5	0	57.7	38.9	42.8	1.49	1.35
Series 4	7	8-8-O12.9-6#5-6	A	6.25	8620	9.8	1.56	13.0	0	79.0	44.0	45.4	1.79	1.74
		8-8-O9.1-6#5-6	B	6.25	8620	10.5	1.68	9.2	0	70.9	44.0	45.4	1.61	1.56
	8	8-8-S6.5-6#5-6	A	6.38	8620	10.0	1.57	5.0	0	73.0	45.1	46.3	1.62	1.58
		8-8-O4.5-6#5-6	B	6.50	8620	10.8	1.65	4.5	0	74.0	46.2	47.3	1.60	1.57
Series 5	9	8-5-S14.9-6#5-6	A	6.50	4200	10.3	1.58	15.0	0	61.8	32.2	39.8	1.92	1.55
		8-5-S6.5-6#5-6	B	6.50	4200	10.0	1.54	5.0	0	49.2	32.2	39.8	1.53	1.24
	10	8-5-O12.9-6#5-6	A	6.63	4200	10.0	1.51	13.0	0	52.4	33.0	40.6	1.59	1.29
		8-5-O4.5-6#5-6	B	6.50	4200	10.1	1.56	4.5	0	50.1	32.2	39.8	1.55	1.26
	11	8-5-S9.5-6#5-6	A	6.50	4200	10.3	1.58	9.5	0	48.9	32.2	39.8	1.52	1.23
		8-5-S9.5-6#5-6	B	6.38	4200	10.1	1.59	9.5	0	54.5	31.5	39.0	1.73	1.40
12	8-5-F4.1-6#5-6 ^[4]	-	8.44	4200	47.3	5.60	4.1	0	39.1	47.3	52.0	0.83	0.75	
Series 6	13	8-5-F4.1-0-6	A	6.50	5180	15.0	2.31	4.1	0	50.5	35.8	41.8	1.41	1.21
		8-5-F4.1-0-6	B	6.25	5180	17.0	2.72	4.1	0	48.9	34.1	40.2	1.43	1.22
		8-5-F4.1-2#5-6	C	6.75	5180	17.0	2.52	4.1	0.78	61.5	38.3	43.5	1.61	1.41
	14	8-5-F4.1-4#5-6	A	6.00	5180	16.8	2.79	4.1	1.57	53.4	31.7	38.5	1.68	1.39
		8-5-F4.1-4#5-6	B	6.13	5180	17.0	2.78	4.1	1.57	52.4	32.5	39.3	1.61	1.33
		8-5-F4.1-4#5-6	C	6.75	5460	17.0	2.52	4.1	1.57	53.5	39.3	44.0	1.36	1.21
	15	8-5-F4.1-6#5-6	A	6.25	5460	17.0	2.72	4.1	2.35	47.3	35.1	40.7	1.35	1.16
		8-5-F4.1-6#5-6	B	6.63	5460	16.8	2.53	4.1	2.35	55.9	37.6	43.2	1.49	1.29
		8-5-F4.1-6#5-6	C	6.88	5460	17.0	2.47	4.1	2.35	52.6	40.2	44.9	1.31	1.17

^[1] SN = specimen number; ℓ_{eh} = embedment length; f_{cm} = measured concrete compressive strength; h_{cl} = distance between the center of headed bar to the inner face of the nearest support plate; A_{brg} = net bearing area of the head (Table 2.3); A_b = area of the headed bar; A_{st} = area of reinforcement in a plane perpendicular to the headed bar within a $1.5\ell_{eh}$ radial distance from the center of the bar (Figures 3.4 and 3.5); T = Force in the headed bar at failure; T_{anc} = anchorage strength calculated using Eq. (3.9) based on anchorage provisions in Chapter 17 of ACI 318-14 (in all cases concrete breakout failure governed the anchorage strength); T_h = anchorage strength of headed bars calculated using Eq. (3.4); a complete descriptions of all notations is provided in Appendix A

^[2] All specimens contained No. 8 headed bars; multiple headed bars in a single specimen are denoted by letters A, B, and C

^[3] In addition to 8 No. 5 bars as reinforcement perpendicular to the headed bar, specimens contained No. 4 bars spaced at 12 in. in a direction perpendicular to the No. 5 bars as shown in Figure 3.6 (details provided in Section B.2 of Appendix B)

^[4] Specimen contained a single centrally placed headed bar

3.1.1 Failure Modes

All specimens exhibited breakout failure in which a region of concrete pulled out of the slab along with the anchored bar, forming a cone-shaped failure surface. The exact failure pattern depended on the placement of the test frame supports, as shown in Figure 3.1. In Figure 3.1a, the support nearest to the headed bar simulating the compression region of a column anchored in the foundation subjected to bending is within the failure region and the other support is away from it, while in Figures 3.1b and c both supports are outside the failure region. The specimen in Figure 3.1b contained a single headed bar anchored at the middle of the slab, while the specimen in Figure 3.1c contained three headed bars embedded sufficiently far apart so that an anchorage failure of one bar did not interfere with the anchorage capacity of the others. When a support was close to the bar it confined, the failure surface extended towards the unconfined region away from the support. The effect of support locations on anchorage strength is described in Section 3.1.2.

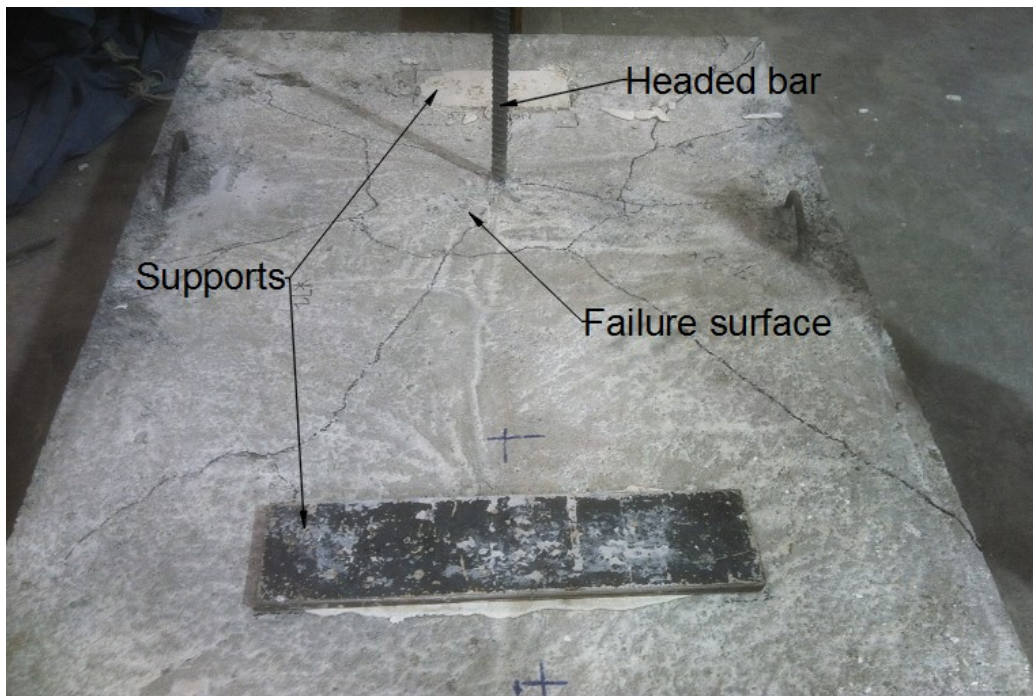


Figure 3.1a Breakout failure of slab specimen 8-5-S14.9-6#5-6 from test Series 5 with one of the supports within the failure region



Figure 3.1b Breakout failure of slab specimen 8-5-F4.1-6#5-6 from test Series 5 with both supports outside the failure region (specimen contained a single bar anchored at the middle of the slab)

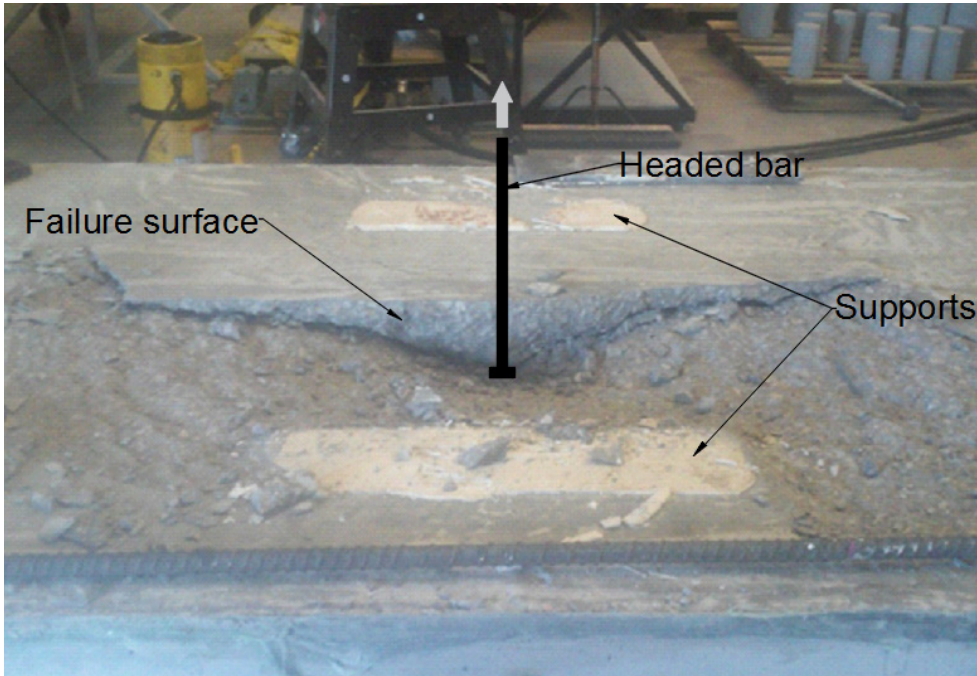


Figure 3.1c Breakout failure of slab specimen 8-5-F4.1-0-6 from test Series 6 with both supports outside the failure region (location of the headed bar is shown)

3.1.2 Effect of Strut Angle

The anchorage strength of a headed bar is dependent on the angle of the strut (Figure 3.2) between the head and the compressive reaction (Eligehausen et al. 2006b). In general, flatter strut angles result in lower anchorage strength. A similar observation was made by Shao et al. (2016) in exterior beam-column joints. To limit the angle, Section R25.4.4.2 of the Commentary to ACI 318-14 suggests that the effective depth of the beam d at a beam-column joint not exceed $1.5\ell_{dt}$, where ℓ_{dt} is the development length of the headed bar. To determine if this behavior is observable in the shallow embedment tests, the anchorage strength of headed bars in the slab specimens, normalized with respect to the concrete compressive strength f_{cm} and the embedment length of the headed bar ℓ_{eh} , is plotted versus the ratio h_{cl}/ℓ_{eh} in Figure 3.3, where h_{cl} is distance from the center of the headed bar to the inside face of the bearing plate at the support (Figure 3.2). This angle is somewhat higher than the actual strut angle (measured from the headed bar to the centroid of the reaction) but is representative of the region susceptible to a breakout failure.

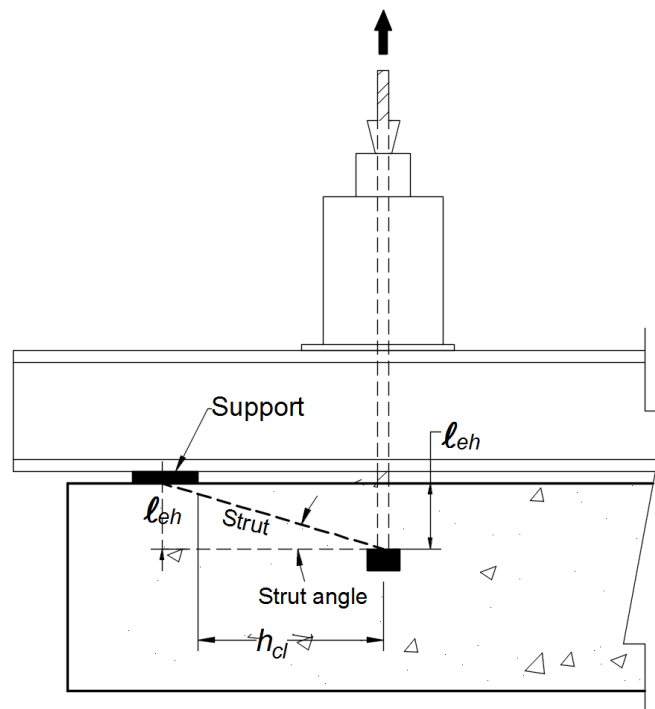


Figure 3.2 Compression region between anchored headed bar and nearest support

A study on the effect of reinforcement in a plane perpendicular to the headed bar, discussed in greater detail in Sections 3.1.3 and 3.3.1.2, showed no effect of such reinforcement on anchorage strength. Therefore, specimens containing reinforcement in a plane perpendicular to the headed

F4.1-6#5-6, with h_{cl}/ℓ_{eh} equal to 5.6, is only about 60% of the average strength of the other specimens. This specimen contained a headed bar located in the middle of the concrete slab and had the lowest strength among the slab specimens. $h_{cl}/\ell_{eh} = 5.6$ is much higher than the maximum ratio of 1.5 suggested in Commentary Section R25.4.4.2 of ACI 318-14 to preclude concrete breakout failure, potentially explaining the low strength relative to that of the other slab specimens.

3.1.3 Effect of Reinforcement in a Plane Perpendicular to Headed Bar

Reinforcement in a plane perpendicular to the headed bar was provided symmetrically on both sides of the bar. The reinforcement within the anticipated concrete breakout failure region (that is, within a $1.5\ell_{eh}$ radial distance from the bar) was expected to confine the concrete by dowel action, preventing a region of concrete from being pulled out of the slab along with the anchored bar, as shown in Figure 3.4. In the first five series, two No. 8, six No. 5, or eight No. 5 bars were placed symmetrically close to the edges parallel to the long direction of the slab with 1.5-in. concrete clear cover (Figures 3.5a and b), with the exception of three specimens in Series 1 and 2 that contained eight No. 5 bars spaced at 6 in. (with two No. 5 bars within a $1.5\ell_{eh}$ radial distance from the headed bar) placed in the long direction and nine No. 4 bars placed on top of the No. 5 bars spaced at 12 in. (with two No. 4 bar within a $1.5\ell_{eh}$ radial distance from the headed bar) placed in the short direction with 1.5-in. concrete clear top cover (see Figure 3.6 and Figure B.10). In Series 6, the reinforcement in a plane perpendicular to the headed bars was placed symmetrically on both sides and close to the bar in the short direction (Figures 3.5c and d). Details of reinforcement in the plane perpendicular to the headed bar for all specimens are provided in Section B.2 of Appendix B.

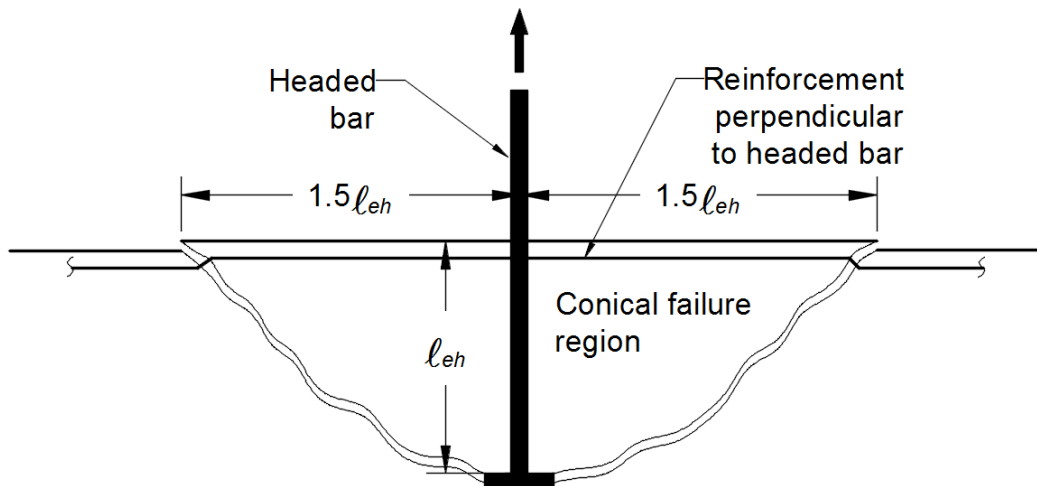


Figure 3.4 Dowel action of reinforcement perpendicular to the headed bar

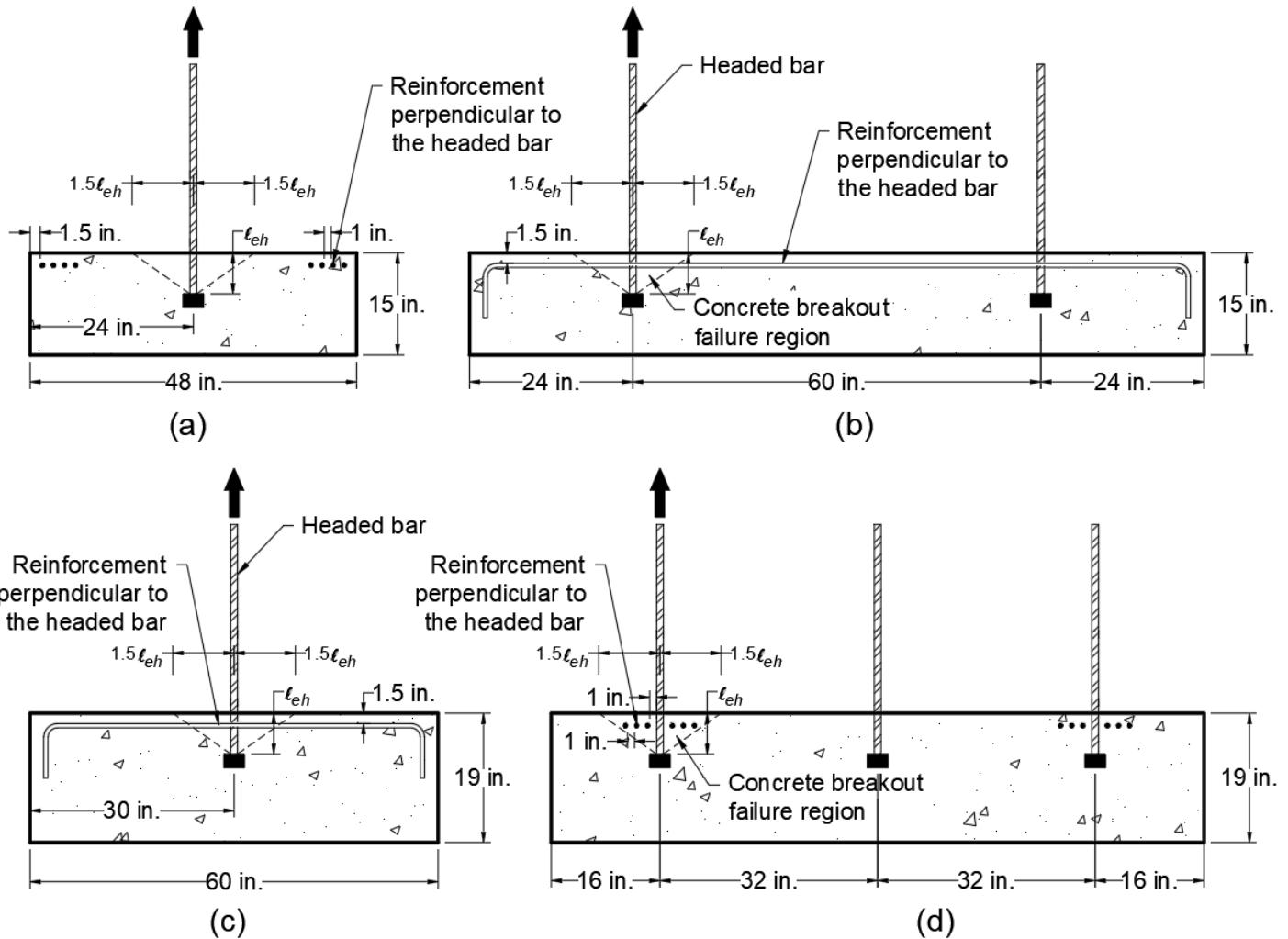


Figure 3.5 Location of headed bars and reinforcement in a plane perpendicular to the headed bar: (a) front and (b) side views of specimens in the first five series, (c) front and (d) side views of specimens in Series 6 (details of reinforcement configuration for all specimens are provided in Section B.2 of Appendix B)



Figure 3.6 Slab specimens in Series 1 and 2 that contained No. 4 and No. 5 bars perpendicular to the headed bar distributed evenly along the long and short direction of the specimen

The normalized bar force at failure T_N based on Eq. (3.1) is plotted versus the amount of reinforcement in a plane perpendicular to the headed bar A_{st} within a $1.5\ell_{eh}$ radial distance from the center of the bar in Figure 3.7. The specimens with $A_{brg} \leq 9.5A_b$ and h_{cl}/ℓ_{eh} ranging from 1.24 to 2.79 are included. The single specimen with h_{cl}/ℓ_{eh} of 5.6, which exhibited lowest strength among the slab specimens (Section 3.1.2), is not included in the figure.

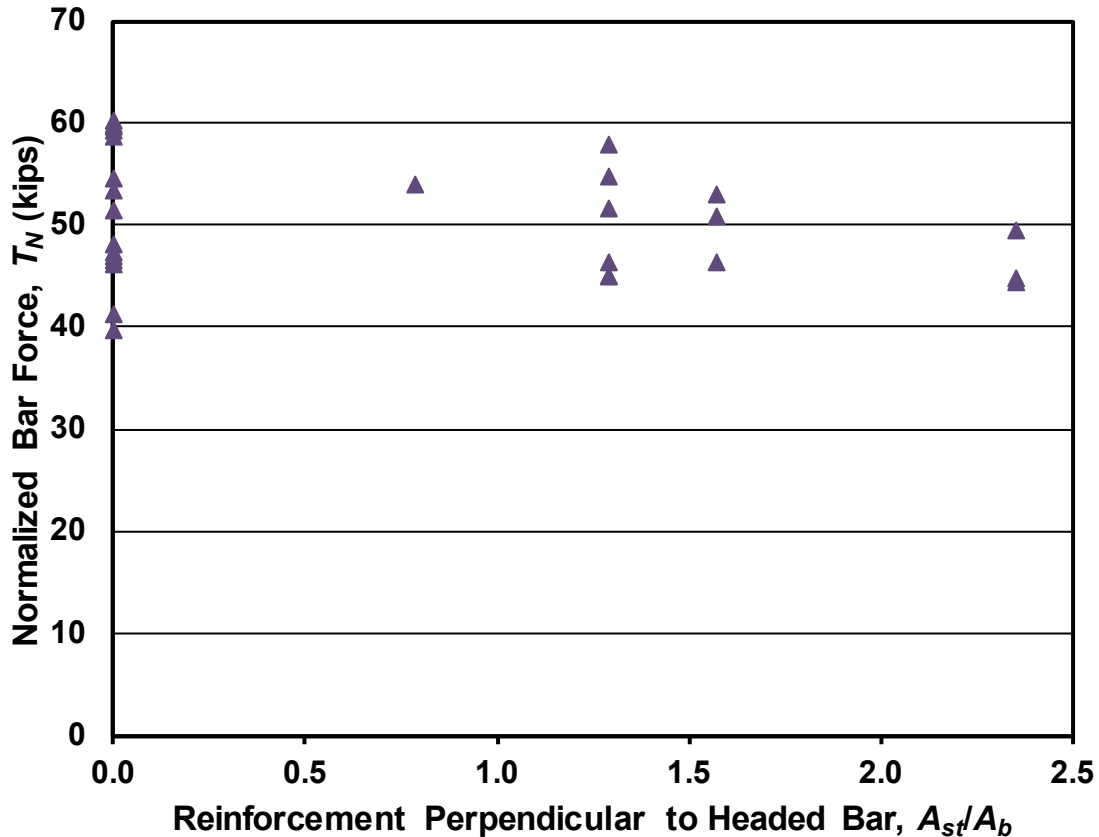


Figure 3.7 Bar force at failure normalized with respect to a concrete compressive strength of 5,000 psi and an embedment length of 6-in. T_N versus area of reinforcement A_{st} , within a $1.5\ell_{eh}$ radial distance from the center of and in a plane perpendicular to the headed bar, normalized with respect to the area of the headed bar A_b [T_N is calculated using Eq. (3.1); specimens with A_{brg} ranging from 4 to $9.5A_b$ and h_{cl}/ℓ_{eh} ranging from 1.24 to 2.79 are included]

For specimens that contained reinforcement perpendicular to the headed bar, Figure 3.7 shows about an 8% decrease in anchorage strength with a two-fold *increase* in the perpendicular reinforcement. A comparison with the specimens that did not contain reinforcement perpendicular to the bar, however, shows that the anchorage strength is virtually unchanged (decreases about 3%). This indicates that the perpendicular reinforcement, which was expected to confine the headed bar by dowel action as shown in Figure 3.4, is not effective in improving the anchorage strength of the headed bar. Choi et al. (2002) and Choi (2006) also investigated the effect of reinforcement perpendicular to the headed bar on anchorage strength in column-like specimens containing two to four headed bars. Choi et al. (2002) showed that an increase in the amount of such reinforcement did not affect the anchorage strength, while Choi (2006) reported a 16% average increase in anchorage strength when doubling the amount of reinforcement perpendicular

to the bar. A detailed discussion on the effect of reinforcement perpendicular to the headed bar based on test results from Choi et al. (2002), Choi (2006), and the current study is presented in Section 3.3.1.2.

3.1.4 Effect of Net Bearing Area of Head

The effect of net bearing area of the head on the anchorage strength of the headed bar is shown in Figure 3.8. A study of the effect of reinforcement in a plane perpendicular to the headed bar, discussed in greater detail in Section 3.1.3 (also in Section 3.3.1.2), showed no effect of such reinforcement on anchorage strength. One specimen with h_{cl}/ℓ_{eh} of 5.6, which exhibited lowest strength among the slab specimens, is not included. Therefore, only specimens with h_{cl}/ℓ_{eh} ranging from 1.24 to 2.79, which appear not to be affected by h_{cl}/ℓ_{eh} , covering entire range of head size (4 to $15A_b$) regardless of the amount of reinforcement perpendicular to the headed bar, are included in Figure 3.8. Since concrete compressive strengths and embedment lengths varied between specimens, the bar force at failure is normalized with respect to a concrete compressive strength of 5,000 psi and an embedment length of 6 in. using Eq. (3.1).

For tests of exterior beam-column joint specimens, Shao et al. (2016) showed that increasing the net bearing area of the headed bars A_{brg} from 3.8 to $9.5A_b$ had no effect on anchorage strength, but that anchorage strength increased by about 15% for larger heads ($A_{brg} = 13$ to $15A_b$). In Figure 3.8, the trendline for specimens with $A_{brg} \leq 9.5A_b$ ($A_{brg} = 4$ to $9.5A_b$) shows that, on average, anchorage strength is little changed (increases on average about 4%) with an increase in the net bearing area from 4 to $9.5A_b$, while the trendline for all specimens shows that the anchorage strength increases by about 15% with an increase in the net bearing area from 4 to $15A_b$. These observations are consistent with the observations made by Shao et al. (2016).

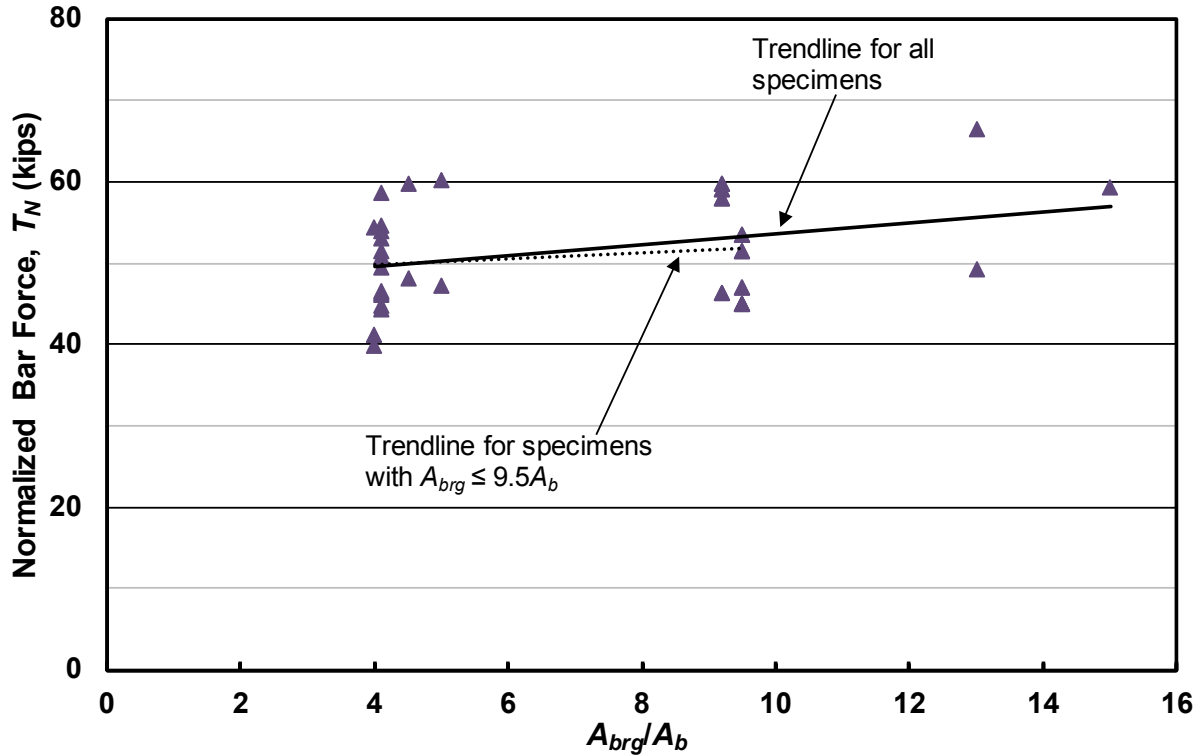


Figure 3.8 Bar force at failure normalized with respect to a concrete compressive strength of 5,000 psi and an embedment length of 6 in. T_N versus the net bearing area of the head A_{brg} [T_N is calculated using Eq. (3.1); only specimens with h_{cl}/ℓ_{eh} ranging from 1.24 to 2.79 are included]

3.1.5 Effect of Concrete Compressive Strength

The effect of concrete compressive strength on the anchorage strength of headed bars is shown in Figure 3.9. Specimens with h_{cl}/ℓ_{eh} ranging from 1.24 to 2.79 and A_{brg} ranging from 4 to $9.5A_b$ are included in the figure. Since the embedment lengths varied between headed bars (ranging from 6 to 8.5 in.), the force in the bar at failure plotted on the vertical axis is normalized with respect to an embedment length of 6 in. using Eq. (3.2).

$$T_N = T \left(\frac{6 \text{ in.}}{\ell_{eh}} \right)^{1.03} \quad (3.2)$$

where T is the measured bar force at failure (kips), and ℓ_{eh} is the embedment length of the headed bar (in.). The power 1.03 in Eq. (3.2) is that for ℓ_{eh} in the descriptive equations [Eq. (1.7) and (1.9)].

Figure 3.9 shows that, on average, increasing the concrete compressive strength from 4,200 to 8,600 psi resulted in an increase in the measured bar force at failure of about 37% (from 46 to

63 kip). This exceeds the value of 18% obtained using Eq. (1.6), which is based on the observations of Shao et al. (2016) for headed bars anchored in beam-column joints.

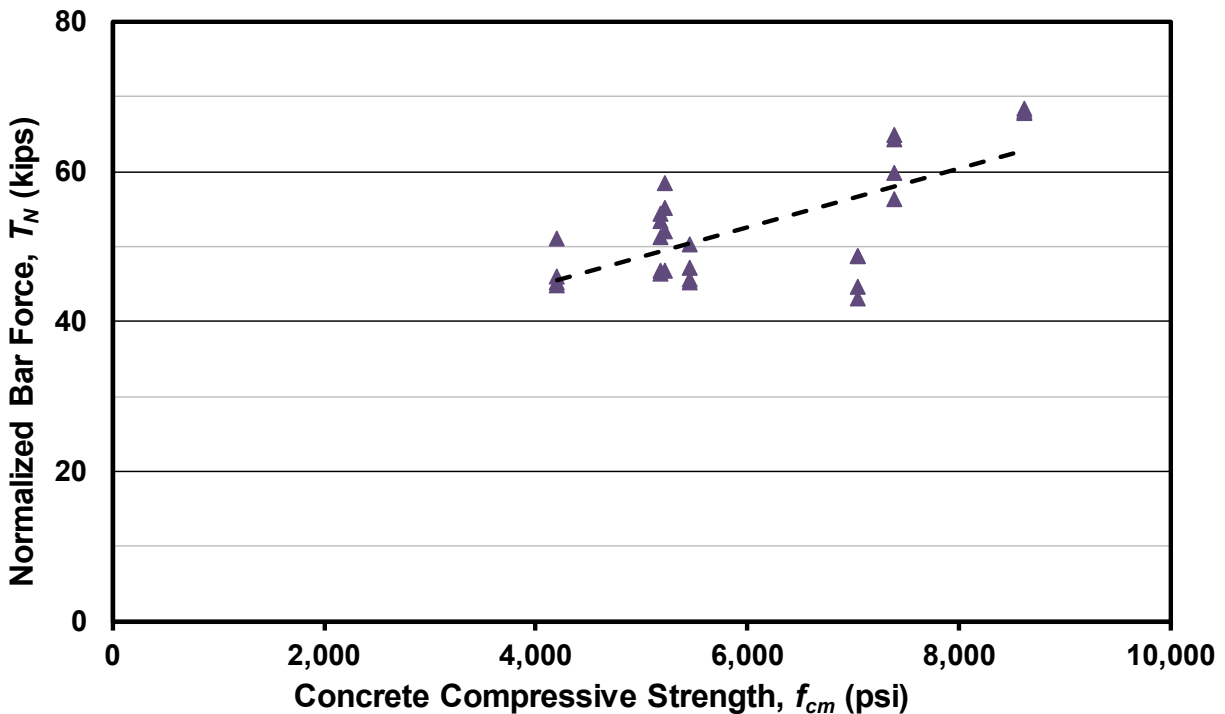


Figure 3.9 Bar force at failure normalized with respect to an embedment length of 6 in. T_N versus concrete compressive strength f_{cm} [T_N is calculated using Eq. (3.2), only specimens with h_{cl}/ℓ_{eh} ranging from 1.24 to 2.79 and A_{brg} ranging from 4 to $9.5A_b$ are included]

The effect of concrete compressive strength can also be evaluated based on the equation for concrete breakout strength in accordance with Section 17.4.2.2 of ACI 318-14. The equation for concrete breakout strength of a single headed bar in tension is given by $N_b = k_c \lambda_a \sqrt{f'_c} h_{ef}^{1.5}$, where k_c is a coefficient for concrete breakout strength in tension, which is equal to 24 for cast-in anchors; λ_a is a modification factor for lightweight concrete, which is equal to 1.0 for normalweight concrete; f'_c is the concrete compressive strength (psi); and h_{ef} is the embedment length of the anchor (in.). Replacing f'_c with measured concrete compressive strength f_{cm} and h_{ef} with the embedment length of headed bars ℓ_{eh} , the equation for the concrete breakout strength of single headed bar in tension becomes $N_b = k_c \lambda_a \sqrt{f_{cm}} \ell_{eh}^{1.5}$.

The effect of concrete compressive strength on the anchorage strength of headed bars is shown in Figure 3.10. The force in the bar at failure plotted on the vertical axis is normalized with respect to an embedment length of 6 in. using Eq. (3.3).

$$T_N = T \left(\frac{6 \text{ in.}}{\ell_{eh}} \right)^{1.5} \quad (3.3)$$

where T is the measured bar force at failure (kips), and ℓ_{eh} is the embedment length of the headed bar (in.). The power 1.5 in Eq. (3.3) is that for h_{ef} in the equation for concrete breakout strength of single headed bar in tension in accordance with Section 17.4.2.2 of ACI 318-14.

Figure 3.10 shows that, on average, increasing the concrete compressive strength from 4,200 to 8,600 psi resulted in an increase in the measured bar force at failure by about 40% (from 43 to 60 kip). This is slightly less than the value of 43% obtained using the equation for concrete breakout strength of single headed bar in tension in accordance with Section 17.4.2.2 of ACI 318-14.

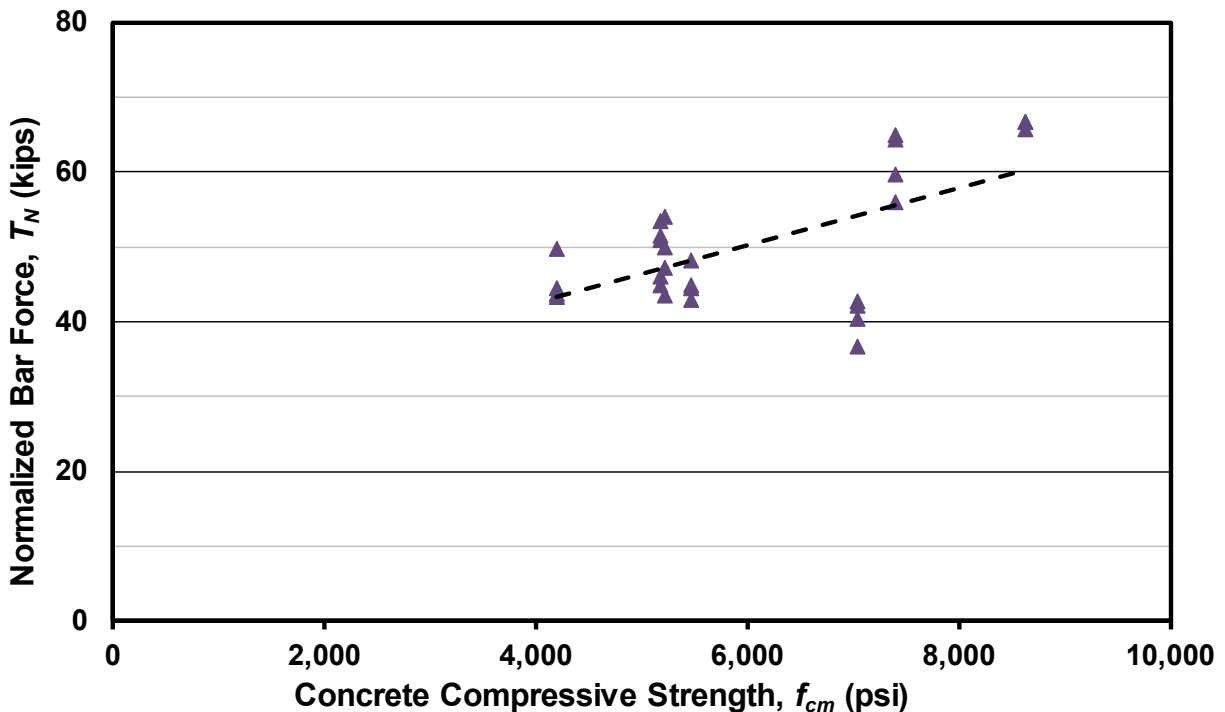


Figure 3.10 Bar force at failure normalized with respect to an embedment length of 6 in. T_N versus concrete compressive strength f_{cm} [T_N is calculated using Eq. (3.3), only specimens with h_{cl}/ℓ_{eh} ranging from 1.24 to 2.79 and A_{brg} ranging from 4 to 9.5 A_b are included]

3.2 HEADED BAR SPLICE TESTS

Six headed bar splice specimens (details in Section 2.3) were tested in two series of three specimens each to investigate the anchorage behavior of headed bars in a lap splice. The specimens contained No. 6 headed bars spliced at mid-span with a lap length ℓ_{st} of 12 in. ($16d_b$). The headed

bars had a net bearing area of $4A_b$ and contained no obstructions. Center-to-center spacing c_{ch} between the bars being spliced was $1\frac{1}{4}$ in. ($1.67d_b$), $1\frac{3}{4}$ in. ($2.33d_b$), or $2\frac{5}{8}$ in. ($3.53d_b$), corresponding to clear spacing between bars c_h of $\frac{1}{2}$ in. ($0.67d_b$), 1 in. ($1.33d_b$), and $1\frac{7}{8}$ in. ($2.53d_b$), respectively. The lowest spacing corresponds to lapped bars with the heads in contact with the adjacent bar. Specimens with clear spacing between the spliced bars of 1 in. and $1\frac{7}{8}$ in. complied with the minimum clear spacing requirements in accordance with Section 25.2.1 of ACI 318-14 for a maximum aggregate size of $\frac{3}{4}$ in., the size used in this study. Both side clear cover c_{so} and top clear cover c_{to} to the lapped bars were 2 in. Measured concrete compressive strengths f_{cm} averaged 6,360 and 10,950 psi for the first and second series, respectively. Strain gauges were mounted on the bars 1 in. outside the splice region. Stresses in the bars at failure ranged from 75,010 to 83,560 psi. A summary of specimens is provided in Table 3.2 with complete details provided in Table B.2 of Appendix B.

Table 3.2 Detail of headed bar splice specimens^[1]

Specimen		n	d_b in.	A_b in ²	f_{cm} psi	ℓ_{st} in.	c_{ch} in.	b_b in.	h_b in.	L_1 in.	L_2 in.	f_{su} ksi	T kips	P kips	M kip-in.
Series 1	(3) 6-5-S4.0-12-0.5	3	0.75	0.44	6330	12	1/2	18.0	20.3	40.1	64.0	77.2	34.0	83.2	1669.2
	(3) 6-5-S4.0-12-1.0	3	0.75	0.44	6380	12	1	18.1	20.3	40.1	64.0	83.6	36.8	90.1	1804.8
	(3) 6-5-S4.0-12-1.9	3	0.75	0.44	6380	12	17/8	18.0	20.1	40.1	64.0	76.3	33.6	82.2	1649.1
Series 2	(3) 6-12-S4.0-12-0.5	3	0.75	0.44	10890	12	1/2	18.0	20.1	40.0	64.1	81.9	36.1	89.1	1782.8
	(3) 6-12-S4.0-12-1.0	3	0.75	0.44	10890	12	1	18.0	20.5	40.1	64.0	75.0	33.0	81.5	1635.9
	(3) 6-12-S4.0-12-1.9	3	0.75	0.44	11070	12	17/8	18.0	20.5	40.0	64.0	82.8	36.4	90.1	1802.4

^[1] n = number of lapped bars; A_b = cross-sectional area of lapped bar; b_b and h_b = width and depth of the beam specimen, respectively; L_1 = average distance between loading points and the nearest supports (Figure 2.7); L_2 = distance between two supports (span length, Figure 2.7); f_{su} = stress in lapped bar at failure calculated from moment-curvature method; T = force in lapped bar at failure ($f_{su}A_b$); P = total load applied on specimen; M = bending moment in splice region; descriptions of all notations are provided in Appendix A.

3.2.1 Failure Modes

The first flexural cracks were observed at about 40% of the ultimate load in the vicinity of the splice region in the constant moment region. Increasing the load resulted in new flexural cracks near the supports as the existing cracks widened. All specimens exhibited a side splitting failure in which the lapped bars closest to the side faces of the beam (edge bars) pushed the cover concrete out; in most cases exposing the head the bar (Figure 3.11), while the middle bar remained confined by concrete. Strain at failure was lower in the outer headed bars than in the middle bar. Strain in

the lapped bars is discussed in greater detail in Section 3.2.3. In five out of six specimens, side splitting occurred predominantly at the end of the splice region closer to the pinned support (described in Section 2.3.5), while one specimen exhibited side splitting at the end of the splice region closer to the roller support.

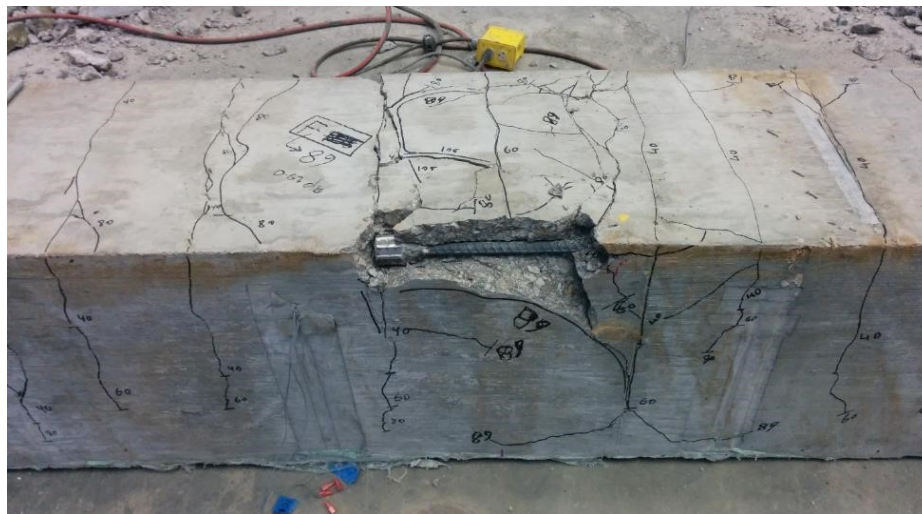
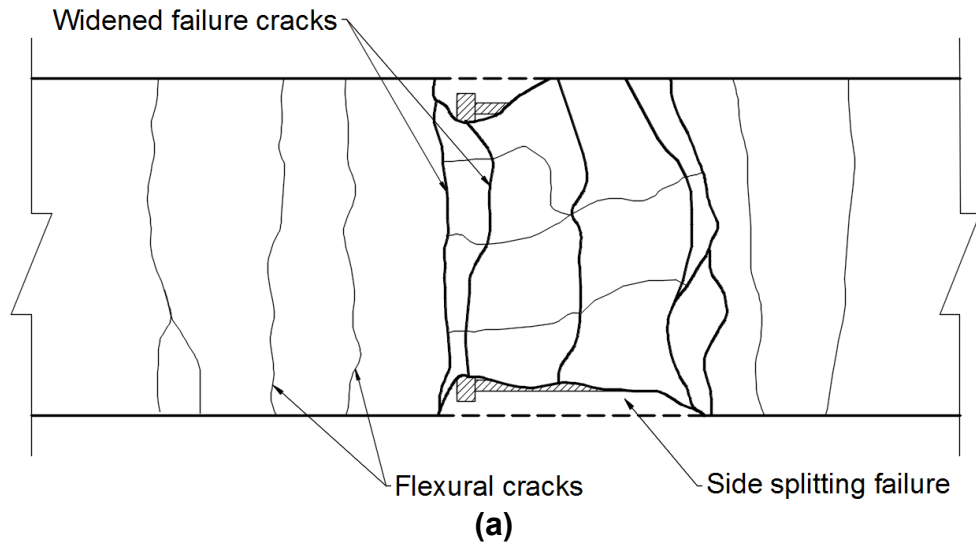


Figure 3.11 (a) Cracking pattern and failure mode of headed splice specimens (top view) (b) cracking patterns and failure mode of Specimen (3) 6-12-S4.0-12-0.5

3.2.2 Effects of Lapped Bar Spacing and Concrete Compressive Strength

The average forces in the headed bars were determined using moment-curvature analysis, as described in ACI 408R-03. The moment-curvature analysis takes into account both concrete and steel stress-strain characteristics to determine the stress in the bar. In this analysis, the stress-strain behavior for concrete was assumed to follow the model proposed by Hognestad (1951); the

stress-strain behavior of the headed bar was obtained from tensile tests (Figure 3.12). Although strain gauges were mounted on the headed bars (see Section 2.3.6), the gauge readings were highly dependent on the location of the gauges with respect to the flexural cracks; when cracks crossed the gauge, the strain readings were higher than when the cracks did not cross the gauge. Therefore, the results from the strain gauges are not reliable and thus not used to determine the average stresses in the lapped bars at failure, which were instead calculated using moment-curvature analysis. The moment M in the splice region is determined by multiplying one-half of the total load applied on the specimen P by the distance between the loading point and the support L_1 (see Figures 2.7 and 2.10a). The moment-curvature analysis was used to convert the moment in the beam to a strain in the bars due to bending. The tensile test results for the headed bars (Figure 3.12) were used to convert the bar strain to stress.

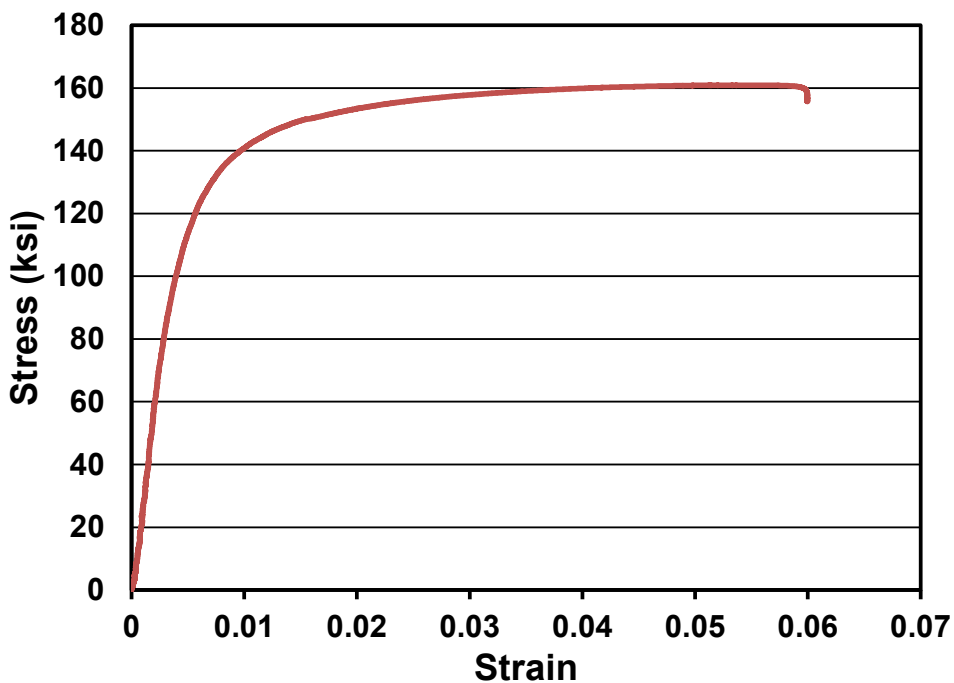


Figure 3.12 Stress-strain behavior for headed bars used in splice specimens

The headed bars in the six splice specimens had a constant lap length of $16d_b$ and were distributed along a fixed width of 18 in. with a center-to-center spacing between the bars of 1.67, 2.33 or $3.53d_b$ (Figure 2.8). For lapped bars spaced closely enough to form a compressive strut spanning between the adjacent bars, the force on the lapped bar is transferred to the adjacent bar through a strut between the bars, as shown in Figure 1.7 (Thompson et al. 2002). Figures 3.13 and

3.14 compare the average maximum forces and average maximum stresses, respectively, in the lapped bars as a function of center-to-center spacing. The figures show that, for a fixed width of concrete and within the range of center-to-center spacing between the lapped bars tested (from 1.67 to $3.53d_b$), the headed bars had nearly constant splice strength, which appears to be unaffected by spacing between the bars. This is likely because the change in bar spacing did not alter the force transfer mechanism between the bars, resulting in similar splice strengths. Furthermore, Student's t-test was used to determine the statistical significance of differences in splice strength as a function of concrete compressive strengths. Based on the average maximum force in the spliced bars in each of the two test series (with average concrete compressive strengths of 6,360 and 10,950 psi), Student's t-test indicates that the differences in splice strength as a function of concrete compressive strength are not statically significant ($p = 0.8$). The effect of headed bar spacing on splice strength in specimens tested by Thompson et al. (2002) and Chun (2015) is discussed in Section 3.3.2.2.

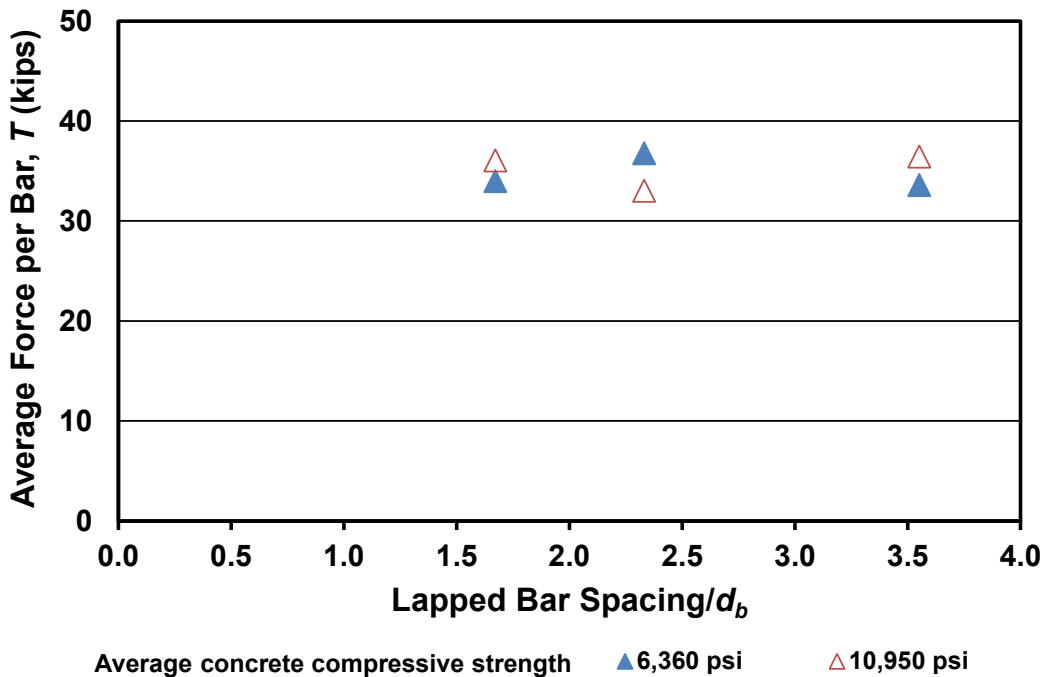


Figure 3.13 Average maximum force T in spliced headed bars versus the center-to-center spacing and concrete compressive strength

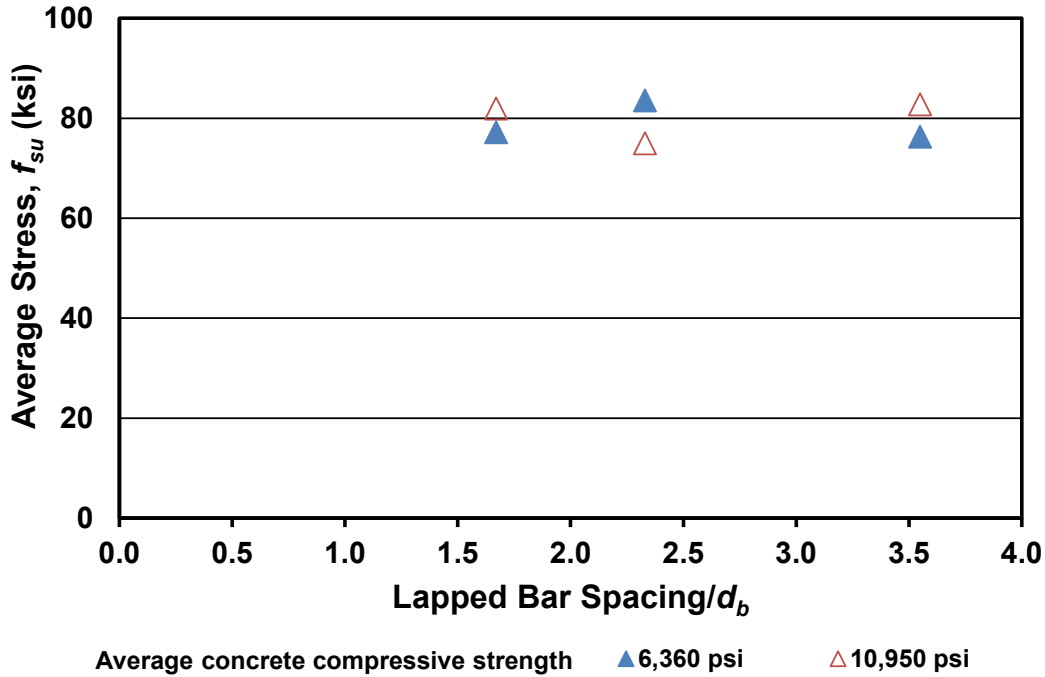


Figure 3.14 Average maximum stress f_{su} in spliced headed bars versus the center-to-center spacing and concrete compressive strength

3.2.3 Load-Deflection and Strain in Lapped Bars

The deflection of specimens was measured using an optical tracking system (see Section 2.3.6). The vertical deflection of the beams was measured with respect to the loading points using infrared markers that are used in the optical tracking system mounted at the mid-span and loading points, as shown in Figure 2.11. The load-deflection diagram for specimen (3) 6-12-4Ab-12-0.5 is presented in Figure 3.15. A decrease in stiffness of the beam (marked by the change in slope of the load-deflection curve at about 40% of the maximum load) corresponds with the formation of the first flexural cracks.

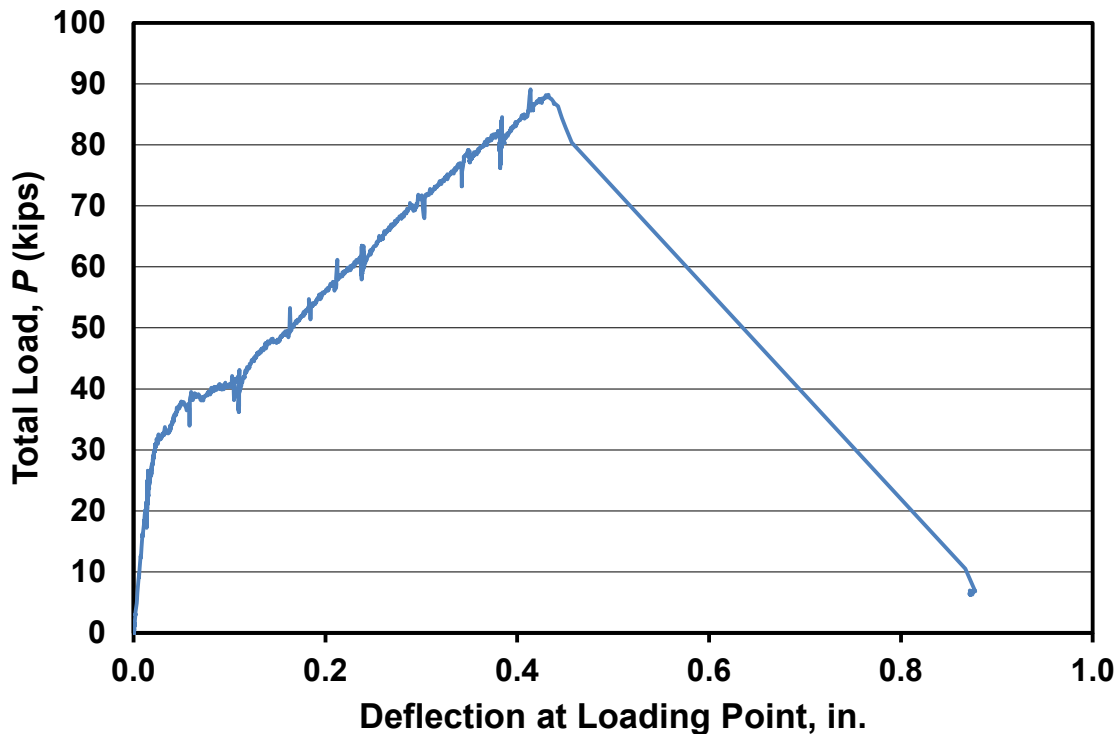


Figure 3.15 Load-deflection diagram for Specimen (3) 6-12-S4.0-12-0.5

The strain in the headed bars was measured using strain gauges mounted 1 in. outside the splice region. As discussed earlier, the sensitivity of the strain gauge reading to crack location did not allow the results to be used in overall strength calculations; however, strain gauge results can be used to evaluate the stress distribution between the middle and edge spliced bars.

Figure 3.16 shows load-strain curves for the three lapped bars in specimen (3) 6-12-S4.0-12-0.5. The load-strain curves for all six specimens are provided in Figures B.14 to B.19 in Appendix B. In this specimen (and in other five specimens tested), the middle bar exhibited greater strain than the edge bars. As discussed in Section 3.2.1, when specimens failed due to splitting of concrete at the edges, in most cases exposing the head of the edge bars, the middle bar was still well confined by the concrete. This likely explains the greater strain in the middle bar. These observations suggest that avoiding the side splitting failure may further increase the splice strength by about 20% as a result of increased stress in the edge bars as high as in the middle bar. The sudden increase in strains at about 40% of the maximum load marks the formation of flexural cracks within the splice region, as reflected in the load-deflection diagram in Figure 3.15.

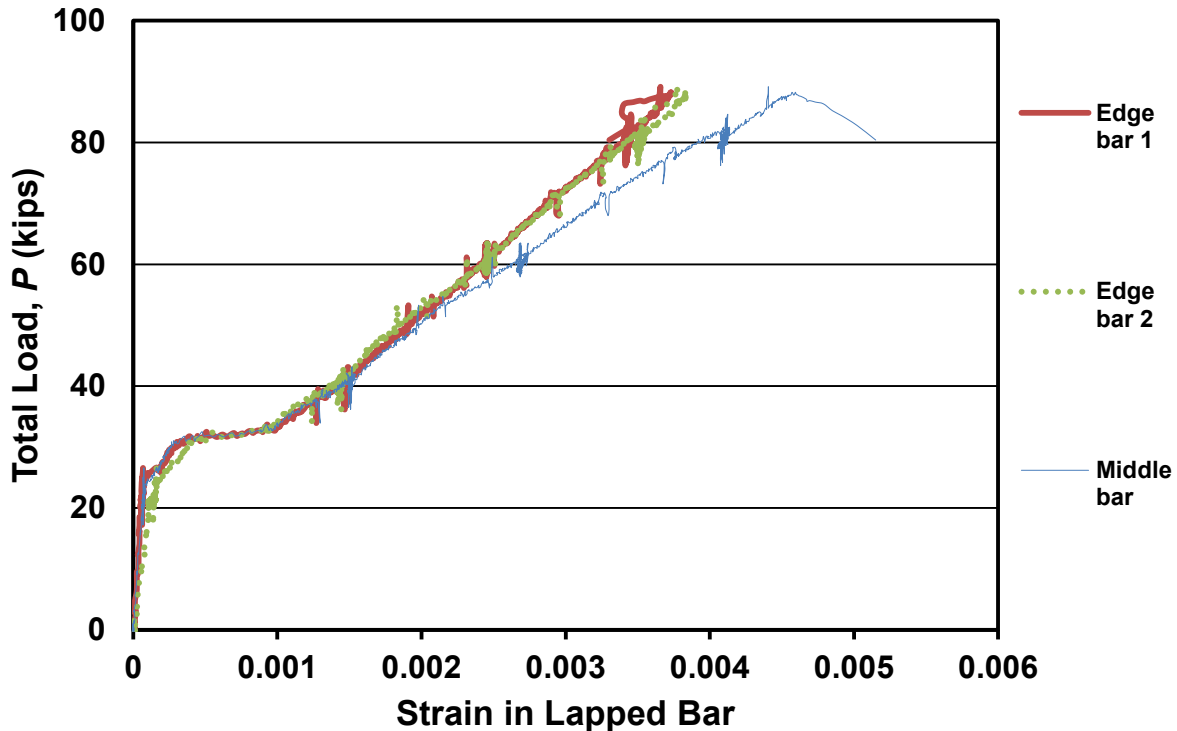


Figure 3.16 Strain in lapped bars in specimen (3) 6-12-S4.0-12-0.5 as a function of total applied load P

3.3 ANALYSIS OF TEST RESULTS FROM OTHER STUDIES AND COMPARISONS WITH THE CURRENT STUDY

Descriptive equations for the anchorage strength of headed bars developed by Shao et al. (2016) and the anchorage provisions in Chapter 17 of ACI 318-14 are used to analyze test results for headed bars anchored in the slab specimens tested by DeVries et al. (1999) and Choi et al. (2002), column-like specimens tested by Choi et al. (2002) and Choi (2006), and headed splice specimens tested by Thompson et al. (2002) and Chun (2015). Results from the current study are also included for comparison.

Descriptive Equations:

Shao et al. (2016) developed descriptive equations and design provisions for the anchorage of headed bars, described in detail in Section 1.4, based on test results of 202 exterior beam-column joint specimens subjected to monotonic loading. Equations (3.4) and (3.5) are the descriptive equations for the anchorage of headed bars without and with confining reinforcement, respectively.

$$T_h = \left(781 f_{cm}^{0.24} \ell_{eh}^{1.03} d_b^{0.35} \right) \left(0.0836 \frac{c_{ch}}{d_b} + 0.3444 \right) \quad (3.4)$$

with $0.0836 \frac{c_{ch}}{d_b} + 0.3444 \leq 1.0$

$$T_h = \left(781 f_{cm}^{0.24} \ell_{eh}^{1.03} d_b^{0.35} + 48,800 \frac{A_{tr}}{n} d_b^{0.88} \right) \left(0.0622 \frac{c_{ch}}{d_b} + 0.5428 \right) \quad (3.5)$$

with $0.0622 \frac{c_{ch}}{d_b} + 0.5428 \leq 1.0$ and $\frac{A_{tr}}{n} \leq 0.3 A_b$

where T_h = anchorage strength of headed bar (lb); f_{cm} = measured concrete compressive strength (psi); ℓ_{eh} = embedment length (in.); and d_b = diameter of headed bar (in.); c_{ch} = center-to-center spacing between the bars (in.); A_{tr} = total cross-sectional area of effective confining reinforcement ($NA_{tr,l}$) parallel to the headed bars being developed (in.²); N = total number of legs of effective confining reinforcement parallel to the headed bars being developed; $A_{tr,l}$ = area of a single leg of confining reinforcement; and n = number of headed bars in tension, with an upper limit on A_{tr}/n of $0.3A_b$.

A modification factor of 0.8 is applied to T_h for headed bars terminating outside a column core (a region of the column cross-section located inside the column longitudinal reinforcement) with clear cover c_{so} to the bar < 2.5 in., or terminating in a member other than beam-column joints with $c_{so} < 8d_b$.

Anchorage Provisions of ACI 318-14 for different failure modes:

The test results are also analyzed using the anchorage provisions in Chapter 17 of ACI 318-14. Concrete breakout strength (Section 17.4.2 of ACI 318-14), concrete side-face blowout strength (Section 17.4.4 of ACI 318-14), and the anchorage strength provided by anchor reinforcement (Section 17.4.2.9 of ACI 318-14) are investigated. The anchorage strength of the headed bars is then determined based on the controlling failure mode, concrete breakout, side-face blowout, or yielding of anchor reinforcement, as explained below. Other failure modes, such as bar pullout, concrete splitting, and bar fracture, are not included in this analysis because none of these failure modes controlled the anchorage strength.

The nominal concrete breakout strength of group of headed bars in tension N_{cbg} (Section 17.4.2 of ACI 318-14) is given by

$$N_{cbg} = \frac{A_{Nc}}{A_{Nco}} \Psi_{ec,N} \Psi_{ed,N} \Psi_{c,N} \Psi_{cp,N} N_b \quad (3.6)$$

where A_{Nc} = projected concrete failure area of group of headed bars (in.²); A_{nco} = projected concrete failure area of a single headed bar equal to $9\ell_{eh}^2$ (in.²); ℓ_{eh} = embedment length of headed bars (in.); $\Psi_{ec,N}$, $\Psi_{ed,N}$, $\Psi_{c,N}$, and $\Psi_{cp,N}$ are modification factors for anchor groups loaded eccentrically in tension, edge effects, cracking of concrete at service load, and post-installed anchors, respectively; N_b is the basic concrete breakout strength of a single headed bar in cracked concrete (equal to $16\lambda_a \sqrt{f'_c} \ell_{eh}^{1.5}$); λ_a is a modification factor for lightweight concrete and is equal to 1.0 because all specimens were cast in normalweight concrete; f'_c is the concrete compressive strength (limited to 10,000 psi). Values of $\Psi_{ec,N}$, $\Psi_{c,N}$, and $\Psi_{cp,N}$ are equal to 1.0 (headed bars loaded simultaneously with no eccentricity), 1.25 (cast-in headed bars with no cracking of concrete before testing), and 1.0 (cast-in headed bars), respectively, and the value of $\Psi_{ed,N}$ is calculated based on minimum concrete cover to the headed bar in accordance with Section 17.4.2.5 of ACI 318-14.

The nominal side-face blowout strength of a single headed bar in tension N_{sb} with embedment length greater than 2.5 times the cover to the center of the bar (Section 17.4.4.1 of ACI 318-14) is given by Eq. (3.7). Concrete breakout failure governs for headed bars with an embedment length less than or equal to 2.5.

$$N_{sb} = 160c_{a1} \sqrt{A_{brg}} \lambda_a \sqrt{f'_c} \quad (3.7)$$

where c_{a1} = cover to the center of the headed bar (in.); A_{brg} = net bearing area of the head (in.²); λ_a is modification factor for lightweight concrete which is equal to 1.0 because all specimens were cast in normalweight concrete; and f'_c is concrete compressive strength (limited to 10,000 psi). A modification factor [equal to $(1+c_{a2}/c_{a1})/4$] for the corner effect in accordance with Section 17.4.4.1 of ACI 318-14 was applied to N_{sb} when the cover to the headed bar c_{a2} in a direction perpendicular to c_{a1} was $\leq 3c_{a1}$.

The nominal anchorage strength of a group of headed bars based on anchor reinforcement N_{arg} is given by Eq. (3.8). Anchor reinforcement is defined in Section 17.4.2.9 of ACI 318-14 as reinforcement parallel to the headed bars within a $0.5\ell_{eh}$ radial distance from the center of the headed bar.

$$N_{arg} = N_{tr} A_{tr,l} f_{yt} \quad (3.8)$$

where N_{tr} is the total number of legs of anchor reinforcement parallel to the headed bars within the $0.5\ell_{eh}$ radial distance from the center of the bar; $A_{tr,l}$ and f_{yt} are the area of a single leg (in.²) and yield strength (psi) of the anchor reinforcement.

The nominal anchorage strength of each headed bar in tension T_{anc} governed by concrete breakout, side-face blowout, or anchor reinforcement is calculated using Eq. (3.9), where n is the number of headed bars loaded simultaneously in tension; N_{cbg} , N_{sb} , and N_{arg} are anchorage strengths calculated using Eq. (3.6), (3.7), and (3.8), respectively.

$$T_{anc} = \min \left\{ \max \left(\frac{N_{cbg}}{n}, \frac{N_{arg}}{n} \right), N_{sb} \right\} \quad (3.9)$$

3.3.1 Headed Bars Tested in Slab and Column-like Specimens

DeVries et al. (1999) tested 18 headed bars in three slab specimens with embedment lengths ranging from 1.4 to 9 in. Tests included eight bars anchored at the center of the slab (center bars), five bars anchored at the edge of the slab (edge bars) with a clear cover c_{so} of 1.6 in. on one side face and 17.6 in. on the adjacent orthogonal side face, and five bars anchored at the corner of the slab (corner bars) with clear cover of 1.6 in. on both adjacent orthogonal side faces. These bars were tested one at a time. During the tests, supports were placed at least $2\ell_{eh}$ from the headed bar to prevent confinement provided by the supports from affecting anchorage strength. Headed bars with side cover of 1.6 in. had 1 in. clear cover to the head. D20 and D35 (20 and 35 mm) headed bars with net bearing areas A_{brg} ranging from 4.7 to $7.4A_b$ (heads had no obstructions) were tested. With the exception of two edge bars (T2B2 and T2B4) and two corner bars (T2B6 and T2B8) with A_{brg} equal to $6.9A_b$, the bars were enclosed by PVC sheathing along the total embedment length ℓ_{eh} , as shown in Figure 3.17, to prevent bond between the embedded portion of the deformed bar and the surrounding concrete. Results from the tests of the 14 headed bars with PVC sheathing are not included in the analysis because the behavior of such unbonded bars is expected to differ from that of fully bonded bars. The center-to-center spacing between the headed bars c_{ch} required to calculate anchorage strength from descriptive equations [Eq. (3.4) and (3.5)] is taken as twice of the minimum concrete cover to the center of the bar. Two specimens (T2B4 and T2B8) contained reinforcement perpendicular to the headed bars, but are considered as having no confining

reinforcement for this analysis. This is consistent with the anchorage design provisions in Section 17.4 in ACI 318-14, which do not consider reinforcement perpendicular to the headed bar as contributing to the anchorage strength.

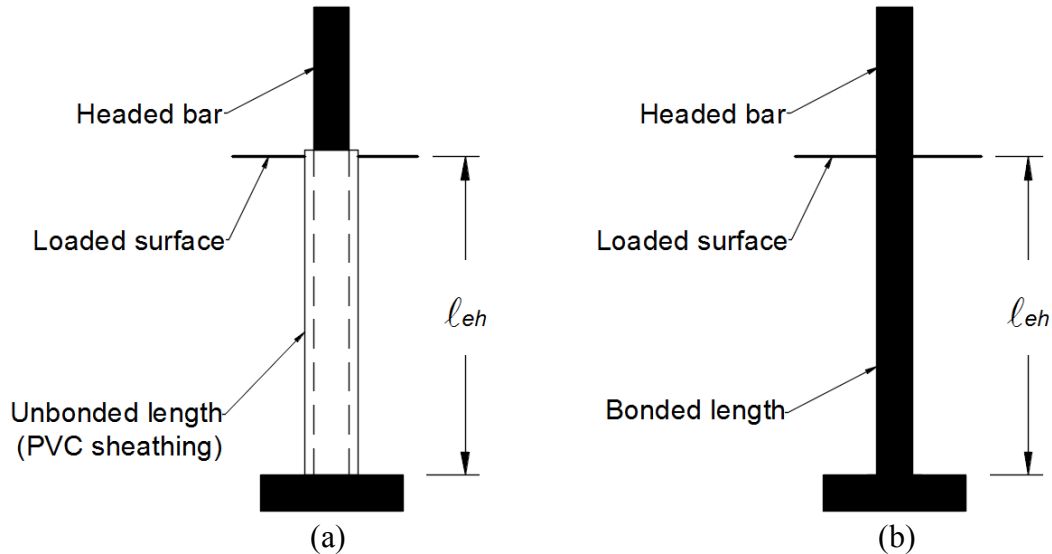


Figure 3.17 (a) Unbonded and (b) bonded lengths of the headed bar tested by DeVries et al. (1999)

Choi et al. (2002) and Choi (2006) conducted 76 tests on No. 5 (D16) through No. 9 (D29) headed bars anchored in slab and column-like specimens, with embedment lengths ℓ_{eh} ranging from 6 to $15d_b$. Sixteen slab specimens (Figure 3.18) contained headed bars anchored at the middle of a concrete slab with a clear cover c_{so} of 35 in. or anchored close to the edge of the slab with a clear cover ranging from 2.5 to 5 in. The remaining 60 specimens contained 2 to 4 headed bars in a layer anchored in column-like members (Figure 3.19), with No. 5 (D16) through No. 8 (D25) bars used as column longitudinal reinforcement. The net bearing area of the headed bars A_{brg} ranged from 2.6 to $3.2A_b$. None of the heads contained obstructions. Most column-like specimens also contained No. 3 (D10) or No. 4 (D13) column ties spaced at 3 to $9.1d_b$ (1.9 to 10.2 in.) as confining reinforcement parallel to the headed bars on both sides. Center-to-center spacing c_{ch} between the headed bars in column-like specimens ranged from 3 to $15d_b$, while the spacing between the bars in slab specimens required to calculate anchorage strength from descriptive equations [Eq. (3.4) and (3.5)] is taken as twice the minimum concrete cover to the center of the bar. During the tests, supports were placed at least $1.5\ell_{eh}$ from the headed bars to prevent the support confinement from affecting anchorage strength.

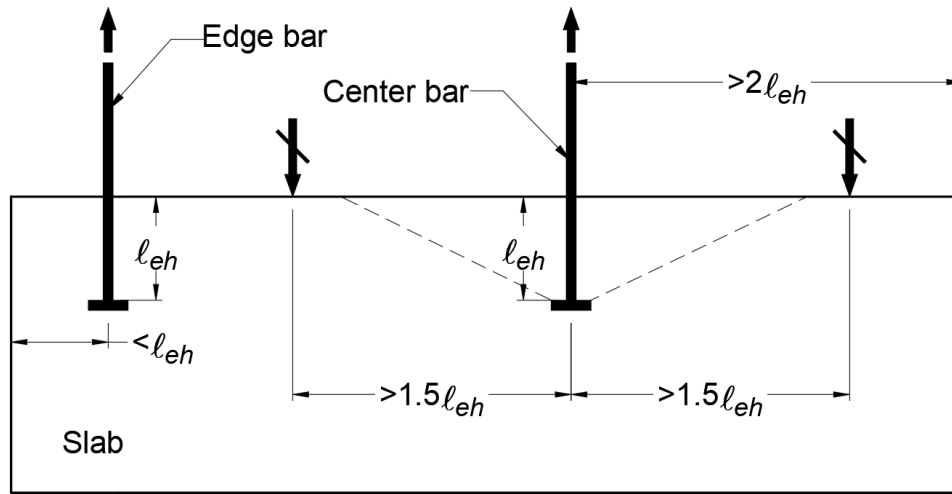


Figure 3.18 Slab specimens tested by Choi et al. (2002)

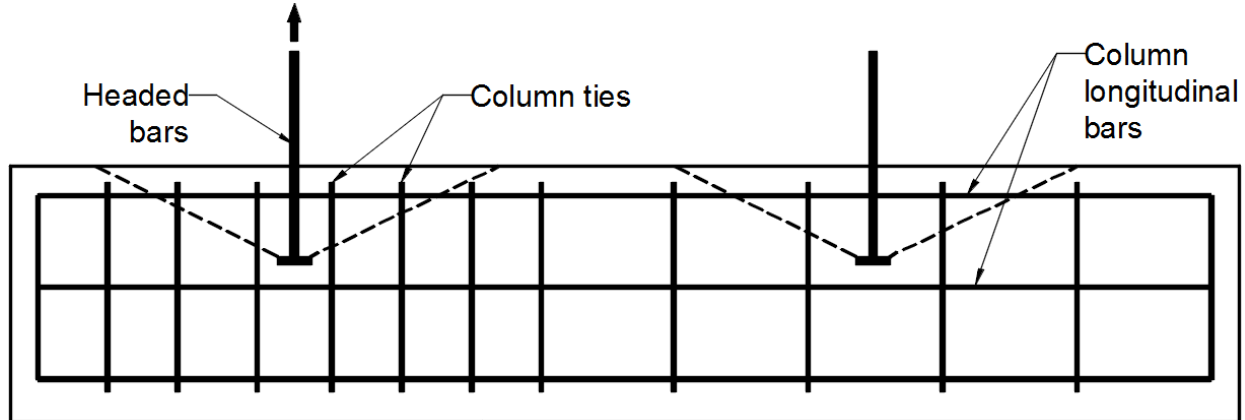


Figure 3.19 Column-like specimens tested by Choi et al. (2002) and Choi (2006)

The anchorage strengths of the headed bars tested by DeVries et al. (1999), Choi et al. (2002), and Choi (2006) are compared with the descriptive equations, Eq. (3.4) and (3.5), and anchorage provisions of Chapter 17 of ACI 318-14.

3.3.1.1 Analysis Based on Descriptive Equations and Anchorage Provisions of ACI 318-14

The net bearing area A_{brg} of the headed bars tested by Choi et al. (2002) and Choi (2006), 2.6 to $3.2A_b$, is less than the minimum net bearing area of $4A_b$ required in ACI 318. The anchorage strengths of these bars are compared with the anchorage strengths T_h calculated using description equations Eq. (3.4) and (3.5) and T_{anc} calculated using anchorage provisions of Chapter 17 of ACI 318-14. The anchorage strengths of headed bars with net bearing areas ranging from 4 to $15A_b$ in the current study and by DeVries et al. (1999) are also compared with T_h calculated using description equation Eq. (3.4) and T_{anc} based on Chapter 17 of ACI 318-14. A 0.8 modification

factor for headed bars with side cover c_{so} less than the required 2.5 in. in column-like specimens and $8d_b$ in slab specimens is applied to T_h from Eq. (3.4) and (3.5). The anchorage strengths T_{anc} were calculated using Eq. (3.9). Only headed bars that did not reach the yield strength (ratio of bars stress at failure to the yield strength $f_{su}/f_y < 1.0$) are included in the analysis. Details of the specimens tested by DeVries et al. (1999), Choi et al. (2002), and Choi (2006) including bar diameter (d_b), embedment length (ℓ_{eh}), cover to the bar (c_{so}), amount of reinforcement perpendicular the headed bar within the failure region (A_{st}), and bar force at failure (T) are provided in Table 3.3 with complete details provided in Table C.1 of Appendix C. Details of the slab specimens and comparison of anchorage strengths of headed bars tested in the current study are provided in Table 3.1 and Table B.1 of Appendix B.

Table 3.3 Test results for headed bars in slab and column-like specimens tested by DeVries et al. (1999), Choi et al. (2002), and Choi (2006) and comparisons with descriptive equations [Eq. (3.4) and (3.5)] and anchorage provisions of ACI 318-14 ^[1] (a modification factor of 0.8 is applied to T_h as appropriate ^[2])

Study	Specimen	d_b ^[3]	$\frac{A_{brg}}{A_b}$	ℓ_{eh} ^[3]	$\frac{c_{so}}{d_b}$	$\frac{A_{st}}{nA_b}$ ^[4]	T ^[3]	T_h ^[5]	T_{anc} ^[5]	$\frac{T}{T_h}$	$\frac{T}{T_{anc}}$	Remarks
		(in.)		(in.)			(kips)	(kips)	(kips)			
Choi et al. (2002)	S16-7db.1	0.625	3.2	4.4	56.7	0.0	16.4	23.9	20.2	0.69	0.81	Center bars in slab specimens
	S16-7db.2	0.625	3.2	4.4	56.2	0.0	18.0	23.9	20.2	0.75	0.89	
	S25-7db.1	1	3.0	6.9	35.1	0.0	36.0	44.6	39.4	0.81	0.91	
	S25-7db.2	1	3.0	6.9	34.9	0.0	33.9	44.6	39.4	0.76	0.86	
	E16-7db.1 ^[2]	0.625	3.2	4.4	2.5	0.0	10.6	16.2	10.2	0.65	1.04	Edge bars in slab specimens
	E16-7db.2 ^[2]	0.625	3.2	4.4	2.5	0.0	10.6	16.2	10.2	0.65	1.04	
	E19-7db.1 ^[2]	0.75	2.6	5.2	3.0	0.0	11.7	21.1	12.1	0.55	0.97	
	E19-7db.2 ^[2]	0.75	2.6	5.2	3.0	0.0	10.8	21.1	12.1	0.51	0.90	
	E19-7db.3 ^[2]	0.75	2.6	5.2	6.5	0.0	17.5	22.7	16.9	0.77	1.04	
	E19-7db.4 ^[2]	0.75	2.6	5.2	6.5	0.0	16.9	22.7	16.9	0.74	1.00	
	E25-7db.1 ^[2]	1	3.0	6.9	2.5	0.0	19.6	29.9	19.9	0.65	0.98	
	E25-7db.2 ^[2]	1	3.0	6.9	2.5	0.0	20.7	29.9	19.9	0.69	1.04	
	C16-6db-1C ^[6]	0.625	3.2	3.8	4.1	2.0	18.0	23.7	26.8	0.76	0.67	Column-like specimens
	C16-6db-1D ^[6]	0.625	3.2	3.8	4.1	2.0	17.5	23.7	26.8	0.74	0.65	
	C16-6db-2A ^[6]	0.625	3.2	3.8	2.5	1.0	18.4	17.5	26.8	1.06	0.69	
	C16-6db-2B ^{[2][6]}	0.625	3.2	3.8	2.5	1.0	16.6	17.5	26.8	0.95	0.62	
	C16-6db-2C ^{[2][6]}	0.625	3.2	3.8	2.5	1.0	14.2	17.5	13.4	0.81	1.06	
	C16-6db-2D ^{[2][6]}	0.625	3.2	3.8	2.5	1.0	9.4	17.5	13.4	0.54	0.70	
	C16-6db-3A ^{[2][6]}	0.625	3.2	3.8	2.5	0.7	12.3	13.9	17.9	0.89	0.69	
	C16-6db-3B ^{[2][6]}	0.625	3.2	3.8	2.5	0.7	13.8	13.9	17.9	0.99	0.77	
C16-6db-3C ^{[2][6]}	0.625	3.2	3.8	2.5	0.7	10.2	13.5	8.9	0.75	1.14		
C16-6db-3D ^{[2][6]}	0.625	3.2	3.8	2.5	0.7	6.6	13.5	8.9	0.49	0.74		
C22-6db-1A ^[6]	0.875	2.7	5.2	3.4	1.5	36.0	40.2	97.4	0.89	0.37		
C22-6db-1B ^[6]	0.875	2.7	5.2	3.4	1.5	34.8	40.2	97.4	0.87	0.36		
C22-6db-1C ^[6]	0.875	2.7	5.2	3.4	1.5	32.4	40.2	48.7	0.81	0.66		
C22-6db-3A ^{[2][6]}	0.875	2.7	5.2	1.9	0.5	24.7	23.4	32.5	1.06	0.76		
C22-6db-3B ^{[2][6]}	0.875	2.7	5.2	1.9	0.5	17.2	23.4	32.5	0.74	0.53		
C22-6db-4A ^{[2][6]}	0.875	2.7	5.2	1.8	0.6	22.2	29.3	24.4	0.76	0.91		
C22-6db-4B ^{[2][6]}	0.875	2.7	5.2	1.8	0.6	24.2	29.3	24.4	0.82	0.99		

^[1] Notation described in Section 3.3.1.1 and Appendix A

^[2] A 0.8 modification factor for clear cover c_{so} less than $8d_b$ in slab specimens and 2.5 in. in column-like specimens is applied when calculating T_h

^[3] Values are converted from the SI unit (1 in. = 25.4 mm; 1 psi = 1/145 MPa; and 1 kip = 4.4484 kN)

^[4] nA_b = total area of headed bars sharing A_{st} (n = number of headed bars loaded simultaneously in tension, A_b = bar area)

^[5] T_h is based on Eq. (3.4) and (3.5) for specimens without and with confining reinforcement parallel to the headed bar, respectively; T_{anc} is based on Eq. (3.9)

^[6] Specimen contained confining reinforcement parallel to the headed bar

Table 3.3 Cont. Test results for headed bars in slab and column-like specimens tested by DeVries et al. (1999), Choi et al. (2002), and Choi (2006) and comparisons with descriptive equations [Eq. (3.4) and (3.5)] and anchorage provisions of ACI 318-14 ^[1] (a modification factor of 0.8 is applied to T_h as appropriate ^[2])

Study	Specimen	d_b ^[3] (in.)	$\frac{A_{brg}}{A_b}$	ℓ_{eh} ^[3] (in.)	$\frac{c_{so}}{d_b}$	$\frac{A_{st}}{nA_b}$ ^[4]	T ^[3] (kips)	T_h ^[5] (kips)	T_{anc} ^[5] (kips)	$\frac{T}{T_h}$	$\frac{T}{T_{anc}}$	Remarks
Choi (2006)	C29-10db-2A-L ^[6]	1.128	3.0	11.4	4.3	0.8	51.4	83.7	48.7	0.61	1.05	Column- like specimens
	C29-10db-2C-L ^[6]	1.128	3.0	11.4	4.3	0.8	49.6	83.7	48.7	0.59	1.02	
	C29-10db-2D-L ^[6]	1.128	3.0	11.4	4.3	0.8	40.8	78.8	24.4	0.52	1.67	
	C29-10db-2E-L	1.128	3.0	11.4	4.3	0.8	39.1	63.5	15.9	0.62	2.47	
	C29-10db-2A-M ^[6]	1.128	3.0	11.4	4.3	1.6	53.2	83.7	48.7	0.63	1.09	
	C29-10db-2C-M ^[6]	1.128	3.0	11.4	4.3	1.6	53.7	83.7	48.7	0.64	1.10	
	C29-10db-2D-M ^[6]	1.128	3.0	11.4	4.3	1.6	53.4	78.8	24.4	0.68	2.19	
	C29-10db-2E-M	1.128	3.0	11.4	4.3	1.6	49.7	63.5	15.9	0.78	3.13	
	C22-15db-3E-L	0.875	3.0	13.0	4.0	0.7	34.6	57.3	9.9	0.60	3.51	
	C25-13db-2E-L	1	3.0	13.0	3.5	0.8	45.9	83.4	14.8	0.55	3.09	
DeVries et al. (1999)	T2B2 ^[2]	0.79	6.9	9.0	2.0	0.0	33.3	32.6	24.0	1.02	1.38	Edge bars in slab specimens
	T2B4 ^[2]	0.79	6.9	9.0	2.0	0.4	38.7	32.6	24.0	1.19	1.61	
	T2B6 ^[2]	0.79	6.9	9.0	2.0	0.0	27.4	32.6	13.8	0.84	1.99	Corner bars in slab specimens
	T2B8 ^[2]	0.79	6.9	9.0	2.0	0.4	28.1	32.6	13.8	0.86	2.04	

^[1] Notation described in Section 3.3.1.1 and Appendix A

^[2] A 0.8 modification factor for clear cover c_{so} less than $8d_b$ in slab specimens and 2.5 in. in column-like specimens is applied when calculating T_h

^[3] Values are converted from the SI unit (1 in. = 25.4 mm; 1 psi = 1/145 MPa; and 1 kip = 4.4484 kN)

^[4] nA_b = total area of headed bars sharing A_{st} (n = number of headed bars loaded simultaneously in tension, A_b = bar area)

^[5] T_h is based on Eq. (3.4) and (3.5) for specimens without and with confining reinforcement parallel to the headed bar, respectively; T_{anc} is based on Eq. (3.9)

^[6] Specimen contained confining reinforcement parallel to the headed bar

In Figure 3.20, measured bar forces at failure T in slab specimens tested by DeVries et al. (1999), Choi et al. (2002), and in the current study are plotted versus the bar forces T_h calculated using Eq. (3.4). The specimens tested by DeVries et al. (1999) and Choi et al. (2002) had h_{cl}/ℓ_{eh} greater than 2 and 1.5, respectively (exact values were not reported). The values of h_{cl}/ℓ_{eh} in slab specimens tested in the current study ranged from 1.24 to 5.60. As discussed in Section 3.1.4, for the slab specimens, the net bearing area A_{brg} between 4 and $9.5A_b$ did not affect the anchorage strength of the headed bars, while larger heads with A_{brg} of 13 and $15A_b$ tended to increase the anchorage strength by about 15%. For that reason, only specimens with $A_{brg} \leq 9.5A_b$ are included in Figure 3.20.

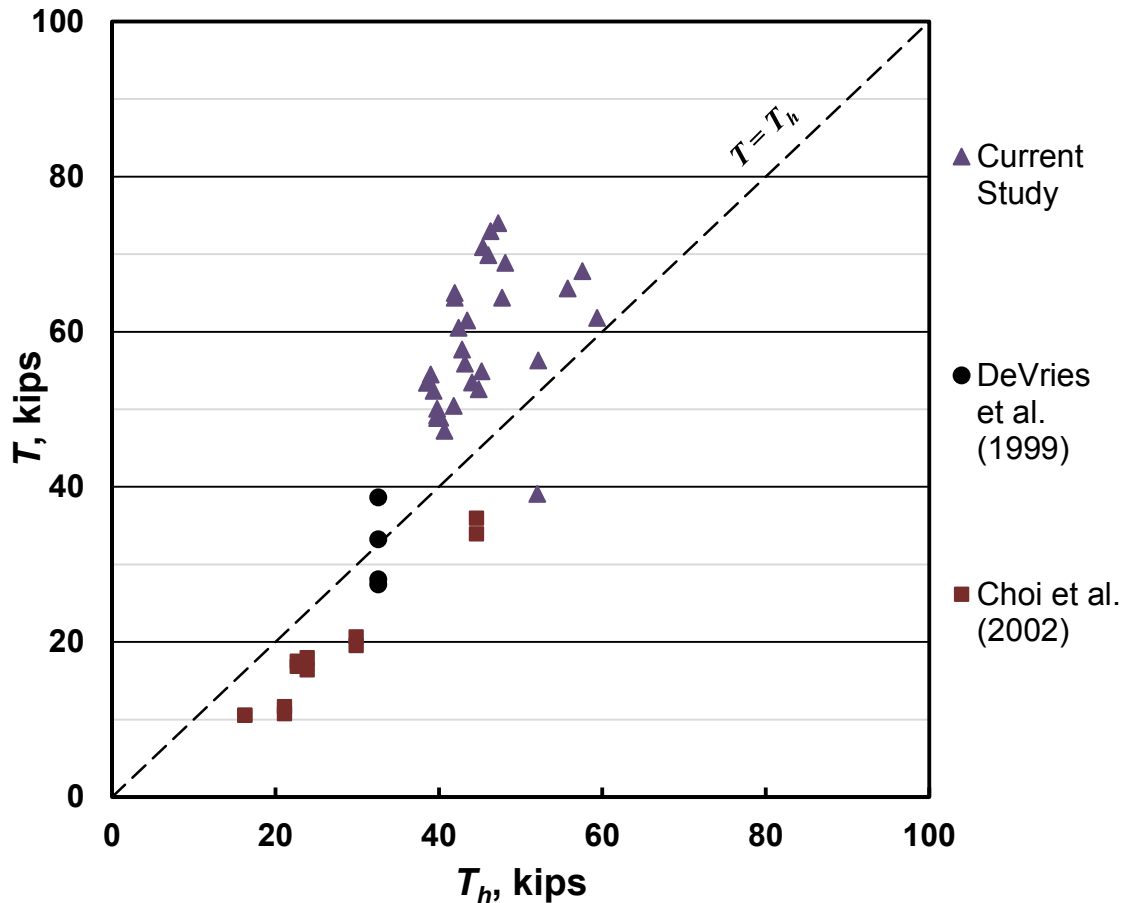


Figure 3.20 Bar force at failure T versus anchorage strength T_h calculated using Eq. (3.4) for slab specimens tested by DeVries et al. (1999) and Choi et al. (2002), and in the current study; a modification factor of 0.8 for headed bars with concrete cover less than $8d_b$ is applied to T_h as appropriate (for specimens tested in the current study, only those with A_{brg} ranging from 4 to $9.5A_b$ are included)

For the specimens shown in Figure 3.20, a 0.8 modification factor for clear cover c_{so} less than $8d_b$ is applied to the four specimens tested by DeVries et al. (1999) and eight out of the 12 specimens tested by Choi et al. (2002). All specimens tested in the current study had $c_{so} > 8d_b$; therefore, the modification factor of 0.8 is not applied in these specimens. The specimens tested by Choi et al. (2002) had a net bearing area A_{brg} ranging from 2.6 to $3.2A_b$, which is less than the minimum net bearing area of $4A_b$ required in ACI 318 and the net bearing areas of 4 to $9.5A_b$ for the headed bars tested in the current study and by DeVries et al. (1999). As shown in the figure, all specimens tested by Choi et al. (2002) exhibited lower anchorage strengths than that predicted by the descriptive equation ($T/T_h < 1.0$). The maximum, minimum, mean, standard deviation (STD), and coefficients of variation (COV) of T/T_h for the headed bars from each study are given

in Table 3.4. The values of T/T_h for the specimens tested by Choi et al. (2002) ranged from 0.51 to 0.81, with an average value of 0.69. The values of T/T_h for the four edge and corner bars tested by DeVries et al. (1999) ranged from 0.84 to 1.19 with an average value of 0.98. For specimens tested in the current study, the average value of T/T_h is equal to 1.33, with a minimum of 0.75 for the specimen containing a single centrally placed headed bar with $h_{cl}/\ell_{eh} = 5.6$, which is the only specimen in this group with a value of T/T_h less than 1.0. These observations suggest that the consistently lower anchorage strengths of the headed bars tested by Choi et al. (2002) are likely due to the small net bearing area of the heads used in those tests.

Table 3.4 Statistical parameters of T/T_h values for slab and column-like specimens tested by DeVries et al. (1999), Choi et al. (2002), Choi (2006), and in the current study

Test/Calculated	T/T_h ^[1] (a modification factor of 0.8 is applied to the calculated strength as appropriate ^[2])							
Specimen type	Slab					Column-like (without confining reinforcement)	Column-like (with confining reinforcement)	
	Current Study [shallow embedment]	Choi et al. (2002) [Center bars]	Choi et al. (2002) [Edge bars]	DeVries et al. (1999) [Edge bars]	DeVries et al. (1999) [Corner bars]	Choi (2006)	Choi et al. (2002)	Choi (2006)
Total number of specimens	32	4	8	2	2	4	17	6
Max	1.74	0.81	0.77	1.19	0.86	0.78	1.06	0.68
Min	0.75	0.69	0.51	1.02	0.84	0.55	0.49	0.52
Mean	1.33	0.75	0.65	1.10	0.85	0.64	0.82	0.61
STD	0.20	0.05	0.09	0.12	0.01	0.10	0.16	0.05
COV	0.15	0.07	0.13	0.11	0.02	0.16	0.19	0.09
Number of specimens with $T/T_h < 1.0$	1	4	8	0	2	4	15	6

^[1] Anchorage strength T_h is calculated using Eq. (3.4) and (3.5)

^[2] A modification factor of 0.8 is applied to T_h for headed bars in slab specimens with cover to the bar $< 8d_b$ and in column-like specimens with cover to the bar < 2.5 in.

The average values of T/T_h for center and edge bars with A_{brg} ranging from 2.6 to $3.2A_b$ tested by Choi et al. (2002) are 0.75 and 0.65, respectively (see Table 3.4); that is, the center bars exhibited 15% greater average anchorage strength than the edge bars with respect to the value T_h . In these tests, the small net bearing area (2.6 to $3.2A_b$) of the headed bars likely resulted in $T/T_h < 1.0$. The average values of T/T_h for edge and corner bars with A_{brg} equal to $6.9A_b$ tested by DeVries et al. (1999) are 1.11 and 0.85, respectively, which suggests that Eq. (3.4) may not properly capture

the lower strength exhibited by headed bars anchored near corners. The 0.8 factor was applied when calculating T_h for the edge bars tested by Choi et al. (2002) and edge and corner bars tested by DeVries et al. (1999), but not for the center bars tested by Choi et al. (2002). If the 0.8 factor had not been applied, the average values of T/T_h for the edge bars tested by Choi et al. (2002) would have been 0.52 and that for edge and corner bars tested by DeVries et al. (1999) would have been 0.89 and 0.68, respectively.

In Figure 3.21, the bar forces at failure T in 27 column-like specimens, 17 tested by Choi et al. (2002) and 10 tested by Choi (2006), are plotted versus the bar forces T_h calculated using Eq. (3.4) and (3.5). The net bearing area of the headed bars in all column-like specimens ranged from 2.7 to $3.2A_b$. The majority of these specimens performed poorly with respect to T_h . Fifteen out of the 17 specimens tested by Choi et al. (2002) and all 10 specimens tested by Choi (2006) had $T/T_h < 1.0$; the average value of T/T_h was 0.75, with a minimum of 0.49. The small net bearing area of 2.6 to $3.2A_b$ likely resulted in the poor performance of these headed bars.

Twenty-three column-like specimens (out of the 27 specimens presented in Table 3.3 and Figure 3.21), all 17 tested by Choi et al. (2002) and six out 10 tested by Choi (2006), with A_{brg} ranging from 2.7 to $3.2A_b$ contained column ties as confining reinforcement parallel to the headed bars. The remaining four (of the 10) column-like specimens tested by Choi (2006) with A_{brg} equal to $3.0A_b$ did not contain such confining reinforcement. The specimens with confining reinforcement parallel to the headed bars had about 20% higher anchorage strength on average with respect to T_h than the specimens without confining reinforcement. The values of T/T_h for specimens containing confining reinforcement ranged from 0.49 to 1.06 with an average of 0.77. The four column-like specimens without confining reinforcement had T/T_h ranging from 0.55 to 0.78 with an average of 0.64.

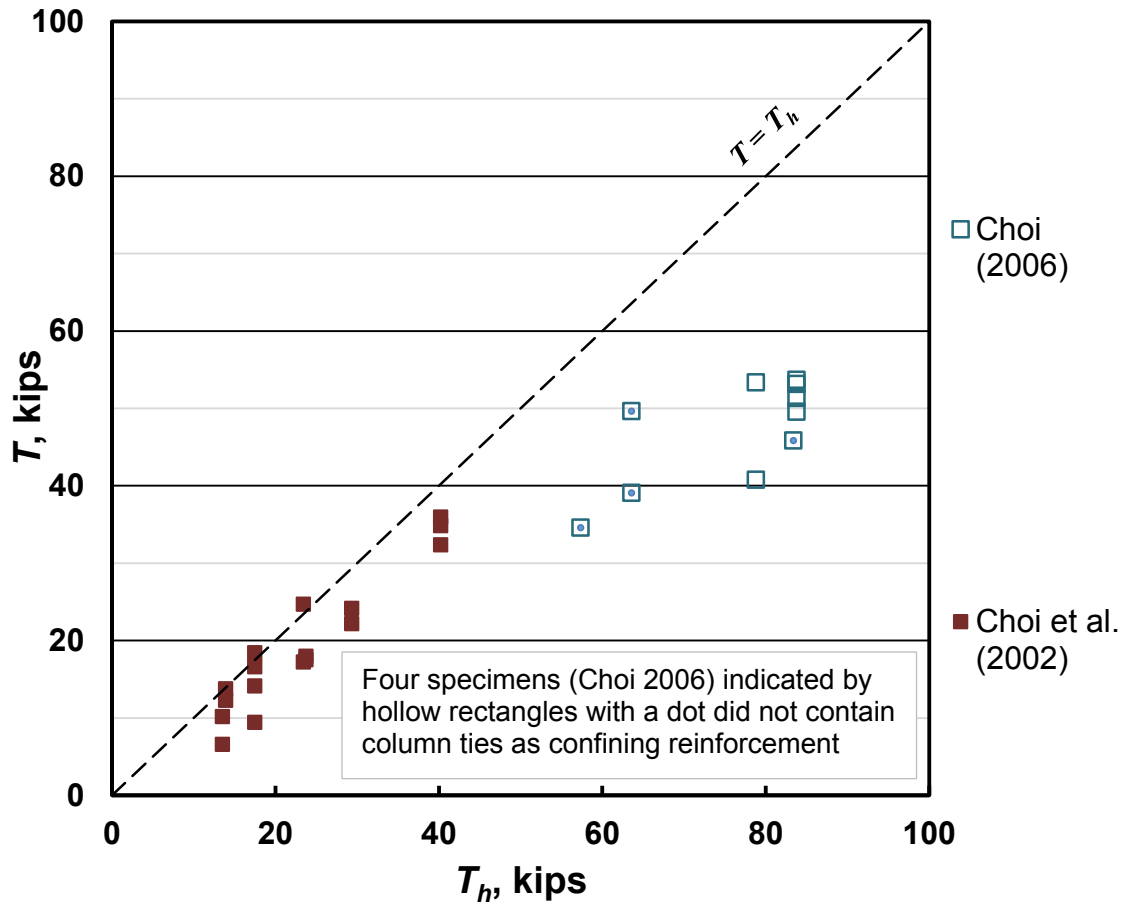


Figure 3.21 Bar force at failure T versus the anchorage strength T_h calculated using Eq. (3.4) and (3.5) for column-like specimens tested by Choi et al. (2002) and Choi (2006); a modification factor of 0.8 for headed bars with concrete cover less than 2.5 in. is applied to T_h

The bar force at failure T in both slab and column-like specimens tested by DeVries et al. (1999), Choi et al. (2002), and in the current study is compared with the anchorage strength T_{anc} . The anchorage strength T_{anc} , governed by concrete breakout strength (N_{cbg}), side-face blowout strength (N_{sb}), or anchorage strength from anchor reinforcement (N_{arg}), is calculated using Eq. (3.9). To calculate N_{arg} [Eq. (3.8)] in column-like specimens, column ties parallel to the headed bar within $0.5\ell_{eh}$ from the center of the bar, as shown in Figure 3.22, are considered as anchor reinforcement.

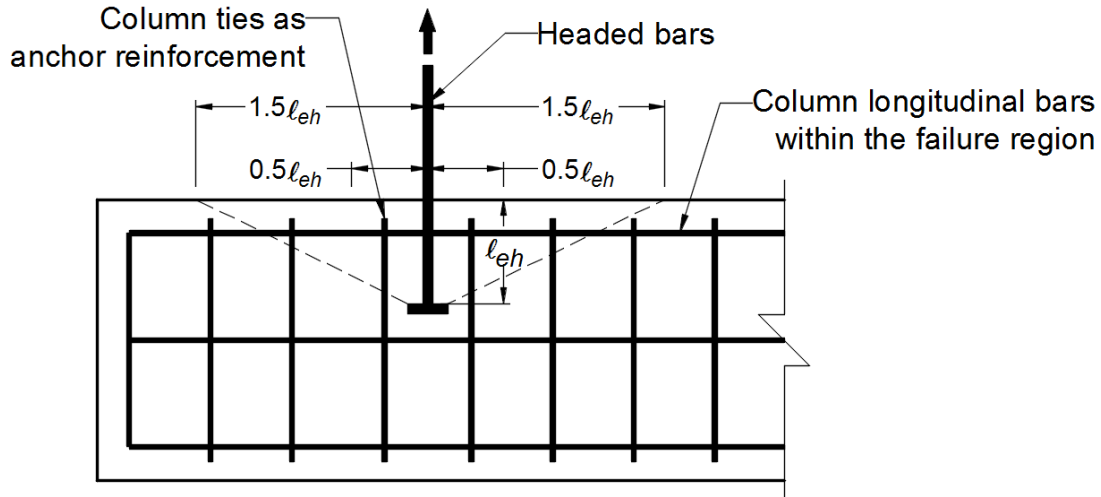


Figure 3.22 Column ties as anchor reinforcement and column longitudinal bars as reinforcement in a plane perpendicular to the headed bars in column-like specimens tested by Choi et al. (2002) and Choi (2006)

The comparison of the bar force at failure T with the anchorage strength T_{anc} is shown in Figure 3.23 for the slab specimens and Figure 3.24 for the column-like specimens tested by DeVries et al. (1999), Choi et al. (2002), Choi (2006), and in the current study. The individual values of T_{anc} are tabulated in Tables 3.1 for the specimens tested in the current study and Table 3.3 for the specimens tested in the other studies. The maximum, minimum, mean, standard deviation (STD), and coefficients of variation (COV) of T/T_{anc} for the headed bars from each study are given in Table 3.5. The comparisons in Figures 3.23 and 3.24 show that the majority of the specimens, including the specimens containing headed bars with net bearing area of 2.6 to $3.2A_b$ (Choi et al. 2002 and Choi 2006), had $T/T_{anc} \geq 1.0$. The average value of T/T_{anc} for headed bars anchored in slab specimens tested by Choi et al. (2002) was 0.96 ; seven out of the 12 bars had $T/T_{anc} < 1.0$ with a minimum of 0.81 . All four edge and corner bars tested by DeVries et al. (1999) had $T/T_{anc} \geq 1.0$ with an average of 1.75 . The headed bars tested in the current study had $T/T_{anc} \geq 1.0$ (average of 1.48), with the exception of two, which had T/T_{anc} equal to 0.83 and 0.99 .

The column-like specimens tested by Choi et al. (2002) and Choi (2006) had an average value of T/T_{anc} of 1.21 but with 15 out of the 27, as shown in Figure 3.24, below 1.0 . Twenty-three of the column-like specimens contained anchor reinforcement on both sides of headed bars (column ties parallel to the headed bars within $0.5\ell_{eh}$ radial distance from the center of the bar, Figure 3.22). In all 23 specimens, the anchorage strength provided by anchor reinforcement N_{arg}

[Eq. (3.8)] was greater than that provided by the concrete breakout strength N_{cbg} [Eq. (3.6)] and, thus, governed the value of T_{anc} .

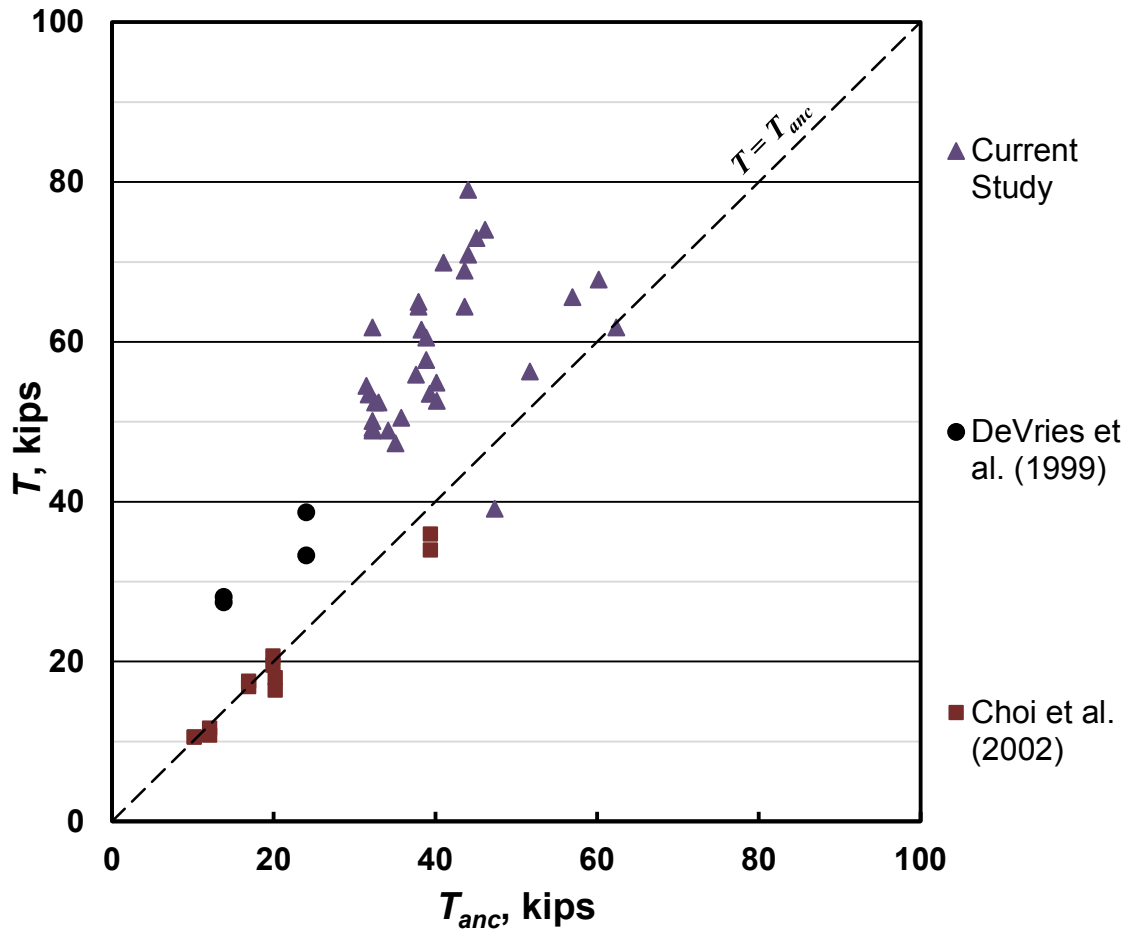


Figure 3.23 Bar force at failure T versus the anchorage strength T_{anc} calculated using Eq. (3.9) for slab specimens tested by DeVries et al. (1999), Choi et al. (2002), Choi (2006), and in the current study

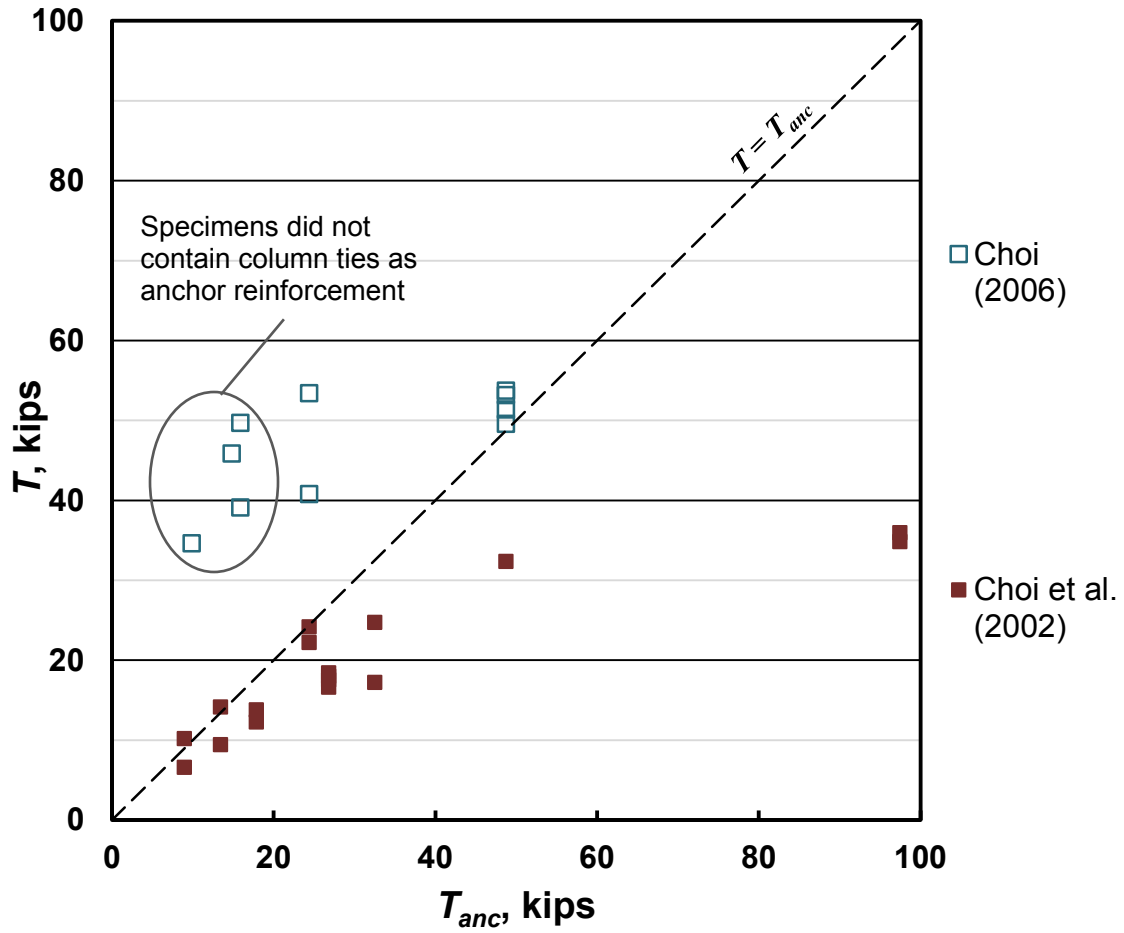


Figure 3.24 Bar force at failure T versus the anchorage strength T_{anc} calculated using Eq. (3.9) for column-like specimens tested by Choi et al. (2002) and Choi (2006)

Table 3.5 Statistical parameters of T/T_{anc} values for slab and column-like specimens tested by DeVries et al. (1999), Choi et al. (2002), Choi (2006), and in the current study

Test/Calculated	T/T_{anc} ^[1]							
Specimen type	Slab					Column-like (without confining reinforcement)	Column-like (with confining reinforcement)	
	Current Study [shallow embedment]	Choi et al. (2002) [Center bars]	Choi et al. (2002) [Edge bars]	DeVries et al. (1999) [Edge bars]	DeVries et al. (1999) [Corner bars]	Choi (2006)	Choi et al. (2002)	Choi (2006)
Total number of specimens	32	4	8	2	2	4	17	6
Max	1.92	0.91	1.04	1.61	2.04	3.51	1.14	2.19
Min	0.83	0.81	0.90	1.38	1.99	2.47	0.36	1.02
Mean	1.48	0.87	1.00	1.50	2.01	3.05	0.72	1.36
STD	0.24	0.04	0.05	0.16	0.03	0.43	0.21	0.48
COV	0.16	0.05	0.05	0.11	0.02	0.14	0.29	0.35
Number of specimens with $T/T_{anc} < 1.0$	2	4	3	0	0	0	15	0

^[1] Anchorage strength T_{anc} is calculated using Eq. (3.9)

Overall, the majority of the specimens had $T/T_h < 1.0$ and $T/T_{anc} \geq 1.0$. This is likely because the anchorage provisions of Chapter 17 of ACI 318-14 used to calculate T_{anc} are based on the 5% fractile of the test results used to develop the anchorage equations, while the descriptive equations for T_h were developed to ensure the *average* ratio of test-to-calculated failure load equal to 1.0. The difference in approach resulted in more conservative estimate of anchorage strength using anchorage provisions of Chapter 17 of ACI 318-14 than the descriptive equations, with $T/T_{anc} > T/T_h$.

Distributions of the ratios T/T_h and T/T_{anc} for specimens tested by DeVries et al. (1999), Choi et al. (2002), Choi (2006), and in the current study are shown in Figures 3.25 through 3.28. The figures show a greater variation in values of T/T_{anc} than those of T/T_h , particularly for the column-like specimens tested by Choi et al. (2002) and Choi (2006). This is likely because in majority of the column-like specimens, T_{anc} was governed by the strength of the anchor reinforcement (Figure 3.22) N_{arg} [Eq. (3.8)], which does not account for the contribution of concrete to anchorage strength. On the other hand, T_h accounts for the contribution of both confining reinforcement and concrete compressive strength on the anchorage strength.

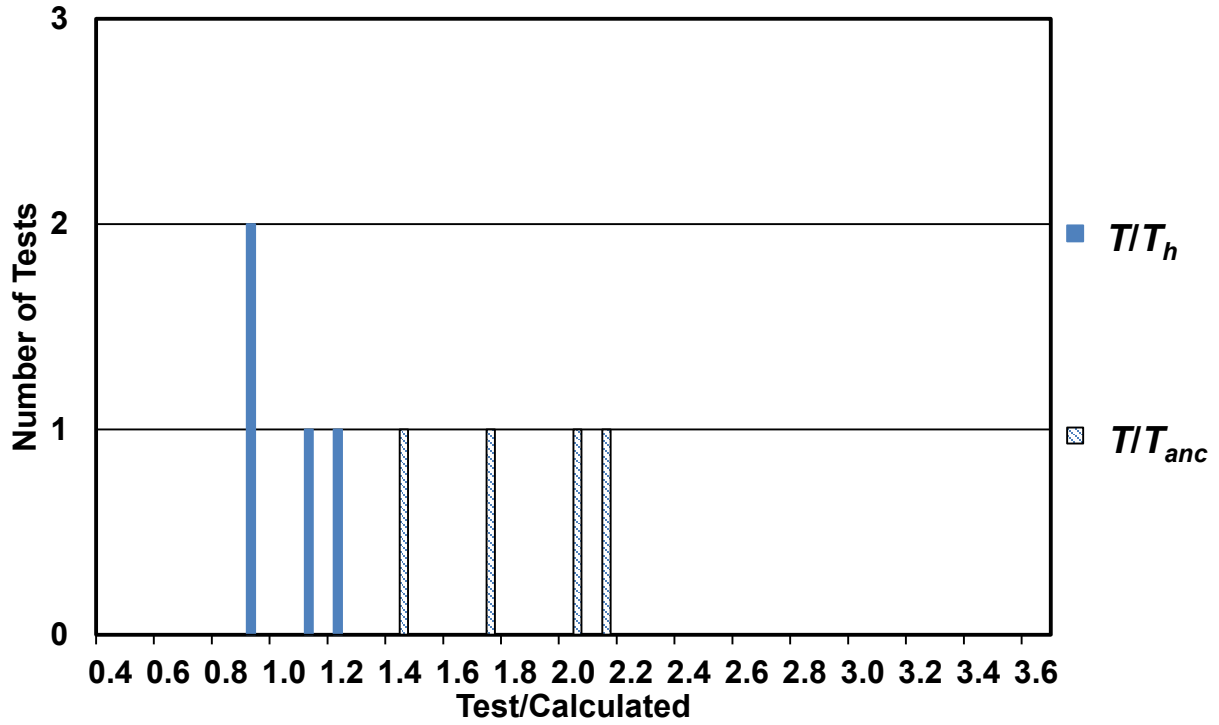


Figure 3.25 Distribution of ratios T/T_h and T/T_{anc} for headed bars in slab specimens tested by DeVries et al. (1999)

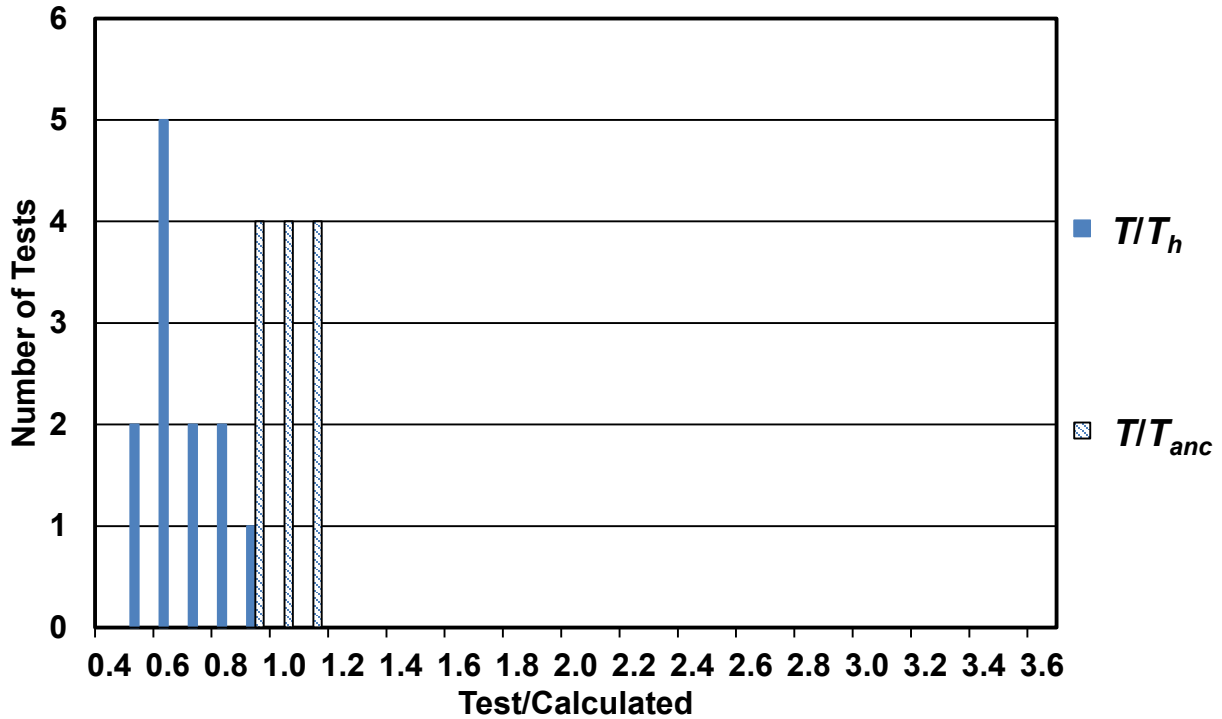


Figure 3.26 Distribution of ratios T/T_h and T/T_{anc} for headed bars in slab specimens tested by Choi et al. (2002)

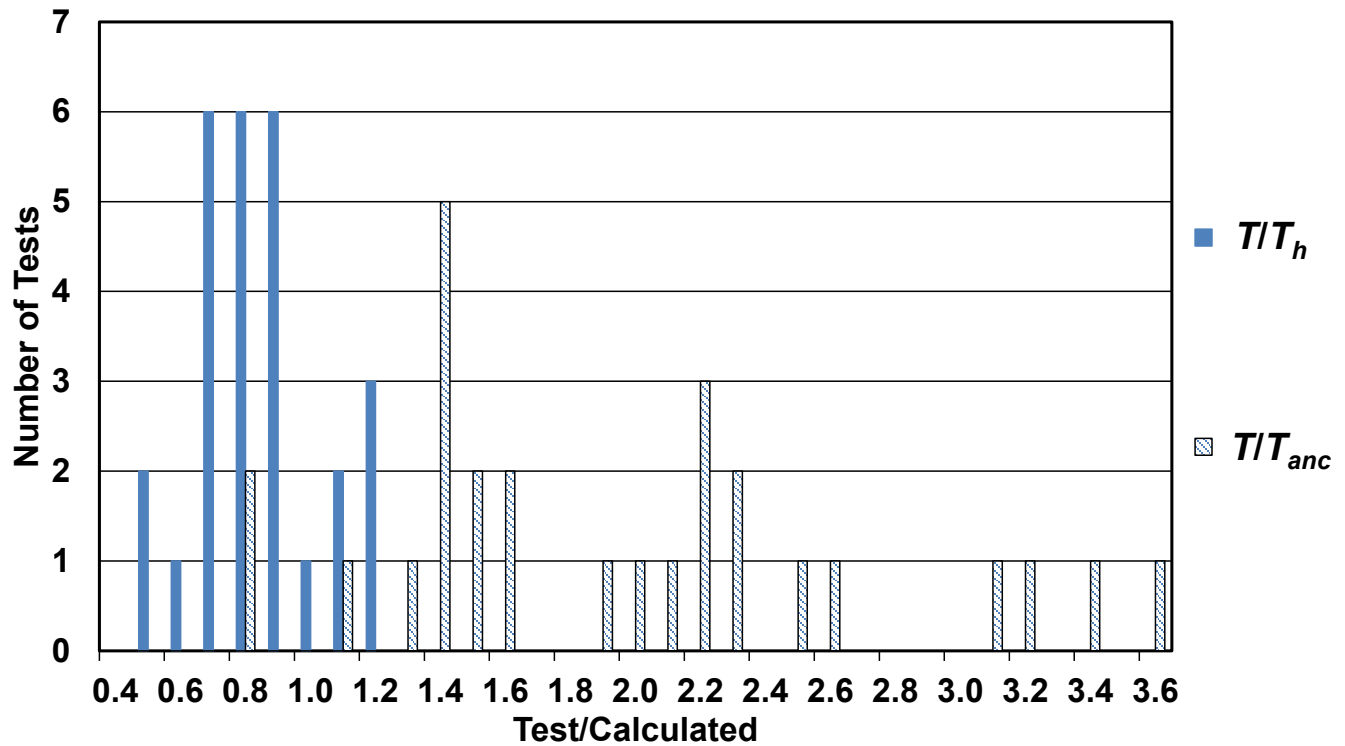


Figure 3.27 Distribution of ratios T/T_h and T/T_{anc} for headed bars in column-like specimens tested by Choi et al. (2002) and Choi (2006)

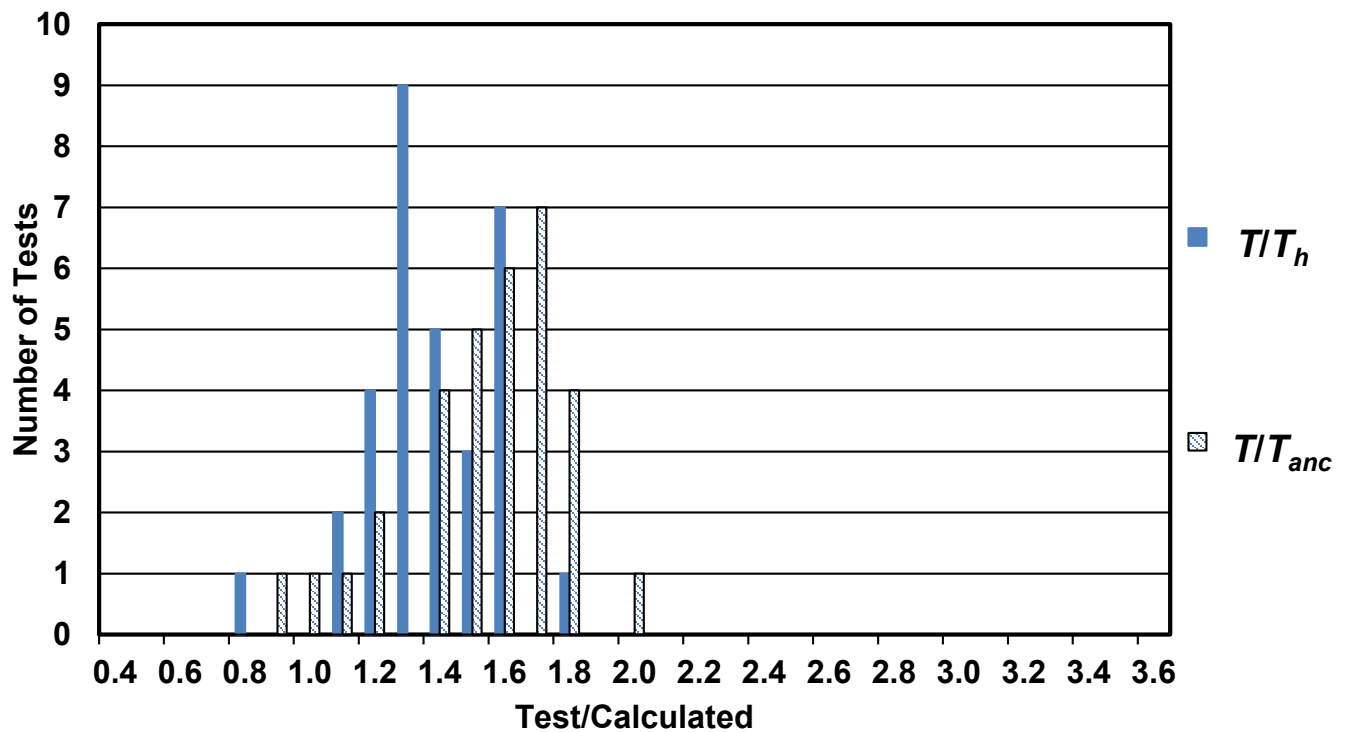


Figure 3.28 Distribution of ratios T/T_h and T/T_{anc} for headed bars in slab specimens tested in the current study

3.3.1.2 Effect of Reinforcement in a Plane Perpendicular to the Headed Bar

Slab specimens tested in the current study (Figure 3.5) and column-like specimens tested by Choi et al. (2002) and Choi (2006) (Figure 3.22) contained reinforcement in a plane perpendicular to the headed bar. These specimens are analyzed to investigate the contribution of such reinforcement to the anchorage strength. Results from the 27 out of the 60 column-like specimens tested by Choi et al. (2002) and Choi (2006) in which the stress in the headed bar did not reach the yield strength ($f_{su}/f_y < 1.0$) are included. The values of h_{cil}/ℓ_{eh} for these specimens was greater than 1.5 (exact values were not reported). The results from the current study for specimens with h_{cil}/ℓ_{eh} ranging from 1.24 to 2.79 and A_{brg} ranging from 4 to $9.5A_b$ are included. None of the headed bars in the current study yielded.

In Figure 3.29, the ratio of bar force at failure T to T_h calculated using Eq. (3.4) and (3.5) is plotted versus the area of reinforcement perpendicular to the headed bar A_{st} normalized to the total area of headed bars loaded simultaneously in tension sharing that reinforcement nA_b . Reinforcement perpendicular to the headed bar within a $1.5\ell_{eh}$ radial distance from the center of the bar (that is, within the failure region as shown in Figures 3.5 and 3.22) is included when calculating A_{st} . The effect of reinforcement perpendicular to the headed bar on anchorage strength is evaluated using dummy variable analysis, “a least-squares regression analysis method that allows differences in populations to be taken into account when formulating relationships between principal variables.”^[1] In the current analysis, changes in T/T_h are assumed to linearly related to changes in $A_{st}/(nA_b)$, independent of bars size, while the absolute value of T/T_h is assumed to be different for different bar sizes (represented by different vertical intercepts of the regression-lines).

^[1] Sperry et al. (2017a)

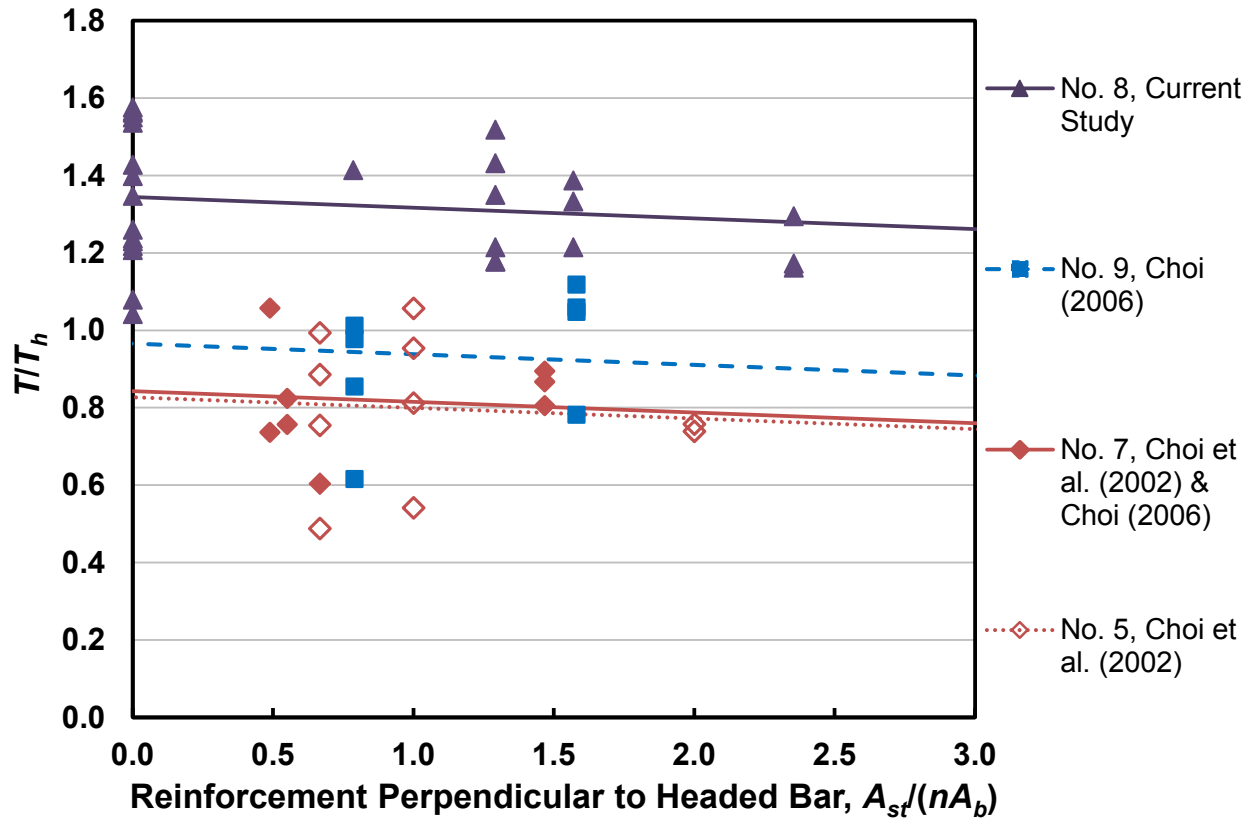


Figure 3.29 Ratio of bar force at failure T to the force calculated using Eq. (3.4) and (3.5) T_h versus reinforcement in a plane perpendicular to the headed bar A_{st} normalized to the total area of the headed bars sharing that reinforcement nA_b for column-like specimens tested by Choi et al. (2002) and Choi (2006) and slab specimens tested in the current study [for specimens tested in the current study, only those with h_{cl}/ℓ_{eh} ranging from 1.24 to 2.79 and A_{brg} ranging from 4 to $9.5A_b$ are included]

In Figure 3.29, the trendlines were obtained from the dummy variable analysis. The slope of these trendlines show a slight decrease in T/T_h with an increase in the reinforcement perpendicular to the headed bars. This is consistent with the observation made in Section 3.1.3 that the anchorage strength of headed bars tested in the current study was virtually unchanged (decreased slightly about 3%) with an increase in reinforcement perpendicular to the bar. On the other hand, Choi et al. (2002) showed that an increase in the amount of such reinforcement did not affect the anchorage strength, while Choi (2006) reported a 16% average increase in anchorage strength when doubling the amount of reinforcement perpendicular to the bar. The observations made by Choi et al. (2002) and Choi (2006) can also be seen in Figure 3.29. Considering the trend of data from the individual studies (not the trend of dummy variable lines), the No. 5 (D16) and

No. 7 (D22) bars tested by Choi et al. (2002) show an almost horizontal trend, suggesting no effect, and No. 9 (D29) bars tested by Choi (2006) show an upward trend, suggesting an increasing effect. Overall, Figure 3.29 shows that the reinforcement perpendicular to the headed bar, in general, has no effect on improving the anchorage strength. This is consistent with the observation made by DeVries et al. (1999) that the reinforcement perpendicular to the headed bar is not effective in confining the bar.

3.3.2 Headed Bar Splice Specimens

Thompson et al. (2002) tested 23 beam specimens, four containing No. 5 spliced headed bars and 19 with No. 8 headed bars. The lap lengths ℓ_{st} ranged from 3 to $14d_b$. The net bearing areas of the headed bars ranged from 1.2 to $4.7A_b$, and heads had no obstructions. The four specimens containing No. 5 headed bars are not included in this analysis because the lapped bars yielded during the test. One of the specimens containing No. 8 headed bars is also not included in the analysis because a bond breaker was used over the lapped bars. The remaining 18 specimens containing No. 8 headed bars included in this analysis had a 2-in. clear top and side covers to the bar c_{so} , with the exception of specimen LS-08-04.70-03-06(N)-1, which had a 1-in. clear side cover and 2-in. clear top cover. The center-to-center spacing c_{ch} between the lapped bars was 2, 3, or $5d_b$.

Chun (2015) studied the anchorage behavior of spliced headed bars based on test results of 24 beam specimens (12 tested by Chun and Lee 2013 and the other 12 tested by Chun 2015) containing splices of Grade 80 No. 8 (D25) or No. 9 (D29) headed bars. The headed bars with circular heads had a gross bearing area of $5A_b$ and contained obstructions with a diameter d_{obs} and a length t_{obs} equal to $1.5d_b$ and $0.75d_b$, respectively, which reduced the net bearing area of the head adjacent to the obstruction (gross head area minus area of the obstruction) to 2.7 and $2.8A_b$. Lap lengths ℓ_{st} ranged from 15 to $30d_b$. The center-to-center spacing c_{ch} between the lapped bars was 3 or $5d_b$ (clear spacing of 2 or $4d_b$), where the latter complied with spacing requirements for headed anchorage in Section 12.6 of ACI 318-11. The side cover c_{so} to the lapped bars was equal to half the clear spacing between the bars, except for three specimens with c_{so} equal to $3.5d_b$ and c_{ch} equal to $3d_b$. Cover to the head c_o ranged from 0.38 to $2.88d_b$; 19 specimens had $1d_b$ side cover to the bar, providing $0.38d_b$ clear cover to the head.

3.3.2.1 Analysis Based on Descriptive Equations

The splice strengths of the headed bars tested by Thompson et al. (2002) and Chun (2015) are calculated using the descriptive equations, Eq. (3.4) and (3.5). When calculating the anchorage strength of lapped bars using the descriptive equations, the value of c_{ch} is taken as the lesser of (1) center-to-center spacing between the adjacent lapped bars and (2) twice the cover to the center of the lapped bar in the direction perpendicular to the plane of the bars. The modification factor of 0.8 is applied when calculating anchorage strength using the descriptive equations because the top and side covers were less than the required $8d_b$ to be treated as anchorage within a region equivalent to a column core.

Details of the specimens tested by Thompson et al. (2002) and a comparison of splice strength T (calculated using the moment-curvature method, as used for the splice specimens in the current study) with the force in the bar calculated using descriptive equation Eq. (3.4) T_h are presented in Table 3.6. Hairpin or hoop tie-down confining reinforcement perpendicular to the headed bars (shown in Figure 1.6) was provided in the last five specimens in Table 3.6. These specimens are not considered as having confining reinforcement because the reinforcement was not parallel to the headed bar, matching the observations by Thompson et al. (2002), and the results shown in Figure 3.29 indicating that confining reinforcement perpendicular to headed bars is ineffective.

As shown in Table 3.6, the values of T/T_h for the lap splice specimens tested by Thompson et al. (2002) ranged from 0.85 to 2.81 (four out of 18 specimens had $T/T_h < 1.0$). The average value of T/T_h was 1.51. The modification factor 0.8 for cover to the bar less than $8d_b$ was applied to calculate T_h . The average value T/T_h for these lap splice specimens would be 1.21 with values ranging from 0.68 to 2.25 (eight out of 18 specimens with $T/T_h < 1.0$) if the modification factor of 0.8 had not been used. Although the values of T/T_h for five specimens with $A_{brg} < 4A_b$ ranged from 0.96 to 2.13 with an average of 1.61, use of headed bars with $A_{brg} < 4A_b$ is not deemed safe without further investigating the performance of such headed bars in lap splices. This point is reinforced by the consistently poor performance of headed bars ($T/T_h < 1.0$) with A_{brg} between 2.6 to $3.2A_b$ tested by Choi et al. (2002) and Choi (2006) (see Section 3.3.1.1).

Table 3.6 Test results for lap splice specimens containing No. 8 headed bars tested by Thompson et al. (2002) and comparisons with descriptive equation [Eq. (3.4)] with 0.8 modification factor applied^[1]

Specimen		d_b	ℓ_{st}	f_{cm}	$\frac{A_{brg}}{A_b}$	$\frac{c_{ch}}{d_b}$	$\frac{c_{so}}{d_b}$	$\frac{c_o}{d_b}$	T ^[2]	T_h ^[3]	$\frac{T}{T_h}$
		(in.)	(in.)	(psi)					(kips)	(kips)	
1	LS-08-01.18-03-06(N)-1	1.0	3	3700	1.2	3	2	1.76	17.6	8.3	2.13
2	LS-08-01.18-05-10(N)-1	1.0	5	3700	1.2	5	2	1.76	23.7	18.0	1.32
3	LS-08-01.18-05-10(C)-1	1.0	5	3700	1.2	2	2	1.76	24.5	12.0	2.03
4	LS-08-01.18-08-10(N)-1	1.0	8	4000	1.2	5	2	1.76	28.6	29.7	0.96
5	LS-08-04.70-03-06(N)-1	1.0	3	3200	4.7	3	1	0.31	21.2	8.0	2.65
6	LS-08-04.70-05-06(N)-1	1.0	5	3700	4.7	3	2	1.31	29.0	14.0	2.07
7	LS-08-04.70-05-10(N)-1	1.0	5	3200	3.7	5	2	1.42	29.0	17.3	1.67
8	LS-08-04.70-05-10(C)-1	1.0	5	3200	4.7	2	2	1.31	32.7	11.6	2.81
9	LS-08-04.70-08-10(N)-1	1.0	8	4000	4.7	5	2	1.31	32.7	29.7	1.10
10	LS-08-04.04-08-10(N)-1	1.0	8	4000	4.0	5	2	1.38	33.4	29.7	1.13
11	LS-08-04.70-12-10(N)-1	1.0	12	4200	4.7	5	2	1.31	48.9	45.6	1.07
12	LS-08-04.04-12-10(N)-1	1.0	12	3800	4.0	5	2	1.38	38.0	44.5	0.85
13	LS-08-04.04-14-10(N)-1	1.0	14	3500	4.0	5	2	1.38	52.0	51.2	1.02
14	LS-08-04.70-08-10(N)-1-H0.25 ^[4]	1.0	8	4200	4.7	5	2	1.31	42.6	30.0	1.42
15	LS-08-04.04-08-10(N)-1-H0.56 ^[4]	1.0	8	3500	4.0	5	2	1.38	42.2	28.8	1.47
16	LS-08-04.04-08-10(N)-1-H1.01 ^[4]	1.0	8	3500	4.0	5	2	1.38	45.2	28.8	1.57
17	LS-08-04.04-12-10(N)-1-H0.56 ^[4]	1.0	12	3800	4.0	5	2	1.38	40.7	44.5	0.91
18	LS-08-04.04-12-10(N)-1-TTD ^[4]	1.0	12	3800	4.0	5	2	1.38	44.1	44.5	0.99

^[1] Notation described in Appendix A

^[2] T is based on moment-curvature method

^[3] T_h is based on Eq. (3.4) with a 0.8 modification factor for cover to the bar being $< 8d_b$ applied

^[4] Specimen had confining reinforcement perpendicular to the headed bars (Figure 1.6)

Details of specimens tested by Chun (2015) and a comparison of splice strength T [calculated by Chun (2015) using the moment-curvature method, as used for the splice specimens in the current study] with the calculated strengths T_h based on Eq. (3.4) are presented in Table 3.7. The last seven specimens listed in Table 3.7 contained confining reinforcement perpendicular to the headed bars in the splice region; in five specimens, the splice region was fully confined with No. 3 (D10) stirrups placed along the entire splice region, while in two specimens, confinement was provided using No. 3 (D10) stirrups only at the ends of the splice region. Chun (2015) observed that the specimens without confining reinforcement failed due to prying of the cover concrete within the splice region characterized by a sudden separation of the cover concrete on a plane parallel to the lapped bars. In specimens containing confining reinforcement, the stirrups perpendicular to the headed bars were effective in confining the bars and, thus, improving the splice strength in the *beam* specimens by limiting the prying effect on the cover concrete within

the splice region and increasing the splice strength relative to the specimens without confining reinforcement. This is in contrast to the findings for headed bar splice specimens tested by Thompson et al. (2002) where the hairpin and hoop tie-down reinforcement perpendicular to the headed bars (Figure 1.6) was shown to be ineffective as confining reinforcement because it had no effect on the prying action within the splice region. Headed lapped bars are considered as a viable alternative to straight lapped bars in closure strips in slabs, where prying of the cover concrete is not the expected failure mode and the use of stirrups as confining reinforcement is highly unlikely. Also, only confining reinforcement parallel to the headed bars are considered when calculating A_t in the descriptive equation Eq. (3.5) for the anchorage strength T_h . Therefore, Eq. (3.4) is used to calculate T_h for all specimens in Table 3.7. Headed bars in one specimen with stirrups placed along the entire splice region reached the yield strength, therefore that specimen is not included in the table.

Table 3.7 Test results for lap splice specimens tested by Chun (2015) and comparisons with descriptive equation [Eq. (3.4)] with 0.8 modification factor applied ^[1]

Specimen		d_b ^[2]	ℓ_{st} ^[2]	f_{cm} ^[2]	$\frac{c_{ch}}{d_b}$	$\frac{c_{so}}{d_b}$	$\frac{c_o}{d_b}$	T ^[3]	T_h ^[4]	$\frac{T}{T_h}$
		(in.)	(in.)	(psi)				(kips)	(kips)	
1	D29-S2-F42-L15	1.14	17.1	6000	3	1	0.38	45.0	57.7	0.78
2	D29-S2-F42-L20	1.14	22.8	6000	3	1	0.38	52.9	77.5	0.68
3	D29-S2-F42-L25	1.14	28.5	6000	3	1	0.38	62.6	97.6	0.64
4	D29-S2-F42-L30	1.14	34.3	5820	3	1	0.38	66.2	116.8	0.57
5	D29-S4-F42-L15	1.14	17.1	6000	5	2	1.38	48.4	73.8	0.66
6	D29-S4-F42-L20	1.14	22.8	6000	5	2	1.38	54.8	99.3	0.55
7	D29-S2-C3.5-F42-L15	1.14	17.1	5820	3	3.5	2.88	52.9	57.2	0.93
8	D29-S2-C3.5-F42-L20	1.14	22.8	5820	3	3.5	2.88	63.8	76.9	0.83
9	D29-S2-C3.5-F42-L25	1.14	28.5	5820	3	3.5	2.88	72.4	96.8	0.75
10	D25-S2-F42-L20	0.98	19.7	6000	3	1	0.38	37.1	65.7	0.57
11	D25-S2-F42-L25	0.98	24.6	6000	3	1	0.38	46.5	82.6	0.57
12	D29-S2-F21-L20	1.14	22.8	2940	3	1	0.38	34.0	65.3	0.52
13	D29-S2-F21-L25	1.14	28.5	2940	3	1	0.38	40.7	82.2	0.50
14	D29-S2-F70-L15	1.14	17.1	9120	3	1	0.38	49.8	63.7	0.78
15	D29-S2-F70-L20	1.14	22.8	9120	3	1	0.38	62.3	85.7	0.73
16	D29-S2-F70-L25	1.14	28.5	9120	3	1	0.38	67.0	107.9	0.62
17	D29-S2-F42-L15-Con. ^[5]	1.14	17.1	6000	3	1	0.38	69.9	57.7	1.22
18	D29-S2-F42-L20-Con. ^[5]	1.14	22.8	6000	3	1	0.38	84.4	77.5	1.09
19	D29-S2-F42-L20-LCon. ^[5]	1.14	22.8	6000	3	1	0.38	70.6	77.5	0.91
20	D29-S2-F42-L25-Lcon. ^[5]	1.14	28.5	5820	3	1	0.38	82.2	96.8	0.85
21	D29-S2-F42-L15-Con.2 ^[5]	1.14	17.1	5820	3	1	0.38	75.4	57.2	1.32
22	D29-S2-F42-L20-Con.2 ^[5]	1.14	22.8	5820	3	1	0.38	98.3	76.9	1.28
23	D29-S2-F70-L15-Con. ^[5]	1.14	17.1	9120	3	1	0.38	81.2	63.7	1.28

^[1] Notation described in Appendix A

^[2] Values are converted from the SI unit (1 in. = 25.4 mm; 1 psi = 1/145 MPa; and 1 kip = 4.4484 kN)

^[3] T is based on moment-curvature method

^[4] T_h is based on Eq. (3.4) with a 0.8 modification factor for cover to the bar being $< 8d_b$ applied

^[5] Specimen was confined by stirrups perpendicular to the spliced headed bars

The headed bars tested by Chun (2015) had a gross bearing area of $5A_b$ and contained obstructions with a diameter d_{obs} and a length t_{obs} equal to $1.5d_b$ and $0.75d_b$, respectively, that reduced the net head bearing area adjacent to the obstruction A_{brg} to values between 2.7 and $2.8A_b$ (similar to the net bearing area of 2.6 to $3.2A_b$ in Choi et al. 2002 and Choi 2006). Also, 18 out of the 23 specimens had a low concrete cover to the head c_o of $0.38d_b$, while the remaining five specimens had covers c_o of 1.38 or $2.88d_b$. Table 3.7 shows that the headed bars with no confining reinforcement within the splice region performed poorly, with all specimens giving $T/T_h < 1.0$. The average value of T/T_h is 0.67 , with a minimum and maximum of 0.50 and 0.93 , respectively. The seven specimens containing confining reinforcement perpendicular to the headed bars had T/T_h ranging from 0.85 to 1.32 with an average of 1.14 . The modification factor 0.8 for cover to

the bar $< 8d_b$ is used to calculate T_h . If the modification factor of 0.8 is not used, the average value of T/T_h for these lap splice specimens without confining reinforcement is 0.53, with values ranging from 0.4 to 0.74 (all specimens with $T/T_h < 1.0$). The low values of T/T_h observed for the splice specimens without confining reinforcement match those for the slab and column-like specimens tested by Choi et al. (2002) and Choi (2006), which contained headed bars without obstructions with net bearing areas A_{brg} between 2.6 and $3.2A_b$. In the slab and column-like specimens tested by Choi et al. (2002) and Choi (2006), the ratio T/T_h had an average value of 0.73 with a value as low as 0.49 after the modification factor of 0.8 was applied to the anchorage strength T_h calculated using Eq. (3.4) and (3.5). These observations are consistent with the observation made by Shao et al. (2016) that the poor performance of the spliced headed bars tested by Chun (2015) was likely due to the small net bearing area of approximately $2.8A_b$ and low concrete cover to the head.

3.3.2.2 Effect of Lapped Bar Spacing on Splice Strength

A comparison of the splice test results from the current study with the results of similar tests conducted by Thompson et al. (2002) and Chun (2015) is made to investigate the effects of spacing of lapped bars. The specimens tested by Thompson et al. (2002) contained No. 8 headed bars with lap lengths ℓ_{st} ranging from 3 to $14d_b$, center-to-center spacing c_{ch} between bars of 2, 3, or $5d_b$, and concrete compressive strengths between 3,200 and 4,200 psi. The clear concrete cover to the bars was 2 in. for all specimens. The specimens tested by Chun (2015) contained No. 9 (D29) headed bars with lap lengths of 15 or $20d_b$, center-to-center spacing between the bars of 2 or $3d_b$, and concrete compressive strengths between 2,940 and 9,120 psi. The specimens tested in the current study contained No. 6 headed bars with a lap length of $16d_b$, center-to-center spacing between the bars of 1.67, 2.33, or $3.53d_b$, and concrete compressive strengths of 6,360 or 10,950 psi. Figure 3.30 shows the effect of lapped bar spacing on splice strength. The specimens tested by Thompson et al. (2002) and Chun (2015) containing no confining reinforcement in the splice region and all of the specimens tested in the current study are included. The forces in the lapped bars, plotted on the vertical axis, are normalized with respect to 5,000 psi concrete compressive strength and 12-in. lap length (lap length of headed bars tested in the current study) using Eq. (3.10).

$$T_N = T \left(\frac{5000 \text{ psi}}{f_{cm}} \right)^{0.24} \left(\frac{12 \text{ in.}}{\ell_{st}} \right)^{1.03} \quad (3.10)$$

where T is force on the lapped bar (kips) calculated from moment-curvature analysis, f_{cm} is the measured concrete compressive strength (psi), and ℓ_{st} is the lap length (in.). The powers of 0.24 and 1.03 in Eq. (3.10) are those for f_{cm} and ℓ_{st} , respectively, in the descriptive equations [Eq. (3.4) and (3.5)].

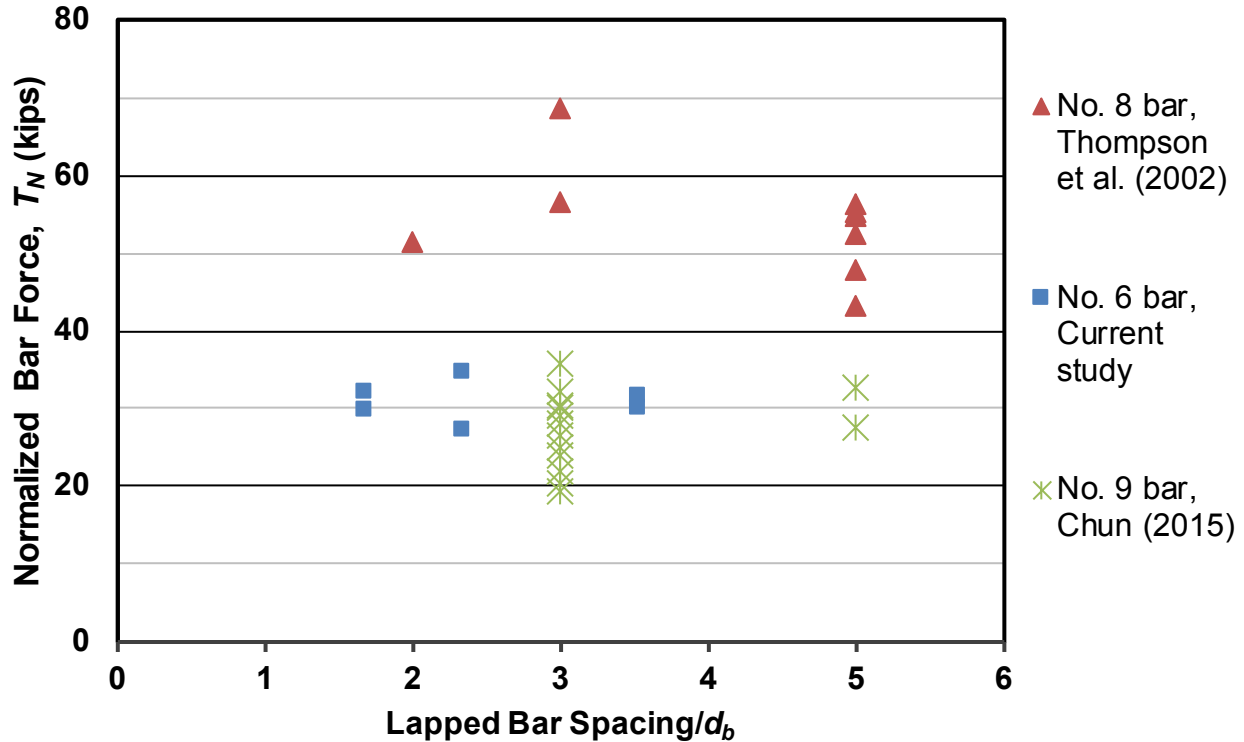


Figure 3.30 Bar force normalized to 5,000 psi concrete compressive strength and 12 in. lap length T_N versus lapped bar spacing for specimens tested by Thompson et al. (2002) and Chun (2015) containing no confining reinforcement and all specimens tested in the current study

As discussed for the splice specimens in the current study in Section 3.2.2, the results for the other two studies also show no significant effect of lapped bar spacing on splice strength (Figure 3.30). This again indicates that within the range of center-to-center spacing between the lapped bars tested (from 1.67 to $5d_b$) an increase in spacing of the lapped bars does not alter the force transfer mechanism between the adjacent bars through a compressive strut, as shown in Figure 1.7, resulting in similar splice strengths of specimens tested within each study. The specimens tested in the current study had a constant width of 18 in., while the specimens tested by Thompson et al. (2002) with a center-to-center spacing c_{ch} of 2 or $5d_b$ had a width of 36 in. and

those with c_{ch} of $3d_b$ had a width of 25 in. The specimens tested by Chun (2015) with c_{ch} of $5d_b$ had a width of 16 in. and those with c_{ch} of $3d_b$ had a width of 8.9, 10.3, or 16 in. An increase in width of the specimens tested by Thompson et al. (2002) and Chun (2015) did not increase the splice strength. All specimens tested in the current study exhibited a side splitting failure in which the lapped bars closest to the side faces of the beam (edge bars) pushed the cover concrete out while the middle bar remained confined by concrete (Figure 3.11). A similar failure mode was observed by Thompson et al. (2002) and Chun (2015). Side splitting failures are more of a function of clear concrete cover to the bar than that of spacing between the bars, which possibly explains the independence of anchorage strength from the width and spacing between the lapped bars. As shown in Figure 3.30, the splice strength of the No. 9 headed bars tested by Chun (2015) was about the same as that of No. 6 headed bars tested in the current study. This further reinforces the observation made in Section 3.3.2.1 and by Shao et al. (2016) that the poor performance of the headed bars tested by Chun (2015) was affected by the small net bearing area of approximately $2.8A_b$ (heads had obstructions with a diameter d_{obs} and a length t_{obs} equal to $1.5d_b$ and $0.75d_b$, respectively), which is less than the minimum net bearing area of $4A_b$ in accordance with ACI 318-14, and low concrete cover to the head (see Table 3.7, 18 out of the 23 specimens had a low concrete cover to the head c_o of $0.38d_b$, and the remaining five specimens had covers c_o of 1.38 or $2.88d_b$).

CHAPTER 4: ANALYSIS OF BEAM-COLUMN JOINT SPECIMENS SUBJECTED TO REVERSED CYCLIC LOADING

4.1 INTRODUCTION

An analysis of exterior, roof-level interior, and knee beam-column joints (Figure 4.1) subjected to reversed cyclic loading is presented in this chapter. In exterior and knee joints, the beam reinforcement was anchored in the column using headed bars, while in roof-level interior joints, the column reinforcement was anchored in the beam using headed bars. A total of 98 specimens from 23 studies were analyzed using descriptive equations for anchorage strength and design provisions for the development length of headed bars (Section 1.4) proposed by Shao et al. (2016). Fifteen out of the 23 studies were published in Japanese. The effects of test parameters, including embedment length, head size, spacing between the headed bars, and joint shear on the performance of the joints under reversed cyclic loading are discussed. An analysis of headed bar anchorage in exterior joints based on anchorage design provisions of Chapter 17 of ACI 318-14 is also included.

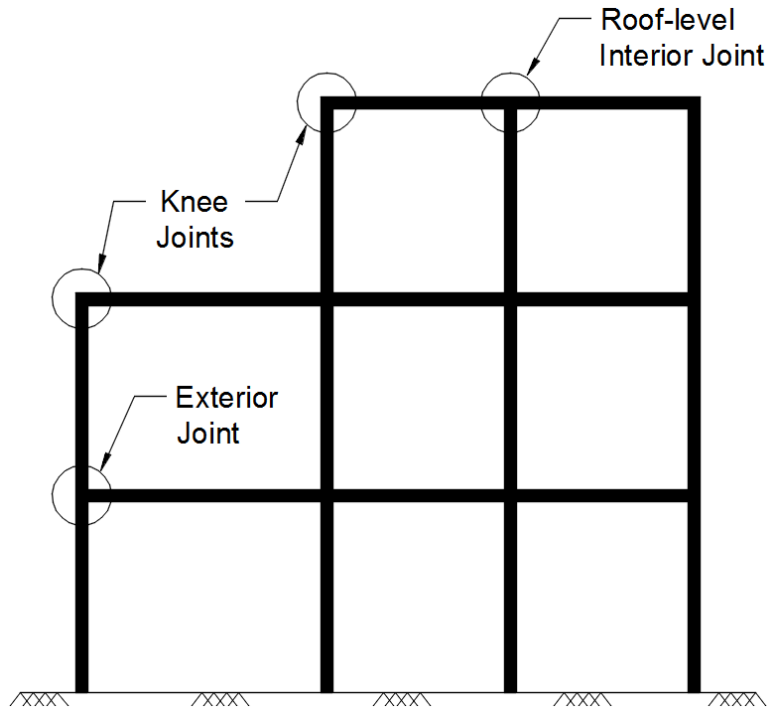


Figure 4.1 Types of beam-column joints studied in the current study

This chapter includes results from studies by Bashandy (1996), Murakami et al. (1998), Wallace et al. (1998), Matsushima et al. (2000), Nakazawa et al. (2000), Tasai et al. (2000), Yoshida et al. (2000), Takeuchi et al. (2001), Ishibashi et al. (2003), Ishibashi and Inokuchi (2004),

Kiyohara et al. (2004), Kiyohara et al. (2005), Kato (2005), Masuo et al. (2006a, 2006b), Adachi and Masuo (2007), Chun et al. (2007), Ishida et al. (2007), Tazaki et al. (2007), Lee and Yu (2009), Kang et al. (2010), Kang et al. (2012), Chun and Shin (2014), and Dhake et al. (2015). Details of these studies are presented in Appendix D.

4.2 ANALYSIS BASED ON NEWLY PROPOSED DESCRIPTIVE AND DESIGN EQUATIONS

Test results from 23 studies on 84 exterior, seven roof-level interior, and seven knee beam-column joints subjected to reversed cyclic loading with significant lateral displacement reversals are analyzed using descriptive equations for anchorage strength and design provisions for the development length of headed bars. The analysis presented in this section evaluates the applicability of the proposed descriptive equations and design provisions to members subjected to reversed cyclic loading.

4.2.1 Descriptive Equations and Design Provisions Proposed by Shao et al. (2016)

Shao et al. (2016) developed descriptive equations and design provisions for the anchorage of headed bars, described in detail in Section 1.4, based on test results of 202 exterior beam-column joint specimens subjected to monotonic loading. Equations (4.1) and (4.2) are the descriptive equations for the anchorage strength of headed bars without and with confining reinforcement, respectively.

$$T_h = \left(781 f_{cm}^{0.24} \ell_{eh}^{1.03} d_b^{0.35} \right) \left(0.0836 \frac{c_{ch}}{d_b} + 0.3444 \right) \quad (4.1)$$

with $0.0836 \frac{c_{ch}}{d_b} + 0.3444 \leq 1.0$

$$T_h = \left(781 f_{cm}^{0.24} \ell_{eh}^{1.03} d_b^{0.35} + 48,800 \frac{A_{tt}}{n} d_b^{0.88} \right) \left(0.0622 \frac{c_{ch}}{d_b} + 0.5428 \right) \quad (4.2)$$

with $0.0622 \frac{c_{ch}}{d_b} + 0.5428 \leq 1.0$ and $\frac{A_{tt}}{n} \leq 0.3 A_b$

where T_h = anchorage strength of headed bar (lb); f_{cm} = measured concrete compressive strength (psi); ℓ_{eh} = embedment length (in.); and d_b = diameter of headed bar (in.); c_{ch} = center-to-center spacing between the bars (in.); A_{tt} = total cross-sectional area of effective confining reinforcement ($NA_{tr,l}$) parallel to the headed bars being developed (in.²); N = total number of legs of effective

confining reinforcement parallel to the headed bars being developed; $A_{tr,l}$ = area of a single leg; and n = number of headed bars in tension, with an upper limit on A_{tr}/n of $0.3A_b$.

A modification factor of 0.8 is applied to T_h for headed bars terminating inside a column core (a region of the column cross-section located inside the column longitudinal reinforcement) with clear cover to the bar $c_{so} < 2.5$ in., or terminating in a member other than beam-column joints with $c_{so} < 8d_b$.

Shao et al. (2016) developed an equation [Eq. (4.3)] for the development length of headed bars based on the descriptive equations [Eq. (4.1) and (4.2)]. The equation includes a strength reduction factor to ensure that no more than 5% of the specimens used to develop the equation have a ratio of test-to-calculated failure load less than 1.0.

$$\ell_{dt} = \left(0.0024 \frac{f_y \psi_e \psi_{cs} \psi_o}{f_c'^{0.25}} \right) d_b^{1.5} \quad (4.3)$$

where ℓ_{dt} = development length of a headed bar in tension (in.) not less than the greater of $8d_b$ and 6 in.; f_y = specified yield strength of the headed bar (psi); ψ_e = modification factor for epoxy-coated or zinc and epoxy dual-coated bars; ψ_{cs} = modification factor for confining reinforcement and bar spacing; ψ_o = modification factor for bar location; f_c' = concrete compressive strength (psi); and d_b = diameter of the headed bar (in.).

The proposed provisions apply to headed bars with yield strengths up to 120,000 psi and concrete compressive strengths up to 16,000 psi. The modification factor ψ_e for the reinforcement coating condition is 1.2 for epoxy-coated or zinc and epoxy dual-coated bars and 1.0 for uncoated or zinc-coated (galvanized) bars, and is retained from ACI 318-14. Values for the modification factor for confining reinforcement and bar spacing ψ_{cs} are given in Table 4.1. The values of ψ_{cs} are permitted to be interpolated for intermediate values of f_y , c_{ch} , and A_{tr}/A_{hs} .

Table 4.1 Modification factor ψ_{cs} for confining reinforcement and spacing

Confinement level	f_y	c_{ch}	
		$2d_b$	$\geq 8d_b$
$\frac{A_{tt}}{A_{hs}} \geq 0.3$	$\leq 60,000$	0.6	0.4
	120,000	0.7	0.45
$\frac{A_{tt}}{A_{hs}} = 0$ (no confining reinforcement)	all	1.0	0.5

where c_{ch} is center-to-center spacing between adjacent headed bars, A_{hs} is the total cross-sectional area of headed bars being developed, and A_{tt} is the total cross-sectional area of all confining reinforcement parallel to ℓ_{dt} for headed bars being developed in beam-column joints (Figure 4.2) and located $8d_b$ of the top (bottom) of the headed bars in direction of the interior of the joint for No. 3 through No. 8 headed bars or within $10d_b$ of the top (bottom) of the bar in direction of the interior of the joint for No. 9 through No. 11; or minimum total cross-sectional area of all confining reinforcement parallel to headed bars being developed in members other than beam-column joints within $7\frac{1}{2}d_b$ on one side of the bar centerline for No. 3 through No. 8 headed bars or within $9\frac{1}{2}d_b$ on one side of the bar centerline for No. 9 through No. 11 headed bars.

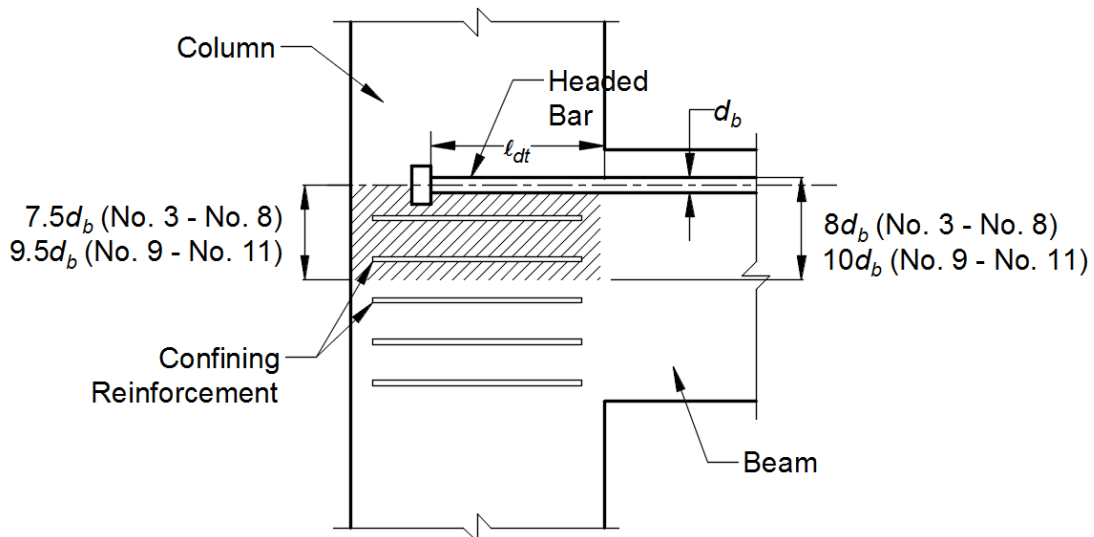


Figure 4.2 Effective confining reinforcement within the joint region of beam-column joints suggested by Shao et al. (2016)

The factor ψ_o is equal to 1.0 for headed bars terminating inside a column core (a region of the column cross-section located inside the column longitudinal reinforcement) with clear cover

to the bar ≥ 2.5 in., or terminating in a member other than beam-column joints with cover to the bar $\geq 8d_b$; in other cases, the value of ψ_o is equal to 1.25.

4.2.2 Exterior and Roof-level Interior Beam-Column Joints

The performance of 84 exterior and seven roof-level interior beam-column joints subjected to reversed cyclic loading is evaluated in this section based on the descriptive equations for the anchorage strength and design provisions for the development length of headed bars. Relevant specimen details are presented in Table 4.2 with complete details and analysis results presented in Table C.2 of Appendix C.

Table 4.2 Detail of exterior and roof-level interior beam-column joint specimens tested under reversed cyclic loading

Study *	Specimen	Bar Size **	$\frac{A_{gross}}{A_b}$	$\frac{A_{obs}}{A_b}$	$\frac{A_{brg}}{A_b}$	$\frac{t_{obs}}{d_b}$	f_y	f_{cm}	c_{so}	$\frac{c_{ch}}{d_b}$	$\frac{A_{tt}}{A_{hs}}$	ℓ_{eh}	ℓ_{ehy}	
			(ksi)	(psi)	(in.)	(in.)	(in.)							
1	Bashandy (1996)	Exterior Joint	D25	9.6	-	8.6	0.0	64.8	4290	3.5	5.1	0.76	11.5	7.8
2	Murakami et al. (1998)	No. 100	D16	2.7	-	1.7	0.0	53.7	5700	2.3	3.5	0.16	8.9	4.7
		No. 101	D16	7.3	-	6.3	0.0	53.7	5700	2.3	3.5	0.16	8.9	4.7
		B8-M	D19	7.0	-	6.0	0.0	74.1	4280	2.3	4.3	0.15	8.9	8.5
		B7-M	D19	7.0	-	6.0	0.0	74.1	4280	2.3	4.3	0.15	8.9	8.5
		No. 102 ‡	D19	3.1	-	2.1	0.0	137.1	5700	2.3	2.9	0.11	8.9	16.7
		No. 103 ‡	D19	6.8	-	5.8	0.0	137.1	5700	2.3	2.9	0.11	8.9	16.7
		No. 104 ‡	D19	4.4	-	3.4	0.0	137.1	5700	2.3	2.9	0.11	8.9	16.7
		M8D16 ‡	D16	7.0	2.6	4.4	0.0	145.1	4100	2.3	3.2	0.04	8.9	14.3
		M4D19 ‡	D19	7.0	3.1	3.9	0.0	145.1	4100	2.3	2.9	0.11	8.9	19.1
		M3D19 ‡	D19	7.0	3.1	3.9	0.0	145.1	4100	2.3	4.3	0.15	8.9	16.9
M2D22 ‡	D22	7.0	3.4	3.6	0.0	141.1	4100	2.2	7.4	0.25	8.9	16.7		
3	Wallace et al. (1998)	BCEJ1 ‡‡	No. 8	5.0	-	4.0	0.0	67.0	5190	-	3.5	0.38	13.9	8.9
4	Matsushima et al. (2000)	H	D25	-	-	-	-	79.9	4770	2.3	5.1	0.19	11.6	13.2
		HS §	D25	-	-	-	-	79.9	4770	2.3	5.1	0.19	7.9	13.2
5	Nakazawa et al. (2000)	J1	D19	6.9	3.0	3.9	1.9	103.0	17400	2.7	3.4	0.14	11.3	7.4
		J2	D19	6.9	-	5.9	0.0	103.0	17400	2.7	3.4	0.14	11.3	7.4
6	Tasai et. al (2000)	No. 6	D25	9.0	3.6	5.4	1.9	105.0	7120	2.4	3.1	0.14	11.8	18.9
		No. 7	D25	9.0	3.6	5.4	1.9	105.0	7120	2.4	4.7	0.28	11.8	15.9
7	Yoshida et al. (2000)	No. 1	D19	6.8	-	5.8	0.0	81.5	5470	2.4	3.7	0.25	10.2	9.1
		No. 2	D19	5.1	-	4.1	0.0	81.5	5470	2.4	3.7	0.25	10.2	9.1
		No. 3	D19	4.1	-	3.1	0.0	81.5	4500	2.4	3.7	0.25	10.2	9.5
8	Takeuchi et al. (2001)	0-1	D25	6.8	-	5.8	0.0	64.5	6400	2.5	4.9	0.19	10.4	7.9
		0-2	D25	6.8	-	5.8	0.0	85.0	8830	2.5	4.9	0.19	10.4	9.8
		0-3	D25	6.8	-	5.8	0.0	54.7	3520	2.5	4.9	0.19	10.4	7.5
		0-4	D25	6.8	-	5.8	0.0	64.5	6400	2.5	4.9	0.19	11.7	7.9
		0-6	D25	6.8	-	5.8	0.0	104.1	6440	2.5	3.3	0.14	10.4	15.2
		0-7	D25	6.8	-	5.8	0.0	104.1	9000	2.5	3.3	0.14	10.4	14.0
9	Ishibashi et. al (2003) §§	T345-30-4S	D19	6.4	3.2	3.2	-	56.3	4830	1.9	7.5	0.34	13.5	4.6
		T345-30-3N	D19	6.4	3.2	3.2	-	56.3	4830	1.9	7.5	0.34	13.5	4.6
		T490-45-4S	D19	6.4	3.2	3.2	-	84.5	7210	1.9	7.5	0.34	13.5	6.6
		T490-45-3N	D19	6.4	3.2	3.2	-	84.5	7210	1.9	7.5	0.34	13.5	6.6

* Values given in SI are converted to in.-lb (1 in. = 25.4 mm; 1 psi = 1/145 MPa; and 1 kip = 4.4484 kN); notation described in Appendix A

** Bar sizes are presented in SI as reported in the original studies (only Wallace et al. 1998 had bar sizes reported in in.-lb)

‡ Analyzed as doubly-reinforced section to calculate M_n ; all other specimens are analyzed as singly-reinforced

‡‡ Specimens contained transverse beams on one or both sides of the test beam. These transverse beams, however, did not meet the dimensional requirements of Section 18.8.4.2 of ACI 318-14 and Section 4.3 of ACI 352R-02 to be considered effective in increasing the joint shear strength.

§ Specimen had $d/\ell_{eh} > 1.5$

§§ Roof-level interior joints; all other specimens are exterior joints

Table 4.2 Cont. Detail of exterior and roof-level interior beam-column joint specimens tested under reversed cyclic loading

Study *	Specimen	$\frac{\ell_{eh}}{\ell_{ehy}}$	ℓ_{dy} (in.)	$\frac{\ell_{eh}}{\ell_{dy}}$	$\frac{d}{\ell_{eh}}$	M_n (kip.in.)	M_{peak} (kip.in.)	$\frac{M_{peak}}{M_n}$	$\frac{V_p}{V_n}$	$\delta_{0.8peak}$	$\frac{T'}{T_h}$	$\frac{T'}{T_{anc}}$	
1	Bashandy (1996)	Exterior Joint	1.46	16.1	0.71	1.4	1443	1593	1.10	0.81	0.053	1.10	2.09
2	Murakami et al. (1998)	No. 100	1.90	6.5	1.36	1.5	859	1031	1.20	0.50	0.080	1.20	2.38
		No. 101	1.90	6.5	1.36	1.5	859	1066	1.24	0.52	0.083	1.24	2.46
		B8-M	1.04	15.1	0.58	1.5	1200	1395	1.16	0.78	0.060	1.16	3.39
		B7-M	1.04	15.1	0.58	1.5	1093	1242	1.14	0.70	0.070	1.14	3.32
		No. 102 ‡	0.53	31.4	0.28	1.5	2838	1957	0.69	0.95	0.040	1.31	4.96
		No. 103 ‡	0.53	31.4	0.28	1.5	2838	1524	0.54	0.74	0.055	1.02	3.87
		No. 104 ‡	0.53	31.4	0.28	1.5	2838	1793	0.63	0.87	0.050	1.20	4.55
		M8D16 ‡	0.62	36.9	0.24	1.5	2918	1793	0.61	1.02	0.040	1.00	4.95
		M4D19 ‡	0.46	37.2	0.24	1.5	2838	1688	0.59	0.97	0.040	1.29	4.53
		M3D19 ‡	0.52	37.2	0.24	1.5	2226	1676	0.75	0.96	0.040	1.43	4.30
M2D22 ‡	0.53	42.0	0.21	1.5	1990	1324	0.67	0.96	0.020	1.21	3.36		
3	Wallace et al. (1998)	BCEJ1 ††	1.56	16.0	0.87	1.5	4448	4950	1.11	0.93	0.048	1.11	2.93
4	Matsushima et al. (2000)	H	0.88	21.2	0.55	1.3	2545	2205	0.87	0.81	0.035	0.98	1.20
		HS §	0.60	21.2	0.37	1.9	2545	2071	0.81	0.76	0.035	1.32	2.25
5	Nakazawa et al. (2000)	J1	1.52	14.7	0.77	1.1	2989	3391	1.13	1.05	0.050	1.13	1.78
		J2	1.52	14.7	0.77	1.1	2989	3344	1.12	1.04	0.058	1.12	1.75
6	Tasai et. al (2000)	No. 6	0.62	27.6	0.43	1.3	4388	2283	0.52	0.89	0.060	0.83	2.09
		No. 7	0.74	27.6	0.43	1.3	2359	1328	0.56	0.55	0.030	0.74	1.13
7	Yoshida et al. (2000)	No. 1	1.13	15.9	0.64	1.4	1818	1681	0.92	0.88	0.040	0.92	2.87
		No. 2	1.13	15.9	0.64	1.4	1818	1696	0.93	0.77	0.040	0.93	2.89
		No. 3	1.08	17.5	0.58	1.4	1797	1665	0.93	0.83	0.040	0.93	2.88
8	Takeuchi et al. (2001)	0-1	1.32	13.5	0.77	1.5	2237	2458	1.10	0.56	0.050	1.10	1.80
		0-2	1.06	18.5	0.56	1.5	2937	2897	0.99	0.56	0.033	0.99	2.13
		0-3	1.38	13.2	0.79	1.5	1821	1927	1.06	0.59	0.050	1.06	1.47
		0-4	1.49	13.5	0.86	1.3	2237	2591	1.16	0.59	0.050	1.16	1.90
		0-6	0.69	27.7	0.38	1.5	4390	3481	0.79	0.79	0.030	1.14	2.80
		0-7	0.74	24.7	0.42	1.5	4598	4106	0.89	0.78	0.030	1.20	3.15
9	Ishibashi et. al (2003) §§	T345-30-4S	2.95	9.2	1.47	1.0	1116	1401	1.25	0.72	0.065	1.25	1.83
		T345-30-3N	2.95	9.2	1.47	1.0	1116	1394	1.25	0.72	0.053	1.25	1.82
		T490-45-4S	2.05	15.2	0.89	1.0	1612	1925	1.19	0.83	0.053	1.19	1.73
		T490-45-3N	2.05	15.2	0.89	1.0	1612	1951	1.21	0.82	0.040	1.21	1.76

* Values given in SI are converted to in.-lb (1 in. = 25.4 mm; 1 psi = 1/145 MPa; and 1 kip = 4.4484 kN); notation described in Appendix A

‡ Analyzed as doubly-reinforced section to calculate M_n ; all other specimens are analyzed as singly-reinforced

†† Specimens contained transverse beams on one or both sides of the test beam. These transverse beams, however, did not meet the dimensional requirements of Section 18.8.4.2 of ACI 318-14 and Section 4.3 of ACI 352R-02 to be considered effective in increasing the joint shear strength.

§ Specimen had $d/\ell_{eh} > 1.5$

§§ Roof-level interior joints; all other specimens are exterior joints

Table 4.2 Cont. Detail of exterior and roof-level interior beam-column joint specimens tested under reversed cyclic loading

Study *	Specimen	Bar Size **	$\frac{A_{gross}}{A_b}$	$\frac{A_{obs}}{A_b}$	$\frac{A_{brg}}{A_b}$	$\frac{t_{obs}}{d_b}$	f_y	f_{cm}	c_{so}	$\frac{c_{ch}}{d_b}$	$\frac{A_{tt}}{A_{hs}}$	ℓ_{eh}	ℓ_{ehy}	
			(ksi)	(psi)	(in.)	(in.)	(in.)							
10	Ishibashi and Inokuchi (2004) §§	2S-2	D29	-	-	-	-	77.1	5180	2.9	7.4	0.14	20.5	13.1
		2S-0 [□]	D29	-	-	-	-	77.1	5180	2.9	7.4	0.00	20.5	14.9
		WN-ST	D29	-	-	-	-	77.1	5420	2.9	7.4	0.36	20.5	11.8
11	Kiyohara et al. (2004)	No. 1	D29	6.7	2.6	4.1	2.0	103.0	13820	3.3	5.4	0.20	14.4	12.3
		No. 2	D29	6.7	2.6	4.1	2.0	103.0	21520	3.3	3.4	0.13	14.4	13.4
		No. 3	D29	6.7	2.6	4.1	2.0	103.0	6440	3.3	5.5	0.26	14.4	14.0
		No. 4	D29	6.7	2.6	4.1	2.0	103.0	13820	3.3	5.4	0.20	18.1	12.3
		No. 5 [§]	D29	6.7	2.6	4.1	2.0	103.0	13820	3.3	5.4	0.20	10.8	12.3
12	Kiyohara et al. (2005)	No. 6	D29	6.7	2.6	4.1	2.0	149.9	15420	3.3	2.9	0.11	14.4	22.2
		No. 7	D29	6.7	2.6	4.1	2.0	149.9	20130	3.3	2.9	0.11	14.4	20.8
		No. 8 [‡]	D29	6.7	2.6	4.1	2.0	149.9	6870	3.3	2.9	0.11	14.4	26.7
		No. 9	D29	6.7	2.6	4.1	2.0	149.9	15360	3.3	2.9	0.11	18.1	22.2
		No. 10 [§]	D29	6.7	2.6	4.1	2.0	149.9	15660	3.3	2.9	0.11	10.8	22.1
		No. 11	D29	6.7	2.6	4.1	2.0	100.1	15000	3.3	2.9	0.16	14.4	14.6
13	Kato (2005)	No. 1	D22	6.3	-	5.3	0.0	75.5	8820	4.3	3.6	0.04	14.2	8.3
		No. 2	D22	6.3	2.7	3.6	1.9	73.2	10270	4.3	3.6	0.04	14.2	7.7
14	Masuo et al. (2006a, 2006b)	AH12-2-45	D25	6.8	3.1	3.7	1.9	148.0	18820	2.5	8.0	0.19	11.8	12.3
		AH12-2-40	D25	6.8	3.1	3.7	1.9	148.0	18820	2.5	8.0	0.19	11.8	12.3
		AH12-2-45A [§]	D25	6.8	3.1	3.7	1.9	148.0	18820	2.5	8.0	0.19	9.8	12.3
		AH8-2-45	D25	6.8	3.1	3.7	1.9	148.0	13140	2.5	8.0	0.19	11.8	13.4
		AH12-8-45	D25	6.8	2.9	3.9	1.9	92.0	18820	3.4	2.7	0.07	11.8	11.2
		AH12-8-40	D25	6.8	2.9	3.9	1.9	92.0	18820	3.4	2.7	0.07	11.8	11.2
		AH12-8-45B	D25	6.8	2.9	3.9	1.9	92.0	18820	3.4	2.7	0.15	11.8	10.9
AH8-6-45	D25	6.8	2.9	3.9	1.9	92.0	13140	3.4	2.7	0.10	11.8	12.1		
15	Adachi and Masuo (2007)	J30-12-0	D25	6.4	2.5	3.9	1.9	76.0	4480	3.4	3.2	0.14	11.8	12.0
		J30-12-P1 ^{‡‡}	D25	6.4	2.5	3.9	1.9	76.0	4480	3.4	3.2	0.14	11.8	12.0
		J30-12-P2 ^{‡‡}	D25	6.4	2.5	3.9	1.9	76.0	4480	-	3.2	0.14	11.8	12.0
		J60-12-0	D25	6.4	2.5	3.9	1.9	76.0	9150	3.4	2.7	0.09	11.8	10.9
		J60-12-P1 ^{‡‡}	D25	6.4	2.5	3.9	1.9	76.0	9150	3.4	2.7	0.09	11.8	10.9
		J60-12-P2 ^{‡‡}	D25	6.4	2.5	3.9	1.9	76.0	9150	-	2.7	0.09	11.8	10.9

* Values given in SI are converted to in.-lb (1 in. = 25.4 mm; 1 psi = 1/145 MPa; and 1 kip = 4.4484 kN); notation described in Appendix A

** Bar sizes are presented in SI as reported in the original studies (only Wallace et al. 1998 had bar sizes reported in in.-lb)

□ Specimens did not contain confining reinforcement parallel to the headed bars within the joint region

‡ Analyzed as doubly-reinforced section to calculate M_n ; all other specimens are analyzed as singly-reinforced

‡‡ Specimens contained transverse beams on one or both sides of the test beam. These transverse beams, however, did not meet the dimensional requirements of Section 18.8.4.2 of ACI 318-14 and Section 4.3 of ACI 352R-02 to be considered effective in increasing the joint shear strength.

§ Specimens had $d/\ell_{eh} > 1.5$

§§ Roof-level interior joints; all other specimens are exterior joints

Table 4.2 Cont. Detail of exterior and roof-level interior beam-column joint specimens tested under reversed cyclic loading

Study *		Specimen	$\frac{\ell_{eh}}{\ell_{ehy}}$	ℓ_{dy}	$\frac{\ell_{eh}}{\ell_{dy}}$	$\frac{d}{\ell_{eh}}$	M_n (kip.in.)	M_{peak} (kip.in.)	$\frac{M_{peak}}{M_n}$	$\frac{V_p}{V_n}$	$\delta_{0.8peak}$	$\frac{T'}{T_h}$	$\frac{T'}{T_{anc}}$
10	Ishibashi and Inokuchi (2004) §§	2S-2	1.56	22.8	0.90	1.0	5740	6272	1.09	0.97	0.030	1.09	2.18
		2S-0 [□]	1.38	22.8	0.90	1.0	5740	6165	1.07	0.96	0.030	1.07	2.76
		WN-ST	1.74	22.4	0.92	1.0	5953	6272	1.05	0.95	0.030	1.05	1.01
11	Kiyohara et al. (2004)	No. 1	1.17	24.3	0.59	1.5	8500	9833	1.16	0.76	0.040	1.16	3.22
		No. 2	1.08	20.6	0.70	1.5	12310	11746	0.95	0.91	0.040	0.95	3.00
		No. 3	1.02	31.7	0.45	1.5	6189	6856	1.11	0.66	0.040	1.11	2.31
		No. 4	1.48	24.3	0.75	1.2	8500	10524	1.24	0.82	0.080	1.24	3.45
		No. 5 [§]	0.88	24.3	0.45	2.0	8500	8876	1.04	0.69	0.033	1.17	4.37
12	Kiyohara et al. (2005)	No. 6	0.65	39.1	0.37	1.5	19538	13792	0.71	1.14	0.040	1.08	3.92
		No. 7	0.69	35.8	0.40	1.5	20094	14350	0.71	1.18	0.040	1.03	3.97
		No. 8 [‡]	0.54	50.3	0.29	1.5	18015	9647	0.54	0.96	0.040	0.99	2.98
		No. 9	0.82	39.1	0.46	1.2	19529	16264	0.83	1.34	0.040	1.02	4.63
		No. 10 [§]	0.49	38.9	0.28	1.9	19575	12836	0.66	1.06	0.040	1.32	7.29
		No. 11	0.99	22.6	0.64	1.5	10265	10391	1.01	0.81	0.040	1.03	3.56
		No. 12	1.29	22.4	0.81	1.2	11747	13686	1.17	1.13	0.040	1.17	3.70
13	Kato (2005)	No. 1	1.72	13.8	1.02	1.1	5273	5744	1.09	0.95	0.040	1.09	2.28
		No. 2	1.83	12.3	1.16	1.1	5391	5582	1.04	0.87	0.080	1.04	2.10
14	Masuo et al. (2006a, 2006b)	AH12-2-45	0.95	30.9	0.38	1.3	3543	4032	1.14	0.77	0.030	1.19	2.79
		AH12-2-40	0.95	30.9	0.38	1.3	3543	3772	1.06	0.81	0.028	1.12	2.61
		AH12-2-45A [§]	0.79	30.9	0.32	1.6	3543	3998	1.13	0.76	0.030	1.41	3.69
		AH8-2-45	0.88	34.8	0.34	1.3	3480	3603	1.04	0.69	0.030	1.18	2.54
		AH12-8-45	1.05	15.6	0.75	1.2	7284	8064	1.11	1.66	0.040	1.11	3.82
		AH12-8-40	1.05	15.6	0.75	1.2	7284	7883	1.08	1.82	0.040	1.08	3.74
		AH12-8-45B	1.08	15.6	0.75	1.2	7284	8550	1.17	1.76	0.040	1.17	3.16
		AH8-6-45	0.97	18.0	0.65	1.3	5654	6302	1.11	1.29	0.040	1.14	2.89
15	Adachi and Masuo (2007)	J30-12-0	0.98	20.2	0.58	1.3	3233	3490	1.08	1.03	0.320	1.10	3.57
		J30-12-P1 ^{**}	0.98	20.2	0.58	1.3	3233	3513	1.09	1.03	0.045	1.11	3.59
		J30-12-P2 ^{**}	0.98	20.2	0.58	1.3	3233	3569	1.10	1.05	0.062	1.13	3.65
		J60-12-0	1.08	15.3	0.77	1.3	4781	4845	1.01	0.77	0.033	1.01	5.02
		J60-12-P1 ^{**}	1.08	15.3	0.77	1.3	4781	5139	1.07	0.81	0.034	1.07	5.33
		J60-12-P2 ^{**}	1.08	15.3	0.77	1.3	4781	5320	1.11	0.84	0.067	1.11	5.52

* Values given in SI are converted to in.-lb (1 in. = 25.4 mm; 1 psi = 1/145 MPa; and 1 kip = 4.4484 kN); notation described in Appendix A

[□] Specimens did not contain confining reinforcement parallel to the headed bars within the joint region

[‡] Analyzed as doubly-reinforced section to calculate M_n ; all other specimens are analyzed as singly-reinforced

^{**} Specimens contained transverse beams on one or both sides of the test beam. These transverse beams, however, did not meet the dimensional requirements of Section 18.8.4.2 of ACI 318-14 and Section 4.3 of ACI 352R-02 to be considered effective in increasing the joint shear strength.

[§] Specimens had $d/\ell_{eh} > 1.5$

^{§§} Roof-level interior joints; all other specimens are exterior joints

Table 4.2 Cont. Detail of exterior and roof-level interior beam-column joint specimens tested under reversed cyclic loading

Study *	Specimen	Bar Size **	$\frac{A_{gross}}{A_b}$	$\frac{A_{obs}}{A_b}$	$\frac{A_{brg}}{A_b}$	$\frac{t_{obs}}{d_b}$	f_y	f_{cm}	c_{so}	$\frac{c_{ch}}{d_b}$	$\frac{A_{tt}}{A_{hs}}$	ℓ_{eh}	ℓ_{ehy}	
			(ksi)	(psi)	(in.)	(in.)	(in.)	(in.)	(in.)					
16	Chun et al. (2007)	JM-1 \diamond	D22	3.9	2.2	2.9	0.5	58.4	8950	5.3	3.4	0.09	15.1	6.3
		JM-2 \diamond	D22	3.9	2.2	2.9	0.5	58.4	8720	5.0	2.0	0.05	15.1	7.4
		WM \diamond, \square	D32	3.9	2.2	2.9	0.6	62.5	8180	4.0	5.2	0.00	18.9	12.8
		JM-No.11-1a	D36	4.9	2.2	2.7	0.7	66.4	4760	4.8	4.2	0.26	17.3	14.1
		JM-No.11-1b	D36	4.9	2.2	2.7	0.7	66.4	4760	4.8	4.2	0.26	17.3	14.1
17	Ishida et al. (2007)	P1 **	D22	-	-	-	-	76.0	3480	1.3	4.5	0.21	11.9	11.2
		P2 **	D22	-	-	-	-	76.0	3480	1.3	4.5	0.21	11.9	11.2
		P3 **	D22	-	-	-	-	76.0	3480	1.3	4.5	0.21	11.9	11.2
		P4 **	D22	-	-	-	-	76.0	3480	1.3	4.5	0.16	11.9	11.5
18	Tazaki et al. (2007)	E1	D16	7.9	-	6.9	0.0	55.0	4410	1.1	2.5	0.11	10.2	5.6
		E2 \S	D16	7.9	-	6.9	0.0	55.0	4410	1.1	2.5	0.05	6.3	5.7
19	Lee and Yu (2009)	W0-M1	D22	6.1	2.9	3.2	2.1	68.6	4450	8.7	2.2	0.14	12.1	9.5
		W150-M1	D22	6.1	2.9	3.2	2.1	68.6	5190	2.6	2.2	0.14	12.1	9.1
		W0-M2	D22	6.1	2.9	3.2	2.1	68.6	4450	8.7	2.2	0.14	12.1	9.5
		W150-M2	D22	6.1	2.9	3.2	2.1	68.6	5190	2.6	2.2	0.14	12.1	9.1
20	Kang et al. (2010)	JD \S	D19	3.6	-	2.6	0.0	69.8	4220	2.7	5.2	0.25	11.3	5.7
21	Kang et al. (2012)	JH-R1	D19	6.3	-	5.3	0.0	69.5	4360	1.2	3.1	0.19	11.3	8.7
		JH-R2	D19	6.3	-	5.3	0.0	69.5	4360	1.2	2.3	0.19	11.3	9.3
22	Chun and Shin (2014) \diamond	M0.7S \ddagger	D16	5.0	-	4.0	0.7	70.8	3710	3.0	2.3	0.29	9.0	7.5
		M1.0S	D16	5.0	-	4.0	0.7	70.8	3710	3.0	2.3	0.58	9.0	7.5
		M1.5S \S	D16	5.0	-	4.0	0.7	70.8	3480	3.0	2.3	0.58	9.0	7.6
		M2.0S \S	D16	5.0	-	4.0	0.7	70.8	3830	3.0	2.3	0.58	9.0	7.4
		M2.5S \S	D16	5.0	-	4.0	0.7	70.8	3830	3.0	2.3	0.58	9.0	7.4
		M0.7U \ddagger	D16	5.0	-	4.0	0.7	70.8	3710	3.0	2.3	0.19	9.0	7.8
23	Dhake et al. (2015)	J4 \square	D12	5.0	-	4.0	0.0	76.1	4350	0.9	7.5	0.00	5.9	3.7
		J5 \square	D12	5.0	-	4.0	0.0	76.1	4350	0.9	7.5	0.00	4.0	3.7
		J9	D12	5.0	-	4.0	0.0	76.1	4350	0.9	7.5	0.56	5.9	3.3

* Values given in SI are converted to in.-lb (1 in. = 25.4 mm; 1 psi = 1/145 MPa; and 1 kip = 4.4484 kN); notation described in Appendix A

** Bar sizes are presented in SI as reported in the original studies (only Wallace et al. 1998 had bar sizes reported in in.-lb)

\diamond Heads contained obstruction with diameter d_{obs} of $1.5d_b$ and length $t_{obs} \leq 0.6d_b$ for \geq No.8 (D25) bars or \leq smaller of 0.6 in. and $0.75d_b$ for $<$ No.8 (D25) bars (also see Section 5.1.7). Therefore, the obstruction is not considered to detract from the net bearing area of the head.

\square Specimens did not contain confining reinforcement parallel to the headed bars within the joint region

\ddagger Analyzed as doubly-reinforced section to calculate M_n ; all other specimens are analyzed as singly-reinforced

** Specimens contained transverse beams on one or both sides of the test beam. These transverse beams, however, did not meet the dimensional requirements of Section 18.8.4.2 of ACI 318-14 and Section 4.3 of ACI 352R-02 to be considered effective in increasing the joint shear strength.

\S Specimens had $d/\ell_{eh} > 1.5$

Table 4.2 Cont. Detail of exterior and roof-level interior beam-column joint specimens tested under reversed cyclic loading

Study *	Specimen	$\frac{\ell_{eh}}{\ell_{ehy}}$	ℓ_{dy}	$\frac{\ell_{eh}}{\ell_{dy}}$	$\frac{d}{\ell_{eh}}$	M_n (kip.in.)	M_{peak} (kip.in.)	$\frac{M_{peak}}{M_n}$	$\frac{V_p}{V_n}$	$\delta_{0.8peak}$	$\frac{T'}{T_h}$	$\frac{T'}{T_{anc}}$	
16	Chun et al. (2007)	JM-1 \diamond	2.41	8.6	1.76	1.1	2358	2965	1.26	0.29	0.068	1.27	2.44
		JM-2 \diamond	2.05	10.0	1.52	1.1	4396	5036	1.15	0.53	0.040	1.16	4.37
		WM \diamond, \square	1.48	14.9	1.27	0.7	4859	5558	1.14	0.52	0.084	1.14	4.89
		JM-No.11-1a	1.23	23.1	0.75	1.0	4637	4894	1.06	0.61	0.079	1.06	3.23
		JM-No.11-1b	1.23	23.1	0.75	1.0	4637	4779	1.03	0.60	0.065	1.03	3.16
17	Ishida et al. (2007)	P1 \ddagger	1.06	19.8	0.60	1.2	3842	3950	1.03	1.35	0.015	1.03	1.63
		P2 \ddagger	1.06	19.8	0.60	1.2	3842	4001	1.04	1.35	0.030	1.04	1.65
		P3 \ddagger	1.06	19.8	0.60	1.2	3842	4399	1.14	0.93	0.030	1.14	1.82
		P4 \ddagger	1.04	19.8	0.60	1.2	4919	4681	0.95	1.60	0.030	0.95	1.94
18	Tazaki et al. (2007)	E1	1.82	11.1	0.92	1.0	901	1084	1.20	0.82	0.060	1.20	4.90
		E2 \S	1.10	11.6	0.54	1.6	901	951	1.06	0.82	0.060	1.06	6.78
19	Lee and Yu (2009)	W0-M1	1.27	21.4	0.56	1.3	2336	2769	1.19	0.55	0.080	1.19	2.01
		W150-M1	1.32	19.5	0.62	1.3	2378	2805	1.18	1.04	0.080	1.18	3.25
		W0-M2	1.27	21.4	0.56	1.3	2378	2805	1.18	0.56	0.080	1.18	3.25
		W150-M2	1.32	19.5	0.62	1.3	2378	2909	1.22	1.07	0.080	1.22	3.37
20	Kang et al. (2010)	JD \S	1.98	13.9	0.81	1.8	2313	2697	1.17	0.53	0.036	1.17	3.15
21	Kang et al. (2012)	JH-R1	1.30	14.8	0.76	1.3	1566	1885	1.20	0.68	0.050	1.20	2.14
		JH-R2	1.21	17.1	0.66	1.2	1458	1708	1.17	0.67	0.050	1.17	2.41
22	Chun and Shin (2014) \diamond	M0.7S \ddagger	1.20	14.9	0.60	0.7	540	564	1.04	1.25	0.100	1.04	1.91
		M1.0S	1.20	14.9	0.60	1.1	970	1068	1.10	1.19	0.090	1.10	2.02
		M1.5S \S	1.18	15.3	0.59	1.7	1689	1872	1.11	1.17	0.060	1.11	2.03
		M2.0S \S	1.21	14.7	0.61	2.4	2448	2580	1.05	1.04	0.050	1.05	1.93
		M2.5S \S	1.21	14.7	0.61	3.1	3183	3264	1.03	0.95	0.035	1.03	1.88
		M0.7U \ddagger	1.15	14.9	0.60	0.7	540	576	1.07	1.46	0.100	1.07	3.23
		M1.0U	1.20	14.9	0.60	1.1	970	1140	1.18	1.26	0.100	1.18	3.56
23	Dhake et al. (2015)	J4 \square	1.61	9.9	0.60	1.0	144	180	1.25	0.31	1.024	1.25	4.75
		J5 \square	1.09	9.9	0.41	1.5	144	157	1.09	0.28	0.768	1.09	4.92
		J9	1.79	9.9	0.60	1.0	144	203	1.41	0.36	1.280	1.41	2.61

* Values given in SI are converted to in.-lb (1 in. = 25.4 mm; 1 psi = 1/145 MPa; and 1 kip = 4.4484 kN); notation described in Appendix A

\diamond Heads contained obstruction with diameter d_{obs} of $1.5d_b$ and length $t_{obs} \leq 0.6d_b$ for \geq No.8 (D25) bars or \leq smaller of 0.6 in. and $0.75d_b$ for $<$ No.8 (D25) bars (also see Section 5.1.7). Therefore, the obstruction is not considered to detract from the net bearing area of the head.

\square Specimens did not contain confining reinforcement parallel to the headed bars within the joint region

\ddagger Analyzed as doubly-reinforced section to calculate M_n ; all other specimens are analyzed as singly-reinforced

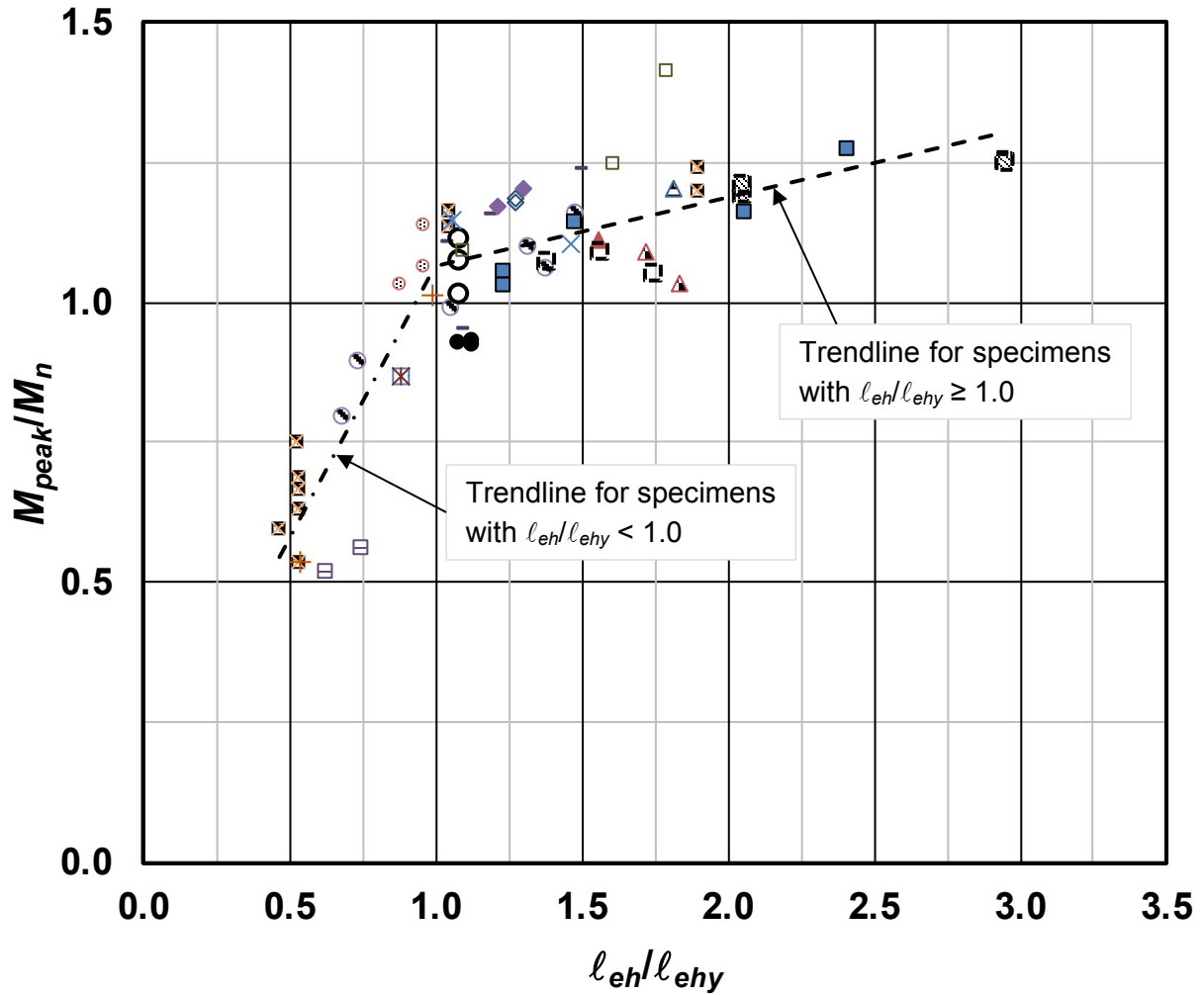
$\ddagger\ddagger$ Specimens contained transverse beams on one or both sides of the test beam. These transverse beams, however, did not meet the dimensional requirements of Section 18.8.4.2 of ACI 318-14 and Section 4.3 of ACI 352R-02 to be considered effective in increasing the joint shear strength.

\S Specimens had $d/\ell_{eh} > 1.5$

The embedment length of headed bars required to yield the bar based on the measured (not specified) yield strength ℓ_{ehy} is calculated using the appropriate descriptive equation, Eq. (4.1) or (4.2), by solving for ℓ_{eh} after replacing T_h with $A_b f_y$. Likewise, the nominal flexural strength M_n of the test beam at an exterior joint (or column at a roof-level interior joint) is calculated based on the measured yield strength using provisions of ACI 318-14. Compression reinforcement is not considered when calculating the nominal flexural strength unless the section is over-reinforced when ignoring such reinforcement, as was the case for specimens No. 102 through No. 104, M8D16, M4D19, M3D19, and M2D22 tested by Murakami et al. (1998); No. 8 tested by Kiyohara et al. (2005); and M0.7S and M0.7U tested by Chun and Shin (2014). These specimens were analyzed as doubly-reinforced sections to calculate M_n . The peak moment M_{peak} applied to a beam at an exterior joint (or column at a roof-level interior joint) during the test is calculated at the beam-column joint interface, which is also the critical section for the headed bars in tension.

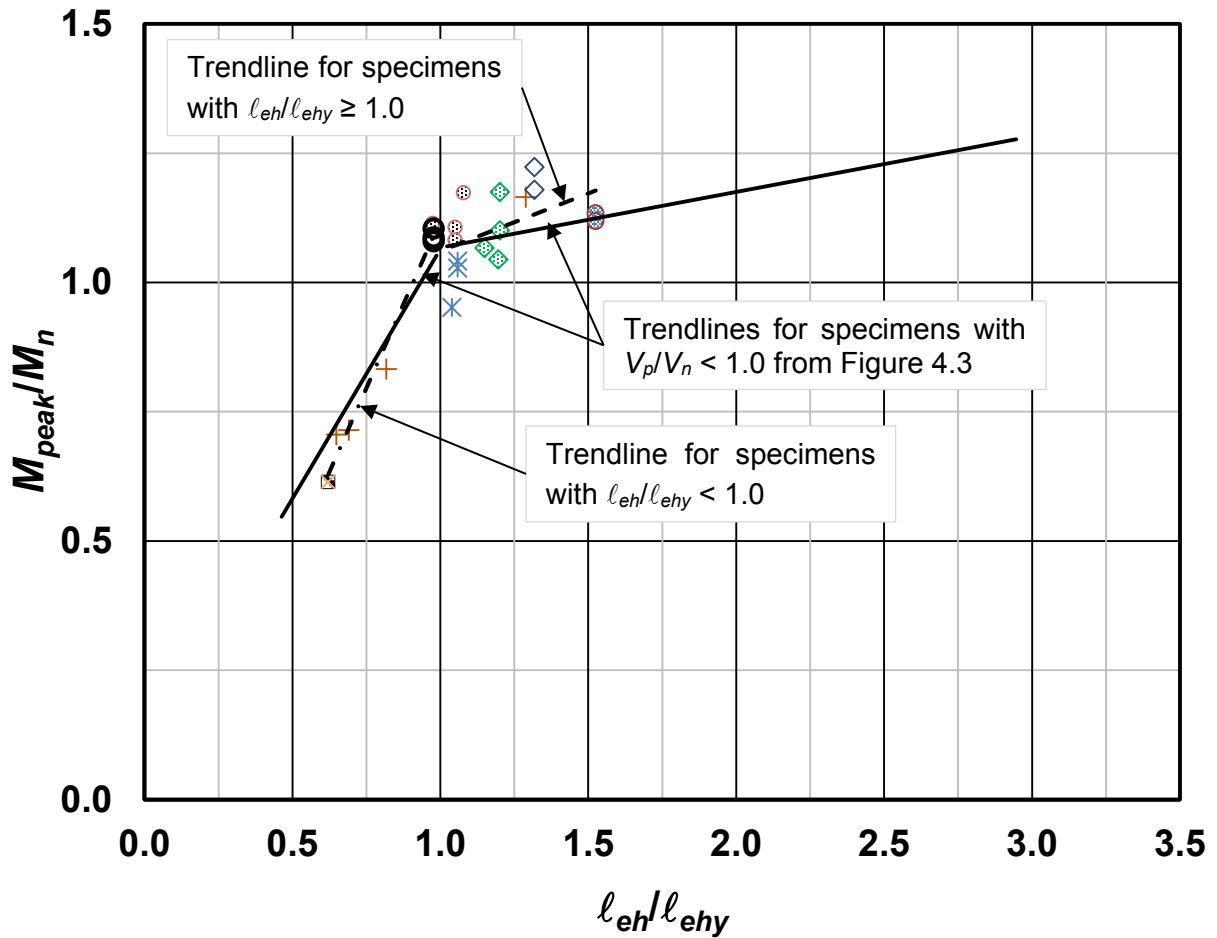
The beam-column joint specimens tested under reversed cyclic loading with a ratio of the peak joint shear to nominal joint shear strength $V_p/V_n < 1.0$ and those with $V_p/V_n \geq 1.0$ are initially analyzed separately because of concern for the potential effect of joint shear on the anchorage performance of the headed bars. The nominal joint shear strength V_n is calculated in accordance with the joint shear strength requirements of Section 18.8.4 of ACI 318-14 as $12\sqrt{f'_c} A_j$, where A_j is an effective cross-sectional area within the beam-column joint in a plane parallel to the headed bars, with an upper limit on f'_c of 10,000 psi. The nominal joint shear strength was also calculated in accordance with Section 4.3 of ACI 352R-02, with an upper limit on concrete compressive strength of 15,000 psi. Values of the nominal joint shear strengths are presented in Table C.2 of Appendix C. The effect of joint shear on the anchorage performance of the headed bar is discussed in detail in Sections 4.2.2.1 and 4.2.2.2. The ratio of the peak moment M_{peak} to the flexural strength M_n is plotted versus the ratio of the actual embedment length of the headed bar ℓ_{eh} to the embedment length required to yield the bar ℓ_{ehy} in Figure 4.3. The figure includes linear trendlines for specimens with (1) $\ell_{eh}/\ell_{ehy} < 1.0$ and (2) $\ell_{eh}/\ell_{ehy} \geq 1.0$. Only specimens with $V_p/V_n < 1.0$ (0.28 to 0.97) are included in the figure. Shao et al. (2016) did not include beam-column joint specimens with a ratio of effective beam depth to embedment length $d/\ell_{eh} > 1.5$ when developing the descriptive and design equations, Eq. (4.1) through (4.3). Therefore, only beam-column joint

specimens with $d/\ell_{eh} \leq 1.5$ (0.7 to 1.5) are included in Figure 4.3; specimens with $d/\ell_{eh} > 1.5$ are analyzed separately in Section 4.2.2.3. The net bearing areas of the headed bars in specimens included in Figure 4.3 ranged from 1.7 to $8.6A_b$. For specimens with high joint shear ($V_p/V_n \geq 1.0$, ranging from 1.02 to 1.82), assumed in this study to undergo significant joint deterioration followed by joint shear failure resulting in poor anchorage performance of the headed bars, M_{peak}/M_n is plotted versus ℓ_{eh}/ℓ_{ehy} in Figure 4.4. The figure includes linear trendlines for specimens with (1) $\ell_{eh}/\ell_{ehy} < 1.0$ and (2) $\ell_{eh}/\ell_{ehy} \geq 1.0$, along with the matching trendlines for specimens with $V_p/V_n < 1.0$ from Figure 4.3. The net bearing areas of the headed bars in specimens included in Figure 4.4 ranged from 3.2 to $5.9A_b$.



- | | |
|---|--|
| × Bashandy (1996) | ⊠ Murakami et al. (1998) |
| ▲ Wallace et al. (1998) | ⊠ Matsushima et al. (2000) |
| ⊠ Tasai et. al (2000) | ● Yoshida et al. (2000) |
| ⊠ Takeuchi et al. (2001) | ⊠ Ishibashi et. al (2003) |
| ⊠ Ishibashi and Inokuchi (2004) | - Kiyohara et al. (2004) |
| + Kiyohara et al. (2005) | ▲ Kato (2005) |
| ⊠ Masuo et al. (2006a, 2006b) | ○ Adachi and Masuo (2007) |
| ■ Chun et. al (2007) | × Ishida et al. (2007) |
| ▲ Tazaki et al. (2007) | ◇ Lee and Yu (2009) |
| ◆ Kang et al. (2012) | □ Dhake et al. (2015) |
| - · - Linear ($l_{eh}/l_{ehy} < 1.0$) | - - - Linear ($l_{eh}/l_{ehy} \geq 1.0$) |

Figure 4.3 M_{peak}/M_n versus l_{eh}/l_{ehy} for specimens with $d/l_{eh} \leq 1.5$ and $V_p/V_n < 1.0$. M_{peak}/M_n is the ratio of peak moment to nominal flexural strength, and l_{eh}/l_{ehy} is the ratio of embedment length to the embedment length required to yield the headed bar calculated using the descriptive equations, Eq. (4.1) and (4.2).



- Murakami et al. (1998)
- Nakazawa et al. (2000)
- Kiyohara et al. (2005)
- Masuo et al. (2006a, 2006b)
- Adachi and Masuo (2007)
- Ishida et al. (2007)
- Lee and Yu (2009)
- Chun and Shin (2014)
- Linear ($l_{eh}/l_{ehy} < 1.0$)
- Linear ($l_{eh}/l_{ehy} \geq 1.0$)
- Linear ($V_p/V_n < 1.0$)

Figure 4.4 M_{peak}/M_n versus l_{eh}/l_{ehy} for specimens with $d/l_{eh} \leq 1.5$ and $V_p/V_n \geq 1.0$. M_{peak}/M_n is the ratio of peak moment to nominal flexural strength, and l_{eh}/l_{ehy} is the ratio of embedment length to the embedment length required to yield the headed bar calculated using the descriptive equations, Eq. (4.1) and (4.2).

Minimum acceptance criteria were established in this study to evaluate the performance of exterior, roof-level interior, and knee beam-column joints subjected to reversed cyclic loading. Specimens were considered to have performed satisfactorily if (1) the ratio of the peak moment to

the nominal flexural strength $M_{\text{peak}}/M_n \geq 1.0$ and (2) the reduction in the peak moment was not more than a 20% at the end of the first complete cycle at 3.5% drift (a ratio of displacement at the loading point in the direction of the load to the distance between the loading point and center of the beam-column joint). Similar acceptance criteria are used in ACI 374.1-05 for weak beam-strong column connections, with the exception that the reduction in the peak moment is permitted to be up to 25% at the end of the *third* complete cycle at 3.5% drift. In addition, as a secondary measure in the current study, an upper limit on joint shear distortion (angular distortion of the joint due to shear calculated from change in length of joint diagonals) Υ_j of 1.2% at 3.5% drift is adopted to distinguish specimens with significant joint deterioration. The same limit on joint shear distortion was also used by Kang et al. (2009). The results shown in Figures 4.3 and 4.4 are discussed next.

4.2.2.1 *Specimens with $d/\ell_{eh} \leq 1.5$ and $\ell_{eh}/\ell_{ehy} < 1.0$*

Exterior beam-column joint specimens with $d/\ell_{eh} \leq 1.5$ tested by Shao et al. (2016) under monotonic loading were used to develop the description equations, Eq. (4.1) and (4.2). Results from beam-column joint specimens tested under reversed cyclic loading with $d/\ell_{eh} \leq 1.5$ and $\ell_{eh}/\ell_{ehy} < 1.0$ are evaluated based on the descriptive equations to investigate the anchorage behavior of the headed bars in these specimens.

Twenty-four exterior beam-column joint specimens with $d/\ell_{eh} \leq 1.5$ (16 with $V_p/V_n < 1.0$ and eight with $V_p/V_n \geq 1.0$) subjected to reversed cyclic loading contained headed bars with embedment lengths ℓ_{eh} less than ℓ_{ehy} calculated using Eq. (4.1) or (4.2). Concrete compressive strengths ranged from 4,100 to 20,130 psi. Headed bar sizes ranged from No. 5 (D16) through No. 9 (D29) with yield strengths ranging from 75,980 to 149,930 psi. Five of the 24 specimens contained headed bars with a yield strength less than 100,000 psi. Clear side concrete cover and minimum center-to-center spacing between the headed bars (minimum of horizontal and vertical spacings) ranged from 2.3 to $3.8d_b$ (2.2 to 3.4 in.) and 2.7 to $8d_b$ (2 to 7.8 in.), respectively. The net bearing areas of headed bars A_{brg} ranged from 2.1 to $5.8A_b$. Two specimens tested by Adachi and Masuo (2007) with $\ell_{eh}/\ell_{ehy} < 1.0$, J30-12-P1 and J30-12-P2, contained transverse beams perpendicular to the test beam at the joint. The transverse beams had widths less than $3/4$ of the effective joint width (defined in Section 18.8.4.3 of ACI 318-14 as the minimum of column width,

beam width plus column depth, and twice the smallest perpendicular distance from beam axis to column sides). Therefore, the transverse beams did not satisfy the minimum dimensional requirement to be considered effective in increasing the joint shear strength in accordance with Section 18.8.4.2 of ACI 318-14.

In Figure 4.3, the trendline for the 16 specimens with $\ell_{eh}/\ell_{ehy} < 1.0$ shows an increase in M_{peak}/M_n with an increase in ℓ_{eh}/ℓ_{ehy} , as expected. This is consistent with the observation made by Shao et al. (2016) that an increase in embedment length increased the anchorage strength of the headed bars. As shown by the trendline in Figure 4.4 ($V_p/V_n \geq 1.0$) for the eight specimens with $\ell_{eh}/\ell_{ehy} < 1.0$, the increase in anchorage strength with an increase in embedment length for those specimens is not significantly different than that for specimens with $V_p/V_n < 1.0$. This indicates that the high joint shear ($V_p/V_n \geq 1.0$) did not have a significant effect on the overall anchorage strength of the headed bars.

Considering Figure 4.3 and Figure 4.4, 16 specimens had $\ell_{eh}/\ell_{ehy} \leq 0.88$ and $M_{peak}/M_n < 1.0$. These specimens exhibited significant joint deterioration, with diagonal cracks between the heads and the compression region of the beam, similar to the failures observed by Shao et al. (2016) for simulated beam-column joints undergoing anchorage failure of headed bars. Headed bars in 15 (of the 16) specimens with $\ell_{eh}/\ell_{ehy} \leq 0.88$ had yield strengths between 104,110 and 149,930 psi and one specimen had a yield strength of 79,900 psi. None of these specimens exhibited flexural hinging within the beam, likely due to embedment lengths that were insufficient to yield the bars. Specimens with embedment lengths ℓ_{eh} ranging from 0.88 to $0.99\ell_{ehy}$ (Adachi and Masuo 2007, Kiyohara et al. 2005, Masuo et al. 2006a, 2006b) had $M_{peak}/M_n \geq 1.0$ with less than a 20% reduction in the peak moment at 3.5% drift. The results shown in Figures 4.3 and 4.4 provide a strong evidence that the descriptive equations Eq. (4.1) and (4.2) are appropriate for members subjected to reversed cyclic loading as well as monotonic loading.

4.2.2.2 Specimens with $d/\ell_{eh} \leq 1.5$ and $\ell_{eh}/\ell_{ehy} \geq 1.0$

Specimens with embedment lengths sufficient to yield the headed bars ($\ell_{eh}/\ell_{ehy} \geq 1.0$) are expected to exhibit post-yield behavior characterized by a slight increase in anchorage strength with an increase in embedment length due to strain hardening of the steel. Beam-column joint

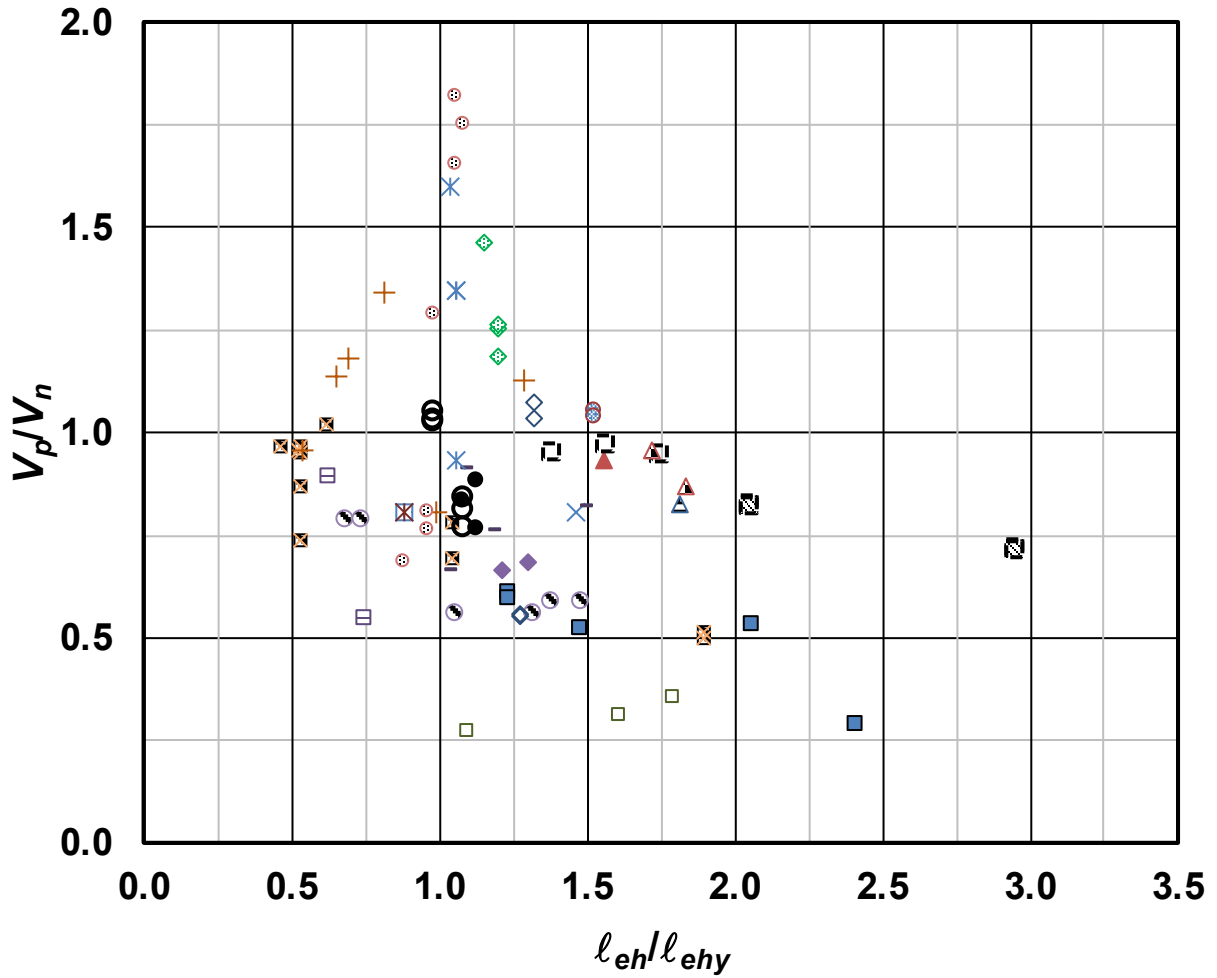
specimens with $\ell_{eh}/\ell_{ehy} \geq 1.0$ subjected to reversed cyclic loading are evaluated based on the descriptive equations to check if such post-yield behavior is realized in these specimens.

Figures 4.3 and 4.4 show the 58 beam-column joint specimens with $\ell_{eh}/\ell_{ehy} \geq 1.0$ (43 with $V_p/V_n < 1.0$ in Figure 4.3 and 15 with $V_p/V_n \geq 1.0$ in Figure 4.4). Four specimens tested by Ishibashi et al. (2003) and three specimens tested by Ishibashi and Inokuchi (2004) were roof-level interior joints. The other specimens were exterior beam-column joints. Concrete compressive strengths ranged from 3,480 to 21,520 psi. Headed bar sizes ranged from No. 4 (D12) through No. 11 (D36) with yield strengths ranging from 53,650 to 103,000 psi. Seven out of the 58 specimens contained headed bars with yield strengths above 100,000 psi. The net bearing area of the headed bars A_{brg} ranged from 1.7 to $8.6A_b$. Clear concrete cover to the bar and minimum center-to-center spacing (minimum of horizontal and vertical spacing) between the headed bars ranged from 1.5 to $9.9d_b$ (0.9 to 8.7 in.) and 2.0 to $7.5d_b$ (1.6 to 8.4 in.), respectively. Seven specimens, one tested by Wallace et al. (1998), two tested by Adachi and Masuo (2007), and four tested by Ishida et al. (2007), contained transverse beams at the joint. The length of the transverse beams measured from the face of the column in specimens tested by Wallace et al. (1998) and Ishida et al. (2007) was less than the overall depth of the beams, and the width of the transverse beams in specimens tested by Adachi and Masuo (2007) was less than $\frac{3}{4}$ of the effective joint width (defined in Section 18.8.4.3 of ACI 318-14 as the minimum of the column width, beam width plus column depth, and twice the smallest perpendicular distance from beam axis to column sides). Therefore, none of the transverse beams satisfied the minimum dimension requirements to be considered effective in increasing the joint shear strength in accordance with Section 18.8.4.2 of ACI 318-14.

The trendline for the 43 specimens with $\ell_{eh}/\ell_{ehy} \geq 1.0$ in Figure 4.3 shows an increase in M_{peak}/M_n with an increase in embedment length, but with a much smaller rate of change with ℓ_{eh}/ℓ_{ehy} compared to the trendline for specimens with $\ell_{eh}/\ell_{ehy} < 1.0$. This is consistent with yielding of the headed bars for $\ell_{eh} \geq \ell_{ehy}$, with the increased strength likely due to strain hardening of the steel. Thirty-eight out of the 43 specimens had $M_{peak}/M_n \geq 1.0$. Of the 38 specimens, 32 exhibited not more than a 20% reduction in the peak moment at about 3.5% drift, while the remaining three roof-level interior joint specimens (2S-2, 2S-0, and WN-ST) tested by Ishibashi and Inokuchi (2004), two exterior joint specimens (J60-12-0 and J60-12-P1) tested by Adachi and Masuo (2007)

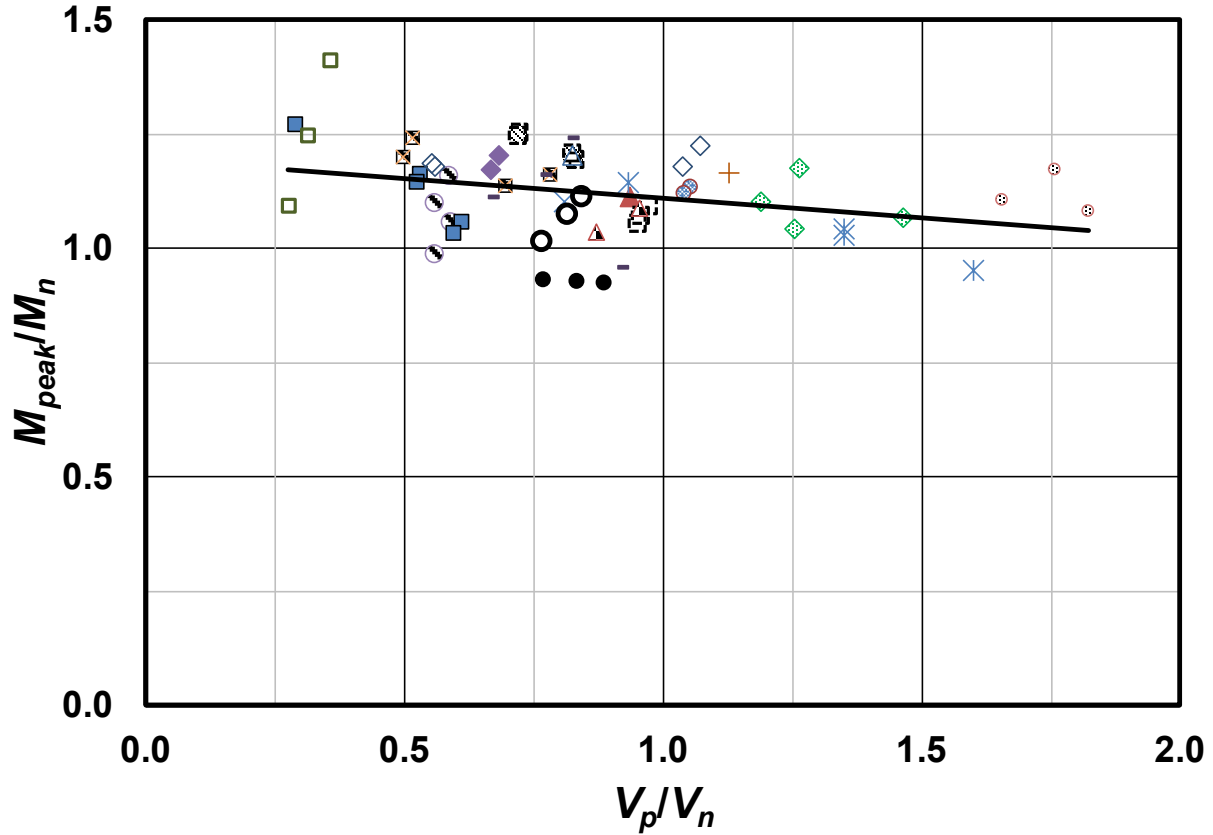
and one exterior joint specimen (P3) tested by Ishida et al. (2007) exhibited 20% reduction in the peak moment at less than 3.5% (3.0 to 3.4%) drift.

Insight into the relationship between M_{peak}/M_n and V_p/V_n is provided by Figures 4.4 through 4.6. In Figure 4.4, the trendlines for the specimens with $V_p/V_n < 1.0$ (trendlines from Figure 4.3) are shown for comparison. As shown in the figure, all but one specimen with $\ell_{eh}/\ell_{ehy} \geq 1.0$ had $M_{peak}/M_n \geq 1.0$. The trendline for specimens with $V_p/V_n \geq 1.0$ and $\ell_{eh}/\ell_{ehy} \geq 1.0$ has a positive slope and is above the trendline for specimens with $V_p/V_n < 1.0$. Over the range of this data, there is little difference between values of the two trendlines. In Figure 4.5, V_p/V_n is plotted versus ℓ_{eh}/ℓ_{ehy} for specimens with $d/\ell_{eh} \leq 1.5$. For values $\ell_{eh}/\ell_{ehy} < 1.0$, there is no clear relationship between V_p/V_n and ℓ_{eh}/ℓ_{ehy} , while for values $\ell_{eh}/\ell_{ehy} \geq 1.0$, V_p/V_n generally decreases with increase in ℓ_{eh}/ℓ_{ehy} . This is likely because as the embedment length increased, the increase in column depth resulted in a greater nominal joint shear strength V_n , which in turn reduced V_p/V_n and presumably improved the response of the specimen to reversed cyclic loading. In Figure 4.6, M_{peak}/M_n is plotted versus V_p/V_n for specimens with $d/\ell_{eh} \leq 1.5$ and $\ell_{eh}/\ell_{ehy} \geq 1.0$. In the figure, the general downward trend in M_{peak}/M_n with increasing V_p/V_n suggests that the increase in M_{peak}/M_n with increase in ℓ_{eh}/ℓ_{ehy} is tied, at least in some extent, to V_p/V_n . At higher values of V_p/V_n , M_{peak}/M_n is clearly associated with deterioration of the joint during cyclic loading.



- | | |
|---------------------------|---------------------------------|
| × Bashandy (1996) | ⊠ Murakami et al. (1998) |
| ▲ Wallace et al. (1998) | ⊠ Matsushima et al. (2000) |
| ⊙ Nakazawa et al. (2000) | □ Tasai et. al (2000) |
| ● Yoshida et al. (2000) | ⊙ Takeuchi et al. (2001) |
| ⊠ Ishibashi et. al (2003) | □ Ishibashi and Inokuchi (2004) |
| - Kiyohara et al. (2004) | + Kiyohara et al. (2005) |
| ▲ Kato (2005) | ⊙ Masuo et al. (2006a, 2006b) |
| ○ Adachi and Masuo (2007) | ■ Chun et. al (2007) |
| × Ishida et al. (2007) | ▲ Tazaki et al. (2007) |
| ◇ Lee and Yu (2009) | ◆ Kang et al. (2012) |
| ◇ Chun and Shin (2014) | □ Dhake et al. (2015) |

Figure 4.5 V_p/V_n versus l_{eh}/l_{ey} for specimens with $d/l_{eh} \leq 1.5$. V_p/V_n is the ratio of peak joint shear to nominal joint shear strength, and l_{eh}/l_{ey} is the ratio of embedment length to the embedment length required to yield the headed bar calculated using the descriptive equations, Eq. (4.1) and (4.2).



- × Bashandy (1996)
- ▲ Wallace et al. (1998)
- Yoshida et al. (2000)
- ▣ Ishibashi et al. (2003)
- Kiyohara et al. (2004)
- ▲ Kato (2005)
- Adachi and Masuo (2007)
- × Ishida et al. (2007)
- ◇ Lee and Yu (2009)
- ◆ Chun and Shin (2014)
- Linear trendline
- ▣ Murakami et al. (1998)
- Nakazawa et al. (2000)
- Takeuchi et al. (2001)
- ▣ Ishibashi and Inokuchi (2004)
- + Kiyohara et al. (2005)
- Masuo et al. (2006a, 2006b)
- Chun et al. (2007)
- ▲ Tazaki et al. (2007)
- ◆ Kang et al. (2012)
- Dhake et al. (2015)

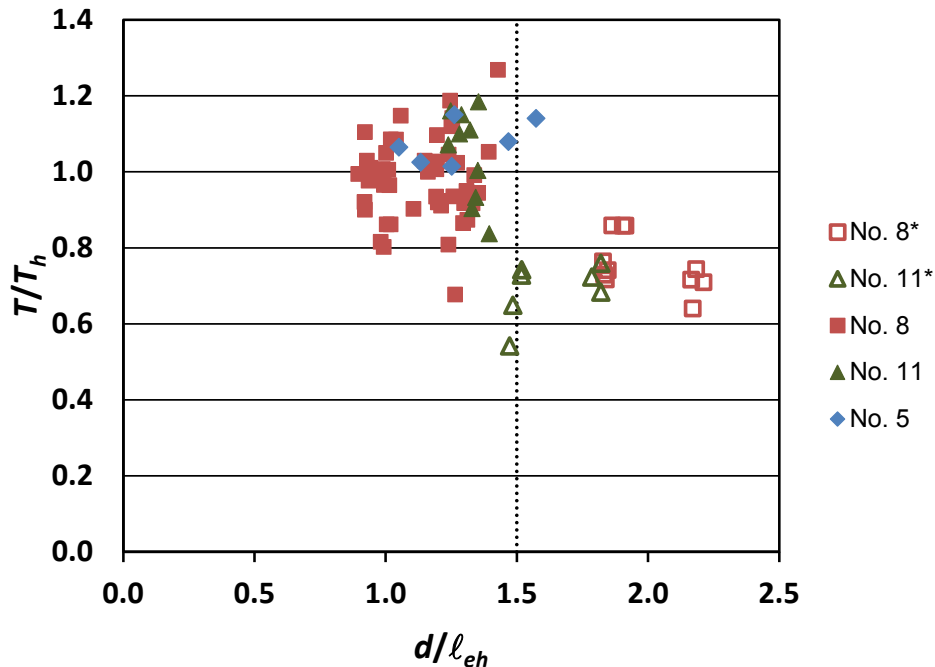
Figure 4.6 M_{peak}/M_n versus V_p/V_n for specimens with $d/\ell_{eh} \leq 1.5$ and $\ell_{eh}/\ell_{ehy} \geq 1.0$. M_{peak}/M_n is the ratio of peak moment to nominal flexural strength, and V_p/V_n is the ratio of peak joint shear to nominal joint shear strength.

4.2.2.3 Specimens with $d/\ell_{eh} > 1.5$

Monotonic loading: Exterior beam-column joint specimens with a ratio of effective beam depth to embedment length $d/\ell_{eh} > 1.5$ tested by Shao et al. (2016) under monotonic loading exhibited 10 to 25% lower anchor strength than the specimens with $d/\ell_{eh} \leq 1.5$. These specimens

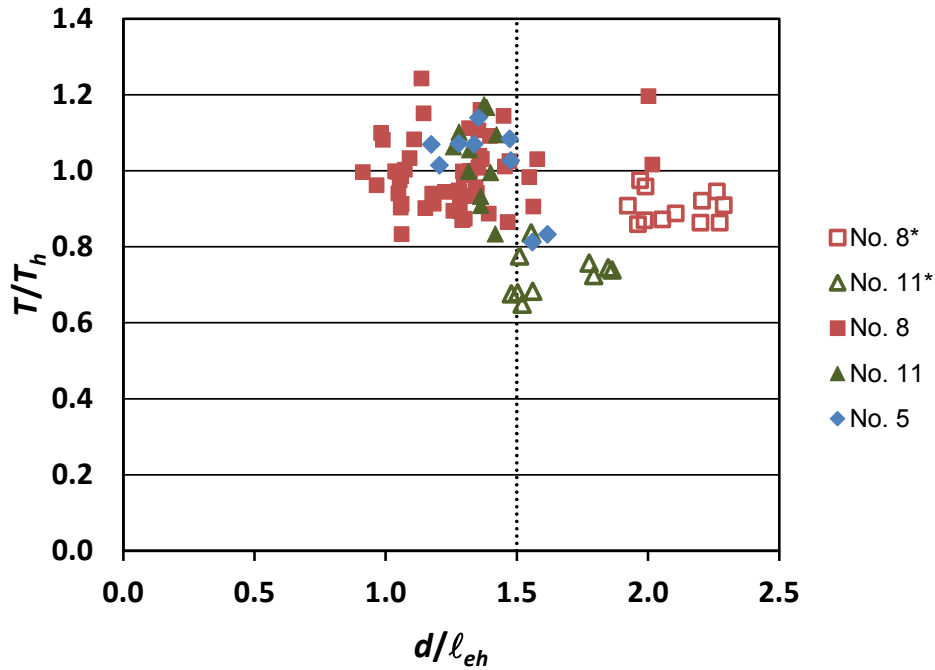
were not used to develop the descriptive equations, Eq. (4.1) and Eq. (4.2). In this section, the beam-column joint specimens tested under reversed cyclic loading with $d/\ell_{eh} > 1.5$ are analyzed to investigate if the joint performance was affected because d/ℓ_{eh} was greater than 1.5.

In Figures 4.7 and 4.8, the values of test-to-calculated strength ratio T/T_h are plotted versus d/ℓ_{eh} for specimens without and with confining reinforcement, respectively, tested by Shao et al. (2016) under monotonic loading. T is the average load on headed bars at failure and T_h is the anchorage strength calculated using Eq. (4.1) or Eq. (4.2). The specimens contained headed bars with $3.8A_b \leq A_{brg} \leq 9.5A_b$. In Figure 4.9, the values of T/T_h are plotted versus confining reinforcement ratio A_{tt}/A_{hs} , where A_{hs} is the total cross-sectional area of headed bars being developed, and A_{tt} is the total cross-sectional area of all confining reinforcement parallel to ℓ_{eh} for headed bars being developed in beam-column joints and located within $8d_b$ of the top of the headed bars in direction of the interior of the joint for No. 3 through No. 8 headed bars or within $10d_b$ of the top of the bar in direction of the interior of the joint for No. 9 through No. 11 (see Figure 4.2). An upper limit on A_{tt}/A_{hs} of 0.3 (Table 4.1) is used when applying Eq. (4.2) to calculate T_h as $A_{tt}/n \leq 0.3A_b$.



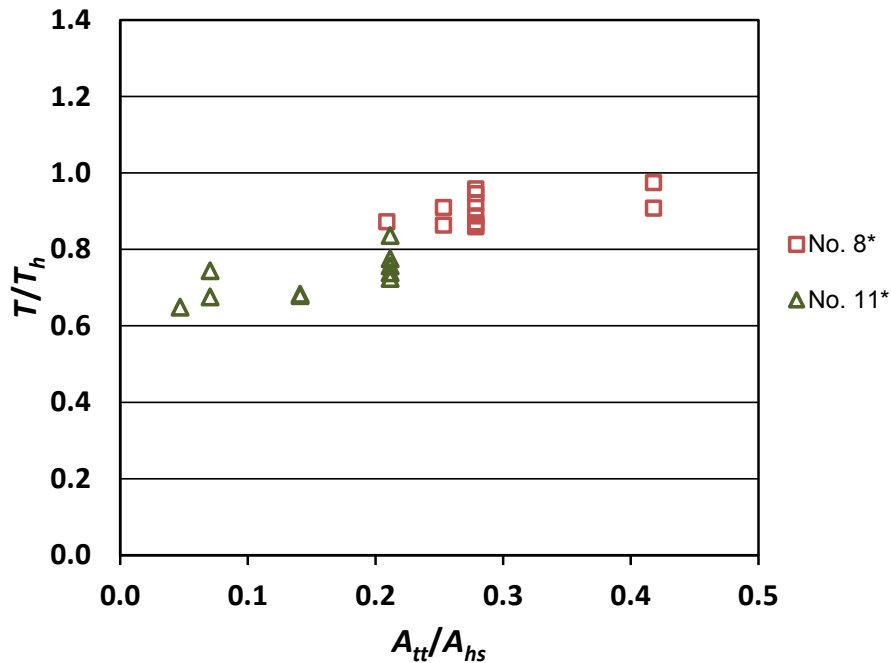
* Specimens not used to develop the descriptive equations [Eq. (4.1) and (4.2)]

Figure 4.7 Ratio of test-to-calculated failure load T/T_h versus ratio of effective beam depth to embedment length d/ℓ_{eh} for specimens without confining reinforcement [T_h is calculated using Eq. (4.1)] (Shao et al. 2016)



* Specimens not used to develop the descriptive equations [Eq. (4.1) and (4.2)]

Figure 4.8 Ratio of test-to-calculated failure load T/T_h versus ratio of effective beam depth to embedment length d/l_{eh} for specimens with confining reinforcement [T_h is calculated using Eq. (4.2)] (Shao et al. 2016)



* Specimens not used to develop the descriptive equations [Eq. (4.1) and (4.2)]

Figure 4.9 Ratio of test-to-calculated failure load T/T_h versus normalized confining reinforcement A_{tt}/A_{hs} for specimens with $d/l_{eh} \geq 1.5$ [T_h is calculated from Eq. (4.2)] (Shao et al. 2016)

As shown in Figures 4.7 and 4.8, specimens without and with confining reinforcement with $d/\ell_{eh} > 1.5$ exhibited about 25 and 10% decreases in anchorage strength on average, respectively, compared to the specimens with $d/\ell_{eh} \leq 1.5$. As shown in Figure 4.9, however, decrease in anchorage strength is progressively less as the amount of confining reinforcement increases. Given these observations, the beam-column joint specimens tested under reversed cyclic loading are also investigated to see if the joint performance was affected by d/ℓ_{eh} being greater than 1.5 and the quantity of confining reinforcement within the joint region.

Reversed cyclic loading: Nine out of the 91 beam-column joint specimens tested under reversed cyclic loading (see Table 4.2) had a ratio of effective beam depth to embedment length $d/\ell_{eh} > 1.5$, with values ranging from 1.6 to 3.1. These included specimens HS tested by Matsushima et al. (2000), No. 5 tested by Kiyohara et al. (2004), No. 10 tested by Kiyohara et al. (2005), AH12-2-45A tested by Masuo et al. (2006a, 2006b), E2 tested by Tazaki et al. (2007), JD tested by Kang et al. (2010), and M1.5S, M2.0S, and M2.5S tested by Chun and Shin (2014). Five of the specimens had $\ell_{eh}/\ell_{ehy} \geq 1.0$, and four had $\ell_{eh}/\ell_{ehy} < 1.0$. Concrete compressive strengths ranged from 3,480 to 18,820 psi. The headed bars were No. 5 (D16), No. 6 (D19), No. 8 (D25), and No. 9 (D29) with yield strengths ranging from 54,960 to 149,930 psi. The net bearing area of the headed bars A_{brg} ranged from 2.6 to $6.9A_b$. Clear side concrete cover and minimum center-to-center spacing between the headed bars (minimum of horizontal and vertical spacings) ranged from 1.7 to $3.9d_b$ (1.1 to 3.3 in.) and 2.3 to $8d_b$ (1.6 to 7.8 in.), respectively. Five out of the nine specimens contained headed bars terminated at 50 to 53% of the column depth, one specimen tested by Kang et al. (2010) contained headed bars terminated at 64% of the column depth, and the remaining three specimens tested by Chun and Shin (2014) contained headed bars terminated at 75% of the column depth.

For the nine specimens, the values of the joint confining reinforcement ratio A_{tt}/A_{hs} , defined in Section 4.2.1, in specimens with $\ell_{eh}/\ell_{ehy} \geq 1.0$ tested by Tazaki et al. (2007) and Kang et al. (2010) were 0.05 and 0.25, respectively, while that in three specimens tested by Chun and Shin (2014) was 0.58 [greater than the upper limit of 0.3 on A_{tt}/A_{hs} allowed to use in descriptive equation Eq. (4.2)]. The other specimens with $\ell_{eh}/\ell_{ehy} < 1.0$ had A_{tt}/A_{hs} ranging from 0.11 to 0.20. The effect

of d/ℓ_{eh} and confining reinforcement within the joint region on the performance of the nine specimens is discussed next.

In accordance with Section R25.4.4.2 of ACI 318-14, for the headed bars in tension in exterior beam-column joints with $d/\ell_{eh} > 1.5$, a concrete breakout failure can be precluded by “providing reinforcement in the form of hoops and ties to establish a load path in accordance with strut-and-tie modeling principles.” To check if there was sufficient confining reinforcement within the joint to prevent concrete breakout failure, anchorage strengths of headed bars with $d/\ell_{eh} > 1.5$ are calculated using the strut-and-tie modeling approach. In this approach, all confining reinforcement within the joint region (not the effective confining reinforcement A_{tt}) is assumed to serve as a single tie with total force of $f_{yt}A_v$ (Figure 4.10) to transfer the force in the headed bars nT' to the compression region of the beam, where f_{yt} is the yield strength of the confining reinforcement (ksi), A_v is the total area of confining reinforcement parallel to the headed bar (in.²), n is the number of headed bars in tension, and T' is the estimated peak force (kips) in each headed bar. The force in the headed bar was not measured directly during the tests and strain measurements at the critical section were available only for nine specimens. The peak force in each headed bar T' is, therefore, approximated using Eq. (4.4).

$$T' = \frac{M_{peak}}{M_n} A_b f_y \quad (4.4)$$

where M_{peak} = peak moment calculated at the beam-column joint interface (kip-in.); M_n = nominal flexural strength (kip-in.); A_b = area of a single headed bar (in.²); and f_y = yield strength of the headed bar (ksi).

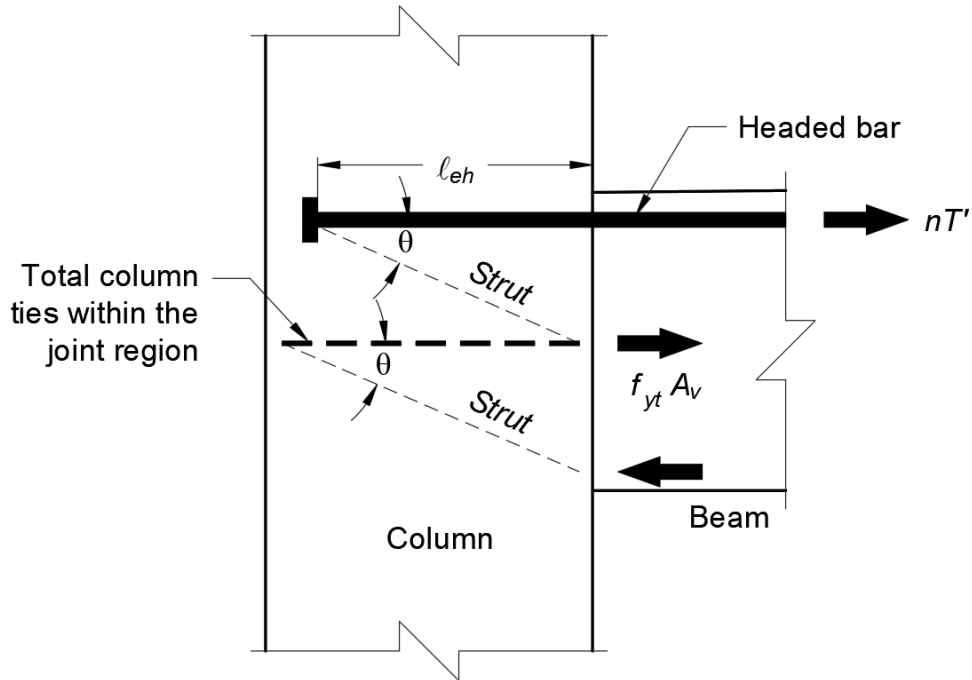


Figure 4.10 Load transfer within the beam-column joint based on strut-and-tie mechanism (column longitudinal reinforcement and beam compression reinforcement are not shown for clarity)

Specimens with $f_{yt} A_v \geq nT$ are considered to have adequate confining reinforcement within the joint region to transfer load through strut-and-tie mechanism. Results from this analysis are presented in Table C.2 of Appendix C. Of the nine specimens, only the three tested by Chun and Shin (2014) (M1.5S, M2.0S, and M2.5S) had $f_{yt} A_v > nT'$. These specimens had ℓ_{eh}/ℓ_{ehy} of 1.18 and 1.21, and a peak shear V_p at the joint equal to 0.95 to 1.17 times the nominal joint shear strength V_n calculated in accordance with the joint shear strength requirements of Section 18.8.4 of ACI 318-14. In the three specimens, M_{peak}/M_n decreased slightly, from 1.11 to 1.03, as d/ℓ_{eh} increased from 1.7 to 3.1. Flexural cracks appeared at the beam-column joint interface at 0.2% drift followed by diagonal cracks at higher drift levels, depending on the value of d/ℓ_{eh} ; the diagonal cracks appeared at lower drift levels as the d/ℓ_{eh} increased. Significant joint deterioration accompanied by substantial spalling of concrete was observed for the three specimens, which was likely due to the high joint shear. The joint shear distortion reported in specimen M1.5S was 1.7% (greater than 1.2%), which also indicates significant joint distress (the distortion values were not reported for specimens M2.0S and M2.5S). These observations, therefore, suggest that the slight decrease in joint strength, M_{peak}/M_n , from 1.11 to 1.03, of these three specimens may be due to a combination of increased joint shear (Figures 4.6) and increase in d/ℓ_{eh} from 1.7 to 3.1. For the specimens with

$d/\ell_{eh} > 1.5$, M_{peak}/M_n is plotted versus ℓ_{eh}/ℓ_{ehy} in Figure 4.10. In the figure, trendlines for the specimens with $d/\ell_{eh} \leq 1.5$ are shown, along with the trendlines for the specimens with $d/\ell_{eh} > 1.5$ for comparison. Of the three specimens tested by Chun and Shin (2014), only the one with d/ℓ_{eh} of 1.7 is above the trend line for specimens with $d/\ell_{eh} \leq 1.5$. Performance of other specimens which had $f_{yt}A_v < nT'$ is discussed next.

In Figure 4.11, for values $\ell_{eh}/\ell_{ehy} < 1.0$, the trendline for specimens with $d/\ell_{eh} > 1.5$ is above and parallel to the trendline for the specimens with $d/\ell_{eh} \leq 1.5$, while for values $\ell_{eh}/\ell_{ehy} \geq 1.0$, the trendline for specimens with $d/\ell_{eh} > 1.5$ is slightly below and almost parallel to the trendline for the specimens with $d/\ell_{eh} \leq 1.5$. All specimens with $\ell_{eh}/\ell_{ehy} \geq 1.0$, including the specimens tested by Tazaki et al. (2007) and Kang et al. (2010), which did not have sufficient confining reinforcement to transfer bar force to the compression region of the beam based on strut-and-tie modeling approach (that is, $f_{yt}A_v < nT'$), had values of $M_{peak}/M_n \geq 1.0$ and exhibited not more than a 20% reduction in the peak moment at 3.5% drift. These results show that given $\ell_{eh} > \ell_{ehy}$, the performance of specimens, including those with $f_{yt}A_v < nT'$, under reversed cyclic loading was not significantly affected in case where d/ℓ_{eh} was greater than 1.5 (up to the maximum value in the tests, 3.1).

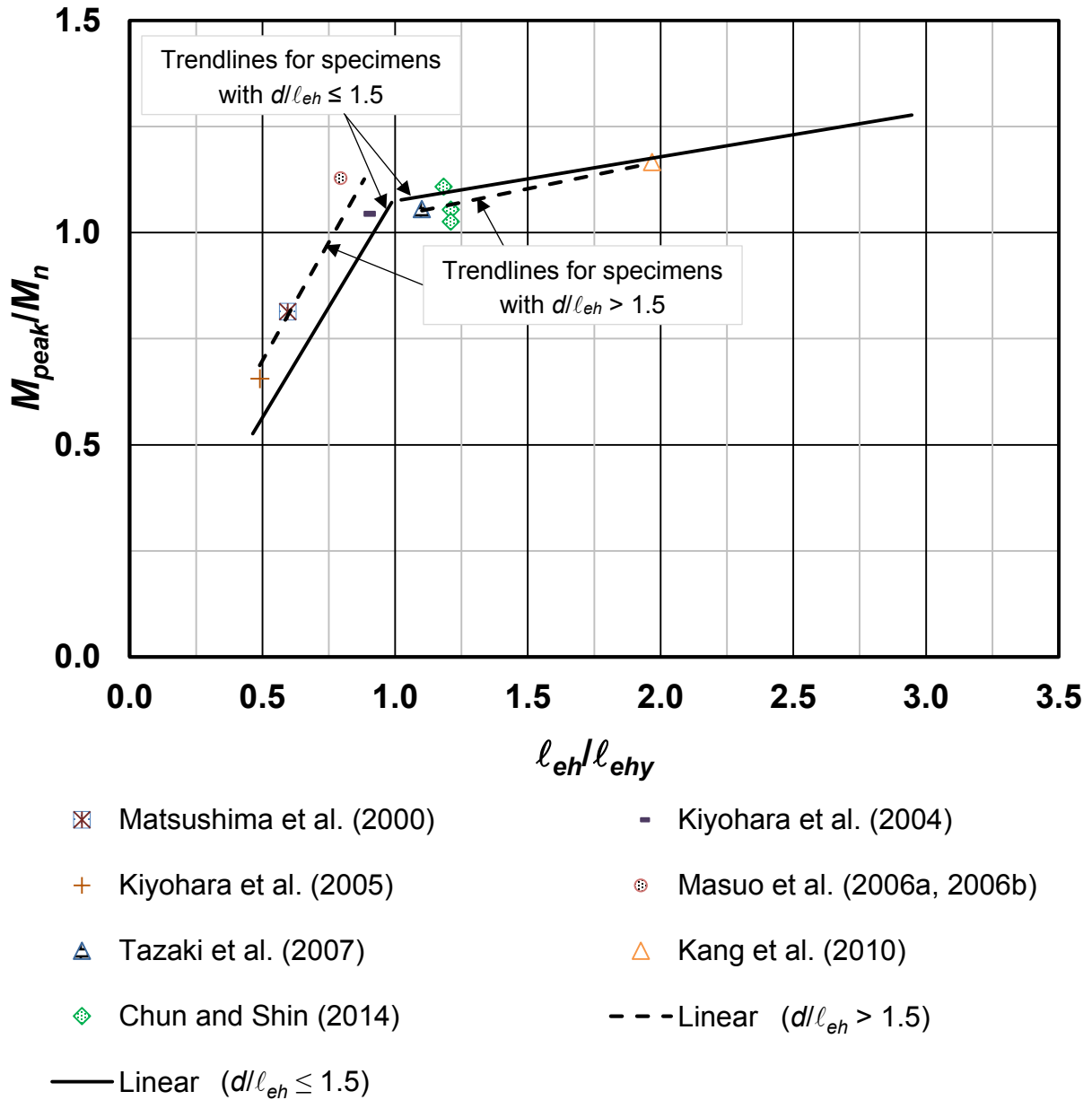


Figure 4.11 M_{peak}/M_n versus l_{eh}/l_{ehy} for specimens with $d/l_{eh} > 1.5$. M_{peak}/M_n is the ratio of peak moment to nominal flexural strength, and l_{eh}/l_{ehy} is the ratio of embedment length to the embedment length required to yield the headed bar calculated from Eq. (4.1) or (4.2).

4.2.2.4 Headed bar spacing

ACI 318-14 specifies a minimum clear spacing of $4d_b$ (center-to-center spacing of $5d_b$) between the headed bars being developed. This minimum clear spacing is specified based on the lower limit on clear spacing between the headed bars used in headed bar splice tests (Thompson et al. 2006b). Section 18.8.5.2 of ACI 318-14, however, allows the minimum clear spacing between the headed bars to be $3d_b$ (center-to-center spacing of $4d_b$) for joints in special moment

frames. These minimum spacing limits for headed bars are significantly greater than the spacing permitted between straight bars in heavily reinforced members in which the clear spacing can be as low as $1d_b$ or 1 in., whichever is greater. The newly proposed descriptive and design equations [Eq. (4.1) through (4.3)], however, account for the spacing between the bars without specifying a minimum limit. In accordance with Section 25.2 of ACI 318-14, the minimum vertical clear spacing between beam bars is greatest of 1 in. and $4/3$ of the maximum size aggregate, and the minimum horizontal spacing between bars is the greatest of $1d_b$, 1 in., and $4/3$ of the maximum size aggregate. For column longitudinal bars, the minimum clear spacing is the greatest of $1.5d_b$, 1.5 in., and $4/3$ of the maximum size aggregate.

Shao et al. (2016) tested beam-column joint specimens under monotonic loading with center-to-center spacing between the headed bars of $2.9d_b$ (clear spacing of $1.9d_b$). Those tests contributed to the development of the descriptive and design equations, Eq. (4.1) through (4.3), which account for spacing between the headed bars with center-to-center spacing as low as $2d_b$ (clear spacing of $1d_b$). Headed bar splice specimens tested in the current study (see Section 3.2) had center-to-center spacing between the bars ranging from 1.67 to $3.53d_b$. These specimens exhibited adequate splice strength, and Eq. (4.1) through (4.3) provide a conservative representation of the test results.

In the exterior and roof-level interior beam-column joint specimens subjected to reversed cyclic loading being evaluated in this chapter, the center-to-center spacing c_{ch} (minimum of horizontal spacing s_h and vertical spacing s_v) between the headed bars ranged from 2 to $8d_b$. The effect of bar spacing on the anchorage performance of headed bars in these specimens is investigated by comparing the bar force at failure with the bar force predicted by the descriptive equations. The force in the headed bars at failure T' (kips) is estimated using Eq. (4.4), and the anchorage strength T_h (kips) is calculated using the descriptive equations, Eq. (4.1) and (4.2), which account for the bar spacing without specifying a minimum limit. The descriptive equations, which include the effects of bar spacing, give an *average* ratio of test-to-calculated failure load equal to 1.0. Thus, the equations can be considered to have effectively captured the spacing effect on the anchorage performance of headed bars subjected to reversed cyclic loading if the average ratio of test to calculated bar force at failure is greater than or equal to 1.0.

Twenty-eight specimens tested under reversed cyclic loading had $\ell_{eh}/\ell_{ehy} < 1.0$. The center-to-center spacing c_{ch} in these specimens ranged from 2.7 to $8d_b$. The net bearing area A_{brg} of the headed bars ranged from 2.1 to $5.8A_b$ (effect of head size is discussed in Section 4.3). Of the 28 specimens, 18 had c_{ch} between 2.7 and $3.3d_b$ (less than $4d_b$, minimum center-to-center spacing permitted for joints in special moment frames in accordance with Section 18.8.5.2 of ACI 318-14). Statistical parameters, including maximum, minimum, mean, standard deviation (STD), and coefficient of variation (COV), of T'/T_h for the specimens with $\ell_{eh}/\ell_{ehy} < 1.0$ are presented in Table 4.3. The values of T'/T_h for the 28 specimens with $\ell_{eh}/\ell_{ehy} < 1.0$ ranged between 0.74 and 1.43 with an average, STD, and COV of 1.13, 0.158, and 0.139, respectively. Of the 28 specimens, the values of T'/T_h for 18 specimens with $c_{ch} < 4d_b$ ranged between 0.83 and 1.32 with an average, STD, and COV of 1.11, 0.126, and 0.114, respectively. For comparison, the statistical parameters for the 10 beam-column joint specimens containing confining reinforcement with $c_{ch} < 4d_b$ tested under monotonic loading by Shao et al. (2016) are also presented in Table 4.3. These specimens contributed to the development of the descriptive equations. Only specimens containing confining reinforcement were considered because all specimens tested under reversed cyclic loading with $\ell_{eh}/\ell_{ehy} < 1.0$ contained confining reinforcement within the joint region. The ratio of test to calculated failure load of headed bars T'/T_h with $c_{ch} < 4d_b$ in the specimens tested by Shao et al. (2016) ranged from 0.83 to 1.15 with an average, STD, and COV of 1.00, 0.107, and 0.108, respectively. These results indicate that the descriptive equations effectively capture the anchorage behavior of the headed bars with $\ell_{eh}/\ell_{ehy} < 1.0$ subjected to reversed cyclic loading, including those with $c_{ch} < 4d_b$.

Table 4.3 Statistical parameters for test-to-calculated ratio in beam-column joint specimens with $\ell_{eh}/\ell_{ehy} < 1.0$ tested under reversed cyclic loading and in beam-column joint specimens containing confining reinforcement tested under monotonic loading by Shao et al. (2016)

Statistical Parameters	T'/T_h		T/T_h
	All specimens with $\ell_{eh}/\ell_{ehy} < 1.0$	Specimens with $\ell_{eh}/\ell_{ehy} < 1.0$ and $c_{ch} < 4d_b$	Specimens containing confining reinforcement with $c_{ch} < 4d_b$ tested by Shao et al. (2016)
Number of specimens with $\ell_{eh}/\ell_{ehy} < 1.0$	28	18	10
Max	1.43	1.32	1.15
Min	0.74	0.83	0.83
Mean	1.13	1.11	1.00
STD	0.158	0.126	0.107
COV	0.139	0.114	0.108

A similar analysis was conducted for the specimens with $\ell_{eh}/\ell_{ehy} \geq 1.0$ tested under reversed cyclic loading. Sixty-three specimens had $\ell_{eh}/\ell_{ehy} \geq 1.0$. The net bearing area A_{brg} of the headed bars ranged from 1.7 to $8.6A_b$ (effect of head size is discussed in detail in Section 4.3). The center-to-center spacing c_{ch} in these specimens ranged from 2 to $11.2d_b$. Thirty-five out of the 63 specimens had c_{ch} between 2 and $3.7d_b$ (less than the $4d_b$ minimum center-to-center spacing permitted in Section 18.8.5.2 of ACI 318-14 for joints in special moment frames). Of the 35 specimens, all but four specimens had $M_{peak}/M_n \geq 1.0$. The statistical parameters, including maximum, minimum, mean, standard deviation (STD), and coefficient of variation (COV), of T'_{mod}/T_h for the specimens with $\ell_{eh}/\ell_{ehy} \geq 1.0$ are presented in Table 4.4. T'_{mod} is the modified bar force at failure T' corresponding to the projected value of M_{peak}/M_n on $\ell_{eh}/\ell_{ehy} = 1.0$ line by extending a line parallel to the trend line for specimens with $\ell_{eh}/\ell_{ehy} \geq 1.0$, as shown in Figure 4.12 for one specimen, and calculated using Eq. (4.5). The anchorage strength of the headed bar T_h (kips) is calculated using the descriptive equations [Eq. (4.1) and (4.2)], corresponding to $\ell_{eh} = \ell_{ehy}$ as for T'_{mod} .

$$T'_{mod} = \left(\frac{M_{peak}}{M_n} \right)_{mod} A_b f_y \quad (4.5)$$

$$\text{with } \left(\frac{M_{peak}}{M_n} \right)_{mod} = \frac{M_{peak}}{M_n} - 0.122 \left(\frac{\ell_{eh}}{\ell_{ehy}} - 1 \right)$$

where the coefficient of 0.122 is the slope of the trendline for specimens with $\ell_{eh}/\ell_{ehy} \geq 1.0$ in Figure 4.12. An example of calculating $(M_{peak}/M_n)_{mod}$ is shown graphically in Figure 4.12.

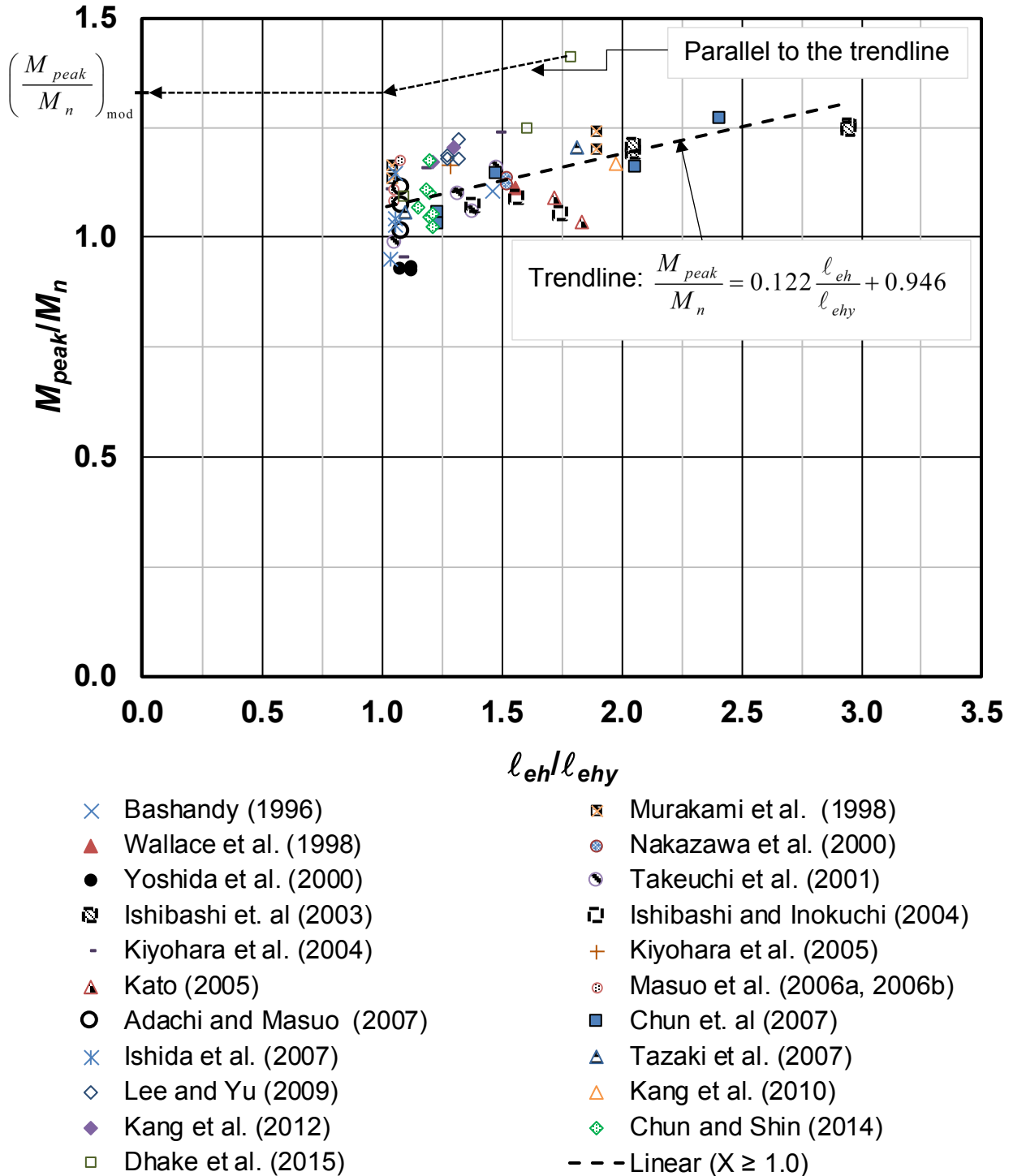


Figure 4.12 M_{peak}/M_n versus ℓ_{eh}/ℓ_{ehy} for exterior and roof-level interior beam-column joint specimens with $\ell_{eh}/\ell_{ehy} \geq 1.0$. M_{peak}/M_n is the ratio of peak moment to nominal flexural strength, and ℓ_{eh}/ℓ_{ehy} is the ratio of embedment length to the embedment length required to yield the headed bar calculated using the descriptive equations, Eq. (4.1) and (4.2).

As shown in the table, the values of T'_{mod}/T_h for the 63 specimens with $\ell_{eh}/\ell_{ehy} \geq 1.0$ ranged between 0.91 and 1.32, with an average, STD, and COV of 1.07, 0.077, and 0.072, respectively. Of the 63 specimens, the values of T'_{mod}/T_h for the 35 specimens with $c_{ch} < 4d_b$ ranged between 0.91 and 1.18 with an average, STD, and COV of 1.07, 0.077, and 0.072, respectively, indicating that the descriptive equations effectively capture the anchorage behavior of the headed bars with $\ell_{eh}/\ell_{ehy} \geq 1.0$ subjected to reversed cyclic loading, including those with $c_{ch} < 4d_b$.

Table 4.4 Statistical parameters for T'_{mod}/T_h in beam-column joint specimens with $\ell_{eh}/\ell_{ehy} \geq 1.0$ tested under reversed cyclic loading

Statistical Parameters	T'_{mod}/T_h	
	All specimens with $\ell_{eh}/\ell_{ehy} \geq 1.0$	Specimens with $\ell_{eh}/\ell_{ehy} \geq 1.0$ and $c_{ch} < 4d_b$
Number of specimens with $\ell_{eh}/\ell_{ehy} < 1.0$	63	35
Max	1.32	1.18
Min	0.91	0.91
Mean	1.07	1.07
STD	0.077	0.077
COV	0.072	0.072

4.2.2.5 Summary

In general, exterior and roof-level interior beam-column joints subjected to reversed cyclic loading exhibited an increase in strength with an increase in embedment length. The rate of increase in strength was approximately proportional to the increase in ℓ_{eh}/ℓ_{ehy} when $\ell_{eh}/\ell_{ehy} < 1.0$ but much lower where $\ell_{eh}/\ell_{ehy} \geq 1.0$. As discussed in Section 4.2.2.2, the lower rate resulted from yielding and subsequent strain hardening of the steel in members where $\ell_{eh}/\ell_{ehy} \geq 1.0$. As shown in Figures 4.3 and 4.4, and discussed in Section 4.2.2.4, the descriptive equations, Eq. (4.1) and (4.2), which were developed based on test results for exterior beam-column joints under monotonic loading, effectively capture the anchorage behavior of the headed bars subjected to reversed cyclic loading in terms of embedment length and bar spacing, independent of whether the bars yielded. As discussed in Section 4.2.2.3, results from a limited number of specimens show that given $\ell_{eh} > \ell_{ehy}$, the performance of specimens, including those with $f_{yt}A_v < nT'$, under reversed cyclic loading was not significantly affected when $d/\ell_{eh} > 1.5$ (up to the maximum value in the tests, 3.1).

4.2.3 Knee Beam-Column Joints

Seven knee beam-column joint specimens, three tested by Wallace et al. (1998) and four tested by Chun et al. (2007), did not perform satisfactorily under reversed cyclic loading. These specimens, in which both beam and column reinforcement were anchored at the joint using headed bars, reached the peak moment between 74 and 86% of the nominal flexural strength of the connecting members during opening cycles (top bars in compression) and had more than a 20% reduction in the peak moment at 3.5% drift during closing cycles (top bars in tension). Such poor performance was likely because of inadequate reinforcement detailing within the joint region. As a result, the reinforcement within the joint did not effectively arrest the cracks radiating inward from the inside corner of the joint during opening cycles and joint lost strength as the cover concrete pried out on the top free surface of the beam during closing cycles. In this section, the knee beam-column joint specimens tested by Wallace et al. (1998) and Chun et al. (2007) are analyzed based on the descriptive equations, Eq. (4.1) and (4.2), and results from tests of knee beam-column joints by Nilsson and Losberg (1976). Specimen details are presented in Table 4.5. Complete details of specimens and analysis results are provided in Table C.3 of Appendix C.

Table 4.5 Detail of knee beam-column joint specimens

Study	Specimen	Loading Direction	Bar Size*	$\frac{A_{gross}}{A_b}$	$\frac{A_{obs}}{A_b}$	$\frac{A_{brg}}{A_b}$	$\frac{t_{obs}}{d_b}$	f_y (ksi)	f_{cm} (psi)	c_{so}^{**} (in.)	$\frac{c_{ch}}{d_b}$	$\frac{A_{tt}}{A_{hs}}$
Wallace et al. (1998)	KJ16	Closing	D16	12.4	-	11.4	0.0	70.6	5390	1.1	4.3	0.27
		Opening	D16	12.4	-	11.4	0.0	70.6	5390	1.1	4.3	0.27
	KJ17	Closing	D16	12.4	-	11.4	0.0	70.6	5450	1.1	4.3	0.27
		Opening	D16	12.4	-	11.4	0.0	70.6	5450	1.1	4.3	0.27
	KJ18	Closing	D20	8.0	-	7.0	0.0	77.2	5540	1.1	3.4	0.17
		Opening	D20	8.0	-	7.0	0.0	77.2	5540	1.1	3.4	0.17
Chun et al. (2007) §	JMT-No. 11-1a	Closing	D36	4.9	2.2	2.7	0.7	67.9	6060	3.1	8.8	1.19
		Opening	D36	4.9	2.2	2.7	0.7	67.9	6060	3.1	8.8	1.19
	JMT-No. 11-1b	Closing	D36	4.9	2.2	2.7	0.7	67.9	6060	3.1	8.8	1.19
		Opening	D36	4.9	2.2	2.7	0.7	67.9	6060	3.1	8.8	1.19
	JMT-No. 11-2a	Closing	D36	4.9	2.2	2.7	0.7	67.9	6060	3.1	8.8	1.19
		Opening	D36	4.9	2.2	2.7	0.7	67.9	6060	3.1	8.8	1.19
	JMT-No. 11-2b	Closing	D36	4.9	2.2	2.7	0.7	67.9	6060	3.1	8.8	1.19
		Opening	D36	4.9	2.2	2.7	0.7	67.9	6060	3.1	8.8	1.19

* Bar sizes are presented in SI as reported in the original studies

** Minimum of side and top clear covers

§ Values given in SI are converted to in.-lb (1 in. = 25.4 mm; 1 psi = 1/145 MPa; and 1 kip = 4.4484 kN)

Table 4.5 Contd. Detail of knee beam-column joint specimens

Study	Specimen	Loading Direction	l_{eh}	l_{ehy}	$\frac{l_{eh}}{l_{ehy}}$	$\frac{d}{l_{eh}}$	M_n (kip.in.)	M_{peak} (kip.in.)	$\frac{M_{peak}}{M_n}$	$\frac{V_p}{V_n}$	$\delta_{0.8 peak}$
			(in.)	(in.)							
Wallace et al. (1998)	KJ16	Closing	14.1	5.7	2.50	1.0	1202	1300	1.08	0.47	0.040
		Opening	14.1	5.7	2.50	1.0	1202	963	0.80	0.47	0.060
	KJ17	Closing	14.1	5.6	2.51	1.0	1203	1460	1.21	0.52	0.060
		Opening	14.1	5.6	2.51	1.0	1203	957	0.80	0.52	0.060
	KJ18	Closing	14.3	9.6	1.49	1.0	1937	2250	1.16	0.79	0.040
		Opening	14.3	9.6	1.49	1.0	1937	1505	0.78	0.79	0.040
Chun et al. (2007) [§]	JMT-No. 11-1a	Closing	15.8	9.8	1.61	1.0	3165	3239	1.02	0.41	0.030
		Opening	15.8	9.8	1.61	1.1	3355	2478	0.74	0.41	0.028
	JMT-No. 11-1b	Closing	15.8	9.8	1.61	1.0	3165	3151	1.00	0.40	0.030
		Opening	15.8	9.8	1.61	1.1	3355	-	-	0.40	-
	JMT-No. 11-2a	Closing	15.8	9.8	1.61	1.0	3165	3664	1.16	0.46	0.035
		Opening	15.8	9.8	1.61	1.1	3355	-	-	0.46	-
	JMT-No. 11-2b	Closing	15.8	9.8	1.61	1.0	3165	3991	1.26	0.50	0.060
		Opening	15.8	9.8	1.61	1.1	3355	2876	0.86	0.50	0.030

[§] Values given in SI are converted to in.-lb (1 in. = 25.4 mm; 1 psi = 1/145 MPa; and 1 kip = 4.4484 kN)

Nilsson and Losberg (1976) studied reinforcement detailing requirements of knee beam-column joints to ensure joint strength at least equal to the strength of connecting members, limited cracking, sufficient ductility, and simplicity of construction. The study involved tests of 78 knee joints containing hooked bars with different reinforcement configurations in the joint region. None of these specimens contained confining reinforcement parallel and perpendicular to the beam or column reinforcement. Specimens were tested under monotonic loading. Specimens with the plane of hooks parallel to the inside face of the joint, as shown in Figure 4.13a, are comparable to the specimens with beam and column reinforcement anchored at the joint using headed bars. Nilsson and Losberg (1976) found that the joint efficiency (ratio of the peak opening moment to the nominal flexural strength of the members framing into the joint) in these specimens was only about 68%. Darwin et al. (2016) have pointed out that the reinforcement configuration shown in Figure 4.13a is ineffective in arresting cracks radiating inward from the inside corner of the joint and cracks perpendicular to the joint diagonal at outside corner, which results in premature failure of the joint under opening moment. Only knee joint specimens with 180° hooked bars intersecting cracks perpendicular to the joint diagonal at outside corner of the joint and additional diagonal reinforcement placed perpendicular to the cracks radiating inward from the inside corner of the joint, as shown in Figure 4.13b, provided a joint efficiency above 100% (about 115%). Based on

the observations by Nilsson and Losberg (1976), necessary changes in joint reinforcement details are recommended for knee joints, in which both beam and column reinforcement are anchored at the joint using headed bars.

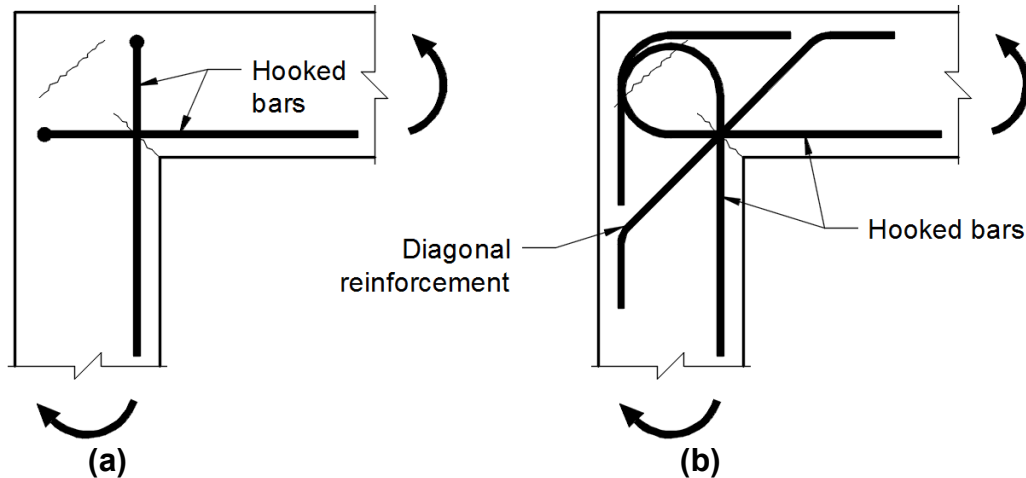


Figure 4.13 Reinforcement detail of knee beam-column joints with joint efficiency (a) 68%, and (b) 115% tested by Nilsson and Losberg (1976)

In the seven knee beam-column joint specimens, three tested by Wallace et al. (1998) and four tested by Chun et al. (2007), concrete compressive strengths ranged from 5,390 to 6,060 psi. Bar size included D16, D20, and D36 (16, 20, and 36 mm) with yield strengths ranging from 67,860 to 77,200 psi. Clear side concrete cover and minimum center-to-center spacing between the headed bars (minimum of horizontal and vertical spacings) ranged from 1.4 to $2.2d_b$ (1.1 to 3.1 in.) and 3.4 to $8.8d_b$ (2.7 to 12.4 in.), respectively. The net bearing areas of the headed bars A_{brg} in specimens tested by Wallace et al. (1998) were 7.0 and $11.4A_b$, while all specimens tested by Chun et al. (2007) had A_{brg} equal to $2.7A_b$.

Wallace et al. (1998) investigated the performance of three knee-joint specimens (KJ16, KJ17, and KJ18) containing headed bars with different joint reinforcement details. In specimen KJ16, in addition to No. 3 hoops serving as confining reinforcement within the joint region parallel to the beam reinforcement, vertical No. 3 bars (identified as U-stirrups in Figure 4.14) were also provided to restrain the headed bars. The specimen reached a peak closing moment (top bars in tension) about 8% greater than the nominal flexural strength of the beam, but the peak opening moment (top bars in compression) was only about 80% of the nominal flexural strength of the beam despite having ℓ_{eh} about 2.5 times ℓ_{ehy} . This is likely because the beam bottom bars did not effectively arrest the cracks radiating inward from the inside corner of the joint, as observed by

Nilsson and Losberg (1976), which resulted in premature joint failure. Wallace et al. (1998) reported that during the closing cycles, “the heads were pulled forward and upward when the top beam bars were in tension” resulting in loss of top concrete cover, which appears to be as a result of prying action of cover concrete on the top free face of the beam. To prevent this, additional No. 4 and No. 5 U-stirrups at the heads of beam top bars were provided in specimens KJ17 and KJ18, respectively, as shown in Figures 4.15 and 4.16. The U-stirrups adjacent to the heads were designed for one half the total tension force corresponding the yield stress in the beam top bars under closing moment. The U-stirrups improved the performance of specimens KJ17 and KJ18 under closing moment, but were ineffective during opening cycles. The performance of these two specimens was superior to specimen KJ16, with peak closing moment M_{peak} exceeding the nominal flexural strength of the beam M_n by 21 and 16%, respectively. Specimen KJ17 maintained 80% of the peak closing moment up to 6% drift. Specimens KJ18, however, exhibited significant loss of strength (about 30% of the peak closing moment) at the end of the third cycle after it reached the peak closing moment at about 2% drift. During opening cycles, none of the specimens reached the nominal flexural strength M_n of the beam, but all maintained more than 80% of the peak opening moment up to 5% drift. Joint shear stress was low, below $6\sqrt{f'_c}$, in all three specimens.

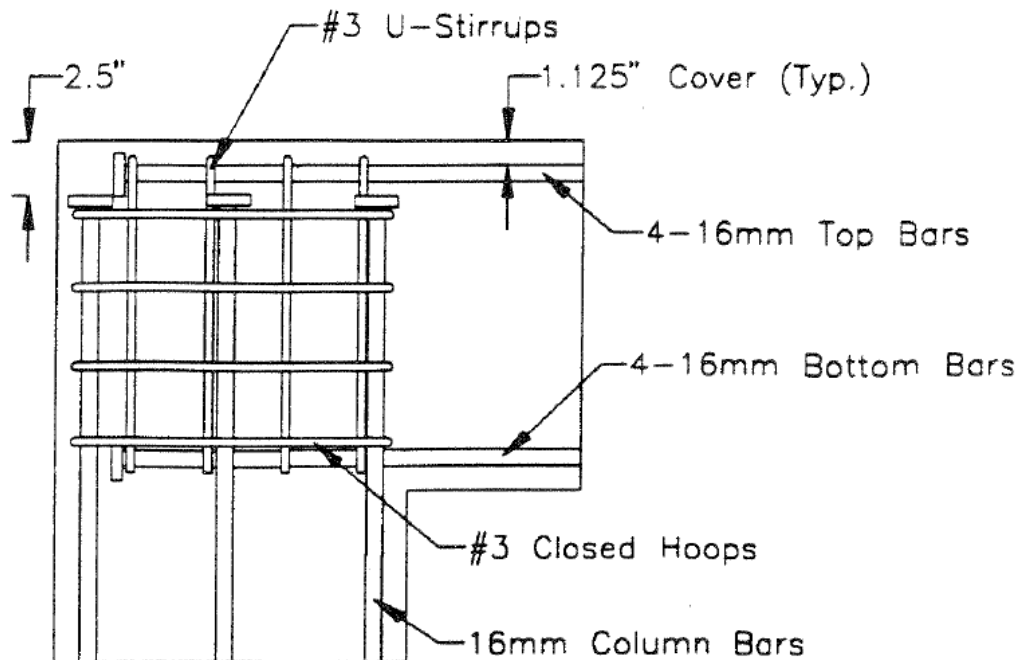


Figure 4.14 Reinforcement details for KJ16 knee beam-column joint specimens (McConnell and Wallace 1995)

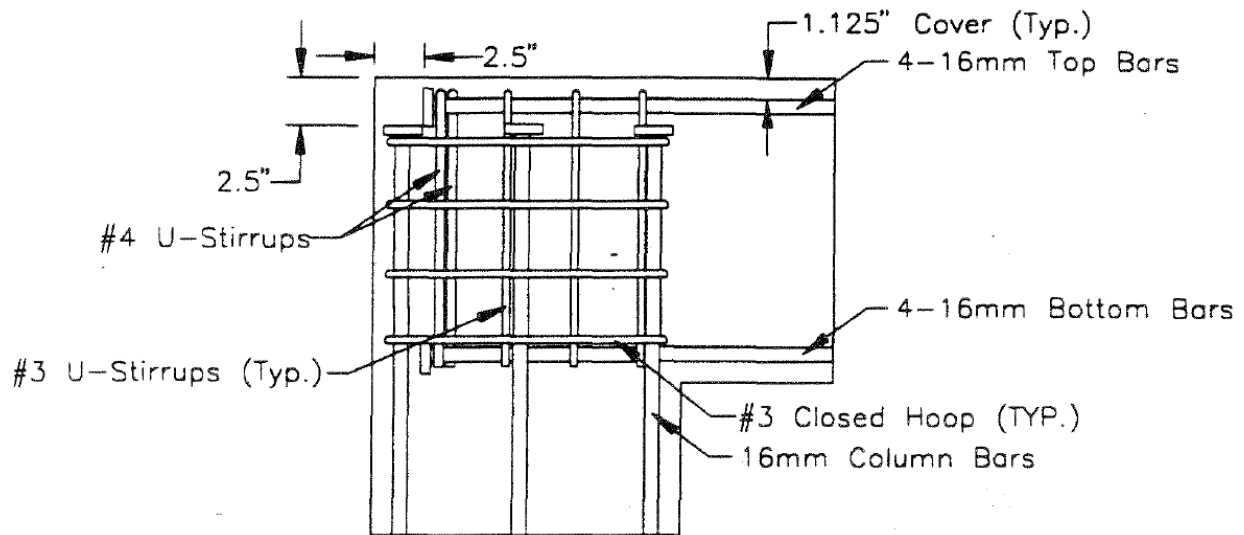


Figure 4.15 Reinforcement details for KJ17 knee beam-column joint specimens (McConnell and Wallace 1995)

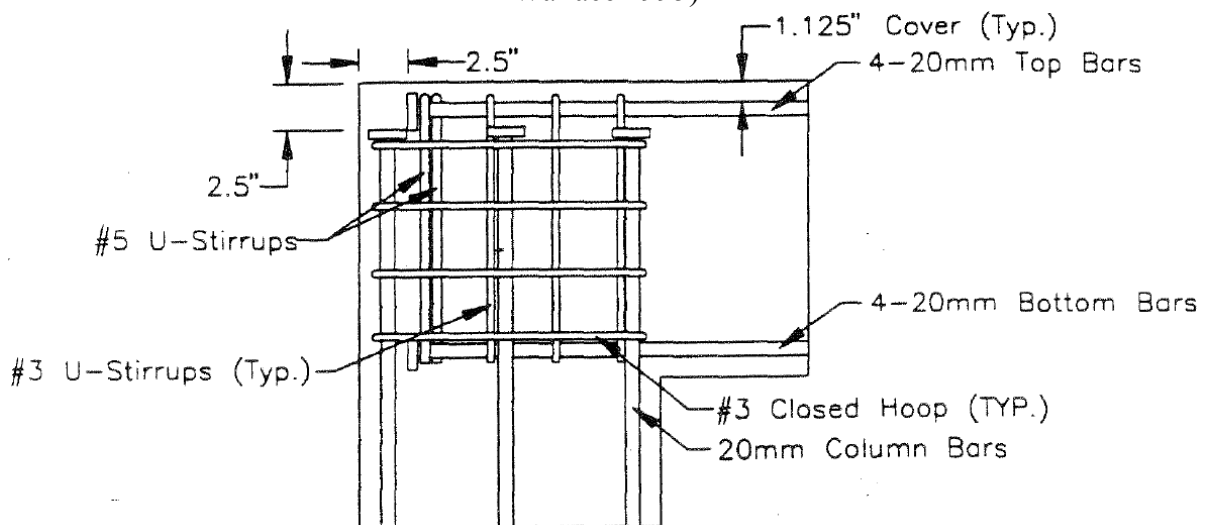


Figure 4.16 Reinforcement details for KJ18 knee beam-column joint specimens (McConnell and Wallace 1995)

The four knee beam-column joint specimens tested by Chun et al. (2007) included two joint reinforcement configurations, as shown in Figure 4.17. In specimens JMT-No.11-1a and JMT-No.11-1b, the beam top bars were placed above the head of the column longitudinal bars (Figure 4.17a), while in specimens JMT-No.11-2a and JMT-No.11-2b, the beam top bars were placed below the head of the column longitudinal bars with a No. 5 (D16) hoop tying the column heads above the beam top bars (Figure 4.17b). D16 hoops were provided as joint confining

reinforcement along with No. 5 (D16) and No. 6 (D19) stirrups, identified as U-bars in Figure 4.17, to confine the beam top reinforcement.

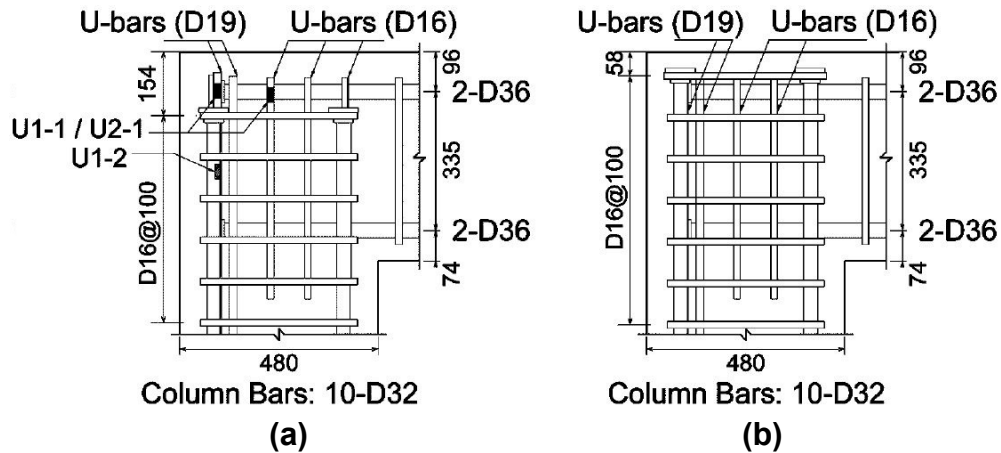


Figure 4.17 Reinforcement detail of knee beam-column joint specimens (a) JMT-No. 11-1a and JMT-No. 11-1b, and (b) JMT-No. 11-2a and JMT-No. 11-2b (Chun et al. 2007)

Performance of these four specimens tested by Chun et al. (2007) was similar to that of the specimens tested by Wallace et al. (1998). During the closing cycles, specimens JMT-No. 11-1a and JMT-No. 11-1b had a peak closing moment equal to 1.02 and 1.0 times the nominal flexural strength of the beam, respectively, while specimens JMT-No. 11-2a and JMT-No. 11-2b had a peak closing moment equal to 1.16 and 1.26 times the nominal flexural strength of the beam, respectively. Chun et al. (2007) suggested that the superior performance of specimens JMT-No. 11-2a and JMT-No. 11-2b during closing cycles was due to the beam top bars being placed below the heads of column bars with a hoop to tie the column heads above the beam top bars (Figure 4.17b). The specimens exhibited pronounced strength degradation in closing cycles with more than a 20% drop in the peak moment at the end of the third cycle at 3.5% drift. During opening cycles, none of the specimens reached the nominal flexural strength of the beam, but did not exhibit loss in strength up to 9% opening drift. Chun et al. (2007) suggested that strength degradation may be further prevented if a longer development length were provided. Figure 4.18, comparing the ratio of peak moment to nominal flexural strength of beam M_{peak}/M_n with ℓ_{eh}/ℓ_{ehy} , however, shows that an increase in embedment length ℓ_{eh} to a value greater than that required to yield the bars ℓ_{ehy} has little effect on the strength of the beam-column joints under reversed cyclic loading. This is especially true under opening moment, in which specimens did not reach M_n despite having sufficient embedment length to yield the bars. Such poor performance is likely because both

headed bars and confining reinforcement parallel and perpendicular to the bars within the joint region were ineffective in arresting cracks at the outer edge of the joint and cracks radiating inward from the inside corner of the joint. This resulted in premature failure of the joint, regardless of the embedment length sufficient to yield the headed bars. Also, an analysis of headed bars anchored in slab specimens tested by DeVries et al. (1999) in Section 3.3.1.1 showed that headed bars anchored at the corner of the slab had a value of T/T_h [T was the bar force at failure and T_h was calculated using the descriptive equations, Eq. (4.1) and (4.2)] about 77% of that of the headed bars anchored at the edge of the slab. The headed bars anchored at the corner and edge of the slab can be considered similar to the headed bars anchored in knee and exterior beam-column joints, respectively, in terms of available concrete around the bar. This observation suggests that the lower strength exhibited by headed bars anchored near corners is a function of the joint detailing, not the embedment length of the headed bars.

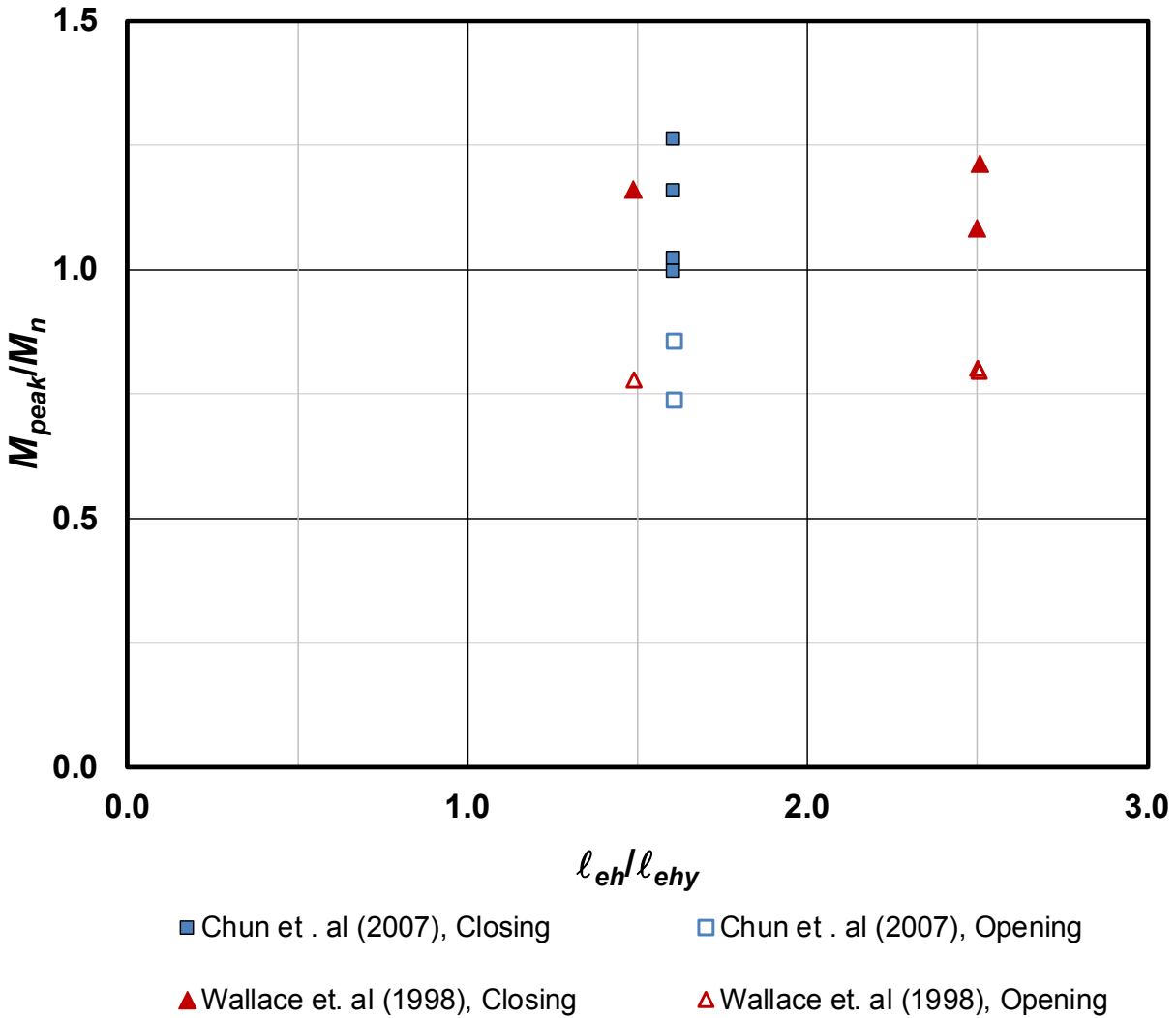


Figure 4.18 Ratio of peak moment to nominal flexural strength M_{peak}/M_n versus ratio l_{eh}/l_{ehy} for knee beam-column joint specimens [l_{ehy} is calculated using Eq. (4.2)]

These observations indicate that achieving a peak opening moment at least equal to the nominal flexural strength of the connecting members with the reinforcement configurations used in the specimens tested by Wallace et al. (1998) and Chun et al. (2007) is unlikely. Therefore, in addition to confining reinforcement parallel and perpendicular to the headed bars restraining the heads on the top free face of the beam, the use of diagonal reinforcement placed perpendicular to the possible cracks radiating inward from the inside corner of the joint, as shown in Figure 4.13, may be helpful to improve the joint performance under opening cycles. None of the knee joint specimens containing headed bars, however, were tested with such reinforcement configurations. The existing evidence strongly suggests that knee joint configurations similar to those tested by Wallace et al. (1998) and Chun et al. (2007) should not be used.

4.3 EFFECT OF HEAD SIZE

Exterior beam-column joint specimens subjected to reversed cyclic loading by Murakami et al. (1998), Matsushima et al. (2000), Nakazawa et al. (2000), Yoshida et al. (2000), Ishibashi et al. (2003), Ishibashi and Inokuchi (2004), Kato (2005), Masuo et al. (2006a, 2006b), Adachi and Masuo (2007), Chun et al. (2007), Ishida et al. (2007), Lee and Yu (2009), and Kang et al. (2010) contained headed bars with a net bearing area A_{brg} less than $4A_b$. In the majority of these cases, the headed bars had obstructions adjacent to the bearing face of the head (see Table 4.2 for area A_{obs} and length t_{obs} of the obstructions). This differs from the provisions in Sections 20.2.1.6 and 25.4.4.1 of ACI 318-14, which require a minimum net bearing area of $4A_b$ and heads with dimensional limits in accordance with ASTM A970-13a that require the length and diameter of the obstruction not exceed 1.5 and $2d_b$, respectively. Shao et al. (2016) suggested that the net bearing area of a head with an obstruction be defined as the gross head area minus the area of the obstruction adjacent to the head and be at least $4A_b$. This requirement has been adopted in ASTM A970-17.

Three specimens tested by Chun et al. (2007) contained D22 or D32 (No. 7 or No. 10) headed bars with a net bearing area of $2.9A_b$. The headed bars contained obstructions adjacent to the bearing face of the head. Details of the obstructions, including area A_{obs} and length t_{obs} , are presented in Table 4.2. These specimens performed satisfactorily despite having bearing areas as small as $2.9A_b$, but the embedment length ℓ_{eh} in these specimens ranged from 1.48 to 2.41 times the embedment length required to yield the bar ℓ_{ehy} calculated using the descriptive equations, Eq. (4.1) and (4.2), and twice the development length calculated in accordance with Section 4.5.3.3 of ACI 352R-02. These long embedment lengths likely reduced the bearing force on the head, resulting in little or no contribution of the head to the anchorage strength. Thus, these tests do not show that heads this small will perform adequately for shorter embedment lengths. Based on the results of these tests, Chun et al. (2007), however, suggested that heads with bearing area of $3A_b$ are sufficient to fully anchor the headed bar.

To investigate if the headed bars with a bearing area less than $4A_b$ performed satisfactorily because of extended embedment lengths, beyond that required to yield the bar, the actual embedment length ℓ_{eh} is compared with the embedment length required to yield a headed bar ℓ_{ehy}

calculated using Eq. (4.1) or (4.2). A similar comparison is made based on the embedment length required to yield a straight bar in tension (headed bars in beam-column joint specimens treated as straight bars by ignoring the head) ℓ_{dy} calculated using Eq. (4.6) for the development length of straight bars in accordance with Section 4.3 of ACI 408R-03.

$$\ell_{dy} = \frac{\left(\frac{f_y}{\phi f_c'^{1/4}} - 2400\omega \right) \alpha \beta \lambda}{76.3 \left(\frac{c\omega + K_{tr}}{d_b} \right)} d_b \quad (4.6)$$

where $K_{tr} = \frac{0.52t_r t_d A_{tr}}{sn} f_c'^{1/2}$

$\omega = 0.1 (c_{max}/c_{min}) + 0.9 \leq 1.25$, $(c\omega + K_{tr})/d_b \leq 4.0$, $c = c_{min} + 0.5d_b$, $s = \ell_{eh}/N$, $t_r = 9.6R_r + 0.28 \leq 1.72$, $t_d = 0.78d_b + 0.22$, $\alpha\beta \leq 1.7$, $c_{max} = \text{maximum}(c_b, c_s)$, $c_{min} = \text{minimum}(c_b, c_s)$, $c_s = \text{minimum}(c_{so}, c_{si} + 0.25 \text{ in.})$, ℓ_{dy} = development length of bar being anchored (in.); f_y = yield strength of the anchored bar (psi); f_c' = concrete compressive strength (psi); d_b = bar diameter (in.); K_{tr} = confining reinforcement index; ϕ = strength reduction factor; α = reinforcement location factor equal to 1.3 for reinforcement with more than 12 in. of fresh concrete cast below the bar, or 1.0 for other reinforcement; β = coating factor equal to 1.5 for epoxy-coated reinforcement with cover less than $3d_b$ or clear spacing less than $6d_b$, 1.2 for other epoxy-coated reinforcement, and 1.0 for uncoated reinforcement; λ = lightweight-concrete factor equal to 1.3 for light weight concrete and 1.0 for normalweight-concrete; A_{tr} = cross-sectional area of confining reinforcement (column longitudinal reinforcement, Figure 4.19) crossing the potential plane of splitting adjacent to the reinforcement being anchored (in.²); N = number of legs of confining reinforcement crossing the potential plane of splitting; s = center-to-center spacing of confining reinforcement (in.); $R_r = 0.0727$ (relative rib area of reinforcement); c_b = bottom clear concrete cover (in.); and c_{so} and c_{si} are side clear concrete cover (in.) and half of clear bar spacing (in.), respectively.

When calculating the required development length for straight bars (headed bars in beam-column joint specimens treated as straight bars by ignoring the head) using Eq. (4.6), the value of reinforcement location factor α is taken as 1.0. The values of coating factor β and lightweight concrete factor λ are taken equal to 1.0 because all specimens were cast with normalweight concrete and contained uncoated bars. The strength reduction factor ϕ is taken equal to 1.0. Column

longitudinal reinforcement (Figure 4.19), which crossed the potential plane of splitting, is counted as confining reinforcement to calculate A_{tr} in Eq. (4.6). Column reinforcement located outside the embedded portion of the headed bar (that is, outside the potential plane of splitting failure) is not considered effective in arresting the potential splitting cracks and, therefore, not included while calculating A_{tr} .

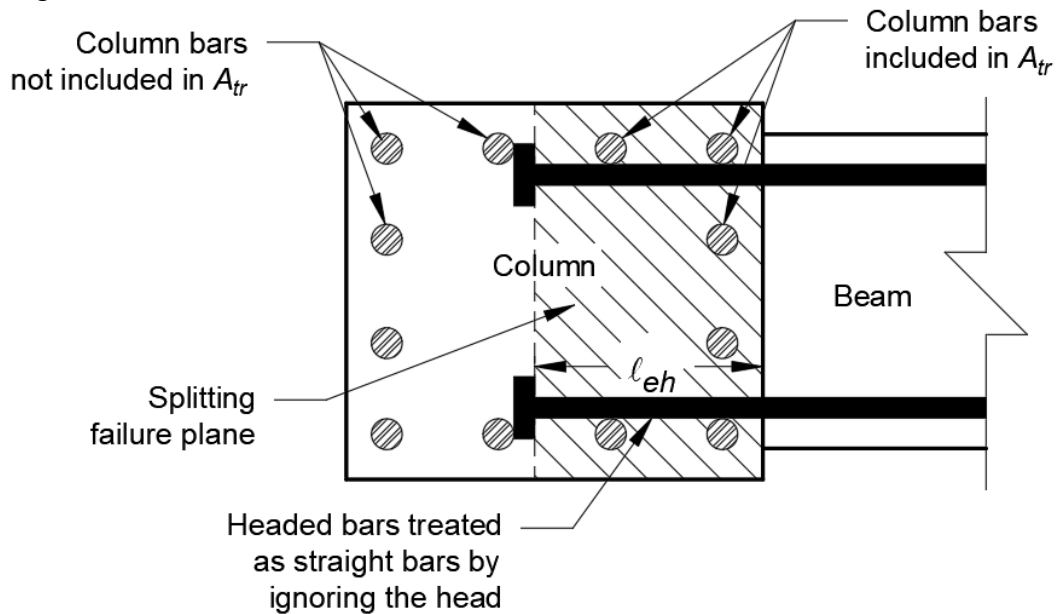


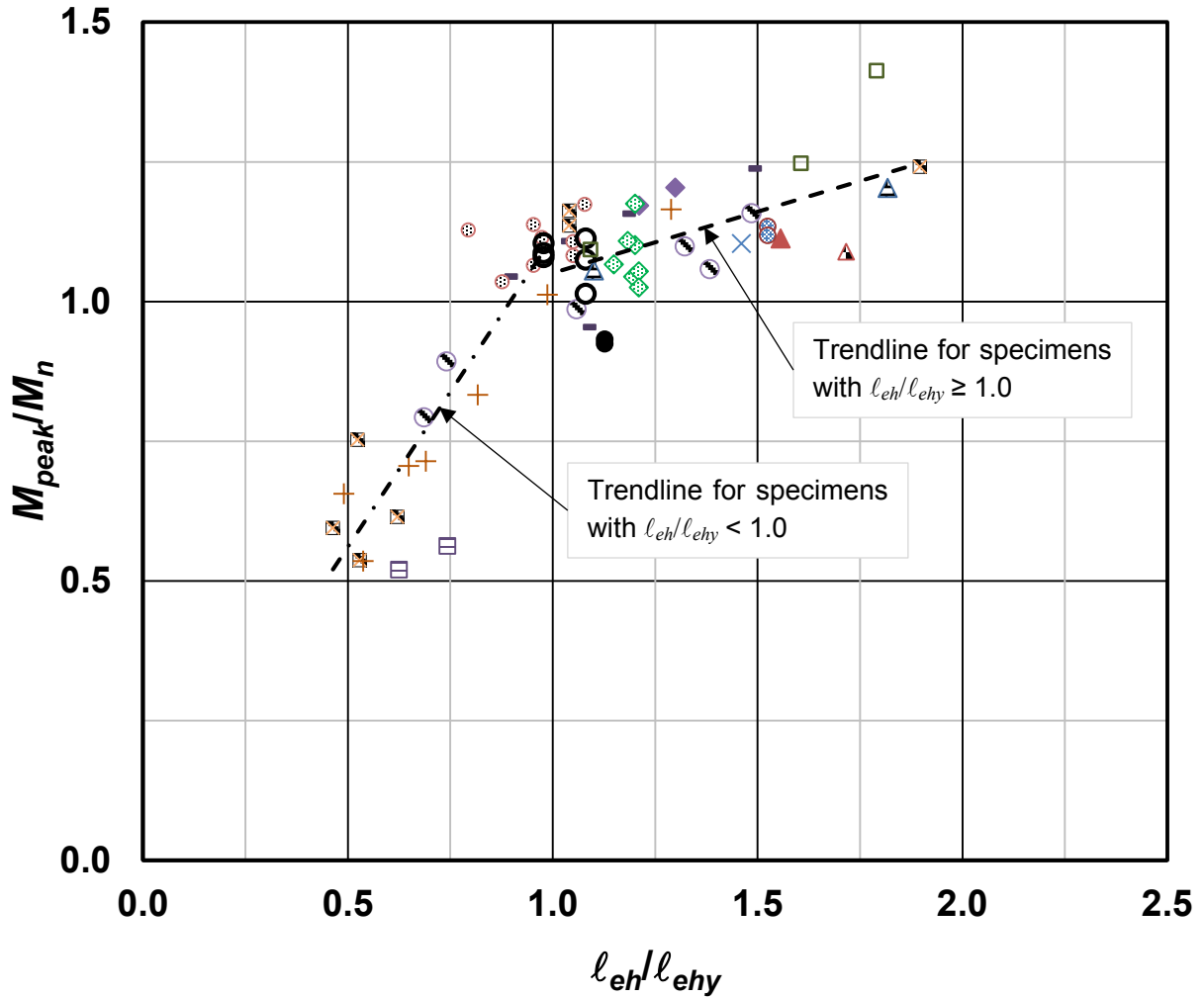
Figure 4.19 Splitting failure plane and column longitudinal reinforcement as confining reinforcement for headed bars anchored in the column treated as straight bars by ignoring the head

4.3.1 Specimens with bearing area $A_{brg} \geq 3.7A_b$

From the tests of exterior beam-column joints under monotonic loading, Shao et al. (2016) observed that heads with A_{brg} as low as $3.8A_b$ provided adequate anchorage to the bar. Based on this observation, the effect of bearing area on the anchorage performance of headed bars in beam-column joints tested under reversed cyclic loading is analyzed separately for the bars with $A_{brg} \geq 3.7A_b$ and $A_{brg} < 3.7A_b$. The bearing area of $3.7A_b$ is slightly less than $3.8A_b$, but is considered close enough to represent the $3.8A_b$ heads tested by Shao et al. (2016).

Sixty-two specimens (23 with $l_{eh}/l_{ehy} < 1.0$ and 39 with $l_{eh}/l_{ehy} \geq 1.0$) contained headed bars with a net bearing area of the head A_{brg} between 3.7 and $8.6A_b$; most of the heads had bearing areas close to $4A_b$. Details of the heads in nine specimens tested by Matsushima et al. (2000), Ishibashi and Inokuchi (2004), and Ishida et al. (2007) are not available and, therefore, these

specimens are excluded from the analysis. Relevant specimen details are presented in Table 4.2 with complete details and analysis results presented in Table C.2 of Appendix C. The ratio of the peak moment to the nominal flexural strength of beam M_{peak}/M_n is plotted versus ℓ_{eh}/ℓ_{ehy} in Figure 4.20 for specimens with $A_{brg} \geq 3.7A_b$. Linear trendlines are shown for specimens with (1) $\ell_{eh}/\ell_{ehy} < 1.0$ and (2) $\ell_{eh}/\ell_{ehy} \geq 1.0$. The maximum value of ℓ_{eh}/ℓ_{ehy} for these specimens was 1.9. As shown in the figure, all but four specimens with $\ell_{eh}/\ell_{ehy} \geq 1.0$ had $M_{peak}/M_n \geq 1.0$. Twenty-three specimens had $\ell_{eh}/\ell_{ehy} < 1.0$. In these specimens, the values of the ratio of force in the headed bar at failure estimated using Eq. (4.4) to the anchorage strength calculated using the descriptive equations [Eq. (4.1) and (4.2)], T'/T_h , ranged between 0.74 and 1.43 with an average, standard deviation, and coefficient of variation of 1.12, 0.161, and 0.144, respectively. None of the specimens were reported to have exhibited bar slip failure due to insufficient bearing on the head. A detailed discussion of the performance of these specimens under reversed cyclic loading is presented in Sections 4.2.2.1 and 4.2.2.2. Fifteen specimens with ℓ_{eh} close to ℓ_{ehy} (ℓ_{eh}/ℓ_{ehy} between 0.95 and 1.10) and joint confining reinforcement ratio A_{jt}/A_{hs} ranging from none to 0.26 [less than the upper limit of 0.3 on A_{jt}/A_{hs} allowed to use in descriptive equation Eq. (4.2)] had A_{brg} between 3.7 and 4.1 A_b . These specimens reached $M_{peak} \geq M_n$ and no loss in strength was reported due to insufficient bearing on the head. These results indicate that the headed bars with bearing area as small as 3.7 A_b provided adequate anchorage during reversed cyclic loading.



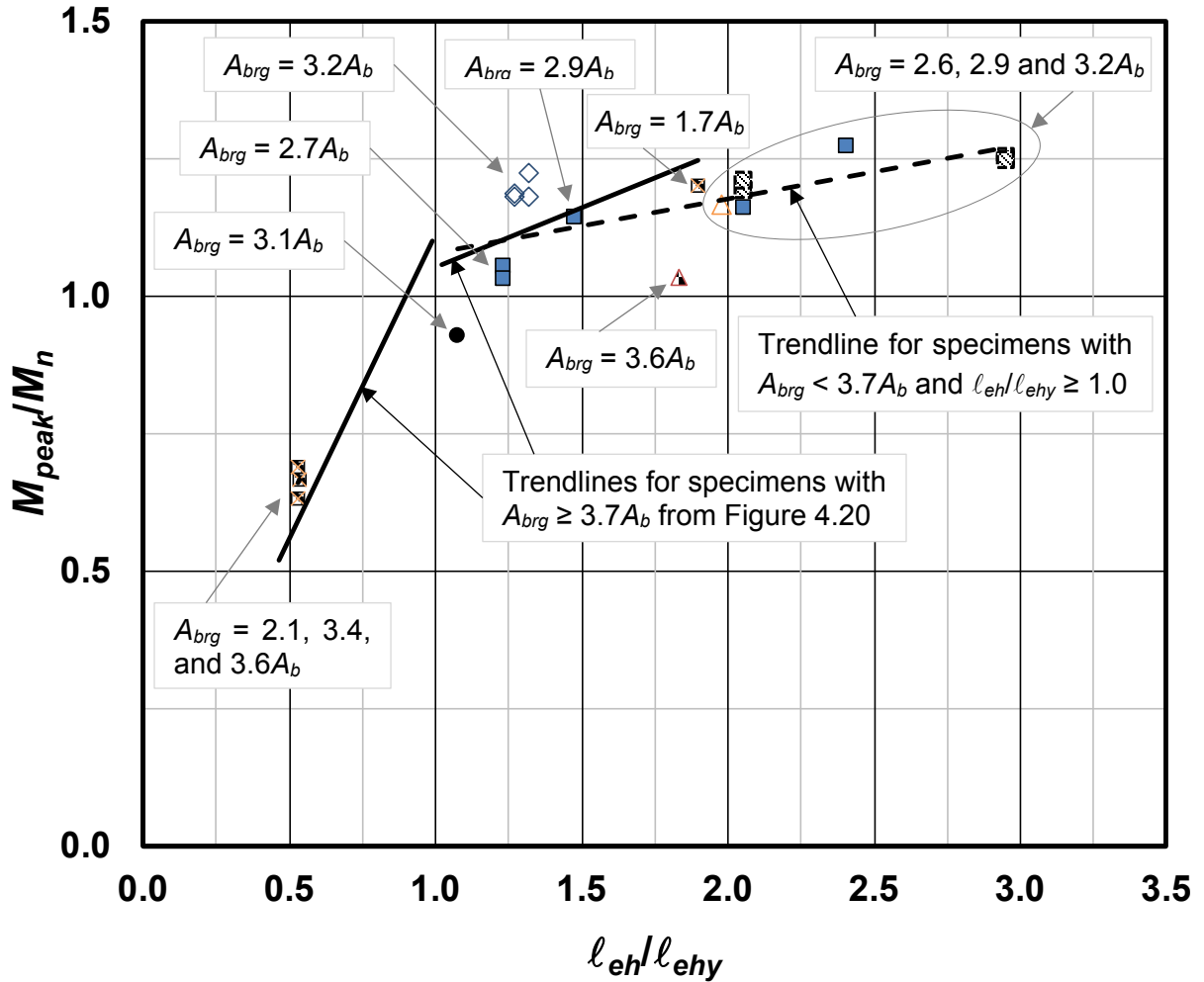
- | | | | |
|-------|-----------------------------------|-------|--------------------------------------|
| × | Bashandy (1996) | ⊠ | Murakami et al. (1998) |
| ▲ | Wallace et al. (1998) | ⊙ | Nakazawa et al. (2000) |
| ⊞ | Tasai et. al (2000) | ● | Yoshida et al. (2000) |
| ⊗ | Takeuchi et al. (2001) | - | Kiyohara et al. (2004) |
| + | Kiyohara et al. (2005) | ▲ | Kato (2005) |
| ⊗ | Masuo et al. (2006a, 2006b) | ○ | Adachi and Masuo (2007) |
| ▲ | Tazaki et al. (2007) | ◆ | Kang et al. (2012) |
| ◇ | Chun and Shin (2014) | □ | Dhake et al. (2015) |
| - · - | Linear ($l_{eh}/l_{ehy} < 1.0$) | - - - | Linear ($l_{eh}/l_{ehy} \geq 1.0$) |

Figure 4.20 M_{peak}/M_n versus l_{eh}/l_{ehy} for exterior and roof-level interior beam-column joint specimens with $A_{brg} \geq 3.7A_b$. M_{peak}/M_n is the ratio of peak moment to nominal flexural strength, and l_{eh}/l_{ehy} is the ratio of embedment length to the embedment length required to yield the headed bar calculated using the descriptive equations, Eq. (4.1) and (4.2).

4.3.2 Specimens with bearing area $A_{brg} < 3.7A_b$

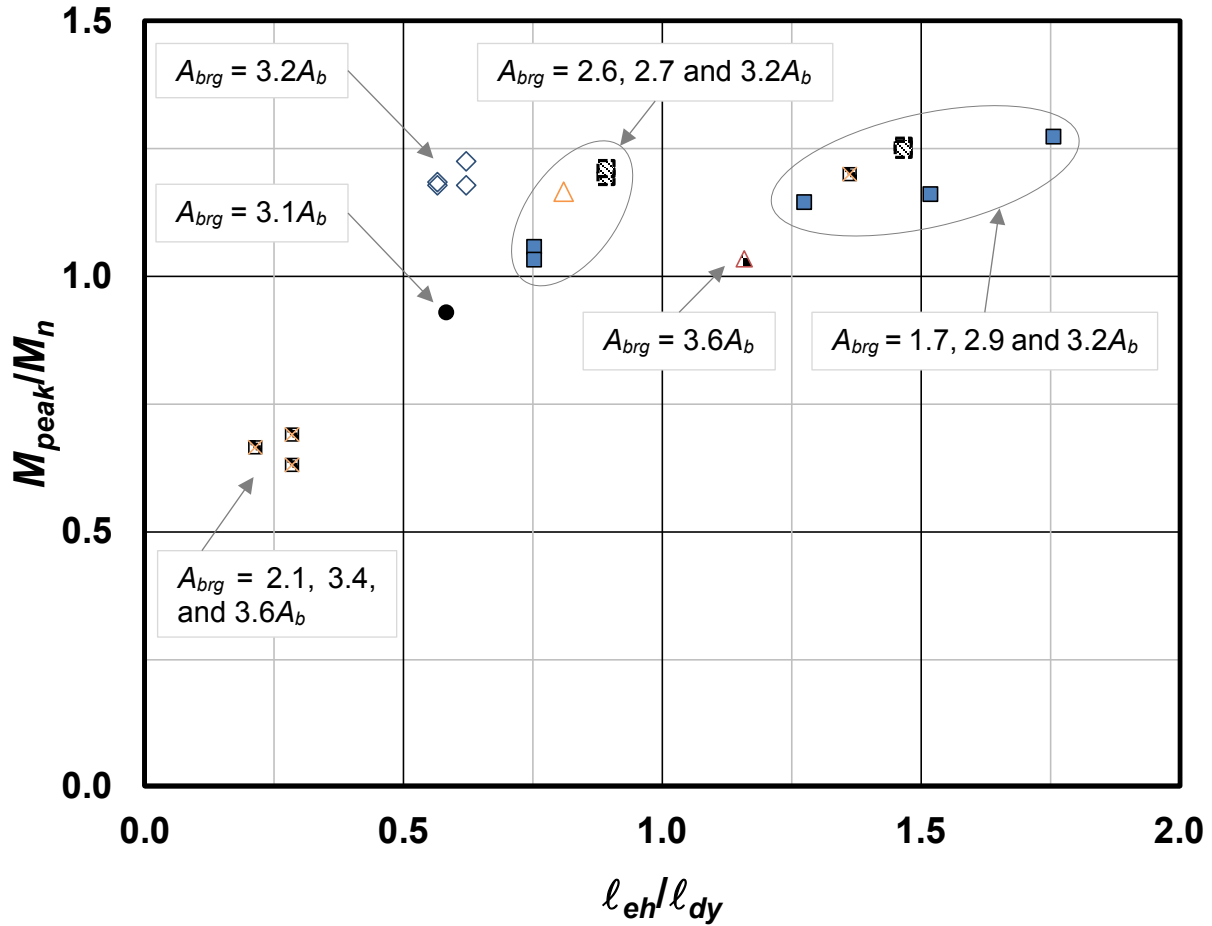
Twenty specimens contained headed bars with a net bearing with values between 1.7 and $3.6A_b$. Three specimens tested by Chun et al. (2007), JM-1, JM-2, and WM, contained headed bars with a net bearing area of $2.9A_b$. Two other specimens tested by Chun et al. (2007), JM-No.11-1a and JM-No.11-1b, contained headed bars with a net bearing area $2.7A_b$. The headed bars in these specimens contained obstructions adjacent to the bearing face of the head. Specimens No. 100 and No. 102 (Murakami et al. 1998) and JD (Kang et al. 2010) contained headed bars with A_{brg} of 1.7, 2.1, and $2.6A_b$, respectively, and had no obstructions. Twelve specimens, four tested by each Ishibashi et al. (2003) and Lee and Yu (2009), two tested by Murakami et al. (1998), and one tested by each Yoshida et al. (2000) and Kato (2005), contained headed bars with A_{brg} between 3.1 and $3.6A_b$ (eight had A_{brg} of $3.2A_b$); the headed bars in all but two of the specimens, with A_{brg} of 3.1 and 3.4, had an obstruction adjacent to the head. Details of the obstructions, including area A_{obs} and length t_{obs} , are presented in Table 4.2. The roof-level interior joint specimens tested by Ishibashi et al. (2003) with A_{brg} of $3.2A_b$ had a joint confining reinforcement ratio A_{tt}/A_{hs} equal to 0.34, which were only the specimens with A_{tt}/A_{hs} greater than the upper limit of 0.3 used in descriptive equation Eq. (4.2). The rest of the specimens had A_{tt}/A_{hs} ranging from none to 0.26.

The ratio of the peak moment to the nominal flexural strength of the beam M_{peak}/M_n is plotted versus the ratios ℓ_{eh}/ℓ_{ehy} in Figure 4.21 and ℓ_{eh}/ℓ_{dy} in Figure 4.22. The embedment length required to yield the headed bars ℓ_{ehy} is calculated using the descriptive equations, Eq. (4.1) and (4.2), and that required to yield straight bars (headed bars in beam-column joint specimens treated as straight bars by ignoring the head) ℓ_{dy} is calculated using Eq. (4.6) in accordance with Section 4.3 of ACI 408R-03. None of the specimens had transverse beams at the joint perpendicular to the test beam. Relevant specimen details are presented in Table 4.2 with complete details and analysis results presented in Table C.2 of Appendix C. A trendline for the specimens with $\ell_{eh}/\ell_{ehy} \geq 1.0$ is shown in Figure 4.21. Trendlines for specimens with $A_{brg} \geq 3.7A_b$ (from Figure 4.20) are also shown with solid lines for comparison. As noted earlier, the maximum value of ℓ_{eh}/ℓ_{ehy} for the specimens with $A_{brg} \geq 3.7A_b$ was 1.9.



- ▣ Murakami et al. (1998)
- ▣ Ishibashi et. al (2003)
- Chun et. al (2007)
- △ Kang et al. (2010)
- Yoshida et al. (2000)
- ▲ Kato (2005)
- ◇ Lee and Yu (2009)
- - Linear ($l_{eh}/l_{ehy} \geq 1.0$)
- Linear ($A_{brg} \geq 3.7A_b$)

Figure 4.21 M_{peak}/M_n versus l_{eh}/l_{ehy} for exterior and roof-level interior beam-column joint specimens with $A_{brg} < 3.7A_b$. M_{peak}/M_n is the ratio of peak moment to nominal flexural strength, and l_{eh}/l_{ehy} is the ratio of embedment length to the embedment length required to yield the headed bar calculated using the descriptive equations, Eq. (4.1) and (4.2).



- Murakami et al. (1998) ● Yoshida et al. (2000) ▣ Ishibashi et. al (2003)
- ▲ Kato (2005) ■ Chun et. al (2007) ◇ Lee and Yu (2009)
- △ Kang et al. (2010)

Figure 4.22 M_{peak}/M_n versus l_{eh}/l_{dy} for exterior and roof-level interior beam-column joint specimens with $A_{brg} < 3.7A_b$. M_{peak}/M_n is the ratio of peak moment to nominal flexural strength, and l_{eh}/l_{dy} is the ratio of embedment length to the development length of straight bar (headed bars treated as straight bars by ignoring the head) calculated using Eq. (4.6) in accordance with Section 4.3 of ACI 408R-03.

All four specimens tested by Ishibashi et al. (2003), three specimens tested by Chun et al. (2007) (JM-1, JM-2, and WM), and the individual specimens tested by Murakami et al. (1998), Kato (2005), and Kang et al. (2010) with A_{brg} ranging from 1.7 to $3.6A_b$ had $M_{peak}/M_n \geq 1.0$. In these specimens, the joint confining reinforcement ratio A_{tj}/A_{hs} ranged from none to 0.34, which is less than or close to the upper limit of 0.3 on A_{tj}/A_{hs} allowed to use in descriptive equation Eq. (4.2). The embedment lengths, however, ranged from 1.48 to 2.95 times l_{ehy} and from 0.98 to 1.97 times l_{dy} . These long embedment lengths likely reduced the bearing force on the head, resulting in

little or no contribution of the head to the anchorage strength. Thus, these tests do not show that heads with $A_{brg} < 3.7A_b$ will perform adequately in specimens with short embedment lengths.

All four specimens tested by Lee and Yu (2009), two specimens, JM-No.11-1a and JM-No.11-1b, tested by Chun et al. (2007), and one specimen, No. 3, tested by Yoshida et al. (2000) with bearing area 2.7 to $3.2A_b$ had ℓ_{eh} 1.08 to 1.32 times ℓ_{ehy} and from 0.56 to 75 times ℓ_{dy} , which is shorter than that of the specimens discussed above. The joint confining reinforcement ratio A_{tl}/A_{hs} in these specimens ranged from 0.14 to 0.26, which is within the range used to develop the descriptive equations. Six out of these seven specimens had $M_{peak}/M_n > 1.0$. Three specimens, No. 102, No. 104, and M2D22, tested by Murakami et al. (1998), had $\ell_{eh} = 0.53\ell_{ehy}$ and are the only specimens with $\ell_{eh}/\ell_{ehy} < 1.0$ in Figure 4.21. The bars contained headed bars with net bearing areas of 2.1, 3.4 and $3.6A_b$. M_{peak}/M_n of these three specimens is above the trendline for specimens with $A_{brg} \geq 3.7A_b$. These limited results suggest that heads with A_{brg} as low as $2.7A_b$ may be sufficient to anchor the headed bars in members subjected to reversed cyclic loading. As discussed in Section 3.3.1, however, headed bars anchored in slab and column-like specimens tested under monotonic loading by Choi et al. (2002) and Choi (2006) with net bearing areas between 2.6 and $3.2A_b$ and no obstruction consistently performed poorly.

4.4 ANALYSIS OF HEADED BARS IN BEAM-COLUMN JOINTS USING ANCHORAGE PROVISIONS IN ACI BUILDING CODE

The anchorage strength of headed bars in exterior and roof-level interior beam-column joints subjected to reversed cyclic loading is analyzed in this section based on the anchorage design provisions in Chapter 17 of ACI 318-14. Concrete breakout strength (Section 17.4.2 of ACI 318-14), concrete side-face blowout strength (Section 17.4.4 of ACI 318-14), and the anchorage strength provided by anchor reinforcement (Section 17.4.2.9 of ACI 318-14) are investigated. The anchorage strength of the headed bars is then determined based on the controlling failure mode, concrete breakout, side-face blowout, or yielding of anchor reinforcement, as explained below. Other failure modes, such as bar pullout, concrete splitting, and bar fracture, are not included in this analysis because none of these failure modes controlled the anchorage strength. Anchorage strengths of the headed bars were also calculated using descriptive equations, Eq. (4.1) and (4.2), for comparison.

The geometric parameters used for anchorage analysis are shown in Figure 4.23. The anticipated concrete breakout failure region, which is within a radial distance of $1.5\ell_{eh}$ from the center of the headed bar anchored in the column (Section R17.4.2.1 of ACI 318-14), overlaps with the projected failure region of the adjacent headed bars [$\max(s_h, s_v)/2 \leq 1.5\ell_{eh}$]. Therefore, a group effect must be considered when calculating the nominal concrete breakout strength. The nominal concrete breakout strength of a group of headed bars in tension N_{cbg} as given in Section 17.4.2 of ACI 318-14 is

$$N_{cbg} = \frac{A_{Nc}}{A_{Nco}} \psi_{ec,N} \psi_{ed,N} \psi_{c,N} \psi_{cp,N} N_b \quad (4.7)$$

where A_{Nc} = projected concrete failure area of group of headed bars (in.²), as shown in Figure 4.23a; A_{Nco} = projected concrete failure area of a single headed bar equal to $9\ell_{eh}^2$ (in.²); ℓ_{eh} = embedment length of headed bars (in.); $\psi_{ec,N}$, $\psi_{ed,N}$, $\psi_{c,N}$, and $\psi_{cp,N}$ are modification factors for anchor groups loaded eccentrically in tension, edge effects, cracking of concrete at service load, and post-installed anchors, respectively; N_b is the basic concrete breakout strength of a single headed bar in cracked concrete (equal to $16\lambda_a \sqrt{f'_c} \ell_{eh}^{1.5}$); λ_a is the modification factor for lightweight concrete and is equal to 1.0 because all specimens were cast in normalweight concrete; f'_c is concrete compressive strength $\leq 10,000$ psi. Values of $\psi_{ec,N}$, $\psi_{c,N}$, and $\psi_{cp,N}$ are equal to 1.0 (headed bars loaded simultaneously with no eccentricity), 1.25 (cast-in headed bars with no cracking of concrete before testing), and 1.0 (cast-in headed bars), respectively, and the value of $\psi_{ed,N}$ is calculated based on minimum concrete cover to the headed bar in accordance with Section 17.4.2.5 of ACI 318-14.

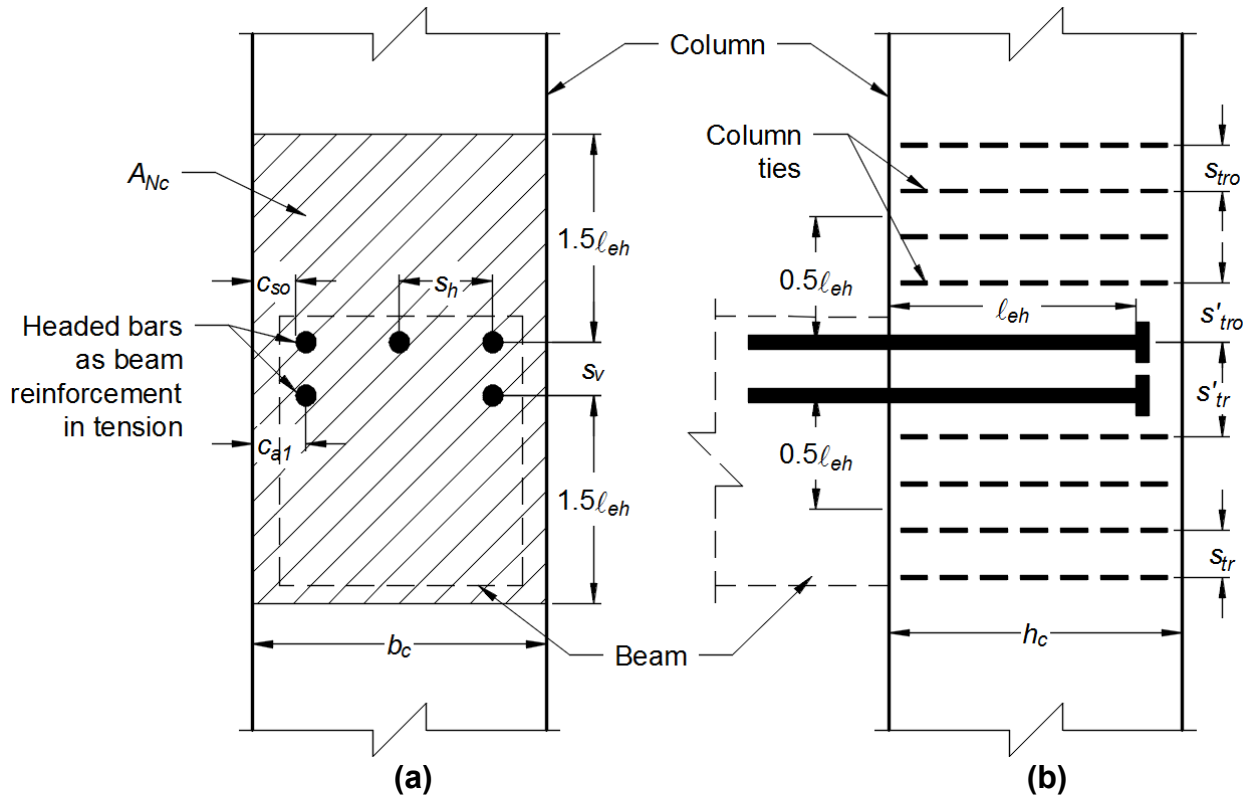


Figure 4.23 Geometric parameters used in the anchorage analysis of beam-column joint specimens (a) front view (b) side view (column longitudinal reinforcement and beam compression reinforcement are not shown for clarity)

In accordance with Section 17.4.4.1 of ACI 318-14, the nominal side-face blowout strength of a single headed bar (adjacent to the side face of the column) in tension N_{sb} with embedment length greater than 2.5 times the cover to the center of the bar is given by Eq. (4.8). Concrete breakout failure governs for headed bars with an embedment length less than or equal to 2.5.

$$N_{sb} = 160c_{al}\sqrt{A_{brg}}\lambda_a\sqrt{f'_c} \quad (4.8)$$

where c_{al} = cover to the center of the headed bar (in.), as shown in Figure 4.23a; A_{brg} = net bearing area of the head (in.²); λ_a is modification factor for lightweight concrete, which is equal to 1.0 because all specimens were cast in normalweight concrete; and f'_c is concrete compressive strength $\leq 10,000$ psi. The modification factor for the corner effect in accordance with Section 17.4.4.1 of ACI 318-14 is not applied to N_{sb} because all specimens had cover to the center of headed bar in a direction perpendicular to c_{al} (parallel to the longitudinal axis of the column) greater than $3c_{al}$.

For specimens containing two layers of headed bars with embedment lengths greater than $2.5c_{al}$ and vertical center-to-center spacing between the bars in different layers s_v less than $6c_{al}$, the group effect must be considered when calculating the nominal side-face blowout strength, as was the case in all specimens. In accordance with Section 17.4.4.2 of ACI 318-14, the nominal side-face blowout strength of multiple headed bars (two headed bars along the side-face of the column) in tension N_{sbg} is given by

$$N_{sbg} = \left(1 + \frac{s_v}{6c_{al}} \right) N_{sb} \quad (4.9)$$

where s_v = center-to-center spacing between the headed bars along the side face of the column (in.), which is also the vertical center-to-center spacing between headed bars in different layers (Figure 4.23); and N_{sb} is the nominal side-face blowout strength of single headed bar calculated from Eq. (4.8).

The nominal anchorage strength of the headed bars is also evaluated based on anchor reinforcement (Section 17.4.2.9 of ACI 318-14). Column ties parallel to the headed bars within $0.5\ell_{eh}$ from the center of the nearest headed bar (inside and outside the joint region), as shown in Figure 4.23b, are considered as anchor reinforcement. The nominal anchorage strength of group of headed bars based on anchor reinforcement N_{arg} is given by Eq. (4.10).

$$N_{arg} = N_{tr} A_{tr,l} f_{yt} + N_{tro} A_{tro,l} f_{yto} \quad (4.10)$$

where N_{tr} and N_{tro} are the total number of legs of column ties inside and outside the joint region parallel to the headed bars within $0.5\ell_{eh}$ of the center of the nearest headed bar, respectively (Figure 4.23b); $A_{tr,l}$ and $A_{tro,l}$ are areas of single legs of anchor reinforcement inside and outside the joint region (in.²), respectively; and f_{yt} and f_{yto} are yield strengths of anchor reinforcement inside and outside the joint region (psi), respectively.

The nominal anchorage strength of each headed bar in tension in beam-column joints T_{anc} governed by concrete breakout, side-face blowout, or anchor reinforcement is calculated using Eq. (4.11), where n is the number of headed bars loaded simultaneously in tension. N_{cbg} , N_{sb} , N_{sbg} , and N_{arg} are anchorage strengths calculated using Eq. (4.7), (4.8), (4.9), and (4.10), respectively.

$$T_{anc} = \min \left\{ \begin{array}{l} \max \left(\frac{N_{cbg}}{n}, \frac{N_{arg}}{n} \right) \\ \min \left(\frac{N_{sbg}}{2}, N_{sb} \right) \end{array} \right\} \quad (4.11)$$

The nominal anchorage strength is compared with the force in headed bars during the test when the specimens reached the peak moment M_{peak} . The force in the bars, however, was not measured directly during the test and strain measurements at the critical section (face of the column) were available only for nine specimens. The peak force in each headed bar is, therefore, approximated using Eq. (4.4), introduced in Section 4.2.2.3.

$$T' = \frac{M_{peak}}{M_n} A_b f_y \quad (4.4)$$

where T' = estimated peak force on the headed bar (kips); M_{peak} = peak moment in the beam calculated at the face of the column (kip-in.); M_n = nominal flexural strength of the beam (kip-in.); A_b = area of the headed bar (in.²); and f_y = yield strength of the headed bar (ksi). Force T' is also compared with the force T_h in the bar calculated using descriptive equations, Eq.(4.1) and (4.2).

Twenty-eight beam-column joint specimens with $\ell_{eh}/\ell_{ehy} < 1.0$ subjected to reversed cyclic loading, in which headed bars are considered not to have reached the yield strength of the bar, were analyzed based on the anchorage design provisions of Chapter 17 of ACI 318-14 and the descriptive equations, Eq. (4.1) and (4.2). All specimens were exterior joints. The estimated bar force T' [Eq. (4.4)] is compared with anchorage strengths T_{anc} [Eq. (4.11)] and T_h [Eq. (4.1) or (4.2)]. Statistical parameters, including maximum, minimum, mean, standard deviation (STD), and coefficient of variation (COV) of the ratios T'/T_{anc} and T'/T_h are presented in Table 4.6. Complete details of specimens and analysis results are provided in Table 4.2 and Table C.2 of Appendix C.

In all 28 specimens, nominal anchorage strength based on anchor reinforcement N_{arg} governed the anchorage strength, which was 1.53 to 4.32 times greater than the concrete breakout strength N_{cbg} . Side-face blowout strength, minimum of N_{sb} and N_{sbg} , was 1.7 to 6.1 times greater than anchorage strength based on anchor reinforcement, indicating that side-face blowout did not control the anchorage strength. This is consistent with none of the specimens were reported to have concrete breakout or side-face blowout as a major failure mode.

The results from the analysis based on the anchorage provisions and descriptive equations show that the estimated peak bar force T' is greater by a factor of 3.54 and 1.13 on average than the anchorage strengths T_{anc} and T_h , respectively. The values of T'/T_{anc} ranged from 1.13 to 7.29 with STD and COV of 1.246 and 0.352, respectively, while the values of T'/T_h ranged from 0.74 to 1.43 with STD and COV of 0.158 and 0.139, respectively. None of the specimens had $T'/T_{anc} < 1.0$, but four specimens, one tested by each Matsushima et al. (2000) (H) and Kiyohara et al. (2005) (No. 8), and two tested by Tasai et al. (2000) (No. 6 and No. 7), had $T'/T_h < 1.0$ (0.74, 0.83, 0.98, and 0.99, respectively). These results show that the anchorage strength calculated using anchorage provisions of Chapter 17 of ACI 318-14 results in more conservative estimate of anchorage strength compared to that calculated using the descriptive equations, with $T'/T_{anc} > T'/T_h$. This occurs because the anchorage provisions of Chapter 17 of ACI 318-14 used to calculate T_{anc} are based on the 5% fractile of the test results used to develop the anchorage equations, while the descriptive equations for T_h were developed to ensure the *average* ratio of test-to-calculated failure load equal to 1.0. Distribution of T'/T_{anc} and T'/T_h is shown in Figures 4.24. The figures show a greater variation in values of T'/T_{anc} compared to that of T'/T_h , as suggested by the coefficients of variation of 35% vs 14% (see Table 4.6). These observations indicate that the descriptive equations, Eq. (4.1) and (4.2), which were developed based on test results of exterior beam-column joints subjected to monotonic loading, capture the anchorage behavior of exterior and roof-level interior beam-column joints subjected to reversed cyclic loading more accurately than do the anchorage provisions.

Table 4.6 Statistical parameters from the comparison of anchorage strengths of headed bars

Statistical Parameters	Specimens with $\ell_{eh}/\ell_{ehy} < 1.0$	
	T'/T_{anc}	T'/T_h
Number of specimens	28	28
Max	7.29	1.43
Min	1.13	0.74
Mean	3.54	1.13
STD	1.246	0.158
COV	0.352	0.139
Number of specimens with T'/T_{anc} or $T'/T_h < 1.0$	0	4

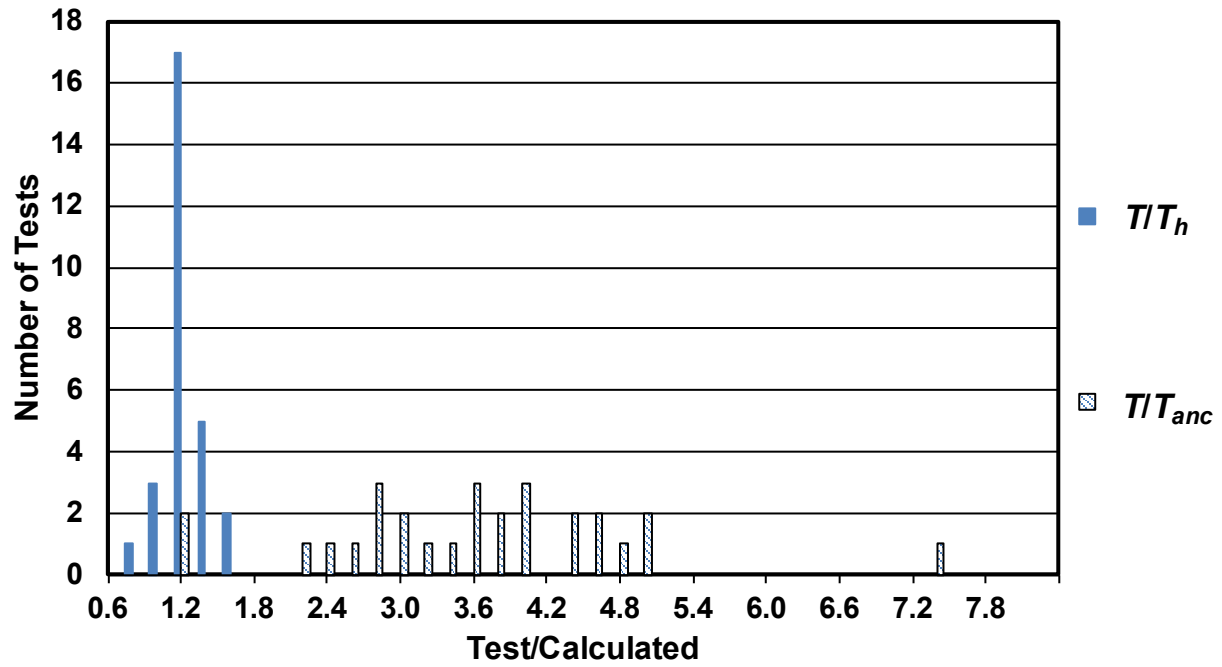


Figure 4.24 Distribution of ratios T/T_h and T/T_{anc} for headed bars with $\ell_{eh}/\ell_{ehy} < 1.0$ in beam-column joint specimens tested under reversed cyclic loading

CHAPTER 5: DESIGN PROVISIONS

Shao et al. (2016) developed a design equation and supporting provisions for the development length ℓ_{dt} of headed bars based on test results from 202 exterior beam-column joint specimens subjected to monotonic loading. In this chapter, an update and simplifications to these design provisions is presented to accommodate the application of headed bars in members subjected to reversed cyclic as well as monotonic loading. Proposed code provisions for the development length of headed bars and head dimension requirements are also presented, along with representative design example problems for headed bar applications.

5.1 DESIGN EQUATION

Design equation Eq. (5.1) for the development length of headed bars is based on the descriptive equations discussed in Section 1.4.1 developed by Shao et al. (2016). In the equation, strength-reduction factors, producing a probability of failure less than one-fifth the probability of a flexural failure ($\beta = 3.5$, versus 3.0 for flexure), are embedded.

$$\ell_{dt} = \left(0.0024 \frac{f_y \Psi_e \Psi_{cs} \Psi_o}{f_c'^{0.25}} \right) d_b^{1.5} \quad (5.1)$$

where ℓ_{dt} = development length of a headed bar in tension (in.) not less than the greater of $8d_b$ and 6 in.; f_y = specified yield strength of the headed bar (psi); Ψ_e = modification factor for epoxy-coated or zinc and epoxy dual-coated bars; Ψ_{cs} = modification factor for confining reinforcement and bar spacing; Ψ_o = modification factor for bar location; f_c' = concrete compressive strength (psi); and d_b = diameter of the headed bar (in.).

Equation (5.1) is further simplified to Eq. (5.2).

$$\ell_{dt} = \left(\frac{f_y \Psi_e \Psi_{cs} \Psi_o}{400 f_c'^{0.25}} \right) d_b^{1.5} \quad (5.2)$$

The proposed provisions apply to headed bars with specified yield strengths up to 120,000 psi and concrete compressive strengths up to 16,000 psi. The modification factor Ψ_e for the reinforcement coating condition is 1.2 for epoxy-coated or zinc and epoxy dual-coated bars and 1.0 for uncoated or zinc-coated (galvanized) bars. This modification factor is retained from ACI 318-14, as is the restriction on not using headed bars in lightweight concrete due to a total lack of data on the use of headed bars in lightweight concrete.

5.1.1 Confinement and spacing factor, ψ_{cs}

The development length is adjusted based on the amount of confining reinforcement parallel to the headed bars within the joint region as well as the spacing between the bars. Requirements for the determination of values for the modification factor for confining reinforcement and bar spacing ψ_{cs} are simplified from those originally suggested in Shao et al. (2016). The simplified values for ψ_{cs} , given in Table 5.1, are permitted to be interpolated for intermediate values of c_{ch} and A_{tt}/A_{hs} .

Table 5.1 Modification factor ψ_{cs} for confining reinforcement and bar spacing

Confinement level	c_{ch}	
	$2d_b$	$\geq 8d_b$
	Value of ψ_{cs}	
$\frac{A_{tt}}{A_{hs}} \geq 0.3$	0.6	0.4
$\frac{A_{tt}}{A_{hs}} = 0$ (no confining reinforcement)	1.0	0.5

where c_{ch} is center-to-center spacing between adjacent headed bars; for splices, c_{ch} is taken as the lesser of (1) center-to-center spacing between the adjacent lapped bars and (2) twice the cover to the center of the lapped bar in the direction perpendicular to the plane of the bars, A_{hs} is the total cross-sectional area of headed bars being developed, and A_{tt} is the total cross-sectional area of all confining reinforcement parallel to ℓ_{dt} for headed bars being developed in beam-column joints and located within $8d_b$ of the center of the headed bars in the direction of the interior of the joint, as shown in Figure 5.1; for members other than beam-column joints, A_{tt} is the minimum total cross-sectional area of all confining reinforcement within $8d_b$ on one side of the bar centerline parallel to the headed bars being developed, as shown in Figure 5.2.

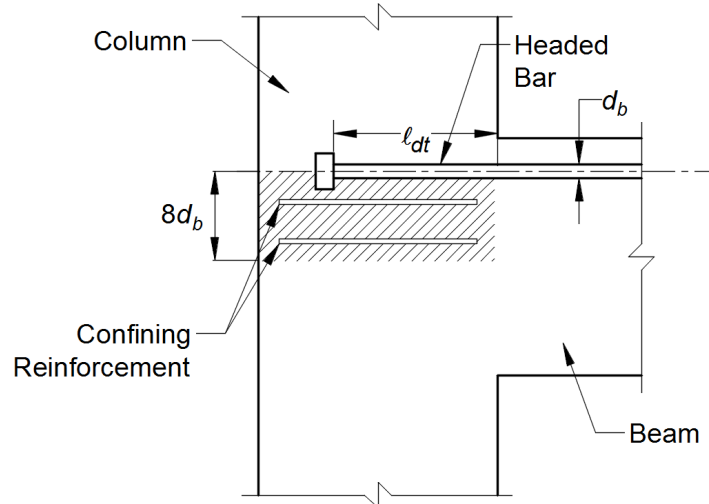


Figure 5.1 Effective confining reinforcement within the joint region of beam-column joints

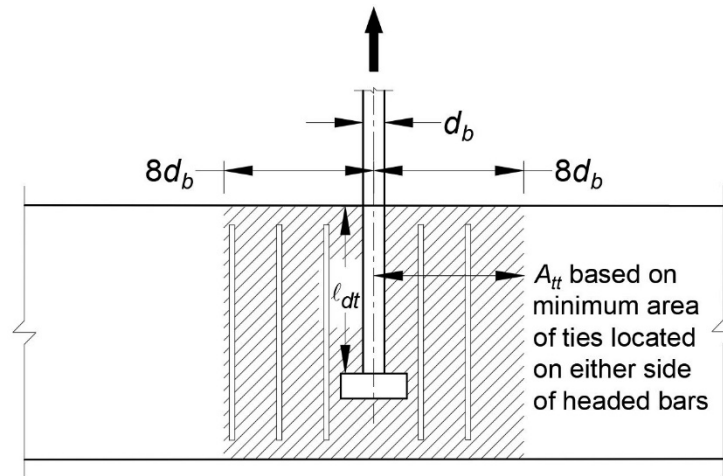


Figure 5.2 Effective confining reinforcement for members other than beam-column joints

Reinforcement perpendicular to headed bars is not considered when calculating A_{tt} . Hairpin or hoop tie-down confining reinforcement perpendicular to the headed bars (see Figure 1.6) was provided in splice specimens (slabs) tested by Thompson et al. (2002), while stirrups were used in splice specimens (beams) tested by Chun (2015) and CCT node specimens (beams) tested by Thompson et al. (2005, 2006a). The hairpin or hoop tie-downs in the splice specimens did not contribute to improve the anchorage strength of headed bars. This is consistent with the findings discussed in Section 3.3.1.2 that reinforcement perpendicular to a headed bar is ineffective in confining the bar. On the other hand, in his splice tests, Chun (2015), observed that stirrups perpendicular to the headed bars were effective in confining the bars in the *beam* specimens by limiting the prying effect on the cover concrete within the splice region and increasing the splice strength relative to the specimens without confining reinforcement. The use of stirrups as confining

reinforcement, however, is highly unlikely for headed bar splices, such as in closure strips in slabs, where prying of the cover concrete is not the expected failure mode. Therefore, reinforcement perpendicular to the headed bars is not considered when calculating A_{tt} .

5.1.2 Bar location factor, ψ_o

The descriptive equations discussed in Section 1.4.1 for the anchorage strength of headed bars were developed from tests of beam-column joint specimens containing headed bars inside the column core (a region of the column cross-section located inside the column longitudinal reinforcement) with 2.5-in. minimum side cover to the bar inside the joint region. These descriptive equations were used to develop the design equation Eq. (5.2). Headed bars anchored inside the column core with side cover to the bar $c_{so} < 2.5$ in., outside the column core, or in members other than beam-column joints with $c_{so} < 8d_b$ exhibited about 20% lower anchorage strength on average compared to the headed bars anchored inside the column core with $c_{so} \geq 2.5$ in. (Shao et al. 2016). The bar location factor ψ_o is, therefore, introduced to accommodate lower anchorage strength of such headed bars. The value of ψ_o is equal to 1.0 for headed bars terminating inside the column core with minimum clear cover to the bar $c_{so} \geq 2.5$ in., or terminating in a supporting member other than beam-column joints with minimum clear cover to the bar $\geq 8d_b$; in other cases, the value of ψ_o is equal to 1.25.

5.1.3 Comparisons of test results

The provisions for headed bars were compared with results for beam-column joint tests by Bashandy (1996), shallow embedment tests by DeVries et al. (1999), CCT node and splice tests by Thompson et al. (2005, 2006a, 2006b), beam-column joint tests by Chun et al. (2009), splice tests by Chun (2015), beam-column joint and CCT node tests by Shao et al. (2016), and splice and shallow embedment tests in the current study.

In Figures 5.3 and 5.4, the ratio of the stress at anchorage failure of headed bars f_{su} to the stress predicted by Eq. (5.2) $f_{s,calc}$ is compared to the measured concrete compressive strength f_{cm} for specimens without and with confining reinforcement tested by Shao et al. (2016), respectively. The results cover both widely-spaced (center-to-center spacing $\geq 8d_b$) and closely-spaced (center-to-center spacing $< 8d_b$) headed bars with head bearing areas A_{brg} between 3.8 and $9.5A_b$. These head sizes are grouped based on observations by Shao et al. (2016) that headed bars with bearing

areas within this range provide approximately the same anchorage capacity. The statistical parameters of $f_{su}/f_{s,calc}$ for the beam-column joint headed-bar specimens without and with confining reinforcement are summarized in Tables 5.2 and 5.3, respectively.

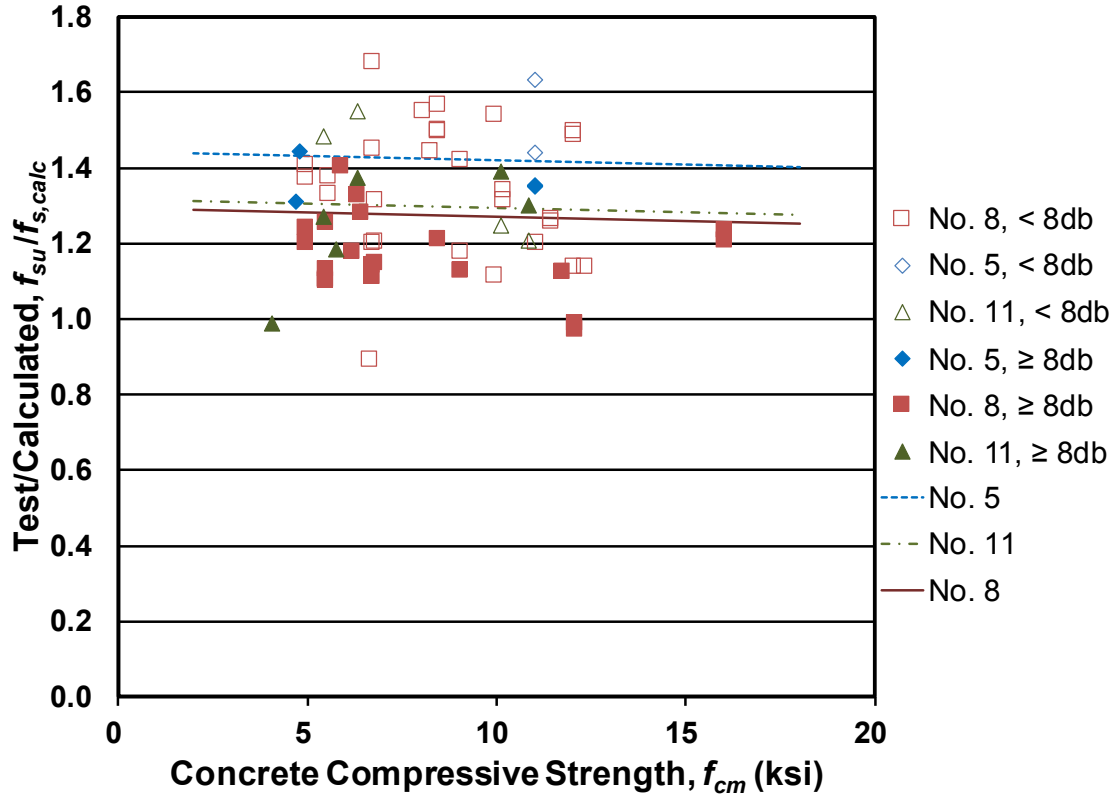


Figure 5.3 Ratio of test-to-calculated stress $f_{su}/f_{s,calc}$ versus concrete compressive strength f_{cm} for beam-column joint specimens with widely-spaced and closely-spaced headed bars without confining reinforcement tested by Shao et al. (2016).

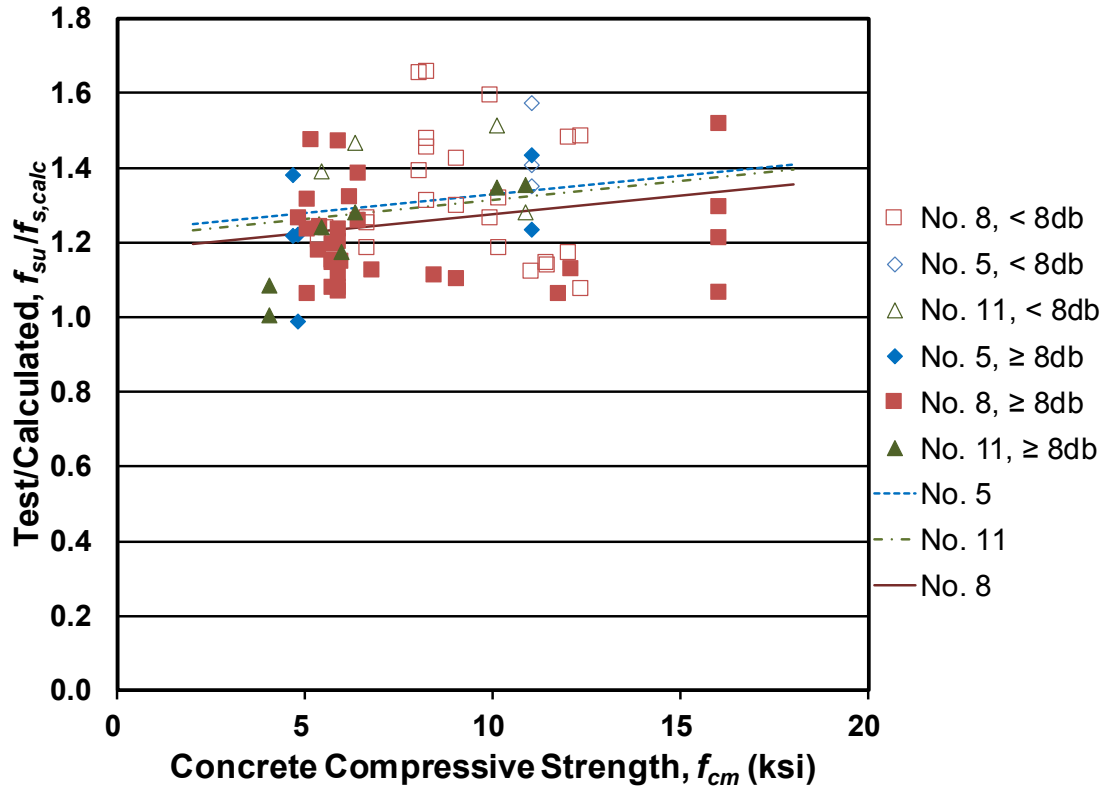


Figure 5.4 Ratio of test-to-calculated stress $f_{su}/f_{s,calc}$ versus concrete compressive strength f_{cm} for beam-column joint specimens with widely-spaced and closely-spaced headed bars enclosed by No. 3 ties spaced at $3d_b$ in the joint region tested by Shao et al. (2016).

Table 5.2 Statistical parameters of $f_{su}/f_{s,calc}$ for headed-bar beam-column joint specimens without confining reinforcement tested by Shao et al. (2016), with $f_{s,calc}$ based on Eq. (5.2)

(Number of specimens)	All	C-C spacing $\geq 8d_b$			$3d_b \leq$ C-C spacing $< 8d_b$		
		No. 5	No. 8	No. 11	No. 5	No. 8	No. 11
	(64)	(4)	(20)	(6)	(2)	(28)	(4)
Max	1.68	1.44	1.40	1.39	1.63	1.68	1.55
Min	0.89	1.31	0.97	0.99	1.44	0.89	1.21
Mean	1.29	1.37	1.17	1.25	1.54	1.35	1.37
STD	0.168	0.055	0.103	0.148	0.135	0.174	0.171
COV	0.130	0.040	0.088	0.118	0.088	0.129	0.125
No. with $f_{su}/f_{s,calc} < 1.0$	4	0	2	1	0	1	0

Table 5.3 Statistical parameters of $f_{su}/f_{s,calc}$ for headed-bar beam-column joint specimens with confining reinforcement tested by Shao et al. (2016), with $f_{s,calc}$ based on Eq. (5.2)

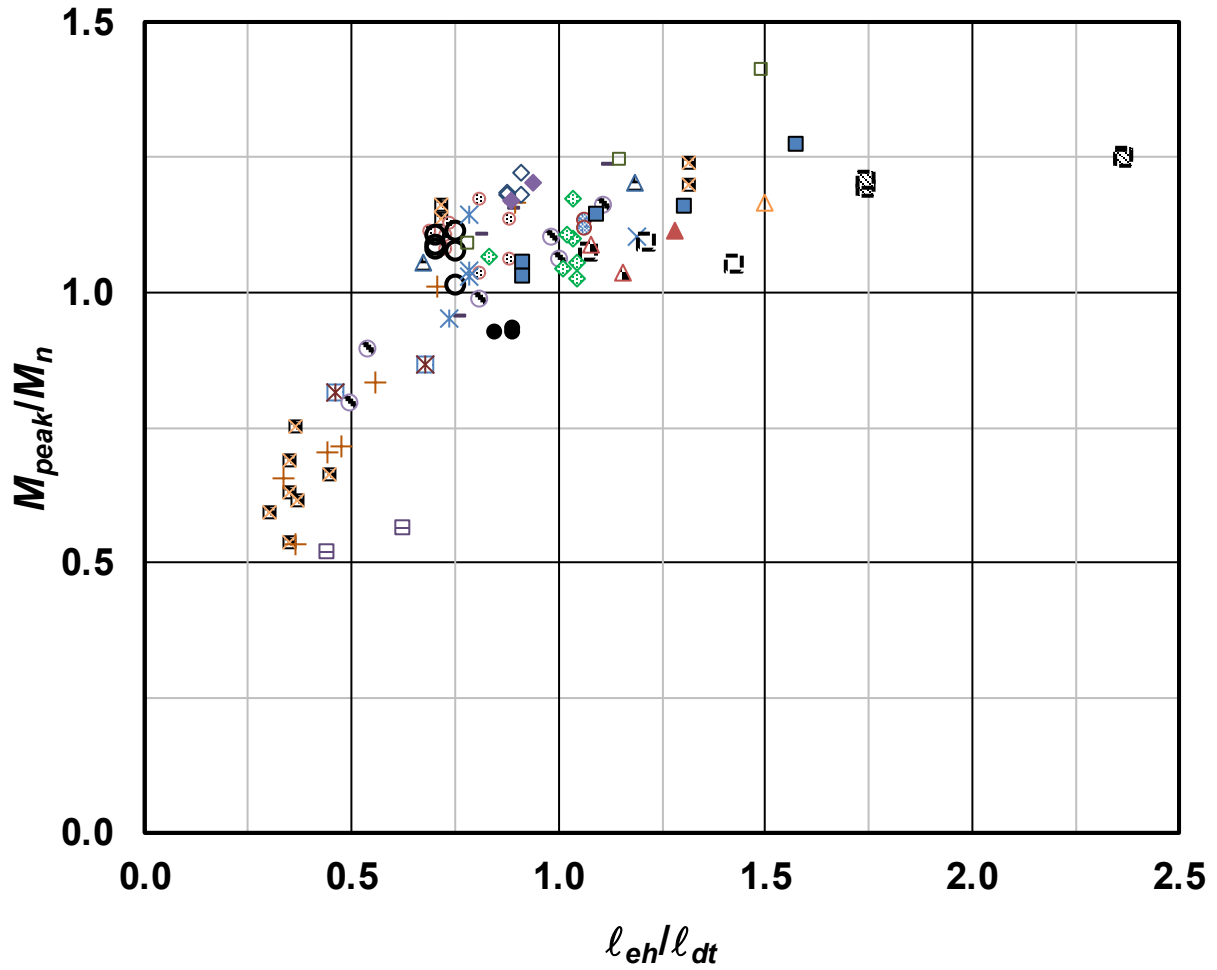
(Number of specimens)	All	C-C spacing $\geq 8d_b$			$3d_b \leq$ C-C spacing $< 8d_b$		
		No. 5	No. 8	No. 11	No. 5	No. 8	No. 11
	(74)	(6)	(30)	(7)	(3)	(24)	(4)
Max	1.66	1.43	1.52	1.35	1.57	1.66	1.51
Min	0.99	0.99	1.06	1.00	1.35	1.07	1.28
Mean	1.27	1.25	1.21	1.21	1.44	1.32	1.41
STD	0.157	0.156	0.128	0.132	0.117	0.170	0.101
COV	0.124	0.125	0.106	0.109	0.081	0.128	0.071
No. with $f_{su}/f_{s,calc} < 1.0$	1	1	0	0	0	0	0

The best-fit lines for headed bars in Figures 5.3 and 5.4 are closely spaced and nearly horizontal. The lines drop slightly with an increase in f_{cm} for headed bars without confining reinforcement and rise slightly for headed bars with confining reinforcement. The order of the lines is not in order of bar size, although the line for No. 5 bars is the highest in each case. The comparisons show that bar diameter to the 1.5 power and concrete compressive strength to the 0.25 power provide realistic representations of the anchorage strength. As shown in Tables 5.2 and 5.3, the mean ratios of $f_{su}/f_{s,calc}$ for headed-bar test specimens without and with confining reinforcement are 1.29 and 1.27, with coefficients of variation of 0.130 and 0.124, respectively. Six percent (4 out of 64) of the test specimens without and 1.5 percent (1 out of 74) of the test specimens with confining reinforcement have values of $f_{su}/f_{s,calc} < 1.0$ - overall less than 4 percent. Of the five specimens with $f_{su}/f_{s,calc} < 1.0$, four have values of 0.97 or greater.

In addition to the results shown in Figures 5.3 and 5.4 and Tables 5.2 and 5.3, Shao et al. (2016) observed that headed bars with A_{brg} between 12.9 and $15A_b$ provide additional capacity that could be used to justify reducing the proposed development lengths by about 10%. For simplicity, however, a provision to take advantage of this higher strength is not being proposed at this time. Based on strain-gage data, no tests indicated that the full load was transferred at that head (Shao et al. 2016).

As observed for the beam-column joints tested under monotonic loading by Shao et al. (2016), a comparison of test results for the beam-column joints tested under reversed cyclic loading with significant inelastic lateral displacement shows that the provisions for headed bars are conservative for reversed cyclic loading as well. In Figure 5.5, the ratio of the peak moment to

flexural strength M_{peak}/M_n is plotted versus the ratio of the actual embedment length ℓ_{eh} to the development length ℓ_{dt} of the headed bars calculated using Eq. (5.2) based on the actual yield strength. As shown in the figure, all specimens with $\ell_{eh}/\ell_{dt} \geq 1.0$ had $M_{peak}/M_n \geq 1.0$. This indicates that the development length calculated using Eq. (5.2) is sufficient to yield the headed bars in members subjected to reversed cyclic loading.



- × Bashandy (1996)
- ▲ Wallace et al. (1998)
- ⊗ Nakazawa et al. (2000)
- Yoshida et al. (2000)
- ▣ Ishibashi et. al (2003)
- Kiyohara et al. (2004)
- ▲ Kato (2005)
- Adachi and Masuo (2007)
- × Ishida et al. (2007)
- ◇ Lee and Yu (2009)
- ◆ Kang et al. (2012)
- Dhake et al. (2015)
- ⊠ Murakami et al. (1998)
- ⊠ Matsushima et al. (2000)
- ▣ Tasai et. al (2000)
- ⊗ Takeuchi et al. (2001)
- ▣ Ishibashi and Inokuchi (2004)
- + Kiyohara et al. (2005)
- ⊗ Masuo et al. (2006a, 2006b)
- Chun et. al (2007)
- △ Tazaki et al. (2007)
- △ Kang et al. (2010)
- ◆ Chun and Shin (2014)

Figure 5.5 M_{peak}/M_n versus l_{eh}/l_{dt} for beam-column joint specimens tested under reversed cyclic loading. M_{peak}/M_n is the ratio of peak moment to nominal flexural strength, and l_{eh}/l_{dt} is the ratio of embedment length to the development length calculated using Eq. (5.2).

Comparisons of test results for specimen types other than beam-column joints also show that the provisions for headed bars are conservative. The results for CCT node (Thompson et al. 2005, 2006a; Shao et al. 2016), splice (Thompson et al. 2006b; current study), and shallow embedment (DeVries et al. 1999; current study) tests are summarized in Table 5.4. The mean values of $f_{su}/f_{s,calc}$ for CCT node, splice and shallow embedment tests are, respectively, 2.00, 1.53, and 1.54, with coefficients of variation of 0.135, 0.217, and 0.150, and no values of $f_{su}/f_{s,calc}$ below 1.0. The high mean value of $f_{su}/f_{s,calc}$ for the CCT node tests is likely due to the compressive reaction acting perpendicular to the headed bars in the beam test specimens.

Table 5.4 Statistical parameters of $f_{su}/f_{s,calc}$ for headed-bar CCT node, splice, and shallow embedment specimens, with $f_{s,calc}$ based on Eq. (5.2)

(Number of specimens)	CCT Node	Splice	Shallow embedment
	$6d_b \leq \text{C-C spacing} < 12d_b$	$1.67d_b \leq \text{C-C spacing} < 5d_b$	NA
	(25)	(21)	(35)
Max	2.81	2.27	2.28
Min	1.29	1.14	1.17
Mean	2.00	1.53	1.54
STD	0.270	0.330	0.231
COV	0.135	0.217	0.150
No. with $f_{su}/f_{s,calc} < 1.0$	0	0	0

Tests on exterior beam-column joint specimens (Shao et al. 2016) showed that the beam-column joints with a ratio of effective beam depth to embedment length $d/\ell_{eh} > 1.5$ generally exhibited lower anchorage strength than the joints with the ratio less than or equal to 1.5 (Section 4.2.2.3). The specimens with $d/\ell_{eh} > 1.5$ were not used to develop the design provisions discussed in Sections 5.1.1 and 5.1.2. An analysis of the specimens with $d/\ell_{eh} > 1.5$ using strut-and-tie method in accordance with Chapter 23 of ACI 318-14 provided a conservative estimate of the anchorage strength of headed bars (Shao et al. 2016). Therefore, the analysis and design of joints with $d/\ell_{eh} > 1.5$ is suggested to be based on the strut-and-tie method in accordance with Chapter 23 of ACI 318-14.

As discussed in Section 3.1.2, tests on headed bars in column-foundation joints showed that the anchorage strength of headed bars was not affected when the ratio of distance from the center of the headed bar to the inside face of the bearing plate (Figure 3.2) to the embedment length h_{cl}/ℓ_{eh} was as high as 2.79, but that the anchorage strength was reduced when h_{cl}/ℓ_{eh} was equal to

5.6. The values of h_{cl}/ℓ_{eh} of 2.79 and 5.6 correspond, respectively, to ratios of the effective depth of the simulated column under bending to the embedment length of the headed bar d/ℓ_{eh} equal to 3 and 5.73, respectively (also see Table 3.1 and Table B.1 of Appendix B). A key difference of these tests from those involving beam-column joints is the fact that little if any of the conical breakout surface at a foundation joint intersects the exterior of the foundation, while the breakout surface in the beam-column joints is truncated by the column. It is, therefore, suggested that the design provisions discussed in Sections 5.1.1 and 5.1.2 be used for headed bars in members anchored to foundations if the effective depth d of the member is no more than 3 times the embedment length of headed bars.

5.1.4 Range of specified yield strength

Because the tests by Shao et al. (2016) show that Eq. (5.2) is valid for bar stresses up to 142 ksi, the proposed provisions could be used for bars with specified yield strengths up to 120 ksi.

5.1.5 Stress multiplier

As discussed in Section 4.2, the strength and deformability of beam-column joints subjected to reversed cyclic loading with embedment lengths sufficient to yield the bar are the functions of the post-yield behavior of the headed bars. The actual yield strength of a typical reinforcing bar is usually 110 to 125% of the specified yield strength (Section 3.3.4 of ACI 352R-02), and strain hardening of the reinforcing bars commonly begins slightly above the actual yield strength of the bar (Wight and Sozen 1973). In accordance with Section 18.8.2.1 of ACI 318-14, for beam-column joints of special moment frames forming part of seismic-force-resisting system, forces in beam longitudinal reinforcement should be calculated assuming a bar stress of $1.25f_y$. This implies that an embedment length sufficient to develop $1.25f_y$ is needed for headed bars anchored in members of special moment frames. The design provisions for the development length of headed bar in Section 18.8.5.2 of ACI 318-14, however, do not specify that the embedment length be calculated assuming bar stress of $1.25f_y$, which is in contrast with the development length requirements of Section 4.5.3.3 of ACI 352R-02. To ensure that the strain hardening of steel at plastic hinge locations can occur in members expected to undergo significant inelastic deformations, such as in special moment frames forming part of seismic-force-resisting system, it

is suggested that the embedment length of the headed bar be calculated using Eq. (5.2) based on a bar stress of $1.25f_y$.

5.1.6 Further simplification of design equation

For ease of design, it is suggested that a simplified alternative to Eq.(5.2) be added to ACI 318:

$$\ell_{dt} = \left(\frac{f_y \Psi_e \Psi_o}{k_t f_c'^{0.25}} \right) d_b \quad (5.3)$$

where k_t is the coefficient for development length of headed bars, values of which are given in Table 5.5.

Table 5.5 Coefficient k_t for headed deformed bars in tension

Clear spacing of headed bars being developed	No. 5 and smaller bars	No. 6, 7, and 8 bars	No. 9, 10, and 11 bars
$\geq 7d_b$	1000	800	670
$\geq 2d_b$ and $< 7d_b$	550	430	365
$\geq 1d_b$ and $< 2d_b$	500	400	330

Equation (5.3) is based on Eq. (5.2) and ψ_{cs} from Table 5.1 for $A_{tt}/A_{hs} = 0$ (no confining reinforcement). The values of k_t cover three cases for bar size (No. 5 and smaller, No. 6 through No. 8, and No. 9 and larger bars) and spacing that are often encountered in practice: (a) widely spaced headed bars, (b) headed deformed bars with a clear spacing of at least $2d_b$, and (c) closely spaced headed deformed bars with a clear spacing of d_b . Using the minimum spacing and maximum bar size in each category shown in Table 5.5, Eq. (5.3) with appropriate value of k_t gives the value of ℓ_{dt} obtained using Eq. (5.2) with the corresponding value of ψ_{cs} for $A_{tt}/A_{hs} = 0$. As a result Eq. (5.3) is in most cases more conservative than Eq. (5.2).

5.1.7 Head size

Cold-swaged threaded coupling sleeve heads used in slab specimens tested in the current study (see Table 2.3) and beam-column joint specimens tested by Shao et al. (2016) contained an obstruction that exceeded the dimensional limits of HA headed bars in ASTM A970-16. These headed bars contained a tapered section (gap) adjacent to the head followed by a larger obstruction, as shown in Figure 5.6. As discussed in Section 2.1.2, the heads used in the beam-column joint specimens tested by Shao et al. (2016) were re-measured. The minimum value of the gross head

area minus the area of maximum size of the obstruction (diameter of $2.2d_b$, equivalently, net area of $3.8A_b$) was $2.8A_b$. The upper limit on the length of the obstruction measured from the bearing face of the head was $5.25d_b$. Shao et al. (2016) observed from autopsies of specimens after tests that concrete was intact around the full bearing face of the head (including the gap), indicating that bearing on the head within the tapered portion of the obstruction was also effective in transferring the load. Shao et al. (2016), therefore, calculated the net bearing area as the gross area of head minus the area of the obstruction adjacent to the bearing face of the head (at the taper section), which was as low as $4.5A_b$. The width of the gap in these headed bars was $3/8$ in. for No. 6 and No. 8 bars, and $5/8$ in. for No. 11 bar, and the depth of the gap was less than the width. No reduction in anchorage strength of these headed bars was observed compared to other headed bars with similar net bearing areas containing no obstructions. In addition, as shown in Figure 5.7, friction-forged heads used in slab specimens tested in the current study (see Table 2.3) and beam-column joint specimens tested by Shao et al. (2016) contained obstructions that had length measured from the bearing face of the head not more than $0.6d_b$ for No. 8 and larger bars or the smaller of 0.6 in. and $0.75d_b$ for bars smaller than No. 8 and did not have a diameter greater than $1.5d_b$. These obstructions, however, did not have any detrimental effects on the anchorage strength of the headed bars and, therefore, are not considered to detract from the net bearing area of the head.

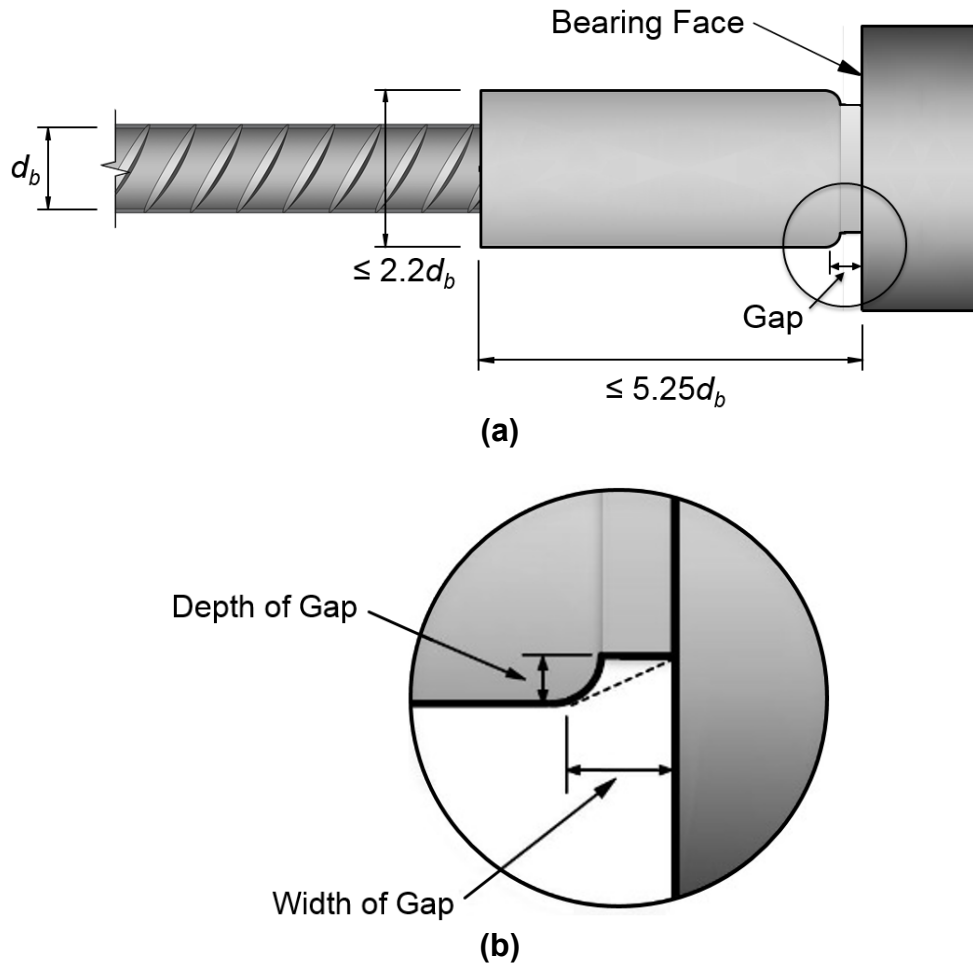


Figure 5.6 (a) Maximum dimensions and non-planar features of the obstruction (b) detail of gap in obstruction adjacent to the bearing face of the head (after Shao et al. 2016)

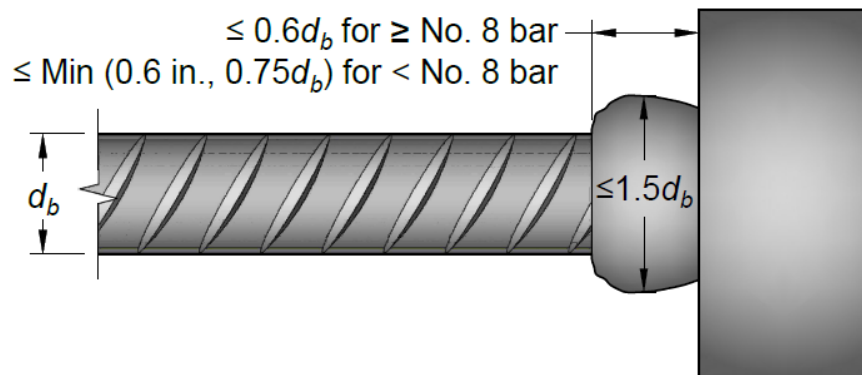
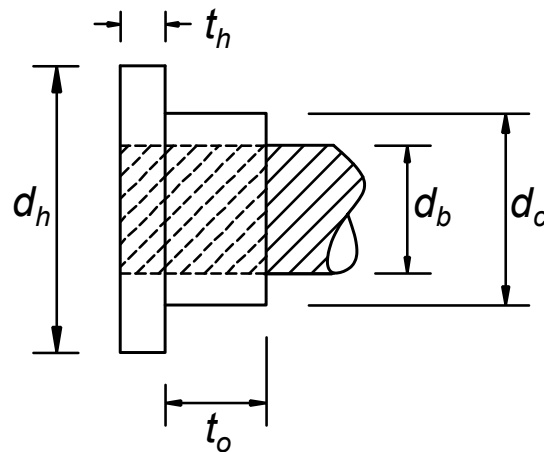


Figure 5.7 Headed bar with an obstruction not considered to detract from the net bearing area of the head

In addition, Shao et al. (2016) analyzed results from beam-column joint specimens tested by Chun et al. (2009) and headed splice specimens tested by Chun (2015). Headed bars in these specimens (Figure 5.8) had a gross head area of $5A_b$ and a bearing area (calculated as gross head

area minus bar area) of $4A_b$, equal to the minimum net bearing area of heads allowed in ACI 318-14 and ASTM A970-16. These heads, however, contained obstructions with a length of $0.75d_b$ and a diameter $1.5d_b$, equal to the upper limit for HA heads, which reduced the head bearing area adjacent to the obstruction (gross head area minus the maximum area of the obstruction) to between 2.7 and $2.8A_b$. Unlike the cold-swaged threaded coupling sleeve headed bars (Figure 5.6) tested in the current study and by Shao et al. (2016), obstructions on headed bars tested by Chun et al. (2009) and Chun (2015) did not contain any tapered section adjacent to the bearing face of the head. Also, the obstructions on headed bars tested by Chun et al. (2009) and Chun (2015) were longer than the friction-forged headed bars tested in the current study and by Shao et al. (2016). The beam-column joint and headed splice specimens containing these headed bars tested by Chun et al. (2009) and Chun (2015) had consistently low anchorage strengths when compared to the headed bars tested in the current study and by Shao et al. (2016) and below those based on both descriptive and design equations.



Bar Size	d_b	d_h	d_c	t_h	t_o
No. 8	1.0	2.24	1.50	0.35	0.79
No. 11	1.41	3.15	2.13	0.47	1.03
No. 18	2.26	5.04	3.31	0.79	1.65

(Unit: in.)

Figure 5.8 Dimensions of heads used in beam-column joint specimens tested by Chun et al. (2009) and headed splice specimens tested by Chun (2015) [figure after Hong et al. (2007)]

The analysis of the effect of head size on the performance of beam-column joints subjected to reversed cyclic loading presented in Section 4.3 shows that headed bars with a net bearing area

less than $3.7A_b$ performed satisfactorily because they had embedment lengths ℓ_{eh} between 1.48 and 2.95 times the embedment length required to yield the bar ℓ_{ehy} calculated using descriptive equations, Eq. (4.1) and (4.2). Thus, these tests do not show that heads with $A_{brg} < 3.7A_b$ will provide adequate anchorage in specimens with embedment lengths just sufficient to yield the bar. On the other hand, results from a limited number of beam-column joint specimens (6) containing headed bars with A_{brg} between 2.7 and $3.2A_b$ and ℓ_{eh} between 1.08 and 1.32 times ℓ_{ehy} showed that A_{brg} as low as $2.7A_b$ may be sufficient to anchor the headed bars in members subjected to reversed cyclic loading. As discussed in Section 3.3.1, however, headed bars anchored in slab and column-like specimens tested under monotonic loading by Choi et al. (2002) and Choi (2006) with net bearing areas between 2.6 and $3.2A_b$ and no obstruction consistently performed poorly. Therefore, the use of headed bars with net bearing area less than $3.7A_b$ cannot ensure adequate anchorage in all cases. Specimens containing headed bars with a net bearing area $\geq 3.7A_b$, however, provided adequate anchorage without requiring an extended development length or a high amount of confining reinforcement.

Based on the performance of headed bars with different head sizes and the re-measurement of the heads used in beam-column joint specimens tested by Shao et al. (2016), it is suggested that in most cases, the net bearing area of the head be calculated as the gross head area minus the maximum area of the obstruction adjacent to the head and should not be less than $4A_b$, as suggested by Shao et al. (2016), with the exception of heads with very short obstructions. The recommended minimum value of A_{brg} of $4A_b$ is retained from ACI 318-14. Headed bars with obstructions should meet the dimensional limits shown in Figure 5.6. For heads with an obstruction containing a gap adjacent to the head, the net bearing area of the head can be calculated as the gross head area minus the area of the obstruction at the gap adjacent to the bearing face of the head, provided that the width of the gap is not less than the larger of $\frac{3}{8}$ in. and $\frac{3}{8}d_b$, the depth of the gap does not exceed width of the gap, and the obstruction everywhere within the gap falls inside a straight line connecting the outer dimension of the obstruction at the initiation of the gap with the dimension of the obstruction at the bearing face of the head (Figure 5.6b). Also, for heads with an obstruction containing a gap satisfying these gap dimension limits, the gross head area minus the maximum obstruction area should not be less than $2.8A_b$. The maximum length measured from the bearing

face of the head should not exceed $5.25d_b$, and the diameter of the obstruction should not exceed $2.2d_b$ (net area of $3.8A_b$), with the exception of obstructions, as shown in Figure 5.7, that do not extend from bearing face of the head more than 0.6 nominal bar diameters for No. 8 and larger bars or the smaller of 0.6 in. and $0.75d_b$ for bars smaller than No. 8 and do not have a diameter greater than 1.5 nominal bar diameters shall not be considered to detract from the net bearing area of the head.

5.2 PROPOSED CODE PROVISIONS

5.2.1 Proposed Changes in ACI 318

The following modifications are recommended for Sections 2.2, 15.4, 16.3, 18.8, and 25.4 of ACI 318-14. The changes are shown using underline and ~~strikeout~~.

2.2—Notation

A_{hs} = total cross-sectional area of hooked or headed bars being developed, in.²

A_{tt} = total cross-sectional area of all ties or stirrups enclosing headed bars in.²

c_{ch} = minimum center-to-center spacing of hooked or headed bars being developed or spliced, in.

k_t = coefficient for development length of headed deformed bars

~~ψ_e~~ = factor used to modify development length based on cover

ψ_{cs} = factor used to modify development length based on center-to-center spacing of and reinforcement enclosing hooked or headed bars

ψ_o = factor used to modify development length based on minimum clear cover and the placement of hooked or headed bars within the confined core of a column

15.4.4 Development of longitudinal reinforcement terminating in the joint shall be in accordance with **25.4**. If the effective depth d of any beam framing into the joint and generating shear exceeds 1.5 times the reinforcement anchorage length, analysis and design of the joint shall be based on the strut-and-tie method in accordance with Chapter 23.

R15.4.4 Tests on exterior beam-column joint specimens (Shao et al. 2016) show that the beam-column joints with a ratio of effective beam depth to embedment length d/ℓ_{eh} greater than 1.5 generally exhibit lower anchorage strength than the joints with the ratio less than or equal to 1.5. Tests of specimens with d/ℓ_{eh} greater than 1.5 were not used to develop the design provisions of 25.4.4. An analysis of the specimens with d/ℓ_{eh} greater than 1.5 using strut-and-tie method in accordance with **Chapter 23** provided a conservative estimate of the anchorage strength of headed bars.

16.3.5.5 Headed deformed bars shall be permitted to be anchored in tension in accordance with 25.4.4 if the effective depth d of the supported member is no more than 3 times the anchorage length.

R16.3.5.5 Tests on headed bars in column-foundation joints (Shao et al. 2016; Ghimire et al. 2018) showed that the anchorage strength of the headed bar was not affected when the ratio of effective depth d of column under bending to the anchorage length of the headed bar was increased up to 3, but the anchorage strength was reduced when the ratio exceeded 3.

18.8.5.2 For headed deformed bars satisfying 20.2.1.6, development in tension shall be in accordance with 25.4.4 based on a bar stress of $1.25f_y$, except clear spacing between bars shall be permitted to be at least $3d_b$ or greater.

R18.8.5.2 The $3d_b$ spacing limit is based on studies of joints confined by transverse reinforcement consistent with special moment frame requirements in this chapter (Kang et al. 2009). To avoid congestion, it may be desirable to stagger the heads. Provisions of 25.4.4 effectively capture the anchorage behavior of the headed bars in beam-column joints subjected to reversed cyclic loading before and after the yielding of the bars (Ghimire et al. 2018). To ensure that the strain hardening of steel at plastic hinge locations can occur in members expected to undergo significant inelastic deformations, as required at the joint face of special moment frames (refer to R18.8.2), the development length of the headed bar is calculated for a stress of $1.25f_y$.

25.4.1.4 The value of $\sqrt[3]{f'_c} f'_c$ used to calculate development length shall not exceed ~~100~~ 16,000 psi, except in 25.4.7 and 25.4.9, where f'_c used to calculate development length shall not exceed 10,000 psi.

Note to readers: Changes in 25.4.1.4 also depend on changes on the development length requirements for straight bars. In this proposed change, 25.4.1.4 has been written to apply to the development of straight, hooked, and headed bars. Since no changes are planned for 25.4.7 (development of plain welded-wire reinforcement in tension) and 25.4.9 (development of deformed bars and deformed wires in compression), the 10,000 psi limit is retained in 25.4.1.4.

R25.4.1.4 Darwin et al. (1996) and Zuo and Darwin (2000) showed that the tension force developed in a straight bars in development and lap splice tests increases at a lesser rate than $\sqrt{f'_c}$ that is close to $f'_c{}^{0.25}$ with increasing compressive strength up to 16,000 psi. Using $\sqrt{f'_c}$, however, is sufficiently accurate for values of $\sqrt{f'_c}$ up to 100 psi, and because of the long standing use of the $\sqrt{f'_c}$ in design, The anchorage strength of standard hooks Sperry et al. (2015a, 2015b, 2017b);

Ajaam et al. 2017) and headed bars (Shao et al. 2016) have also been shown to increase at a lesser rate than $\sqrt{f'_c}$ that is close to $f'_c{}^{0.25}$. ACI Committee 318 has chosen retained $\sqrt{f'_c}$ not to change the exponent applied to the compressive strength used to calculate development and lap splice lengths for welded plain wire reinforcement in tension and deformed bars and deformed wires in compression in a number of cases, but rather to set an upper limit of 10,000 psi on $\sqrt{f'_c}$ f'_c .

25.4.4 Development of headed deformed bars in tension

25.4.4.1 Use of heads to develop deformed bars in tension shall be permitted if conditions (a) through (g) are satisfied:

- (a) Bar shall conform to 20.2.1.6
- (b) Bar f_y shall not exceed 60,000 psi
- (c) Bar size shall not exceed No. 11
- (d) Net bearing area of head A_{brg} shall be at least $4A_b$
- (e) Concrete shall be normalweight
- (f) Clear cover for bar shall be at least $2d_b$
- (g) Clear spacing between bars shall be at least $4d_b$

R25.4.4.1 As used in this section, development describes cases in which the force in the bar is transferred to the concrete through a combination of a bearing force at the head and bond forces along the bar. In contrast, Chapter 17 anchorage provisions describes cases in which the force in the bar is transferred through bearing to the concrete at the head alone. Headed bars are limited to those types that meet the requirements of Class HA heads in ASTM A970 because a wide variety of methods are used to attach heads to bars, some of which involve significant obstructions or interruptions of the bar deformations. Headed bars with significant obstructions or interruptions of the bar deformations were not evaluated in the tests used to formulate the provisions in 25.4.4.2. The headed bars evaluated in the tests were limited to those types that meet the criteria in 20.2.1.6 for Class HA heads.

The provisions for headed deformed bars were formulated based on the evaluation of a large number of tests involving headed bars in a variety of applications with due consideration of the provisions for anchorage in Chapter 17 and the bearing strength provisions of 22.8 (Thompson et

al. 2005, 2006a; Shao et al. 2016). Chapter 17 contains provisions for headed anchors related to the individual failure modes of concrete breakout, side-face blowout, and pullout. These failure modes are also applicable to headed and hooked reinforcing bars, and were considered in the formulation of 25.4.4.2. Nevertheless, some cases may require explicit calculation of the concrete breakout or side-face blowout strength, particularly where multiple bars are terminated in close proximity. The restrictions on the upper limit of 60,000 psi for f_y to maximum bar size of No. 11 bars; and normalweight concrete are based on the available data from tests (Thompson et al. 2005, 2006a,b; Shao et al. 2016). The upper limit of 60,000 psi on f_y that appeared prior to the 2019 edition of ACI 318 has been deleted because the provisions in 25.4.4.2 were developed based on headed bars exhibiting anchorage failures at stresses ranging between 26,000 and 153,000 psi (Shao et al. 2016).

For bars in tension, heads allow the bars to be developed in a shorter length but otherwise perform in a similar manner to bars anchored by standard hooks (Thompson et al. 2005, 2006a,b; Shao et al. 2016). The minimum limits on head size, clear cover, and clear spacing are based on the lower limits of these parameters on head sizes used in the tests to establish the expression for ℓ_{dt} in 25.4.4.2. The clear cover and clear spacing requirements in 25.4.4.1 are based on dimensions measured to the bar, not to the head. The head is considered to be part of the bar for the purposes of satisfying the specified cover requirements in 20.6.1.3, and aggregate size requirements of 26.4.2.1(a)(4). To avoid congestion, it may be desirable to stagger the heads.

Headed bars with $A_{brg} < 4A_b$ have been used in practice, but their performance is not accurately represented by the provisions in 25.4.4.2, and they should be used only with designs that are supported by test results under 25.4.5. These provisions do not address the design of studs or headed stud assemblies used for shear reinforcement.

25.4.4.2 Development length ℓ_{dt} for headed deformed bars in tension shall be the greatest of (a) through (c).

(a) $\left(\frac{0.016 f_y \psi_e}{\sqrt{f'_c}} \right) d_b$ with ψ_e given in 25.4.4.3 and the value of f'_c shall not exceed 6,000 psi

(a) Length calculated in accordance with 25.4.4.3 or 25.4.4.4 using the applicable modification factors of 25.4.3.7

(b) $8d_b$

(c) 6 in.

R25.4.4.2 This provision gives a two-tier approach for the calculation of the development length of headed deformed bars in tension. The user can either use the simplified equation of 25.4.4.3 (Eq. (25.4.4.3)) in which development length is calculated in multiples of bar diameter or the general equation (Eq. (25.4.4.4)), which more accurately represents the factors that affect the force that can be developed by headed deformed bars.

25.4.4.3 The development length for headed deformed bars in tension ℓ_{dt} shall be calculated by:

$$\ell_{dt} = \left(\frac{f_y \Psi_e \Psi_o}{k_t f_c'^{0.25}} \right) d_b \quad (25.4.4.3)$$

where k_t shall be in accordance with Table 25.4.4.3.

Table 25.4.4.3 - Coefficient k_t for headed deformed bars in tension

<u>Clear spacing of headed bars being developed</u>	<u>No. 5 and smaller bars</u>	<u>No. 6, 7, and 8 bars</u>	<u>No. 9, 10, and 11 bars</u>
$\geq 7d_b$	<u>1000</u>	<u>800</u>	<u>670</u>
$\geq 2d_b$ and $< 7d_b$	<u>550</u>	<u>430</u>	<u>365</u>
$\geq 1d_b$ and $< 2d_b$	<u>500</u>	<u>400</u>	<u>330</u>

R25.4.4.3 This provision, which is based on Eq. (25.4.4.4) and Ψ_{cs} from Table 25.4.4.7b for the no confining reinforcement within the joint region, covers three cases that are often encountered in the application of headed deformed bars: (a) widely spaced hooked bars, (b) headed deformed bars with a clear spacing of at least $2d_b$, and (c) closely spaced headed deformed bars with a clear spacing of d_b . Using the minimum spacing and maximum bar size in each category shown in Table 25.4.4.3, Eq. (25.4.4.3) with appropriate value of k_t , reflects the value of ℓ_{dt} obtained using Eq. (25.4.4.4) using the corresponding value of Ψ_{cs} for $A_{tt}/A_{hs} = 0$.

25.4.4.4 The development length for headed deformed bars in tension ℓ_{dt} shall be calculated by:

$$\ell_{dt} = \left(\frac{f_y \Psi_e \Psi_{cs} \Psi_o}{400 f_c'^{0.25}} \right) d_b^{1.5} \quad (25.4.4.4)$$

R25.4.4.24 The provisions for developing headed deformed bars give the length of the bar, ℓ_{dt} , measured from the critical section to the bearing face of the head, as shown in Fig. R25.4.4.2a.

As observed for hooked bars, for a given bar size, the stress developed in a headed reinforcing bar increases slightly more rapidly than the embedded length, but a linear relation between the two provides the satisfactory representation. Also like hooked bars, the required development length increases with bar diameter to the 1.5 power.

The upper limit on the value of f'_c in 25.4.4.24 for use in calculating ℓ_{dt} that appeared prior to the 2019 edition of ACI 318 has been removed based on the work of Shao et al. (2016) who demonstrated that the provisions of now included in 25.4.4.24 can be applied to concrete with f'_c up to and above 16,000 psi. ~~is based on the concrete strengths used in the tests (Thompson et al. 2005, 2006a,b). Because transverse reinforcement has been shown to be largely ineffective in improving the anchorage of headed deformed bars (Thompson et al. 2005, 2006a,b), additional reductions in development length, such as those allowed for standard hooks with additional confinement provided by transverse reinforcement in 25.4.3.2, are not used for headed deformed reinforcing bars. Transverse reinforcement, however, helps limit splitting cracks in the vicinity of the head and for that reason is recommended.~~

Where longitudinal headed deformed bars from a beam or a slab terminate at a supporting member, such as the column shown in Fig. R25.4.4.24b, the bars should extend through the joint to the far face of the confined core of the supporting member, allowing for cover and avoidance of interference with column reinforcement, even though the resulting anchorage length exceeds ℓ_{dt} . Extending the bar to the far side of the column core helps to transfer compressive forces (as identified in a strut-and-tie model) that are likely to form in such a connection and improves the performance of the joint.

Where closely spaced headed bars are used, the potential for concrete breakout failure exists. For joints as shown in Fig. R25.4.4.24c and R25.4.4.24d, concrete breakout failure can be precluded by providing anchorage length equal to or greater than $d/1.5$ (Eligehausen 2006b), as shown in Fig. R25.4.4.24c, or by providing reinforcement in the form of hoops and ties to establish a load path in accordance with strut-and-tie modeling principles, as shown in Fig. R25.4.4.24d. Strut-

and-tie models should be verified in accordance with Chapter 23. Note that the strut-and-tie models illustrated in Fig. R25.4.4.24c and R25.4.4.24d rely on a vertical strut from a column extending above the joint. Beam-column joints at roof-level and portal frames are vulnerable to joint failure and should be properly detailed to restrain diagonal cracking through the joint and breakout of the bars through the top surface.

For cases where concrete breakout is not prevented, as shown in Fig. R25.4.4.24e, this failure mode should be considered in accordance with the provisions of Chapter 17.

~~25.4.4.3 Modification factor ψ_e in 25.4.4.2(a) shall be 1.2 for epoxy coated or zinc and epoxy dual coated bars and 1.0 for uncoated or zinc coated (galvanized) bars.~~

~~R25.4.4.3 A 1.2 factor is conservatively used for epoxy coated headed deformed reinforcing bars, the same value used for epoxy coated standard hooks.~~

25.4.4.5 In beam-column joints, the total cross-sectional area of all ties or stirrups enclosing headed bars A_{tt} , shall be defined as those ties or stirrups parallel to ℓ_{dt} and located within $8d_b$ of centerline of the headed bars in direction of the interior of the joint

R25.4.4.5 Confining reinforcement oriented parallel to the development length and located within the regions defined in 25.4.4.5 and 25.4.4.6 (refer to Fig. R25.4.4.5 and R25.4.4.6) contributes to anchorage strength in proportion to the area of the confining reinforcement for headed bars (Shao et al. 2016). Confining reinforcement oriented perpendicular to the development length has been shown to be largely ineffective in improving the anchorage of headed deformed bars in a number of cases (Thompson et al. 2005, 2006a,b). Confining reinforcement perpendicular to the development length ~~Transverse reinforcement~~, however, helps limit splitting cracks in the vicinity of the head and for that reason is recommended.

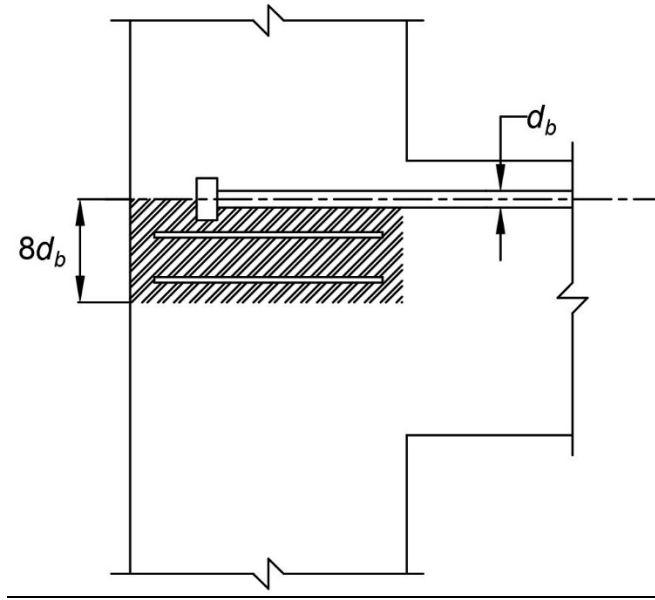


Fig. R25.4.4.5 —Ties or stirrups placed parallel to the headed beam bars being developed in a beam-column joint that contribute to anchorage strength.

25.4.4.6 In members other than beam-column joints, the total cross-sectional area of all ties or stirrups acting enclosing headed bars A_{tt} shall be defined as the minimum on either side of the headed bars located within $8d_b$ on one side of the centerline of the headed bars.

R25.4.4.6 The minimum value of confining on one side (see Fig. R25.4.4.6) governs because the anchorage failure will be governed by the weaker side of the failure region.

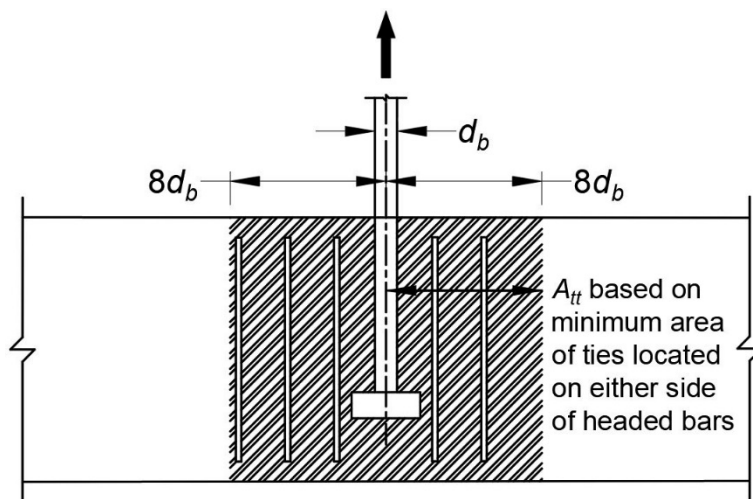


Fig. R25.4.4.6 —Ties or stirrups placed parallel to the headed bars being developed in other than a beam-column joint that contribute to anchorage strength.

25.4.4.7 For the calculation of ℓ_{dt} , modification factors ψ_e and ψ_o shall be in accordance with Table 25.4.4.7a and modification factor ψ_{cs} shall be in accordance with Table 25.4.4.7b. Factor ψ_{cs} shall be permitted to be taken as 1.0.

Table 25.4.4.7a—Modification factors for development of headed bars in tension

Modification Factor	Condition	Value of Factor
ψ_e	Epoxy-coated or zinc and epoxy dual-coated reinforcement	1.2
	Uncoated or zinc-coated (galvanized) reinforcement	1.0
ψ_o ^[1]	For headed bars (1) terminating inside a column core with clear side cover to bar ≥ 2.5 in., or (2) terminating in a member with clear side cover to bar $\geq 8d_b$ ^[2]	1.0
	Other	1.25

^[1] In cases where clear cover is less than 2.5 in., such as in slabs, splices, and joints where both beam and column terminate, ψ_o shall be 1.25.

^[2] d_b is the nominal diameter of the headed bar

Table 25.4.4.7b—Modification factor ψ_{cs} for confining reinforcement and spacing^[1]

Confinement level	c_{ch}^[2]	
	$2d_b$^[3]	$\geq 8d_b$
	Value of Factor	
$\frac{A_{tr}}{A_{hs}} \geq 0.3$	0.6	0.4
$\frac{A_{tr}}{A_{hs}} = 0$ (no confining reinforcement)	1.0	0.5

^[1] ψ_{cs} is permitted to be linearly interpolated for values of A_{tr}/A_{hs} between 0 and 0.3 and for spacing c_{ch} between $2d_b$ and $8d_b$

^[2] For splices, c_{ch} shall be taken as the lesser of (1) center-to-center spacing between the adjacent lapped bars and (2) twice the cover to the center of the lapped bar in the direction perpendicular to the plane of the bars

^[3] d_b is the nominal diameter of the headed bar

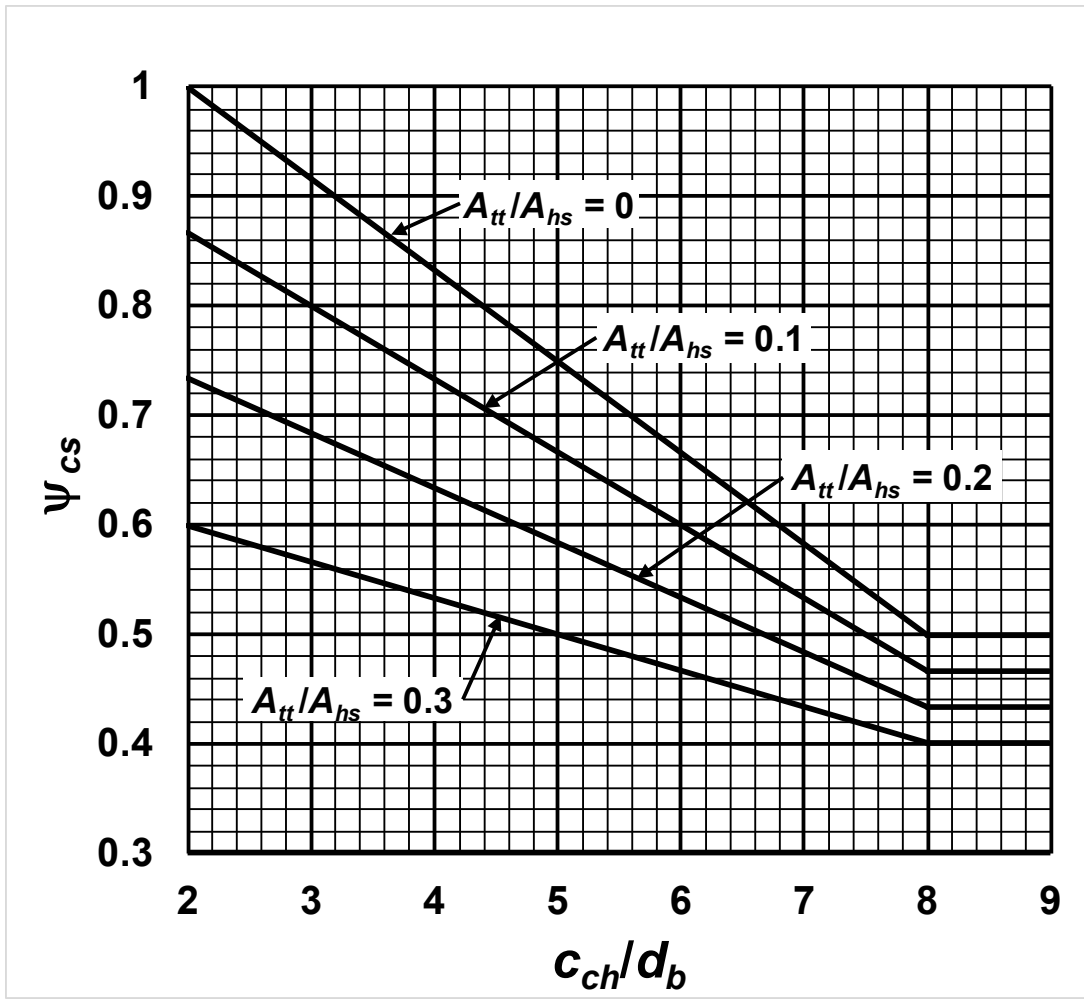
R25.4.4.7 A 1.2 factor ψ_e is conservatively used for epoxy-coated headed deformed reinforcing bars, the same value used for epoxy-coated standard hooks. The placement factor ψ_o accounts for

the confinement provided by longitudinal reinforcement within columns and high side cover for other supporting members.

The confining reinforcement and spacing factor ψ_{cs} is similar to that used for hooked bars (Shao et al. 2016). Unlike hooked bars, however, data indicate that only reinforcement parallel to and enclosing headed bar contribute to anchorage strength and is considered as reducing development length (Thompson et al. 2005, 2006a,b). For headed bars anchored in members other than beam column joints, A_{tf} is based on the minimum confining reinforcement on either side of the centerline of the headed bars rather than as the total confining reinforcement located on both sides of the headed bars. This provision is based on observations showing that the minimum confining reinforcement on one side of a bar controls anchorage strength (Shao et al 2016). Further, unlike anchors, for which confining steel and concrete are not considered to share load, this provisions is based on observations that indicate that confining reinforcement and concrete do share load.

The confining reinforcement and spacing factor ψ_{cs} is applied as it is for standard hooks. Anchorage capacity increases as the center-to-center spacing of the bars c_{ch} increases up to $8d_b$, rather than $6d_b$ as used for standard hooks, and as the ratio of the area of confining reinforcement A_{tf} to the area of the headed bars A_{hs} increases. The minimum values of ψ_{cs} for headed bars are lower than those for hooked bars. The upper limit on A_{tf}/A_{hs} in Table 25.4.4.7b is based on limited data for values above 0.3.

The relationship between the confining reinforcement and spacing factor ψ_{cs} and c_{ch}/d_b , and values of function of A_{tf}/A_{hs} of 0 and 0.3 are shown in Fig. R25.4.3.7. Interpolation is permitted for intermediate values of c_{ch}/d_b and A_{tf}/A_{hs} .



R25.4.4.7— Relationship between the confining reinforcement and spacing ψ_{cs} and c_{ch}/d_b for A_{tt}/A_{hs} equal to 0, 0.1, 0.2 and 0.3. Interpolation is permitted for intermediate values of values of A_{tt}/A_{hs}

25.4.4.8 Where beam negative moment reinforcement is provided by headed deformed bars that terminate in the joint, the column shall extend above the top of the joint a distance at least the depth h of the joint. Alternatively, the beam reinforcement shall be enclosed by additional vertical joint reinforcement providing equivalent confinement to the top face of the joint.

R25.4.4.8 Refer to R18.8.3.4.

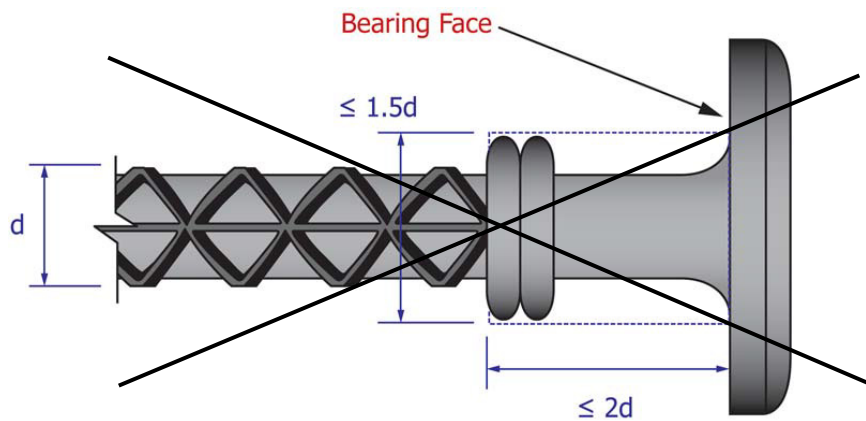
5.2.2 Proposed Changes in ASTM A970

Changes for the requirements for class HA head dimensions in Section A.1.1 of Annex A1 of ASTM A970/A970M-16 are proposed as follows. The changes are shown using underline and strikeout. These proposed changes, with the exception of Fig. A1.3, were approved through an ASTM ballot and appear in ASTM A970-17. Figure A1.3 will appear in an upcoming ballot.

A1. Requirements for Class HA head dimensions

Introduction

The following requirements shall apply only when specified in the purchase order or contract. When specified, this Annex A1 replaces 5.3, 6.3.1.1, and 14.2.2 with the following.



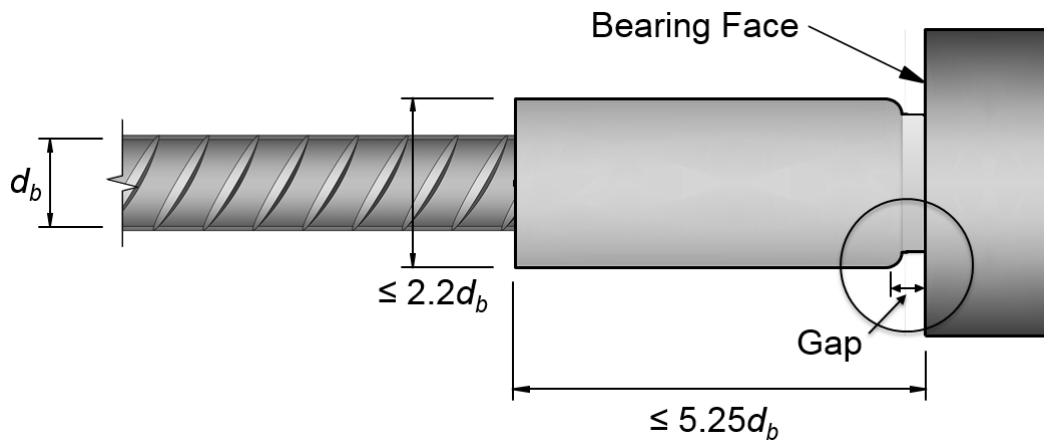


FIG. A1.1 Maximum Dimensions and Non-Planar Features of Obstruction or Interruptions of Bar Deformations and Non-Planar Features of the Bearing Surface

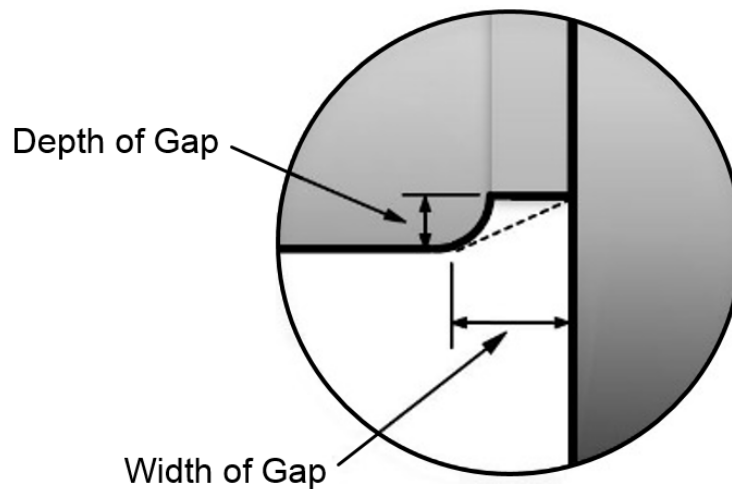


FIG. A1.2 Details of Gap in Obstruction Adjacent to Head

A1.1 Replacement Requirements for 5.3

A1.1.1 Head dimensions for headed bars conforming to Class HA shall be provided by the purchaser in the purchase order.

A1.1.1.1 Head dimensions shall define the head geometry including thickness, diameter or height and width of the head (Fig. 1).

A1.1.1.2 Class HA head dimensions shall comply with A1.1.1.3 through A1.1.1.5.

A1.1.1.3 ~~The net bearing area of the head shall not be less than four times the nominal cross-sectional area of the bar.~~ The net bearing area of a bars without an obstruction meeting the requirements of this annex is the gross area of the head minus the area of the deformed reinforcing bar and shall not be less than four times the nominal cross-sectional area of the bar.

A1.1.1.4 The net bearing area of a bar with an obstruction meeting the requirements of this annex is the gross area of the head minus the maximum area of the obstruction and shall not be less than four times the nominal cross-sectional area of the bar (Fig. A1.1).

A1.1.1.5 For heads with an obstruction with a gap adjacent to the head, the net bearing area is the gross area of the head minus the area of the obstruction adjacent to the bearing face, provided that the gap has a width not less than the larger of 3/8 in. and 3/8 bar diameters, the depth of the gap does not exceed the width of the gap, and the obstruction everywhere within the gap falls inside a straight line connecting the outer dimension of the obstruction at the initiation of the gap with the dimension of the obstruction at the bearing face of the head (Fig. A1.2), and shall not be less than four times the nominal cross-sectional area of the bar (Fig. A1.1). In addition, the gross area of the head minus the maximum area of the obstruction shall not be less than 2.8 times the nominal cross-sectional area of the bar

Note A1.1—The criteria for the size of a gap, the shape of the obstruction within a gap, and the minimum values for the gross area of the head minus the maximum area of the obstruction are based on successful performance in tests. Shao, Y., Darwin, D., O’Reilly, M., Lequesne, R. D., Ghimire, K., and Hano, M., 2016, “Anchorage of Conventional and High-Strength Headed Reinforcing Bars,” *SM Report* No. 117, University of Kansas Center for Research, Lawrence, Kansas, August, 234 pp.

A1.1.1.46 The bearing face shall consist of a single, nominally flat surface that lies in a plane perpendicular to the longitudinal axis of the bar.

A1.1.1.57 Obstructions or interruptions of the bar deformations and non-planar features on the bearing face of the head shall not extend more than ~~two~~ 5.25 nominal bar diameters from the bearing face and shall not have a diameter greater than ~~1.5~~ 2.2 nominal bar diameters (Fig. A1.1). ~~Such obstructions shall not be considered to detract from the net bearing area of the head.~~ Obstructions exceeding any of these limits are not permitted, with the exception that obstructions that do not extend from bearing face of the head more than 0.6 nominal bar diameters for No. 8 (No. 25) and larger bars or the smaller of 0.6 in. (15 mm) and $0.75d_b$ for bars smaller than No. 8 (No. 25) and do not have a diameter greater than 1.5 nominal bar diameters shall not be considered to detract from the net bearing area of the head (Fig. A1.3).

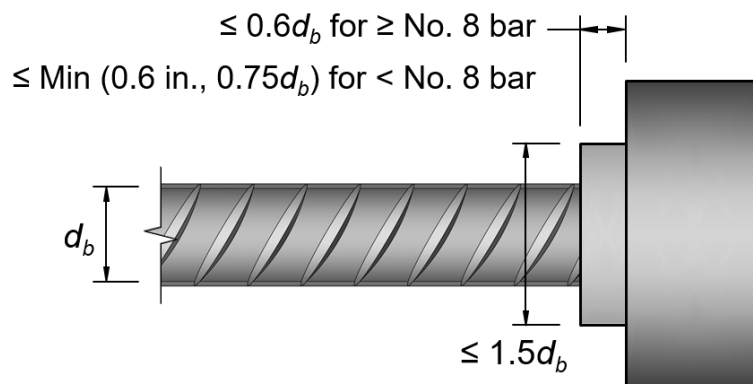


FIG. A1.3 Obstruction not considered to detract from the net bearing area of the head

A1.2 Replacement Requirements for 6.3.1.1

A1.2.1 *Class HA*—Develop the minimum specified tensile strength of the reinforcing bar.

A1.3 Replacement Requirements for 14.2.2

A1.3.1 *Type of Headed Reinforcing Bar*—Letter *H* indicating that the headed bar was manufactured in accordance with this Annex A1.

5.3 EXAMPLE DESIGN PROBLEMS

Application of the proposed design provisions for the development length of headed bars is illustrated using two example problems that demonstrate most of the aspects in applying the proposed provisions for headed deformed bars. The first example illustrates application of the simplified expression for ℓ_{dt} to a beam-column joint that requires no additional confining reinforcement. The second example illustrates application of the general expression for ℓ_{dt} to a beam-column joint that requires additional confining reinforcement.

Example 1: Headed bars anchored in exterior beam-column joint:

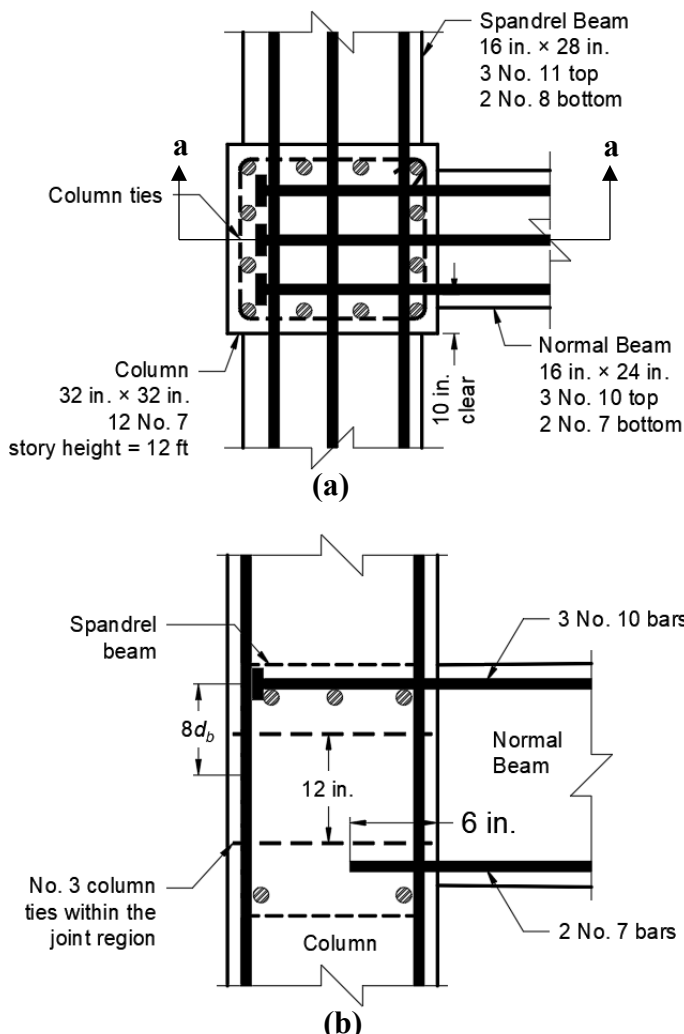


Figure 5.9 Beam-column joint for Example 1. (a) Plan view; (b) Section a-a (For column bars, only corner bars are shown)

Exterior beam-column joint shown in Figure 5.9. $f_y = 60,000$ psi, $f'_c = 4000$ psi. Width of beam $b_b = 16$ in., depth of beam $h_b = 24$ in., and width and depth of column $b_c = h_c = 32$ in. Normalweight concrete and uncoated reinforcement. Two No. 3 column ties within the joint region (minimum confining reinforcement per Section 15.4). Check development of No. 10 top bars from beam using headed bars.

The available length (assuming No. 3 bar ties and head thickness = 1.0 in.) for $\ell_{dt} = h_c - 1.5 - 0.375 - 0.875 - 1 = 32 - 3.8 = 28.2$ in.

Calculate center-to-center spacing c_{ch} based on No. 4 stirrups.

$$c_{ch} = \frac{b_b - 2 \left(1.5 + 0.5 + \frac{1.27}{2} \right) \text{ in.}}{2} = 5.4 \text{ in.}$$

$$c_{ch}/d_b = 5.4/1.27 = 4.25$$

First use Eq. (25.4.4.3):

From Table 25.4.4.3 for No. 10 bars with $c_{ch} = 4.25d_b$, $k_t = 365$. $\psi_e = \psi_o = 1.0$

$$\ell_{dt} = \left(\frac{f_y \psi_e \psi_o}{k_t f_c'^{0.25}} \right) d_b = \left(\frac{60,000 \times 1.0 \times 1.0}{365 \times 4000^{0.25}} \right) 1.27 = 26.3 \text{ in.} < 28.2 \text{ in. (Okay)}$$

Example 2: Headed bars anchored in exterior beam-column joint:

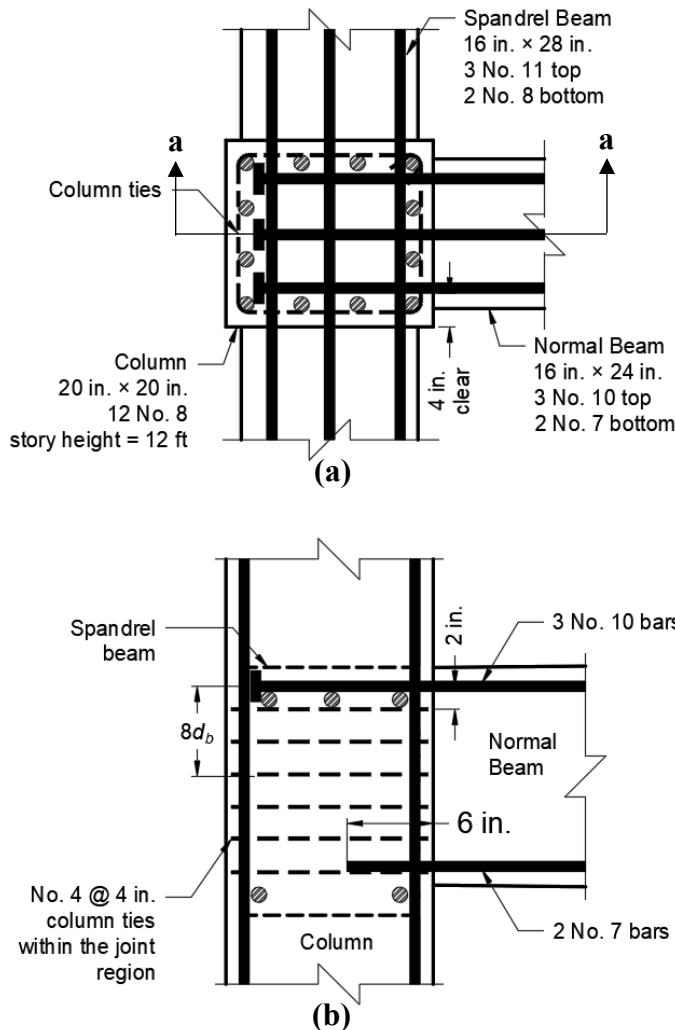
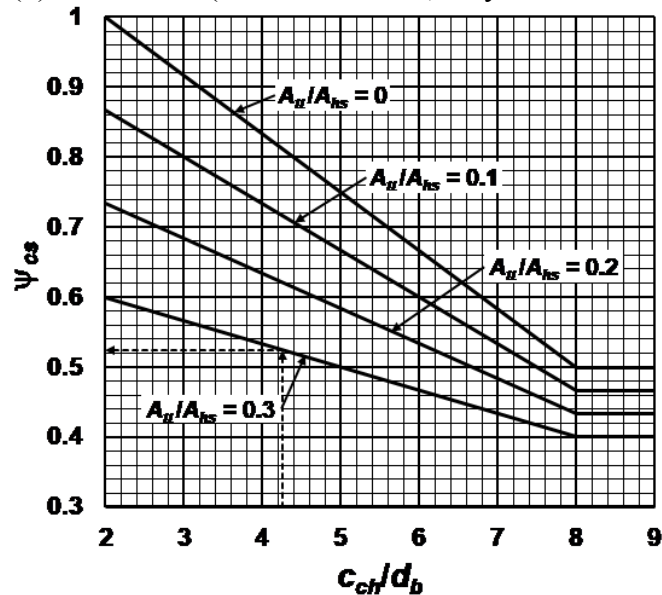


Figure 5.10 Beam-column joint for Example 2. (a) Plan view; (b) Section a-a (For column bars, only corner bars are shown)



Exterior beam-column joint similar to Example 1, but the column is 20×20 in. with No. 8 longitudinal bars, as shown in Figure 5.10. $f_y = 60000$ psi, $f'_c = 4000$ psi. Normalweight concrete and uncoated reinforcement. Check development of No. 10 top bars from beam using headed bars.

Based on Example 1, it is clear that two No. 3 ties will not be satisfactory to anchor the bars within the available length (assuming No. 4 bar ties) for $\ell_{dt} = h_c - 1.5 - 0.5 - 1 - 1 = 20 - 4 = 16$ in.

As shown in Figure 5.10, there are three No. 4 bar ties (six legs parallel to the headed bar) within $8d_b$ of the centerline of the beam headed bars, giving $A_{tt} = 6 \times 0.2 = 1.2$ in². For three headed bars, $A_{hs} = 3 \times 1.27 = 3.81$ in². $A_{tt}/A_{hs} = 1.2/3.81 = 0.31 > 0.3$ maximum value permitted in Table 25.4.4.7b to calculate ψ_{cs} , so use 0.3.

From Table 25.4.4.7b or Figure R25.4.4.7, for $c_{ch} = 4.25d_b$ and $A_{th}/A_{hs} = 0.3$, $\psi_{cs} = 0.53$. $\psi_e = \psi_o = 1.0$

Using Eq. (25.4.4.4),

$$\begin{aligned} \ell_{dt} &= \left(\frac{f_y \psi_e \psi_{cs} \psi_o}{400 f'_c{}^{0.25}} \right) d_b^{1.5} \\ &= \left(\frac{60,000 \times 1.0 \times 0.53 \times 1.0}{400 \times 4000^{0.25}} \right) 1.27^{1.5} \\ &= 14.3 \text{ in.} < 16 \text{ in. (Okay)} \end{aligned}$$

Fig. R25.4.4.7— Relationship between the confining reinforcement and spacing ψ_{cs} and c_{ch}/d_b for A_{th}/A_{hs} equal to 0, 0.1, 0.2 and 0.3. Interpolation is permitted for intermediate values of values of A_{th}/A_{hs}

CHAPTER 6: SUMMARY AND CONCLUSIONS

6.1 SUMMARY

This study assesses the anchorage behavior of headed bars subjected to monotonic loading in column-foundation joints and splices, and reversed cyclic loading in beam-column joints. The major test parameters include embedment length, concrete compressive strength, spacing between bars, bearing area of heads, reinforcement perpendicular to headed bars, distance between compression reaction and headed bar, and in the case of beam-column joints, joint shear. Design provisions to accommodate the application of headed bars in members subjected to monotonic and reversed cyclic loading are presented, including proposed code provisions for the development length of headed bars and specifications for head dimensions.

Headed bars anchored in slab specimens were tested under monotonic loading to investigate the anchorage behavior of the bars in a simulated column-foundation joint with the column subjected to bending. Thirty-two No. 8 headed bars with embedment lengths ranging between 6 and 8.5 in. were tested. The net bearing areas of the heads ranged from 4 to 15 times the area of the bar A_b . Some headed bars had large obstructions adjacent to the bearing face of the head that exceeded the dimensional limits for HA heads in ASTM A970-16. Reinforcement in a plane perpendicular to the headed bars ranged from none to quantities including two No. 8 or six or eight No. 5 bars placed symmetrically about the headed bar, parallel and close to the long edges of the specimen; two to six No. 5 bars placed symmetrically about and close to the headed bar in the short direction of the specimen; and nine No. 4 and eight No. 5 bars distributed evenly and oriented in, respectively, the long and short directions of the specimen. Concrete compressive strengths ranged from 4,200 to 8,620 psi and stresses in the bars at failure ranged from 49,500 to 117,000 psi. Six headed bar splice specimens without confining reinforcement were tested under monotonic loading to investigate the anchorage behavior of headed bars in a lap splice. The splice specimens contained No. 6 headed bars with a net bearing area of $4A_b$ and lap length of 16 bar diameters d_b . The center-to-center spacing between the lapped bars was 1.67, 2.33, or $3.53d_b$. Both side and top clear covers to the bar were 2 in. Concrete compressive strengths averaged 6,360 and 10,950 psi and stresses in the bars at failure ranged from 75,010 to 83,560 psi. The current study also evaluated the applicability of the descriptive equations and design provisions proposed by

Shao et al. (2016) to members subjected to reversed cyclic loading. To do this, test results from 23 studies of 84 exterior, 7 roof-level interior, and 7 knee beam-column joints subjected to reversed cyclic loading were analyzed. Concrete compressive strengths and steel yield strengths ranged from 3,480 to 21,520 psi and from 53,650 to 149,930 psi, respectively. Headed bar sizes ranged between D12 (No. 4) and D36 (No. 11) with net bearing areas ranging from 1.7 to $11.4A_b$. The embedment lengths of the headed bars ranged from 8 to $22.6d_b$ (4 to 18.9 in.). Clear cover and minimum center-to-center spacing between the bars ranged from 1.5 to $9.9d_b$ (0.9 to 8.7 in.) and from 2 to $11.2d_b$ (1.6 to 8.4 in.), respectively. All but four specimens contained hoops, spaced at 2.2 to $6.8d_b$ (1.8 to 5.9 in.), as confining reinforcement parallel to the headed bar within the joint region. Column axial load applied during the test ranged from none to $0.20A_g f'_c$. The study also includes an evaluation to test results from studies of headed bars in lap splice specimens by Thompson et al. (2002) and Chun (2015), slab specimens by DeVries et al. (1999) and Choi et al. (2002), and column-like specimens by Choi et al. (2002) and Choi (2006).

6.1 CONCLUSIONS

The following conclusions can be drawn from the results and analyses presented in this report.

1. Reinforcement perpendicular to the headed bar does not improve the anchorage strength of the bar.
2. An increase in net bearing area of the head from 4 to $9.5A_b$ has no effect on the anchorage strength, while the anchorage strength increases slightly (less than 15%) for heads with net bearing areas of 13 to $15A_b$. This is consistent with the observation made by Shao et al. (2016).
3. Headed bars with net bearing areas of 2.6 to $3.2A_b$ tested under monotonic loading had anchorage strength less than that of the bars with a minimum net bearing area of $4A_b$. Results from a limited number of specimens tested under reversed cyclic loading, however, suggest that heads with a net bearing area as low as $2.7A_b$ may be sufficient to anchor headed bars in certain circumstances.
4. Results from slab specimens tested under monotonic loading and beam-column joint specimens tested under reversed cyclic loading show that the distance between the headed bar and compression reaction (nearest support in slab specimens and compression region

of the beam in beam-column joint specimens), with a test range of up to 3.1 times the embedment length, had no effect on the anchorage strength. But the strength decreased for the single slab specimen for which distance between the headed bar and compression reaction equaled 5.6 times the embedment length.

5. Descriptive equations developed based on beam-column joint specimens tested under monotonic loading, in which the anchorage strength of the headed bar is a function of embedment length, concrete compressive strength, bar spacing, bar diameter, and confining reinforcement within the joint region, can be used to represent the anchorage strength of headed bars in beam-column joints subjected to reversed cyclic loading.
6. The anchorage provisions of Chapter 17 of ACI 318-14 with a strength reduction factor of 1.0 provide a more conservative estimate of anchorage strength of headed bars than do the descriptive equations. The provisions of Chapter 17 of ACI 318-14 also result in a greater variation in the estimated anchorage strengths than the descriptive equations.
7. The performance of headed bars terminated in knee beam-column joints is a function of the joint detailing. The headed bars, evaluated in this study, did not provide sufficient anchorage in such joints when subjected to reversed cyclic loading.
8. The proposed design provisions for the development length of headed bars are appropriate for members subjected to monotonic and reversed cyclic loading.
9. As included in the proposed design provisions, the minimum clear spacing of $3d_b$ between headed bars permitted in joints in special moment frames in accordance with Section 18.8.5.2 of ACI 318-14 can be reduced to $1d_b$, allowing for the use of more closely spaced headed bars.
10. Test results show that headed bars with large obstructions, exceeding the dimensional limits for HA heads in ASTM A970-16, provide adequate anchorage strength. The findings are incorporated in ASTM A970-17.

6.2 FUTURE WORK

Neither the proposed design provisions nor those in ACI 318-14 for the development length of headed bars allow headed bars to be used in lightweight concrete because of a total lack of data. Therefore, it is recommended that tests be performed to investigate the anchorage behavior of headed bars in lightweight concrete.

The maximum size of the headed bars evaluated in the current study is No. 11. A limited number of tests have been performed on larger size headed bars. Chun et al. (2009) tested No. 18 headed bars, but these bars contained heads with a net bearing area of just $2.8A_b$ (less than $4A_b$) and had small clear cover to the head ($0.38d_b$). The headed bars tested by Chun exhibited low strength compared to that obtained with the descriptive equations developed by Shao et al (2016). It is hypothesized that the low strength resulted from the small bearing area and clear cover. It is, therefore, recommended that more tests be performed to investigate the anchorage strength of larger headed bars.

REFERENCE

ACI Committee 318, 1999, *Building Code Requirements for Structural Concrete (ACI 318-99) and Commentary (ACI 318R-99)*, American Concrete Institute, Farmington Hills, Michigan, 369 pp.

ACI Committee 318, 2011, *Building Code Requirements for Structural Concrete (ACI 318-11) and Commentary (ACI 318R-11)*, American Concrete Institute, Farmington Hills, Michigan, 503 pp.

ACI Committee 318, 2014, *Building Code Requirements for Structural Concrete (ACI 318-14) and Commentary (ACI 318R-14)*, American Concrete Institute, Farmington Hills, Michigan, 520 pp.

ACI Committee 352, 1991, *Recommendations for Design of Beam-Column Joints in Monolithic Reinforced Concrete Structures (ACI 352R-91, reapproved 1997)*, American Concrete Institute, Farmington Hills, Michigan, 18 pp.

ACI Committee 352, 2002, *Recommendation for Design of Beam-Column Connections in Monolithic Reinforced Concrete Structures (ACI 352R-02, reapproved 2010)*, American Concrete Institute, Farmington Hills, Michigan, 38 pp.

ACI Committee 374, 2005, *Acceptance Criteria for Moment Frames Based on Structural Testing and Commentary (ACI 374.1-05, Reapproved 2014)*, American Concrete Institute, Farmington Hills, Michigan, 9 pp.

ACI Committee 408, 2003, *Bond and Development of Straight Reinforcement in Tension (ACI 408R-03)*, American Concrete Institute, Farmington Hills, Michigan, 49 pp.

Adachi, M., and Masuo, K., 2007, "The Effect of Orthogonal Beams on Ultimate Strength of R/C Exterior Beam-Column Joint using Mechanical Anchorages," *Proc., Architectural Institute of Japan*, Aug., pp. 633-634 (in Japanese).

Ajaam, A., Darwin, D., and O'Reilly, M. O., 2017, "Anchorage Strength Reinforcing Bars with Standard Hooks," *SM Report No. 125*, University of Kansas Center for Research, Inc., Lawrence, Kansas, Apr., 346 pp.

ASTM A615, 2014, *Standard Specification for Deformed and Plain Carbon-Steel Bars for Concrete Reinforcement (ASTM A615/A615M-14)*, ASTM International, West Conshohocken, PA, 7 pp.

ASTM A615, 2016, *Standard Specification for Deformed and Plain Carbon-Steel Bars for Concrete Reinforcement (ASTM A615/A615M-16)*, ASTM International, West Conshohocken, PA, 8 pp.

ASTM A706, 2015, *Standard Specification for Deformed and Plain Low-Alloy Steel Bars for Concrete Reinforcement (ASTM A706/A706M-15)*, ASTM International, West Conshohocken, PA, 7 pp.

ASTM A970, 2013, *Standard Specification for Headed Steel Bars for Concrete Reinforcement (ASTM A970/A970M-13a)*, ASTM International, West Conshohocken, PA, 9 pp.

ASTM A970, 2016, *Standard Specification for Headed Steel Bars for Concrete Reinforcement (ASTM A970/A970M-16)*, ASTM International, West Conshohocken, PA, 9 pp.

ASTM A970, 2017, *Standard Specification for Headed Steel Bars for Concrete Reinforcement (ASTM A970/A970M-17)*, ASTM International, West Conshohocken, PA, 9 pp.

ASTM A1035, 2015, *Standard Specification for Deformed and Plain, Low-Carbon, Chromium, Steel Bars for Concrete Reinforcement (ASTM A1035/A1035M-14)*, ASTM International, West Conshohocken, PA, 7 pp.

Bashandy, T. R., 1996, "Application of Headed Bars in Concrete Members," *Ph.D. dissertation*, The University of Texas at Austin, Austin, TX, Dec., 303 pp.

Choi, D.-U., 2006, "Test of Headed Reinforcement in Pullout II: Deep Embedment," *International Journal of Concrete Structures and Materials*, Vol. 18, No. 3E, Aug., pp. 151-159.

Choi, D.-U., Hong, S.-G., and Lee, C.-Y., 2002, "Test of Headed Reinforcement in Pullout," *KCI Concrete Journal*, Vol. 14, No. 3, Sep., pp. 102-110.

Chun, S. C., 2015, "Lap Splice Tests Using High-Strength Headed Bars of 550 MPa (80 ksi) Yield Strength," *ACI Structural Journal*, Vol. 112, No. 6, Nov.-Dec., pp. 679-688.

Chun, S. C., and Lee, J. G., 2013, "Anchorage Strengths of Lap Splices Anchored by High-Strength Headed Bars," *Proc., VIII International Conference on Fracture Mechanics of Concrete and Concrete Structures*, Toledo, Spain, pp. 1-7.

Chun, S. C., Lee, S. H., Kang, T. H., Oh, B., and Wallace, J. W., 2007, "Mechanical Anchorage in Exterior Beam-Column Joints Subjected to Cyclic Loading," *ACI Structural Journal*, Vol. 104, No. 1, Jan.-Feb., pp. 102-112.

Chun, S. C., Oh, B., Lee, S. H., and Naito, C. J., 2009, "Anchorage Strength and Behavior of Headed Bars in Exterior Beam-Column Joints," *ACI Structural Journal*, Vol. 106, No. 5, Sep.-Oct., pp. 579-590.

Chun, S. C., and Shin, Y.-S., 2014, "Cyclic Testing of Exterior Beam-Column Joints with Varying Joint Aspect Ratio," *ACI Structural Journal*, Vol. 111, No. 3, May-June, pp. 693-704.

Darwin, D., Dolan, C. W., and Nilson, A. H., 2016, *Design of Concrete Structures*, 15th ed., McGraw-Hill, New York, 776 pp.

Darwin, D., Zuo, J., Tholen, M. L., and Idun, E. K., 1996, "Development Length Criteria for Conventional and High Relative Rib Area Reinforcing Bars," *ACI Structural Journal*, Vol. 93, No. 3, May-June, pp. 1-13.

DeVries, R. A., 1996, "Anchorage of Headed Reinforcement in Concrete," *PhD Dissertation*, The University of Texas at Austin, Austin, Texas, Dec., 314 pp.

DeVries, R. A., Jirsa, J. O., and Bashandy, T., 1999, "Anchorage Capacity in Concrete of Headed Reinforcement with Shallow Embedments," *ACI Structural Journal*, Vol. 96, No. 5, Sep.-Oct., pp. 728-736.

Dhake, P. D., Patil, H. S., and Patil, Y. D., 2015, "Anchorage Behaviour and Development Length of Headed Bars in Exterior Beam-Column Joints," *Magazine of Concrete Research*, Vol. 67, No. 2, Aug., pp. 53-62.

Dilger, W. H., and Ghali, A., 1981, "Shear Reinforcement for Concrete Slabs," *Journal of the Structural Division*, Vol. 107, No. 12, Dec., pp. 2403-2420.

Eligehausen, R., Mallée, R., and Silva, J., 2006b, "Anchorage in Concrete Construction," Ernst & Sohn (J. T. Wiley), Berlin, Germany, May, 380 pp.

Ghimire, K., Darwin, D., and O'Reilly, M., 2018, "Anchorage of Headed Reinforcing Bars in Concrete," *SM Report No. 127*, University of Kansas Center for Research, Inc., Lawrence, KS, Jan., 278 pp.

Hognestad, E., 1951, "A Study of Combined Bending and Axial Load in Reinforced Concrete Members," *Bulletin Series No 399*, University of Illinois Engineering Experiment Station, Urbana, pp.

Hong, S. G., Chun, S. C., Lee, S. H., and Oh, B., 2007, "Strut-and-Tie Model for Development of Headed Bars in Exterior Beam-Column Joint," *ACI Structural Journal*, Vol. 104, No. 5, Sep.-Oct., pp. 590-600.

Ishibashi, K., and Inokuchi, R., 2004, "Experimental Study on T-shaped Joints with Anchor-Heads on Column's Rebars—Part 3: Loading Capacity and Ductility of Full-Scale Specimens," *Proc., Architectural Institute of Japan*, Aug., pp. 819-820 (in Japanese).

Ishibashi, K., Inokuchi, R., Ono, H., and Masuo, K., 2003, "Experimental Study on T-shaped Beam-Column Joints with Anchor-Heads on Column's Rebars—Part 1: Ductilities and Strength and Part 2: Deformations," *Proc., Architectural Institute of Japan*, Sep., pp. 533-536 (in Japanese).

Ishida, Y., Fujiwara, A., Adachi, T., Matsui, T., and Kuramoto, H., 2007, "Structural Performance of Exterior Beam-Column Joint with Wide Width Beam Using Headed Bars—Part 1: Outline of Test and Failure modes and Part 2: Test Results and Discussion," *Proc., Architectural Institute of Japan*, Aug., pp. 657-660 (in Japanese).

Kang, T. H., Ha, S.-S., and Choi, D.-U., 2010, "Bar Pullout Tests and Seismic Tests of Small-Headed Bars in Beam-Column Joints," *ACI Structural Journal*, Vol. 107, No. 1, Jan.-Feb., pp. 32-42.

Kang, T. H., Kim, W., and Shin, M., 2012, "Cyclic Testing for Seismic Design Guide of Beam-Column Joints with Closely Spaced Headed Bars," *Journal of Earthquake Engineering*, Vol. 16, No. 2, May, pp. 211-230.

Kang, T. H., Shin, M., Mitra, N., and Bonacci, J. F., 2009, "Seismic Design of Reinforced Concrete Beam-Column Joints with Headed Bars," *ACI Structural Journal*, Vol. 106, No. 6, Nov.-Dec., pp. 868-877.

Kato, T., 2005, “Mechanical Anchorage Using Anchor Plate for Beam/ Column Joints of R/C Frames—Part 2: Pull-out Behavior and Structural Behavior of T-shaped Frame Using Frictional Anchor Plate,” *Proc., Architectural Institute of Japan*, Sep., pp. 277-278 (in Japanese).

Kiyohara, T., Hasegawa, Y., Fujimoto, T., Akane, J., Amemiya, M., Tasai, A., and Adachi, T., 2005, “Seismic Performance of High Strength RC Exterior Beam Column Joint with Beam Main Bars Anchored Mechanically—Part 5: Anchorage Performance and Estimation for Strength; Part 6: Experimental Result on Shear Failure Models; Part 7: Anchorage Performance and Estimation for Strength No. 6-10; Part 8: Experimental Study and Estimation for Strength No. 11, No. 12; and Part 9: Behavior of Crack,” *Proc., Architectural Institute of Japan*, Sep., pp. 35-42 (in Japanese).

Kiyohara, T., Tasai, A., Watanabe, K., Hasegawa, Y., and Fujimoto, T., 2004, “Seismic Capacity of High Strength RC Exterior Beam Column Joint with Beam Main Bars Anchored Mechanically—Part 1: Anchorage Performance and Estimation of Strength; Part 2: Restoring Force Characteristics and Displacement Component; Part 3; Failure Modes and Width of Crack; and Part 4: Anchorage Performance and Estimation of Strength,” *Proc., Architectural Institute of Japan*, Aug., pp. 27-34 (in Japanese).

Lee, H.-J., and Yu, S.-Y., 2009, “Cyclic Response of Exterior Beam-Column Joints with Different Anchorage Methods,” *ACI Structural Journal*, Vol. 106, No. 3, May-June, pp. 329-339.

Masuo, K., Adachi, M., and Imanishi, T., 2006a, “Ultimate Strength of R/C Exterior Beam-Column Joint Using Mechanical Anchorage for Beam Reinforcement USD590—Part 1: Experiment on Anchorage Strength of Beam Reinforcement,” *Proc., Architectural Institute of Japan*, Sep., pp. 25-26 (in Japanese).

Masuo, K., Adachi, M., and Imanishi, T., 2006a, 2006b, “Ultimate Strength of R/C Exterior Beam-Column Joint Using Mechanical Anchorage for Beam Reinforcement USD590—Part 1: Experiment on Anchorage Strength of Beam Reinforcement and Part 2: Experiment on Shear Strength of Beam-Column Joint,” *Proc., Architectural Institute of Japan*, Sep., pp. 25-28 (in Japanese).

Masuo, K., Adachi, M., and Imanishi, T., 2006b, “Ultimate Strength of R/C Exterior Beam-Column Joint Using Mechanical Anchorage for Beam Reinforcement USD590—Part 2: Experiment on Shear Strength of Beam-Column Joint,” *Proc., Architectural Institute of Japan*, Sep., pp. 27-28 (in Japanese).

Matsushima, M., Kuramoto, H., Maeda, M., Shindo, K., and Ozone, S., 2000, “Test on Corner Beam-Column Joint under Tri-axial Loadings— Outline fo Test: Study on Structural Performance of Mechanical Anchorage (No. 10); Discussion of Test Results: Study on Structural Performance of Mechanical Anchorage (No. 11),” *Proc., Architectural Institute of Japan*, Sep., pp. 861-864 (in Japanese).

McConnell, S. W., and Wallace, J. W., 1995, “Behavior of Reinforced Concrete Beam-Column Knee-Joints Subjected to Reversed Cyclic Loading,” *Report No. CU/CEE-95-07*, Department of Civil and Environmental Engineering, Clarkson University, June, 209 pp.

McMackin, P. J., Slutter, R. G., and Fisher, J. W., 1973, “Headed Steel Anchor under Combined Loading,” *AISC Engineering Journal*, Vol. 10, No. 2, Apr.-Jun., pp. 43-52.

Murakami, M., Fuji, T., and Kubota, T., 1998, "Failure Behavior of Beam-Column Joints with Mechanical Anchorage in Subassemblage Frames," *Concrete Research and Technology*, Vol. 9, No. 1, Jan., pp. 1-9 (in Japanese).

Nakazawa, H., Kumagai, H., Saito, H., Kurose, Y., and Yabe, Y., 2000, "Development on the Ultra-High-Strength Reinforced Concrete Structure—Part 3: Loading Tests on Exterior Beam-Column Joints," *Proc., Architectural Institute of Japan*, Sep., pp. 611-612 (in Japanese).

Nilsson, I. H. E., and Losberg, A., 1976, "Reinforced Concrete Corners and Joints Subjected to Bending Moment," *J Struct Div-Asce*, Vol. 102, No. ST6, June, pp. 1229-1254.

Shao, Y., Darwin, D., O'Reilly, M., Lequesne, R. D., Ghimire, K., and Hano, M., 2016, "Anchorage of Conventional and High-Strength Headed Reinforcing Bars," *SM Report No. 117*, University of Kansas Center for Research, Inc., Lawrence, KS, Aug., 234 pp.

Sperry, J., Al-Yasso, S., Searle, N., DeRubeis, M., Darwin, D., O'Reilly, M., Matamoros, A., Feldman, L., Lepage, A., Lequesne, R., and Ajaam, A., 2015a, "Anchorage of High-Strength Reinforcing Bars with Standard Hooks," *SM Report No. 111*, University of Kansas Center for Research, Inc., Lawrence, Kansas, June, 243 pp.

Sperry, J., Darwin, D., O'Reilly, M., and Lequesne, R., 2015b, "Anchorage Strength of Conventional and High-Strength Hooked Bars in Concrete," *SM Report No. 115*, University of Kansas Center for Research, Inc., Lawrence, Kansas, Dec., 266 pp.

Sperry, J., Darwin, D., O'Reilly, M., Matamoros, A., Feldman, L., Lepage, A., Lequesne, R., and Yasso, S., 2017b, "Conventional and High-Strength Hooked Bars—Part 2: Data Analysis," *ACI Structural Journal*, Vol. 114, No. 1, Jan.-Feb., pp. 267-276.

Sperry, J., Yasso, S., Searle, N., DeRubeis, M., Darwin, D., O'Reilly, M., Matamoros, A., Feldman, L., Lepage, A., and Lequesne, R., 2017a, "Conventional and High-Strength Hooked Bars—Part 1: Anchorage Tests," *ACI Structural Journal*, Vol. 114, No. 1, Jan.-Feb., pp. 255-266.

Stoker, J., Boulware, R., Crozier, W., and Swirsky, R., 1974, "Anchorage Devices for Large Diameter Reinforcing Bars," *Report No. CA-DOT-TL-6626-1-73-30*, Transportation Laboratory California Division of Highways, Sacramento, CA, Sep., 75 pp.

Takeuchi, H., Kishimoto, T., Hattori, S., Nakamura, K., Hosoya, H., and Ichikawa, M., 2001, "Development of Mechanical Anchorage Used Circular Anchor Plate—Part 3: Outline of Exterior Beam-Column Joint Test and Experimental Results and Part 4: Experimental Results and Discussion of Exterior Beam-Column Joint Test," *Proc., Architectural Institute of Japan*, Sep., pp. 111-114 (in Japanese).

Tasai, A., Kawakatsu, K., Kiyohara, T., and Murakami, M., 2000, "Shear Performance of Exterior Beam Column Joint with Beam Main Bars Anchored Mechanically—Part 1: Study on Structural Performance of Mechanical Anchorage (No. 8)," *Proc., Architectural Institute of Japan*, Sep., pp. 857-864 (in Japanese).

Tazaki, W., Kusuhara, F., and Shiohara, H., 2007, "Tests of R/C Beam-Column Joints with Irregular Details on Anchorage of Beam Longitudinal Bars—Part 1: Outline of Tests and Part 2:

Test Results and Discussions,” *Proc., Architectural Institute of Japan*, Aug., pp. 653-656 (in Japanese).

Thompson, M. K., 2002, “The Anchorage Behavior of Headed Reinforcement in CCT Nodes and Lap Splices,” *PhD Dissertation*, The University of Texas at Austin, Austin, TX, 529 pp.

Thompson, M. K., Jirsa, J. O., and Breen, J. E., 2006, “Behavior and Capacity of Headed Reinforcement,” *ACI Structural Journal*, Vol. 103, No. 4, July-Aug., pp. 522-530.

Thompson, M. K., Jirsa, J. O., and Breen, J. E., 2006a, “CCT Nodes Anchored by Headed Bars-Part 2: Capacity of Nodes,” *ACI Structural Journal*, Vol. 103, No. 1, Jan.-Feb., pp. 65-73.

Thompson, M. K., Jirsa, J. O., Ledesma, A. L., Breen, J. E., and Klinger, R. E., 2002, “Anchorage Behaviour of Headed Reinforcement,” *Report No. 1855-3*, Center for Transportation Research, The University of Texas at Austin, Austin, TX, May, 117 pp.

Thompson, M. K., Ledesma, A., Jirsa, J. O., and Breen, J. E., 2006b, “Lap Splices Anchored by Headed Bars,” *ACI Structural Journal*, Vol. 103, No. 2, Mar.-Apr., pp. 271-279.

Thompson, M. K., Ziehl, M. J., Jirsa, J. O., and Breen, J. E., 2005, “CCT Nodes Anchored by Headed Bars-Part 1: Behavior of Nodes,” *ACI Structural Journal*, Vol. 102, No. 6, Nov.-Dec., pp. 808-815.

Viest, I. M., 1956, “Investigation of Stud Shear Connectors for Composite Concrete and Steel T-Beams,” *Journal of American Concrete Institute*, Vol. 27, No. 8, Apr., pp. 875-892.

Wallace, J. W., McConnell, S. W., Gupta, P., and Cote, P. A., 1998, “Use of Headed Reinforcement in Beam-Column Joints Subjected to Earthquake Loads,” *ACI Structural Journal*, Vol. 95, No. 5, Sep.-Oct., pp. 590-602.

Wight, J. K., and Sozen, M. A., 1973, “Shear Strength Decay in Reinforced Concrete Columns Subjected to Large Deflection Reversals,” *Report No. SRS 403*, Department of Civil Engineering, University of Illinois, Urbana-Champaign, IL, Aug., 290 pp.

Yoshida, J., Ishibashi, K., and Nakamura, K., 2000, “Experimental Study on Mechanical Anchorage Using Bolt and Nut in Exterior Beam-Column Joint—Part 1: Specimens and Outline of Experiment and Part 2: Analysis of Experiment,” *Proc., Architectural Institute of Japan*, Sep., pp. 635-638 (in Japanese).

Zuo, J., and Darwin, D., 2000, “Splice Strength of Conventional and High Relative Rib Area Bars in Normal and High Strength Concrete,” *ACI Structural Journal*, Vol. 97, No. 4, July-Aug., pp. 630-641.

APPENDIX A: NOTATION

A_b	Cross-sectional area of an individual headed deformed bar
A_{brg}	Net bearing area of the head of headed deformed bar calculated as the gross head area minus maximum area of the obstruction adjacent to the head; net bearing area of the head calculated as gross head area minus bar area if no obstruction is present or the obstruction, as shown in Figure 5.7, has length measured from the bearing face of the head not more than $0.6d_b$ for No. 8 and larger bars or the smaller of 0.6 in. and $0.75d_b$ for bars smaller than No. 8 and does not have a diameter greater than $1.5d_b$
A_g	Gross cross-sectional area of column in exterior beam-column joint or beam in roof-level interior beam-column joint
A_{gross}	Gross cross-sectional area of the head
A_{hs}	Total cross-sectional area of headed deformed bars being developed (nA_b)
A_j	Effective cross-sectional area within the beam-column joint in a plane parallel to the headed bars (Section 4.2.2)
A_{Nc}	Projected concrete failure area of group of headed bars
A_{Nco}	Projected concrete failure area of a single headed bar ($9\ell_{eh}^2$)
A_{obs}	Gross cross-sectional area of the obstruction adjacent to the bearing face of the head
A_{st}	Total cross-sectional area of reinforcement perpendicular to the headed bar within a failure region
A_{tr}	Cross-sectional area of confining reinforcement crossing the potential plane of splitting [Eq. (4.6), Figure 4.19]
$A_{tr,l}$	Cross-sectional area of a single leg of confining reinforcement (or anchor reinforcement) parallel to the headed bar within the joint region
$A_{tro,l}$	Cross-sectional area of a single leg of confining reinforcement (or anchor reinforcement) parallel to the headed bar outside the joint region
A_{tt}	Total cross-sectional area of effective confining reinforcement ($NA_{tr,l}$) parallel to ℓ_{dt} for headed bars being developed (Sections 1.4, 3.3, 4.2.1, 5.1.1, and 5.2.1)
A_{st}	Total cross-sectional area of reinforcement perpendicular to the headed bar within a $1.5\ell_{eh}$ radial distance from the center of the bar (Sections 3.1 and 3.3.1.2)
A_v	Total cross-sectional area of confining reinforcement parallel to the headed bar ($N_{total} A_{tr,l}$) assumed to serve as a single tie (Section 4.2.2.3)
b	Width of the head (Table 2.3); width of slab specimens (Figures 2.3 and 2.4)
b_b	Width of beam in exterior and knee beam-column joints; width of column in roof-level interior beam-column joints; width of splice specimens
b_c	Width of column in exterior and knee beam-column joints; width of beam in roof-level interior beam-column joints

b_j	Effective width of beam-column joint perpendicular to the headed bars in tension calculated based on Section 18.8.4.3 of ACI 318-14
$b_{j,ACI352}$	Effective width of beam-column joint perpendicular to the headed bars in tension calculated based on Section 4.3.1 of ACI 352R-02
c_{a1}	Minimum distance from the center of the headed bar to the edge of concrete
c_{a2}	Minimum distance from the center of the headed bar to the edge of concrete in the direction perpendicular to c_{a1}
c_{bc}	Clear cover measured from the back of the head to the back of the member
c_{ch}	Center-to-center spacing between adjacent headed bars
c_h	Clear spacing between adjacent headed bars
c_o	Clear cover measured from the head to the nearest free concrete face of the member
c_{si}	Half of clear spacing between bars [Eq. (4.6)]
c_{so}	Clear cover measured from the headed bar to the nearest free concrete face of the member within the anchorage region
c_{to}	Clear cover measured from the headed bar to the top free concrete face of splice specimens within the anchorage region
c_b	Clear cover measured from the headed bar to the bottom free concrete face of member [Eq. (4.6)]
d	Distance from the centroid of the tension bar to the extreme compression fiber of the beam in exterior and knee joints or column in roof-level interior and column foundation joints; diameter of the head (Table 2.3)
d'	Distance from the centroid of the compression bar to the extreme compression fiber of the beam in exterior and knee joints (or column in roof-level interior joints)
d_1	Diameter of the head (Table 2.3)
d_2	Diameter of the obstruction (Table 2.3)
d_b	Nominal diameter of the headed bar
$d_{b,sprt}$	Nominal diameter of reinforcement in the support - column in exterior joint and beam in roof-level interior joint
d_c	Diameter of the obstruction (Figure 5.8)
d_h	Diameter of the head (Figure 5.8)
d_{obs}	Diameter of the obstruction adjacent to the bearing face of the head
f'_c	Specified compressive strength of concrete
f_{cm}	Measured compressive strength of concrete
f_{su}	Stress in the headed bar at failure
$f_{s,calc}$	Stress in the headed bar calculated using Eq. (5.2)
f_y	Measured yield strength of the headed bar
$f_{y,sprt}$	Measured yield strength of reinforcing bars in the support- column in exterior joint and beam in roof-level interior joint - passing through the joint

f_{yt}	Measured yield strength of confining reinforcement (hoops) parallel to the headed bar within the joint region
f_{yto}	Measured yield strength of hoops parallel to the headed bar outside the joint region
h	Height of the head (Table 2.3), height of slab and splice specimens (Figures 2.3 and 2.4)
h_b	Depth of beam in exterior and knee beam-column joints; depth of column in roof-level interior beam-column joints; depth of splice specimens
h_c	Depth of column in exterior and knee beam-column joints; depth of beam in roof-level interior beam-column joints
h_{cl}	Distance between the center of headed bar to the inner face of the nearest support plate (Figure 3.2)
h_{ef}	Embedment length of the anchor (Section 3.1.5)
k_c	Coefficient for concrete breakout strength in tension
k_t	Coefficient for development length of headed deformed bars (Sections 5.1.6 and 5.2.1)
K_{tr}	Confining reinforcement index [Eq. (4.6)]
L_1	Distance between loading point and nearest support in splice specimens (Figure 2.7)
L_2	Distance between two supports in splice specimens (Figure 2.7)
ℓ_{dh}	Development length in tension of deformed bar or deformed wire with a standard hook, measured from outside end of hook, point of tangency, toward critical section
ℓ_{dt}	Development length in tension of headed deformed bar, measured from the critical section to the bearing face of the head
ℓ_{dy}	Development length in tension of straight deformed bar (headed bar treated as straight bar by ignoring the head) calculated using Eq. (4.6)
ℓ_{eh}	Embedment length measured from the critical section to the bearing face of the head
ℓ_{ehy}	Embedment length required to yield the headed bars calculated using the descriptive equations, Eq. (4.1) and (4.2)
ℓ_{st}	Lap length of headed bars in splice specimens
M	Bending moment in the splice region
M_{peak}	Peak moment at critical section of headed bars in beam-column joints subjected to reversed cyclic loading
M_n	Nominal flexural strength of beam in exterior and knee joints and column in roof-level interior joints
n	Number of headed bars loaded simultaneously in tension; number of headed bars at the tension face of the beam in exterior and knee joints and column in roof-level interior joints when the applied moment reached M_{peak}
$n_{l,sprt}$	Number of longitudinal bars around the perimeter of a column core within the joint region that are laterally supported by the corner of hoops or cross-ties
n_{sprt}	Total number of longitudinal bars in the support - column in exterior joints and beam in roof-level interior joints

N	Number of legs of effective confining reinforcement A_u in the joint region; total number of column (or beam) reinforcement, considered as confining reinforcement, crossing the potential plane of splitting [Eq. (4.6), Figure 4.19]
N_{ar}	Nominal anchorage strength of a single headed bar based on anchor reinforcement
N_{arg}	Nominal anchorage strength of a group of headed bars based on anchor reinforcement
N_b	Basic concrete breakout strength of a single headed bar in tension
N_{cb}	Nominal concrete breakout strength of a single headed bar in tension
N_{cbg}	Nominal concrete breakout strength of a group of headed bars in tension
N_{sb}	Nominal side-face blowout strength of a single headed bar in tension
N_{sbg}	Nominal side-face blowout strength of a group of headed bars in tension
N_{split}	Total number of column (or beam) reinforcement, considered as confining reinforcement, crossing the potential plane of splitting (Figure 4.19), used as N in Eq. (4.6)
N_{total}	Total number of legs of confining reinforcement within a beam-column joint
N_{tr}	Total number of legs of anchor reinforcement parallel to the headed bars within $0.5\ell_{eh}$ radial distance from the center of the bar in column-like specimens (Figure 3.22); total number of legs of anchor reinforcement parallel to the headed bars within $0.5\ell_{eh}$ from the center of the headed bar in the direction of the interior of beam-column joint (Figure 4.23)
N_{tro}	Total number of legs of anchor reinforcement parallel to the headed bars within $0.5\ell_{eh}$ from the center of the headed bar in the direction outside of the beam-column joint (Figure 4.23)
P	Total load applied on splice specimens at failure; column axial load applied during the test of beam-column joints
p	Probability value from student t-test
R_r	Relative rib area of the anchored bar [Eq. (4.6)]
s	Center-to-center spacing of confining reinforcement in Eq. (4.6) crossing the potential plane of splitting
s_h	Center-to-center spacing between headed bars in a layer (Figure 4.23)
s_{tr}	Center-to-center spacing of confining reinforcement (hoops) within the joint region (Figure 4.23)
s'_{tr}	Center-to-center spacing between the first confining reinforcement (hoop) within the joint region and the top headed bar in tension (Figure 4.23)
s_{tro}	Center-to-center spacing of hoops outside joint region (Figure 4.23)
s'_{tro}	Center-to-center spacing between the first hoop outside the joint region and the nearest headed bar in tension (Figure 4.23)
s_v	Center-to-center spacing between headed bars in adjacent layers (Figure 4.23)
T	Test failure load on a headed bar
T_{dgn}	Force on a headed bar calculated using design equation, Eq. (5.2)

T'	Estimated test failure load on a headed bar in beam-column joints subjected to reversed cyclic loading calculated using Eq. (4.4)
T'_{mod}	Modified bar force T' in beam-column joint specimens with $\ell_{eh} \geq \ell_{ehy}$ calculated using Eq. (4.5)
T_{anc}	Nominal anchorage strength of each headed bar in tension in beam-column joints governed by concrete breakout, side-face blowout, or anchor reinforcement, calculated using Eq. (3.9) and (4.11) based on anchorage design provisions in Chapter 17 of ACI 318-14
T_c	Anchorage strength of a headed bar without confining reinforcement in Eq. (1.6), (1.7) and (1.10); contribution of concrete to anchorage strength of a headed bar
T_h	Anchorage strength of a headed bar with confining reinforcement in Eq. (1.8), (1.9) and (1.11); anchorage strength of a headed bar calculated using descriptive equations in Sections 3.3 and 4.2.1
T_N	Normalized load on a headed bar at failure calculated using Eq. (3.1) through (3.3) and (3.10)
t, t_1	Thickness of the head (Tables 2.3)
t_2	Length of the obstruction measured from the bearing face of the head (Table 2.3)
t_h	Thickness of the head (Figure 5.8)
t_{obs}	Length of the obstruction measured from the bearing face of the head
V_n	Nominal joint shear strength calculated in accordance with the joint shear strength requirements of Section 18.8.4 of ACI 318-14
$V_{n,ACI352}$	Nominal joint shear strength calculated in accordance with Section 4.3 of ACI 352R-02
V_p	Peak joint shear applied at the beam-column joint
w/c	Water-to-cement ratio by weight
α	Stress multiplier in Eq. (1.2) and (1.3); reinforcement location factor in Eq. (4.6)
β	Bar coating factor [Eq. (4.6)]; reliability index (Section 5.1)
$\delta_{0.8peak}$	Drift ratio at drop to 80% from the peak load
δ_y	Drift ratio at first bar yielding (measured)
ϕ	Strength reduction factor [Eq. (4.6)]
Υ_j	Angular distortion of a beam-column joint due to shear approximately at 3.5% drift
Ψ_{cs}	Factor used to modify development length based on confining reinforcement and bar spacing
Ψ_e	Factor used to modify development length based on reinforcement coating
$\Psi_{ec,N}$	Factor used to modify tensile strength of anchors based on eccentricity of applied loads
$\Psi_{ed,N}$	Factor used to modify tensile strength of anchors based on proximity to edges of concrete member
$\Psi_{c,N}$	Factor used to modify tensile strength of anchors based on presence or absence of cracks in concrete

$\Psi_{cp,N}$	factor used to modify tensile strength of postinstalled anchors intended for use in uncracked concrete without supplementary reinforcement to account for the splitting tensile stresses due to installation
Ψ_o	Factor used to modify development length based on bar location within member
θ	Strut angle in beam-column joints (Figure 4.10)
λ, λ_a	Modification factor to reflect the reduced mechanical properties of lightweight concrete relative to normalweight concrete of the same compressive strength

Acronym list

ACI	American Concrete Institute
ASTM	American Society of Testing and Materials - International
BSG	Bulk Specific Gravity
BSG (SSD)	Bulk Saturated Surface Dry Specific Gravity
CCT	Compression-Compression-Tension
COV	Coefficient of Variation
HA	Class of head satisfying head dimension requirements detailed in Section 5.2.2
MAX	Maximum
MIN	Minimum
PVC	Polyvinyl Chloride
SG	Specific Gravity
SN	Specimen Number
SSD	Saturated Surface Dry
STD	Standard Deviation

APPENDIX B: DETAILS OF SLAB AND SPLICE SPECIMENS TESTED IN THE CURRENT STUDY

B.1 STRESS-STRAIN CURVES FOR HEADED BARS

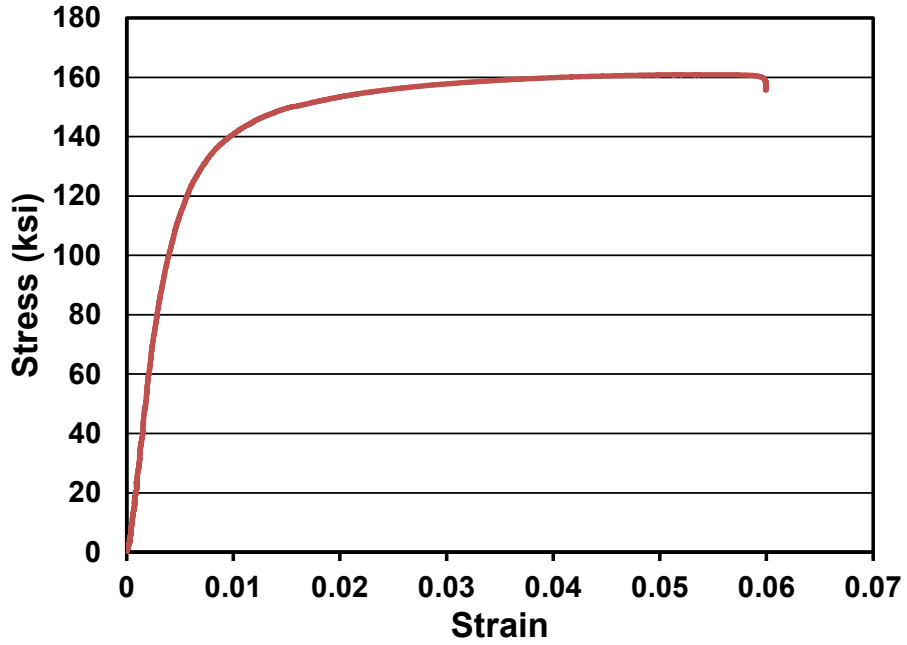


Figure B.1 Stress-strain curve for No. 6 headed bar

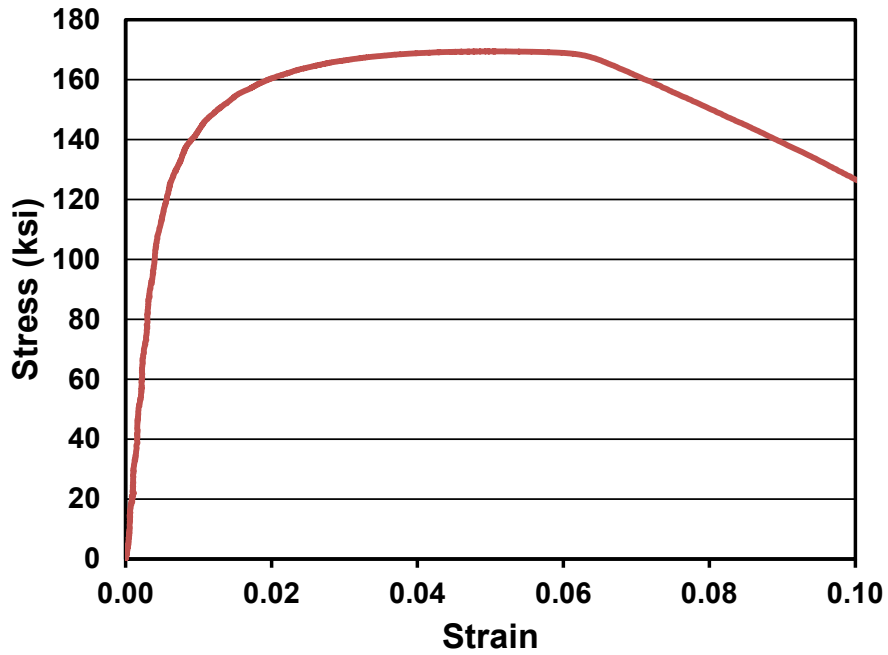


Figure B.2 Stress-strain curve for No. 8 headed bar

B.2 SCHEMATICS OF SLAB SPECIMENS

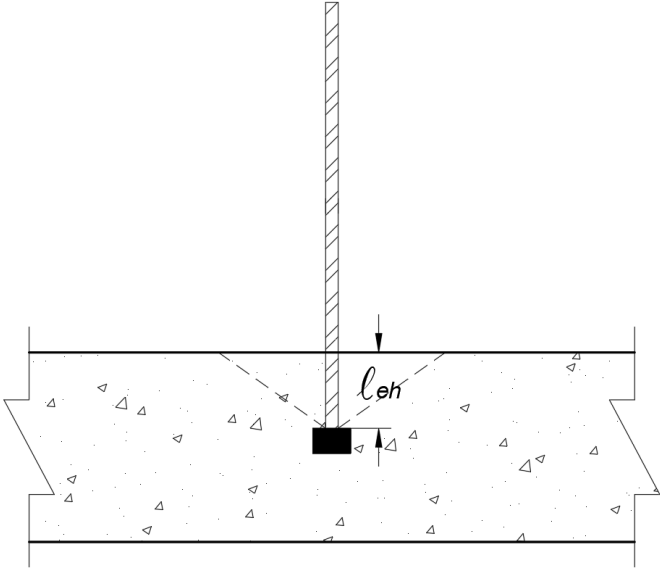


Figure B.3 Cross-section view of slab specimen 8-5-F4.1-0-6 with no reinforcement perpendicular to the headed bar

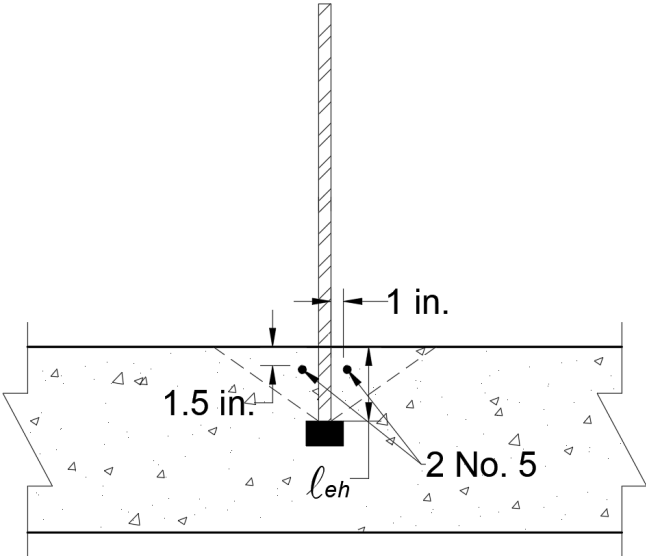


Figure B.4 Cross-section view of slab specimen 8-5-F4.1-2#5-6 with 2 No. 5 bars as reinforcement perpendicular to the headed bar

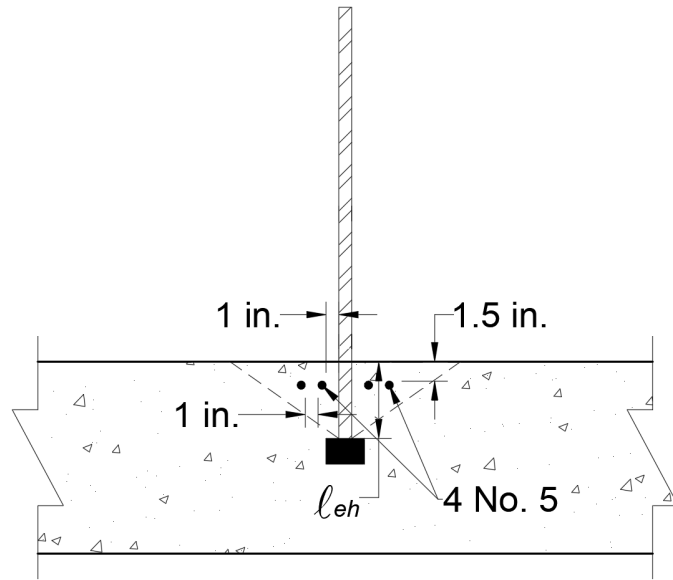


Figure B.5 Cross-section view of slab specimen 8-5-F4.1-4#5-6 with 4 No. 5 bars as reinforcement perpendicular to the headed bar

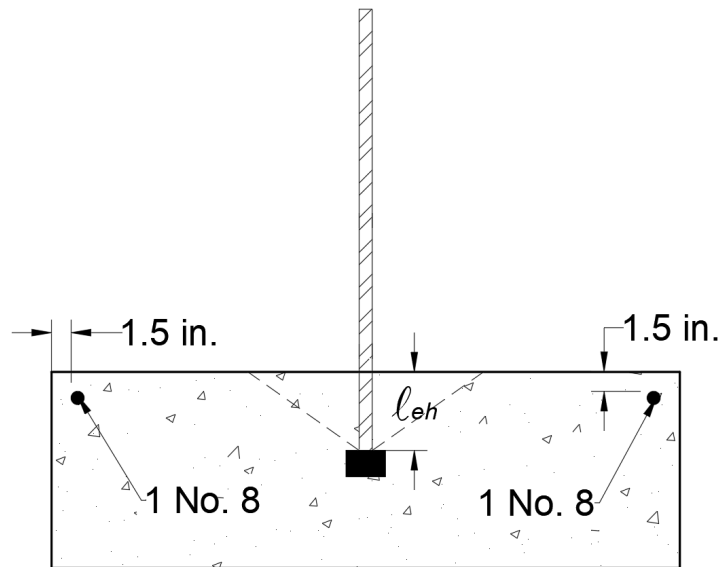


Figure B.6 End view of slab specimens 8-5-F4.1-2#8-6, 8-5-F9.1-2#8-6, 8-5-T4.0-2#8-6, and 8-5-T9.5-2#8-6 with 2 No. 8 bars as reinforcement perpendicular to the headed bar

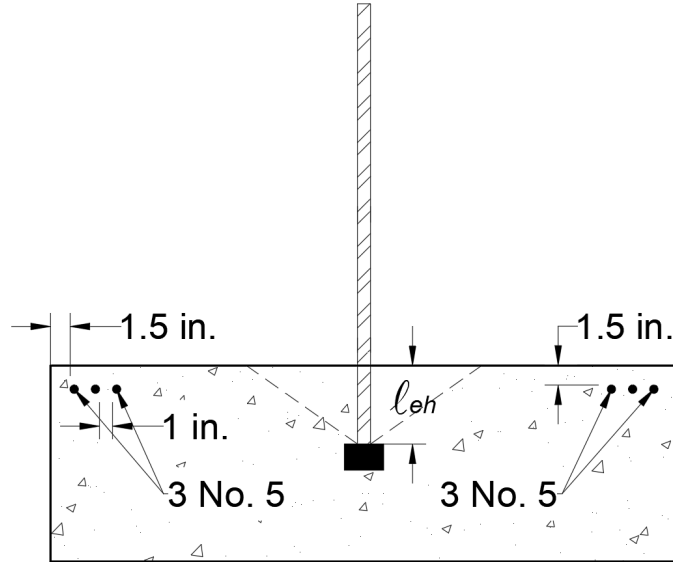


Figure B.7 End view of slab specimens 8-8-O12.9-6#5-6, 8-8-O9.1-6#5-6, 8-8-S6.5-6#5-6, 8-8-O4.5-6#5-6, 8-5-S14.9-6#5-6, 8-5-S6.5-6#5-6, 8-5-O12.9-6#5-6, 8-5-O4.5-6#5-6, 8-5-S9.5-6#5-6, 8-5-S9.5-6#5-6, and 8-5-F4.1-6#5-6 with 6 No. 5 bars as reinforcement perpendicular to the headed bar

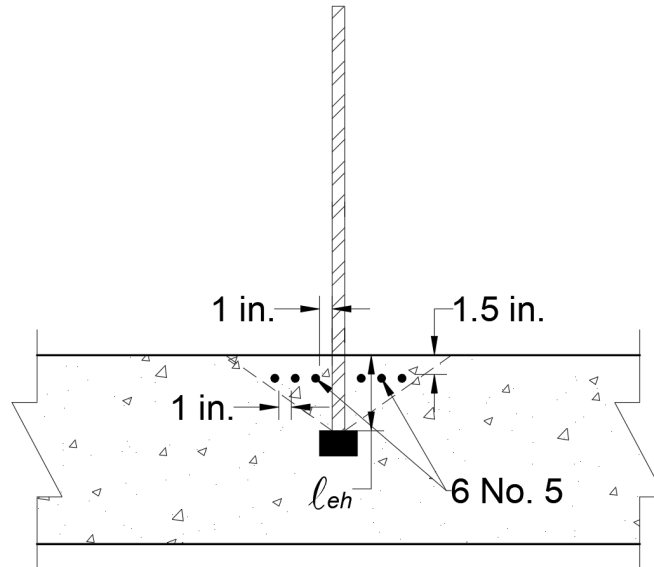


Figure B.8 Cross-section view of slab specimen 8-5-F4.1-6#5-6 with 6 No. 5 bars as reinforcement perpendicular to the headed bar

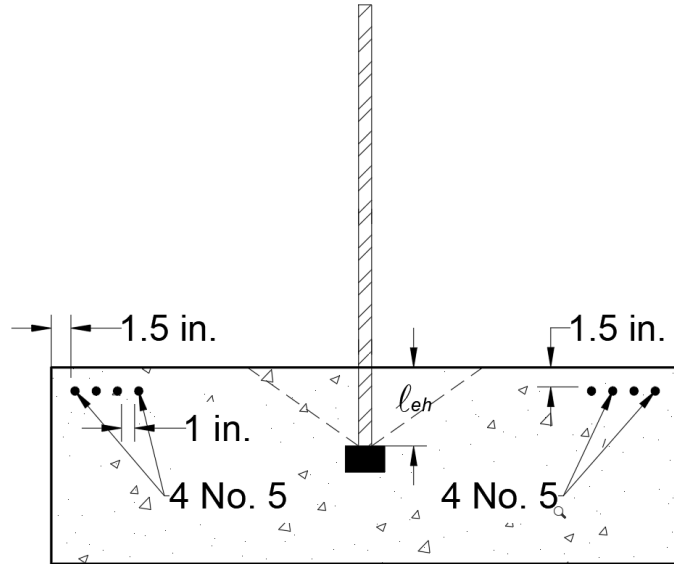


Figure B.9 End view of slab specimen 8-5-T4.0-8#5-6 with 8 No. 5 bars as reinforcement perpendicular to the headed bar

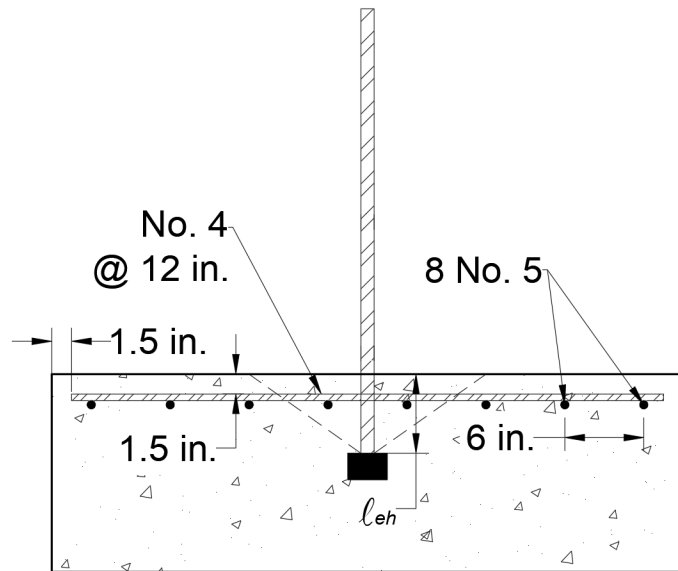


Figure B.10 End view of slab specimens 8-5-T9.5-8#5-6, 8-5-F4.1-8#5-6, and 8-5-F9.1-8#5-6 with 8 No. 5 bars and No. 4 bars spaced at 12 in. as reinforcement perpendicular to the headed bar

Table B.1 Slab specimens tested in the current study [§]

	Specimens			Head Type [‡]	A_{brg}/A_b	A_{st} (in.)	A_{st}/A_b	c_{bc} (in.)	c_{ch} [□] (in.)	c_{so} (in.)	d/ℓ_{eh}
	SN	Designation	Headed bar ^{§§}								
Series 1	1	8-5-T9.5-8#5-6 ^{‡‡}	A	T9.5	9.5	1.02	1.29	7.0	48	23.5	1.48
		8-5-T9.5-8#5-6 ^{‡‡}	B	T9.5	9.5	1.02	1.29	6.8	48	23.5	1.44
	2	8-5-T4.0-8#5-6	A	T4.0	4.0	0	0	6.5	48	23.5	1.38
		8-5-T4.0-8#5-6	B	T4.0	4.0	0	0	7.5	48	23.5	1.55
Series 2	3	8-5-F4.1-8#5-6 ^{‡‡}	A	F4.1	4.1	1.02	1.29	7.6	48	23.5	1.63
		8-5-F4.1-8#5-6 ^{‡‡}	B	F4.1	4.1	1.02	1.29	7.6	48	23.5	1.63
	4	8-5-F9.1-8#5-6 ^{‡‡}	A	F9.1	9.2	1.02	1.29	7.9	48	23.5	1.71
		8-5-F9.1-8#5-6 ^{‡‡}	B	F9.1	9.2	1.02	1.29	8.0	48	23.5	1.69
Series 3	5	8-5-F4.1-2#8-6	A	F4.1	4.1	0	0	9.0	48	23.5	1.96
		8-5-F9.1-2#8-6	B	F9.1	9.2	0	0	9.0	48	23.5	1.96
	6	8-5-T4.0-2#8-6	A	T4.0	4.0	0	0	8.9	48	23.5	1.93
		8-5-T9.5-2#8-6	B	T9.5	9.5	0	0	8.9	48	23.5	1.90
Series 4	7	8-8-O12.9-6#5-6	A	O12.9	13.0	0	0	8.8	48	23.5	1.79
		8-8-O9.1-6#5-6	B	O9.1	9.2	0	0	8.8	48	23.5	1.89
	8	8-8-S6.5-6#5-6	A	S6.5	5.0	0	0	8.6	48	23.5	1.78
		8-8-O4.5-6#5-6	B	O4.5	4.5	0	0	8.5	48	23.5	1.86
Series 5	9	8-5-S14.9-6#5-6	A	S14.9	15.0	0	0	8.5	48	23.5	1.84
		8-5-S6.5-6#5-6	B	S6.5	5.0	0	0	8.5	48	23.5	1.75
	10	8-5-O12.9-6#5-6	A	O12.9	13.0	0	0	8.4	48	23.5	1.73
		8-5-O4.5-6#5-6	B	O4.5	4.5	0	0	8.5	48	23.5	1.77
	11	8-5-S9.5-6#5-6	A	S9.5	9.5	0	0	8.5	48	23.5	1.79
		8-5-S9.5-6#5-6	B	S9.5	9.5	0	0	8.6	48	23.5	1.83
12	8-5-F4.1-6#5-6 ^{□□}	-	F4.1	4.1	0	0	6.6	48	23.5	5.73	
Series 6	13	8-5-F4.1-0-6	A	F4.1	4.1	0	0	12.0	32	15.5	2.49
		8-5-F4.1-0-6	B	F4.1	4.1	0	0	12.0	32	15.5	2.91
		8-5-F4.1-2#5-6	C	F4.1	4.1	0.62	0.78	12.0	32	15.5	2.74
	14	8-5-F4.1-4#5-6	A	F4.1	4.1	1.24	1.57	12.0	32	15.5	3.00
		8-5-F4.1-4#5-6	B	F4.1	4.1	1.24	1.57	12.0	32	15.5	2.98
		8-5-F4.1-4#5-6	C	F4.1	4.1	1.24	1.57	12.0	32	15.5	2.70
	15	8-5-F4.1-6#5-6	A	F4.1	4.1	1.86	2.35	12.0	32	15.5	2.89
		8-5-F4.1-6#5-6	B	F4.1	4.1	1.86	2.35	12.0	32	15.5	2.72
		8-5-F4.1-6#5-6	C	F4.1	4.1	1.86	2.35	12.0	32	15.5	2.65

[§] Notation described in Appendix A; all specimens contained No. 8 headed bars

^{§§} Multiple headed bars in a single specimen are denoted by letters A, B, and C; specimen dimensions shown in Figures 2.3 and 2.4

[‡] Details of heads provided in Section 2.1.2

^{‡‡} In addition to 8 No. 5 bars as reinforcement perpendicular to the headed bar, specimens contained No. 4 bars spaced at 12 in. in a direction perpendicular to the No. 5 bars as shown in Figure B.10

[□] c_{ch} is taken as twice of the minimum concrete cover to the center of the bar [that is, $c_{ch} = 2 \times (c_{so} + d_b/2)$]

^{□□} Specimen contained a single headed bar at the middle

Table B.1 Cont. Slab specimens tested in the current study [§]

	Specimens			f_{cm} (ksi)	f_{su} (ksi)	h_{cl} (in.)	ℓ_{eh} (in.)	h_{cl}/ℓ_{eh}	T (kips)	T_{anc} (kips)	T_h (kips)
	SN	Designation	Headed bar ^{§§}								
Series 1	1	8-5-T9.5-8#5-6 ^{‡‡}	A	7040	83.0	10.5	8.00	1.31	65.6	57.0	55.8
		8-5-T9.5-8#5-6 ^{‡‡}	B	7040	85.8	10.5	8.25	1.27	67.8	60.2	57.5
	2	8-5-T4.0-8#5-6	A	7040	78.2	10.5	8.50	1.24	61.8	62.4	59.3
		8-5-T4.0-8#5-6	B	7040	71.3	10.5	7.50	1.40	56.3	51.7	52.2
Series 2	3	8-5-F4.1-8#5-6 ^{‡‡}	A	5220	87.2	10.5	7.44	1.41	68.9	43.6	48.1
		8-5-F4.1-8#5-6 ^{‡‡}	B	5220	81.5	10.5	7.38	1.42	64.4	43.6	47.7
	4	8-5-F9.1-8#5-6 ^{‡‡}	A	5220	88.5	10.5	7.13	1.47	69.9	41.0	46.1
		8-5-F9.1-8#5-6 ^{‡‡}	B	5220	69.5	10.5	7.00	1.50	54.9	40.1	45.2
Series 3	5	8-5-F4.1-2#8-6	A	7390	81.5	10.5	6.00	1.75	64.4	37.9	41.9
		8-5-F9.1-2#8-6	B	7390	82.3	10.5	6.00	1.75	65.0	37.9	41.9
	6	8-5-T4.0-2#8-6	A	7390	76.6	10.5	6.06	1.73	60.5	38.9	42.4
		8-5-T9.5-2#8-6	B	7390	73.0	10.5	6.13	1.71	57.7	38.9	42.8
Series 4	7	8-8-O12.9-6#5-6	A	8620	100.0	9.8	6.25	1.56	79.0	44.0	45.4
		8-8-O9.1-6#5-6	B	8620	89.7	10.5	6.25	1.68	70.9	44.0	45.4
	8	8-8-S6.5-6#5-6	A	8620	92.4	10.0	6.38	1.57	73.0	45.1	46.3
		8-8-O4.5-6#5-6	B	8620	93.7	10.8	6.50	1.65	74.0	46.2	47.3
Series 5	9	8-5-S14.9-6#5-6	A	4200	78.2	10.3	6.50	1.58	61.8	32.2	39.8
		8-5-S6.5-6#5-6	B	4200	62.3	10.0	6.50	1.54	49.2	32.2	39.8
	10	8-5-O12.9-6#5-6	A	4200	66.3	10.0	6.63	1.51	52.4	33.0	40.6
		8-5-O4.5-6#5-6	B	4200	63.4	10.1	6.50	1.56	50.1	32.2	39.8
	11	8-5-S9.5-6#5-6	A	4200	61.9	10.3	6.50	1.58	48.9	32.2	39.8
		8-5-S9.5-6#5-6	B	4200	69.0	10.1	6.38	1.59	54.5	31.5	39.0
	12	8-5-F4.1-6#5-6 [Ⓜ]	-	4200	49.5	47.3	8.44	5.60	39.1	47.3	52.0
	Series 6	13	8-5-F4.1-0-6	A	5180	63.9	15.0	6.50	2.31	50.5	35.8
8-5-F4.1-0-6			B	5180	61.9	17.0	6.25	2.72	48.9	34.1	40.2
8-5-F4.1-2#5-6			C	5180	77.8	17.0	6.75	2.52	61.5	38.3	43.5
14		8-5-F4.1-4#5-6	A	5180	67.6	16.8	6.00	2.79	53.4	31.7	38.5
		8-5-F4.1-4#5-6	B	5180	66.3	17.0	6.13	2.78	52.4	32.5	39.3
		8-5-F4.1-4#5-6	C	5460	67.7	17.0	6.75	2.52	53.5	39.3	44.0
15		8-5-F4.1-6#5-6	A	5460	59.8	17.0	6.25	2.72	47.3	35.1	40.7
		8-5-F4.1-6#5-6	B	5460	70.8	16.8	6.63	2.53	55.9	37.6	43.2
		8-5-F4.1-6#5-6	C	5460	66.6	17.0	6.88	2.47	52.6	40.2	44.9

[§] Notation described in Appendix A; all specimens contained No. 8 headed bars

^{§§} Multiple headed bars in a single specimen are denoted by letters A, B, and C; specimen dimensions shown in Figures 2.3 and 2.4

^{‡‡} In addition to 8 No. 5 bars as reinforcement perpendicular to the headed bar, specimens contained No. 4 bars spaced at 12 in. in a direction perpendicular to the No. 5 bars as shown in Figure B.10

[Ⓜ] Specimen contained a single headed bar at the middle

[#] Detail of reinforcement in a plane perpendicular to the headed bar shown in Figures B.3 through B.10 of Appendix B

Table B.1 Cont. Slab specimens tested in the current study [§]

	Specimens			T_{dgn}^{\diamond} (kips)	T/T_{anc}	T/T_h	T/T_{dgn}	Ψ_{cs}^{∞}	Ψ_o	Reinf. Layout #
	SN	Designation	Headed bar ^{§§}							
Series 1	1	8-5-T9.5-8#5-6 ^{‡‡}	A	46.3	1.15	1.18	1.42	0.5	1.0	B.10
		8-5-T9.5-8#5-6 ^{‡‡}	B	47.8	1.13	1.18	1.42	0.5	1.0	B.10
	2	8-5-T4.0-8#5-6	A	49.2	0.99	1.04	1.26	0.5	1.0	B.9
		8-5-T4.0-8#5-6	B	43.4	1.09	1.08	1.30	0.5	1.0	B.9
Series 2	3	8-5-F4.1-8#5-6 ^{‡‡}	A	40.0	1.58	1.43	1.72	0.5	1.0	B.10
		8-5-F4.1-8#5-6 ^{‡‡}	B	39.6	1.48	1.35	1.63	0.5	1.0	B.10
	4	8-5-F9.1-8#5-6 ^{‡‡}	A	38.3	1.70	1.52	1.83	0.5	1.0	B.10
		8-5-F9.1-8#5-6 ^{‡‡}	B	37.6	1.37	1.21	1.46	0.5	1.0	B.10
Series 3	5	8-5-F4.1-2#8-6	A	35.2	1.70	1.54	1.83	0.5	1.0	B.6
		8-5-F9.1-2#8-6	B	35.2	1.71	1.55	1.85	0.5	1.0	B.6
	6	8-5-T4.0-2#8-6	A	35.5	1.56	1.43	1.70	0.5	1.0	B.6
		8-5-T9.5-2#8-6	B	35.9	1.49	1.35	1.61	0.5	1.0	B.6
Series 4	7	8-8-O12.9-6#5-6	A	38.1	1.79	1.74	2.08	0.5	1.0	B.7
		8-8-O9.1-6#5-6	B	38.1	1.61	1.56	1.86	0.5	1.0	B.7
	8	8-8-S6.5-6#5-6	A	38.8	1.62	1.58	1.88	0.5	1.0	B.7
		8-8-O4.5-6#5-6	B	39.6	1.60	1.57	1.87	0.5	1.0	B.7
Series 5	9	8-5-S14.9-6#5-6	A	33.1	1.92	1.55	1.87	0.5	1.0	B.7
		8-5-S6.5-6#5-6	B	33.1	1.53	1.24	1.49	0.5	1.0	B.7
	10	8-5-O12.9-6#5-6	A	33.7	1.59	1.29	1.55	0.5	1.0	B.7
		8-5-O4.5-6#5-6	B	33.1	1.55	1.26	1.51	0.5	1.0	B.7
	11	8-5-S9.5-6#5-6	A	33.1	1.52	1.23	1.48	0.5	1.0	B.7
		8-5-S9.5-6#5-6	B	32.4	1.73	1.40	1.68	0.5	1.0	B.7
	12	8-5-F4.1-6#5-6 [⊠]	-	42.9	0.83	0.75	0.91	0.5	1.0	B.7
	Series 6	13	8-5-F4.1-0-6	A	34.9	1.41	1.21	1.45	0.5	1.0
8-5-F4.1-0-6			B	33.5	1.43	1.22	1.46	0.5	1.0	B.3
8-5-F4.1-2#5-6			C	36.2	1.61	1.41	1.70	0.5	1.0	B.4
14		8-5-F4.1-4#5-6	A	32.2	1.68	1.39	1.66	0.5	1.0	B.5
		8-5-F4.1-4#5-6	B	32.8	1.61	1.33	1.60	0.5	1.0	B.5
		8-5-F4.1-4#5-6	C	36.7	1.36	1.21	1.46	0.5	1.0	B.5
15		8-5-F4.1-6#5-6	A	34.0	1.35	1.16	1.39	0.5	1.0	B.8
		8-5-F4.1-6#5-6	B	36.0	1.49	1.29	1.55	0.5	1.0	B.8
		8-5-F4.1-6#5-6	C	37.3	1.31	1.17	1.41	0.5	1.0	B.8

[§] Notation described in Appendix A; all specimens contained No. 8 headed bars

^{§§} Multiple headed bars in a single specimen are denoted by letters A, B, and C; specimen dimensions shown in Figures 2.3 and 2.4

^{‡‡} In addition to 8 No. 5 bars as reinforcement perpendicular to the headed bar, specimens contained No. 4 bars spaced at 12 in. in a direction perpendicular to the No. 5 bars as shown in Figure B.10

[⊠] Specimen contained a single headed bar at the middle

[◇] T_{dgn} is based on Eq. (5.2)

[∞] Ψ_{cs} is based on Table 5.1

[#] Detail of reinforcement in a plane perpendicular to the headed bar shown in Figures B.3 through B.10 of Appendix B

B.3 CROSS-SECTIONS OF HEADED SPLICE SPECIMENS

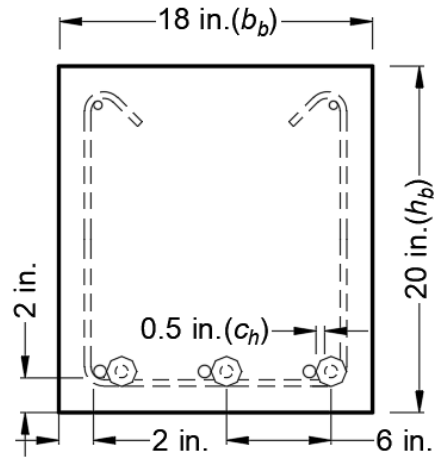


Figure B.11 Lapped bars with clear spacing of 0.5 in.

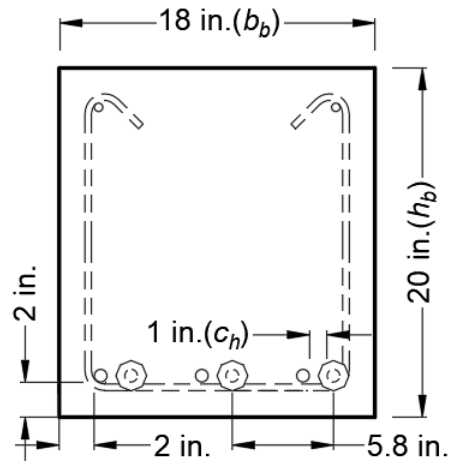


Figure B.12 Lapped bars with clear spacing of 1 in.

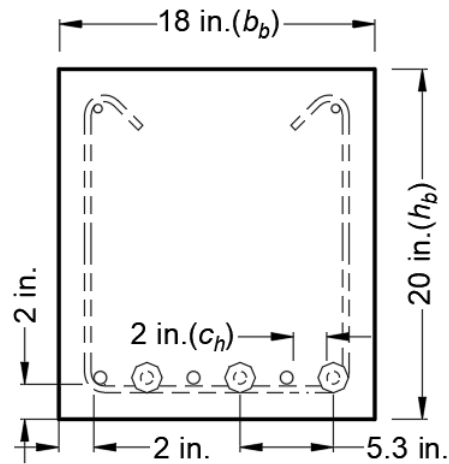


Figure B.13 Lapped bars with clear spacing of 1.9 in.

Table B.2 Headed splice specimens tested in the current study §

Specimen		Head Type §§	A_b (in. ²)	b (in.)	c_{ch} (in.)	c_h (in.)	c_{so} (in.)	d (in.)	d_b (in.)	f_{cm} (psi)	f_{su}^\ddagger (ksi)
1	2	3	4	5	6	7	8	9	10	11	12
Series 1	(3) 6-5-S4.0-12-0.5	S4.0	0.44	18	1.25	0.5	2	17.9	0.75	6330	77.2
	(3) 6-5-S4.0-12-1.0	S4.0	0.44	18.1	1.75	1	2	17.9	0.75	6380	83.6
	(3) 6-5-S4.0-12-1.9	S4.0	0.44	18	2.65	1.9	2	17.8	0.75	6380	76.3
Series 2	(3) 6-12-S4.0-12-0.5	S4.0	0.44	18	1.25	0.5	2	17.8	0.75	10890	81.9
	(3) 6-12-S4.0-12-1.0	S4.0	0.44	18	1.75	1	2	18.1	0.75	10890	75.0
	(3) 6-12-S4.0-12-1.9	S4.0	0.44	18	2.65	1.9	2	18.1	0.75	11070	82.8

Table B.2 Cont. Headed splice specimens tested in the current study §

Specimen		h (in.)	ℓ_{st} (in.)	L_1 (in.)	L_2 (in.)	M (kip.in.)	n	P (kips)	T (kips)	T_h (kips)
1	2	13	14	15	16	17	18	19	20	21
Series 1	(3) 6-5-S4.0-12-0.5	20.3	12	40.1	64	1669	3	83.2	34.0	30.5
	(3) 6-5-S4.0-12-1.0	20.3	12	40.1	64	1804	3	90.1	36.8	32.3
	(3) 6-5-S4.0-12-1.9	20.1	12	40.1	64	1649	3	82.2	33.6	38.3
Series 2	(3) 6-12-S4.0-12-0.5	20.1	12	40.0	64.1	1783	3	89.1	36.1	34.8
	(3) 6-12-S4.0-12-1.0	20.5	12	40.1	64	1636	3	81.5	33.0	36.7
	(3) 6-12-S4.0-12-1.9	20.5	12	40.0	64	1802	3	90.1	36.4	43.7

Table B.2 Cont. Headed splice specimens tested in the current study §

Specimen		$T_{dgn}^{\ddagger\ddagger}$ (kips)	T/T_h	T/T_{dgn}	Ψ_{cs}^\diamond	Ψ_o	Section Detail ^{◇◇}
1	2	22	23	24	25	26	27
Series 1	(3) 6-5-S4.0-12-0.5	23.2	1.11	1.46	1.00	1.25	B.11
	(3) 6-5-S4.0-12-1.0	23.9	1.14	1.54	0.97	1.25	B.12
	(3) 6-5-S4.0-12-1.9	26.7	0.88	1.26	0.87	1.25	B.13
Series 2	(3) 6-12-S4.0-12-0.5	26.6	1.04	1.36	1.00	1.25	B.11
	(3) 6-12-S4.0-12-1.0	27.3	0.90	1.21	0.97	1.25	B.12
	(3) 6-12-S4.0-12-1.9	30.6	0.83	1.19	0.87	1.25	B.13

§ Notation described in Appendix A; all specimens contained No. 6 headed bars

§§ Details of the heads provided in Section 2.1.2

* Stress in lapped bar at failure calculated from moment-curvature method

** T_{dgn} is based on Eq. (5.2)

◇ Ψ_{cs} is based on Table 5.1

◇◇ Reinforcement detail at splice region shown in Figures B.11 through B.13 of Appendix B

B.4 STRAIN IN LAPPED BARS IN HEADED SPLICE SPECIMENS

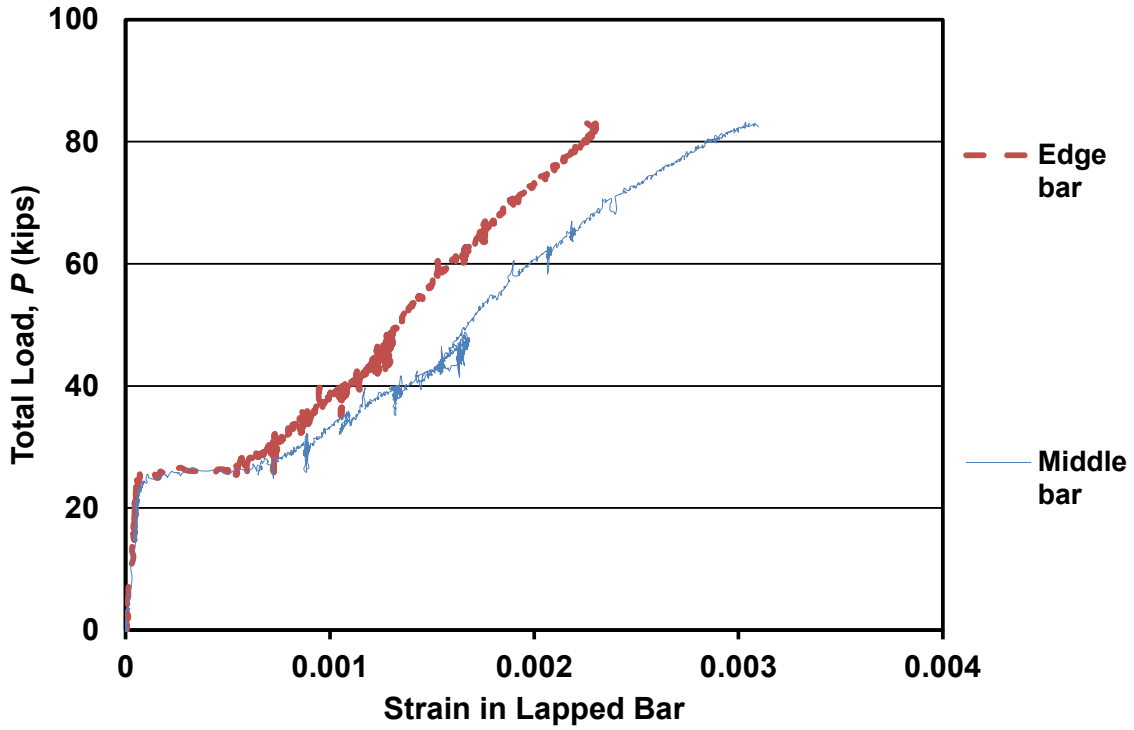


Figure B.14 Strain in lapped bars in specimen (3) 6-5-S4.0-12-0.5 as a function of applied load

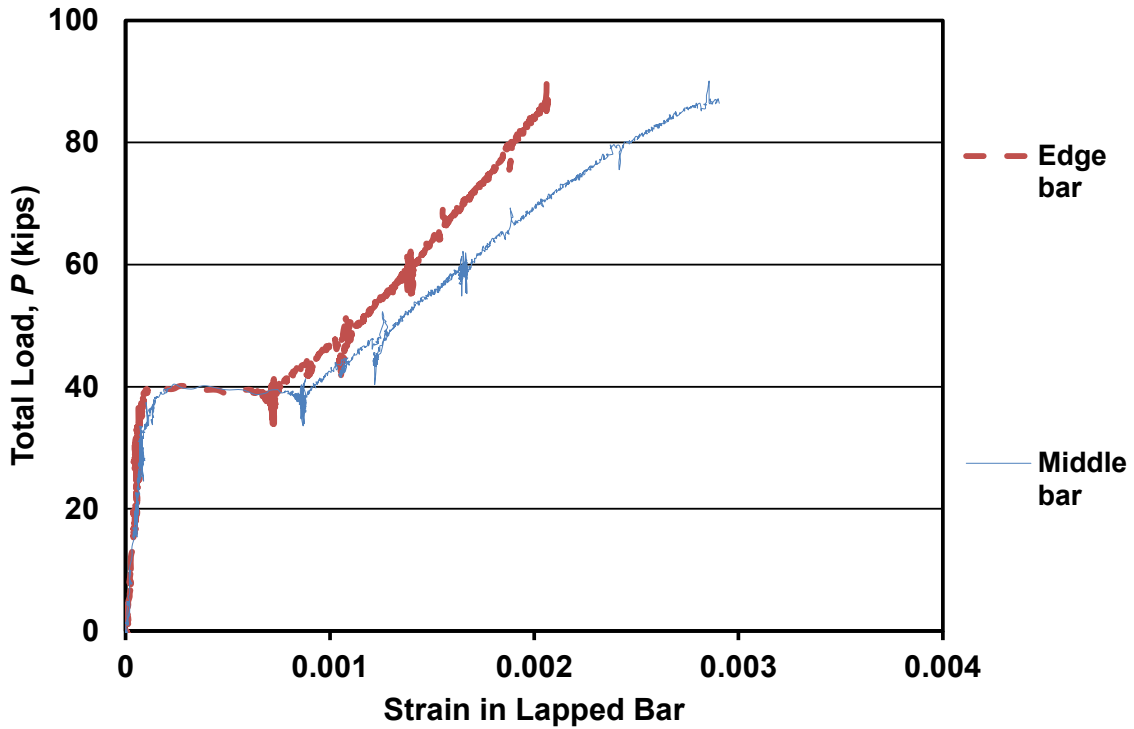


Figure B.15 Strain in lapped bars in specimen (3) 6-5-S4.0-12-1.0 as a function of applied load

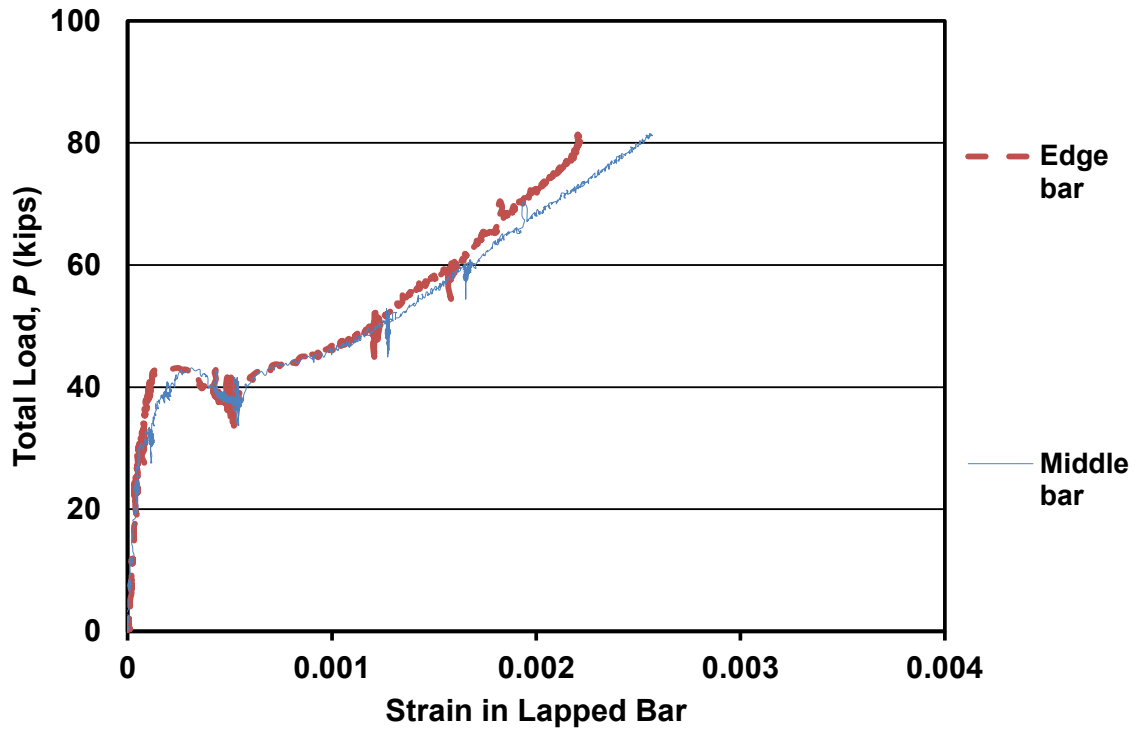


Figure B.16 Strain in lapped bars in specimen (3) 6-5-S4.0-12-1.9 as a function of applied load

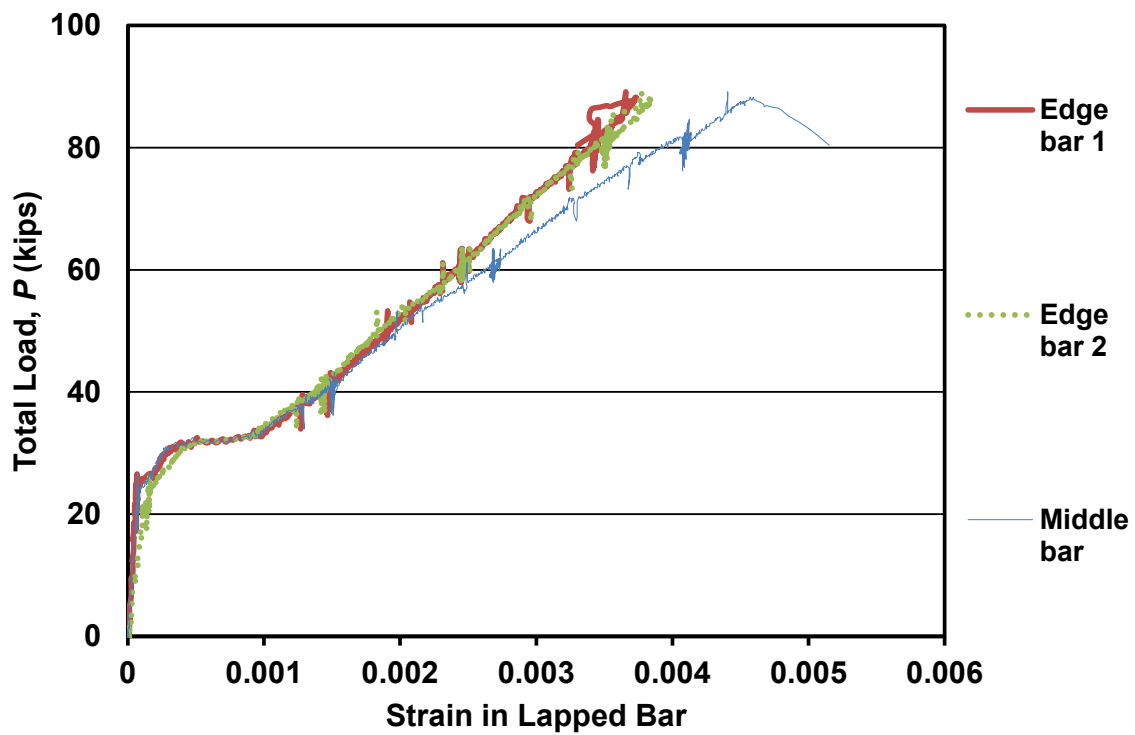


Figure B.17 Strain in lapped bars in specimen (3) 6-12-S4.0-12-0.5 as a function of applied load

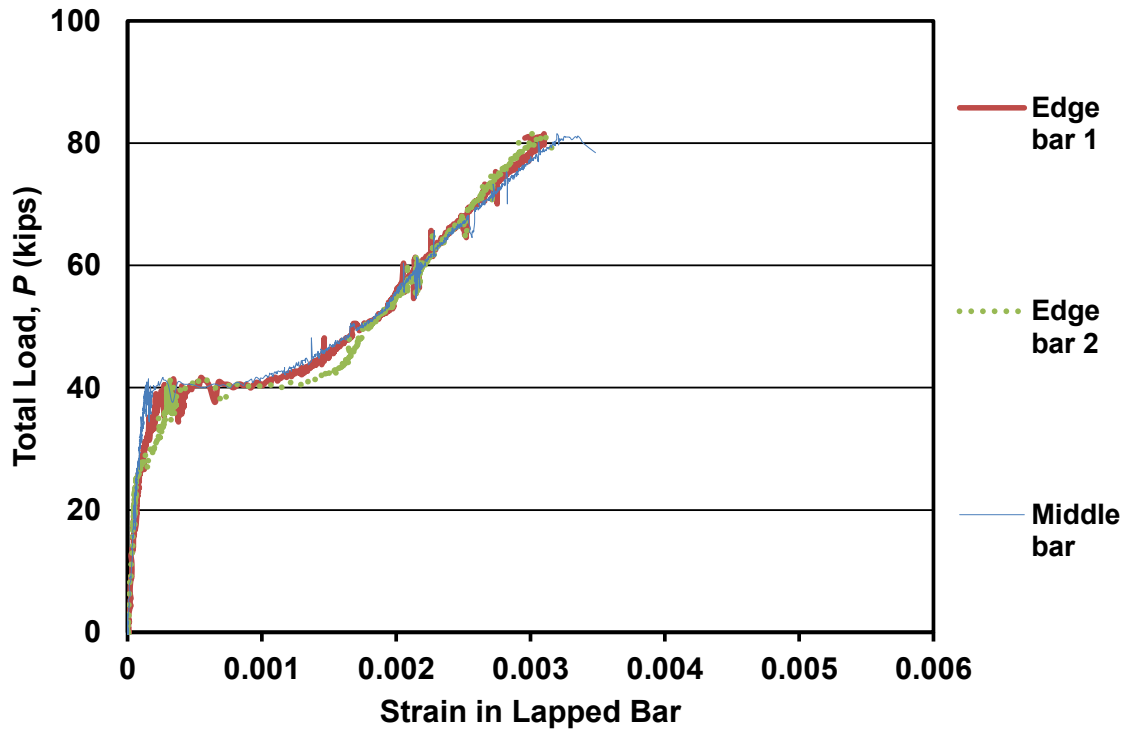


Figure B.18 Strain in lapped bars in specimen (3) 6-12-S4.0-12-1.0 as a function of applied load

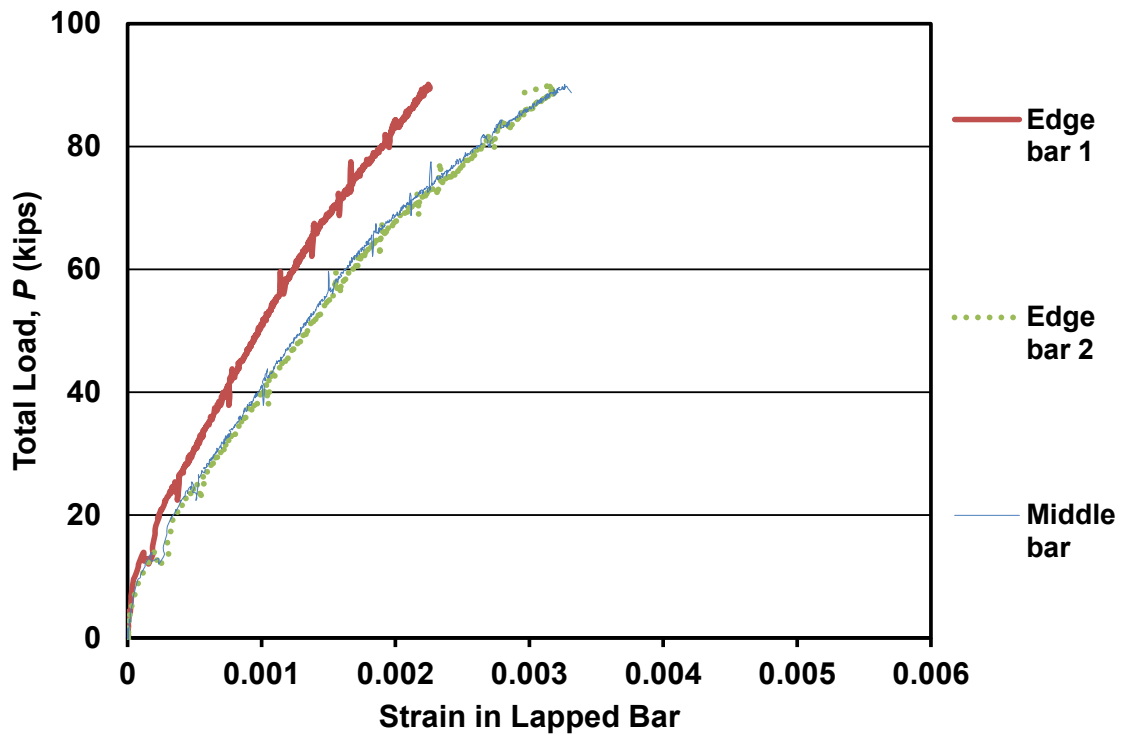


Figure B.19 Strain in lapped bars in specimen (3) 6-12-S4.0-12-1.9 as a function of applied load (strains were measured when the specimen was reloaded after loading to 65 kips)

**APPENDIX C: TEST RESULTS AND SPECIMENS FROM OTHER STUDIES
INCLUDED IN THE CURRENT STUDY**

C.1 SLAB AND COLUMN-LIKE SPECIMENS

Table C.1 Data for specimens tested by Devries et al. (1999), Choi et al. (2002), and Choi (2006)[§]

Study	Specimen	Bar size ^{§§}	A_b (in. ²)	A_{brg}/A_b	A_{hs} (in. ²)	A_{Nc} (in. ²)	$A_{tr,t}$ (in. ²)	$A_{tro,t}$ (in. ²)	A_{tt} (in. ²)	A_{st}/nA_b	A_{tt}/A_{hs}	c_{ch}^{\square}/d_b	c_{so}/d_b	d_b^{\ddagger} (in.)	
1	2	3	4	5	6	7	8	9	10	11	12	13	14	15	
	S16-7db.1	D16	0.31	3.2	0.31	175	0	0	0	0	0	114.4	56.7	0.625	
	SI6-7db.2	D16	0.31	3.2	0.31	175	0	0	0	0	0	113.4	56.2	0.625	
	S25-7db.1	D25	0.79	3.0	0.79	427	0	0	0	0	0	71.1	35.1	1	
	S25-7db.2	D25	0.79	3.0	0.79	427	0	0	0	0	0	70.9	34.9	1	
	E16-7db.1	D16	0.31	3.2	0.31	112	0	0	0	0	0	6.0	2.5	0.625	
	EI6-7db.2	D16	0.31	3.2	0.31	112	0	0	0	0	0	6.0	2.5	0.625	
	E19-7db.1	D19	0.44	2.6	0.44	165	0	0	0	0	0	7.0	3.0	0.75	
	EI9-7db.2	D19	0.44	2.6	0.44	165	0	0	0	0	0	7.0	3.0	0.75	
	E19-7db.3	D19	0.44	2.6	0.44	206	0	0	0	0	0	14.0	6.5	0.75	
	E19-7db.4	D19	0.44	2.6	0.44	206	0	0	0	0	0	14.0	6.5	0.75	
	E25-7db.1	D25	0.79	3.0	0.79	275	0	0	0	0	0	5.9	2.5	1	
	E25-7db.2	D25	0.79	3.0	0.79	275	0	0	0	0	0	5.9	2.5	1	
	Choi et al. (2002)	C16-6db-1C	D16	0.31	3.2	0.31	65	0.11	0.11	0.22	2.0	0.71	15.1	4.1	0.625
		C16-6db-1D	D16	0.31	3.2	0.31	65	0.11	0.11	0.22	2.0	0.71	15.1	4.1	0.625
		C16-6db-2A	D16	0.31	3.2	0.62	85	0.11	0.11	0.44	1.0	0.71	6.0	2.5	0.625
		C16-6db-2B	D16	0.31	3.2	0.62	85	0.11	0.11	0.44	1.0	0.71	6.0	2.5	0.625
		C16-6db-2C	D16	0.31	3.2	0.62	85	0.11	0.11	0.22	1.0	0.35	6.0	2.5	0.625
		C16-6db-2D	D16	0.31	3.2	0.62	85	0.11	0.11	0.22	1.0	0.35	6.0	2.5	0.625
		C16-6db-3A	D16	0.31	3.2	0.93	85	0.11	0.11	0.44	0.7	0.47	3.0	2.5	0.625
C16-6db-3B		D16	0.31	3.2	0.93	85	0.11	0.11	0.44	0.7	0.47	3.0	2.5	0.625	
C16-6db-3C		D16	0.31	3.2	0.93	85	0.11	0.11	0.22	0.7	0.24	3.0	2.5	0.625	
C16-6db-3D		D16	0.31	3.2	0.93	85	0.11	0.11	0.22	0.7	0.24	3.0	2.5	0.625	
C22-6db-1A		D22	0.60	2.7	0.60	107	0.20	0.20	0.80	1.5	1.33	10.8	3.4	0.875	
C22-6db-1B		D22	0.60	2.7	0.60	107	0.20	0.20	0.80	1.5	1.33	10.8	3.4	0.875	
C22-6db-1C		D22	0.60	2.7	0.60	107	0.20	0.20	0.40	1.5	0.67	10.8	3.4	0.875	
C22-6db-3A		D22	0.60	2.7	1.80	147	0.20	0.20	0.80	0.5	0.44	3.0	1.9	0.875	
C22-6db-3B	D22	0.60	2.7	1.80	147	0.20	0.20	0.80	0.5	0.44	3.0	1.9	0.875		
C22-6db-4A	D22	0.60	2.7	2.40	307	0.20	0.20	0.80	0.6	0.33	5.9	1.8	0.875		
C22-6db-4B	D22	0.60	2.7	2.40	307	0.20	0.20	0.80	0.6	0.33	5.9	1.8	0.875		

[§] Columns arranged in alphabetical order of notation; notation described in Appendix A

^{§§} Bar sizes are presented in SI as reported in the original studies

[□] c_{ch} is taken as twice of the minimum concrete cover to the center of the bar [that is, $c_{ch} = 2 \times (c_{so} + d_b/2)$]

[‡] Values are converted from the SI unit (1 in. = 25.4 mm; 1 psi = 1/145 MPa; and 1 kip = 4.4484 kN)

Table C.1 Contd. Data for specimens tested by Devries et al. (1999), Choi et al. (2002), and Choi (2006)[§]

Study	Specimen	f_{cm}^{\ddagger}	f_{su}	f_y^{\ddagger}	f_{su}/f_y	f_{yt}^{\ddagger}	f_{yto}^{\ddagger}	ℓ_{eh}^{\ddagger}	N	N_{ar}	N_{cb}	N_{sb}	N_{tr}	N_{tro}
		(ksi)	(ksi)	(ksi)		(ksi)	(ksi)	(in.)		(kips)	(kips)	(kips)		
1	2	16	17	18	19	20	21	22	23	24	25	26	27	28
Choi et al. (2002)	S16-7db.1	5270	52.9	60.9	0.87	60.9	60.9	4.4	0	0.0	20.2	-	0	0
	S16-7db.2	5270	58.0	60.9	0.95	60.9	60.9	4.4	0	0.0	20.2	-	0	0
	S25-7db.1	5270	45.5	60.9	0.75	60.9	60.9	6.9	0	0.0	39.4	-	0	0
	S25-7db.2	5270	43.0	60.9	0.71	60.9	60.9	6.9	0	0.0	39.4	-	0	0
	E16-7db.1	5270	34.1	60.9	0.56	60.9	60.9	4.4	0	0.0	10.2	-	0	0
	E16-7db.2	5270	34.1	60.9	0.56	60.9	60.9	4.4	0	0.0	10.2	-	0	0
	E19-7db.1	3930	26.6	52.2	0.51	60.9	60.9	5.2	0	0.0	12.1	-	0	0
	E19-7db.2	3930	24.5	52.2	0.47	60.9	60.9	5.2	0	0.0	12.1	-	0	0
	E19-7db.3	3930	39.9	52.2	0.76	60.9	60.9	5.2	0	0.0	16.9	-	0	0
	E19-7db.4	3930	38.3	52.2	0.73	60.9	60.9	5.2	0	0.0	16.9	-	0	0
	E25-7db.1	5270	24.8	60.9	0.41	60.9	60.9	6.9	0	0.0	19.9	-	0	0
	E25-7db.2	5270	26.2	60.9	0.43	60.9	60.9	6.9	0	0.0	19.9	-	0	0
	C16-6db-1C	5670	58.0	60.9	0.95	60.9	60.9	3.8	2	26.8	7.1	-	2	2
	C16-6db-1D	5670	56.6	60.9	0.93	60.9	60.9	3.8	2	26.8	7.1	-	2	2
	C16-6db-2A	5670	59.5	60.9	0.98	60.9	60.9	3.8	4	26.8	4.4	-	4	4
	C16-6db-2B	5670	53.7	60.9	0.88	60.9	60.9	3.8	4	26.8	4.4	-	4	4
	C16-6db-2C	5670	45.7	60.9	0.75	60.9	60.9	3.8	2	13.4	4.4	-	2	2
	C16-6db-2D	5670	30.5	60.9	0.50	60.9	60.9	3.8	2	13.4	4.4	-	2	2
	C16-6db-3A	5670	39.6	60.9	0.65	60.9	60.9	3.8	4	17.9	2.9	-	4	4
	C16-6db-3B	5670	44.5	60.9	0.73	60.9	60.9	3.8	4	17.9	2.9	-	4	4
	C16-6db-3C	5670	32.9	60.9	0.54	60.9	60.9	3.8	2	8.9	2.9	-	2	2
	C16-6db-3D	5670	21.3	60.9	0.35	60.9	60.9	3.8	2	8.9	2.9	-	2	2
	C22-6db-1A	5670	59.9	60.9	0.98	60.9	60.9	5.2	4	97.4	9.8	-	4	4
	C22-6db-1B	5670	58.1	60.9	0.95	60.9	60.9	5.2	4	97.4	9.8	-	4	4
	C22-6db-1C	5670	54.0	60.9	0.89	60.9	60.9	5.2	2	48.7	9.8	-	2	2
	C22-6db-3A	5670	41.2	60.9	0.68	60.9	60.9	5.2	4	32.5	4.2	-	4	4
	C22-6db-3B	5670	28.7	60.9	0.47	60.9	60.9	5.2	4	32.5	4.2	-	4	4
	C22-6db-4A	5670	37.0	60.9	0.61	60.9	60.9	5.2	4	24.4	6.6	31.6	4	4
C22-6db-4B	5670	40.3	60.9	0.66	60.9	60.9	5.2	4	24.4	6.6	31.6	4	4	

[§] Columns arranged in alphabetical order of notation; notation described in Appendix A

[‡] Values are converted from the SI unit (1 in. = 25.4 mm; 1 psi = 1/145 MPa; and 1 kip = 4.4484 kN)

Table C.1 Contd. Data for specimens tested by Devries et al. (1999), Choi et al. (2002), and Choi (2006)[§]

Study	Specimen	<i>n</i>	<i>S'_{tr}</i> [‡] (in.)	<i>S_{tr}</i> [‡] (in.)	<i>S'_{tro}</i> [‡] (in.)	<i>S_{tro}</i> [‡] (in.)	<i>T</i> [‡] (kips)	<i>T_{unc}</i> (kips)	<i>T_h</i> (kips)	<i>T</i> / <i>T_h</i>	<i>T</i> / <i>T_{unc}</i>	ψ_o	Remarks
1	2	29	30	31	32	33	34	35	36	37	38	39	40
Choi et al. (2002)	S16-7db.1	1	-	-	-	-	16.4	20.2	23.9	0.69	0.81	1.0	Center bars in slab specimens
	S16-7db.2	1	-	-	-	-	18.0	20.2	23.9	0.75	0.89	1.0	
	S25-7db.1	1	-	-	-	-	36.0	39.4	44.6	0.81	0.91	1.0	
	S25-7db.2	1	-	-	-	-	33.9	39.4	44.6	0.76	0.86	1.0	
	E16-7db.1	1	-	-	-	-	10.6	10.2	16.2	0.65	1.04	1.25	Edge bars in slab specimens
	E16-7db.2	1	-	-	-	-	10.6	10.2	16.2	0.65	1.04	1.25	
	E19-7db.1	1	-	-	-	-	11.7	12.1	21.1	0.55	0.97	1.25	
	E19-7db.2	1	-	-	-	-	10.8	12.1	21.1	0.51	0.90	1.25	
	E19-7db.3	1	-	-	-	-	17.5	16.9	22.7	0.77	1.04	1.25	
	E19-7db.4	1	-	-	-	-	16.9	16.9	22.7	0.74	1.00	1.25	
	E25-7db.1	1	-	-	-	-	19.6	19.9	29.9	0.65	0.98	1.25	
	E25-7db.2	1	-	-	-	-	20.7	19.9	29.9	0.69	1.04	1.25	
	C16-6db-1C	1	1.9	3.8	1.9	3.8	18.0	26.8	23.7	0.76	0.67	1.0	Column-like specimens
	C16-6db-1D	1	2.8	5.7	2.8	5.7	17.5	26.8	23.7	0.74	0.65	1.0	
	C16-6db-2A	2	0.9	1.9	0.9	1.9	18.4	26.8	17.5	1.06	0.69	1.25	
	C16-6db-2B	2	1.4	2.8	1.4	2.8	16.6	26.8	17.5	0.95	0.62	1.25	
	C16-6db-2C	2	1.9	3.8	1.9	3.8	14.2	13.4	17.5	0.81	1.06	1.25	
	C16-6db-2D	2	2.8	5.7	2.8	5.7	9.4	13.4	17.5	0.54	0.70	1.25	
	C16-6db-3A	3	0.9	1.9	0.9	1.9	12.3	17.9	13.9	0.89	0.69	1.25	
	C16-6db-3B	3	1.4	2.8	1.4	2.8	13.8	17.9	13.9	0.99	0.77	1.25	
C16-6db-3C	3	1.9	3.8	1.9	3.8	10.2	8.9	13.5	0.75	1.14	1.25		
C16-6db-3D	3	2.8	5.7	2.8	5.7	6.6	8.9	13.5	0.49	0.74	1.25		
C22-6db-1A	1	1.3	2.6	1.3	2.6	36.0	97.4	40.2	0.89	0.37	1.0		
C22-6db-1B	1	1.9	3.9	1.9	3.9	34.8	97.4	40.2	0.87	0.36	1.0		
C22-6db-1C	1	2.6	5.2	2.6	5.2	32.4	48.7	40.2	0.81	0.66	1.0		
C22-6db-3A	3	1.3	2.6	1.3	2.6	24.7	32.5	23.4	1.06	0.76	1.25		
C22-6db-3B	3	1.9	3.9	1.9	3.9	17.2	32.5	23.4	0.74	0.53	1.25		
C22-6db-4A	4	1.3	2.6	1.3	2.6	22.2	24.4	29.3	0.76	0.91	1.25		
C22-6db-4B	4	1.9	3.9	1.9	3.9	24.2	24.4	29.3	0.82	0.99	1.25		

[§] Columns arranged in alphabetical order of notation; notation described in Appendix A

[‡] Values are converted from the SI unit (1 in. = 25.4 mm; 1 psi = 1/145 MPa; and 1 kip = 4.4484 kN)

Table C.1 Contd. Data for specimens tested by Devries et al. (1999), Choi et al. (2002), and Choi (2006)[§]

Study	Specimen	Bar size ^{§§}	A_b (in. ²)	A_{brg}/A_b	A_{hs} (in. ²)	A_{Nc} (in. ²)	$A_{tr,t}$ (in. ²)	$A_{tro,t}$ (in. ²)	A_{tt} (in. ²)	A_{st}/nA_b	A_{tr}/A_{hs}	c_{so}/d_b	c_{ch}^{\square}/d_b	d_b^{\ddagger} (in.)
1	2	3	4	5	6	7	8	9	10	11	12	13	14	15
Choi (2006)	C29-10db-2A-L	D29	1.00	3.0	2.00	607	0.20	0.20	0.80	0.8	0.40	4.3	6.0	1.128
	C29-10db-2C-L	D29	1.00	3.0	2.00	607	0.20	0.20	0.80	0.8	0.40	4.3	6.0	1.128
	C29-10db-2D-L	D29	1.00	3.0	2.00	607	0.20	0.20	0.40	0.8	0.20	4.3	6.0	1.128
	C29-10db-2E-L	D29	1.00	3.0	2.00	607	0	0	0	0.8	0	4.3	6.0	1.128
	C29-10db-2A-M	D29	1.00	3.0	2.00	607	0.20	0.20	0.80	1.6	0.40	4.3	6.0	1.128
	C29-10db-2C-M	D29	1.00	3.0	2.00	607	0.20	0.20	0.80	1.6	0.40	4.3	6.0	1.128
	C29-10db-2D-M	D29	1.00	3.0	2.00	607	0.20	0.20	0.40	1.6	0.20	4.3	6.0	1.128
	C29-10db-2E-M	D29	1.00	3.0	2.00	607	0	0	0	1.6	0	4.3	6.0	1.128
	C22-15db-3E-L	D22	0.60	3.0	1.80	614	0	0	0	0.7	0	4.0	4.5	0.875
C25-13db-2E-L	D25	0.79	3.0	1.58	614	0	0	0	0.8	0	3.5	8.0	1	
DeVries et al. (1999)	T2B2	D20	0.49	6.9	0.49	420	0	0	0	0.0	0	2.0	5.1	0.79
	T2B4	D20	0.49	6.9	0.49	420	0	0	0	0.4	0	2.0	5.1	0.79
	T2B6	D20	0.49	6.9	0.49	241	0	0	0	0.0	0	2.0	5.1	0.79
	T2B8	D20	0.49	6.9	0.49	241	0	0	0	0.4	0	2.0	5.1	0.79

Table C.1 Contd. Data for specimens tested by Devries et al. (1999), Choi et al. (2002), and Choi (2006)[§]

Study	Specimen	f_{cm}^{\ddagger} (ksi)	f_{su} (ksi)	f_y^{\ddagger} (ksi)	f_{su}/f_y	f_{yt}^{\ddagger} (ksi)	f_{yto}^{\ddagger} (ksi)	ℓ_{ch}^{\ddagger} (in.)	N	N_{ar} (kips)	N_{cb} (kips)	N_{sb} (kips)	N_{tr}	N_{tro}
1	2	16	17	18	19	20	21	22	23	24	25	26	27	28
Choi (2006)	C29-10db-2A-L	4450	51.4	60.9	0.84	60.9	60.9	11.4	4	48.7	15.9	-	4	4
	C29-10db-2C-L	4450	49.6	60.9	0.81	60.9	60.9	11.4	4	48.7	15.9	-	4	4
	C29-10db-2D-L	4450	40.8	60.9	0.67	60.9	60.9	11.4	2	24.4	15.9	-	2	2
	C29-10db-2E-L	4450	39.1	60.9	0.64	60.9	60.9	11.4	0	0.0	15.9	-	0	0
	C29-10db-2A-M	4450	53.2	60.9	0.87	60.9	60.9	11.4	4	48.7	15.9	-	4	4
	C29-10db-2C-M	4450	53.7	60.9	0.88	60.9	60.9	11.4	4	48.7	15.9	-	4	4
	C29-10db-2D-M	4450	53.4	60.9	0.88	60.9	60.9	11.4	2	24.4	15.9	-	2	2
	C29-10db-2E-M	4450	49.7	60.9	0.82	60.9	60.9	11.4	0	0.0	15.9	-	0	0
	C22-15db-3E-L	4700	57.7	60.9	0.95	60.9	60.9	13.0	0	0.0	9.9	57.9	0	0
C25-13db-2E-L	4700	58.0	60.9	0.95	60.9	60.9	13.0	0	0.0	14.8	67.5	0	0	
DeVries et al. (1999)	T2B2	4790	67.9	80.3	0.84	60.9	60.9	9.0	0	0.0	24.0	40.9	0	0
	T2B4	4790	78.9	80.3	0.98	60.9	60.9	9.0	0	0.0	24.0	40.9	0	0
	T2B6	4790	56.0	80.3	0.70	60.9	60.9	9.0	0	0.0	13.8	40.9	0	0
	T2B8	4790	57.3	80.3	0.71	60.9	60.9	9.0	0	0.0	13.8	40.9	0	0

[§] Columns arranged in alphabetical order of notation; notation described in Appendix A

^{§§} Bar sizes are presented in SI as reported in the original studies

[□] c_{ch} is taken as twice of the minimum concrete cover to the center of the bar [that is, $c_{ch} = 2 \times (c_{so} + d_b/2)$]

[‡] Values are converted from the SI unit (1 in. = 25.4 mm; 1 psi = 1/145 MPa; and 1 kip = 4.4484 kN)

Table C.1 Contd. Data for specimens tested by Devries et al. (1999), Choi et al. (2002), and Choi (2006)[§]

Study	Specimen	<i>n</i>	<i>S'_{tr}</i> [‡] (in.)	<i>S_{tr}</i> [‡] (in.)	<i>S'_{tro}</i> [‡] (in.)	<i>S_{tro}</i> [‡] (in.)	<i>T</i> [‡] (kips)	<i>T_{anc}</i> (kips)	<i>T_h</i> (kips)	<i>T/ T_h</i>	<i>T/ T_{anc}</i>	ψ_o	Remarks
1	2	29		30	31	32	33	34	35	36	37	38	39
Choi (2006)	C29-10db-2A-L	2	1.7	3.4	1.7	3.4	51.4	48.7	83.7	0.61	1.05	1.0	Column- like specimens
	C29-10db-2C-L	2	3.4	6.8	3.4	6.8	49.6	48.7	83.7	0.59	1.02	1.0	
	C29-10db-2D-L	2	5.1	10.2	5.1	10.2	40.8	24.4	78.8	0.52	1.67	1.0	
	C29-10db-2E-L	2	-	-	-	-	39.1	15.9	63.5	0.62	2.47	1.0	
	C29-10db-2A-M	2	1.7	3.4	1.7	3.4	53.2	48.7	83.7	0.63	1.09	1.0	
	C29-10db-2C-M	2	3.4	6.8	3.4	6.8	53.7	48.7	83.7	0.64	1.10	1.0	
	C29-10db-2D-M	2	5.1	10.2	5.1	10.2	53.4	24.4	78.8	0.68	2.19	1.0	
	C29-10db-2E-M	2	-	-	-	-	49.7	15.9	63.5	0.78	3.13	1.0	
	C22-15db-3E-L	3	-	-	-	-	34.6	9.9	57.3	0.60	3.51	1.0	
	C25-13db-2E-L	2	-	-	-	-	45.9	14.8	83.4	0.55	3.09	1.0	
DeVries et al. (1999)	T2B2	1	-	-	-	-	33.3	24.0	32.6	1.02	1.38	1.25	Edge bars in slab specimens
	T2B4	1	-	-	-	-	38.7	24.0	32.6	1.19	1.61	1.25	
	T2B6	1	-	-	-	-	27.4	13.8	32.6	0.84	1.99	1.25	Corner bars in slab specimens
	T2B8	1	-	-	-	-	28.1	13.8	32.6	0.86	2.04	1.25	

[§] Columns arranged in alphabetical order of notation; notation described in Appendix A

[‡] Values are converted from the SI unit (1 in. = 25.4 mm; 1 psi = 1/145 MPa; and 1 kip = 4.4484 kN)

C.2 EXTERIOR AND ROOF-LEVEL INTERIOR BEAM-COLUMN JOINT SPECIMENS

Table C.2 Data for beam-column joint specimens (exterior and roof-level interior joints) tested under reversed cyclic loading *

Study	Specimen	Bar Size **	A_b (in. ²)	A_{brg}/A_b	A_{gross}/A_b	A_{hs} (in. ²)	A_{Nc} (in. ²)	A_{obs}/A_b	A_{tr} (in. ²)	$A_{tr,l}$ (in. ²)	$A_{tro,l}$ (in. ²)	A_{tt} (in. ²)	A_{tt}/A_{hs}	
1	2	3	4	5	6	7	8	9	10	11	12	13	14	
1	Bashandy (1996)	Exterior Joint	D25	0.79	8.6	9.6	1.58	412	-	0.60	0.20	0.20	1.20	0.76
2	Murakami et al. (1998)	No. 100	D16	0.31	1.7	2.7	1.24	314	-	0.44	0.05	0.05	0.20	0.16
		No. 101	D16	0.31	6.3	7.3	1.24	314	-	0.44	0.05	0.05	0.20	0.16
		B8-M	D19	0.44	6.0	7.0	1.32	314	-	0.44	0.05	0.05	0.20	0.15
		B7-M	D19	0.44	6.0	7.0	1.32	314	-	0.44	0.05	0.05	0.20	0.15
		No. 102 ‡	D19	0.44	2.1	3.1	1.76	314	-	0.44	0.05	0.05	0.20	0.11
		No. 103 ‡	D19	0.44	5.8	6.8	1.76	314	-	0.44	0.05	0.05	0.20	0.11
		No. 104 ‡	D19	0.44	3.4	4.4	1.76	314	-	0.44	0.05	0.05	0.20	0.11
		M8D16 ‡	D16	0.31	4.4	7.0	2.48	337	2.6	0.44	0.05	0.05	0.10	0.04
		M4D19 ‡	D19	0.44	3.9	7.0	1.76	314	3.1	0.44	0.05	0.05	0.20	0.11
		M3D19 ‡	D19	0.44	3.9	7.0	1.32	314	3.1	0.44	0.05	0.05	0.20	0.15
M2D22 ‡	D22	0.60	3.6	7.0	1.20	314	3.4	0.44	0.05	0.05	0.29	0.25		
3	Wallace et al. (1998)	BCEJ1 ††	No. 8	0.79	4.0	5.0	3.16	751	-	1.00	0.20	0.20	1.20	0.38
4	Matsushima et al. (2000)	H	D25	0.79	-	-	2.37	549	-	0.60	0.11	0.11	0.44	0.19
		HS §	D25	0.79	-	-	2.37	372	-	0.60	0.11	0.11	0.44	0.19
5	Nakazawa et al. (2000)	J1	D19	0.44	3.9	6.9	2.64	515	3.0	0.44	0.05	0.05	0.37	0.14
		J2	D19	0.44	5.9	6.9	2.64	515	-	0.44	0.05	0.05	0.37	0.14
6	Tasai et al. (2000)	No. 6	D25	0.79	5.4	9.0	3.16	558	3.6	1.58	0.11	0.11	0.44	0.14
		No. 7	D25	0.79	5.4	9.0	1.58	558	3.6	1.58	0.11	0.11	0.44	0.28
7	Yoshida et al. (2000)	No. 1	D19	0.44	5.8	6.8	1.76	361	-	0.44	0.11	0.11	0.44	0.25
		No. 2	D19	0.44	4.1	5.1	1.76	361	-	0.44	0.11	0.11	0.44	0.25
		No. 3	D19	0.44	3.1	4.1	1.76	361	-	0.44	0.11	0.11	0.44	0.25
8	Takeuchi et al. (2001)	0-1	D25	0.79	5.8	6.8	2.37	491	-	0.60	0.11	0.11	0.44	0.19
		0-2	D25	0.79	5.8	6.8	2.37	491	-	0.60	0.11	0.11	0.44	0.19
		0-3	D25	0.79	5.8	6.8	2.37	491	-	0.60	0.11	0.11	0.44	0.19
		0-4	D25	0.79	5.8	6.8	2.37	551	-	0.60	0.11	0.11	0.44	0.19
		0-6	D25	0.79	5.8	6.8	3.16	491	-	0.60	0.11	0.11	0.44	0.14
		0-7	D25	0.79	5.8	6.8	3.16	491	-	0.60	0.11	0.11	0.44	0.14
9	Ishibashi et al. (2003) §§	T345-30-4S	D19	0.44	3.2	6.4	1.32	545	3.2	0.75	0.11	0.11	0.44	0.34
		T345-30-3N	D19	0.44	3.2	6.4	1.32	545	3.2	0.75	0.11	0.11	0.44	0.34
		T490-45-4S	D19	0.44	3.2	6.4	1.32	545	3.2	0.75	0.11	0.11	0.44	0.34
		T490-45-3N	D19	0.44	3.2	6.4	1.32	545	3.2	0.75	0.11	0.11	0.44	0.34

* Columns arranged in alphabetical order of notation; notation described in Appendix A; values given in SI are converted to in.-lb (1 in. = 25.4 mm; 1 psi = 1/145 MPa; and 1 kip = 4.4484 kN)

** Bar sizes are presented in SI as reported in the original studies (only Wallace et al. 1998 had bar sizes reported in in.-lb)

‡ Analyzed as doubly-reinforced section to calculate M_n ; all other specimens are analyzed as singly-reinforced

†† Specimens contained transverse beams on one or both sides of the test beam. These transverse beams, however, did not meet the dimensional requirements of Section 18.8.4.2 of ACI 318-14 and Section 4.3 of ACI 352R-02 to be considered effective in increasing the joint shear strength.

§ Specimen had $d/\ell_{eh} > 1.5$

§§ Roof-level interior joints; all other specimens are exterior joints

Table C.2 Cont. Data for beam-column joint specimens (exterior and roof-level interior joints) tested under reversed cyclic loading *

Study	Specimen	A_v	b_b	b_c	b_j	$b_{j,ACI352}$	c_{ch}	c_{ch}/d_b	c_o	c_o/d_b	c_{so}	c_{so}/d_b	d	d/ℓ_{eh}	
		(in. ²)	(in.)	(in.)	(in.)	(in.)	(in.)		(in.)		(in.)		(in.)		
	1	2	15	16	17	18	19	20	21	22	23	24	25	26	27
1	Bashandy (1996)	Exterior Joint	2.00	10.0	12	12.0	11.0	5.0	5.1	2.4	2.5	3.5	3.6	15.5	1.4
2	Murakami et al. (1998)	No. 100	0.39	10.2	12	11.8	11.0	2.2	3.5	2.1	3.4	2.3	3.8	13.6	1.5
		No. 101	0.39	10.2	12	11.8	11.0	2.2	3.5	1.8	2.9	2.3	3.8	13.6	1.5
		B8-M	0.39	10.2	12	11.8	11.0	3.2	4.3	1.7	2.2	2.3	3.0	13.6	1.5
		B7-M	0.39	10.2	12	11.8	11.0	3.2	4.3	1.7	2.2	2.3	3.0	13.6	1.5
		No. 102 †	0.39	10.2	12	11.8	11.0	2.2	2.9	2.0	2.7	2.3	3.0	13.6	1.5
		No. 103 †	0.39	10.2	12	11.8	11.0	2.2	2.9	1.7	2.2	2.3	3.0	13.6	1.5
		No. 104 †	0.39	10.2	12	11.8	11.0	2.2	2.9	1.9	2.5	2.3	3.0	13.6	1.5
		M8D16 †	0.39	10.2	12	11.8	11.0	2.0	3.2	1.8	2.9	2.3	3.8	13.0	1.5
		M4D19 †	0.39	10.2	12	11.8	11.0	2.2	2.9	1.7	2.2	2.3	3.0	13.6	1.5
		M3D19 †	0.39	10.2	12	11.8	11.0	3.2	4.3	1.7	2.2	2.3	3.0	13.6	1.5
M2D22 †	0.39	10.2	12	11.8	11.0	6.5	7.4	1.5	1.7	2.2	2.5	13.6	1.5		
3	Wallace et al. (1998)	BCEJ1 ††	2.40	18.0	18	18.0	18.0	3.5	3.5	-	-	-	-	21.5	1.5
4	Matsushima et al. (2000)	H	0.66	13.8	16	15.7	14.8	5.0	5.1	-	-	2.3	2.3	15.1	1.3
		HS §	0.66	13.8	16	15.7	14.8	5.0	5.1	-	-	2.3	2.3	15.1	1.9
5	Nakazawa et al. (2000)	J1	0.56	11.0	14	14.2	12.6	2.6	3.4	2.1	2.8	2.7	3.6	11.8	1.1
		J2	0.56	11.0	14	14.2	12.6	2.6	3.4	2.1	2.8	2.7	3.6	11.8	1.1
6	Tasai et. al (2000)	No. 6	0.66	13.8	16	15.7	14.8	3.1	3.1	1.4	1.4	2.4	2.4	15.2	1.3
		No. 7	0.66	13.8	16	15.7	14.8	4.7	4.7	1.4	1.4	2.4	2.4	15.2	1.3
7	Yoshida et al. (2000)	No. 1	1.11	11.8	12	11.8	11.8	2.8	3.7	1.8	2.4	2.4	3.2	14.0	1.4
		No. 2	1.11	11.8	12	11.8	11.8	2.8	3.7	1.9	2.5	2.4	3.2	14.0	1.4
		No. 3	1.11	11.8	12	11.8	11.8	2.8	3.7	2.0	2.7	2.4	3.2	14.0	1.4
8	Takeuchi et al. (2001)	0-1	0.66	13.8	16	15.7	14.8	4.8	4.9	1.7	1.7	2.5	2.6	15.6	1.5
		0-2	0.66	13.8	16	15.7	14.8	4.8	4.9	1.7	1.7	2.5	2.6	15.6	1.5
		0-3	0.66	13.8	16	15.7	14.8	4.8	4.9	1.7	1.7	2.5	2.6	15.6	1.5
		0-4	0.66	13.8	16	15.7	14.8	4.8	4.9	1.7	1.7	2.5	2.6	15.6	1.3
		0-6	0.66	13.8	16	15.7	14.8	3.2	3.3	1.7	1.7	2.5	2.6	15.6	1.5
		0-7	0.66	13.8	16	15.7	14.8	3.2	3.3	1.7	1.7	2.5	2.6	15.6	1.5
9	Ishibashi et. al (2003) §§	T345-30-4S	0.66	15.7	12	11.8	11.8	5.6	7.5	1.3	1.7	1.9	2.5	13.5	1.0
		T345-30-3N	0.66	15.7	12	11.8	11.8	5.6	7.5	1.3	1.7	1.9	2.5	13.5	1.0
		T490-45-4S	0.66	15.7	12	11.8	11.8	5.6	7.5	1.3	1.7	1.9	2.5	13.5	1.0
		T490-45-3N	0.66	15.7	12	11.8	11.8	5.6	7.5	1.3	1.7	1.9	2.5	13.5	1.0

* Columns arranged in alphabetical order of notation; notation described in Appendix A; values given in SI are converted to in.-lb (1 in. = 25.4 mm; 1 psi = 1/145 MPa; and 1 kip = 4.4484 kN)

† Analyzed as doubly-reinforced section to calculate M_n ; all other specimens are analyzed as singly-reinforced

†† Specimens contained transverse beams on one or both sides of the test beam. These transverse beams, however, did not meet the dimensional requirements of Section 18.8.4.2 of ACI 318-14 and Section 4.3 of ACI 352R-02 to be considered effective in increasing the joint shear strength.

§ Specimen had $d/\ell_{eh} > 1.5$

§§ Roof-level interior joints; all other specimens are exterior joints

Table C.2 Cont. Data for beam-column joint specimens (exterior and roof-level interior joints) tested under reversed cyclic loading *

Study	Specimen	d'	d_b	$d_{b,sprt}$	f_{cm}	f_y	$f_{y,sprt}$	f_{yt}	$f_{yt}A_v$	f_{yto}	h_b	h_c	
		(in.)	(in.)	(in.)	(psi)	(ksi)	(ksi)	(ksi)	(kips)	(ksi)	(in.)	(in.)	
1	2	28	29	30	31	32	33	34	35	36	37	38	
1	Bashandy (1996)	Exterior Joint	2.5	0.98	0.875	4290	64.8	65.3	45.1	90.2	45.1	18.0	15.0
2	Murakami et al. (1998)	No. 100	2.2	0.625	-	5700	53.7	-	113.8	44.7	113.8	15.7	11.8
		No. 101	2.2	0.625	-	5700	53.7	-	113.8	44.7	113.8	15.7	11.8
		B8-M	2.2	0.75	-	4280	74.1	-	113.8	44.7	113.8	15.7	11.8
		B7-M	2.2	0.75	-	4280	74.1	-	113.8	44.7	113.8	15.7	11.8
		No. 102 ‡	2.2	0.75	-	5700	137.1	-	113.8	44.7	113.8	15.7	11.8
		No. 103 ‡	2.2	0.75	-	5700	137.1	-	113.8	44.7	113.8	15.7	11.8
		No. 104 ‡	2.2	0.75	-	5700	137.1	-	113.8	44.7	113.8	15.7	11.8
		M8D16 ‡	2.8	0.625	-	4100	145.1	-	113.8	44.7	113.8	15.7	11.8
		M4D19 ‡	2.2	0.75	-	4100	145.1	-	113.8	44.7	113.8	15.7	11.8
		M3D19 ‡	2.2	0.75	-	4100	145.1	-	113.8	44.7	113.8	15.7	11.8
M2D22 ‡	2.2	0.875	-	4100	141.1	-	113.8	44.7	113.8	15.7	11.8		
3	Wallace et al. (1998)	BCEJ1 ‡‡	2.5	1	1.128	5190	67.0	67.0	67.0	160.8	67.0	24.0	18.0
4	Matsushima et al. (2000)	H	3.8	0.98	0.875	4770	79.9	75.5	57.6	38.2	126.4	18.9	15.7
		HS §	3.8	0.98	0.875	4770	79.9	75.5	57.6	38.2	126.4	18.9	15.7
5	Nakazawa et al. (2000)	J1	2.3	0.75	0.75	17400	103.0	99.5	184.9	103.8	184.9	14.2	14.2
		J2	2.3	0.75	0.75	17400	103.0	99.5	184.9	103.8	184.9	14.2	14.2
6	Tasai et al. (2000)	No. 6	2.5	1	0.875	7120	105.0	76.1	49.6	32.7	108.3	17.7	15.7
		No. 7	2.5	1	0.875	7120	105.0	76.1	49.6	32.7	108.3	17.7	15.7
7	Yoshida et al. (2000)	No. 1	1.8	0.75	0.75	5470	81.5	81.5	52.3	58.0	52.3	15.7	13.8
		No. 2	1.8	0.75	0.75	5470	81.5	81.5	52.3	58.0	52.3	15.7	13.8
		No. 3	1.8	0.75	0.75	4500	81.5	81.5	52.3	58.0	52.3	15.7	13.8
8	Takeuchi et al. (2001)	0-1	2.2	0.98	0.875	6400	64.5	80.2	141.4	93.3	141.4	17.7	15.7
		0-2	2.2	0.98	0.875	8830	85.0	80.2	141.4	93.3	141.4	17.7	15.7
		0-3	2.2	0.98	0.875	3520	54.7	80.2	141.4	93.3	141.4	17.7	15.7
		0-4	2.2	0.98	0.875	6400	64.5	80.2	141.4	93.3	141.4	17.7	15.7
		0-6	2.2	0.98	0.875	6440	104.1	80.2	141.4	93.3	141.4	17.7	15.7
		0-7	2.2	0.98	0.875	9000	104.1	80.2	141.4	93.3	141.4	17.7	15.7
9	Ishibashi et al. (2003) §§	T345-30-4S	2.2	0.75	0.75	4830	56.3	49.0	57.7	38.3	57.7	15.7	15.7
		T345-30-3N	2.2	0.75	0.75	4830	56.3	49.0	57.7	38.3	57.7	15.7	15.7
		T490-45-4S	2.2	0.75	0.75	7210	84.5	61.9	154.9	102.9	154.9	15.7	15.7
		T490-45-3N	2.2	0.75	0.75	7210	84.5	61.9	154.9	102.9	154.9	15.7	15.7

* Columns arranged in alphabetical order of notation; notation described in Appendix A; values given in SI are converted to in.-lb (1 in. = 25.4 mm; 1 psi = 1/145 MPa; and 1 kip = 4.4484 kN)

‡ Analyzed as doubly-reinforced section to calculate M_n ; all other specimens are analyzed as singly-reinforced

‡‡ Specimens contained transverse beams on one or both sides of the test beam. These transverse beams, however, did not meet the dimensional requirements of Section 18.8.4.2 of ACI 318-14 and Section 4.3 of ACI 352R-02 to be considered effective in increasing the joint shear strength.

§ Specimen had $d/\ell_{eh} > 1.5$

§§ Roof-level interior joints; all other specimens are exterior joints

Table C.2 Cont. Data for beam-column joint specimens (exterior and roof-level interior joints) tested under reversed cyclic loading *

Study	Specimen	$\ell_{dt}^{\#}$	ℓ_{dt}/d_b	ℓ_{dy}	ℓ_{dy}/d_b	ℓ_{eh}	ℓ_{eh}/d_b	ℓ_{ehy}	ℓ_{ehy}/d_b	ℓ_{eh}/h_c	ℓ_{eh}/ℓ_{dt}	ℓ_{eh}/ℓ_{dy}	ℓ_{eh}/ℓ_{ehy}	
		(in.)		(in.)		(in.)		(in.)						
1	2	39	40	41	42	43	44	45	46	47	48	49	50	
1	Bashandy (1996)	Exterior Joint	9.6	9.8	16.1	16.4	11.5	11.7	7.8	8.0	0.76	1.19	0.71	1.46
2	Murakami et al. (1998)	No. 100	6.7	10.8	6.5	10.4	8.9	14.2	4.7	7.5	0.75	1.32	1.36	1.90
		No. 101	6.7	10.8	6.5	10.4	8.9	14.2	4.7	7.5	0.75	1.32	1.36	1.90
		B8-M	12.4	16.5	15.1	20.2	8.9	11.8	8.5	11.4	0.75	0.72	0.58	1.04
		B7-M	12.4	16.5	15.1	20.2	8.9	11.8	8.5	11.4	0.75	0.72	0.58	1.04
		No. 102 ‡	25.4	33.9	31.4	41.9	8.9	11.8	16.7	22.3	0.75	0.35	0.28	0.53
		No. 103 ‡	25.4	33.9	31.4	41.9	8.9	11.8	16.7	22.3	0.75	0.35	0.28	0.53
		No. 104 ‡	25.4	33.9	31.4	41.9	8.9	11.8	16.7	22.3	0.75	0.35	0.28	0.53
		M8D16 ‡	23.9	38.3	36.9	59.1	8.9	14.2	14.3	22.8	0.75	0.37	0.24	0.62
		M4D19 ‡	29.2	39.0	37.2	49.6	8.9	11.8	19.1	25.5	0.75	0.30	0.24	0.46
		M3D19 ‡	24.5	32.6	37.2	49.6	8.9	11.8	16.9	22.6	0.75	0.36	0.24	0.52
M2D22 ‡	20.0	22.8	42.0	48.0	8.9	10.1	16.7	19.0	0.75	0.44	0.21	0.53		
3	Wallace et al. (1998)	BCEJ1 ††	10.9	10.9	16.0	16.0	13.9	13.9	8.9	8.9	0.77	1.28	0.87	1.56
4	Matsushima et al. (2000)	H	17.2	17.5	21.2	21.7	11.6	11.9	13.2	13.5	0.74	0.68	0.55	0.88
		HS §	17.2	17.5	21.2	21.7	7.9	8.0	13.2	13.5	0.50	0.46	0.37	0.60
5	Nakazawa et al. (2000)	J1	10.6	14.1	14.7	19.5	11.3	15.0	7.4	9.8	0.79	1.06	0.77	1.52
		J2	10.6	14.1	14.7	19.5	11.3	15.0	7.4	9.8	0.79	1.06	0.77	1.52
6	Tasai et. al (2000)	No. 6	26.7	26.7	27.6	27.6	11.8	11.8	18.9	18.9	0.75	0.44	0.43	0.62
		No. 7	18.9	18.9	27.6	27.6	11.8	11.8	15.9	15.9	0.75	0.63	0.43	0.74
7	Yoshida et al. (2000)	No. 1	11.4	15.3	15.9	21.2	10.2	13.6	9.1	12.1	0.74	0.89	0.64	1.13
		No. 2	11.4	15.3	15.9	21.2	10.2	13.6	9.1	12.1	0.74	0.89	0.64	1.13
		No. 3	12.0	16.0	17.5	23.4	10.2	13.6	9.5	12.6	0.74	0.85	0.58	1.08
8	Takeuchi et al. (2001)	0-1	10.5	10.7	13.5	13.8	10.4	10.6	7.9	8.0	0.66	0.99	0.77	1.32
		0-2	12.8	13.0	18.5	18.9	10.4	10.6	9.8	10.0	0.66	0.81	0.56	1.06
		0-3	10.3	10.5	13.2	13.4	10.4	10.6	7.5	7.7	0.66	1.01	0.79	1.38
		0-4	10.5	10.7	13.5	13.8	11.7	11.9	7.9	8.0	0.74	1.11	0.86	1.49
		0-6	20.8	21.2	27.7	28.2	10.4	10.6	15.2	15.5	0.66	0.50	0.38	0.69
		0-7	19.1	19.5	24.7	25.2	10.4	10.6	14.0	14.3	0.66	0.54	0.42	0.74
9	Ishibashi et. al (2003) §§	T345-30-4S	5.7	7.6	9.2	12.3	13.5	18.0	4.6	6.1	0.86	2.37	1.47	2.95
		T345-30-3N	5.7	7.6	9.2	12.3	13.5	18.0	4.6	6.1	0.86	2.37	1.47	2.95
		T490-45-4S	7.8	10.3	15.2	20.2	13.5	18.0	6.6	8.8	0.86	1.74	0.89	2.05
		T490-45-3N	7.8	10.3	15.2	20.2	13.5	18.0	6.6	8.8	0.86	1.74	0.89	2.05

* Columns arranged in alphabetical order of notation; notation described in Appendix A; values given in SI are converted to in.-lb (1 in. = 25.4 mm; 1 psi = 1/145 MPa; and 1 kip = 4.4484 kN)

‡ Analyzed as doubly-reinforced section to calculate M_n ; all other specimens are analyzed as singly-reinforced

†† Specimens contained transverse beams on one or both sides of the test beam. These transverse beams, however, did not meet the dimensional requirements of Section 18.8.4.2 of ACI 318-14 and Section 4.3 of ACI 352R-02 to be considered effective in increasing the joint shear strength.

§ Specimen had $d/\ell_{eh} > 1.5$

§§ Roof-level interior joints; all other specimens are exterior joints

ℓ_{dt} based on Eq. (5.2)

Table C.2 Cont. Data for beam-column joint specimens (exterior and roof-level interior joints) tested under reversed cyclic loading *

Study	Specimen	M_n	M_{peak}	M_{peak}/M_n	N	N_{arg}	N_{cbg}	N_{sb}	N_{sbg}	N_{splt}^\diamond	N_{total}	N_{tr}	
		(kip.in.)	(kip.in.)			(kips)	(kips)	(kips)	(kips)				
	1	2	51	52	53	54	55	56	57	58	59	60	61
1	Bashandy (1996)	Exterior Joint	1443	1593	1.10	6	54.1	20.5	109.1	-	2	10	4
2	Murakami et al. (1998)	No. 100	859	1031	1.20	4	33.5	20.2	23.3	-	6	8	2
		No. 101	859	1066	1.24	4	33.5	20.2	44.9	-	6	8	2
		B8-M	1200	1395	1.16	4	33.5	17.5	45.2	-	6	8	2
		B7-M	1093	1242	1.14	4	33.5	17.5	45.2	-	6	8	2
		No. 102 ‡	2838	1957	0.69	4	33.5	20.2	30.9	-	6	8	2
		No. 103 ‡	2838	1524	0.54	4	33.5	20.2	51.3	-	6	8	2
		No. 104 ‡	2838	1793	0.63	4	33.5	20.2	39.0	-	6	8	2
		M8D16 ‡	2918	1793	0.61	2	44.7	18.4	31.8	35.8	6	8	4
		M4D19 ‡	2838	1688	0.59	4	33.5	17.1	35.7	-	6	8	2
		M3D19 ‡	2226	1676	0.75	4	33.5	17.1	35.7	-	6	8	2
M2D22 ‡	1990	1324	0.67	6	33.5	17.1	40.0	-	6	8	2		
3	Wallace et al. (1998)	BCEJ1 ‡‡	4448	4950	1.11	6	80.4	48.3	-	-	5	12	3
4	Matsushima et al. (2000)	H	2545	2205	0.87	4	136.8	27.7	-	-	8	6	4
		HS §	2545	2071	0.81	4	68.4	23.5	-	-	8	6	2
5	Nakazawa et al. (2000)	J1	2989	3391	1.13	8	173.5	38.6	64.5	73.4	6	12	8
		J2	2989	3344	1.12	8	173.5	38.6	79.3	90.3	6	12	8
6	Tasai et. al (2000)	No. 6	4388	2283	0.52	4	82.4	34.2	80.9	-	2	6	2
		No. 7	2359	1328	0.56	4	82.4	34.2	80.9	-	2	6	2
7	Yoshida et al. (2000)	No. 1	1818	1681	0.92	4	46.2	21.0	52.1	-	4	10	4
		No. 2	1818	1696	0.93	4	46.2	21.0	43.8	-	4	10	4
		No. 3	1797	1665	0.93	4	46.2	19.1	34.6	-	4	10	4
8	Takeuchi et al. (2001)	0-1	2237	2458	1.10	4	93.3	30.8	81.9	-	6	6	2
		0-2	2937	2897	0.99	4	93.3	36.1	96.2	-	6	6	2
		0-3	1821	1927	1.06	4	93.3	22.8	60.8	-	6	6	2
		0-4	2237	2591	1.16	4	93.3	32.3	81.9	-	6	6	2
		0-6	4390	3481	0.79	4	93.3	30.9	82.2	-	6	6	2
		0-7	4598	4106	0.89	4	93.3	36.5	97.1	-	6	6	2
9	Ishibashi et. al (2003) §§	T345-30-4S	1116	1401	1.25	4	51.0	25.2	29.6	42.0	4	6	4
		T345-30-3N	1116	1394	1.25	4	51.0	25.2	29.6	42.0	4	6	4
		T490-45-4S	1612	1925	1.19	4	170.8	30.8	36.2	51.3	4	6	4
		T490-45-3N	1612	1951	1.21	4	170.8	30.8	36.2	51.3	4	6	4

* Columns arranged in alphabetical order of notation; notation described in Appendix A; values given in SI are converted to in.-lb (1 in. = 25.4 mm; 1 psi = 1/145 MPa; and 1 kip = 4.4484 kN)

‡ Analyzed as doubly-reinforced section to calculate M_n ; all other specimens are analyzed as singly-reinforced

‡‡ Specimens contained transverse beams on one or both sides of the test beam. These transverse beams, however, did not meet the dimensional requirements of Section 18.8.4.2 of ACI 318-14 and Section 4.3 of ACI 352R-02 to be considered effective in increasing the joint shear strength.

§ Specimen had $d/\ell_{eh} > 1.5$

§§ Roof-level interior joints; all other specimens are exterior joints

◊ N_{splt} is used as N in Eq. (4.6)

Table C.2 Cont. Data for beam-column joint specimens (exterior and roof-level interior joints) tested under reversed cyclic loading *

Study	Specimen	N_{tro}	n	nT' (kips)	$n_{l,sprt}$	n_{sprt}	$P/A_g f'_c$	s_h/d_b	s'_{tr} (in.)	s_{tr} (in.)	s'_{tro} (in.)	s_{tro} (in.)	s_v/d_b	T_{anc} (kips)	
															62
1	Bashandy (1996)	Exterior Joint	2	2	113.1	4	4	0.00	5.1	2.2	2.2	3.1	6.0	-	27.1
2	Murakami et al. (1998)	No. 100	4	4	79.8	4	12	0.04	3.5	1.6	3.1	1.5	3.0	-	8.4
		No. 101	4	4	82.6	4	12	0.04	3.5	1.6	3.1	1.5	3.0	-	8.4
		B8-M	4	3	113.7	4	12	0.06	4.3	1.6	3.1	1.5	3.0	-	11.2
		B7-M	4	3	111.2	4	12	0.06	4.3	1.6	3.1	1.5	3.0	-	11.2
		No. 102 ‡	4	4	166.4	4	12	0.04	2.9	1.6	3.1	1.5	3.0	-	8.4
		No. 103 ‡	4	4	129.6	4	12	0.04	2.9	1.6	3.1	1.5	3.0	-	8.4
		No. 104 ‡	4	4	152.5	4	12	0.04	2.9	1.6	3.1	1.5	3.0	-	8.4
		M8D16 ‡	4	8	221.1	4	12	0.06	3.5	2.8	1.8	1.5	3.0	3.2	5.6
		M4D19 ‡	4	4	151.9	4	12	0.06	2.9	1.6	3.1	1.5	3.0	-	8.4
		M3D19 ‡	4	3	144.2	4	12	0.06	4.3	1.6	3.1	1.5	3.0	-	11.2
M2D22 ‡	4	2	112.7	4	12	0.06	7.4	1.6	3.1	1.5	3.0	-	16.8		
3	Wallace et al. (1998)	BCEJ1 ‡‡	3	4	235.6	4	8	0.00	3.5	3.3	4.0	4.5	8.0	-	20.1
4	Matsushima et al. (2000)	H	8	3	164.1	4	12	0.11	5.1	1.0	4.7	1.8	3.9	-	45.6
		HS §	4	3	154.1	4	13	0.11	5.1	1.0	4.7	1.8	3.9	-	22.8
5	Nakazawa et al. (2000)	J1	12	6	308.3	8	12	0.00	3.7	0.8	3.0	0.8	2.0	3.4	28.9
		J2	12	6	304.1	8	12	0.00	3.7	0.8	3.0	0.8	2.0	3.4	28.9
6	Tasai et. al (2000)	No. 6	6	4	172.6	8	12	0.00	3.1	2.6	3.9	0.7	3.9	-	20.6
		No. 7	6	2	93.3	8	12	0.00	4.7	2.6	3.9	0.7	3.9	-	41.2
7	Yoshida et al. (2000)	No. 1	4	4	132.6	4	8	0.00	3.7	1.5	3.0	1.8	2.0	-	11.6
		No. 2	4	4	133.8	4	8	0.00	3.7	1.5	3.0	1.8	2.0	-	11.6
		No. 3	4	4	132.9	4	8	0.00	3.7	1.5	3.0	1.8	2.0	-	11.6
8	Takeuchi et al. (2001)	0-1	4	3	168.0	4	12	0.10	4.9	3.0	3.9	1.1	3.9	-	31.1
		0-2	4	3	198.6	4	12	0.10	4.9	3.0	3.9	1.1	3.9	-	31.1
		0-3	4	3	137.1	4	12	0.10	4.9	3.0	3.9	1.1	3.9	-	31.1
		0-4	4	3	177.1	4	12	0.10	4.9	3.0	3.9	1.1	3.9	-	31.1
		0-6	4	4	260.9	4	12	0.10	3.3	3.0	3.9	1.1	3.9	-	23.3
		0-7	4	4	293.8	4	12	0.10	3.3	3.0	3.9	1.1	3.9	-	23.3
9	Ishibashi et. al (2003) §§	T345-30-4S	4	3	93.2	4	8	0.00	7.5	0.6	5.1	0.6	3.5	7.5	17.0
		T345-30-3N	4	3	92.8	4	8	0.00	7.5	0.6	5.1	0.6	3.5	7.5	17.0
		T490-45-4S	6	3	133.2	4	8	0.00	7.5	0.6	5.1	0.6	2.4	7.5	25.7
		T490-45-3N	6	3	135.1	4	8	0.00	7.5	0.6	5.1	0.6	2.4	7.5	25.7

* Columns arranged in alphabetical order of notation; notation described in Appendix A; values given in SI are converted to in.-lb (1 in. = 25.4 mm; 1 psi = 1/145 MPa; and 1 kip = 4.4484 kN)

‡ Analyzed as doubly-reinforced section to calculate M_n ; all other specimens are analyzed as singly-reinforced

‡‡ Specimens contained transverse beams on one or both sides of the test beam. These transverse beams, however, did not meet the dimensional requirements of Section 18.8.4.2 of ACI 318-14 and Section 4.3 of ACI 352R-02 to be considered effective in increasing the joint shear strength.

§ Specimen had $d/\ell_{eh} > 1.5$

§§ Roof-level interior joints; all other specimens are exterior joints

Table C.2 Cont. Data for beam-column joint specimens (exterior and roof-level interior joints) tested under reversed cyclic loading *

Study	Specimen	T_h	T'	T'_{mod}	T'/T_{unc}	T'/T_h	T'_{mod}/T_h	t_{obs}/d_b	V_n	$V_{n,ACI352}$	V_p	
		(kips)	(kips)	(kips)					(kips)	(kips)	(kips)	
	1	2	75	76	77	78	79	80	81	82	83	84
1	Bashandy (1996)	Exterior Joint	51.2	56.5	53.7	2.09	1.10	1.05	0.0	141	130	114
2	Murakami et al. (1998)	No. 100	16.6	20.0	18.1	2.38	1.20	1.09	0.0	126	118	63
		No. 101	16.6	20.6	18.8	2.46	1.24	1.13	0.0	126	118	65
		B8-M	32.6	37.9	37.7	3.39	1.16	1.16	0.0	110	102	86
		B7-M	32.6	37.1	36.9	3.32	1.14	1.13	0.0	110	102	76
		No. 102 ‡	31.8	41.6	-	4.96	1.31	-	0.0	126	118	120
		No. 103 ‡	31.8	32.4	-	3.87	1.02	-	0.0	126	118	94
		No. 104 ‡	31.8	38.1	-	4.55	1.20	-	0.0	126	118	110
		M8D16 ‡	27.6	27.6	-	4.95	1.00	-	0.0	107	100	109
		M4D19 ‡	29.5	38.0	-	4.53	1.29	-	0.0	107	100	104
M3D19 ‡	33.6	48.1	-	4.30	1.43	-	0.0	107	100	103		
M2D22 ‡	46.6	56.3	-	3.36	1.21	-	0.0	107	100	103		
3	Wallace et al. (1998)	BCEJ1 ††	52.9	58.9	55.3	2.93	1.11	1.04	0.0	280	280	262
4	Matsushima et al. (2000)	H	55.8	54.7	-	1.20	0.98	-	-	206	193	166
		HS §	39.0	51.4	-	2.25	1.32	-	-	206	193	156
5	Nakazawa et al. (2000)	J1	45.3	51.4	48.5	1.78	1.13	1.07	1.9	242	263	255
		J2	45.3	50.7	47.8	1.75	1.12	1.05	0.0	242	263	251
6	Tasai et al. (2000)	No. 6	52.3	43.2	-	2.09	0.83	-	1.9	251	235	224
		No. 7	63.0	46.7	-	1.13	0.74	-	1.9	251	235	137
7	Yoshida et al. (2000)	No. 1	35.9	33.1	32.6	2.87	0.92	0.91	0.0	144	144	128
		No. 2	35.9	33.4	32.9	2.89	0.93	0.92	0.0	144	144	111
		No. 3	35.9	33.2	32.9	2.88	0.93	0.92	0.0	131	131	109
8	Takeuchi et al. (2001)	0-1	51.0	56.0	54.0	1.80	1.10	1.06	0.0	238	223	133
		0-2	67.1	66.2	65.7	2.13	0.99	0.98	0.0	280	262	156
		0-3	43.2	45.7	43.7	1.47	1.06	1.01	0.0	177	166	104
		0-4	51.0	59.0	56.0	1.90	1.16	1.10	0.0	238	223	140
		0-6	57.0	65.2	-	2.80	1.14	-	0.0	239	224	188
		0-7	61.4	73.4	-	3.15	1.20	-	0.0	282	265	221
9	Ishibashi et al. (2003) §§	T345-30-4S	24.8	31.1	25.2	1.83	1.25	1.02	-	155	155	112
		T345-30-3N	24.8	30.9	25.0	1.82	1.25	1.01	-	155	155	111
		T490-45-4S	37.2	44.4	39.7	1.73	1.19	1.07	-	190	190	157
		T490-45-3N	37.2	45.0	40.3	1.76	1.21	1.08	-	190	190	156

* Columns arranged in alphabetical order of notation; notation described in Appendix A; values given in SI are converted to in.-lb (1 in. = 25.4 mm; 1 psi = 1/145 MPa; and 1 kip = 4.4484 kN)

‡ Analyzed as doubly-reinforced section to calculate M_n ; all other specimens are analyzed as singly-reinforced

†† Specimens contained transverse beams on one or both sides of the test beam. These transverse beams, however, did not meet the dimensional requirements of Section 18.8.4.2 of ACI 318-14 and Section 4.3 of ACI 352R-02 to be considered effective in increasing the joint shear strength.

§ Specimen had $d/\ell_{eh} > 1.5$

§§ Roof-level interior joints; all other specimens are exterior joints

Table C.2 Cont. Data for beam-column joint specimens (exterior and roof-level interior joints) tested under reversed cyclic loading *

Study	Specimen	V_p / V_n	$\delta_{0.8peak}$	δ_y	Υ_j	$\Psi_{cs}^{##}$	Ψ_o	
	1	2	85	86	87	88	89	90
1	Bashandy (1996)	Exterior Joint	0.81	0.053	0.009	0.005	0.50	1.00
2	Murakami et al. (1998)	No. 100	0.50	0.080	-	-	0.71	1.25
		No. 101	0.52	0.083	-	-	0.71	1.25
		B8-M	0.78	0.060	-	-	0.67	1.25
		B7-M	0.70	0.070	-	-	0.67	1.25
		No. 102 ‡	0.95	0.040	-	-	0.79	1.25
		No. 103 ‡	0.74	0.055	-	-	0.79	1.25
		No. 104 ‡	0.87	0.050	-	-	0.79	1.25
		M8D16 ‡	1.02	0.040	-	-	0.86	1.25
		M4D19 ‡	0.97	0.040	-	-	0.79	1.25
		M3D19 ‡	0.96	0.040	-	-	0.67	1.25
M2D22 ‡	0.96	0.020	-	-	0.44	1.25		
3	Wallace et al. (1998)	BCEJ1 ‡‡	0.93	0.048	0.015	-	0.55	1.00
4	Matsushima et al. (2000)	H	0.81	0.035	-	0.022	0.59	1.25
		HS §	0.76	0.035	-	0.031	0.59	1.25
5	Nakazawa et al. (2000)	J1	1.05	0.050	0.020	0.001	0.73	1.00
		J2	1.04	0.058	0.020	0.001	0.73	1.00
6	Tasai et. al (2000)	No. 6	0.89	0.060	0.010	0.000	0.75	1.25
		No. 7	0.55	0.030	0.020	0.000	0.53	1.25
7	Yoshida et al. (2000)	No. 1	0.88	0.040	0.020	0.007	0.59	1.25
		No. 2	0.77	0.040	0.020	0.006	0.59	1.25
		No. 3	0.83	0.040	0.020	0.007	0.59	1.25
8	Takeuchi et al. (2001)	0-1	0.56	0.050	0.005	0.008	0.60	1.00
		0-2	0.56	0.033	0.010	-	0.60	1.00
		0-3	0.59	0.050	0.005	-	0.60	1.00
		0-4	0.59	0.050	0.006	0.003	0.60	1.00
		0-6	0.79	0.030	-	0.040	0.74	1.00
		0-7	0.78	0.030	-	-	0.74	1.00
9	Ishibashi et. al (2003) §§	T345-30-4S	0.72	0.065	0.010	0.009	0.42	1.25
		T345-30-3N	0.72	0.053	0.010	0.008	0.42	1.25
		T490-45-4S	0.83	0.053	0.010	0.010	0.42	1.25
		T490-45-3N	0.82	0.040	0.010	0.011	0.42	1.25

* Columns arranged in alphabetical order of notation; notation described in Appendix A; values given in SI are converted to in.-lb (1 in. = 25.4 mm; 1 psi = 1/145 MPa; and 1 kip = 4.4484 kN)

‡ Analyzed as doubly-reinforced section to calculate M_n ; all other specimens are analyzed as singly-reinforced

‡‡ Specimens contained transverse beams on one or both sides of the test beam. These transverse beams, however, did not meet the dimensional requirements of Section 18.8.4.2 of ACI 318-14 and Section 4.3 of ACI 352R-02 to be considered effective in increasing the joint shear strength.

§ Specimen had $d/\ell_{eh} > 1.5$

§§ Roof-level interior joints; all other specimens are exterior joints

Ψ_{cs} is based on Table 5.1

Table C.2 Cont. Data for beam-column joint specimens (exterior and roof-level interior joints) tested under reversed cyclic loading *

Study	Specimen	Bar Size **	A_b	A_{brg}/A_b	A_{gross}/A_b	A_{hs}	A_{Nc}	A_{obs}/A_b	A_{tr}	$A_{tr,l}$	$A_{tro,l}$	A_{tr}	A_{tr}/A_{hs}	
			(in. ²)			(in. ²)	(in. ²)		(in. ²)	(in. ²)	(in. ²)	(in. ²)		
	1	2	3	4	5	6	7	8	9	10	11	12	13	14
10	Ishibashi and Inokuchi (2004) §§	2S-2	D29	1.02	-	-	3.06	1102	-	1.02	0.11	0.11	0.44	0.14
		2S-0 □	D29	1.02	-	-	3.06	1102	-	1.02	0.11	0.11	0.00	0.00
		WN-ST	D29	1.02	-	-	3.06	1102	-	1.02	0.11	0.11	1.11	0.36
11	Kiyohara et al. (2004)	No. 1	D29	1.00	4.1	6.7	4.00	933	2.6	0.79	0.20	0.20	0.79	0.20
		No. 2	D29	1.00	4.1	6.7	6.00	1017	2.6	0.79	0.20	0.20	0.79	0.13
		No. 3	D29	1.00	4.1	6.7	3.00	933	2.6	0.79	0.20	0.20	0.79	0.26
		No. 4	D29	1.00	4.1	6.7	4.00	1177	2.6	0.79	0.20	0.20	0.79	0.20
		No. 5 §	D29	1.00	4.1	6.7	4.00	704	2.6	0.79	0.20	0.20	0.79	0.20
12	Kiyohara et al. (2005)	No. 6	D29	1.00	4.1	6.7	7.00	1017	2.6	0.79	0.20	0.20	0.79	0.11
		No. 7	D29	1.00	4.1	6.7	7.00	1017	2.6	0.79	0.20	0.20	0.79	0.11
		No. 8 ‡	D29	1.00	4.1	6.7	7.00	1017	2.6	0.79	0.20	0.20	0.79	0.11
		No. 9	D29	1.00	4.1	6.7	7.00	1260	2.6	0.79	0.20	0.20	0.79	0.11
		No. 10 §	D29	1.00	4.1	6.7	7.00	787	2.6	0.79	0.20	0.20	0.79	0.11
		No. 11	D29	1.00	4.1	6.7	5.00	933	2.6	0.79	0.20	0.20	0.79	0.16
13	Kato (2005)	No. 1	D22	0.60	5.3	6.3	4.80	858	-	0.60	0.05	0.08	0.20	0.04
		No. 2	D22	0.60	3.6	6.3	4.80	858	2.7	0.60	0.05	0.08	0.20	0.04
14	Masuo et al. (2006a, 2006b)	AH12-2-45	D25	0.79	3.7	6.8	1.58	486	3.1	0.60	0.08	0.08	0.31	0.19
		AH12-2-40	D25	0.79	3.7	6.8	1.58	486	3.1	0.60	0.08	0.08	0.31	0.19
		AH12-2-45A §	D25	0.79	3.7	6.8	1.58	405	3.1	0.60	0.08	0.08	0.31	0.19
		AH8-2-45	D25	0.79	3.7	6.8	1.58	486	3.1	0.60	0.08	0.08	0.31	0.19
		AH12-8-45	D25	0.79	3.9	6.8	6.32	523	2.9	0.79	0.08	0.08	0.46	0.07
		AH12-8-40	D25	0.79	3.9	6.8	6.32	523	2.9	0.79	0.08	0.08	0.46	0.07
		AH12-8-45B	D25	0.79	3.9	6.8	6.32	523	2.9	0.79	0.08	0.08	0.92	0.15
AH8-6-45	D25	0.79	3.9	6.8	4.74	523	2.9	0.60	0.08	0.08	0.46	0.10		
15	Adachi and Masuo (2007)	J30-12-0	D25	0.79	3.9	6.4	3.16	625	2.5	0.60	0.11	0.11	0.44	0.14
		J30-12-P1 ‡‡	D25	0.79	3.9	6.4	3.16	625	2.5	0.60	0.11	0.11	0.44	0.14
		J30-12-P2 ‡‡	D25	0.79	3.9	6.4	3.16	625	2.5	0.60	0.11	0.11	0.44	0.14
		J60-12-0	D25	0.79	3.9	6.4	4.74	672	2.5	0.60	0.11	0.11	0.44	0.09
		J60-12-P1 ‡‡	D25	0.79	3.9	6.4	4.74	672	2.5	0.60	0.11	0.11	0.44	0.09
		J60-12-P2 ‡‡	D25	0.79	3.9	6.4	4.74	672	2.5	0.60	0.11	0.11	0.44	0.09

* Columns arranged in alphabetical order of notation; notation described in Appendix A; values given in SI are converted to in.-lb (1 in. = 25.4 mm; 1 psi = 1/145 MPa; and 1 kip = 4.4484 kN)

** Bar sizes are presented in SI as reported in the original studies (only Wallace et al. 1998 had bar sizes reported in in.-lb)

□ Specimens did not contain confining reinforcement parallel to the headed bars within the joint region

‡ Analyzed as doubly-reinforced section to calculate M_n ; all other specimens are analyzed as singly-reinforced

‡‡ Specimens contained transverse beams on one or both sides of the test beam. These transverse beams, however, did not meet the dimensional requirements of Section 18.8.4.2 of ACI 318-14 and Section 4.3 of ACI 352R-02 to be considered effective in increasing the joint shear strength.

§ Specimens had $d/\ell_{ch} > 1.5$

§§ Roof-level interior joints; all other specimens are exterior joints

Table C.2 Cont. Data for beam-column joint specimens (exterior and roof-level interior joints) tested under reversed cyclic loading *

Study	Specimen	A_v	b_b	b_c	b_j	$b_{j,ACI352}$	c_{ch}	c_{ch}/d_b	c_o	c_o/d_b	c_{so}	c_{so}/d_b	d	d/ℓ_{eh}	
		(in. ²)	(in.)	(in.)	(in.)	(in.)	(in.)	(in.)	(in.)	(in.)	(in.)	(in.)	(in.)	(in.)	
	1	2	15	16	17	18	19	20	21	22	23	24	25	26	27
10	Ishibashi and Inokuchi (2004) ^{§§}	2S-2	0.89	23.6	16	15.7	15.7	8.4	7.4	-	-	2.9	2.5	20.2	1.0
		2S-0 [□]	0.00	23.6	16	15.7	15.7	8.4	7.4	-	-	2.9	2.5	20.2	1.0
		WN-ST	1.33	23.6	16	15.7	15.7	8.4	7.4	-	-	2.9	2.5	20.2	1.0
11	Kiyohara et al. (2004)	No. 1	1.18	17.7	22	21.7	19.7	6.2	5.4	2.4	2.1	3.3	2.9	21.6	1.5
		No. 2	1.18	17.7	22	21.7	19.7	3.9	3.4	2.4	2.1	3.3	2.9	20.9	1.5
		No. 3	1.18	17.7	22	21.7	19.7	6.3	5.5	2.4	2.1	3.3	2.9	21.6	1.5
		No. 4	1.18	17.7	22	21.7	19.7	6.2	5.4	2.4	2.1	3.3	2.9	21.6	1.2
		No. 5 [§]	1.18	17.7	22	21.7	19.7	6.2	5.4	2.4	2.1	3.3	2.9	21.6	2.0
12	Kiyohara et al. (2005)	No. 6	1.18	17.7	22	21.7	19.7	3.3	2.9	2.4	2.1	3.3	2.9	20.9	1.5
		No. 7	1.18	17.7	22	21.7	19.7	3.3	2.9	2.4	2.1	3.3	2.9	20.9	1.5
		No. 8 [‡]	1.18	17.7	22	21.7	19.7	3.3	2.9	2.4	2.1	3.3	2.9	20.9	1.5
		No. 9	1.18	17.7	22	21.7	19.7	3.3	2.9	2.4	2.1	3.3	2.9	20.9	1.2
		No. 10 [§]	1.18	17.7	22	21.7	19.7	3.3	2.9	2.4	2.1	3.3	2.9	20.9	1.9
		No. 11	1.18	17.7	22	21.7	19.7	3.3	2.9	2.4	2.1	3.3	2.9	21.6	1.5
13	Kato (2005)	No. 1	0.79	12.8	19	18.7	15.7	3.1	3.6	3.6	4.1	4.3	4.9	15.5	1.1
		No. 2	0.79	12.8	19	18.7	15.7	3.1	3.6	3.6	4.1	4.3	4.9	15.5	1.1
14	Masuo et al. (2006a, 2006b)	AH12-2-45	0.61	11.8	14	13.8	12.8	7.8	8.0	1.7	1.7	2.5	2.6	15.7	1.3
		AH12-2-40	0.61	11.8	14	13.8	12.8	7.8	8.0	1.7	1.7	2.5	2.6	15.7	1.3
		AH12-2-45A [§]	0.61	11.8	14	13.8	12.8	7.8	8.0	1.7	1.7	2.5	2.6	15.7	1.6
		AH8-2-45	0.61	11.8	14	13.8	12.8	7.8	8.0	1.7	1.7	2.5	2.6	15.7	1.3
		AH12-8-45	0.77	13.8	14	13.8	13.8	2.7	2.7	2.6	2.7	3.4	3.5	14.4	1.2
		AH12-8-40	0.77	13.8	14	13.8	13.8	2.7	2.7	2.6	2.7	3.4	3.5	14.4	1.2
		AH12-8-45B	0.77	13.8	14	13.8	13.8	2.7	2.7	2.6	2.7	3.4	3.5	14.4	1.2
AH8-6-45	0.77	13.8	14	13.8	13.8	2.7	2.7	2.6	2.7	3.4	3.5	14.9	1.3		
15	Adachi and Masuo (2007)	J30-12-0	0.89	13.8	18	17.7	15.7	3.1	3.2	2.7	2.7	3.4	3.5	15.7	1.3
		J30-12-P1	0.89	13.8	18	17.7	15.7	3.1	3.2	2.7	2.7	3.4	3.5	15.7	1.3
		J30-12-P2 ^{**}	0.89	13.8	18	17.7	15.7	3.1	3.2	-	-	-	-	15.7	1.3
		J60-12-0	0.89	13.8	18	17.7	15.7	2.6	2.7	2.7	2.7	3.4	3.5	15.0	1.3
		J60-12-P1	0.89	13.8	18	17.7	15.7	2.6	2.7	2.7	2.7	3.4	3.5	15.0	1.3
		J60-12-P2 ^{**}	0.89	13.8	18	17.7	15.7	2.6	2.7	-	-	-	-	15.0	1.3

* Columns arranged in alphabetical order of notation; notation described in Appendix A; values given in SI are converted to in.-lb (1 in. = 25.4 mm; 1 psi = 1/145 MPa; and 1 kip = 4.4484 kN)

□ Specimens did not contain confining reinforcement parallel to the headed bars within the joint region

‡ Analyzed as doubly-reinforced section to calculate M_n ; all other specimens are analyzed as singly-reinforced

** Specimens contained transverse beams on one or both sides of the test beam. These transverse beams, however, did not meet the dimensional requirements of Section 18.8.4.2 of ACI 318-14 and Section 4.3 of ACI 352R-02 to be considered effective in increasing the joint shear strength.

§ Specimens had $d/\ell_{eh} > 1.5$

§§ Roof-level interior joints; all other specimens are exterior joints

Table C.2 Cont. Data for beam-column joint specimens (exterior and roof-level interior joints) tested under reversed cyclic loading *

Study	Specimen	d'	d_b	$d_{b,sprt}$	f_{cm}	f_y	$f_{y,sprt}$	f_{yt}	$f_{yt}A_v$	f_{yto}	h_b	h_c	
		(in.)	(in.)	(in.)	(psi)	(ksi)	(ksi)	(ksi)	(kips)	(ksi)	(in.)	(in.)	
	1	2	28	29	30	31	32	33	34	35	36	37	38
10	Ishibashi and Inokuchi (2004) ^{§§}	2S-2	3.4	1.14	1.14	5180	77.1	77.1	60.2	53.3	139.3	23.6	23.6
		2S-0 [□]	3.4	1.14	1.14	5180	77.1	77.1	0.0	0.0	139.3	23.6	23.6
		WN-ST	3.4	1.14	1.14	5420	77.1	77.1	139.3	185.2	139.3	23.6	23.6
11	Kiyohara et al. (2004)	No. 1	2.0	1.14	1	13820	103.0	103.1	124.0	146.3	124.0	23.6	21.7
		No. 2	2.8	1.14	1	21520	103.0	103.1	124.0	146.3	124.0	23.6	21.7
		No. 3	2.0	1.14	1	6440	103.0	103.1	124.0	146.3	124.0	23.6	21.7
		No. 4	2.0	1.14	1	13820	103.0	103.1	124.0	146.3	124.0	23.6	21.7
		No. 5 [§]	2.0	1.14	1	13820	103.0	103.1	124.0	146.3	124.0	23.6	21.7
12	Kiyohara et al. (2005)	No. 6	2.8	1.14	1	15420	149.9	102.2	119.0	140.5	119.0	23.6	21.7
		No. 7	2.8	1.14	1	20130	149.9	102.2	119.0	140.5	119.0	23.6	21.7
		No. 8 [‡]	2.8	1.14	1	6870	149.9	102.2	119.0	140.5	119.0	23.6	21.7
		No. 9	2.8	1.14	1	15360	149.9	102.2	119.0	140.5	119.0	23.6	21.7
		No. 10 [§]	2.8	1.14	1	15660	149.9	102.2	119.0	140.5	119.0	23.6	21.7
		No. 11	2.0	1.14	1	15000	100.1	102.2	119.0	140.5	119.0	23.6	21.7
13	Kato (2005)	No. 1	2.3	0.875	0.875	8820	75.5	99.3	113.8	89.4	113.8	17.7	18.7
		No. 2	2.3	0.875	0.875	10270	73.2	99.3	113.8	89.4	113.8	17.7	18.7
14	Masuo et al. (2006a, 2006b)	AH12-2-45	2.0	0.98	0.875	18820	148.0	83.2	155.3	95.3	155.3	17.7	17.7
		AH12-2-40	2.0	0.98	0.875	18820	148.0	83.2	155.3	95.3	155.3	17.7	15.7
		AH12-2-45A [§]	2.0	0.98	0.875	18820	148.0	83.2	155.3	95.3	155.3	17.7	17.7
		AH8-2-45	2.0	0.98	0.875	13140	148.0	83.2	155.3	95.3	155.3	17.7	17.7
		AH12-8-45	3.3	0.98	1	18820	92.0	79.6	155.3	119.2	155.3	17.7	17.7
		AH12-8-40	3.3	0.98	1	18820	92.0	79.6	155.3	119.2	155.3	17.7	15.7
		AH12-8-45B	3.3	0.98	1	18820	92.0	79.6	155.3	119.2	155.3	17.7	17.7
AH8-6-45	2.8	0.98	0.875	13140	92.0	83.2	155.3	119.2	155.3	17.7	17.7		
15	Adachi and Masuo (2007)	J30-12-0	2.0	0.98	0.875	4480	76.0	60.0	54.8	48.6	109.9	17.7	17.7
		J30-12-P1	2.0	0.98	0.875	4480	76.0	60.0	54.8	48.6	109.9	17.7	17.7
		J30-12-P2 ^{**}	2.0	0.98	0.875	4480	76.0	60.0	54.8	48.6	109.9	17.7	17.7
		J60-12-0	2.8	0.98	0.875	9150	76.0	60.0	54.8	48.6	109.9	17.7	17.7
		J60-12-P1	2.8	0.98	0.875	9150	76.0	60.0	54.8	48.6	109.9	17.7	17.7
		J60-12-P2 ^{**}	2.8	0.98	0.875	9150	76.0	60.0	54.8	48.6	109.9	17.7	17.7

* Columns arranged in alphabetical order of notation; notation described in Appendix A; values given in SI are converted to in.-lb (1 in. = 25.4 mm; 1 psi = 1/145 MPa; and 1 kip = 4.4484 kN)

□ Specimens did not contain confining reinforcement parallel to the headed bars within the joint region

‡ Analyzed as doubly-reinforced section to calculate M_n ; all other specimens are analyzed as singly-reinforced

** Specimens contained transverse beams on one or both sides of the test beam. These transverse beams, however, did not meet the dimensional requirements of Section 18.8.4.2 of ACI 318-14 and Section 4.3 of ACI 352R-02 to be considered effective in increasing the joint shear strength.

§ Specimens had $d/\ell_{ch} > 1.5$

§§ Roof-level interior joints; all other specimens are exterior joints

Table C.2 Cont. Data for beam-column joint specimens (exterior and roof-level interior joints) tested under reversed cyclic loading *

Study	Specimen	ℓ_{dt} [#]	ℓ_{dt}/d_b	ℓ_{dy}	ℓ_{dy}/d_b	ℓ_{eh}	ℓ_{eh}/d_b	ℓ_{ehy}	ℓ_{ehy}/d_b	ℓ_{eh}/h_c	ℓ_{eh}/ℓ_{dt}	ℓ_{eh}/ℓ_{dy}	ℓ_{eh}/ℓ_{ehy}	
		(in.)		(in.)		(in.)		(in.)						
	1	2	39	40	41	42	43	44	45	46	47	48	49	50
10	Ishibashi and Inokuchi (2004) ^{§§}	2S-2	16.9	14.9	22.8	20.0	20.5	18.0	13.1	11.5	0.87	1.21	0.90	1.56
		2S-0 [□]	19.1	16.8	22.8	20.0	20.5	18.0	14.9	13.0	0.87	1.07	0.90	1.38
		WN-ST	14.4	12.6	22.4	19.6	20.5	18.0	11.8	10.3	0.87	1.42	0.92	1.74
11	Kiyohara et al. (2004)	No. 1	16.4	14.3	24.3	21.3	14.4	12.6	12.3	10.7	0.66	0.88	0.59	1.17
		No. 2	19.1	16.8	20.6	18.0	14.4	12.6	13.4	11.7	0.66	0.75	0.70	1.08
		No. 3	17.9	15.7	31.7	27.8	14.4	12.6	14.0	12.3	0.66	0.80	0.45	1.02
		No. 4	16.4	14.3	24.3	21.3	18.1	15.9	12.3	10.7	0.84	1.11	0.75	1.48
		No. 5 [§]	16.4	14.3	24.3	21.3	10.8	9.5	12.3	10.7	0.50	0.66	0.45	0.88
12	Kiyohara et al. (2005)	No. 6	32.4	28.4	39.1	34.3	14.4	12.6	22.2	19.4	0.66	0.44	0.37	0.65
		No. 7	30.3	26.6	35.8	31.4	14.4	12.6	20.8	18.3	0.66	0.47	0.40	0.69
		No. 8 [‡]	39.7	34.8	50.3	44.1	14.4	12.6	26.7	23.5	0.66	0.36	0.29	0.54
		No. 9	32.5	28.5	39.1	34.3	18.1	15.9	22.2	19.5	0.84	0.56	0.46	0.82
		No. 10 [§]	32.3	28.3	38.9	34.1	10.8	9.5	22.1	19.4	0.50	0.34	0.28	0.49
		No. 11	20.3	17.8	22.6	19.8	14.4	12.6	14.6	12.8	0.66	0.71	0.64	0.99
		No. 12	20.3	17.8	22.4	19.7	18.1	15.9	14.0	12.3	0.84	0.89	0.81	1.29
13	Kato (2005)	No. 1	13.1	15.0	13.8	15.8	14.2	16.2	8.3	9.4	0.76	1.08	1.02	1.72
		No. 2	12.3	14.0	12.3	14.0	14.2	16.2	7.7	8.8	0.76	1.16	1.16	1.83
14	Masuo et al. (2006a, 2006b)	AH12-2-45	13.3	13.6	30.9	31.6	11.8	12.0	12.3	12.6	0.66	0.88	0.38	0.95
		AH12-2-40	13.3	13.6	30.9	31.6	11.8	12.0	12.3	12.6	0.75	0.88	0.38	0.95
		AH12-2-45A [§]	13.3	13.6	30.9	31.6	9.8	10.0	12.3	12.6	0.55	0.73	0.32	0.79
		AH8-2-45	14.6	14.9	34.8	35.5	11.8	12.0	13.4	13.7	0.66	0.81	0.34	0.88
		AH12-8-45	16.2	16.5	15.6	15.9	11.8	12.0	11.2	11.4	0.66	0.73	0.75	1.05
		AH12-8-40	16.2	16.5	15.6	15.9	11.8	12.0	11.2	11.4	0.75	0.73	0.75	1.05
		AH12-8-45B	14.5	14.8	15.6	15.9	11.8	12.0	10.9	11.1	0.66	0.81	0.75	1.08
		AH8-6-45	17.1	17.5	18.0	18.3	11.8	12.0	12.1	12.3	0.66	0.69	0.65	0.97
15	Adachi and Masuo (2007)	J30-12-0	16.7	17.0	20.2	20.6	11.8	12.0	12.0	12.3	0.66	0.70	0.58	0.98
		J30-12-P1	16.7	17.0	20.2	20.6	11.8	12.0	12.0	12.3	0.66	0.70	0.58	0.98
		J30-12-P2 ^{**}	16.7	17.0	20.2	20.6	11.8	12.0	12.0	12.3	0.66	0.70	0.58	0.98
		J60-12-0	15.6	15.9	15.3	15.6	11.8	12.0	10.9	11.1	0.66	0.75	0.77	1.08
		J60-12-P1	15.6	15.9	15.3	15.6	11.8	12.0	10.9	11.1	0.66	0.75	0.77	1.08
		J60-12-P2 ^{**}	15.6	15.9	15.3	15.6	11.8	12.0	10.9	11.1	0.66	0.75	0.77	1.08

* Columns arranged in alphabetical order of notation; notation described in Appendix A; values given in SI are converted to in.-lb (1 in. = 25.4 mm; 1 psi = 1/145 MPa; and 1 kip = 4.4484 kN)

□ Specimens did not contain confining reinforcement parallel to the headed bars within the joint region

‡ Analyzed as doubly-reinforced section to calculate M_n ; all other specimens are analyzed as singly-reinforced

** Specimens contained transverse beams on one or both sides of the test beam. These transverse beams, however, did not meet the dimensional requirements of Section 18.8.4.2 of ACI 318-14 and Section 4.3 of ACI 352R-02 to be considered effective in increasing the joint shear strength.

§ Specimens had $d/\ell_{eh} > 1.5$

§§ Roof-level interior joints; all other specimens are exterior joints

ℓ_{dt} based on Eq. (5.2)

Table C.2 Cont. Data for beam-column joint specimens (exterior and roof-level interior joints) tested under reversed cyclic loading *

Study	Specimen	M_n	M_{peak}	M_{peak} / M_n	N	N_{arg}	N_{cbg}	N_{sb}	N_{sbg}	N_{splt}^\diamond	N_{total}	N_{tr}	
		(kip.in.)	(kip.in.)			(kips)	(kips)	(kips)	(kips)				
	1	2	51	52	53	54	55	56	57	58	59	60	61
10	Ishibashi and Inokuchi (2004) ^{§§}	2S-2	5740	6272	1.09	4	118.6	42.8	-	-	4	8	4
		2S-0 [□]	5740	6165	1.07	0	92.0	42.8	-	-	4	0	0
		WN-ST	5953	6272	1.05	10	246.3	43.8	-	-	4	12	10
11	Kiyohara et al. (2004)	No. 1	8500	9833	1.16	4	147.9	61.9	125.6	-	8	6	2
		No. 2	12310	11746	0.95	4	196.7	67.4	125.6	146.5	8	6	4
		No. 3	6189	6856	1.11	4	147.9	49.7	100.8	-	8	6	2
		No. 4	8500	10524	1.24	4	147.9	68.5	125.6	-	8	6	2
		No. 5 [§]	8500	8876	1.04	4	98.4	55.0	125.6	-	6	6	2
12	Kiyohara et al. (2005)	No. 6	19538	13792	0.71	4	188.9	67.5	125.6	146.5	10	6	4
		No. 7	20094	14350	0.71	4	188.9	67.5	125.6	146.5	10	6	4
		No. 8 [‡]	18015	9647	0.54	4	188.9	55.9	104.1	121.4	10	6	4
		No. 9	19529	16264	0.83	4	188.9	73.3	125.6	146.5	10	6	4
		No. 10 [§]	19575	12836	0.66	4	94.4	61.5	125.6	146.5	8	6	2
		No. 11	10265	10391	1.01	4	142.1	61.9	125.6	-	10	6	2
13	Kato (2005)	No. 1	5273	5744	1.09	4	173.6	54.7	126.6	141.6	6	16	12
		No. 2	5391	5582	1.04	4	173.6	58.2	111.1	124.2	6	16	12
14	Masuo et al. (2006a, 2006b)	AH12-2-45	3543	4032	1.14	4	95.3	35.5	81.8	-	5	8	4
		AH12-2-40	3543	3772	1.06	4	95.3	35.5	81.8	-	5	8	4
		AH12-2-45A [§]	3543	3998	1.13	4	71.5	32.8	81.8	-	5	8	2
		AH8-2-45	3480	3603	1.04	4	95.3	35.5	81.8	-	5	8	4
		AH12-8-45	7284	8064	1.11	6	168.4	39.0	110.6	123.1	6	10	6
		AH12-8-40	7284	7883	1.08	6	168.4	39.0	110.6	123.1	6	10	6
		AH12-8-45B	7284	8550	1.17	12	216.1	39.0	110.6	123.1	6	10	10
15	Adachi and Masuo (2007)	J30-12-0	3233	3490	1.08	4	72.6	31.2	73.7	-	6	8	4
		J30-12-P1	3233	3513	1.09	4	72.6	31.2	73.7	-	6	8	4
		J30-12-P2 ^{**}	3233	3569	1.10	4	72.6	40.7	-	-	6	8	4
		J60-12-0	4781	4845	1.01	4	72.6	47.9	105.3	117.2	6	8	4
		J60-12-P1	4781	5139	1.07	4	72.6	47.9	105.3	117.2	6	8	4
		J60-12-P2 ^{**}	4781	5320	1.11	4	72.6	62.5	-	-	6	8	4

* Columns arranged in alphabetical order of notation; notation described in Appendix A; values given in SI are converted to in.-lb (1 in. = 25.4 mm; 1 psi = 1/145 MPa; and 1 kip = 4.4484 kN)

□ Specimens did not contain confining reinforcement parallel to the headed bars within the joint region

‡ Analyzed as doubly-reinforced section to calculate M_n ; all other specimens are analyzed as singly-reinforced

** Specimens contained transverse beams on one or both sides of the test beam. These transverse beams, however, did not meet the dimensional requirements of Section 18.8.4.2 of ACI 318-14 and Section 4.3 of ACI 352R-02 to be considered effective in increasing the joint shear strength.

§ Specimens had $d/\ell_{ch} > 1.5$

§§ Roof-level interior joints; all other specimens are exterior joints

◇ N_{splt} is used as N in Eq. (4.6)

Table C.2 Cont. Data for beam-column joint specimens (exterior and roof-level interior joints) tested under reversed cyclic loading *

Study	Specimen	N_{tro}	n	nT' (kips)	n_{sprt}	n_{sprt}	$P/A_g f'_c$	S_h/d_b	s'_{tr} (in.)	s_{tr} (in.)	s'_{tro} (in.)	s_{tro} (in.)	s_v/d_b	T_{anc} (kips)	
	1	2	62	63	64	65	66	67	68	69	70	71	72	73	74
10	Ishibashi and Inokuchi (2004) ^{§§}	2S-2	6	3	258.1	4	8	0.00	7.4	1.8	4.8	1.8	3.5	7.4	39.5
		2S-0 [□]	6	3	253.7	0	8	0.00	7.4	0.0	0.0	1.8	3.5	7.4	30.7
		WN-ST	6	3	248.9	4	8	0.00	7.4	1.8	1.8	1.8	3.5	7.4	82.1
11	Kiyohara et al. (2004)	No. 1	4	4	476.6	4	16	0.00	5.4	3.9	5.9	2.0	3.9	-	37.0
		No. 2	4	6	589.7	4	16	0.00	5.4	2.0	3.9	2.0	3.9	3.4	32.8
		No. 3	4	3	342.3	4	16	0.00	5.5	3.9	5.9	2.0	3.9	-	49.3
		No. 4	4	4	510.1	4	16	0.00	5.4	3.9	5.9	2.0	3.9	-	37.0
		No. 5 [§]	2	4	430.2	4	16	0.00	5.4	3.9	5.9	2.0	3.9	-	24.6
12	Kiyohara et al. (2005)	No. 6	4	7	740.9	4	20	0.00	2.9	2.0	3.9	2.0	3.9	3.4	27.0
		No. 7	4	7	749.5	4	20	0.00	2.9	2.0	3.9	2.0	3.9	3.4	27.0
		No. 8 [‡]	4	7	562.0	4	20	0.00	2.9	2.0	3.9	2.0	3.9	3.4	27.0
		No. 9	4	7	874.0	4	20	0.00	2.9	2.0	3.9	2.0	3.9	3.4	27.0
		No. 10 [§]	2	7	688.2	4	20	0.00	2.9	2.0	3.9	2.0	3.9	3.4	13.5
		No. 11	4	5	506.4	4	20	0.00	2.9	3.9	5.9	2.0	3.9	-	28.4
13	Kato (2005)	No. 1	12	8	395.0	12	12	0.00	3.6	2.4	2.4	1.6	2.4	3.8	21.7
		No. 2	12	8	363.9	12	12	0.00	3.6	2.4	2.4	1.6	2.4	3.8	21.7
14	Masuo et al. (2006a, 2006b)	AH12-2-45	4	2	266.1	4	8	0.02	8.0	2.0	3.3	2.0	2.4	-	47.7
		AH12-2-40	4	2	249.0	4	8	0.02	8.0	2.0	3.3	2.0	2.4	-	47.7
		AH12-2-45A [§]	4	2	263.9	4	8	0.02	8.0	2.0	3.3	2.0	2.4	-	35.8
		AH8-2-45	4	2	242.1	4	10	0.02	8.0	2.0	3.3	2.0	2.4	-	47.7
		AH12-8-45	8	8	643.7	4	12	0.02	3.2	1.3	2.8	2.0	2.0	2.7	21.1
		AH12-8-40	8	8	629.3	4	12	0.02	3.2	1.3	2.8	2.0	2.0	2.7	21.1
		AH12-8-45B	8	8	682.5	4	12	0.02	3.2	1.3	2.8	2.0	2.0	2.7	27.0
AH8-6-45	8	6	486.1	4	12	0.02	3.2	1.3	2.8	2.0	2.0	2.7	28.1		
15	Adachi and Masuo (2007)	J30-12-0	4	4	259.2	4	12	0.06	3.2	2.0	3.3	2.4	3.1	-	18.2
		J30-12-P1	4	4	260.9	4	12	0.06	3.2	2.0	3.3	2.4	3.1	-	18.2
		J30-12-P2 ^{**}	4	4	265.0	4	12	0.06	3.2	2.0	3.3	2.4	3.1	-	18.2
		J60-12-0	4	6	365.0	4	12	0.04	3.2	1.7	2.4	2.4	3.1	2.7	12.1
		J60-12-P1	4	6	387.1	4	12	0.04	3.2	1.7	2.4	2.4	3.1	2.7	12.1
		J60-12-P2 ^{**}	4	6	400.7	4	12	0.04	3.2	1.7	2.4	2.4	3.1	2.7	12.1

* Columns arranged in alphabetical order of notation; notation described in Appendix A; values given in SI are converted to in.-lb (1 in. = 25.4 mm; 1 psi = 1/145 MPa; and 1 kip = 4.4484 kN)

□ Specimens did not contain confining reinforcement parallel to the headed bars within the joint region

‡ Analyzed as doubly-reinforced section to calculate M_n ; all other specimens are analyzed as singly-reinforced

** Specimens contained transverse beams on one or both sides of the test beam. These transverse beams, however, did not meet the dimensional requirements of Section 18.8.4.2 of ACI 318-14 and Section 4.3 of ACI 352R-02 to be considered effective in increasing the joint shear strength.

§ Specimens had $d/\ell_{ch} > 1.5$

§§ Roof-level interior joints; all other specimens are exterior joints

Table C.2 Cont. Data for beam-column joint specimens (exterior and roof-level interior joints) tested under reversed cyclic loading *

Study	Specimen	T_h	T'	T'_{mod}	T'/T_{anc}	T'/T_h	T'_{mod}/T_h	t_{obs}/d_b	V_n	$V_{n,ACI352}$	V_p	
		(kips)	(kips)	(kips)					(kips)	(kips)	(kips)	
	1	2	75	76	77	78	79	80	81	82	83	84
10	Ishibashi and Inokuchi (2004) ^{§§}	2S-2	78.7	86.0	80.6	2.18	1.09	1.02	-	321	321	312
		2S-0 [□]	78.7	84.6	80.9	2.76	1.07	1.03	-	321	321	307
		WN-ST	78.7	83.0	75.8	1.01	1.05	0.96	-	329	329	312
11	Kiyohara et al. (2004)	No. 1	103.0	119.2	117.0	3.22	1.16	1.14	2.0	563	601	430
		No. 2	103.0	98.3	97.3	3.00	0.95	0.94	2.0	563	626	514
		No. 3	103.0	114.1	113.8	2.31	1.11	1.11	2.0	452	410	300
		No. 4	103.0	127.5	121.5	3.45	1.24	1.18	2.0	563	601	460
		No. 5 [§]	91.8	107.6	-	4.37	1.17	-	2.0	563	601	388
12	Kiyohara et al. (2005)	No. 6	97.6	105.8	-	3.92	1.08	-	2.0	563	626	639
		No. 7	103.7	107.1	-	3.97	1.03	-	2.0	563	626	665
		No. 8 [‡]	81.2	80.3	-	2.98	0.99	-	2.0	466	424	447
		No. 9	122.5	124.9	-	4.63	1.02	-	2.0	563	626	754
		No. 10 [§]	74.3	98.3	-	7.29	1.32	-	2.0	563	626	595
		No. 11	98.8	101.3	-	3.56	1.03	-	2.0	563	626	455
13	Kato (2005)	No. 1	45.3	49.4	45.4	2.28	1.09	1.00	0.0	394	332	376
		No. 2	43.9	45.5	41.0	2.10	1.04	0.93	1.9	420	358	366
14	Masuo et al. (2006a, 2006b)	AH12-2-45	111.6	133.1	-	2.79	1.19	-	1.9	293	333	225
		AH12-2-40	111.6	124.5	-	2.61	1.12	-	1.9	260	296	211
		AH12-2-45A [§]	93.7	131.9	-	3.69	1.41	-	1.9	293	333	224
		AH8-2-45	103.0	121.1	-	2.54	1.18	-	1.9	293	312	201
		AH12-8-45	72.7	80.5	80.0	3.82	1.11	1.10	1.9	293	359	485
		AH12-8-40	72.7	78.7	78.2	3.74	1.08	1.08	1.9	260	319	474
		AH12-8-45B	72.7	85.3	84.6	3.16	1.17	1.16	1.9	293	359	515
		AH8-6-45	70.8	81.0	-	2.89	1.14	-	1.9	293	336	379
15	Adachi and Masuo (2007)	J30-12-0	58.7	64.8	-	3.57	1.10	-	1.9	252	224	259
		J30-12-P1	58.7	65.2	-	3.59	1.11	-	1.9	252	224	261
		J30-12-P2 ^{**}	58.7	66.3	-	3.65	1.13	-	1.9	252	224	265
		J60-12-0	60.0	60.8	60.2	5.02	1.01	1.00	1.9	360	320	276
		J60-12-P1	60.0	64.5	63.9	5.33	1.07	1.07	1.9	360	320	293
		J60-12-P2 ^{**}	60.0	66.8	66.2	5.52	1.11	1.10	1.9	360	320	304

* Columns arranged in alphabetical order of notation; notation described in Appendix A; values given in SI are converted to in.-lb (1 in. = 25.4 mm; 1 psi = 1/145 MPa; and 1 kip = 4.4484 kN)

□ Specimens did not contain confining reinforcement parallel to the headed bars within the joint region

‡ Analyzed as doubly-reinforced section to calculate M_n ; all other specimens are analyzed as singly-reinforced

** Specimens contained transverse beams on one or both sides of the test beam. These transverse beams, however, did not meet the dimensional requirements of Section 18.8.4.2 of ACI 318-14 and Section 4.3 of ACI 352R-02 to be considered effective in increasing the joint shear strength.

§ Specimens had $d/\ell_{ch} > 1.5$

§§ Roof-level interior joints; all other specimens are exterior joints

Table C.2 Cont. Data for beam-column joint specimens (exterior and roof-level interior joints) tested under reversed cyclic loading *

Study		Specimen	V_p / V_n	$\delta_{0.8peak}$	δ_y	Υ_j	$\Psi_{cs}^{##}$	Ψ_o
	1	2	85	86	87	88	89	90
10	Ishibashi and Inokuchi (2004) ^{§§}	2S-2	0.97	0.030	0.010	0.004	0.49	1.25
		2S-0 [□]	0.96	0.030	0.010	0.003	0.55	1.25
		WN-ST	0.95	0.030	0.010	0.005	0.42	1.25
11	Kiyohara et al. (2004)	No. 1	0.76	0.040	0.017	0.018	0.57	1.00
		No. 2	0.91	0.040	0.017	0.018	0.74	1.00
		No. 3	0.66	0.040	0.013	0.011	0.51	1.00
		No. 4	0.82	0.080	0.017	0.008	0.57	1.00
		No. 5 [§]	0.69	0.033	0.015	0.018	0.57	1.00
12	Kiyohara et al. (2005)	No. 6	1.14	0.040	0.040	0.012	0.79	1.00
		No. 7	1.18	0.040	0.040	0.013	0.79	1.00
		No. 8 [‡]	0.96	0.040	0.040	0.017	0.79	1.00
		No. 9	1.34	0.040	0.040	0.012	0.79	1.00
		No. 10 [§]	1.06	0.040	0.040	0.013	0.79	1.00
		No. 11	0.81	0.040	0.018	0.014	0.74	1.00
13	Kato (2005)	No. 1	0.95	0.040	0.013	-	0.82	1.00
		No. 2	0.87	0.080	0.110	-	0.82	1.00
14	Masuo et al. (2006a, 2006b)	AH12-2-45	0.77	0.030	0.013	-	0.44	1.00
		AH12-2-40	0.81	0.028	0.019	-	0.44	1.00
		AH12-2-45A [§]	0.76	0.030	0.016	-	0.44	1.00
		AH8-2-45	0.69	0.030	0.020	-	0.44	1.00
		AH12-8-45	1.66	0.040	0.010	-	0.85	1.00
		AH12-8-40	1.82	0.040	0.012	-	0.85	1.00
		AH12-8-45B	1.76	0.040	0.012	-	0.76	1.00
AH8-6-45	1.29	0.040	0.012	-	0.82	1.00		
15	Adachi and Masuo (2007)	J30-12-0	1.03	0.320	-	-	0.74	1.00
		J30-12-P1	1.03	0.045	-	-	0.74	1.00
		J30-12-P2 ^{**}	1.05	0.062	-	-	0.74	1.00
		J60-12-0	0.77	0.033	-	-	0.83	1.00
		J60-12-P1	0.81	0.034	-	-	0.83	1.00
		J60-12-P2 ^{**}	0.84	0.067	-	-	0.83	1.00

* Columns arranged in alphabetical order of notation; notation described in Appendix A; values given in SI are converted to in.-lb (1 in. = 25.4 mm; 1 psi = 1/145 MPa; and 1 kip = 4.4484 kN)

□ Specimens did not contain confining reinforcement parallel to the headed bars within the joint region

‡ Analyzed as doubly-reinforced section to calculate M_n ; all other specimens are analyzed as singly-reinforced

** Specimens contained transverse beams on one or both sides of the test beam. These transverse beams, however, did not meet the dimensional requirements of Section 18.8.4.2 of ACI 318-14 and Section 4.3 of ACI 352R-02 to be considered effective in increasing the joint shear strength.

§ Specimens had $d/\ell_{ch} > 1.5$

§§ Roof-level interior joints; all other specimens are exterior joints

Ψ_{cs} is based on Table 5.1

Table C.2 Cont. Data for beam-column joint specimens (exterior and roof-level interior joints) tested under reversed cyclic loading *

Study	Specimen	Bar Size **	A_b	A_{brg} / A_b	A_{gross} / A_b	A_{hs}	A_{nc}	A_{obs} / A_b	A_{tr}	$A_{tr,l}$	$A_{tro,l}$	A_{tt}	A_{tt} / A_{hs}	
			(in. ²)			(in. ²)	(in. ²)		(in. ²)	(in. ²)	(in. ²)	(in. ²)		
1	2	3	4	5	6	7	8	9	10	11	12	13	14	
16	Chun et al. (2007)	JM-1 [∞]	D22	0.60	2.9	3.9	2.40	1162	2.2	0.60	0.11	0.11	0.22	0.09
		JM-2 [∞]	D22	0.60	2.9	3.9	4.80	1206	2.2	0.60	0.11	0.11	0.22	0.05
		WM ^{□,∞}	D32	1.27	2.9	3.9	6.35	1788	2.2	1.27	0.11	0.11	0.00	0.00
		JM-No.11-1a	D36	1.56	2.7	4.9	4.68	1331	2.2	1.56	0.20	0.20	1.20	0.26
		JM-No.11-1b	D36	1.56	2.7	4.9	4.68	1331	2.2	1.56	0.20	0.20	1.20	0.26
17	Ishida et al. (2007)	P1 ^{‡‡}	D22	0.60	-	-	4.20	562	-	0.79	0.11	0.11	0.89	0.21
		P2 ^{‡‡}	D22	0.60	-	-	4.20	562	-	0.79	0.11	0.11	0.89	0.21
		P3 ^{‡‡}	D22	0.60	-	-	4.20	562	-	0.79	0.11	0.11	0.89	0.21
		P4 ^{‡‡}	D22	0.60	-	-	5.40	562	-	0.79	0.11	0.11	0.89	0.16
18	Tazaki et al. (2007)	E1	D16	0.31	6.9	7.9	1.85	379	-	0.44	0.05	0.04	0.20	0.11
		E2 [§]	D16	0.31	6.9	7.9	1.85	240	-	0.44	0.05	0.04	0.10	0.05
19	Lee and Yu (2009)	W0-M1	D22	0.60	3.2	6.1	2.40	868	2.9	0.60	0.11	0.11	0.33	0.14
		W150-M1	D22	0.60	3.2	6.1	2.40	868	2.9	0.60	0.11	0.11	0.33	0.14
		W0-M2	D22	0.60	3.2	6.1	2.40	868	2.9	0.60	0.11	0.11	0.33	0.14
		W150-M2	D22	0.60	3.2	6.1	2.40	868	2.9	0.60	0.11	0.11	0.33	0.14
20	Kang et al. (2010)	JD [§]	D19	0.44	2.6	3.6	1.77	598	-	0.79	0.11	0.11	0.44	0.25
21	Kang et al. (2012)	JH-R1	D19	0.44	5.3	6.3	1.76	505	-	0.44	0.11	0.11	0.33	0.19
		JH-R2	D19	0.44	5.3	6.3	1.76	531	-	0.44	0.11	0.11	0.33	0.19
22	Chun and Shin (2014) [∞]	M0.7S [‡]	D16	0.44	4.0	5.0	1.76	324	-	0.71	0.17	0.20	0.51	0.29
		M1.0S	D16	0.44	4.0	5.0	1.76	324	-	0.71	0.20	0.20	1.02	0.58
		M1.5S [§]	D16	0.44	4.0	5.0	1.76	324	-	0.71	0.20	0.20	1.02	0.58
		M2.0S [§]	D16	0.44	4.0	5.0	1.76	324	-	0.71	0.20	0.20	1.02	0.58
		M2.5S [§]	D16	0.44	4.0	5.0	1.76	324	-	0.71	0.20	0.20	1.02	0.58
		M0.7U [‡]	D16	0.44	4.0	5.0	1.76	324	-	0.71	0.11	0.20	0.33	0.19
		M1.0U	D16	0.44	4.0	5.0	1.76	324	-	0.71	0.11	0.20	0.66	0.38
23	Dhake et al. (2015)	J4 [□]	D12	0.18	4.0	5.0	0.35	105	-	0.35	0.05	0.05	0.00	0.00
		J5 [□]	D12	0.18	4.0	5.0	0.35	71	-	0.35	0.05	0.05	0.00	0.00
		J9	D12	0.18	4.0	5.0	0.35	105	-	0.35	0.05	0.05	0.20	0.56

* Columns arranged in alphabetical order of notation; notation described in Appendix A; values given in SI are converted to in.-lb (1 in. = 25.4 mm; 1 psi = 1/145 MPa; and 1 kip = 4.4484 kN)

** Bar sizes are presented in SI as reported in the original studies (only Wallace et al. 1998 had bar sizes reported in in.-lb)

□ Specimens did not contain confining reinforcement parallel to the headed bars within the joint region

∞ Heads contained obstruction with diameter d_{obs} of $1.5d_b$ and length $l_{obs} \leq 0.6d_b$ for \geq No.8 (D25) bars or \leq smaller of 0.6 in. and $0.75d_b$ for $<$ No.8 (D25) bars (also see Section 5.1.7). Therefore, the obstruction is not considered to detract from the net bearing area of the head.

‡ Analyzed as doubly-reinforced section to calculate M_n ; all other specimens are analyzed as singly-reinforced

‡‡ Specimens contained transverse beams on one or both sides of the test beam. These transverse beams, however, did not meet the dimensional requirements of Section 18.8.4.2 of ACI 318-14 and Section 4.3 of ACI 352R-02 to be considered effective in increasing the joint shear strength.

§ Specimens had $d/\ell_{ch} > 1.5$

Table C.2 Cont. Data for beam-column joint specimens (exterior and roof-level interior joints) tested under reversed cyclic loading *

Study	Specimen	A_v	b_b	b_c	b_j	$b_{j,ACI}$	c_{ch}	c_{ch}/d_b	c_o	c_{ol}/d_b	c_{so}	c_{sol}/d_b	d	d/ℓ_{eh}	
		(in. ²)	(in.)	(in.)	(in.)	(in.)	(in.)	(in.)	(in.)	(in.)	(in.)	(in.)	(in.)	(in.)	
1	2	15	16	17	18	19	20	21	22	23	24	25	26	27	
16	Chun et al. (2007)	JM-1 [∞]	0.44	13.8	26	25.6	18.7	3.0	3.4	4.9	5.6	5.3	6.1	17.3	1.1
		JM-2 [∞]	0.44	13.8	26	25.6	18.7	1.7	2.0	4.6	5.2	5.0	5.7	16.8	1.1
		WM ^{□,∞}	0.00	31.5	31	31.5	31.5	6.6	5.2	3.4	2.7	4.0	3.1	13.1	0.7
		JM-No.11-1a	1.20	17.7	26	25.6	21.7	5.9	4.2	3.9	2.8	4.8	3.4	17.1	1.0
		JM-No.11-1b	1.20	17.7	26	25.6	21.7	5.9	4.2	3.9	2.8	4.8	3.4	17.1	1.0
17	Ishida et al. (2007)	P1 ^{**}	1.33	31.5	16	15.7	15.7	3.9	4.5	-	-	1.3	1.5	13.7	1.2
		P2 ^{**}	1.33	31.5	16	15.7	15.7	3.9	4.5	-	-	1.3	1.5	13.7	1.2
		P3 ^{**}	1.33	31.5	16	15.7	15.7	3.9	4.5	-	-	1.3	1.5	13.7	1.2
		P4 ^{**}	1.33	39.5	16	15.7	15.7	3.9	4.5	-	-	1.3	1.5	13.7	1.2
18	Tazaki et al. (2007)	E1	0.29	11.8	12	11.8	11.8	1.6	2.5	0.5	0.8	1.1	1.7	10.0	1.0
		E2 [§]	0.29	11.8	12	11.8	11.8	1.6	2.5	0.5	0.8	1.1	1.7	10.0	1.6
19	Lee and Yu (2009)	W0-M1	0.99	12.0	24	24.0	16.0	2.0	2.2	8.0	9.2	8.7	9.9	16.0	1.3
		W150-M1	0.99	12.0	24	12.0	14.4	2.0	2.2	2.0	2.3	2.6	3.0	16.0	1.3
		W0-M2	0.99	12.0	24	24.0	16.0	2.0	2.2	8.0	9.2	8.7	9.9	16.0	1.3
		W150-M2	0.99	12.0	24	12.0	14.4	2.0	2.2	2.0	2.3	2.6	3.0	16.0	1.3
20	Kang et al. (2010)	JD [§]	1.32	17.7	18	17.7	17.7	3.9	5.2	2.4	3.2	2.7	3.6	19.8	1.8
21	Kang et al. (2012)	JH-R1	0.99	10.0	15	15.0	12.5	2.3	3.1	0.6	0.8	1.2	1.6	14.4	1.3
		JH-R2	0.99	10.0	15	15.0	12.5	1.7	2.3	0.6	0.8	1.2	1.6	13.6	1.2
22	Chun and Shin (2014) [∞]	M0.7S [‡]	0.43	9.8	12	12.0	10.9	1.7	2.3	2.5	3.3	3.0	3.9	5.9	0.7
		M1.0S	1.56	9.8	12	12.0	10.9	1.7	2.3	2.5	3.3	3.0	3.9	9.8	1.1
		M1.5S [§]	2.60	9.8	12	12.0	10.9	1.7	2.3	2.5	3.3	3.0	3.9	15.7	1.7
		M2.0S [§]	3.64	9.8	12	12.0	10.9	1.7	2.3	2.5	3.3	3.0	3.9	21.6	2.4
		M2.5S [§]	4.68	9.8	12	12.0	10.9	1.7	2.3	2.5	3.3	3.0	3.9	27.5	3.1
		M0.7U [‡]	0.33	9.8	12	12.0	10.9	1.7	2.3	2.5	3.3	3.0	3.9	5.9	0.7
		M1.0U	0.99	9.8	12	12.0	10.9	1.7	2.3	2.5	3.3	3.0	3.9	9.8	1.1
23	Dhake et al. (2015)	J4 [□]	0.00	5.9	6	5.9	5.9	3.5	7.5	0.7	1.4	0.9	2.0	5.9	1.0
		J5 [□]	0.00	5.9	6	5.9	5.9	3.5	7.5	0.7	1.4	0.9	2.0	5.9	1.5
		J9	0.29	5.9	6	5.9	5.9	3.5	7.5	0.7	1.4	0.9	2.0	5.9	1.0

* Columns arranged in alphabetical order of notation; notation described in Appendix A; values given in SI are converted to in.-lb (1 in. = 25.4 mm; 1 psi = 1/145 MPa; and 1 kip = 4.4484 kN)

□ Specimens did not contain confining reinforcement parallel to the headed bars within the joint region

∞ Heads contained obstruction with diameter d_{obs} of $1.5d_b$ and length $t_{obs} \leq 0.6d_b$ for \geq No.8 (D25) bars or \leq smaller of 0.6 in. and $0.75d_b$ for $<$ No.8 (D25) bars (also see Section 5.1.7). Therefore, the obstruction is not considered to detract from the net bearing area of the head.

‡ Analyzed as doubly-reinforced section to calculate M_n ; all other specimens are analyzed as singly-reinforced

** Specimens contained transverse beams on one or both sides of the test beam. These transverse beams, however, did not meet the dimensional requirements of Section 18.8.4.2 of ACI 318-14 and Section 4.3 of ACI 352R-02 to be considered effective in increasing the joint shear strength.

§ Specimens had $d/\ell_{eh} > 1.5$

Table C.2 Cont. Data for beam-column joint specimens (exterior and roof-level interior joints) tested under reversed cyclic loading *

Study	Specimen	d' (in.)	d_b (in.)	$d_{b,sprt}$ (in.)	f_{cm} (psi)	f_y (ksi)	$f_{y,sprt}$ (ksi)	f_{yt} (ksi)	$f_{yt}A_v$ (kips)	f_{yto} (ksi)	h_b (in.)	h_c (in.)	
1	2	28	29	30	31	32	33	34	35	36	37	38	
16	Chun et al. (2007)	JM-1 [∞]	2.4	0.875	0.875	8950	58.4	58.4	55.7	24.5	55.7	19.7	19.7
		JM-2 [∞]	2.4	0.875	0.875	8720	58.4	58.4	55.7	24.5	55.7	19.7	19.7
		WM ^{□,∞}	2.6	1.27	1.27	8180	62.5	62.5	0.0	0.0	55.7	15.7	23.6
		JM-No.11-1a	2.8	1.41	1.41	4760	66.4	66.4	72.5	87.0	72.5	19.9	20.5
		JM-No.11-1b	2.8	1.41	1.41	4760	66.4	66.4	72.5	87.0	72.5	19.9	20.5
17	Ishida et al. (2007)	P1 ^{**}	2.0	0.875	1	3480	76.0	76.0	113.8	151.2	113.8	15.7	15.7
		P2 ^{**}	2.0	0.875	1	3480	76.0	76.0	113.8	151.2	113.8	15.7	15.7
		P3 ^{**}	2.0	0.875	1	3480	76.0	76.0	113.8	151.2	113.8	15.7	15.7
		P4 ^{**}	2.0	0.875	1	3480	76.0	76.0	113.8	151.2	113.8	15.7	15.7
18	Tazaki et al. (2007)	E1	1.9	0.625	0.625	4410	55.0	55.0	53.1	15.6	53.1	11.8	11.8
		E2 [§]	1.9	0.625	0.625	4410	55.0	55.0	53.1	15.6	53.1	11.8	11.8
19	Lee and Yu (2009)	W0-M1	2.0	0.875	0.875	4450	68.6	68.6	68.0	67.3	68.0	18.0	16.0
		W150-M1	2.0	0.875	0.875	5190	68.6	68.6	68.0	67.3	68.0	18.0	16.0
		W0-M2	2.0	0.875	0.875	4450	68.6	68.6	68.0	67.3	68.0	18.0	16.0
		W150-M2	2.0	0.875	0.875	5190	68.6	68.6	68.0	67.3	68.0	18.0	16.0
20	Kang et al. (2010)	JD [§]	1.5	0.75	1	4220	69.8	59.0	83.0	109.6	83.0	21.3	17.7
21	Kang et al. (2012)	JH-R1	1.5	0.75	0.75	4360	69.5	69.5	69.5	68.8	69.5	15.9	15.0
		JH-R2	2.7	0.75	0.75	4360	69.5	69.5	69.5	68.8	69.5	15.9	15.0
22	Chun and Shin (2014) [∞]	M0.7S [‡]	2.5	0.75	0.875	3710	70.8	66.8	66.7	28.9	66.7	7.9	12.0
		M1.0S	2.5	0.75	0.875	3710	70.8	66.8	66.7	104.1	66.7	11.8	12.0
		M1.5S [§]	2.5	0.75	0.875	3480	70.8	66.8	66.7	173.5	66.7	17.7	12.0
		M2.0S [§]	2.5	0.75	0.875	3830	70.8	66.8	66.7	242.9	66.7	23.6	12.0
		M2.5S [§]	2.5	0.75	0.875	3830	70.8	66.8	66.7	312.3	66.7	29.5	12.0
		M0.7U [‡]	2.5	0.75	0.875	3710	70.8	66.8	62.4	20.6	62.4	7.9	12.0
		M1.0U	2.5	0.75	0.875	3710	70.8	66.8	62.4	61.8	62.4	11.8	12.0
23	Dhake et al. (2015)	J4 [□]	1.2	0.47	0.472	4350	76.1	76.1	0.0	0.0	0.0	7.1	7.9
		J5 [□]	1.2	0.47	0.472	4350	76.1	76.1	0.0	0.0	0.0	7.1	7.9
		J9	1.2	0.47	0.472	4350	76.1	76.1	73.6	21.7	73.6	7.1	7.9

* Columns arranged in alphabetical order of notation; notation described in Appendix A; values given in SI are converted to in.-lb (1 in. = 25.4 mm; 1 psi = 1/145 MPa; and 1 kip = 4.4484 kN)

□ Specimens did not contain confining reinforcement parallel to the headed bars within the joint region

∞ Heads contained obstruction with diameter d_{obs} of $1.5d_b$ and length $l_{obs} \leq 0.6d_b$ for \geq No.8 (D25) bars or \leq smaller of 0.6 in. and $0.75d_b$ for $<$ No.8 (D25) bars (also see Section 5.1.7). Therefore, the obstruction is not considered to detract from the net bearing area of the head.

‡ Analyzed as doubly-reinforced section to calculate M_n ; all other specimens are analyzed as singly-reinforced

** Specimens contained transverse beams on one or both sides of the test beam. These transverse beams, however, did not meet the dimensional requirements of Section 18.8.4.2 of ACI 318-14 and Section 4.3 of ACI 352R-02 to be considered effective in increasing the joint shear strength.

§ Specimens had $d/\ell_{eh} > 1.5$

Table C.2 Cont. Data for beam-column joint specimens (exterior and roof-level interior joints) tested under reversed cyclic loading *

Study	Specimen	$\ell_{dt}^{\#}$ (in.)	ℓ_{dt}/d_b	ℓ_{dy} (in.)	ℓ_{dy}/d_b	ℓ_{eh} (in.)	ℓ_{eh}/d_b	ℓ_{ehy} (in.)	ℓ_{ehy}/d_b	ℓ_{eh}/h_c	ℓ_{eh}/ℓ_{dt}	ℓ_{eh}/ℓ_{dy}	ℓ_{eh}/ℓ_{ehy}	
1	2	39	40	41	42	43	44	45	46	47	48	49	50	
16	Chun et al. (2007)	JM-1 [∞]	9.6	11.0	8.6	9.9	15.1	17.3	6.3	7.2	0.77	1.58	1.76	2.41
		JM-2 [∞]	11.6	13.3	10.0	11.4	15.1	17.3	7.4	8.4	0.77	1.30	1.52	2.05
		WM ^{□,∞}	17.3	13.6	14.9	11.7	18.9	14.9	12.8	10.1	0.80	1.09	1.27	1.48
		JM-No.11-1a	19.0	13.5	23.1	16.4	17.3	12.3	14.1	10.0	0.85	0.91	0.75	1.23
		JM-No.11-1b	19.0	13.5	23.1	16.4	17.3	12.3	14.1	10.0	0.85	0.91	0.75	1.23
17	Ishida et al. (2007)	P1 ^{**}	15.1	17.3	19.8	22.6	11.9	13.6	11.2	12.9	0.76	0.79	0.60	1.06
		P2 ^{**}	15.1	17.3	19.8	22.6	11.9	13.6	11.2	12.9	0.76	0.79	0.60	1.06
		P3 ^{**}	15.1	17.3	19.8	22.6	11.9	13.6	11.2	12.9	0.76	0.79	0.60	1.06
		P4 ^{**}	16.2	18.5	19.8	22.6	11.9	13.6	11.5	13.1	0.76	0.73	0.60	1.04
18	Tazaki et al. (2007)	E1	8.6	13.7	11.1	17.7	10.2	16.3	5.6	8.9	0.86	1.18	0.92	1.82
		E2 [§]	9.3	14.8	11.6	18.6	6.3	10.0	5.7	9.1	0.53	0.68	0.54	1.10
19	Lee and Yu (2009)	W0-M1	13.8	15.8	21.4	24.4	12.1	13.8	9.5	10.8	0.75	0.87	0.56	1.27
		W150-M1	13.3	15.2	19.5	22.3	12.1	13.8	9.1	10.5	0.75	0.91	0.62	1.32
		W0-M2	13.8	15.8	21.4	24.4	12.1	13.8	9.5	10.8	0.75	0.87	0.56	1.27
		W150-M2	13.3	15.2	19.5	22.3	12.1	13.8	9.1	10.5	0.75	0.91	0.62	1.32
20	Kang et al. (2010)	JD [§]	7.5	10.0	13.9	18.5	11.3	15.0	5.7	7.6	0.64	1.50	0.81	1.98
21	Kang et al. (2012)	JH-R1	12.0	16.0	14.8	19.7	11.3	15.0	8.7	11.5	0.75	0.94	0.76	1.30
		JH-R2	12.7	17.0	17.1	22.8	11.3	15.0	9.3	12.4	0.75	0.88	0.66	1.21
22	Chun and Shin (2014) [∞]	M0.7S [‡]	8.9	11.8	14.9	19.9	9.0	12.0	7.5	10.0	0.75	1.01	0.60	1.20
		M1.0S	8.7	11.6	14.9	19.9	9.0	12.0	7.5	10.0	0.75	1.04	0.60	1.20
		M1.5S [§]	8.8	11.8	15.3	20.4	9.0	12.0	7.6	10.1	0.75	1.02	0.59	1.18
		M2.0S [§]	8.6	11.5	14.7	19.7	9.0	12.0	7.4	9.9	0.75	1.04	0.61	1.21
		M2.5S [§]	8.6	11.5	14.7	19.7	9.0	12.0	7.4	9.9	0.75	1.04	0.61	1.21
		M0.7U [‡]	10.8	14.4	14.9	19.9	9.0	12.0	7.8	10.4	0.75	0.83	0.60	1.15
		M1.0U	8.7	11.6	14.9	19.9	9.0	12.0	7.5	10.0	0.75	1.04	0.60	1.20
23	Dhake et al. (2015)	J4 [□]	5.2	10.9	9.9	20.9	5.9	12.5	3.7	7.8	0.75	1.15	0.60	1.61
		J5 [□]	5.2	10.9	9.9	20.9	4.0	8.5	3.7	7.8	0.51	0.78	0.41	1.09
		J9	4.0	8.4	9.9	20.9	5.9	12.5	3.3	7.0	0.75	1.49	0.60	1.79

* Columns arranged in alphabetical order of notation; notation described in Appendix A; values given in SI are converted to in.-lb (1 in. = 25.4 mm; 1 psi = 1/145 MPa; and 1 kip = 4.4484 kN)

□ Specimens did not contain confining reinforcement parallel to the headed bars within the joint region

∞ Heads contained obstruction with diameter d_{obs} of $1.5d_b$ and length $t_{obs} \leq 0.6d_b$ for \geq No.8 (D25) bars or \leq smaller of 0.6 in. and $0.75d_b$ for $<$ No.8 (D25) bars (also see Section 5.1.7). Therefore, the obstruction is not considered to detract from the net bearing area of the head.

‡ Analyzed as doubly-reinforced section to calculate M_n ; all other specimens are analyzed as singly-reinforced

** Specimens contained transverse beams on one or both sides of the test beam. These transverse beams, however, did not meet the dimensional requirements of Section 18.8.4.2 of ACI 318-14 and Section 4.3 of ACI 352R-02 to be considered effective in increasing the joint shear strength.

§ Specimens had $d/\ell_{eh} > 1.5$

ℓ_{dt} based on Eq. (5.2)

Table C.2 Cont. Data for beam-column joint specimens (exterior and roof-level interior joints) tested under reversed cyclic loading *

Study	Specimen	M_n	M_{peak}	M_{peak}/M_n	N	N_{arg}	N_{cbg}	N_{sb}	N_{sbg}	N_{spl}^\diamond	N_{total}	N_{tr}	
		(kip.in.)	(kip.in.)			(kips)	(kips)	(kips)	(kips)				
	1	2	51	52	53	54	55	56	57	58	59	60	61
16	Chun et al. (2007)	JM-1 [∞]	2358	2965	1.26	2	30.6	73.1	88.3	-	9	4	2
		JM-2 [∞]	4396	5036	1.15	2	30.6	74.5	81.9	86.2	9	4	2
		WM ^{□,∞}	4859	5558	1.14	0	-	92.8	98.6	-	5	0	0
		JM-No.11-1a	4637	4894	1.06	6	101.5	56.1	124.6	-	6	6	4
		JM-No.11-1b	4637	4779	1.03	6	101.5	56.1	124.6	-	6	6	4
17	Ishida et al. (2007)	P1 ^{**}	3842	3950	1.03	8	201.0	32.0	-	-	8	12	8
		P2 ^{**}	3842	4001	1.04	8	201.0	32.0	-	-	8	12	8
		P3 ^{**}	3842	4399	1.14	8	201.0	32.0	-	-	8	12	8
		P4 ^{**}	4919	4681	0.95	8	201.0	32.0	-	-	8	12	8
18	Tazaki et al. (2007)	E1	901	1084	1.20	4	25.0	19.1	21.3	25.4	4	6	6
		E2 [§]	901	951	1.06	2	15.1	15.8	21.3	25.4	2	6	4
19	Lee and Yu (2009)	W0-M1	2336	2769	1.19	3	97.2	47.3	-	-	3	9	3
		W150-M1	2378	2805	1.18	3	59.8	45.1	48.9	-	3	9	3
		W0-M2	2378	2805	1.18	3	59.8	47.3	-	-	3	9	3
		W150-M2	2378	2909	1.22	3	59.8	45.1	48.9	-	3	9	3
20	Kang et al. (2010)	JD [§]	2313	2697	1.17	4	45.7	29.1	34.3	-	6	12	2
21	Kang et al. (2012)	JH-R1	1566	1885	1.20	3	68.8	24.1	25.1	-	5	9	3
		JH-R2	1458	1708	1.17	3	68.8	25.4	25.1	29.7	5	9	3
22	Chun and Shin (2014) [∞]	M0.7S [‡]	540	564	1.04	3	68.0	17.0	43.0	-	5	3	6
		M1.0S	970	1068	1.10	5	68.0	17.0	43.0	-	5	8	6
		M1.5S [§]	1689	1872	1.11	5	68.0	16.4	41.7	-	5	13	6
		M2.0S [§]	2448	2580	1.05	5	68.0	17.2	43.7	-	5	18	6
		M2.5S [§]	3183	3264	1.03	5	68.0	17.2	43.7	-	5	23	6
		M0.7U [‡]	540	576	1.07	3	41.2	17.0	43.0	-	5	3	6
		M1.0U	970	1140	1.18	6	41.2	17.0	43.0	-	5	9	6
23	Dhake et al. (2015)	J4 [□]	144	180	1.25	0	-	7.0	10.4	-	2	0	0
		J5 [□]	144	157	1.09	0	-	5.9	10.4	-	2	0	0
		J9	144	203	1.41	4	14.4	7.0	10.4	-	2	6	4

* Columns arranged in alphabetical order of notation; notation described in Appendix A; values given in SI are converted to in.-lb (1 in. = 25.4 mm; 1 psi = 1/145 MPa; and 1 kip = 4.4484 kN)

□ Specimens did not contain confining reinforcement parallel to the headed bars within the joint region

∞ Heads contained obstruction with diameter d_{obs} of $1.5d_b$ and length $t_{obs} \leq 0.6d_b$ for \geq No.8 (D25) bars or \leq smaller of 0.6 in. and $0.75d_b$ for $<$ No.8 (D25) bars (also see Section 5.1.7). Therefore, the obstruction is not considered to detract from the net bearing area of the head.

‡ Analyzed as doubly-reinforced section to calculate M_n ; all other specimens are analyzed as singly-reinforced

** Specimens contained transverse beams on one or both sides of the test beam. These transverse beams, however, did not meet the dimensional requirements of Section 18.8.4.2 of ACI 318-14 and Section 4.3 of ACI 352R-02 to be considered effective in increasing the joint shear strength.

§ Specimens had $d/\ell_{ch} > 1.5$

◇ N_{spl} is used as N in Eq. (4.6)

Table C.2 Cont. Data for beam-column joint specimens (exterior and roof-level interior joints) tested under reversed cyclic loading *

Study	Specimen	N_{tro}	n	nT' (kips)	$n_{l,sprt}$	n_{sprt}	$P/A_g f'_c$	s_h/d_b	s'_{tr} (in.)	s_{tr} (in.)	s'_{tro} (in.)	s_{tro} (in.)	s_v/d_b	T_{anc} (kips)	
	1	2	62	63	64	65	66	67	68	69	70	71	72	73	74
16	Chun et al. (2007)	JM-1 [∞]	3	4	178.4	4	16	0.05	3.4	4.5	5.9	5.4	5.9	-	18.3
		JM-2 [∞]	3	8	325.4	4	16	0.05	3.4	2.8	5.9	5.4	5.9	2.0	9.3
		WM ^{□,∞}	0	5	453.9	0	8	0.05	5.2	0.0	0.0	5.9	11.8	-	18.6
		JM-No.11-1a	3	3	328.0	4	10	0.00	4.2	2.4	4.7	6.0	4.7	-	33.8
		JM-No.11-1b	3	3	320.3	4	10	0.00	4.2	2.4	4.7	6.0	4.7	-	33.8
17	Ishida et al. (2007)	P1 ^{**}	8	7	328.2	8	12	0.12	4.5	2.0	3.9	2.0	3.9	-	28.7
		P2 ^{**}	8	7	332.4	8	12	0.12	4.5	2.0	3.9	2.0	3.9	-	28.7
		P3 ^{**}	8	7	365.5	8	12	0.12	4.5	2.0	3.9	2.0	3.9	-	28.7
		P4 ^{**}	8	9	390.5	8	12	0.12	4.5	2.0	3.9	2.0	3.9	-	22.3
18	Tazaki et al. (2007)	E1	4	6	122.3	4	16	0.08	4.0	0.9	2.0	1.4	2.0	2.5	4.2
		E2 [§]	2	6	107.3	4	16	0.08	4.0	0.9	2.0	1.4	2.0	2.5	2.6
19	Lee and Yu (2009)	W0-M1	10	4	195.2	12	12	0.10	2.2	3.0	4.0	1.5	4.0	-	24.3
		W150-M1	5	4	194.2	12	12	0.10	2.2	3.0	4.0	1.5	5.0	-	15.0
		W0-M2	5	4	194.2	12	12	0.10	2.2	3.0	4.0	1.5	6.0	-	15.0
		W150-M2	5	4	201.4	12	12	0.10	2.2	3.0	4.0	1.5	7.0	-	15.0
20	Kang et al. (2010)	JD [§]	3	4	143.7	8	12	0.00	5.2	1.2	4.7	1.5	5.9	-	11.4
21	Kang et al. (2012)	JH-R1	6	4	147.1	8	8	0.00	3.1	2.2	3.5	1.3	3.5	-	17.2
		JH-R2	6	4	143.2	8	8	0.00	3.1	2.2	3.5	1.3	3.5	2.3	14.9
22	Chun and Shin (2014) [∞]	M0.7S [‡]	0	4	130.1	6	8	0.00	2.3	1.1	3.0	4.9	6.0	-	17.0
		M1.0S	0	4	137.2	6	8	0.00	2.3	1.1	3.0	4.9	6.0	-	17.0
		M1.5S [§]	0	4	138.1	6	8	0.00	2.3	1.1	3.0	4.9	6.0	-	17.0
		M2.0S [§]	0	4	131.3	6	8	0.00	2.3	1.1	3.0	4.9	6.0	-	17.0
		M2.5S [§]	0	4	127.8	6	8	0.00	2.3	1.1	3.0	4.9	6.0	-	17.0
		M0.7U [‡]	0	4	132.9	6	8	0.00	2.3	1.1	3.0	4.9	6.0	-	10.3
		M1.0U	0	4	146.4	6	8	0.00	2.3	1.1	3.0	4.9	6.0	-	10.3
23	Dhake et al. (2015)	J4 [□]	0	2	33.3	0	4	0.20	7.5	0.0	0.0	3.1	3.9	-	3.5
		J5 [□]	0	2	29.1	0	4	0.20	7.5	0.0	0.0	3.1	3.9	-	3.0
		J9	0	2	37.7	4	4	0.20	7.5	0.4	2.6	3.1	3.9	-	7.2

* Columns arranged in alphabetical order of notation; notation described in Appendix A; values given in SI are converted to in.-lb (1 in. = 25.4 mm; 1 psi = 1/145 MPa; and 1 kip = 4.4484 kN)

□ Specimens did not contain confining reinforcement parallel to the headed bars within the joint region

∞ Heads contained obstruction with diameter d_{obs} of $1.5d_b$ and length $t_{obs} \leq 0.6d_b$ for \geq No.8 (D25) bars or \leq smaller of 0.6 in. and $0.75d_b$ for $<$ No.8 (D25) bars (also see Section 5.1.7). Therefore, the obstruction is not considered to detract from the net bearing area of the head.

‡ Analyzed as doubly-reinforced section to calculate M_n ; all other specimens are analyzed as singly-reinforced

** Specimens contained transverse beams on one or both sides of the test beam. These transverse beams, however, did not meet the dimensional requirements of Section 18.8.4.2 of ACI 318-14 and Section 4.3 of ACI 352R-02 to be considered effective in increasing the joint shear strength.

§ Specimens had $d/\ell_{eh} > 1.5$

Table C.2 Cont. Data for beam-column joint specimens (exterior and roof-level interior joints) tested under reversed cyclic loading *

Study	Specimen	T_h	T'	T'_{mod}	T'/T_{anc}	T'/T_h	T'_{mod}/T_h	t_{obs}/d_b	V_n	$V_{n,ACI352}$	V_p	
		(kips)	(kips)	(kips)					(kips)	(kips)	(kips)	
	1	2	75	76	77	78	79	80	81	82	83	84
16	Chun et al. (2007)	JM-1 [∞]	35.1	44.6	38.6	2.44	1.27	1.10	0.5	572	418	166
		JM-2 [∞]	35.1	40.7	36.2	4.37	1.16	1.03	0.5	564	413	300
		WM ^{□,∞}	79.4	90.8	86.2	4.89	1.14	1.09	0.6	807	807	423
		JM-No.11-1a	103.6	109.3	106.4	3.23	1.06	1.03	0.7	434	367	265
		JM-No.11-1b	103.6	106.8	103.8	3.16	1.03	1.00	0.7	434	367	258
17	Ishida et al. (2007)	P1 ^{**}	45.6	46.9	46.6	1.63	1.03	1.02	-	176	176	237
		P2 ^{**}	45.6	47.5	47.2	1.65	1.04	1.03	-	176	176	237
		P3 ^{**}	45.6	52.2	51.9	1.82	1.14	1.14	-	176	176	164
		P4 ^{**}	45.6	43.4	43.2	1.94	0.95	0.95	-	176	176	281
18	Tazaki et al. (2007)	E1	16.9	20.4	18.7	4.90	1.20	1.10	0.0	111	111	92
		E2 [§]	16.9	17.9	17.7	6.78	1.06	1.04	0.0	111	111	92
19	Lee and Yu (2009)	W0-M1	41.2	48.8	47.4	2.01	1.19	1.15	2.1	307	205	170
		W150-M1	41.2	48.5	47.0	3.25	1.18	1.14	2.1	166	199	172
		W0-M2	41.2	48.5	47.2	3.25	1.18	1.15	2.1	307	205	172
		W150-M2	41.2	50.4	48.8	3.37	1.22	1.18	2.1	166	199	178
20	Kang et al. (2010)	JD [§]	30.8	35.9	32.3	3.15	1.17	1.05	0.0	245	245	129
21	Kang et al. (2012)	JH-R1	30.6	36.8	35.7	2.14	1.20	1.17	0.0	177	148	121
		JH-R2	30.6	35.8	35.0	2.41	1.17	1.15	0.0	177	148	118
22	Chun and Shin (2014) [∞]	M0.7S [‡]	31.2	32.5	31.8	1.91	1.04	1.02	0.7	105	96	132
		M1.0S	31.2	34.3	33.5	2.02	1.10	1.08	0.7	105	96	125
		M1.5S [§]	31.2	34.5	33.8	2.03	1.11	1.09	0.7	102	93	119
		M2.0S [§]	31.2	32.8	32.0	1.93	1.05	1.03	0.7	107	97	111
		M2.5S [§]	31.2	31.9	31.1	1.88	1.03	1.00	0.7	107	97	102
		M0.7U [‡]	31.2	33.2	32.7	3.23	1.07	1.05	0.7	105	96	154
		M1.0U	31.2	36.6	35.8	3.56	1.18	1.15	0.7	105	96	133
23	Dhake et al. (2015)	J4 [□]	13.3	16.6	15.6	4.75	1.25	1.17	0.0	37	37	12
		J5 [□]	13.3	14.6	14.4	4.92	1.09	1.08	0.0	37	37	10
		J9	13.3	18.8	17.6	2.61	1.41	1.32	0.0	37	37	13

* Columns arranged in alphabetical order of notation; notation described in Appendix A; values given in SI are converted to in.-lb (1 in. = 25.4 mm; 1 psi = 1/145 MPa; and 1 kip = 4.4484 kN)

□ Specimens did not contain confining reinforcement parallel to the headed bars within the joint region

∞ Heads contained obstruction with diameter d_{obs} of $1.5d_b$ and length $t_{obs} \leq 0.6d_b$ for \geq No.8 (D25) bars or \leq smaller of 0.6 in. and $0.75d_b$ for $<$ No.8 (D25) bars (also see Section 5.1.7). Therefore, the obstruction is not considered to detract from the net bearing area of the head.

‡ Analyzed as doubly-reinforced section to calculate M_n ; all other specimens are analyzed as singly-reinforced

** Specimens contained transverse beams on one or both sides of the test beam. These transverse beams, however, did not meet the dimensional requirements of Section 18.8.4.2 of ACI 318-14 and Section 4.3 of ACI 352R-02 to be considered effective in increasing the joint shear strength.

§ Specimens had $d/\ell_{ch} > 1.5$

Table C.2 Cont. Data for beam-column joint specimens (exterior and roof-level interior joints) tested under reversed cyclic loading *

Study		Specimen	V_p/V_n	$\delta_{0.8peak}$	δ_y	Υ_j	$\psi_{cs}^{##}$	ψ_o
	1	2	85	86	87	88	89	90
16	Chun et al. (2007)	JM-1 [∞]	0.29	0.068	0.005	0.001	0.78	1.00
		JM-2 [∞]	0.53	0.040	0.009	0.011	0.94	1.00
		WM ^{□,∞}	0.52	0.084	0.013	-	0.74	1.00
		JM-No.11-1a	0.61	0.079	0.016	0.003	0.57	1.00
		JM-No.11-1b	0.60	0.065	0.018	0.006	0.57	1.00
17	Ishida et al. (2007)	P1 ^{**}	1.35	0.015	0.012	-	0.60	1.25
		P2 ^{**}	1.35	0.030	0.010	-	0.60	1.25
		P3 ^{**}	0.93	0.030	0.012	-	0.60	1.25
		P4 ^{**}	1.60	0.030	0.013	-	0.64	1.25
18	Tazaki et al. (2007)	E1	0.82	0.060	0.005	0.008	0.82	1.25
		E2 [§]	0.82	0.060	0.015	0.007	0.89	1.25
19	Lee and Yu (2009)	W0-M1	0.55	0.080	0.010	-	0.80	1.00
		W150-M1	1.04	0.080	0.010	0.001	0.80	1.00
		W0-M2	0.56	0.080	0.013	-	0.80	1.00
		W150-M2	1.07	0.080	0.080	-	0.80	1.00
20	Kang et al. (2010)	JD [§]	0.53	0.036	0.006	0.001	0.53	1.00
21	Kang et al. (2012)	JH-R1	0.68	0.050	0.019	0.008	0.69	1.25
		JH-R2	0.67	0.050	0.015	0.010	0.73	1.25
22	Chun and Shin (2014) [∞]	M0.7S [‡]	1.25	0.100	0.030	0.003	0.60	1.00
		M1.0S	1.19	0.090	0.020	0.005	0.59	1.00
		M1.5S [§]	1.17	0.060	0.020	0.017	0.59	1.00
		M2.0S [§]	1.04	0.050	0.020	-	0.59	1.00
		M2.5S [§]	0.95	0.035	0.020	-	0.59	1.00
		M0.7U [‡]	1.46	0.100	0.030	0.002	0.73	1.00
23	Dhake et al. (2015)	J4 [□]	0.31	1.024	0.304	-	0.54	1.25
		J5 [□]	0.28	0.768	0.336	-	0.54	1.25
		J9	0.36	1.280	0.236	-	0.42	1.25

* Columns arranged in alphabetical order of notation; notation described in Appendix A; values given in SI are converted to in.-lb (1 in. = 25.4 mm; 1 psi = 1/145 MPa; and 1 kip = 4.4484 kN)

□ Specimens did not contain confining reinforcement parallel to the headed bars within the joint region

∞ Heads contained obstruction with diameter d_{obs} of $1.5d_b$ and length $t_{obs} \leq 0.6d_b$ for \geq No.8 (D25) bars or \leq smaller of 0.6 in. and $0.75d_b$ for $<$ No.8 (D25) bars (also see Section 5.1.7). Therefore, the obstruction is not considered to detract from the net bearing area of the head.

‡ Analyzed as doubly-reinforced section to calculate M_n ; all other specimens are analyzed as singly-reinforced

** Specimens contained transverse beams on one or both sides of the test beam. These transverse beams, however, did not meet the dimensional requirements of Section 18.8.4.2 of ACI 318-14 and Section 4.3 of ACI 352R-02 to be considered effective in increasing the joint shear strength.

§ Specimens had $d/\ell_{eh} > 1.5$

ψ_{cs} is based on Table 5.1

C.3 KNEE BEAM-COLUMN JOINT SPECIMENS

Table C.3 Data for knee beam-column joint specimens tested by Wallace et al. (1998) and Chun et al. (2007) under reversed cyclic loading *

Study	Specimen	Loading Direction	Bar Size**	A_b	A_{brg}/A_b	A_{gross}/A_b	A_{hs}	A_{obs}/A_b	$A_{tr,l}$	A_u	A_u/A_{hs}	b_b	b_c
				(in. ²)			(in. ²)		(in. ²)		(in.)	(in.)	
1	2	3	4	5	6	7	8	9	10	11	12	13	14
Wallace et al. (1998)	KJ16	Closing	D16	0.31	11.4	12.4	1.24	-	0.11	0.33	0.27	11	16
		Opening	D16	0.31	11.4	12.4	1.24	-	0.11	0.33	0.27	11	16
	KJ17	Closing	D16	0.31	11.4	12.4	1.24	-	0.11	0.33	0.27	11	16
		Opening	D16	0.31	11.4	12.4	1.24	-	0.11	0.33	0.27	11	16
	KJ18	Closing	D20	0.48	7.0	8.0	1.92	-	0.11	0.33	0.17	11	16
		Opening	D20	0.48	7.0	8.0	1.92	-	0.11	0.33	0.17	11	16
Chun et al. (2007) §	JMT-No. 11-1a	Closing	D36	1.56	2.7	4.9	3.12	2.2	0.31	3.72	1.19	17.7	29.5
		Opening	D36	1.56	2.7	4.9	3.12	2.2	0.31	3.72	1.19	17.7	29.5
	JMT-No. 11-1b	Closing	D36	1.56	2.7	4.9	3.12	2.2	0.31	3.72	1.19	17.7	29.5
		Opening	D36	1.56	2.7	4.9	3.12	2.2	0.31	3.72	1.19	17.7	29.5
	JMT-No. 11-2a	Closing	D36	1.56	2.7	4.9	3.12	2.2	0.31	3.72	1.19	17.7	29.5
		Opening	D36	1.56	2.7	4.9	3.12	2.2	0.31	3.72	1.19	17.7	29.5
	JMT-No. 11-2b	Closing	D36	1.56	2.7	4.9	3.12	2.2	0.31	3.72	1.19	17.7	29.5
		Opening	D36	1.56	2.7	4.9	3.12	2.2	0.31	3.72	1.19	17.7	29.5

Table C.3 Contd. Data for knee beam-column joint specimens tested by Wallace et al. (1998) and Chun et al. (2007) under reversed cyclic loading *

Study	Specimen	Loading Direction	c_{ch}	c_{ch}/d_b	c_o	c_o/d_b	c_{so}	c_{so}/d_b	d	d/ℓ_{eh}	d'	d_b	f_{cm}
			(in.)		(in.)		(in.)		(in.)		(in.)	(in.)	(psi)
1	2	3	15	16	17	18	19	20	21	22	23	24	25
Wallace et al. (1998)	KJ16	Closing	2.7	4.3	0.3	0.5	1.125	1.8	14.6	1.0	1.4	0.625	5390
		Opening	2.7	4.3	0.3	0.5	1.125	1.8	14.6	1.0	1.4	0.625	5390
	KJ17	Closing	2.7	4.3	0.3	0.5	1.125	1.8	14.6	1.0	1.4	0.625	5450
		Opening	2.7	4.3	0.3	0.5	1.125	1.8	14.6	1.0	1.4	0.625	5450
	KJ18	Closing	2.7	3.4	0.4	0.5	1.125	1.4	14.5	1.0	1.5	0.79	5540
		Opening	2.7	3.4	0.4	0.5	1.125	1.4	14.5	1.0	1.5	0.79	5540
Chun et al. (2007) §	JMT-No. 11-1a	Closing	12.4	8.8	2.2	1.6	3.1	2.2	16.1	1.0	3.8	1.41	6060
		Opening	12.4	8.8	2.2	1.6	3.1	2.2	17.0	1.1	2.9	1.41	6060
	JMT-No. 11-1b	Closing	12.4	8.8	2.2	1.6	3.1	2.2	16.1	1.0	3.8	1.41	6060
		Opening	12.4	8.8	2.2	1.6	3.1	2.2	17.0	1.1	2.9	1.41	6060
	JMT-No. 11-2a	Closing	12.4	8.8	2.2	1.6	3.1	2.2	16.1	1.0	3.8	1.41	6060
		Opening	12.4	8.8	2.2	1.6	3.1	2.2	17.0	1.1	2.9	1.41	6060
	JMT-No. 11-2b	Closing	12.4	8.8	2.2	1.6	3.1	2.2	16.1	1.0	3.8	1.41	6060
		Opening	12.4	8.8	2.2	1.6	3.1	2.2	17.0	1.1	2.9	1.41	6060

* Columns arranged in alphabetical order of notation; notation described in Appendix A

** Bar sizes are presented in SI as reported in the original studies

§ Values given in SI are converted to in.-lb (1 in. = 25.4 mm; 1 psi = 1/145 MPa; and 1 kip = 4.4484 kN)

Table C.3 Contd. Data for knee beam-column joint specimens tested by Wallace et al. (1998) and Chun et al. (2007) under reversed cyclic loading *

Study	Specimen	Loading Direction	f_y (ksi)	f_{yt} (ksi)	h_b (in.)	h_c (in.)	$\ell_{dt}^{\#}$ (in.)	ℓ_{dt}/d_b	ℓ_{eh} (in.)	ℓ_{eh}/d_b	ℓ_{ehy} (in.)	ℓ_{ehy}/d_b	ℓ_{eh}/h_c	
	1	2	26	27	28	29	30	31	32	33	34	35	36	
1	Wallace et al. (1998)	KJ16	Closing	70.6	70.0	16.0	16.0	7.1	11.3	14.1	22.6	5.7	9.0	2.50
			Opening	70.6	70.0	16.0	16.0	7.1	11.3	14.1	22.6	5.7	9.0	2.50
		KJ17	Closing	70.6	70.0	16.0	16.0	7.0	11.3	14.1	22.6	5.6	9.0	2.51
			Opening	70.6	70.0	16.0	16.0	7.0	11.3	14.1	22.6	5.6	9.0	2.51
		KJ18	Closing	77.2	70.0	16.0	16.0	13.6	17.3	14.3	18.1	9.6	12.2	1.49
			Opening	77.2	70.0	16.0	16.0	13.6	17.3	14.3	18.1	9.6	12.2	1.49
2	Chun et al. (2007) §	JMT-No. 11-1a	Closing	67.9	57.4	19.9	18.9	12.9	9.1	15.8	11.2	9.8	7.0	1.61
			Opening	67.9	57.4	19.9	18.9	12.9	9.1	15.8	11.2	9.8	7.0	1.61
		JMT-No. 11-1b	Closing	67.9	57.4	19.9	18.9	12.9	9.1	15.8	11.2	9.8	7.0	1.61
			Opening	67.9	57.4	19.9	18.9	12.9	9.1	15.8	11.2	9.8	7.0	1.61
		JMT-No. 11-2a	Closing	67.9	57.4	19.9	18.9	12.9	9.1	15.8	11.2	9.8	7.0	1.61
			Opening	67.9	57.4	19.9	18.9	12.9	9.1	15.8	11.2	9.8	7.0	1.61
		JMT-No. 11-2b	Closing	67.9	57.4	19.9	18.9	12.9	9.1	15.8	11.2	9.8	7.0	1.61
			Opening	67.9	57.4	19.9	18.9	12.9	9.1	15.8	11.2	9.8	7.0	1.61

Table C.3 Contd. Data for knee beam-column joint specimens tested by Wallace et al. (1998) and Chun et al. (2007) under reversed cyclic loading *

Study	Specimen	Loading Direction	ℓ_{eh}/ℓ_{dt}	ℓ_{eh}/ℓ_{ehy}	M_n (kip.in.)	M_{peak} (kip.in.)	M_{peak}/M_n	N	n	$P/A_g f'_c$	s_h/d_b	s'_{tr} (in.)	s_{tr} (in.)	
	1	2	37	38	39	40	41	42	43	44	45	46	47	
1	Wallace et al. (1998)	KJ16	Closing	2.00	2.50	1202	1300	1.08	3	4	0	4.3	1.5	1.8
			Opening	2.00	2.50	1202	963	0.80	3	4	0	4.3	1.5	1.8
		KJ17	Closing	2.01	2.51	1203	1460	1.21	3	4	0	4.3	1.5	1.8
			Opening	2.01	2.51	1203	957	0.80	3	4	0	4.3	1.5	1.8
		KJ18	Closing	1.05	1.49	1937	2250	1.16	3	4	0	3.4	1.5	1.8
			Opening	1.05	1.49	1937	1505	0.78	3	4	0	3.4	1.5	1.8
2	Chun et al. (2007) §	JMT-No. 11-1a	Closing	1.23	1.61	3165	3239	1.02	12	2	0	8.8	2.1	3.9
			Opening	1.23	1.61	3355	2478	0.74	12	2	0	8.8	2.1	3.9
		JMT-No. 11-1b	Closing	1.23	1.61	3165	3151	1.00	12	2	0	8.8	2.1	3.9
			Opening	1.23	1.61	3355	-	-	12	2	0	8.8	2.1	3.9
		JMT-No. 11-2a	Closing	1.23	1.61	3165	3664	1.16	12	2	0	8.8	2.1	3.9
			Opening	1.23	1.61	3355	-	-	12	2	0	8.8	2.1	3.9
		JMT-No. 11-2b	Closing	1.23	1.61	3165	3991	1.26	12	2	0	8.8	2.1	3.9
			Opening	1.23	1.61	3355	2876	0.86	12	2	0	8.8	2.1	3.9

* Columns arranged in alphabetical order of notation; notation described in Appendix A

§ Values given in SI are converted to in.-lb (1 in. = 25.4 mm; 1 psi = 1/145 MPa; and 1 kip = 4.4484 kN)

ℓ_{dt} based on Eq. (5.2)

Table C.3 Contd. Data for knee beam-column joint specimens tested by Wallace et al. (1998) and Chun et al. (2007) under reversed cyclic loading *

Study	Specimen	Loading Direction	T' (kips)	t_{obs}/d_b	V_n (kips)	$V_{n,ACI352}$ (kips)	V_p (kips)	V_p/V_n	$\delta_{0.8peak}$	δ_y	Υ_j	$\psi_{cs}^{##}$	ψ_o	
	1	2	3	48	49	50	51	52	53	54	55	56	57	58
1	Wallace et al. (1998)	KJ16	Closing	23.7	0.00	226	190	105	0.47	0.040	0.017	-	0.55	1.25
			Opening	17.5	0.00	226	190	105	0.47	0.060	-	-	0.55	1.25
		KJ17	Closing	26.6	0.00	227	191	118	0.52	0.060	0.012	-	0.55	1.25
			Opening	17.4	0.00	227	191	118	0.52	0.060	-	-	0.55	1.25
		KJ18	Closing	43.0	0.00	229	193	182	0.79	0.040	0.017	-	0.70	1.25
			Opening	28.8	0.00	229	193	182	0.79	0.040	-	-	0.70	1.25
2	Chun et al. (2007) §	JMT-No. 11-1a	Closing	108.3	0.73	521	396	213	0.41	0.030	-	0.003	0.40	1.00
			Opening	78.2	0.73	521	396	213	0.41	0.028	-	-	0.40	1.00
		JMT-No. 11-1b	Closing	105.4	0.73	521	396	206	0.40	0.030	0.020	0.025	0.40	1.00
			Opening	-	0.73	521	396	206	0.40	-	-	-	0.40	1.00
		JMT-No. 11-2a	Closing	122.5	0.73	521	396	240	0.46	0.035	0.019	0.003	0.40	1.00
			Opening	-	0.73	521	396	240	0.46	-	-	-	0.40	1.00
		JMT-No. 11-2b	Closing	133.5	0.73	521	396	262	0.50	0.060	0.024	0.002	0.40	1.00
			Opening	90.8	0.73	521	396	262	0.50	0.030	0.000	-	0.40	1.00

* Columns arranged in alphabetical order of notation; notation described in Appendix A

§ Values given in SI are converted to in.-lb (1 in. = 25.4 mm; 1 psi = 1/145 MPa; and 1 kip = 4.4484 kN)

ψ_{cs} is based on Table 5.1

APPENDIX D: SUMMARY OF STUDIES ON BEAM-COLUMN JOINTS TESTED UNDER REVERSED CYCLIC LOADING

The current study includes results from tests of exterior, roof-level interior, and knee beam-column joint specimens subjected to reversed cyclic loading by Bashandy (1996), Murakami et al. (1998), Wallace et al. (1998), Matsushima et al. (2000), Nakazawa et al. (2000), Tasai et al. (2000), Yoshida et al. (2000), Takeuchi et al. (2001), Ishibashi et al. (2003), Ishibashi and Inokuchi (2004), Kiyohara et al. (2004), Kiyohara et al. (2005), Kato (2005), Masuo et al. (2006a, 2006b), Adachi and Masuo (2007), Chun et al. (2007), Ishida et al. (2007), Tazaki et al. (2007), Lee and Yu (2009), Kang et al. (2010), Kang et al. (2012), Chun and Shin (2014), and Dhake et al. (2015). This appendix includes a detailed summary of these 23 studies.

Bashandy (1996)

Bashandy (1996) tested an exterior beam-column joint specimen to investigate the anchorage behavior of headed bars under reversed cyclic loading. The specimen consisted of a 254 × 457 mm (10 × 18 in.) beam anchored in a 330 × 381 mm (13 × 15 in.) column using two No. 25 (No. 8) headed bars as top and bottom beam reinforcement. The embedment length was $11.7d_b$, which resulted in an effective beam depth to embedment length ratio of 1.4. The net bearing area of the headed bars was $8.6A_b$, and the heads had no obstruction adjacent to the bearing face. Clear cover to the bar and center-to-center spacing between the bars were 3.6 and $5.1d_b$, respectively. The concrete compressive strength and steel yield strength were 29.6 and 447 MPa (4,290 and 64,820 psi), respectively. Five No. 13 (No. 4) ties spaced at 56 mm (2.2 in.) were provided as confining reinforcement parallel to the headed bars within the joint region. Specimen was loaded for one cycle in each drift level from 0.75 to 6% drifts. No column axial load was applied during the test.

Bashandy (1996) observed that after the first two cycles of loading, cracks formed within the joint region and in the beam. Splitting cracks along the column longitudinal reinforcement and spalling of cover concrete from the side face of the column were observed. The specimen reached its peak moment at 6.1% drift (7.8 times the drift at the first yield) and maintained about 90% of the peak moment at 6% drift.

Murakami et al. (1998)

Murakami et al. (1998) tested 11 exterior beam-column joint specimens to investigate the anchorage performance of headed bars subjected to reversed cyclic loading. Two specimens containing 90° hooked bars and one specimen containing straight bars were also tested for comparison. The major test parameters included head bearing area and type of anchorage (headed, hooked, or straight bar). The net bearing areas of heads ranged from 1.7 to $6.3A_b$ (headed bars with gross head area of $7A_b$ contained obstructions adjacent to the bearing face of the head which reduced the net bearing area, calculated as gross head area minus obstruction area, to between 3.6 and $4.4A_b$). Two to four D16 (No. 5), D19 (No. 6), or D22 (No. 7) headed bars in a single layer were used as top and bottom beam reinforcement, with the exception of one specimen that contained two layers of four D16 (No. 5) bars. The clear cover to the bar and the center-to-center spacing between the bars in a layer ranged from 2.5 to $3.8d_b$ and 2.9 to $7.4d_b$, respectively. The specimen containing two layers of headed bars had a vertical center-to-center spacing between the bars in different layers equal to $3.2d_b$. Four specimens designed to ensure flexural yielding of the beam reinforcement contained headed bars with yield strengths of 370 and 511 MPa (53,650 and 74,110 psi), while the other seven specimens, designed to investigate shear at the joint region, contained headed bars with yield strengths ranging from 946 to 1,000 MPa (137,120 to 145,090 psi). Concrete compressive strengths ranged from 28.3 to 39.3 MPa (4,100 to 5,700 psi). The beam and column cross-sections were 275×300 mm (10.2×15.7 in.) and 300×300 mm (11.8×11.8 in.), respectively, in all specimens. An embedment length of 225 mm (8.9 in.), equivalent to 10.1 to $14.2d_b$ depending on bar diameter, was provided. The effective beam depth to embedment length ratio was 1.5. Four hoops with an area of single leg equal to 0.049 in.^2 (Japanese bar size D6) spaced at 46 or 80 mm (1.8 or 3.1 in.) within the joint region were provided as confining reinforcement parallel to the headed bars. Specimens were loaded for one cycle in each drift level (0.25, 0.5, 1, 2, 4, and 8.3 %). A column axial load of 0.04 or 0.06 times $A_g f'_c$ was applied during the test.

The specimens designed to ensure flexural yielding of the beam reinforcement had peak moments that were 14 to 24% greater than the nominal flexural strength of the test beam. These specimens had a drop of less than 20% of the peak load up to 8.3% drift. The specimens designed

to investigate shear in the joint, which had the same embedment length as that of other specimens but with 2 to 2.5 times higher yield strengths of the bars, reached 54 to 75% of the nominal flexural strength and had more than a 20% drop in the peak load at 8.3% drift. Murakami et al. (1998) did not find significant difference in anchorage behavior of hooked and headed bars. Specimens containing headed bars, however, exhibited slightly improved energy dissipation capacity than did the companion specimens containing hooked bars.

Wallace et al. (1998)

Wallace et al. (1998) conducted a comparative study of the performance of hooked and headed bars under reversed cyclic loading in beam-column joints. In the study, two full-scale exterior and three two-third scale knee beam-column joint specimens were tested using headed bars containing circular heads with a net bearing area of $4A_b$ along with two companion knee beam-column joint specimens containing hooked bars. The headed bars had no obstructions. All specimens were tested under reversed cyclic loading, except one exterior beam-column joint specimen which was tested under monotonic loading. The exterior beam-column joint specimens (Figure D.1) consisted of an 18×24 in. beam anchored with headed bars in an 18×18 in. column. Stub beams connected at the joint perpendicular to the plane of the test beam and column were provided to simulate the three-dimensional effect in an exterior beam-column joint. Beam and column longitudinal reinforcement consisted of ASTM A706 or A615 Grade 60 No. 8 and No. 9 bars, respectively. Four No. 4 bar ties were used as confining reinforcement in the joint region. Headed bars from the beam were embedded $13d_b$ into the column, equal to 82% of the embedment length of the 90° hooked bars in the companion specimen required to develop 1.25 times the yield strength of the bar without applying modification factors for joint confinement and side cover in accordance with Section 4.5 of ACI 352R-91. The center-to-center spacing between headed bars was $3.5d_b$. The full-scale exterior beam-column joint specimens had concrete compressive strengths of 4,870 and 5,190 psi.

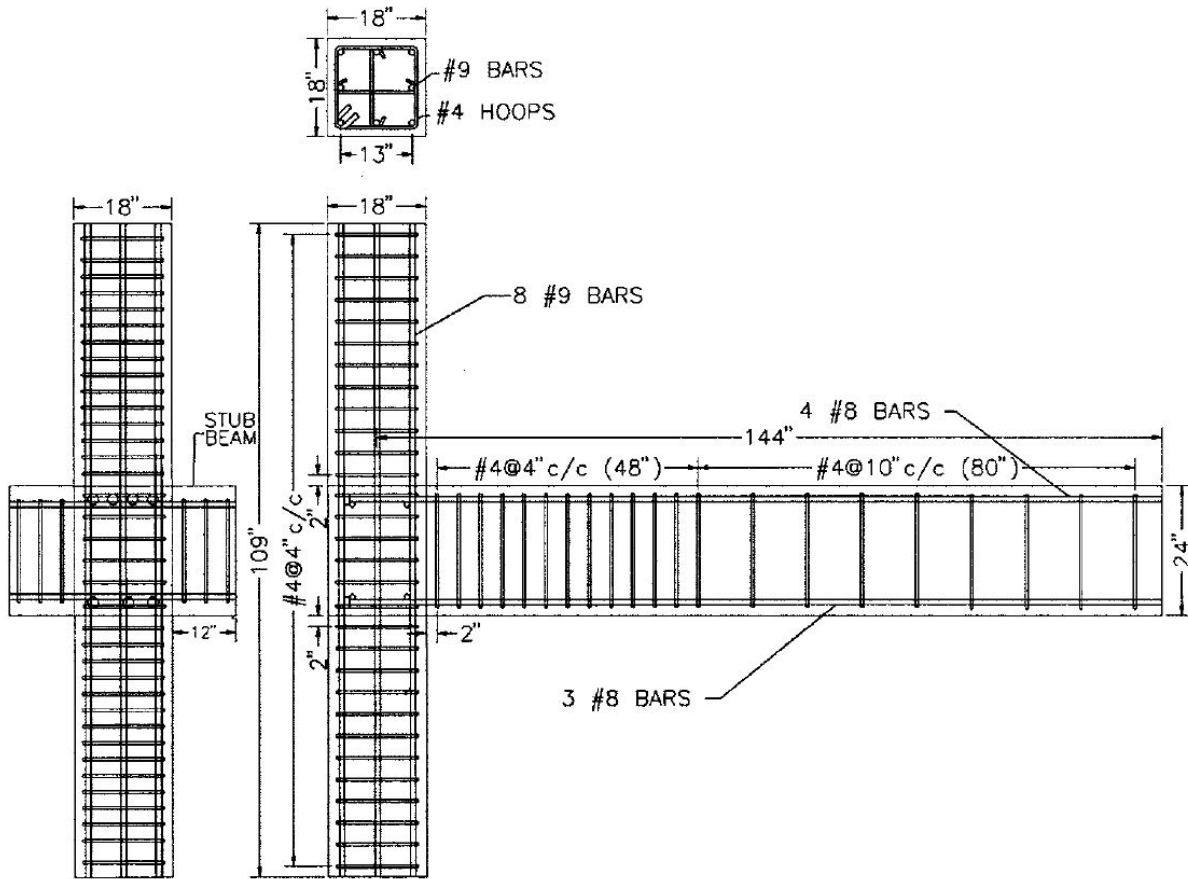


Figure D.1 Reinforcement details for exterior beam-column joint specimens (Wallace et al. 1998)

The knee beam-column joint specimens consisted of an 11×16 in. beam and a 16×16 in. column, as shown in Figure D.2. Concrete compressive strengths ranged from 4,760 to 7,480 psi. Grade 60 D16 (16 mm) and D20 (20 mm) headed bars were used as beam and column reinforcement. Grade 60 No. 3 hoops with a cross-tie spaced at 3.5 in. ($5.6d_b$) were provided in the joint region parallel to the headed bars as confining reinforcement. In the exterior beam-column joint specimens, the ratio of the flexural strength of the column to that of the beam was 1.72, where the ratio is defined as the sum of the nominal flexural strengths of columns to the summation of nominal flexural strengths of beams framing into a joint. For the corner beam-column joint specimens, the flexural strength ratio was approximately unity, with the column slightly stronger than the beam. Each specimen underwent at least two cycles of loading at each increasing drift level (0.5, 1, 2, 3, and 4%), where drift is the ratio of lateral displacement of a member at the loading point to the distance between the loading point and center of the beam-column joint.

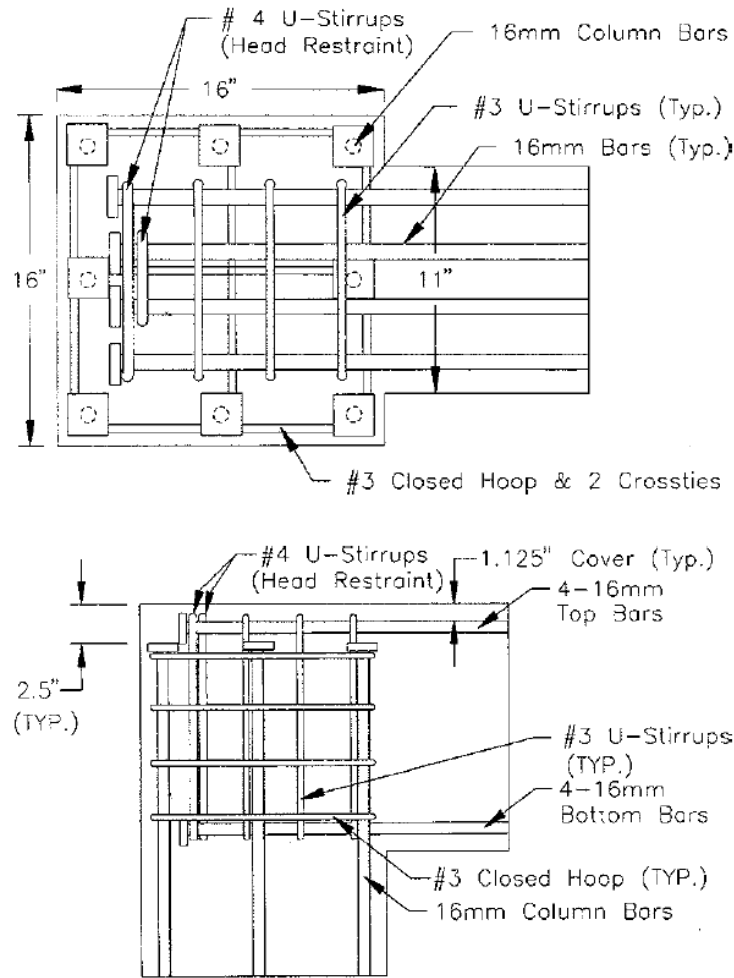


Figure D.2 Reinforcement details for knee beam-column joint specimens (Wallace et al. 1998)

Wallace et al. (1998) proposed confinement requirements for knee joints and limits on joint shear stress. Their study showed that the headed bars in exterior beam-column joint specimens performed satisfactorily. However, in knee beam-column joints, the headed bars in the beams could not be fully developed without confining reinforcement (identified as U-stirrups in Figure D.2) perpendicular to the bars because the bars prematurely pushed out of the top face of the joint. The knee joint specimens, therefore, required U-stirrups as additional confining reinforcement within the joint region, compared with exterior joints, to confine the headed bars throughout the loading cycles. Wallace et al. (1998) recommended a minimum embedment length of $12d_b$ for bar sizes from No. 5 to No. 8. They also suggested limiting shear stress to $6\sqrt{f'_c}$ on knee joints with no transverse beams (beams connected at the joint perpendicular to the plane of the test beam and column) to avoid premature shear failure.

Matsushima et al. (2000)

Matsushima et al. (2000) investigated the anchorage performance of headed bars under reversed cyclic loading in two exterior beam-column joint specimens. One exterior beam-column joint specimen containing 90° hooked bars, but otherwise identical to a specimen containing headed bars, was also tested for comparison. In these tests, the embedment length of the headed bars was the major test parameter. The embedment lengths were 8 and $11.9d_b$ (corresponding to 50% and 75% of column depth) with beam effective depth to embedment length ratios equal to 1.9 and 1.3, respectively. The specimens consisted of two 350×480 mm (13.8×18.9 in.) orthogonal beams anchored in a 400×400 mm (15.7×15.7 in.) column at the same level. Two D25 (No. 8) headed bars spaced center-to-center at $5.1d_b$ were provided as top and bottom beam reinforcement. Details of the heads were not available. Clear side concrete cover to the headed bars in the joint region was $2.3d_b$. Concrete compressive strength and steel yield strength were 32.9 and 551 MPa (4,770 and 79,900 psi), respectively. Three D10 (No. 3) hoops spaced at 120 mm (4.7 in.) were provided as confining reinforcement parallel to the headed bars within the joint region. Load was applied transversely in combination on both orthogonal beams for two reversed cycles in each drift level (0.25 to 4%). A column axial load of $0.11A_g f'_c$ was applied during the test.

During the tests, flexural cracks on the beam occurred close to the column face at 0.25% drift, while diagonal cracks at joint region appeared at 0.75% drift. Matsushima et al. (2000) observed that none of the specimens reached the nominal flexural strength of the beam; specimens with embedment lengths of 8 and $11.9d_b$ reached maximums of 81 and 87% of nominal flexural strength at about 3.5% drift, respectively, from which Matsushima et al. (2000) concluded that increase in embedment length would have improved the joint performance.

Nakazawa et al. (2000)

Nakazawa et al. (2000) tested two exterior beam-column joint specimens to investigate the anchorage behavior of headed bars in high-strength concrete. The concrete compressive strength was 120 MPa (17,400 psi). The specimens consisted of a 280×360 mm (11×14.2 in.) beam and a 360×360 mm (14.2×14.2 in.) column. Two layers of six D19 (No. 6) headed bars (four bars on the outside layer and two bars on the inside layer) were provided as top and bottom beam reinforcement. One specimen contained threaded headed bars with a gross head area of $6.9A_b$ with

an obstruction adjacent to the bearing face, which reduced the net bearing area (gross head area minus obstruction area) to $3.9A_b$. The other specimen contained headed bars with net bearing area of $5.9A_b$ with no obstruction. The yield strength of the headed bar was 685 MPa (99,330 psi). An embedment length of $15d_b$ was provided in both specimens, with beam effective depth to embedment length ratio equal to 1.1. Clear cover to the headed bars was $3.6d_b$. Center-to-center spacing between the bars in a layer was $3.7d_b$, and the spacing between the bars in different layers was $3.4d_b$. Three sets of one hoop and two single-leg ties with an area of a single leg equal to 0.047 in.^2 (Japanese bar size U6.2), spaced at 75 mm (3 in.) within the joint region, were provided as confining reinforcement parallel to the headed bars. Additionally, two single-leg ties of the same bar size were also provided perpendicular to the headed bars at a spacing of 75 mm (3 in.) within the joint region. Specimens were loaded for one cycle at 0.25, 0.5, and 0.75% drift levels and for two cycles at 1, 1.5, 2, 3, and 5% drift levels. No column axial load was applied during the test.

Nakazawa et al. (2000) observed that diagonal cracks at the joint region occurred in the vicinity of the heads and extended toward the compression region of the beam. Both specimens exhibited flexural hinging within the beam at a peak moment equal to about 15% more than the nominal flexural strength of the beam. Nakazawa et al. (2000) also observed high deformability of the specimens; the specimens reached their peak load at 3% drift and maintained more than 90% of the peak load at the end of the first cycle at 5% drift. At the end of second cycle at the same drift level, the specimen containing threaded headed bars maintained about 85% of the peak load, while the other specimen maintained about 70% of the peak load.

Tasai et al. (2000)

Tasai et al. (2000) tested six half-scale exterior beam-column joint specimens to investigate the shear behavior of the joints. The major test parameters included embedment length and joint shear. The specimens consisted of $350 \times 450 \text{ mm}$ ($13.8 \times 17.7 \text{ in.}$) beams and $450 \times 450 \text{ mm}$ ($15.7 \times 15.7 \text{ in.}$) columns. Four specimens contained a single layer of four D25 (No. 8) headed bars, one specimen contained a single layer of two D25 (No. 8) headed bars, and one specimen contained two layers of nine D19 (No. 6) headed bars (five bars on the outside and four bars on the inside layer) as top and bottom beam reinforcement. The headed bars (gross head area of $9A_b$) contained obstructions adjacent to the head, which reduced the net bearing area (gross head area minus

obstruction area) to $5.4d_b$. Embedment lengths ranged from 10.6 to $15.8d_b$. The yield strengths of the headed bars were 545 and 724 MPa (70,030 and 105,000 psi). Concrete compressive strengths were 49.1 and 57.4 MPa (7,120 and 8,320 psi). Clear side cover to the headed bars from the free face of the column was $2.4d_b$. Four-leg ties (two hoops in a layer) of D10 (No. 3) bars spaced at 100 mm (4 in.) were provided as confining reinforcement parallel to the headed bars within the joint region. Specimens were loaded for two cycles in each drift level (0.25, 0.5, 1, 2, and 4%). No column axial load was applied during the test. Tasai et al. (2000) observed significant joint deterioration in the specimens with rapid loss of strength in higher drift levels. Specimens reached lateral drift as high as 4% drift, but the full joint strength was not realized.

Yoshida et al. (2000)

Yoshida et al. (2000) investigated the anchorage performance headed bars in three exterior beam-column joints in which joint shear was expected to reach the nominal joint shear strength. The major test parameters included concrete compressive strength [31 and 37.7 MPa (4,500 and 5,470 psi)] and head size (net bearing area equal to 3.1, 4.1, and $5.8A_b$). The headed bars had no obstructions adjacent to the heads. The specimens consisted of a 300×400 (11.8 \times 15.7 in.) beam and a 300×350 mm (11.8 \times 13.8 in.) column. Single layers of four No. 6 (D19) headed bars were provided as top and bottom beam reinforcement. An embedment length of $13.5d_b$ was provided in the specimens, giving an effective beam depth to embedment length ratio of 1.4. The steel yield strength was 562 MPa (81,500 psi). Clear side concrete cover to the headed bars in the joint region was $3.2d_b$ and the center-to-center spacing between the bars was $3.7d_b$. Five No. 3 (D10) hoops spaced at 75 mm (3 in.) within the joint region were provided as confining reinforcement parallel to the headed bars. Specimens were loaded for 2 cycles at the initial drift of 0.5% and final drift of 4%, while the specimens were loaded for 3 cycles each at intermediate drifts of 1 and 2%. No column axial load was applied during the test.

Yoshida et al. (2000) observed similar cracking patterns in all specimens. Until the final loading cycle, most of the cracking occurred in the joint region. Joint diagonal cracks formed between the heads and compression region of the beam at 0.5% drift, which became dominant failure cracks with widths exceeding 0.2 in. after 2% drift. Splitting cracks were observed at the back face of the columns along the longitudinal reinforcement. Yoshida et al. (2000) reported that

the splitting cracks were due to the extension of joint diagonal cracks toward the back face of the column. Two specimens with 37.7 MPa (5,470 psi) concrete compressive strength maintained the peak load at the end of the first cycle at 4% drift, while the specimen with 31 MPa (4,500 psi) concrete compressive strength maintained only approximately 80% of its peak load at the same drift level at the end of the first cycle. Yoshida et al. (2000) observed that the anchorage of headed bars was not affected by the decrease in net bearing area of the heads from 5.8 to $3.1A_b$; this observation is likely due to the fact that the embedment lengths in these specimens were more than sufficient to yield the bars, which reduced the stress demand on the head.

Takeuchi et al. (2001)

Takeuchi et al. (2001) studied the anchorage of headed bars in six exterior beam-column joint specimens subjected to reversed cyclic loading. One exterior beam-column joint specimen with hooked bars, but otherwise identical to a headed bar specimen, was also tested for comparison. The major test parameters included concrete compressive strength and embedment length. Specimens consisted of a 350×450 mm (13.8×17.7 in.) beam and a 400×400 mm (15.7×15.7 in.) column. A single layer of three or four D25 (No. 8) headed bars was provided as both top and bottom beam reinforcement. Heads had a gross head area of $6.8A_b$ and an obstruction adjacent to the bearing face that reduced the net bearing area (gross head area minus obstruction area) to $3.8A_b$. The yield strength of the headed bars ranged from 54,660 to 104,110 psi. The embedment length was $10.6d_b$ (67% of the column depth), with the exception of one specimen that had an embedment length of $11.9d_b$ (75% of the column depth). Beam effective depth to embedment length ratios were 1.3 and 1.5. Five specimens, including the specimen containing hooked bars, were designed to ensure flexural yielding of the beam reinforcement, while the other two specimens were designed to investigate shear behavior within the joint. Concrete compressive strengths ranged from 24.3 to 62.1 MPa (3,520 to 9,000 psi). The clear cover to the headed bar was $2.6d_b$ in the joint region, while the center-to-center spacing between headed bars was 3.3 and $4.9d_b$. Three D10 (No. 3) hoops spaced at $3.9d_b$ within the joint region were provided as confining reinforcement parallel to the headed bars. Specimens were loaded for one reversed cycle to 0.25, 0.5, 3, and 4% drift levels and three reversed cycles to 1, 1.5, and 2% drift levels. A column axial load of $0.10A_g f'_c$ was applied during the test.

Takeuchi et al. (2001) observed that all specimens exhibited similar cracking patterns. Flexural cracks on the beam formed at 0.25% drift and diagonal cracks formed between the head and compression region of the beam at 0.5% or higher drift levels. Diagonal cracks also extended along column longitudinal reinforcement. Test results showed that specimens designed for flexural yielding of the beam reinforcement reached the peak moment 6 to 16% greater than the nominal flexural strength of the beam and maintained at least 80% of the peak load up to 4% drift. The other specimens designed to investigate shear at the joint failed at 10 to 20% below the nominal flexural strength partly because these specimens did not have sufficient embedment length to yield the headed bars. The specimen containing hooked bars had a peak load about 8% greater than the nominal flexural strength and exhibited brittle failure at the joint. An increase in concrete compressive strength from 24.3 to 60.9 MPa (3,520 to 8,830 psi) increased the anchorage strength of headed bars by about 50%. Specimens with higher concrete compressive strength exhibited brittle failure. Takeuchi et al. (2001) also observed that an increase in embedment length improved the joint anchorage strength and energy dissipation capacity, and decreased the head slip relative to the surrounding concrete. A decrease in head slip was also observed for specimens with increased concrete compressive strength.

Ishibashi et al. (2003) and Ishibashi and Inokuchi (2004)

Ishibashi et al. (2003) and Ishibashi and Inokuchi (2004) investigated the anchorage behavior of headed bars in roof-level interior beam-column joints, where the column reinforcement was anchored in the beam using headed bars. The major test parameters included concrete compressive strength and confining reinforcement within the joint region. A total of eight specimens (four in each study) were tested; seven specimens contained regular headed bars and one specimen had the column reinforcement anchored in the beam using headed bars with spirals along the embedment length of the bar. Specimens consisted of 300×400 mm (11.8×15.7 in.) to 400×600 mm (15.7×23.6 in.) beams and 400×400 mm (15.7×15.7 in.) to 600×600 mm (23.6×23.6 in.) columns. Three D19 (No. 6) (Ishibashi et al. 2003) and three D29 (No. 9) (Ishibashi and Inokuchi 2004) headed bars in each face of the column (a total of eight bars) were used as column reinforcement. An embedment length of $18d_b$ was used in all specimens with an effective column depth to embedment length ratio of 1.05 to 1.25 depending on the depth of the column. In

specimens tested by Ishibashi et al. (2003), headed bars (gross head area of $6.4A_b$) contained obstructions adjacent to the head, which reduced the net bearing area (gross head area minus obstruction area) to $3.2A_b$. Ishibashi and Inokuchi (2004) did not provide details of the heads. Measured yield strengths of the headed bars ranged from 388 to 583 MPa (56,260 to 84,540 psi), and concrete compressive strengths ranged from 33.3 to 49.7 MPa (4,830 to 7,210 psi). Clear concrete cover to the bar within the joint region was $2.5d_b$. The center-to-center spacing between the headed bars in specimens tested by Ishibashi et al. (2003) was $7.5d_b$ and that in specimens tested by Ishibashi and Inokuchi (2004) was $7.4d_b$. Three to six D10 (No. 3) hoops with spacings ranging from 6.8 to $2.4d_b$ were provided as confining reinforcement parallel to the headed bars within the joint region. One specimen tested by Ishibashi and Inokuchi (2004) contained no joint confining reinforcement.

The specimens tested by Ishibashi et al. (2003) reached peak moment 1.19 to 1.25 times the flexural strength of the column, with less than a 20% decrease in peak moment at 3.5% drift. The specimens tested by Ishibashi and Inokuchi (2004) reached peak moment 1.05 to 1.09 times the flexural strength of the column. These specimens, however, lost more than 20% of the peak load at 3.5% drift, with the exception of one specimen containing headed bars with spiral deformation, which maintained 80% of the peak load up to 6% drift. In both studies, a significant slip of head relative to the surrounding concrete at the onset of failure was observed.

Kiyohara et al. (2004) and Kiyohara et al. (2005)

Kiyohara et al. (2004, 2005) tested 12 exterior beam-column joint specimens to investigate the anchorage performance of headed bars subjected to reversed cyclic loading. The major test parameters included embedment length and concrete compressive strength. Specimens consisted of a 450×600 mm (17.7×23.6 in.) beam and a 550×550 mm (21.7×21.7 in.) column. Three to seven D29 (No. 9) headed bars were provided as top and bottom beam reinforcement. Embedment lengths ranged from 9.5 to $15.9d_b$ with effective beam depth to embedment length ratios ranging from 1.2 to 2 (two specimens a ratio > 1.5). The gross head area of the headed bars was $5.7A_b$ with a net bearing area (gross head area minus obstruction area) of $4.1A_b$. The center-to-center spacing of headed bars in a layer ranged from 2.9 to $5.5d_b$, while in specimens containing two layers of headed bars, the center-to-center spacing between the bars in different layers was $3.4d_b$.

Clear concrete side cover to the headed bar within the joint region was 2.6 or $2.9d_b$. Concrete compressive strengths ranged from 44.4 to 148.4 MPa ($6,440$ to $21,520$ psi), and the steel yield strengths ranged from 690 to 1034 MPa ($102,520$ to $149,930$ psi). Three D13 (No. 4) hoops spaced at 100 or 150 mm (3.9 or 5.9 in.) within the joint region were used as confining reinforcement parallel to the headed bars. Specimens were loaded for one reversed cycle at 0.125% and for two reversed cycles in each subsequent higher drift level (0.25 , 0.5 , 1 , 2 , 3 , and 4%). No column axial load was applied.

Kiyohara et al. (2004) found that concrete compressive strength did not have a significant effect on the anchorage performance of headed bars, while an increase in the center-to-center spacing between bars from 3.4 to $5.5d_b$ increased the peak moment to nominal flexural strength ratio from 0.95 to 1.10 . Specimens with an embedment length of $9.5d_b$ did not reach the nominal flexural strength of the beam, while the specimen with an embedment length of $15.9d_b$ exceeded the nominal flexural strength by 20% and maintained 80% of the peak load at 4% drift level. The longer embedment length also delayed the strength degradation after the specimen reached its peak load.

Kato (2005)

Kato (2005) tested two exterior beam-column joint specimens to investigate the anchorage behavior of friction welded and threaded headed bars with gross head area of $6.3A_b$. The friction welded headed bars had no obstructions adjacent to the head giving a net head bearing area of $5.3A_b$. However, the threaded headed bars had obstructions adjacent to the head which reduced the net bearing area (gross head area minus obstruction area) to $3.6A_b$. The specimens consisted of 325×450 mm (12.8×17.7 in.) beams and 475×475 mm (18.7×18.7 in.) columns. Two layers of four D22 (No. 7) headed bars at both the top and bottom of the beam were anchored in the column. The yield strengths of the friction welded and threaded headed bars were 521 and 505 MPa ($75,550$ and $73,230$ psi), respectively. The respective concrete compressive strengths were 60.8 and 70.8 MPa ($8,820$ and $10,270$ psi). The center-to-center spacing between headed bars in a layer was $3.6d_b$, while the spacing between the bars in different layers was $3.8d_b$. Clear side cover to the bar was $4.9d_b$ in the joint region. Two hoops in a layer with an area of a single leg equal to 0.049 in.² (Japanese bar size D6) spaced at $2.7d_b$ within the joint region were provided as confining

reinforcement parallel to the headed bars. The embedment length was $16.2d_b$, which resulted in beam effective depth to embedment length ratio of 1.1. No column axial load was applied.

Kato (2005) observed similar cracking patterns in the specimens. Diagonal cracks within the joint region formed close to the heads and extended toward the compression region of the beam. Both specimens exhibited flexural hinging of the beam. The specimen containing the friction welded headed bars (5.3A_b) had about 15% higher peak load than the specimen containing the threaded headed bars (3.6A_b). The specimen containing the friction welded headed bars maintained the peak load at the end of the first cycle at 4% drift, and the load dropped to about 80% of the peak load at the end of second cycle at the same drift level. The specimen containing the threaded headed bars maintained the peak load throughout two loading cycles at 4% drift level.

Masuo et al. (2006a)

Masuo et al. (2006a) tested four exterior beam-column joint specimens to investigate the performance of high-strength headed bars under reversed cyclic loading. The major test parameters included concrete compressive strength, column depth, and embedment length. The study involved headed bars with a yield strength of 1,022 MPa (148,000 psi). Concrete compressive strengths were 90.6 and 129.8 MPa (13,140 and 18,820 psi). Specimens consisted of 350×400 mm (13.8×15.7 in.) or 350×450 mm (13.8×17.7 in.) columns and 300×450 mm (11.8×17.7 in.) beams anchored in the column using headed bars. Embedment lengths were 10 and $12d_b$, giving an effective beam depth to embedment length ratio of 1.3, with the exception of one specimen for which the ratio was 1.6. Embedment length to column depth ratios ranged from 0.55 to 0.75. All specimens contained a single layer of two D25 (No. 8) headed bars spaced center-to-center at $8d_b$ as top and bottom beam reinforcement. Clear side concrete cover to the bar was $2.6d_b$ in the joint region. The headed bars had gross head area of $6.8A_b$, and the heads contained obstructions adjacent to the bearing face, which reduced the net bearing area (gross head area minus obstruction area) to $3.9A_b$. Four hoops with an area of single leg equal to 0.077 in.^2 (Japanese bar size S8) spaced at 83 mm (3.3 in.) within the joint region were provided as confining reinforcement parallel to the headed bars. A column axial load of $0.02A_g f'_c$ was applied during the test.

All specimens reached the peak load at 2.5 to 3% drift, with the exception of one specimen with a $10d_b$ embedment length, which reached the peak load at 2% drift. Specimens exceeded

nominal flexural strength by 4 to 14%. Masuo et al. (2006a) found that an increase in concrete compressive strength from 90.6 to 129.8 MPa (13,140 to 18,830 psi) increased the drift at the peak load from 2 to 3% and anchorage strength by about 12%. Specimens with a concrete compressive strength of 90.6 MPa (13,140 psi), however, exhibited a more ductile failure compared to the specimens with concrete compressive strength of 129.8 MPa (18,830 psi). An increase in column depth from 400 mm (15.7 in.) ($16d_b$) to 450 mm (17.7 in.) ($18d_b$) for an embedment length of $12d_b$ increased the peak load by about 7%, an increase that may have resulted because of the increase in joint shear strength as the column depth increased. Specimens with embedment lengths of both 10 and $12d_b$ maintained the peak load at the end of the first cycle at 3% drift, but specimens with $12d_b$ embedment lengths maintained 80% of the peak load at the second loading cycle, while the specimen with $10d_b$ embedment length maintained only about 30% of the peak load at the second loading cycle. Masuo et al. (2006a) concluded that an increase in embedment length improved the post-peak failure behavior of the specimens and an increase in column depth did not significantly affect the joint performance.

Masuo et al. (2006b)

Masuo et al. (2006b) investigated the joint shear strength of four exterior beam-column joints containing headed bars. The major test parameters included embedment length, concrete compressive strength, column depth, and joint shear. Concrete compressive strengths were 90.6 and 129.8 MPa (13,140 and 18,820 psi). Specimens consisted of 350×450 mm (13.8×17.7 in.) beams anchored with headed bars in 450×400 mm (17.7×15.7 in.) or 450×450 mm (17.7×17.7 in.) columns. Two layers of four D25 (No. 8) headed bars were used as both top and bottom beam reinforcement, with the exception of one specimen that had four bars in the outside layer and two bars on the inside layer as top and bottom beam reinforcement. The horizontal center-to-center spacing between headed bars in a layer was $3.2d_b$, and the vertical center-to-center spacing was $2.7d_b$. The yield strength of the headed bars was 634 MPa (91,930 psi). The embedment length of the headed bars was $12d_b$, with a ratio of beam effective depth to embedment length of 1.2 or 1.3 and an embedment length to column depth ratio of 0.67 or 0.75. The clear side concrete cover to the bar was $3.4d_b$ in the joint region. The gross head area of the headed bars was $6.8A_b$ with an obstruction adjacent to the bearing face that reduced the net bearing area (gross head area minus

obstruction area) to $3.9A_b$. Hoops with an area of a single leg equal to 0.078 in.^2 (Japanese bar size S8) spaced at 71 mm (2.8 in.) within the joint region were provided as confining reinforcement parallel to the headed bar, with the exception of one specimen that contained, in addition to the hoops, two single-leg ties of the same bar size and spacing parallel to the headed bars. A column axial load of $0.02A_g f'_c$ was applied during the test.

During the test, specimens reached the peak moment 8 to 7% greater than the nominal flexural strength of the beam at about 3% drift and maintained 80% of the peak load up to 4% drift. Specimens with column depths of 400 and 450 mm (15.7 and 17.7 in.) had similar peak moments and post-peak behavior. The specimen containing hoops and two single-leg ties as confining reinforcement had 6% higher peak load than the specimens containing only hoops. The joint shear at failure was 29 to 82% greater than the nominal joint shear strength. Differences in concrete compressive strength did not significantly affect joint performance. Masuo et al. (2006b) concluded that the specimens performed satisfactorily even if the joint shear stress was significantly higher than the nominal joint shear strength.

Adachi and Masuo (2007)

Adachi and Masuo (2007) tested six exterior beam-column joint specimens to investigate the effect of transverse beams (beams perpendicular to the test beam at the joint) on the anchorage performance of headed bars. The major test parameters included concrete compressive strength and the presence or absence of transverse beams. Four specimens consisted of one or two transverse beams eccentric to the column centerline by 56 mm (2.2 in.). Two specimens did not contain transverse beams. In specimens containing a single transverse beam, headed bars were used to anchor the transverse beam reinforcement into the column, while in specimens containing two transverse beams, the transverse beam reinforcement on one side of the column was continued through the joint into the transverse beam on the opposite side of the column. For the test beam, headed bars with an embedment length of $12d_b$ were used providing an effective beam depth to embedment length ratio of 1.3. The headed bars had a gross head area of $6.4A_b$, and the heads contained obstructions adjacent to the bearing face, which reduced the net bearing area (gross head area minus obstruction area) to $3.9A_b$. The specimen dimensions were $350 \times 450 \text{ mm}$ ($13.8 \times 17.7 \text{ in.}$) for the test beams, $225 \times 450 \text{ mm}$ ($8.9 \times 17.7 \text{ in.}$) for the transverse beams, and $450 \times 450 \text{ mm}$

(17.7 × 17.7 in.) for the columns. Concrete compressive strengths were 30.9 and 63.1 MPa (4,480 and 9,150 psi), and the steel yield strength was 524 MPa (75,980 psi). The specimens with 63.1 MPa (9,150 psi) concrete compressive strength contained six D25 (No. 8) headed bars in two layers (four bars in the outside layer and two bars in the inside layer) as top and bottom beam reinforcement, while specimens with concrete compressive strength of 30.9 MPa (4,480 psi) contained a single layer of four No. 8 (D25) headed bars as both the top and bottom beam reinforcement. The transverse beams contained two No. 8 (D25) bars on top and bottom face of the beam. The center-to-center spacing between headed bars in a layer in test beams was $3.2d_b$, while the spacing in transverse beams was $5d_b$. In the specimens containing two layers of headed bars, the center-to-center spacing between bars in different layers was $2.7d_b$. Clear side concrete cover to the bar at the free face of the column was $3.5d_b$. Four D10 (No. 3) hoops spaced at 60 or 85 mm (2.4 or 3.3 in.) within the joint region were provided as confining reinforcement parallel to the headed bars. The specimens were loaded for two reversed cycles in each drift level (0.5, 1, 2, 3, 4, and 6%). A column axial load of $0.04A_g f'_c$ was applied during the test.

Adachi and Masuo (2007) observed that the joint cracks in the vicinity of heads were confined by the transverse beams. The specimens containing transverse beams had higher peak loads (20-35% greater) compared to the specimens without transverse beams. The presence of transverse beams also improved the post-peak behavior of the joint; specimens with transverse beams were more ductile than those without. Adachi and Masuo (2007) suggested that the improved performance of specimens containing transverse beams resulted from reduced joint deterioration due to confinement by the transverse beams. Also, the specimens with a concrete compressive strength of 30.9 MPa (4,480 psi) exhibited a more ductile failure mode than those with a compressive strength of 63.1 MPa (9,150 psi). Adachi and Masuo (2007) concluded that the presence of transverse beams improved joint performance by confining the concrete within the joint and, as a result, reducing the joint deterioration.

Chun et al. (2007)

Chun et al. (2007) studied the effects of bar size and reinforcement detailing on the anchorage strength of exterior beam-column joints subjected to reversed cyclic loading. Three exterior and one knee beam-column joint specimen containing 90° standard hooks (Section 7.1 of

ACI 318-05), and four exterior and four knee beam-column joint specimens containing headed bars were tested. Two wide-beam-to-wall joint specimens containing hooked or headed bars were also tested. Concrete compressive strengths ranged from 32.8 to 61.7 MPa (4,760 to 8,950 psi). The hooked and headed beam reinforcement consisted of D22 (No. 7), D25 (No. 8), or D36 (No. 11) bars with actual yield strength between 403 and 468 MPa (58,450 and 67,880 psi). Headed bars contained circular heads with gross head area of 3.9 , 4.9 , and $6.2A_b$ for the No. 7, No. 8, and No. 11 bars, respectively. The heads had obstructions adjacent to the bearing face with a diameter of $1.5d_b$ and lengths ranging from 0.5 to $0.7d_b$ giving net bearing areas of 1.7 to $2.7A_b$. The horizontal center-to-center spacing of the anchored bars ranged from 3 to $4.5d_b$, while the vertical center-to-center spacing between the bars in layers ranged from 2.1 to $2.7d_b$ (1.9 to 3.4 in.). The beam bars were arranged in one or two layers, as shown in Figure D.3. The joint region was detailed in accordance with the requirements of ACI 352R-02 for Type 1 and Type 2 joints. Type 1 joints are detailed for non-seismic requirements, without considering significant inelastic deformation, while Type 2 joints are detailed for seismic loading, considering deformation under load reversals into the inelastic range. Two or three layers of hoops placed parallel to the headed bars were used as confining reinforcement between the top and bottom beam bars. D10 (No. 3), D13 (No. 4), and D16 (No. 5) bars were used as the confining reinforcement for the exterior beam-column joints, wide-beam-to-wall joints, and knee beam-column joints, respectively.

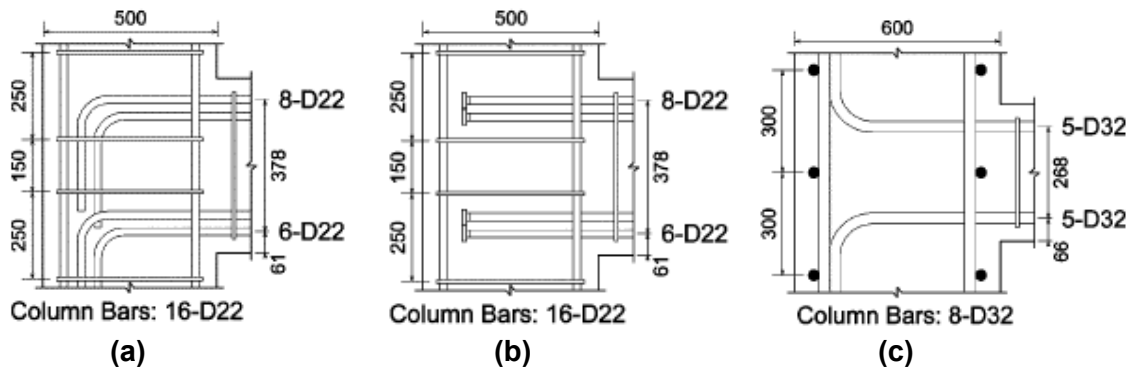


Figure D.3 Side view showing configuration of beam bars in exterior beam-column joint (a) 90° standard hooks, (b) headed bars, and (c) 90° standard hooks anchored in wall (Chun et al. 2007)

Chun et al (2007) designed the specimens to ensure yielding of the anchored bars. The embedment lengths of the hooked bars were at least the development length for standard hooks ℓ_{dh} calculated in accordance with Section 4.5.2.4 of ACI 352R-02 (see Eq. (1.2) in Section 1.3).

Specimens containing No. 7 and No. 8 bars were tested under a constant column axial load of 110 kips ($0.05A_g f'_c$, where A_g is the gross cross-sectional area of the column). Three complete cycles of reversed cyclic loading were applied to the beam at each (increasing) drift level under displacement control. Except for the specimens containing No. 11 bars (which were loaded monotonically while increasing the drift level from 0.5 to 10%), specimens were loaded to five drift levels corresponding to 1, 2, 4, 8, and 12 times the displacement at first yield. In all cases, the first drift level was within the elastic range.

Chun et al. (2007) found that the exterior beam-column joint specimen containing headed bars with a gross area of $3.9A_b$ (net bearing area of $2.9A_b$ in accordance with ASTM A970), and bearing area adjacent to the obstruction of $1.7A_b$ in a Type 1 joint, which had an embedment length equal to twice the development length calculated in accordance with Section 4.5.2.4 of ACI 352R-02 (see Eq. (1.2) in Section 1.3), maintained the peak load up to 4.5% drift and reached up to 6.8% drift maintaining 80% of the peak load when the compression reinforcement yielded. This performance was superior to the companion hooked bar specimen, which maintained peak load up to 4.9% drift, but maintained only 60% of the peak load at 3.5% drift when the compression reinforcement yielded. Based on these observations and without addressing the high value of the embedment length used in the tests, Chun et al. (2007) suggested that headed bars with a net bearing area of $3A_b$ would be sufficient to provide adequate ductility under seismic loading. The Type 2 joint containing headed bars with gross head area of $3.9A_b$ (net bearing area adjacent to the obstruction of $1.7A_b$), and an embedment length equal to twice the development length calculated in accordance with Section 4.5.2.4 of ACI 352R-02 (see Eq. (1.2) in Section 1.3), also performed satisfactorily.

Ishida et al. (2007)

Ishida et al. (2007) tested four exterior beam-column joint specimens to investigate the anchorage performance of headed bars in beams wider than columns. An exterior beam-column joint specimen containing standard 90° hooked bars, but otherwise identical to a specimen containing headed bars, was also tested for comparison. Specimens consisted of test beams 2 to 2.5 times wider than the columns. The beams had dimensions of 800×400 mm (31.5×15.7 in.) and 1000×400 mm (39.4×15.7 in.); transverse beams had dimensions ranging from 250×400

mm (9.8×15.7 in.) to 400×400 mm (15.7×15.7 in.). The columns were 400×400 mm (15.7×15.7 in.). The beams contained seven or eight No. 7 (D22) headed bars as top and bottom beam reinforcement spaced center-to-center at $4.5d_b$. The beam extending outside the column width was anchored in the transverse beams using headed bars; four out of seven bars were anchored outside the column. No vertical reinforcement at the top free face of the joint was provided to restrain the headed bars anchored in the transverse beams. Headed bars had an embedment length of $13.6d_b$, giving an effective beam depth to embedment length ratio of 1.2. The concrete compressive strength and steel yield strength were 24 MPa (3,480 psi) and 524 MPa (76,000 psi), respectively. Two D10 (No. 3) hoops in a layer spaced at 100 mm (3.9 in.) within the joint region were provided as confining reinforcement parallel to the headed bars. Load was applied for two reversed cycles in each drift level (0.5, 1, 1.5, 2, 3, and 4%). A column axial load of $0.12A_g f'_c$ was applied during the test.

Ishida et al. (2007) observed that headed bars anchored in the column reached the yield strength but that the stress in headed bars anchored in the transverse beams was up to 35% lower than yield. Specimens with 800 mm (31.5 in.) wide (2 times the column width) beams had peak moment to nominal flexural strength ratios ranging from 1.03 to 1.14. The specimen with peak moment equal to 1.14 times the nominal flexural strength of the beam had a joint shear demand equal to 74% of the nominal joint shear strength, while other specimens had joint shear demands that exceeded the joint shear strength by 8%. The specimen with a 1000 mm (39.4 in.) wide (2.5 times the column width) beam had a peak moment to nominal flexural strength ratio of 0.95 and a shear that exceeded the nominal joint shear strength by 28%. The specimen containing hooked bars reached peak load about 4% greater than that of the companion specimen containing headed bars. Unlike the companion headed bar specimen, the hooked bar specimen exhibited a sharp decline in strength once it reached the peak load. Ishida et al. (2007) concluded that beams wider than the column did not significantly affect the joint performance, but decreased the stress demand in headed bars anchored outside the column.

Tazaki et al. (2007)

Tazaki et al. (2007) tested two exterior and two interior beam-column joints to investigate the joint performance under reversed cyclic loading. In the exterior beam-column joint specimens, four D16 (No. 5) headed bars in the outside layer and two D16 (No. 5) headed bars in the inside layer were provided as top and bottom beam reinforcement. Interior beam-column joint specimens contained similar reinforcement, but in one specimen the beam reinforcement was continued through the joint, while in the other specimen a steel plate was used at the middle of the joint to connect the bars from the approaching beams. The specimens consisted of 300×300 mm (11.8×11.8 in.) beams and columns. The embedment lengths in exterior joint specimens were 10 and $16.3d_b$, giving effective beam depth to embedment length ratios equal to 1.6 and 1.0, respectively. The concrete compressive strength and the yield strength of headed bars were 30.4 and 379 MPa (4,410 and 54,960 psi), respectively. Clear concrete cover to the headed bars was $1.7d_b$. Center-to-center spacing between bars in a layer was $4d_b$, while the spacing between bars in different layers was $2.5d_b$. Three hoops with an area of single leg equal to 0.049 in.^2 (Japanese bar size D6) spaced at 2 in. within the joint region were provided as confining reinforcement parallel to the headed bars. Specimens were loaded for one cycle at 0.0625, 0.125, and 0.25% drift levels and for two cycles at 0.5, 1, 2, 3, and 4% drift levels. A column axial load of $0.08A_g f'_c$ was applied during the test.

Tazaki et al. (2007) observed extensive joint deterioration at the intersection of diagonal cracks in the interior joint specimens. In the exterior joint specimens, cracks occurred in the vicinity of heads and extended toward the compression region of the beam. The joint deterioration in these specimens was not as significant as in interior joint specimens. The peak moment in interior joint specimens was about twice the peak load in exterior joint specimens. Both exterior joint specimens reached the peak load at 3% drift and maintained at least 90% of the peak load at 4% drift. The exterior joint specimen with an embedment length of $16.3d_b$ had about 14% higher peak moment than that of the specimen with an embedment length of $10d_b$.

Kang et al. (2009)

Kang et al. (2009) investigated the anchorage behavior of headed bars in beam-column joints subjected to reversed cyclic loading using test results from 22 studies. Most of the papers describing the studies were in Japanese. The specimens included exterior beam-column joints, roof level interior beam-column joints (column terminating at a continuous beam), and knee joints (both beam and column terminating at a joint). The specimens were subjected to reversed cyclic loading with considerable inelastic lateral displacement reversals. Both the top and bottom beam reinforcing steel consisted of headed bars terminating in the joint. Kang et al. (2009) focused on the effects of embedment length, bar size, bar spacing, and net bearing area of the head. Based on an analysis of the test results, Kang et al. (2009) suggested that the minimum clear spacing between headed bars (ACI 318-08) could be reduced from 4 to $2d_b$. Their analysis showed that the equation for the development length of headed bars in Section 4.5.3 of ACI 352R-02 was less conservative than the equation in Section 21.7.5 of ACI 318-08. Kang et al. (2009) also found that joints containing headed bars with development lengths based on ACI 352R-02 performed satisfactorily in reversed cyclic loading tests. Kang et al. (2009), therefore, suggested that the provisions in ACI 352R-02 be included in ACI 318-08. Those provisions are discussed in detail in Section 1.3. Four specimens containing headed bars with a net bearing of the head less than $4A_b$ (most of them close to $3A_b$) performed satisfactorily, based on which, Kang et al. (2009) suggested that the minimum net bearing area of head may be reduced to $3A_b$. Two of the four specimens containing $2.9A_b$ heads, however, had embedment lengths 1.7 and 2.0 times the development length required in accordance with Section 25.4.4 of ACI 318-14 and Section 4.5.3 of ACI 352R-02, respectively. One specimen containing headed bars with a net bearing area equal to $2.6A_b$ had an embedment length equal to 0.9 and 1.1 times the development length required in accordance with Section 25.4.4 of ACI 318-14 and Section 4.5.3 of ACI 352R-02, respectively, but had a significant amount of confining reinforcement. The other specimen with $1.7A_b$ heads had embedment length 1.2 and 1.6 times the development length required in accordance with Section 25.4.4 of ACI 318-14 and Section 4.5.3 of ACI 352R-02, respectively.

Lee and Yu (2009)

Lee and Yu (2009) tested six simulated beam-column joints; three containing concentric beams and three containing eccentric beams anchored with standard hooks or heads in a column. Two specimens contained standard 90° hooks, two specimens contained headed bars with single head in each bar, and two specimens contained double-headed bars, as shown in Figure D.3. The double-headed bars had one head close to the critical section (outer edge of confining reinforcement as per Section 4.5.1 of ACI 352R-02) and the other at the far end of the embedment length (Figure D.3c). The headed bars consisted of circular heads with a gross head area of $6.1A_b$, but obstructions reduced the net bearing area adjacent to the head (gross area of head minus obstruction area) to $3.2A_b$. Beam reinforcement consisted of Grade 60 D22 (No. 7) bars. Concrete compressive strengths equaled 4,190 to 4,280 psi. The yield strengths of the hooked and headed bars were 66,000 psi and 68,600 psi, respectively. The center-to-center spacing between the bars and the concrete cover to the center of the bar were $2.2d_b$ and $3.5d_b$, respectively. No. 3 hoops spaced at 4 in. center-to-center were provided throughout the column and within the joint region. An embedment length of $14.9d_b$ and tail cover of 2.8 in. were used for all specimens. The embedment length was less than the development length for hooked bars required by ACI 318-08 but was greater than that recommended in ACI 352R-02. The development length requirements for headed bars in ACI 318-08 do not account for the effect of confining reinforcement. The specimens were tested under displacement control with three fully reversed cycles at each drift ratio, which increased from 0.25 to 8%. The axial stress on the column was one-tenth of the measured concrete compressive strength.

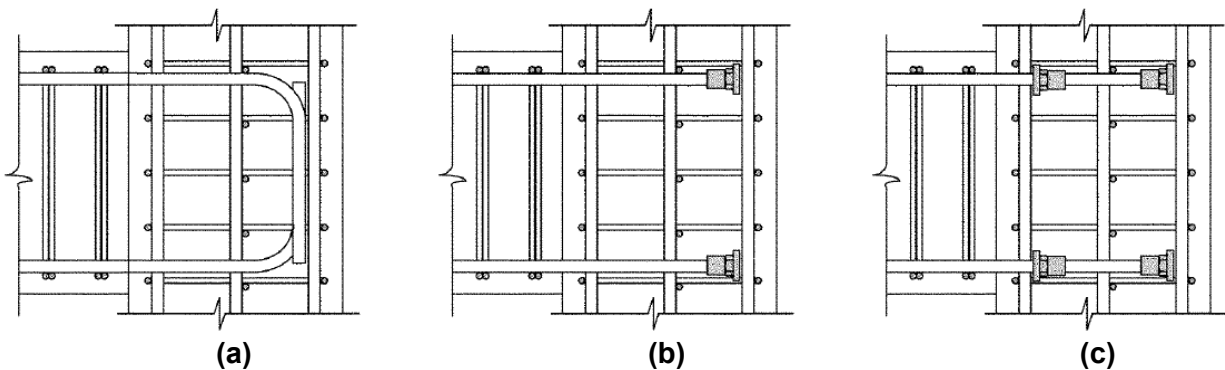


Figure D.4 Configuration of hooked and headed bars in beam-column joints (a) standard 90° hooked bars (b) single-headed bars, and (c) double-headed bars (Lee and Yu 2009)

The test results show that the specimens failed by flexural yielding, followed by the formation of cracks within the joint region along the compressive strut between the head and the compressive zone of the beam. All specimens maintained at least 80% of the peak load at the end of the third cycle at 3.5% drift. This is an acceptable level of performance under the provisions of ACI 374.1-05, which provides minimum acceptance criteria to validate results for tests of weak beam-strong column connections. Test results from beam-column joint specimens under reversed cyclic loading complying with the criteria in ACI 374.1-05 are considered adequate to be used in moment frames in high seismic regions. The eccentric beam-column joint specimen containing hooked bars (Figure D.4a) maintained only 50% of the peak load at 5% drift, while the concentric beam-column joint specimen with hooked bars maintained 80% of the peak load at the same drift level. Both the concentric and the eccentric beam-column joint specimens containing headed bars (Figure D.4b) maintained 80% of the peak load at 5% drift. The specimens containing double-headed bars, shown in Figure D.4c, exhibited improved performance under reversed cyclic loading compared to the other specimens. In these specimens, the *peak load* was maintained at 5% drift level (the concentric specimen maintained the peak load up to 7% drift). The performance of the eccentric beam-column joint specimen was similar to that of the concentric specimen up to 4 or 5% drift, but the eccentric beam-column joint specimen deteriorated more rapidly than the concentric specimen at higher drift levels. These results were achieved with $2.2d_b$ of center-to-center spacing between the anchored bars; as a result, Lee and Yu (2009) suggested that the minimum $4d_b$ center-to-center spacing between headed bars required by Section 12.6 of ACI 318-08 could be reduced. They did not, however, tie their recommendation to a value of embedded length. They also concluded that the use of headed bars with a single head at the end of the embedment length is sufficient to provide adequate strength up to 4% drift, while double headed bars improve performance up to 7% drift.

Kang et al. (2010)

Kang et al. (2010) tested a single beam-column joint specimen to investigate the anchorage behavior of small headed bars under reversed cyclic loading. The headed bars consisted of circular heads with a net bearing area of $2.6A_b$, below the value of $4A_b$ required by ACI 318, and had no obstructions adjacent to the head. The specimen contained four No. 6 headed bars as top and

bottom beam reinforcement was embedded $15d_b$ into the column (Figure D.5). Three D10 (No. 3) hoops were used as confining reinforcement in the joint region. The concrete compressive strength was 29.1MPa (4,220 psi), and the yield strength of the headed bars was 481 MPa (69,750 psi). A beam-column joint specimen containing standard 90° hooked bars, but otherwise identical to the headed bar specimen, was also tested for comparison. The specimens were loaded to drift levels of 0.4 to 3.5%, with three complete cycles at each drift level. Kang et al. (2010) included test results from Choi et al. (2002) and Choi (2006) that included 80 tests with single and multiple headed bars embedded in reinforced concrete column-like members with embedment lengths ranging from 6 to $15d_b$. In these tests, D19 (No. 6) square headed bars with a net bearing area of $3A_b$ and thickness of $1d_b$ were used. To design the beam-column joint specimens, Kang et al. (2010) relied on the following conclusions by Choi et al. (2002) and Choi (2006):

- Anchorage behavior of multiple headed bars is independent to the clear bar spacing within the range they tested (clear bar spacing from 3.5 to $8d_b$).
- If the clear side concrete cover is greater than or equal to $3.5d_b$ and if confining reinforcement spaced at $3d_b$ within a distance of 0.45 times the embedment length from the headed bar is provided, an embedment length of at least $13d_b$ is required to develop 125% of yield strength on a headed bar.
- For side cover greater than $2.8d_b$, anchorage strength increases as side cover increases.

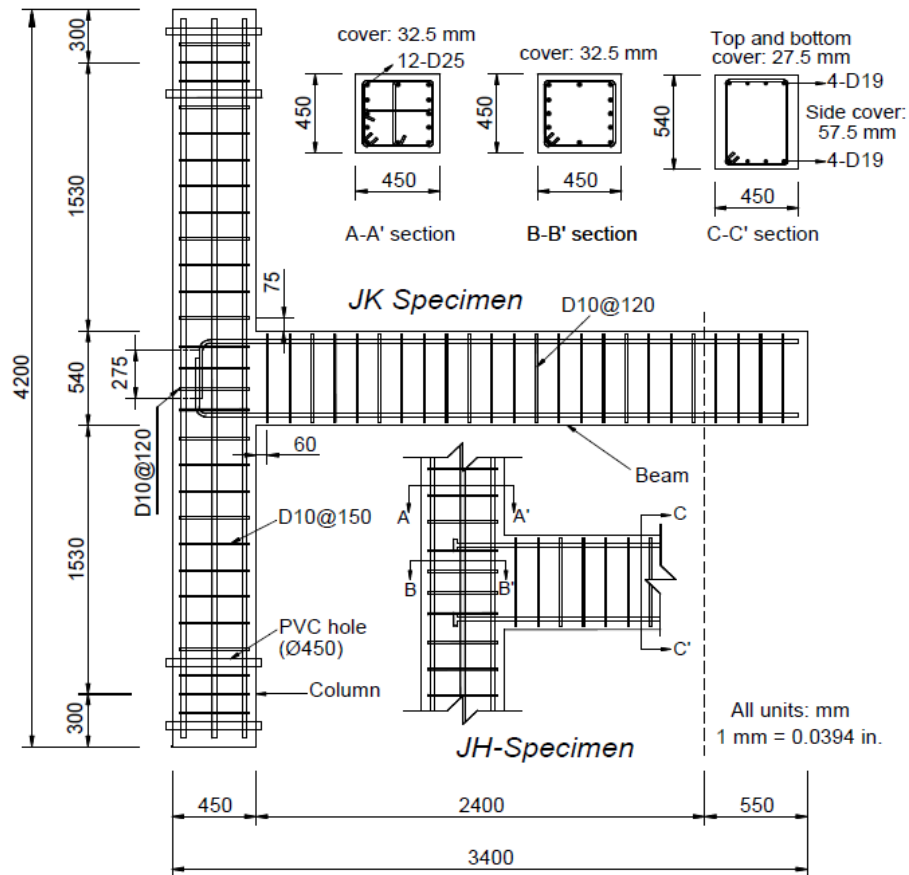


Figure D.5 Detail of exterior beam-column joint specimens containing hooked bars and headed bars (Kang et al. 2010)

The performance of the exterior beam-column joint containing headed bars with a net bearing area of $2.6A_b$ was superior to that of the companion specimen containing hooked bars. Both specimens failed by flexural yielding; however, the specimen containing hooked bars exhibited more severe joint deterioration. Both specimens had similar peak loads at about 2.2% drift. However, the specimen containing headed bars maintained the peak load up to 3.5% drift, while the specimen containing hooked bars maintained only 75% of the peak load at 3.25% drift. Kang et al. (2010) also observed that the specimen containing headed bars had greater energy dissipation capacity during each drift cycle after first yield. Kang et al. (2010) concluded that headed bars with a net bearing area of $2.6A_b$ performed satisfactorily under reversed cyclic loading.

Kang et al. (2012)

Kang et al. (2012) tested two exterior beam-column joint specimens subjected to reversed cyclic loading to investigate the effect of bar clear spacing and multiple layers of headed bars on anchorage performance. As shown in Figure D.6, one specimen (JH-R1) contained four D19 (No.

6) headed bars as top and bottom beam reinforcement in a single layer spaced center-to-center at $3.1d_b$, while the other specimen (JH-R2) contained two layers of two D19 (No. 6) headed bars with a center-to-center spacing between the bars in different layers of $2.3d_b$. The net bearing area of the head was $5.3A_b$, and the head had no obstruction. The specimens consisted of 255×405 mm (10×15.9 in.) beams and 380×380 mm (15×15 in.) columns. The concrete compressive strength and yield strength of the headed bars were 30.1 and 183.4 MPa (4,360 and 69,460 psi), respectively. Then embedment length of the headed bars was $15d$, and the effective beam depth to embedment length ratios were 1.2 and 1.3. The clear concrete cover to the headed bars was $1.6d_b$. Three D10 (No. 3) hoops with single-leg ties spaced at 90 mm (3.5 in.) were provided as confining reinforcement parallel to the headed bars within the joint region. Specimens were loaded for three cycles each at 0.5, 0.75, 1, 1.5, 2, 3, 4, and 5% drift levels. No column axial load was applied during the test.

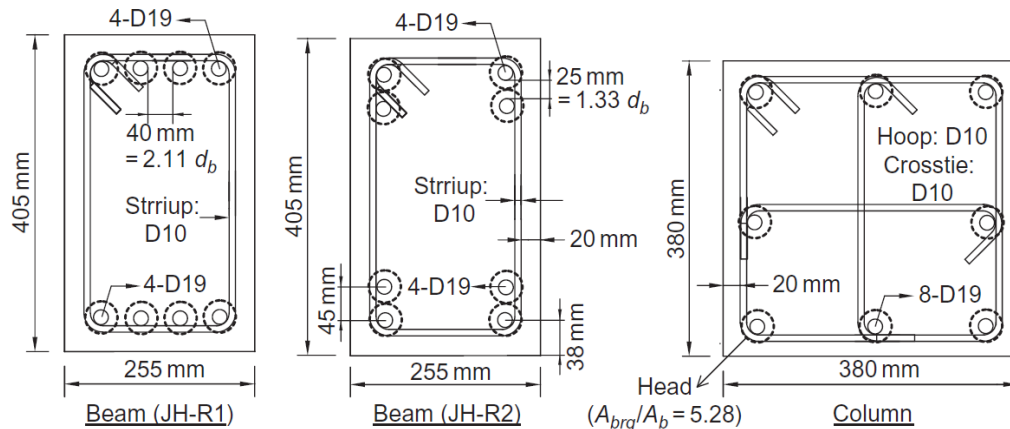


Figure D.6 Reinforcement detail for exterior beam-column joint specimens (Kang et al. 2012)

Kang et al. (2012) observed flexural cracks at the beam-column joint interface at drifts of 1 to 1.5%. Diagonal cracks at the joint region formed around the heads and extended toward the compression region of the beam. Both specimens exhibited flexural hinging in the beams. The specimens reached a nominal flexural strength of the beam at 1.7 to 2.8% drift. The peak moments occurred at 3.5 to 4.9% drift and were 17 to 20% greater than the nominal flexural strength of the beams. Kang et al. (2012) concluded that the headed bars with clear spacing of about $2d_b$ or placed in two layers may be permitted for the anchorage of headed bars in beam-column joint subjected to reversed cyclic loading. These specimens, however, had embedment lengths that were 21 and 30% greater than required to yield the headed bars based on the descriptive equations discussed in

the current study for bars with the spacing used in the specimens. Thus, the specimens by themselves, do not demonstrate that $2d_b$ spacing can be used.

Chun and Shin (2014)

Chun and Shin (2014) studied the effects of joint aspect ratio (beam depth-to-column depth ratio) and confining reinforcement on the anchorage strength of headed bars in beam-column joints subject to reversed cyclic loading. Seven exterior beam-column joints with joint aspect ratios ranging from 0.67 to 2.5 were tested. The specimens consisted of a 300×300 mm (12×12 in.) column and 250 mm (9.8 in.) wide beam; beam depths ranged from 200 to 750 mm (7.9 to 29.5 in.) depending on the joint aspect ratio. Five of the specimens contained five D13 (No. 4) hoops and D10 (No. 3) single-leg ties spaced at 3 in. as confining reinforcement within the joint region, in accordance with the joint confining reinforcement requirement of Section 4.2.2.2 of ACI 352R-02. The other two specimens contained five D10 (No. 3) hoops and D10 (No. 3) single-leg ties spaced at 75 mm (3 in.) within the joint region, two-thirds of the amount of confining reinforcement required in Section 4.2.2.2 of ACI 352R-02. The beams contained D19 (No. 6) headed bars with a bearing area, calculated as gross head area minus bar area, of $4A_b$ (complying with ASTM A970). However, the heads had obstructions (with a diameter of $1.5d_b$ and a length of $0.68d_b$), which reduced the net bearing area adjacent to the obstruction (gross head area minus obstruction area) to $2.7A_b$. The clear spacing between the headed bars was $1.3d_b$. Embedment lengths were $12d_b$ for all specimens. Concrete compressive strengths were between 25.6 and 26.4 MPa (3,710 and 3,830 psi). No column axial load was applied during the test. Seven other exterior beam-column joints containing standard 90° hooked bars, but otherwise identical to the specimens containing headed bars, were also tested for comparison.

The test results showed that specimens reached a peak moment 1.5% to 17% greater than the nominal moment capacity based on the yield strength of the beam reinforcement. All specimens maintained their peak load at 3.5% drift. Specimens with a joint aspect ratio (beam depth-to-column depth) less than or equal to 1.0 failed by flexural hinging at the beam away from the joint with limited joint deterioration; specimens with a joint aspect ratio greater than 1.5 also failed by hinging at the beam but with extensive joint deterioration characterized by substantial spalling of the joint cover concrete. The specimens containing the lower amount of confining reinforcement

showed similar behavior to the specimens containing confining reinforcement in accordance with ACI 352R-02. Chun and Shin (2014) found no significant difference between the specimens containing headed bars and the specimens containing hooked bars in terms of failure modes, joint deterioration, energy dissipation, or moment-drift relationship.

Dhake et al. (2015)

Dhake et al. (2015) tested six one-third scale exterior beam-column joint specimens to investigate the anchorage of headed bars with and without confining reinforcement within the joint region. Of the six specimens, beam reinforcement was anchored in the column using 90° hooked bars or straight bars in two specimens. The remaining four specimens contained headed bars with circular heads. One of the four headed bar specimens contained PVC sheathing along the total embedment length to prevent any bond between the embedded portion of the bar and the surrounding concrete. The net bearing area of the heads was $4A_b$, and the heads had no obstructions adjacent to the bearing face. The major test parameters included embedment length and confining reinforcement within the joint region. The specimens consisted of 150×180 mm (5.9×7.1 in.) beams and 150×200 mm (5.9×7.9 in.) columns. A single layer of two D12 (No. 4) bars with a yield strength of 525 MPa (76,100 psi) were used as top and bottom beam reinforcement. The concrete compressive strength was 4,350 psi. Embedment lengths were 8.5 and $12.5d_b$, which resulted in effective beam depth to embedment length ratios of 1.5 and 1.0, respectively. Three hoops of D6 bars (with an area of a single leg equal to 0.049 in.^2) spaced at 100 mm (4 in.) were provided as confining reinforcement parallel to the anchored bars within the joint region in the specimen containing hooked bar and in one of the four specimens containing headed bars. The other specimens contained no confining reinforcement within the joint region. The clear side concrete cover to the bar at the free face of the column and the center-to-center spacing between the bars were $2d_b$ and $7.5d_b$, respectively. The specimens were loaded for two reversed cycles at each drift level from 0.5 to 5% with an increment of 0.5% from the first to second drift level and 1% for higher drift levels. A column axial load of $0.2A_g f'_c$ was applied during the test.

None of the specimens exhibited side blowout failure, leading Dhake et al. (2015) to conclude that a side clear cover of $2d_b$ is sufficient to prevent such failure. All specimens containing headed bars, including the one with PVC sheathing as bond breaker, exhibited flexural

hinging of the beam with less than 20% drop in the peak load at 3.5% drift, indicating an acceptable level of performance under reversed cyclic loading. Headed bar specimens without confining reinforcement within the joint region exhibited greater joint deterioration than the specimens with confining reinforcement. The performance of the specimen containing hooked bars was comparable with that of the companion headed bar specimen, with flexural hinging of the beam accompanied by less than 20% drop in peak load at 3.5% drift. The hooked bar specimen, however, exhibited a drop in the peak load by 18% at 4% drift, while the companion headed bar specimen maintained the peak load up to 5% drift. The specimen with the beam bars anchored by straight bars performed poorly, with the peak load equal to only 60% of the peak load of the companion headed bar specimen at 3% drift. Since the behavior of unbonded bars is expected to differ from that of fully bonded bars, only three out of four specimens containing headed bars without PVC sheathing are included in the current study.

